

AD-A280 273

AGARD-R-797

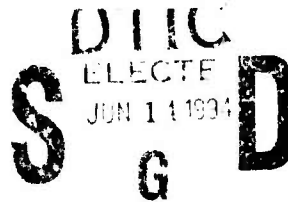


AGARD-R-797

# AGARD

ADVISORY GROUP FOR AEROSPACE RESEARCH & DEVELOPMENT  
7 RUE ANCELLE 92200 NEUILLY SUR SEINE FRANCE

AGARD REPORT 797



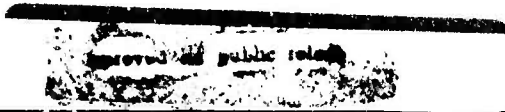
## An Assessment of Fatigue Damage and Crack Growth Prediction Techniques

(L'Evaluation de l'Endommagement en Fatigue  
et les Techniques de Prédiction  
de la Propagation des Fissures)

*Papers presented at the 77th Meeting of the AGARD Structures and Materials Panel,  
held in Bordeaux, France 29th—30th September 1993.*



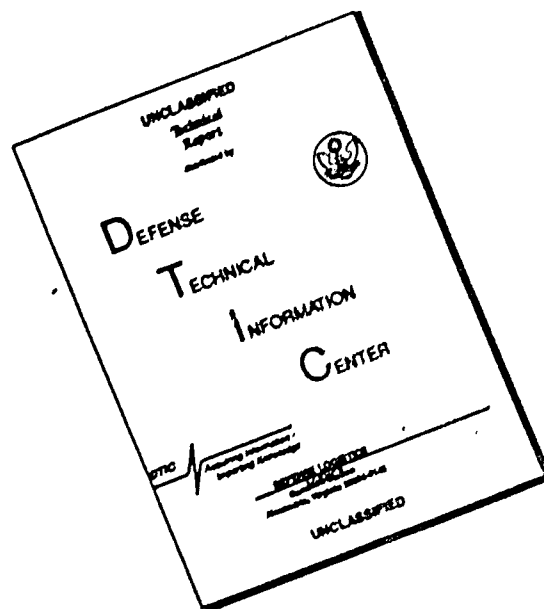
NORTH ATLANTIC TREATY ORGANIZATION



Published March 1994

*Distribution and Availability on Back Cover*

# DISCLAIMER NOTICE



THIS DOCUMENT IS BEST QUALITY AVAILABLE. THE COPY FURNISHED TO DTIC CONTAINED A SIGNIFICANT NUMBER OF PAGES WHICH DO NOT REPRODUCE LEGIBLY.

# AGARD

ADVISORY GROUP FOR AEROSPACE RESEARCH & DEVELOPMENT

7 RUE ANCELLE 92200 NEUILLY SUR SEINE FRANCE

**AGARD REPORT 797**

## An Assessment of Fatigue Damage and Crack Growth Prediction Techniques

(L'Evaluation de l'Endommagement en Fatigue  
et les Techniques de Prédiction  
de la Propagation des Fissures)

Accession For	
NTIS CRA&I	<input checked="" type="checkbox"/>
DTIC TAB	<input checked="" type="checkbox"/>
Unannounced	<input type="checkbox"/>
Justification	
By	
Distribution /	
Availability Codes	
Dist	Avail and/or Special
A-1	

DTIC QUANTITY INCLUDED 2

Papers presented at the 77th Meeting of the AGARD Structures and Materials Panel,  
held in Bordeaux, France 29th—30th September 1993.



North Atlantic Treaty Organization  
Organisation du Traité de l'Atlantique Nord

2770  
94-18167

94 3 13 000

# The Mission of AGARD

According to its Charter, the mission of AGARD is to bring together the leading personalities of the NATO nations in the fields of science and technology relating to aerospace for the following purposes:

- Recommending effective ways for the member nations to use their research and development capabilities for the common benefit of the NATO community;
- Providing scientific and technical advice and assistance to the Military Committee in the field of aerospace research and development (with particular regard to its military application);
- Continuously stimulating advances in the aerospace sciences relevant to strengthening the common defence posture;
- Improving the co-operation among member nations in aerospace research and development;
- Exchange of scientific and technical information;
- Providing assistance to member nations for the purpose of increasing their scientific and technical potential;
- Rendering scientific and technical assistance, as requested, to other NATO bodies and to member nations in connection with research and development problems in the aerospace field.

The highest authority within AGARD is the National Delegates Board consisting of officially appointed senior representatives from each member nation. The mission of AGARD is carried out through the Panels which are composed of experts appointed by the National Delegates, the Consultant and Exchange Programme and the Aerospace Applications Studies Programme. The results of AGARD work are reported to the member nations and the NATO Authorities through the AGARD series of publications of which this is one.

Participation in AGARD activities is by invitation only and is normally limited to citizens of the NATO nations.

The content of this publication has been reproduced directly from material supplied by AGARD or the authors.

Published March 1994

Copyright © AGARD 1994  
All Rights Reserved

ISBN 92-835-0734-7



Printed by Specialised Printing Services Limited  
40 Chigwell Lane, Loughton, Essex IG10 3TZ

## Preface

Fatigue is an important consideration in structural design and monitoring of continued airworthiness of military aircraft. During a previous AGARD Meeting, held in Bath in 1991, a need was identified to review the efficacies of the several methods that are used for assessment of fatigue damage and crack growth in airframe components by comparing their predictions against full-scale test and service experiences, to thereby categorize the degree of conservatism inherent in each method. The latter consideration is essential to sound management of fatigue consumption. Towards that end, the Structures and Materials Panel (SMP) within AGARD organized a Workshop in the Fall of 1993, titled "An Assessment of Fatigue Damage and Crack Growth Prediction Techniques".

The Workshop provided a forum for an in-depth discussion of the correlation between in-service experience and results from analytical predictive models, specimen level tests, component tests and full-scale tests. Additionally, the Workshop made possible an examination of the operating standards that different countries adopt with respect to various elements in the design process such as load spectrum, exceedance diagram, algorithm for calculating fatigue damage, and in-service monitoring protocol — all contributing to refinement of the requirements of an aircraft monitoring system.

## Préface

La fatigue est une considération importante pour la conception structurale et le suivi permanent de l'aptitude au vol des avions militaires. Lors d'une réunion de l'AGARD à Bath en 1991, le Panel AGARD SMP a identifié le besoin de revoir l'efficacité des différentes méthodes utilisées pour l'évaluation de l'endommagement en fatigue et la propagation des fissures dans les éléments de cellule, en comparant les prévisions obtenues par ces méthodes aux résultats des essais en vraie grandeur et aux données d'exploitation, afin de catégoriser le degré conservatoire propre à chaque méthode. Cette dernière considération est essentielle pour la bonne gestion de l'endurance en fatigue. Dans cette optique, le Panel AGARD des structures et matériaux (SMP) a organisé un atelier sur "l'évaluation de l'endommagement en fatigue" et les techniques de prédiction de la propagation des fissures" en automne 1993.

L'atelier a servi de forum pour des discussions approfondies de la corrélation qui existe entre le fonctionnement en service et les résultats obtenus des modèles prédictifs analytiques, des essais sur échantillon, des essais de composants et des essais en vraie grandeur. En outre, l'atelier a permis l'étude des normes d'exploitation adoptées par les différents pays en ce qui concerne les divers éléments du processus de conception tels que le spectre de charge, le schéma d'exécédent, l'algorithme de calcul de l'endommagement en fatigue et le protocole de contrôle en service — autant d'aspects qui concourent à l'optimisation de la spécification d'un système de contrôle d'avion.

Dr S.G. Sampath  
Sub-Committee Chairman

# Structures and Materials Panel

**Chairman:** Mr Roger Labourdette  
Directeur Scientifique des  
Structures  
ONERA  
29, Avenue de la Div. Leclerc  
92322 Châtillon  
France

**Deputy Chairman:** Dipl.Ing. O. Sensburg  
Deutsche Aerospace Structures  
Militärflugzeuge  
LME 202  
Postfach 80 11 60  
8000 Munich 80  
Germany

## SUB-COMMITTEE

**Chairman:** Dr S. Sampath  
Federal Aviation Administration  
Technical Center  
Atlantic City International Airport  
Code ACD-200  
Atlantic City, NJ 08405  
United States

## Members

P. Armando	FR	H.H. Ottens	NE
M. Curbillon	FR	D.B. Paul	US
W. Elber	US	R.J. Pax	SP
H. Goncalo	PO	C. Perron	UK
C.R. Gostelow	UK	A. Salvetti	IT
P. Heuler	GE	E. Sanchiz	SP
A.R. Humble	UK	O. Sensburg	GE
M.J. Kilst w	UK	D.L. Simpson	CA
R. Labourdette	FR	T.P. Watterson	UK
C. Moura Branco	PO		

## PANEL EXECUTIVE

Dr Jose M. Carballal, Spain

**Mail from Europe:**  
AGARD—OTAN  
Attn: SMP Executive  
7, rue Ancelle  
92200 Neuilly-sur-Seine  
France

**Mail from US and Canada:**  
AGARD—NATO  
Attn: SMP Executive  
Unit 21551  
APO AE 09777

Tel: 33(1)47 38 57 90 & 57 92  
Telex: 610176 (France)  
Telefax: 33(1)47 38 57 99

# Contents

	Page
<b>Preface/Préface</b>	iii
<b>Structures and Materials Panel</b>	iv
	Reference
<b>Technical Evaluation Report</b> by T. Swift	T
<b>Lead Paper: Overview of the Structural Integrity Process</b> by J.W. Lincoln	LP
<b>SESSION I – MEASUREMENTS AND PREDICTIVE METHODOLOGIES</b>	
<b>Miner's Rule Revisited</b> by W. Schütz and P. Heuler	1
<b>Fatigue Life and Crack Growth Prediction Methodology</b> by J.C. Newman, Jr, E.P. Phillips and R.A. Everett, Jr	2
<b>Crack Growth Predictions using a Crack Closure Model</b> by R.L. Hewitt and P.G. Collins	3
<b>Paper 4 withdrawn</b>	
<b>The Crack Severity Index of Monitored Load Spectra</b> by J.B. de Jonge	5
<b>SESSION II – MEASUREMENTS AND PREDICTIVE METHODOLOGIES</b>	
<b>An Assessment of Fatigue Crack Growth Prediction Models for Aerospace Structures</b> by A. Salvetti, L. Iazzeri and A. Pieracci	6
<b>A Combined Approach to Buffet Response Analyses and Fatigue Life Prediction</b> by J.H. Jacobs and R. Perez	7
<b>Paper 8 withdrawn</b>	
<b>Notch Fatigue Assessment of Aircraft Components using a Fracture Mechanics Based Parameter</b> by Chr. Boller and M. Buderath, P. Heuler and M. Vormwald	9
<b>Growth of Artificially and Naturally Initiating Notch Root Cracks under FALSTAFF Spectrum Loading</b> by R. Sunder, R.V. Prakash and E.I. Mitchenko	10
<b>SESSION III – DESIGN EXPERIENCES</b>	
<b>Rotorcraft Fatigue Life-Prediction: Past, Present and Future</b> by R.A. Everett Jr, and W. Elber	11
<b>Fatigue Management and Verification of Airframes</b> by A.F. Blom and H. Ansell	12

	<b>Reference</b>
<b>Risk Analysis of the C-141 WS405 Inner-to-Outer Wing Joint</b> by R.E. Alford, R.P. Bell, J.B. Cochran and D.O. Hammond	13
<b>Assessment of In-Service Aircraft Fatigue Monitoring Process</b> by R.J. Cazes	14
<b>The Role of Fatigue Analysis for Design of Military Aircraft</b> by R. Bochmann and D. Weisgerber	15

**SESSION IV – DESIGN EXPERIENCES**

<b>Damage Tolerance Management of the X-29 Vertical Tail</b> by J. Harter	16
<b>Harrier II: A Comparison of US and UK Approaches to Fatigue Clearance</b> by F.S. Perry	17
<b>Fatigue Design, Test and In-Service Experience of the BAe Hawk</b> by J. O'Hara	18
<b>Reduction of Fatigue Load Experience as Part of the Fatigue Management Program for F-16 Aircraft of the RNLAf</b> by D.J. Spiekhout	19
<b>An Overview of the F-16 Service Life Approach</b> by J. Morrow and G. F. Herrick	20

# Technical Evaluation Report

by

**I. Swift**

Chief Scientific Technical Advisor  
Fracture Mechanics Metallurgy  
Federal Aviation Administration  
3229F Spring Street  
Long Beach, CA 92630  
United States

The following report attempts to provide a summary of the Workshop on "An Assessment of Fatigue Damage and Crack Growth Prediction Techniques" sponsored by the Structures and Materials Panel of the Advisory Group for Aerospace Research and Development (AGARD).

The theme of this Workshop, chaired by Dr. S.G. Sampath (FAA United States) was to assess fatigue damage and crack growth to categorize the degree of conservatism inherent in each method with respect to full-scale test and service experience. The Workshop was intended to provide a discussion about all aspects of the fatigue process from spectra development through the crack initiation and propagation phases to in-service monitoring. Eighteen papers were presented in four sessions, two of which were related to Measurements and Predictive Methods/techniques, and two related to Design Experiences. In addition, a lead paper was presented by Dr. J.W. Lincoln from the USAF which provided an overview of the overall structural integrity process for US military aircraft. It is believed the theme of the Workshop was amply satisfied by the 19 technical papers presented followed by, in some cases, animated discussions which again reinforced the scientific communities view that there is more than one way to solve an engineering problem. The papers covered a wide historical segment of variable amplitude fatigue initiation and propagation development from the early 1920s to modern Neural Network Monitoring Technology. The overview paper by Dr. Lincoln emphasized the importance of considering all the five links of the structural integrity process (i.e. Design Information through Design Analysis and Development Tests, Full Scale Testing, Force Management Data Package to Force Management. Dr. Lincoln outlined all the potential threats to structural integrity encountered from material, manufacturing, environmental and service operations. He also emphasized the political threats often encountered during the procurement of military aircraft in today's economic environment.

The first paper of Session I, entitled "Miner's Rule Revisited", was appropriately chosen to "start the ball rolling" and was presented by Dr. W. Schatz of IABG. Dr. Schatz described a very large fatigue test program which included five types of automotive components tested under constant amplitude and variable amplitude loading. He indicated that predictions by Miner's Rule were, in most cases, unconservative and in one case damage to failure was as low as 0.044, corresponding to an overestimation of fatigue life using Miner's Rule by a factor of 23. He indicated that many attempts to improve Miner's Rule have been made but in retrospect all have been unsuccessful. Dr. Schatz emphasized that quite surprisingly this

fact has not deterred industrial (including aeronautical users) from still calculating the fatigue life of their products to this day by Miner's Rule with a cumulative damage sum of 1.0. He indicated that fatigue life prediction by calculation alone can never be employed for critical components; fatigue tests with the component and/or inspections and damage tolerance or fail safe design are necessary.

In contrast to these results, Dr. James Newman of NASA, presenting a paper entitled "Fatigue Life and Crack Growth Prediction Methodologies", by himself et al. described prediction of total fatigue life of notched specimens subjected to constant and variable amplitude loading within a factor of two. The total fatigue life prediction approach based solely on crack growth phenomena uses a plasticity induced crack closure model together with initial microstructural features such as inclusion particle sizes. As the first two sessions proceeded the crack closure concept appeared to emerge as the most popular in accounting for load sequence effects in crack propagation analysis.

Crack growth predictions for through and corner cracks in T65 D551 plate under constant amplitude loading and corner cracks under two variable amplitude loadings were described by Mr. H.H. Hewson of the National Research Council of Canada. A crack closure model embedded in what was described as a "Black Box" program was used. Excellent predictions for both life and final crack length could be obtained if crack growth data were into the program in tubular form were modified to increase growth rates at higher values of stress intensity factor range. Life prediction ratios were within 0.57 to 1.34. In the ensuing discussion, Dr. Newman cautioned that  $d_a/d_N$  can be different than  $d_s/d_N$  for surface crack growth.

A description of the development and validation of the "Crack Severity Index" (CSI) as a means of expressing relative damage in terms of crack growth potential of stress spectra was given by Mr. J.H. de Jong of NLR, Netherlands. The CSI which takes into account spectrum shape, is a crack closure model. The method has been validated with a very large number of tests under a wide variety of spectra for a wide variety of locations in the F-16 aircraft used by the RNLAF. The CSI used as a standard tool in the RNLAF F-16 Fatigue Load Monitoring Program appears to provide a reasonably accurate measure of the relative severity of maneuver dominated fighter spectra.

In a paper by himself et al. Dr. E. Lazzari of the University of Pisa described an ongoing research program in the Department of Aerospace Engineering to assess fatigue and crack



gram is supported by full scale fatigue testing to several lifetimes. A second fatigue test of the JAS 39 is planned to at least four lifetimes.

A presentation was made by Dr J.W. Lincoln, on behalf of Mr J.B. Cochran et al. from Lockheed Aeronautical Systems, on a fracture based risk assessment of the C-141 transport wing joint at WS 405. This wing joint suffered both multi-element and multi-site fatigue damage. The aircraft was designed to provide 30,000 flight hours and the force is currently averaging 34,000 hours. Dr Lincoln explained that it is not inconceivable to expect this aircraft to provide reliable service well into the 21st century and stated that the current tools of structural analysis must go beyond the specifics of strength, durability and fracture mechanics into the realm of statistics and reliability. The acceptable single flight risk after structural member failure, as adopted by the USAF Scientific Advisory Board (SAB) for this evaluation, was  $1.0 \times 10^{-4}$ . Dr Lincoln mentioned that the intact structural risk should be no greater than  $1.0 \times 10^{-4}$ . The risk assessment provided valuable input into the decision process for implementing actions in a timely manner to protect the safety of the force.

The assessment of an in-service monitoring process to maintain structural integrity was described by Mr R.J. Cazes of Dassault Aviation. The process uses a test-calibrated Miner's cumulative damage law (Miner's relative law) to establish crack initiation followed by damage tolerance evaluation. The approach is supported by in-flight integrated calculations considering load signal precision, elimination of low amplitude variations and cycle counting methods. Use is made of already available Electric Flight Control Systems (EFCS) to obtain real forces on the aircraft in use. This on-board monitoring revealed that the Mirage 2000 aircraft was being used more severely than considered during design. The structure has been subsequently strengthened in aircraft in current production.

The role of fatigue analysis for the design of military aircraft was described by Dr R. Bochmann in a paper by himself and Mr D. Weisgerber of Deutsche Aerospace Military Aircraft (DASA). Dr Bochmann stated that, despite many reservations expressed in numerous publications, the Miner's cumulative damage rule is still used at DASA and widely used in Europe due to its simple and universal applicability. Studies have revealed that the cause of fatigue cracks developed during tornado full-scale fatigue testing were due to the lack of accuracy in stress analysis. It was concluded that a change in design philosophy from "safe life" to "damage tolerance" would not have automatically improved efficiency of the analysis. Dr Bochmann indicated that it is doubtful if Miner's rule will be replaced by more sophisticated methods for safe life design.

Damage tolerance management of the X-29 vertical tail in the presence of severe buffet loads was described by Mr J. Harter of the USAF. Fin tip acceleration levels of 110 Gs at 16 Hz were experienced during initial flight testing of the aircraft. Although the aircraft was not initially designed according to damage tolerance principles, it was possible to apply these principles to manage the safety of the aircraft through completion of the flight test program. A crack growth prediction model (MODGRO) was developed and three-dimensional crack growth analysis performed at a critical location near the root of the fin between flight days. The minimum crack growth life in terms of buffet events was determined from a  $0.01 \times 0.01$  inch corner crack at the critical hole. Time in buffet and

the number of buffet events were monitored and allowed safe completion of the flight test program.

A comparison of US and UK approaches to fatigue clearance of the Harrier II aircraft was presented by Mr E.S. Perry of the Military Aircraft Division of British Aerospace Defence Ltd. The UK requirements for fatigue clearance include analysis using the nominal stress Miner's cumulative damage rule together with an S-N equation for bolted joints derived at the Royal Aeronautical Establishment (RAE) by R.B. Heywood. The US method used by McDonnell Aircraft Company (MCAIR) is based on a stress concentration factor/design limit stress (KtDLS) approach. This method is based on local strain analysis using Neuber's rule. The two methods are different in that the nominal stress approach cannot account for notch residual stresses whereas the KtDLS approach accounts for this. However, the paper debates whether this is important. In fact the results from a comparison lead to a conclusion that there is little to choose between the two methods.

A paper, entitled "Fatigue Design, Test and In-Service Experience of the BAe Hawk by Mr J. O'Hara of British Aerospace Defence Ltd. was presented by Mr Alan Humble who described design of the Hawk to AP 970 safe life requirements for a 6000 hour life with scatter factor of 5. A full-scale fatigue test has been used to lead the fleet. Incidents arising on the test are handled by several approaches including S-N and fracture mechanics analyses with modifications and/or routine inspections. Although fatigue analyses are based on the Miner's rule approach, the key to good fatigue (damage tolerant) design is the choice of materials possessing good resistance to crack growth.

Reduction of fatigue load experience as part of the fatigue management program for F-16 aircraft of the RNLAf was presented by Mr D.J. Spiekhout of NLR. The loads monitoring program for this aircraft uses an electronic device capable of analyzing a calibrated strain gage on one of the major carry-through bulkheads of the fuselage. This is done on a sample of the fleet and, by using a large centralized data base system, individual airplane tracking is performed. The fatigue damage per flight is calculated in terms of crack growth through the use of a "Crack Severity Index" (CSI) using a crack closure model. The RNLAf F-16s are flown more severely than other fleets of F-16s and attempts are made to reduce crack growth damage through reductions in stress per G by take off store configuration manipulation. Thus, reductions in fatigue load experience are achieved on individual aircraft.

An overview of the F-16 service life approach by Mr J.W. Morrow of Lockheed Ft Worth was presented by Dr J.W. Lincoln. The F-16 was the first aircraft designed to the USAF fracture requirements from its inception to an 8000 hour life with a factor of two. The safe life approach, abandoned in the early 70s, did not account for initial flaws and had shown poor correlation between test and service. The presentation covered all aspects of the structural integrity program with an introduction to the F-16 airframe, design/prediction approaches, test policy comparisons, fracture control plan, force management approach and a considerable list of lessons learned from which subsequent programs have gained considerable benefit.

In reviewing the 19 excellent papers presented during the Workshop and listening to subsequent discussions, it became abundantly clear that, even after 150 years of fatigue analysis methodology development, the hope for a universal approach to future fatigue life prediction is not in sight in the foresee-

able future. Many still feel comfortable with the Miner's cumulative damage rule approach, perhaps on account of its simplicity, even though it has been demonstrated to be unconservative in its predictions, in some cases by an order of magnitude. This fact surprises Dr Schütz and me but is adamantly defended by current users. Other researchers, recognizing that total fatigue life is a crack propagation process from the first load application, are plowing new ground by developing total fatigue life crack growth models that include cracks initiating from microstructural inclusions. Such models appear to offer a prediction capability within a factor of 2. It was noted during discussion that the damage tolerance philosophy is used world wide for commercial transport certification and for aircraft designed for the US Air Force. It was generally thought that the safe life approach was confined to military aircraft designed in Europe. This of course is not the case in Sweden nor is it the case in the Netherlands for life management of military aircraft. However, Miner's rule analysis appeared to be generally favored by military aircraft designers in other countries in Europe. Significantly though, considerable effort appears to be exerted in these countries and others to make sure material selection provides for slow crack growth and high residual strength, a property characteristic of damage tolerant structures. The need for paying attention to geometric details, manufacturing quality and full-scale fatigue testing — ingredients of good fatigue quality — is also a common refrain among all groups. This has not always been the case in the past. As mentioned earlier the crack closure concept appears

to be emerging as the most popular for variable amplitude crack growth predictions to support the rapidly growing damage tolerance philosophy. Still, I have confidence in some of the simpler models such as the Generalized Willenborg model. As a member of the Certification Service for the FAA one thing is clear, clarified even further by Workshop 2, irrespective of the fatigue method used whether safe life, or damage tolerance, whether Miner's rule or KitDLS, whether crack closure or Generalized Willenborg model, all fatigue analysis methodology used to certify an aircraft type must be validated by test.

Another personal observation: as we look at recent developments in static and rotating engine components, rotorcraft dynamic components, new commuter aircraft, bridges, nuclear reactors, aging tankers, tractors — and on-and-on, it is inevitable that damage tolerance will emerge as the safest and/or the most cost-effective means for maintaining structural integrity. However, this statement assumes that an infrastructure exists for performing inspections either during initial manufacturing or according to a maintenance program. Nevertheless, particularly in airframe components, because of the widespread damage mode with its tough elements, multi site damage and multi element damage, we will need to combine all three philosophies: safe life, fail safe and damage tolerance.

In the interim, are we not all fortunate that "there is more than one way to solve an engineering problem"?

## OVERVIEW OF THE STRUCTURAL INTEGRITY PROCESS

John W. Lincoln  
 Aeronautical Systems Center of USAF/AFMC  
 ASC/ENFS BLDG 125  
 2335 SEVENTH STREET STE6  
 Wright-Patterson AFB, Ohio 45433-7809  
 USA

### SUMMARY

The development process for a new aircraft requires the successful completion of a number of tasks established to ensure that the structure of an aircraft will meet its design objectives. In addition, for aircraft that have been deployed, there are a number of tasks that must be accomplished to ensure its operational success. For both military and commercial aircraft, the tasks to be performed are largely dictated by acquisition or certification agency requirements. There is considerable historical evidence to prove that when the requirements were lacking in some respect, the structural integrity of the resulting aircraft was also found to be lacking. Many of the problems with aircraft structures can be traced back to a failure to understand the threat to their integrity. In addition, many of structural problems can be identified with an unrealistic assessment of the operational usage and weight growth of the aircraft. Fighter and attack aircraft, in particular, have demonstrated significantly more severe average usage and more variability in usage than predicted during its design. It is the purpose of this paper to explore the processes that are used to ensure a safe and operationally economic structural design for an aircraft. The USAF Aircraft Structural Integrity Program (ASIP) is used to illustrate the various aspects of the process. The current approach used for the ASIP by the United States Air Force is discussed along with a discussion of problems encountered in practice. In addition, some recommendations for improvement of the integrity process are included.

### INTRODUCTION

Aircraft structural integrity is the characteristic of an airplane that enables it to withstand the loads environment and usage imposed during service. The need for formalizing an aircraft structural integrity in the Air Force was first recognized in 1958 when there were a series of catastrophic wing failures on B-47s that were caused by fatigue. The Air Force Chief of Staff, Gen Curtis LeMay, approved the initiation of the program in a May 1958 memorandum. He issued a policy directive on 19 November 1958 that required a commitment from the major commands. A complete history of the origin of the program may be found in reference 1. The objectives of the structural integrity program were to control structural failure of operational

aircraft, determine methods of accurately predicting aircraft service life, and provide a design and test approach that will avoid structural fatigue problems in future weapon systems. These objectives still constitute the basis of the present USAF Aircraft Structural Integrity Program (ASIP).

The original ASIP used a reliability based approach to establish the operational life. This was referred to as the "safe life approach." The safe life approach relied upon the results of the laboratory "fatigue test" of a full-scale article to the spectrum of loading that simulated the service operational environment of the aircraft. The "safe life" of the airplane was established by dividing the number of successfully test simulated flight hours by a factor (e.g., four was commonly used by the USAF). The intent of the factor was to account for article to article variation in materials and manufacturing quality and was thought to be sufficient to preclude structural failure in service aircraft attributable to materials, or manufacturing quality. This concept was the basis for all new designs during the 1960's. It was also the concept used to establish the "safe life" for earlier designs when these aircraft were subjected to a fatigue test. The approach appeared to be successful as exemplified by systems such as the C-141. The C-141 has generally had an excellent safety and overall service record, although some of the materials chosen and some of the structural details used in this aircraft have caused service problems in its later life.

There were, however, some cases during the 1960's where service experience was unsatisfactory and the "safe life" approach became suspect. Catastrophic loss of an F-111 in 1969 demonstrated the "safe life" method had not precluded the use of low ductility materials operating at high stresses. Consequently, this design was intolerant to manufacturing and service induced defects. This was evidenced, also, by failures in cold proof test. Since the program was initiated after the 1969 accident, there have been over ten significant failures in cold proof test in aircraft that were considerably short of their test demonstrated safe life. Some of these were found to be the result of small defects induced by maintenance actions. Other losses (e.g., F-5, B-52 and F-38) and incidents of serious cracking (e.g., KC-135) during this period confirmed this shortcoming. The ability to inspect these early "safe life" aircraft was significantly impacted by this

intolerance to defects and cracks. In many applications, it was found to be extremely difficult to inspect the aircraft. Since inspectability of the aircraft was not required as a part of this approach, many details were found to be outside the 1960's inspection capability. Relatively small cracks and defects could readily escape detection with dramatic consequences. In these situations, a modification program was usually the only viable alternative.

The shortcomings of the safe life process as illustrated by the cited service incidents demanded a fundamental change be made in the approach to design, qualification, and inspection of aircraft. An improved reliability approach and a damage tolerance approach emerged as the candidates for this change. The damage tolerance approach recognized an aircraft was subject to a wide range of initial quality from the manufacturing process and from service induced damage and it had to be inspectable. To ensure the design could be operated safely in the presence of such anomalies, the structure is designed to be tolerant to these defects for some period of service usage before there is a need for an inspection. The damage tolerance approach can be used to determine the period of safe operation, called the safety limit, and required inspection intervals. The same approach is used for existing designs as well as new. The difference is that inspection intervals may be more easily controlled in a new design. The damage tolerance approach was used to upgrade the structural integrity of several operational aircraft (e.g., the F-111, C-5A and F-4) in the early 1970's. It influenced the design of the F-15, and was a basis for the design criteria for the B-1A. The success of these endeavors convinced the Air Force damage tolerance should be the basis for all future designs. In December of 1975, the damage tolerance approach was formally made a part of ASIP with the publication of reference 2. During the 1970's and 1980's, the Air Force performed an assessment on every major aircraft weapon system using the damage tolerance approach to develop appropriate inspection/modification programs to maintain operational safety. As an indicator of success, the failure rate for all systems designed to and/or maintained to the damage tolerance policy is one aircraft lost due to structural reasons in more than ten million flight hours. This is significantly less than the overall aircraft loss rate from all causes by two orders of magnitude.

The current version of the ASIP includes five separate tasks that cover all aspects of the development and support of an aircraft structure. These tasks, some of which are shown in figure 1 are identified as follows:

1. Design Information
2. Design Analyses and Development Tests
3. Full-Scale Testing
4. Force Management Data Package

## 5. Force Management

The primary focus of the program is to ensure the structural safety of Air Force aircraft. As indicated above, this has been accomplished such that the pilot is exposed to less risk from aircraft structural failure than he normally accepts in other activities (e.g., driving an automobile). Much of this success has been attained through the utilization of the results of the individual tail number tracking program. This program is a main feature of the ASIP. This tracking capability has long been recognized as an essential feature of the integrity program since experience has shown aircraft are often used differently than they were designed. There are many examples of this. One of these is the F-16, which is being used approximately a factor of eight times more severely than it was designed. It would be impossible to operate this aircraft safely without the data being derived from the aircraft tracking program. The F-16A/B tracking program has been adversely affected by the operator removing the flight data recorder and replacing it with a video camera. In spite of this problem, there has been sufficient data to adequately support this program. Another program where the tracking program has proved to be invaluable is the F-15. The current usage on the F-15 is approximately four times more severe than that used in design. The tracking program has revealed this is mainly attributed to weight increases and to operations at Mach numbers that are higher than originally expected. The normal load factor experience is quite close to the design estimates. The tracking program has been able to identify the extent of operational usage where buffet loading on the wing and the vertical tail has caused a significant maintenance cost for the user. This information was used to design and test modifications to the components. The A-10 early operational service data, as derived from the tracking program, showed the usage was approximately three times more severe than the original design usage. This was partly due to an increase in the normal load factor spectrum and partly due to fuel loadings that were in excess of design. These usage changes were successfully compensated for by modifications to in-service aircraft and by changes in the production aircraft.

The recording device that was the standard in the past for the tracking program, and is still being used, is a tape system. It has been proven by operational experience this device is not technically able to attain, by a considerable margin, the data capture that was potentially possible. The new microprocessor systems have eliminated the past problems and the current evidence shows the data capture is near the maximum potential.

The other main focus of the program is to ensure the aircraft are being operated in the most economical manner possible. The ASIP has evolved over the years,

primarily through the efforts of the Aeronautical Systems Center, into a process that develops aircraft that are tolerant to both manufacturing and service induced damage throughout their design life and usage. Experience has shown it is rare for an Air Force aircraft to be retired because of structural degradation due to fatigue cracking. This type of degradation normally occurs on a single component of the aircraft rather than the entire aircraft. The damage tolerance approach is directed towards repair, modification, or retirement of a component only when in-service inspections reveal one of these actions should be taken. There have been many cases of structural modification to preclude retirement of the aircraft. Examples of this include the B-52D, C-5A, KC-135, F-16, and C-130.

During the seventies and eighties, damage tolerance assessments were performed on all major weapon systems to update their Force Structural Maintenance Plans (FSMP) and their tracking programs. These assessments are discussed at length in reference 3. It is believed the damage tolerance approach incorporated in the integrity process in the seventies is still the cornerstone for protecting the safety of aging aircraft. Service experience has demonstrated this. Since these assessments have been successful in maintaining safe and economic operations, it has been extremely difficult to maintain the level of funding for the ASIP that is needed to ensure the continued success of the program.

Another problem is the constraints placed on the ASIP managers by program management. Program management faces pressures of schedule and cost that does not always permit adequate attention to integrity concerns such as corrosion control. Also, these ASIP managers are so burdened with detail maintenance problems they have little time to devote to the consideration of broader issues for their aircraft. An example of a broader issue is the determination of when to expect the onset of widespread fatigue damage such as that revealed in the inner to outer wing joint of the C-141. Another example is the unanticipated cracking in the A-7D wings that led to a structural failure in December of 1988. Still another example is the identification of nondestructive inspection capability that will enable them to inspect more accurately and economically in the future.

The operational usage of USAF aircraft is often found to be considerably different from that used in design. This was primarily the result of increased weight and mission changes. Many aircraft, such as the B-52, C-130 and C-141 are flying in a low level environment where the damage from cyclic loading is approximately ten times worse than a high altitude mission. It was found aircraft were being flown much more aggressively than that assumed for the design. Also, as was found in the case of the F-16, the weight was

changed without compensating changes to the structure of the aircraft.

### THE ACQUISITION PROCESS

System acquisition programs in the U.S. Air Force typically go through a total of five phases. These are:

- Concept Exploration and Definition
- Demonstration/Validation
- Engineering and Manufacturing Development
- Production and Deployment
- Operations and Support

It is not essential that all of these phases be included. In some cases some of the phases may be combined. Circumstances such as a decision to procure an aircraft that has already been certified by another agency would eliminate and/or combine some of the phases above.

There is very little structural effort required in the Concept Exploration and Definition phase. In this phase paper studies are typically performed to explore alternatives. These studies allow comparison of each alternative on the basis of cost and operational effectiveness. This phase would conclude with a decision on the need for proceeding to the Demonstration/Validation phase.

The Demonstration/Validation phase is used to reduce the technical risk or cost uncertainty. The program office will often task the contractor to build a prototype and/or request tests and paper studies to accomplish these goals. It is anticipated that the early part of this phase would be used for a screening process so that the final stage of this phase could be used to develop data for the selected technologies. It is in this phase that a structural technology is transitioned from the laboratory to the Engineer and Manufacturing Development (EMD) phase. If a prototype is required, it places an additional burden on the structural engineer. It is likely that structure of the prototype would be different from the structure of the EMD aircraft because the EMD structural concepts may have not matured. Therefore, the structural engineer has the task of providing a prototype structure that would enable a meaningful aircraft capability demonstration.

The structural effort in EMD is completely defined in reference 2. At the successful completion of this phase the aircraft structure will be approved for production. The data will have been generated to write the Strength Summary and Operating Restrictions Report and to finalize the Force Structural Maintenance Plan (i.e., the how, when, and where to perform the structural inspections required to maintain safety and economic operation). The methodology will have been developed to perform the tail number tracking required to obtain individual usage data.

The schedule of these phases is, of course, dependent on many considerations. One of the more important considerations is the scope of technologies development required before EMD. Another important consideration is the requirement for a prototype. If there is no significant technology development or prototype required then the time required for the Demonstration/Validation phase may be as short as three years. A prototype could stretch this time by approximately two years. If significant technology development is required then up to an additional five years may be required. Therefore, a program involving a prototype and technology development may impose a ten year interval from the start of Concept Exploration and Definition to EMD start. The EMD schedule is subject to considerable variation because of effects of airframe size and complexity. A spread of five to nine years from the start of EMD to IOC (initial operational capability) is not unreasonable. In the EMD schedule there are several milestones that are crucial to technology development. The milestone before which the technology must be completely matured is the start of the flight test program with an 80 percent of limit load restriction. By this point, the stress analysis will be submitted and approved. Therefore the final loads are available and final allowables for the materials must have been established. However, before this milestone is reached, the program would have had its Critical Design Review (CDR). At this point in the development the contractor should have completed approximately 95 percent of the drawings. That is, the final sizing should have essentially been completed. If the material allowables are not completed by this time the contractor (and correspondingly the government) is operating with some risk to both schedule and cost. Therefore, the contractor should aim his technology development program to be completed (i.e., final allowables, etc.) by the Preliminary Design Review (PDR). This milestone would provide approximately nine to twelve months after start of EMD to complete the technology development. This time could be used as a gage to estimate the degree of completion needed at EMD start.

### Technology Transition

To be successful in the development of a new aircraft, the structural integrity effort must begin before the Engineering and Manufacturing Development phase of the program. In the USAF, the structural activity starts in earnest in the Wright Laboratories even before the Demonstration/Validation phase. However, it is normally the Demonstration/Validation phase that is particularly critical for the transition of structural technology from the laboratory to the aircraft. There are many examples of successful transitions of technology from the laboratory to full-scale development. Many of these successes were derived

from a well-conceived plan or "road map" that formed the basis or criteria for technology transition. In general, these road maps have included programs directed at several levels of technology maturity. These levels are referred to as basic research, exploratory development, advanced development and manufacturing technology development. Most of the advanced development and manufacturing technology development program effort is directed towards the demonstration of the technology by means of the manufacture and testing of a specific piece of hardware.

A key element in the development of the road maps was a knowledge of the threats to structural integrity from the environment in which the structure must be able to perform its function. The understanding of these threats typically is derived from experiences with other materials. There are situations, however, where a new material may be sensitive to a threat that in the past has not been a major factor. The types of threats that one should consider in the development of a new material or process are shown in figure 2.

A study of those successful road maps for transition of technology to full-scale development reveals that they had certain factors in common. These factors may be combined to form a criterion for the transition process to be successful.

From a study of the successful transitions of structural technologies from the laboratory to full-scale development it was found that five factors constituted a common thread among these successes. Also, it was found that these five factors were essential to the successful completion of the tasks of the United States Air Force Structural Integrity Program (ASIP). These five factors are

- Stabilized material and/or material processes
- Producibility
- Characterized mechanical properties
- Predictability of structural performance
- Supportability

In this listing there was no attempt to establish a ranking of importance of these factors. A deficiency in any one of the factors could constitute a fatal defect. A description of each of these five factors involved in the transition of structural technologies to full-scale development is given in reference 4. The relation between the phases of the acquisition process, technology transition, and the ASIP is shown in figure 3.

### DISCUSSION OF THE TASKS OF THE ASIP

Since structural failure from fatigue was the motivating factor for the ASIP initiative in 1958, it is reasonable that a number of elements of the ASIP are associated

with the influence of repeated loads on the structure. This is shown by figure 1. In all five tasks of ASIP, there are significant elements related to repeated loads.

Every element of Task I of the ASIP is critical for the aircraft to be successful in the repeated loads environment. The ASIP master plan provides a living document on what is planned to be accomplished and the results of tests after they are performed. The preparation of this document is typically started in the Demonstration/Validation phase of acquisition. The first draft of this document is submitted with the proposal for the Engineering and Manufacturing Development phase and is updated regularly throughout the development and operational life of the aircraft. Task I could be considered the most important of the tasks of ASIP. The reason for this is that mistakes made here in structural design criteria for durability and damage tolerance, for example, could jeopardize the entire development. The same is also true for establishment of the design service life and usage of the aircraft. The burden for the success in Task I rests mainly with the acquisition authority. The operating command that is to use the aircraft also has a major role. The using command specifies the usage environment for which the aircraft is expected to operate. This is a particularly difficult task in that if the usage they specify is less severe than that to be experienced in operational service then there could be a significant economic burden for structural modifications. One of several examples of this is the case of the A-10. In this case, the initial fuel weight was based on mission requirements rather than using full initial fuel as was experienced in service. If the usage they specify is too severe or if there are missions specified that are not operationally flown, then the weight of the aircraft could have an adverse impact on performance. An obvious example of this is the C-5A. A major function in Task I where the contractor is involved is the selection of materials and processes. It is of utmost importance that the material and process selection be essentially complete by the end of the Demonstration/Validation phase in order to proceed with confidence in the EMD phase and meet the EMD milestones.

It is in Task II of the ASIP that the sizing of the structure is accomplished to meet its operational requirements. This is accomplished through numerous analyses and tests. These analyses and tests are directed at specific structural details that could be subject to an inspection during the operational life of the aircraft. These details are called critical locations. It is one of the functions of Task II to make an initial identification these locations. It is difficult to say that one of the elements of Task II is any more critical than the other. However, the loads analysis is certainly a strong candidate for this distinction. The reason for this, of course, is the severe impact of an error in loads on the

durability and damage tolerance capability of the aircraft. Further, some of the important operational load cases involve high angles of attack and/or side slip. Consequently, there is often considerable difficulty in making an accurate load predictions. The generation of the design service loads spectra is usually straight forward in the case of fighter and attack aircraft. That is, aircraft where the effect of turbulence can be ignored. There are cases, however, where buffet loads may have a significant impact on structural integrity and consequently can not be ignored. Such a case is the F-15 that has suffered buffet load damage on both the wing and the vertical tail. A description of how this was solved on the F-15 vertical tail is found in reference 5. In the case of bomber and transport category aircraft, there is the added problem that the loads and consequently the phasing of the components of the loads can only be represented by their probability distribution functions. This significantly complicates the generation of the design service loads that are to be applied to the full-scale test article. A method for accounting for the load phasing associated with turbulence is described in reference 6. This approach was used in generating the loading sequence used on the C-17 durability test. After the design service loads spectra has been generated for an aircraft, the stress spectra for each of the critical locations can be derived. This effort uses the results from the stress analysis.

The USAF guidance for the damage tolerance analysis for the metallic structure is based on an initial flaw concept. The initial flaw concept and the derivation of currently used initial flaws is discussed in reference 3. The guidance on the size of the initial flaws is given in reference 7. The USAF guidance for most of the durability analyses is that they also be performed using an initial flaw concept. The initial flaw used for these analyses is based on the largest defect that could be expected to be in any given aircraft (see reference 7). Consequently, it is smaller than the damage tolerance initial flaw size.

It is worthy of note that many of the elements of Task II are oriented towards a fracture mechanics oriented damage tolerance approach. However, there is, in fact, little difference in the scope of the effort associated with a safe life analysis. It is essential in both approaches to perform the loads analyses, stress analyses and obtain the stress spectra for each critical location. These are the time consuming, and consequently the costly tasks. It is usually a small difference in computer time that causes the difference in analysis cost between the two approaches.

Under certain restrictions, the safe life approach for ensuring safety can be demonstrated to be adequate. In most examples of the use of safe life on modern military aircraft, testing of the full-scale aircraft is accomplished. If this type of testing is not

accomplished, then the structural engineer is forced to make a judgment on the "effective stress concentration factor", or  $K_t$ , to use in the fatigue analysis. The fatigue data displayed in reference 8 appears to have an effective stress concentration of about five. As shown in reference 9, there is a significant difference in the computed life derived from a change in  $K_t$  from five to six, for example. Without an adequate test, that is truly representative of the expected flight-by-flight usage and stress distributions in the airframe, there is no method of determining the magnitude of the effective  $K_t$  of the structure. Therefore, the results of a safe life analysis without supporting test data are subject to such uncertainty that they are not usable. Another restriction on the use of safe life is that its use should be restricted to materials that are reasonably insensitive to the defects that could have resulted from the manufacturing process or as a result of operational service. An example of the sensitivity of a steel engine mount to small defects is described in reference 9. The failure of the safe life approach for early USAF aircraft is attributed to the fact that they, in most cases, did not have an adequate fatigue test. This was the case for the F-4 and the C-130, as examples. Also, as evidenced by aircraft such as the KC-135, the USAF accepted designs with low toughness materials that operated at stresses that made them flaw sensitive. Finally, the structure should be designed to be inspectable. It is impossible to represent all of the potential environmental effects in a laboratory fatigue test. It is also difficult to know whether the safe life scatter factor adequately accounts for the variation in quality of production aircraft. For these reasons, it is essential that aircraft be subjected to inspection during the course of their operational service. In the event that an aircraft has been subjected to a representative fatigue test, is constructed with materials at stress levels that would satisfy the damage tolerance guidance, and is inspectable, then it could be qualified by the safe life process. If all of these stipulations are incorporated, it is evident that the materials and stresses and configuration would be little different from a design based on damage tolerance principles.

Another critical effort in Task II is the design development tests. These are the coupon, element, subcomponent, and component tests that form the building blocks for the understanding of the structural performance under environmental loading. The costs of these tests can be a significant part of the entire structural development program. Consequently, these tests may fall victim to funding shortfalls in the program. Experience has shown that a successful design development test program is the only way to ensure that the risk is acceptable for the full-scale test program in Task III. It should be a program objective to enter the full-scale test program with low risk. Failures in full-scale testing can create very serious program schedule disruptions and cause a financial

burden far in excess of what would have been spent on a sound design development test program.

The successful completion of the full-scale testing in Task III is essential for keeping the acquisition process on schedule. There is never enough time and money available to ensure that there will be no risk of structural failure. However, as indicated above, with proper attention to the design development testing in Task II, the risk of a major failure could be made to be low.

It has long been recognized that early testing of the full-scale structure was important. Although the early airframes are generally not completely representative of the final configurations, it is essential to get early information on deficiencies so they can be corrected in production. The C-5A program is an example where both the static and fatigue tests were performed after a significant number of production aircraft had been produced. Both of these tests resulted in serious failures that occurred significantly short of the design requirements. Because of the lateness of the tests, no changes were incorporated in any of the production aircraft. As a result, the aircraft had to operate under severe restriction until the entire fleet could be retrofitted with new wings. This, of course, was a major expense to the government.

As indicated in reference 3, a precept of the damage tolerance approach is the safety of the aircraft and its economic operation should be independently proven. The damage tolerance analysis, supported by testing, was the basis for safe operations and the full-scale durability test was the basis for establishing the economic burden associated with service usage. The damage tolerance analysis, supported by testing, has been effective in identifying areas of the aircraft that could potentially cause a safety problem. It is desirable, however, to ensure they have been identified through the full-scale durability test. The spectrum used by the USAF for both the damage tolerance and durability analyses and testing is the expected average usage MIL-A-8867B(USAF) (reference 10), which was released 22 August 1975, stated the full scale durability test should be run for a minimum of two lifetimes unless the economic life was reached prior to two lifetimes. The economic life of a structural component is reached when that component is more economic to replace than repair. The economic life of a component is extremely difficult to determine analytically. It may be, however, demonstrated in durability testing. The same guidance that was given in MIL-A-8867B(USAF) was given later in AF-GS-87221A (reference 7). There was no guidance given, however, on the rationale for a need for testing for more than two lifetimes. Consequently, it has been a program decision to test every aircraft for two lifetimes since 1975. All the known service experience demonstrates that an aircraft, after successfully passing a two lifetime flight-by-flight

durability test, will not reach its economic life in one lifetime of service usage representative of the test spectrum. There is a question, however, whether a full-scale durability test that simulates two lifetimes of planned operational usage will adequately interrogate the structure to determine all the areas in all aircraft that could potentially cause a safety problem.

Experience with operational aircraft has revealed they are typically not flown to the loading spectrum for which they were designed. Data from flight load recorders have shown, in general, that there are considerable differences in usage severity among aircraft with the same designation. Further, it is often found the average aircraft usage is more severe than originally perceived early in the design process. This problem is aggravated by the fact the damage tolerance analysis may have not identified an area which would be a concern if the aircraft usage was more severe than that assumed for design. Also, experience has shown the mass of an aircraft increases as a result of additional equipment or modification after an aircraft enters operational service. In addition, there are differences because (1) pilot technique changes as they become more familiar with the aircraft, and (2) mission changes because of new weapons and tactics. The aircraft-to-aircraft variability comes from several sources such as base to base variations in distance to test ranges and training. These experiences tend to degrade the capability of the full-scale durability test that consisted of two lifetimes of average usage to identify all the areas of the aircraft that could potentially cause a safety problem. Consequently, the structural engineer should, based on historical evidence, make some allowances for increased usage severity occurring as a result of mission severity changes and aircraft to aircraft variations in operational usage. To ensure aircraft durability, this should be done both in the design of the aircraft and in the test. The historical evidence of usage differences derived from changes in pilot technique and mission changes is generally not easily translatable to new designs.

A procedure is described in reference 11 that is believed to be useful for establishing the duration and/or the severity of testing that should be performed in a full-scale durability test to ensure that all of the significant regions of the structure have been identified. It is based primarily on data that could be derived from the existing analyses and development testing. An example problem discussed in reference 11 indicates that the length of testing required using an average spectrum may be uneconomical. However, it appears practical to increase the severity of the spectrum to provide for an adequate test and to complete the test in a timely manner.

The procedure also provides a basis for the success of the test. During or at the end of the full-scale durability

test, a crack may be found that initially appears to be significant. This would not automatically indicate that the structure has failed to pass the test. It would, however, indicate additional investigation should be undertaken. A fractographic examination should be conducted to determine if the crack growth was faster than predicted. If it was found to be faster than predicted based on the earlier analyses and tests, then an investigation should be conducted to determine the local stresses and the fracture data (crack growth rate) for the material used in the full-scale test article. An assessment should also be made to determine the implication on the damage tolerance derived inspection program. After a study of all available information, a judgment is then made on the need for aircraft modification or additional inspections to maintain economic and safe operational aircraft.

It is often found that a region or part of the aircraft needs to be redesigned based on failure in the durability test. There may be occasions where the redesigned part is obviously robust enough such that additional testing is not required. However, in general, the redesign should be subjected to the same rigors of testing as the original airframe. This can often be accomplished with a component test. However, there are some cases where this is not practical. This retesting generally results in significant costs that were not part of the original finding. The prospect of retesting the aircraft should be adequate motivation to take the necessary precautions to ensure that the risk is low at the start of testing.

Another critical element in Task III is the flight and ground operation tests. As indicated above, the analytical determination of loads is a process that requires considerable precision. In many cases, however, this precision is hard to achieve because of the nonlinear character of the loading process. It is rare that the loads are calculated with sufficient accuracy such that no changes are derived from the flight and ground operation testing. It is important to get the information from these load tests early enough to influence the full-scale static and durability testing. The aircraft is released to an envelope of 80 percent of limit load based on analysis only to provide the capability to perform the flight loads testing.

One of the critical elements of Task IV is the development of the Force Structural Maintenance Plan (FSMP). This plan tells the maintainer of the aircraft how, when and where the aircraft are to be inspected and/or modified as they proceed through their operational lives. For new aircraft, the guidance in reference 7 is to establish the stresses such that no inspections are mandatory to provide flight safety. This means that the stresses are established such that there are two lifetimes of slow crack growth capability from the damage tolerance initial flaw to critical crack length. However, an inspection should be developed

that could be used in the case of usage severity or mass increases. For most military aircraft, experience has shown that there is a considerable difference in usage severity among the individual aircraft. The accounting for the actual usage of the aircraft is determined by the individual aircraft tracking program and the loads/environment spectra survey. These two elements work together to obtain an estimate of the stress spectra for a number of control points in the structure. For aircraft that are designed according to the damage tolerance philosophy, the generated stress spectrum is used to determine the time at which the damage tolerance initial flaws would grow to critical. This time is divided by a factor of two to determine the number of flight hours that the inspection should be performed. For aircraft that are operated under a safe life approach, the tracking program is used to determine, for the various tracking control points, the life expended relative to the fatigue test demonstrated life.

There are several approaches that have been used to monitor the aircraft for inputs to the individual tracking program and for the loads/environment spectra survey. One of these is the use of strain gages to make direct measurements of strain and correspondingly stress on the structure. Another approach is to measure certain functions, such as linear and angular accelerations, surface positions, and fuel states to make an estimate of the stress at any desired control point of the structure. It is the position of the USAF that each of these methods has their own advantages and disadvantages for a particular location. Therefore, the choice will be made on what appears to be the best for the particular area to be monitored.

As the aircraft ages, the effort in Task V provides the basis for making modifications to the structural program through the interpretation of inspection results and the results of the individual aircraft tracking program. As an aircraft ages, it is then exposed to multiple threats to its integrity. One example of this is crack growth aggravated by corrosion. Another example that is threat of discrete source damage for a structure with widespread fatigue damage. The latter example has been a problem with several USAF aircraft such as the wings of the KC-135, C-5A, and C-141. The problem is that widespread fatigue damage can degrade the fail safe capability of an aircraft. The approach that has been used to assess this problem is based on determination of the probability of failure given that the discrete damage has occurred. A method for determining this conditional probability of failure is discussed in reference 12.

#### SUMMARY

The integrity process called the USAF Aircraft Structural Integrity Program is believed to contain all of the elements required to ensure that aircraft structure

designed with this process will be successful in meeting their operational requirements. It is further believed that other approaches could be used to achieve structural integrity. The successful deployment of numerous aircraft has proved this to be true. One key feature, however, of any approach is that the structural engineer needs to exercise prudent judgment that will contain the risk of failure to an acceptably low level as the program proceeds to higher and higher levels of funding requirements. Another key feature of any program is to anticipate the threat to structural integrity for a particular design. New threats will appear as increases in performance requirements place pressure on decreases in weight. As the demand for performance increases such that the thermal loading is a significant factor, there will be a need to use probabilistic methods for the assessment of structural integrity. Also, as the performance increases, there will be an expanded role for "smart structures." For the foreseeable future, testing will remain the primary basis for acceptance of the structure. The advent of composite structures has certainly reinforced this position. The test requirement places a discipline in the entire structural design program that probably can not be achieved by any other means.

#### REFERENCES

1. Negaard, Gordon R., "The History of the Aircraft Structural Integrity Program," Aerospace Structures Information and Analysis Center (ASIAC), Report No. 680.1B, 1980.
2. Department of the Air Force, "Aircraft Structural Integrity Program, Airplane Requirements," Military Standard MIL-STD-1530A, 1975.
3. Lincoln, J.W., "Damage Tolerance - USAF Experience," Proceeding of the 13th Symposium of the International Committee on Aeronautical Fatigue, Pisa, Italy, 1985.
4. Lincoln, J.W., "Structural Technology Transition to New Aircraft," Proceeding of the 14th Symposium of the International Committee on Aeronautical Fatigue, Ottawa, Ontario, Canada, 1987.
5. Muliere, R. and Resnick, J., "Dynamic Fatigue Testing of F-15 Vertical Tail to Simulate Buffet Environment," Proceedings of the 1989 USAF Structural Integrity Conference, San Antonio, Texas.
6. Eastin, R., Lercwick, J., and Soedel, S., "The Phase Load Sequence Generator System," Journal of Aircraft.
7. Department of the Air Force, "Air Force Guide Specification, Aircraft Structures, General Specification for," AF-GS-87221A, 1990.

8. "Fatigue Evaluation of Wing and Associated Structure on Small Airplanes," AFS-120-73 2, Airframe Branch, Engineering and Manufacturing Division, Federal Aviation Administration Flight Standards Service, May 1973.

9. Lincoln, J.W., "Damage Tolerance for Commuter Aircraft," Presented at the 1991 International Conference on Aging Aircraft and Structural Airworthiness, Washington, D.C., November 1991.

10. Department of the Air Force, "Airplane Strength and Rigidity Ground Tests," Military Specification MIL-A-008867B(USAF), 1975.

11. Lincoln, J.W., "Assessment of Structural Reliability Derived from Durability Testing," Proceeding of the 17th Symposium of the International Committee on Aeronautical Fatigue," Stockholm, Sweden, 1993.

12. Lincoln, J.W., "Risk Assessments-USA: Experience," Proceeding of the International Workshop on Structural Integrity of Aging Airplanes, Atlanta, March 31 - 2 April 1992

# USAF STRUCTURAL INTEGRITY PROGRAM

TASK I	TASK II	TASK III	TASK IV	TASK V
<b>DESIGN INFORMATION</b> ASIP MASTER PLAN STRUCTURAL DESIGN CRITERIA DAMAGE TOLERANCE & DURABILITY CONTROL PLANS SELECTION OF MAT'L'S PROCESSES & JOINING METHODS DESIGN SERVICE LIFE AND DESIGN USAGE	<b>DESIGN ANALYSES AND DEVELOPMENT TESTS</b> MATERIALS AND JOINT ALLOWABLES LOADS ANALYSIS DESIGN SERVICE LOADS SPECTRA DESIGN CHEMICAL/THERMAL ENVIRONMENT SPECTRA STRESS ANALYSIS DAMAGE TOLERANCE ANALYSIS DURABILITY ANALYSIS SONIC ANALYSIS VIBRATION ANALYSIS FLUTTER ANALYSIS NUCLEAR WEAPONS EFFECTS ANALYSIS NON NUCLEAR WEAPONS EFFECTS ANALYSIS DESIGN REQUIREMENT TESTS	<b>FULL SCALE TESTING</b> STATIC TESTS DURABILITY TESTS DAMAGE TOLERANCE TESTS FLIGHT & GROUND OPERATIONS TESTS SONIC TESTS FLIGHT VIBRATION TESTS FLUTTER TESTS INTERPRETATION & EVALUATION OF TEST RESULTS	<b>FORCE MANAGEMENT DATA PACKAGE</b> FINAL ANALYSES STRENGTH SUMMARY FORCE STRUCTURAL MAINTENANCE PLAN LOADS/ENVIRONMENT SPECTRA SURVEY INDIVIDUAL AIRPLANE TRACKING PROGRAM	<b>FORCE MANAGEMENT</b> LOADS/ENVIRONMENT SPECTRA SURVEY INDIVIDUAL AIRPLANE TRACKING DATA INDIVIDUAL AIRPLANE MAINTENANCE TIMES STRUCTURAL MAINTENANCE RECORDS

Figure 1. The Tasks of the Structural Integrity Program

# POTENTIAL THREATS TO STRUCTURAL INTEGRITY

- MATERIAL/MANUFACTURING
  - VOIDS
  - INCLUSIONS
  - DELAMINATIONS
  - IMPACT DAMAGE
  - SCRATCHES
  - MANUFACTURING ANOMALIES
- ENVIRONMENTAL
  - CORROSION
  - STRESS CORROSION
  - TEMPERATURE
  - MOISTURE
  - CHEMICAL
- SERVICE OPERATIONS
  - FATIGUE CRACKING
  - IMPACT DAMAGE - HIGH ENERGY/LOW ENERGY
  - MAINTENANCE/ACCIDENTAL DAMAGE
  - OVERLOAD
  - RAIN EROSION
  - HAIL
  - LIGHTNING
  - NUCLEAR AND NON-NUCLEAR BATTLE DAMAGE
  - WEAR

Figure 2. Identification of Threats to Structural Integrity



# TYPICAL SEQUENCE OF DEVELOPMENT ACTIVITIES

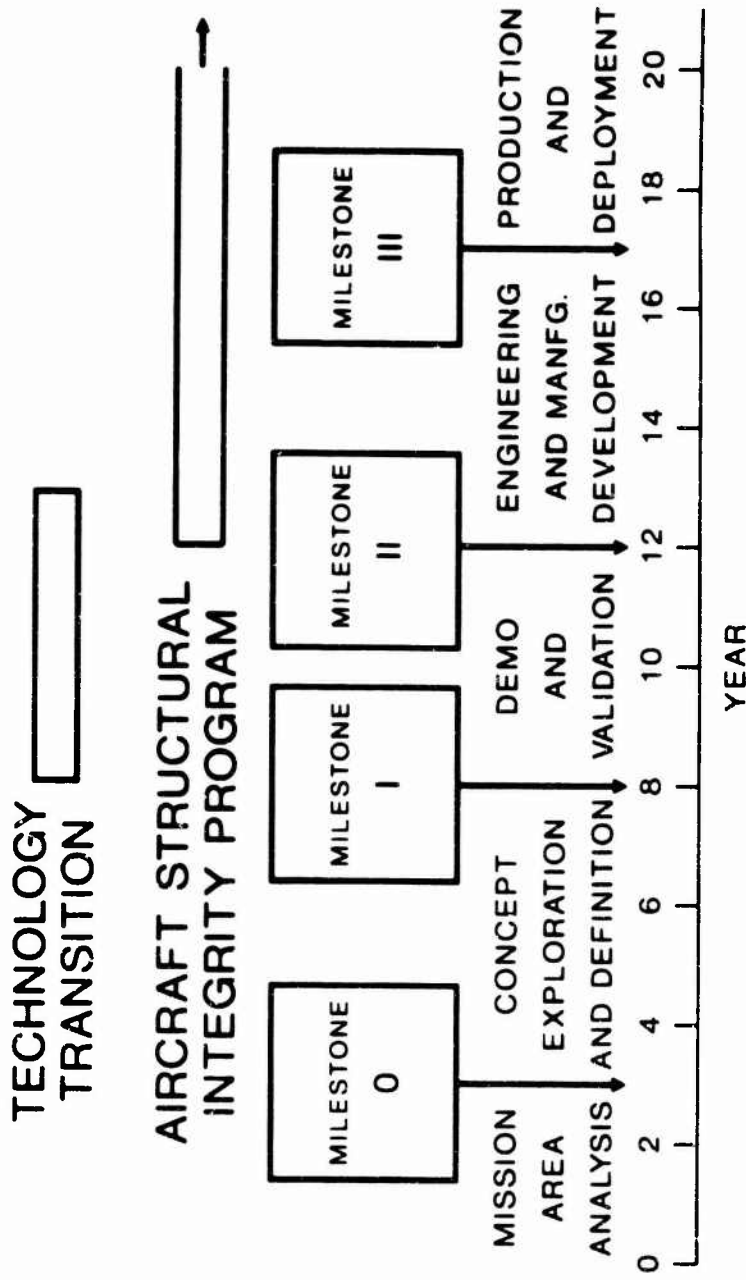


Figure 3. The Acquisition Process Milestones and Tasks

## MINER'S RULE REVISITED

by

W. Schütz and P. Heuler  
 Industrieanlagen-Betriebsgesellschaft mbH  
 Einsteinstrasse 20  
 D-85571 Ottobrunn  
 Germany

### SUMMARY

In the first sections, the requirements to be met by hypotheses for fatigue life prediction (including those for the crack initiation and crack propagation phases) are discussed in detail. These requirements are shown to be different for "scientific" and for "industrial" fatigue life prediction. Aspects with regard to an assessment of fatigue life prediction hypotheses are discussed.

The last section presents the results of a large co-operative programme between IABG and several automobile manufacturers, in which Miner's Rule in several versions was assessed against spectrum tests with five different actual automobile components namely:

- Forged steel stub axle
- Forged steel stub axle, induction hardened
- Sheet steel welded rear axle (front wheel drive car)
- Cast aluminium wheel
- Welded sheet steel wheel.

Since up to 80 components each were available, and two different, but typical, automotive stress-time histories were employed, the assessment was very thorough, avoiding many of the drawbacks of previous assessments.

It is shown that

- damage sums to failure were usually far below 1.0,
- they also depended on the component in question, the aluminium wheel resulting in the lowest damage sums to failure,
- the damage sums to failure were always lower for a mild spectrum than for a severe one
- the influence of spectrum variation was predicted best – among the hypotheses tested – by use of a recent proposal of Zenner and Liu.

### 1 INTRODUCTION

The fatigue life under variable stress amplitudes has been calculated since 1924 (Palmgren [1]), 1937 (Langer [2]) and 1945 (Miner [3]). Langer suggested a damage sum of 1.0 for the crack initiation phase and an additional one of 1.0 for the crack propagation phase; Miner proposed a damage sum of  $\geq 1.0$  to crack initiation.

However, this was generally overlooked by later users, including Miner himself [4] and the total life encompassing crack initiation and crack propagation<sup>1)</sup> was for many years calculated employing Miner's Rule

$$\sum \frac{n_i}{N_i} = 1.0.$$

Since about 1950, the accuracy of Miner's Rule was assessed by unsuitable two-step- or "overload"-tests, at best by blocked programme tests [5], and damage sums between 0.1 and 10 were obtained. Quite surprisingly, this did not deter industrial - including aeronautical - users from still calculating the fatigue life of their products to this day by Miner's Rule with a damage sum of 1.0. In the same time period, many attempts to improve Miner's Rule were made (for example [6]), but, in retrospect, all were unsuccessful.

In 1961 Paris [7] published his crack propagation hypothesis

$$\frac{da}{dN} = C \cdot \Delta K^n$$

which he later [8] extended to variable amplitudes.

After a period in which simple linear [9] or retardation [10] hypotheses were proposed for the prediction of crack propagation life under variable amplitudes, Elber

<sup>1)</sup> Here crack "initiation" means a crack of an "engineering" size of some tenths to some millimetres. From a fundamental point of view, fatigue is sometimes interpreted as crack propagation process exclusively.

published his crack closure measurements [11] in 1968 and model [12] in 1971, on which all significant hypotheses for crack propagation subsequently were based.

In the meantime, servo hydraulic test machines had become available [13], somewhat later with computer control [14], so that for the first time the fatigue life prediction hypotheses, including those to crack initiation and for crack propagation, could be assessed by realistic tests, i.e. tests with realistic stress-time histories. But such assessments even today are quite rare in the open literature, probably because they are very expensive and time-consuming, if they are to be meaningful, see Chapter 4. Most assessments known to the authors employed specimens, not components, although in the end the objective is to predict the fatigue life of components.

## 2 SCIENTIFIC AND INDUSTRIAL FATIGUE LIFE PREDICTION

Although this paper is mainly concerned with Miner's Rule, the following chapters contain general remarks valid for all hypotheses for fatigue life prediction, including those for crack propagation and to crack initiation. "Fatigue life" in this paper therefore comprises the crack initiation or the crack propagation life and also total life to failure. Deliberately most examples given do not concern aerospace applications.

The validity and limitations of fatigue life prediction hypotheses can only be assessed when all relevant input parameters are known. This is typically the case in the development phase where one may use the term "scientific fatigue life prediction" which is characterized as follows:

- The prediction is usually carried out for small specimens;
- basic data (or materials constants), for example the S-N curve(s) for a Miner-type calculation, have been determined with a sufficient number of specimens;
- the stress-time sequences employed are exactly known, often no mean stress variations are considered;
- in many cases the stress level is unrealistically high;
- the critical section of the specimen is known as well as the crack or notch shape;
- therefore the stress intensity factor or stress concentration factor is known, as is the nominal and the local stress, if necessary for the prediction;
- if such a prediction is to be assessed, the required variable amplitude tests are carried out with identical specimens from the same batch of material. Strictly speaking, the result of the assessment is only valid for this batch of material, this specimen type, this stress-time-history and so on.

An important aspect of scientific fatigue life prediction is, that no damage is done if the prediction fails; the pre-

diction can always be repeated with an "improved" hypothesis. In fact, this happened with Miner's Rule in its numerous versions as well as with many crack propagation or local approach hypotheses.

For industrial applications the story is completely different in many aspects:

- The fatigue life of components and structures often of considerable size and complex design has to be predicted.
- The exact stress time history in service is not known, the stress level is inaccurately known.
- Very often, the basic data characterizing fatigue strength are incomplete or not available with sufficient accuracy. It may well be that only 3 to 5 S-N tests, sometimes at one stress level only, are available for a Miner type prediction requiring assumptions to be made with regard to the slope of the S-N curve or the fatigue limit or mean stress effects. In such a case any prediction could be off by a large factor even if the hypothesis itself were perfect.

Even if complete S-N- or  $da/dn$ - vs.  $\Delta K$ -curves were available, these are valid only for the one batch of material or components tested. In reality the structure of even one individual aircraft consists of many batches and the tens of thousand of cars of one type manufactured in even one month contain only nominally identical components manufactured by several different suppliers from many batches of material. This problem has nothing to do with the prediction hypothesis itself and is normally solved by statistical quality control fatigue tests with components from every incoming shipments.

The importance of correct and reliable basic data has been emphasized in a qualitative way by the first author since at least 1980 [15]. Recently the large effect of even small variations of, for example, the exponent  $n$  in the Paris equation on the prediction has been quantified in [16] where the example of a hypothetical designer of an offshore structure was presented who had to assume or take from books, tables etc. all of the necessary input data for a prediction of crack propagation. Not surprisingly large differences in the calculated crack propagation lives resulted, depending on the numerical values assumed.

- For specimen oriented life prediction concepts such as the local strain approach, further severe problems arise from transferability (equivalence) aspects. Usually small polished smooth specimens are used to determine base line fatigue data, but one may well ask for the relevance of those data for a real component such as a forged stub axle which has been subjected to very different forging and machining processes. Furthermore, large components such as truck axles often show a considerable variability of the static strength and cycl. properties as discussed in some detail in [17, 18]. An adequate consideration of

such transferability aspects appears to be essential for such approaches.

- For crack propagation hypotheses, transferability problems may similarly occur with regard to the dependence of the basic crack growth curves on the product form of the material. Examples are the typical irregular crack paths found in Al-Li alloys which appears to be texture-dependent. In [19] limitations with regard to transferability hindered a realistic prediction of crack propagation and residual strength of landing gear forgings.
  - Often the critical sections of the components are usually not known before the basic constant amplitude tests. It is also not certain that these sections critical under constant amplitude tests are identical to those under realistic variable amplitudes [20].
  - Finite element calculations, even with very many degrees of freedom, usually employ too coarse meshes to reliably find these critical sections in complex components, even if the usually multiaxial service loads were known with sufficient accuracy. In fact, if the critical section and the corresponding (too low) fatigue life were known early enough in the development phase, the component design would be improved and the critical section would thus move somewhere else. A good example is given in [21] of the divergence of F.E. calculations and test results, where the calculation correctly predicted the critical section of the original, but not of the final, improved wing joint.
- It is also not generally true that the component cracks or fails where the local strain is highest. Rather the component will fail where the strain due to the service loads is higher than the local allowable strain, which may well be different in different regions of a complex component, for example, at weldments and which may be strongly influenced by environmental conditions (e.g. corrosion).
- Very often, assumptions on input parameters have to be made which control the prediction results to a large extent. An example is the assumed initial crack size for crack propagation prediction. Large efforts are, therefore, made to better quantify these data by use of test and/or in-service experience within an FHS approach.

The largest difference to scientific fatigue life prediction, however, is the consequence of a wrong prediction: Consider the failure of an aircraft wing or of 1.000 automobile axle spindles due to fatigue. Therefore industry can not rely on such predictions alone, but usually requires fatigue tests, inspections and/or fail safe or damage tolerant design.

### 3 VALIDITY REQUIREMENTS FOR FATIGUE LIFE PREDICTION HYPOTHESES

These requirements are different for scientific and industrial fatigue life prediction.

A "scientific" hypothesis should be able to predict the fatigue life under all possible spectra to be expected in service, i.e. gust or manoeuvre spectra for aircraft, wave spectra for oil rigs, and for all materials, specimen shapes, stress levels and fatigue lives, etc.<sup>2</sup>. It should do this with high reliability i.e. the average (mean) prediction should be close to the actual fatigue life in all cases, and with a small scatter (standard deviation). Ideally, all predictions should be exact in every case, with a mean prediction of 1.0 and a standard deviation of zero. This, however, is neither possible nor necessary in view of the many other unknowns.

In the literature a number of quantitative requirements as to the accuracy of such a hypothesis can be found:

According to Buch [23], it is good if the ratio  $N_{test}/N_{pred}$  for all predictions lies within the range of 0.5 to 2.0.

According to Gassner [24], 90 percent of the prediction results should fall into a range of 1.0:2.0 on the safe side, i.e. should always be conservative.

The first author stated in [25] that 90 % of all predictions should lie between 0.66 and 1.5 of the actual life, which corresponds to a standard deviation of  $s \leq 1.35$ .

Schijve in 1987 [26] required all crack propagation predictions to fall within 0.6 to 1.3 for a "good" hypothesis and between 0.5 and 2.0 for an "acceptable" one. In 1991 [27] he stiffened this requirement and required a crack propagation hypothesis to correctly predict the crack growth of every individual flight in a flight by flight sequence.

An **Industrial** fatigue life prediction hypothesis would be good enough if it were able to predict reliably the life for the products, the fatigue lives and the spectra in question. A truck manufacturer for example only needs to predict the life of truck components etc. and only at the long fatigue lives corresponding to  $> 500,000$  km or  $> 10^8$  cycles under a typical, severe customer spectrum; he is not interested in riveted aluminium structure typical for aircraft. The prediction also should always be on

<sup>2</sup> In the authors' opinion it is not necessary, however, to be able to predict unrealistic "overload" or "two step" fatigue lives, because such stress time histories do not occur in service and an otherwise useful hypothesis might be rejected in this way. This view is not shared by other experts, see for example [22].

the conservative side, although not to far to avoid over-design.

However, even a perfect hypothesis would only give the fatigue life with a probability of survival  $P_s = 50\%$ . For industrial application much lower probabilities of failure have to be considered. This aspect must either be incorporated in the fatigue life prediction itself (as is the case for some welding fatigue standards [28, 29]) or it must be obtained by some other means. In [28] and [29] an S-N curve with  $P_s = 97.7\%$  per cent is used, corresponding to the mean minus two standard deviations. The Miner calculations (with a damage sum of 1.0) are carried out with this S-N curve as a basis. Even neglecting the problem with what confidence these S-N curves could have been determined for the many different welding classes in these standards, this approach is fundamentally flawed in the authors' opinion, because it assumes the scatter to be equal under constant and under variable amplitudes. This, however, is not generally true [20]. It is a much better solution to separate the problem of the prediction hypothesis from that of the probability by first calculating the fatigue life under variable amplitudes for  $P_s = 50\%$ , i.e. based on the mean S-N curve, and afterwards applying a statistically derived scatter factor. This must be chosen according to experience with variable amplitude tests on components. Haibach in [30] gives some numerical examples with regard to surface quality.

"What is a good industrial fatigue life prediction" poses a dilemma. On one hand all the parameters necessary for the predictions are often not known with sufficient accuracy, as discussed in Chapter 2, and many other details also influence the result: so it is logical to assume that for the same hypothesis the overall accuracy of the prediction should be much lower than under laboratory conditions; if 0.5 to 2.0 is good for scientific purposes, probably 1.0 to 8.0 should be considered "good enough" for industrial predictions. However, no prospective industrial user could live with the statement that just because of the inaccuracy of the prediction his oil rig might last for 10, but maybe also for 80 years. As mentioned before, this is the reason why a fatigue life prediction by calculation alone can never be employed for critical components; fatigue tests with the component and/or inspections and damage tolerant or fail safe design are necessary.

#### 4 REQUIREMENTS FOR THE ASSESSMENT OF FATIGUE LIFE PREDICTION HYPOTHESES

After the question "What is a good (enough) prediction?" has been settled, the hypothesis in question must be validated. This is only possible by comparison with the results of realistic variable amplitude tests. This may sound trivial, but it is here that most errors are made, often by overly optimistic inventors of new hypotheses. "Realistic" tests mean tests with realistic stress-time

histories and at realistic stress levels and lives to failure. The former requirement can be met easily, because for many applications standardized stress-time histories are now available, like "Gauss" (general), "Twist" (transport aircraft), "Falstaff" (tactical aircraft), "Helix-Felix" (helicopters), "Turbistan" (gas turbines), "Carlos" (automobiles), "Wash" (offshore rig) and "Wisper" (wind turbines).

The second requirement is very difficult to meet, because it is very expensive and time-consuming in particular for long fatigue lives. For example, the 20 or more years' life of an oil rig is equivalent to about  $10^8$  cycles; similar numbers of cycles occur in trucks and cars. Although a considerable percentage of these numbers of cycles can be omitted in test without influencing the results, the "omission dilemma" [21] has not generally been solved. Based on large number of tests, stress amplitudes  $< 50\%$  of the fatigue limit as an upper omission limit have been suggested [31, 32].

Anyway, realistic stress levels in assessment tests are absolutely necessary, because while a hypothesis might be good at high stress levels and, say,  $10^7$  cycles this does not necessarily prove it is good at more realistic stress levels and cycles to failure [33]. A recent example can be found in [34], where Miner's Rule and a crack propagation calculation showed good agreement with test results under Felix/28 at very short fatigue lives/high stresses, but were unconservative by factors of 4 to 7 at longer, more realistic fatigue lives.

Some authors give the impression that their hypotheses have been assessed and found to be "good", but close inspection by independent assessors shows this to be incorrect. An example is the large SAI-Programme [35] where none of the many hypotheses presented could be considered good by a large margin. Another example can be found in [22], where the authors claim their hypothesis to be superior to several others, because it also predicted the fatigue life under very simple "overload" and "underload" sequences better than others while all hypotheses "fit generally well with the test results". On closer inspection, however, none of the hypotheses assessed was good or even acceptable for the realistic stress time histories and the authors' hypothesis was no better than the others.

One aspect of the assessment needs further discussion: Both the constant amplitude as well as the spectrum loading tests show scatter. Deterministic life prediction concepts deliver a prediction for a selected probability, generally for  $P_s = 50\%$ , because this value has the highest confidence. It is self-evident that predictions should be compared to the corresponding experimental values i.e. e.g. for  $P_s = 50\%$ . Very often, however, individual test results are compared to the predicted value because only few variable amplitude test results

are available, in particular at long lives. Thus experimental scatter and the scatter due to the hypotheses themselves are mixed which hinders the assessment with regard to the requirements mentioned in Chapter 3. A better solution would be to evaluate the ratio of predicted vs. mean experimental lives at selected load levels or fatigue life intervals. Only if several different hypotheses are checked and ranked against a fixed set of experimental data, both ways are meaningful. An example is given and discussed in the following chapter.

## 5 FATIGUE LIFE PREDICTION FOR AUTOMOTIVE COMPONENTS

### 5.1 Background

During the eighties, a large test programme was conducted at IABG supported by several German car manufacturers [36, 37]. Five different components of the suspension system were selected from actual production lines including

- a forged steel stub axle
- a forged steel stub axle with an induction hardened critical section
- a sheet steel welded rear axle from a front wheel drive car
- a cast aluminium wheel
- a welded sheet steel wheel.

These components were tested under constant amplitude and spectrum loading to provide a broad basis for an assessment of fatigue life prediction according to different versions of Miner's Rule. Moreover typical life ratios (damage sums at failure) were determined for these components which have to be designed for a spectrum loading environment, since the expected maximum loads are well beyond the endurance limit.

### 5.2 Test Details

The components were tested predominantly in a bending mode since loading in the vertical as well as the lateral direction induces bending moments into the components in the built-in position. The wheels were tested in a special test rig where the wheel fixed to a plate is rotated with a constant frequency of 25 Hz whereas a (variable) bending moment is introduced by a servo hydraulic actuator. Here the loading was kept constant for 4 sec per individual load level which translates to 100 cycles at  $R = -1$  for each step.

Besides constant amplitude loading at  $R = -1$  and partly  $R = -0.4$  two different spectra were applied, Fig. 1. Spectrum I, typical for customer usage, can be described by a straight line in a log-lin diagram; spectrum II, being dominated by higher load ranges, is typical for race or test track driving. It is similar to a Gaussian spectrum. Both sequences were generated by a pseudo-random generator and repeated until failure. The  $R$  ratio was deliberately set to  $R = -1$  for all of the cycles, i.e. mean load changes did not occur. The failure criteria

was total failure or the occurrence of one or several large cracks (in the range of 30 to 100 mm) where no substantial further life increments could be expected. Typical results showing the amount of test data are plotted in Fig. 2 for the sheet steel welded rear axle part.

### 5.3 Miner Hypotheses

Three versions of Miner's Rule were included in the evaluation procedure differing in the handling of load ranges below the fatigue limit, Fig. 3, designated as

- Miner-original (MO), no damage below the fatigue limit
- Miner-modified according to Haibach [38] (MH) where a fictitious  $S-N$  curve below the fatigue limit with a reduced slope  $2k-1$  is assumed
- Miner-elementary (ME), with a fictitious  $S-N$  curve prolonged below the fatigue limit i.e. any fatigue limit is neglected.

Finally a fourth method recently proposed by Zenner and Liu [39] (ZL) was included which consists of a linear Miner type prediction based on an artificial  $S-N$  curve. That  $S-N$  curve is constructed as follows, Fig. 4: Since it has been observed that even elementary Miner predictions can produce unconservative results, a steeper slope than the original slope  $k$  should be applied. With regard to the crack propagation phase which often considerably contributes to total life, a fictitious slope

$k' = \frac{1}{2}(3.5 + k)$  is proposed which is the average of the actual slope  $k$  and  $k = 3.5$  which would be typical for crack propagation. Based on results from omission tests [31, 32], a cut-off level, i.e. a new "fatigue limit", is considered which is 50% of the actual fatigue limit. The artificial  $S-N$  curve starts for the maximum load range of the spectrum at the original  $S-N$  curve. Thus for each overall stress level a new artificial  $S-N$  curve is constructed and used for prediction. It is obvious that some of the elements of that proposal are similar to previous methods [6], but more recent knowledge appears to be incorporated to the new method which is easy to implement.

### 5.4 Results and Discussion

Gassner curves, i.e.  $S-N$  curves for spectrum loading, were predicted for each of the components applying the four versions of Miner type damage calculations mentioned above. Examples are shown in Figs. 5 and 6. For each test result the life ratio  $D = N_{\text{test}}/N_{\text{pred}}$  was determined which is equivalent to an individual damage sum  $D_i$  for that specimen. These life ratios were compiled and mean and standard deviation of their logarithms were established for individual and grouped data sets. From the standard deviations, a scatter factor  $T = D_{10\%}/D_{90\%}$  was derived assuming a log normal distribution for the life ratios,  $D_i$ . Thus these scatter factors include both the scatter due to eventually inadequate hypotheses and the experimental scatter. Since

different hypotheses are checked against a common data pool, that procedure appears to be tolerable.

In Fig. 7 all prediction results are compiled in terms of the respective mean life ratios,  $\bar{D}$ , and the associated scatter factors,  $T$ . These have been obtained individually for each of the five components and each of the two spectra.

The most significant value for an assessment of hypotheses is the scatter factor which in this case gives a measure how good the characteristics of the Gassner curve, i.e. the effect of the overall load level, is predicted. A small scatter factor may well be accompanied by a relatively large error of the overall position of the predicted Gassner curve. Fig. 7 indicates that none of the hypotheses tested exhibits a clear superiority above the others with respect to scatter factors,  $T$ , as an assessment criterion. The smallest scatter values are found for the recent proposal of Zenner/Liu as well as for the original and modified Miner predictions, respectively.

It is interesting to note that the influence of the overall load level is predicted most accurately by the original Miner rule when the maximum load ranges are close to the fatigue limit, Fig. 6. In this case, the method of Zenner/Liu is worst due to a significant difference between the predicted and actual slope of the Gassner curves, respectively.

In most cases the predictions are unconservative ranging down to  $\bar{D} = 0.053$  for the cast aluminium wheel, which corresponds to an overestimation of fatigue life by a factor of 19.

Still more important, however, the mean life ratios are significantly different for the two spectra when the conventional Miner type predictions are considered. For spectrum I characterizing customer usage  $\bar{D}_{\text{mean}} = 0.14$  is found on an average using Miner original whereas for test track usage (spectrum II)  $\bar{D}_{\text{mean}} = 0.56$ . This means that experimental experience collected on test or race tracks cannot directly be used for design for customer usage by a relative Miner approach. With regard to that criterion the Zenner/Liu proposal works best because the range of mean life ratios observed for the two spectra is significantly smaller than those found for the other hypotheses.

Up to now predictions for individual test results were separately evaluated for each of the components and the two spectra, respectively. Thus the overall load levels which were selected for the described test programme were considered. Taking the view of industrial application, a different criterion would perhaps be more significant where an overall load level is chosen for evaluation which can be called a design load level. This load level is the maximum load range which is expected for

the design life excluding, however, overloads resulting from mis-use or near-accident situations. Here the predictions are compared to the respective mean experimental spectrum fatigue lives. The mean life ratios and associated scatter factors for that load level are compiled in Fig. 8 where the results for all five components are combined.

The most striking conclusion from that figure is the superiority of the Zenner/Liu proposal when both spectra are commonly evaluated. Besides the lowest scatter factor for the predictions, a mean life ratio near unity is found.

It is obvious that different criteria may be employed for an assessment of fatigue life prediction hypotheses leading to sometimes contradicting conclusions. It is essential, therefore, to clearly state the criteria used when such hypotheses are evaluated on the basis of relevant experimental data.

## 6 CONCLUDING REMARKS

For an assessment of fatigue life prediction hypotheses several requirements have to be fulfilled which are not easily met. Since the conditions, prerequisites and consequences of an application of fatigue life predictions are extremely varying, it is not realistic to expect or look for prediction concepts which are generally applicable.

When fatigue life prediction is applied in industry Miner's Rule is still in use partly due to its simplicity, but also due to incorporation of basic fatigue data which inherently reflect many of the fatigue-relevant features such as size, surface finish etc. It is, however, evident that the complex process of fatigue (crack) initiation and accumulation (crack propagation) under variable amplitude loading is oversimplified by the linear damage accumulation rule. This has been confirmed again on the basis of the large test programme on actual components from automotive suspension systems as shown in the paper.

## 7 REFERENCES:

- [1] Palmgren, A.: Die Lebensdauer von Kugellagern. VDI-Zeitschrift, Bd. 68 (1924), 339 - 341.
- [2] Langer, B. F.: Fatigue Failure from Stress Cycles of Varying Amplitude. Trans. ASME: Journal of Applied Mechanics, Vol. 59 (1937) p. A 160-A 162.
- [3] Miner, M. A.: Cumulative Damage in Fatigue. Trans. ASME: Journal of Applied Mechanics, Vol. 12 (1945), p A159-164.
- [4] Miner, M. A.: Estimation of Fatigue Life with Particular Emphasis on Cumulative Damage. in: Metal Fatigue, Editors: G. Sines, J.L. Waisman,

McGraw-Hill Book Company, Inc., pp. 278-289, 1959.

- [15] Schütz, W. und H. Zenner: Schadensakkumulationshypothese zur Lebensdauer vorhersage bei schwingender Beanspruchung - ein kritischer Überblick. Z. f. Werkstofftech. 4, 1973 H.1, S. 25-33 u. H.2, S. 97 - 102).
- [16] Corten, H. T., and T. J. Dolan: Cumulative Fatigue Damage. Proceedings of the International Conference on Fatigue of Metals (London, September 1956). Institution of Mechanical Engineers, London.
- [17] Paris, P. C., M. P. Gomez and W. E. Anderson: A Rational Analytic Theory of Fatigue. The Trend in Engineering, 1961, Vol. 13, p. 9.
- [18] Paris, P. C.: The Fracture Mechanics Approach to Fatigue. in: Fatigue - An Interdisciplinary Approach: Editors: J.H. Burke, N.L. Reed, V. Weiss, Syracuse University Press, 1964.
- [19] Forman, R. G., V. E. Kearney and R. M. Engle: Numerical Analysis of crack propagation in cyclic loaded structures. J. of Basic Eng. 89 (1967) 459.
- [10] Willenborg, J., R.M. Engle, H.A. Wood: A Crack Growth Retardation Model Using an Effective Stress Concept. AFFDL-TR-71-1, 1971
- [11] Elber, W.: Fatigue Crack Propagation: Some Effects of Crack Closure on the Mechanics of Fatigue Crack Propagation and Cyclic Tensile Loading. Ph. D. Thesis, University of New South Wales, 1968.
- [12] Elber, W.: The Significance of Fatigue Crack Closure. In: Damage Tolerance in Aircraft Structures ASTM STP 486, 1971 pp 230 - 242.
- [13] Melcon, M.A. and W. Crichlow: Investigation of the Representation of Aircraft Service Loadings in Fatigue Tests. Technical Report No. ASD-TR-61-435.
- [14] Schütz, W., R. Weber: Steuerung von Schwingprüfmaschinen durch Prozeßrechner. Materialprüfung 12 (1970) Nr. 11, S. 369-377.
- [15] Schütz, W.: Lebensdauer vorhersage schwingend beanspruchter Bauteile. in: Werkstoffermüdung und Bauteilfestigkeit, DVM-Kolloquium 1980, DVM, Berlin.
- [16] Wästberg, S.: Variabilities and Uncertainties in Fatigue Life Predictions for Offshore Structures. Paper at the WG2-meeting, Delft, March 1983.
- [17] Hoffmann, J.: Die experimentelle Untersuchung des Einflusses von Werkstoffkennwerten, geometrie- und fertigungsbedingungen auf die rechnerisch ermittelte Lebensdauer nach dem Kerbgrundkonzept. in: Bauteillebensdauer: Rechnung und Versuch. To be published by DVM, Berlin, 1993.
- [18] Hoffmann, J.: Streuverhalten von Anrißwöhlerlinien. Materialprüfung, Heft 3, pp 46 - 51, 1993.
- [19] Schütz, W.: Forgings, Including Landing Gears. In: Practical applications of fracture mechanics, H. Liebowitz editor. Agard AG 257, pp 6.1 - 6.52.
- [20] Schütz, D. and P. Heuler: The Significance of Variable Amplitude Testing. In: Automation in Fatigue and Fracture Analysis. ASTM-STP, to be published.
- [21] Crichlow, W.: On Fatigue Analysis and Testing for the Design of the Airframe. In: AGARD LS 62, 1973.
- [22] Bleuzent, C., M. Chaudonneret, J. Flavenot, N. Paganathan and M. Robert: Validation of Life Prediction Models from Representative Testings on Aluminium Alloy Specimens. Paper presented at the ICAF-Symposium, 1993, Stockholm.
- [23] Buch, A.: Verification of Fatigue Crack Initiation Life Prediction Results. Israel Inst. of Techn., Haifa, IAE No. 400, 1980.
- [24] Gassner, U. und H. Lowak: Wechselverformungsverhalten metallischer Werkstoffe und Lebensdauer bauteilähnlicher gekerbter Probestabe. Materialprüfung 22 (1980), Nr. 8.
- [25] Schütz, W.: Lebensdauer vorhersage schwingend beanspruchter Bauteile. In: Werkstoffermüdung und Bauteilfestigkeit, DVM 1980, Berlin
- [26] Schijve, J.: Fatigue Crack Growth Predictions for Variable Amplitude and Spectrum Loading. In: Proceedings of "Fatigue '87", Charlottesville, 1987.
- [27] Siegl, J., J. Schijve and U.H. Padmadnata: Fractographic observations and predictions on fatigue crack growth in an aluminium alloy under Mini-Twist flight-simulation loading. Int. J. Fatigue 13, No. 2 (1991), pp 139 - 147.
- [28] British Standards Institution: Steel, Concrete and Composite Bridges. BS 5400, Part 10, Code of Practice Fatigue. British Standard Institution, London, 1980.
- [29] Eurocode 3, Design of Steel Structures. Part 1 General Rules and Rules for Buildings. Provisional, Commission of the European Communities, EC3-88-CEE-104.

- [30] Haibach, E.: Betriebsfestigkeit. Verfahren und Daten zur Bauteilberechnung. VDI-Verlag Düsseldorf 1989.
- [31] Heuler, P. and T. Seeger: A criterion for omission of variable amplitude loading histories. Int. J. Fatigue 8, No. 4 (1986), pp. 225-230.
- [32] Oppermann, H.: Zulässige Verkürzung zufallsartiger Lastfolgen für Betriebsfestigkeitsversuche. in: Buxbaum, O., Vorträge des 5. LBF-Koll., LBF-Bericht Nr. TB-180, 1988.
- [33] Jarfall, L.: Fatigue and Damage Tolerance Work during the Aircraft Design Process. In: Durability and Damage Tolerance in Aircraft Design. A. Salvetti and G. Cavallini (Eds.), EMAS, 1985, pp. 1-31.
- [34] Everett, R. A., Jr: A Comparison of Fatigue Life Prediction Methodologies for Rotorcraft. NASA TM 102759, Dec. 1990
- [35] Fatigue under Complex Loading, Analyses and Experiments. R.M. Wetzel, (Ed.), Society of Automotive Engineers, 1977.
- [36] Hück, M., J. Bergmann, and W. Schütz: Gemeinschaftsarbeit Pkw-Industrie/IABG. Relative Miner-Regel. Teil I, Zu den gängigen Verfahren der Lebensdauersicherung ermüdungskritischer Pkw-Bauteile. IABG-Report 2022, 1 December 1988.
- [37] Hück, M., J. Bergmann und P. Heuler: Gemeinschaftsarbeit Pkw-Industrie/IABG. Relative Miner-Regel. Teil II, Bauteilversuche. IABG-Report TF-2904; 9. October 1991.
- [38] Haibach, E.: Modifizierte Schadensakkumulationshypothese zur Berücksichtigung des Dauerfestigkeitsabfalls mit fortschreitender Schädigung. LBF-report TM-50/70, Darmstadt, 1970.
- [39] Zenner, H., Liu, J.: Vorschlag zur Verbesserung der Lebensdauerabschätzung nach dem Nennspannungskonzept. Konstruktion 1/92, S. 9-17, 1992

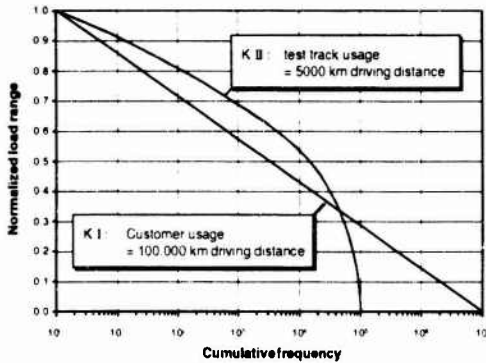


Fig. 1 Cumulative frequency distributions of test spectra

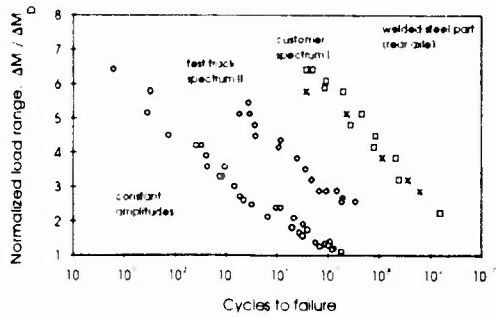


Fig. 2 Fatigue strength of sheet steel welded rear axle under constant amplitude and spectrum bending loading

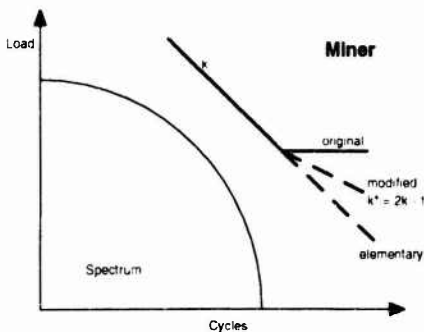


Fig. 3 Representation of S-N curves for different versions of Miner's Rule

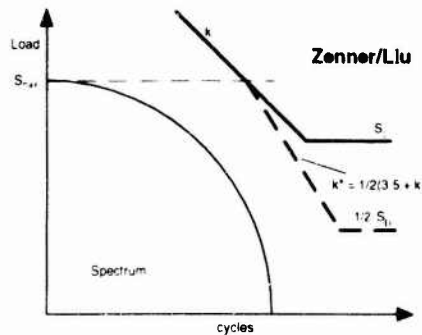


Fig. 4 Representation of S-N curve according to Zenner and Liu [39]

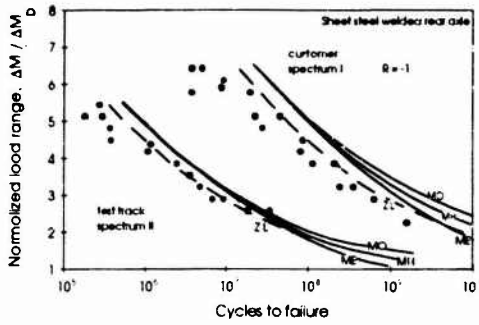


Fig. 5 Test results and predictions for a welded rear axle part under spectrum loading (MO = Miner original, MH = Miner mod. Haibach, ME = Miner elem., ZL = Zenner/Liu)

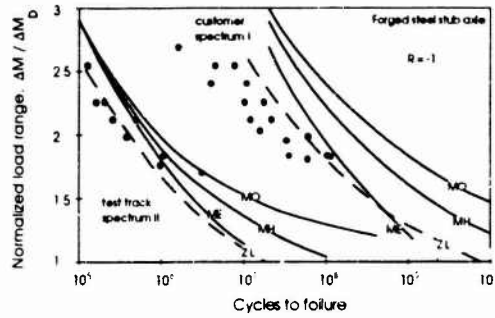
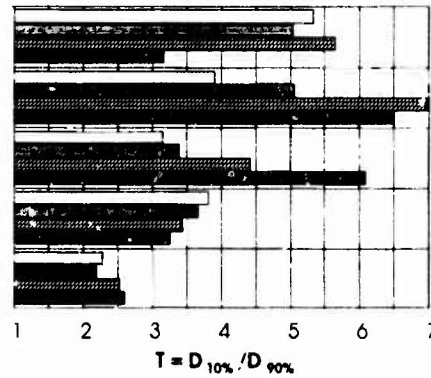
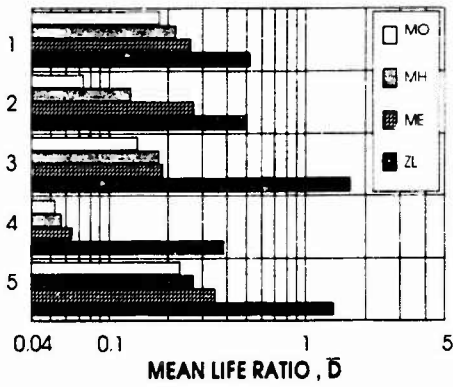


Fig. 6 Test results and predictions for a forged steel stub axle under spectrum loading (MO = Miner original, MH = Miner mod. Haibach, ME = Miner elem., ZL = Zenner/Liu)

**Spectrum I Customer Usage**



**Spectrum II Test Track Usage**

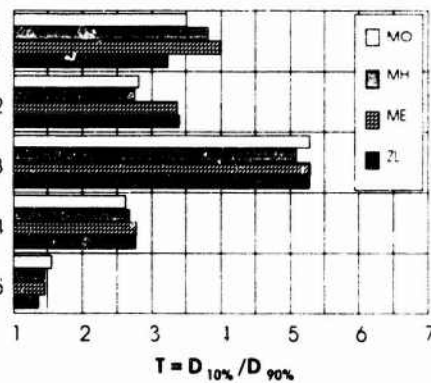
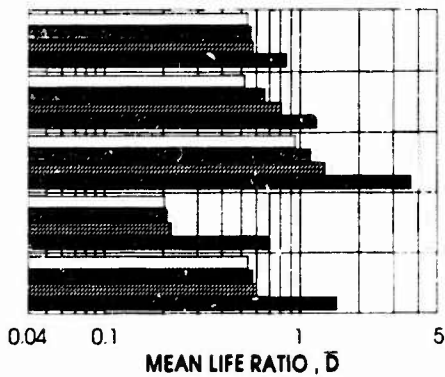
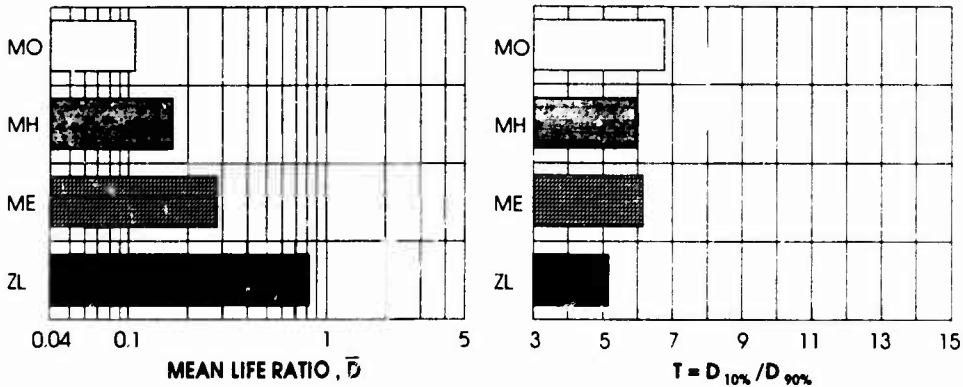
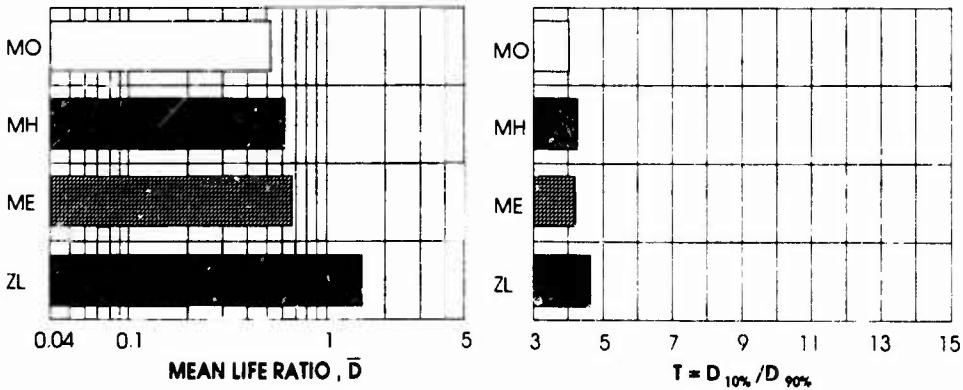


Fig. 7 Evaluation of different Miner hypotheses based on individual test results of five automotive components (1 = stub axle, 2 = stub axle induct. hard., 3 = welded rear axle, 4 = cast al wheel, 5 = welded steel wheel)

**Spectrum I Customer Usage**



**Spectrum II Test Track Usage**



**Spectra I + II**

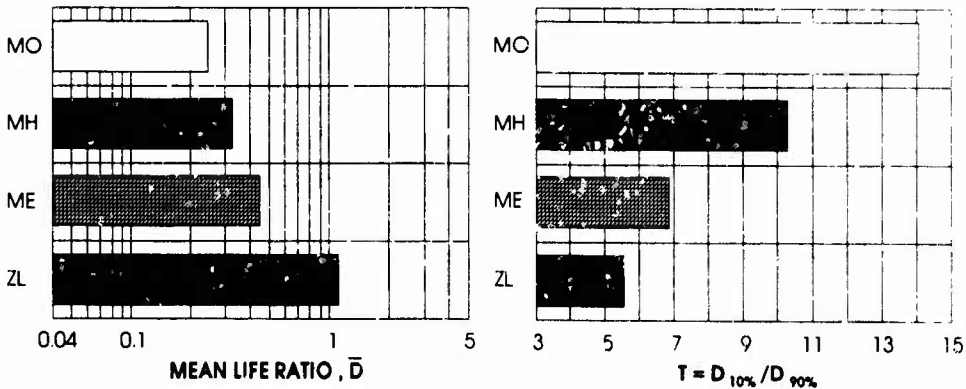


Fig. 8 Evaluation of different Miner hypotheses combining results of five automotive components at design load level (MO = Miner original, MH = Miner mod. Haibach, ME = Miner elem., ZL = Zenner/Liu)

## FATIGUE LIFE AND CRACK GROWTH PREDICTION METHODOLOGY

J. C. Newman, Jr.  
E. P. Phillips  
Mechanics of Materials Branch  
NASA Langley Research Center  
Hampton, Virginia 23681  
USA

R. A. Everett, Jr.  
Vehicle Structures Directorate  
U. S. Army Research Laboratory  
Hampton, Virginia 23681  
USA

### SUMMARY

This paper reviews the capabilities of a plasticity-induced crack-closure model and life-prediction code to predict fatigue crack growth and fatigue lives of metallic materials. Crack-tip constraint factors, to account for three-dimensional effects, were selected to correlate large-crack growth rate data as a function of the effective-stress-intensity factor range ( $\Delta K_{\text{eff}}$ ) under constant-amplitude loading. Some modifications to the  $\Delta K_{\text{eff}}$ -rate relations were needed in the near-threshold regime to fit small-crack growth rate behavior and endurance limits. The model was then used to calculate small- and large-crack growth rates, and in some cases total fatigue lives, for several aluminum and titanium alloys under constant-amplitude, variable-amplitude, and spectrum loading. Fatigue lives were calculated using the crack-growth relations and microstructural features like those that initiated cracks. Results from the tests and analyses agreed well.

### LIST OF SYMBOLS

a	Crack length in thickness (B) direction
a <sub>j</sub>	Initial defect or crack length in B-direction
b	Defect or void half-height
B	Specimen thickness
c	Crack length in width (w) direction
c <sub>j</sub>	Initial defect or crack length in w-direction
F <sub>j</sub>	Boundary correction factor
K <sub>max</sub>	Maximum stress-intensity factor
K <sub>OL</sub>	Overload stress-intensity factor
K <sub>UL</sub>	Underload stress-intensity factor
N	Number of cycles
N <sub>f</sub>	Number of cycles to failure
R	Stress ratio ( $S_{\text{min}}/S_{\text{max}}$ )
r	Notch or hole radius
S	Applied stress
S' <sub>o</sub>	Crack-opening stress
S <sub>max</sub>	Maximum applied stress
S <sub>mf</sub>	Mean flight stress
S <sub>min</sub>	Minimum applied stress
t	Specimen thickness for through or corner crack; half-thickness for surface crack
α	Constraint factor
α <sub>g</sub>	Global constraint factor from finite-element analysis
Δc	Crack extension in c-direction
ΔK	Stress-intensity factor range
ΔK <sub>eff</sub>	Effective stress-intensity factor range
(ΔK <sub>eff</sub> ) <sub>th</sub>	Small-crack ΔK <sub>eff</sub> threshold
ΔK <sub>th</sub>	Large-crack ΔK threshold
ρ	Plastic-zone size
σ <sub>o</sub>	Flow stress (average of σ <sub>ys</sub> and σ <sub>u</sub> )

σ <sub>ys</sub>	Yield stress (0.2 percent offset)
σ <sub>u</sub>	Ultimate tensile strength
ω	Cyclic-plastic-zone size

### 1. INTRODUCTION

The use of damage-tolerance and durability design concepts based on fatigue-crack growth in aircraft structures is well established (Ref 1 and 2). The safe-life approach, using standard fatigue analyses, is also used in many designs. In conventional metallic materials, crack-growth anomalies such as the small-crack effect and the various crack-tip shielding mechanisms (Ref 3 and 4) have improved our understanding of the crack-growth process but have complicated life-prediction methods. In the new metallic materials, such as the aluminum-lithium alloys, crack shielding and failure mechanisms are more complex than in conventional materials due to crack growth along tortuous crack paths (Ref 5). Over the past decade, the intense experimental studies on small or short crack growth behavior in these metallic materials have led to the realization that fatigue life of many materials is primarily "crack growth" from microstructural features, such as inclusion particles, voids or slip-band formation. Concurrently, the improved fracture-mechanics analyses of some of the crack-tip shielding mechanisms, such as plasticity- and roughness-induced crack closure, and analyses of surface- or corner-crack configurations have led to more accurate crack growth and fatigue life prediction methods.

On the basis of linear-elastic fracture mechanics (LEFM), studies on small cracks (10 μm to 1 mm) have shown that small cracks grow much faster than would be predicted from large crack data (Ref 3 and 4). This behavior is illustrated in Figure 1, where the crack-growth rate, da/dN or dc/dN, is plotted against the linear-elastic stress-intensity factor range, ΔK. The solid (sigmoidal) curve shows typical results for large cracks in a given material and environment under constant-amplitude loading ( $R = S_{\text{min}}/S_{\text{max}} = \text{constant}$ ). The solid curve is usually obtained from tests with large cracks. At low growth rates, the threshold stress-intensity factor range, ΔK<sub>th</sub> is usually obtained from load-reduction (ΔK-decreasing) tests. Some typical results for small cracks in plates and at notches are shown by the dashed curves. These results show that small cracks grow at ΔK levels below the large-crack threshold and that they also can grow faster than large cracks at the same ΔK level above threshold. Small-crack effects have been shown to be more prevalent in tests which

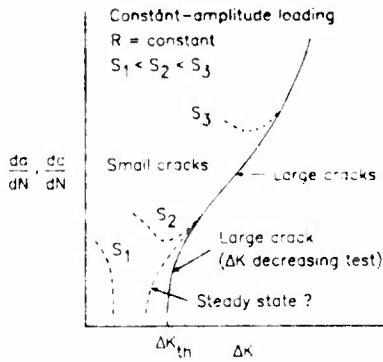


Fig. 1 Typical fatigue-crack-growth rate data for small and large cracks.

have compressive loads, such as negative stress ratios (Refs 6-8).

During the last decade, research on small- or short-crack effects has concentrated on three possible explanations for the behavior of such cracks. They are plasticity effects, metallurgical effects and crack closure (Ref 3 and 4). All of these features contribute to an inadequacy of LEFM and the use of the  $\Delta K$ -concept to correlate fatigue crack growth rates.

Some of the earliest small-crack experiments were conducted at high stress levels which were expected to invalidate LEFM methods. Nonlinear or elastic-plastic fracture mechanics concepts, such as the J-integral and an empirical length parameter (Ref 9), were developed to explain the observed small-crack effects. Recent research on the use of  $\Delta J$  as a crack-driving parameter suggest that plasticity effects are small for many of the early and more recent small-crack experiments (Ref 10). But the influence of plasticity on small-crack growth and the appropriate crack-driving parameter is still being debated.

Small cracks tend to initiate in metallic materials at inclusion particles or voids, in regions of intense slip, or at weak interfaces and grains. In these cases, metallurgical similitude (see Ref 11) breaks down for these cracks (which means that the growth rate is no longer an average taken over many grains). Thus, the local crack growth behavior is controlled by metallurgical features. If the material is markedly anisotropic (differences in modulus and yield stress in different crystallographic directions), the local grain orientation will strongly influence the rate of growth. Crack front irregularities and small particles or inclusions affect the local stresses and, therefore, the crack growth response. In the case of large cracks (which have large fronts), all of these metallurgical effects are averaged over many grains, except in very coarse-grained materials. LEFM and nonlinear fracture mechanics concepts are only beginning to explore the influence of metallurgical features on stress-intensity factors, strain-energy densities, J-integrals and other crack-driving parameters.

Very early in small-crack research, the phenomenon of fatigue-crack closure (Ref 12) was recognized as a possible explanation for rapid small-crack growth rates (see Ref 13). Fatigue crack closure is caused by residual plastic deformations left in the wake of an advancing crack. Only that portion of the load cycle for which the crack is fully open is used in computing an effective stress-intensity factor range ( $\Delta K_{eff}$ ) from LEFM solutions. A small crack initiating at an inclusion particle, a void or a weak grain does not have the prior plastic history to develop closure. Thus, a small crack may not be closed for as much of the loading cycle as a larger crack. If a small crack is fully open, the stress-intensity factor range is fully effective and the crack-growth rate will be greater than steady-state crack-growth rates. (A steady-state crack is one in which the residual plastic deformations and crack closure along the crack surfaces are fully developed and stabilized under steady-state loading.) Small-crack growth rates are also faster than steady-state behavior because these cracks may initiate and grow in weak microstructure. In contrast to small-crack growth behavior, the development of the large-crack threshold, as illustrated in Figure 1, has also been associated with a rise in crack-opening load as the applied load is reduced (Ref 14 and 15). Thus, the steady-state crack-growth behavior may lie between the small-crack and large-crack threshold behavior, as illustrated by the dash-dot curve.

The purpose of this paper is to review the capabilities of a plasticity-induced crack-closure model (Ref 16 and 17) to correlate and to predict small- and large-crack growth rate behavior in several aluminum and titanium alloys under various load histories. Test results from the literature on aluminum alloys 2024-T3 (Refs 7, 18 and 19), 7075-T6 (Ref 20), LC9cs (Ref 20) and 7475-T7351 (Refs 21 and 22) and on titanium alloys Ti-6Al-4V (Ref 23 and 24), IMI-685 (Refs 23-25) and Ti-17 (Refs 23 and 24) under constant-amplitude loading were analyzed with the closure model to establish an effective stress-intensity factor range against crack growth rate relation. The effective stress-intensity factor range against crack growth rate relations were then used in the closure model to predict large-crack growth under a single spike overload, an overload and underload, repeated spike overloads every 1000 cycles, TWIST (Ref 26) and Mini-TWIST (Ref 27) loading. Using the closure model and some microstructural features, a total fatigue life prediction method is demonstrated on a titanium alloy under constant-amplitude loading and on several aluminum alloys under various load histories. The load histories considered were the FALSTAFF (Ref 28), Gaussian (Ref 29), TWIST (Ref 26) and Mini-TWIST (Ref 27). The crack configurations used in these analyses were through-crack configurations, such as center-crack and compact specimens, and three-dimensional crack configurations, such as a corner crack in a bar and a surface or corner crack at a semi-circular notch.

## 2. CRACK-CLOSURE MODEL

The crack-closure model (Refs 16 and 30) was developed for a central through crack in a finite-width specimen subjected to remote applied stress. The model was later extended to a through crack emanating from a circular hole and applied to the growth of small cracks (Ref 15 and 31). The model was based on the Dugdale model (Ref 32), but modified to leave plastically deformed material in the wake of the crack. A schematic of the model is shown in Figure 2. Here a crack is growing from a hole in an elastic body (Region 1). At the maximum applied stress,  $S_{max}$ , the material in the plastic zone,  $p$ , (Region 2) carries the stress,  $\alpha\sigma_0$ . The constraint factor,  $\alpha$ , accounts for the influence of stress state on tensile yielding at the crack front

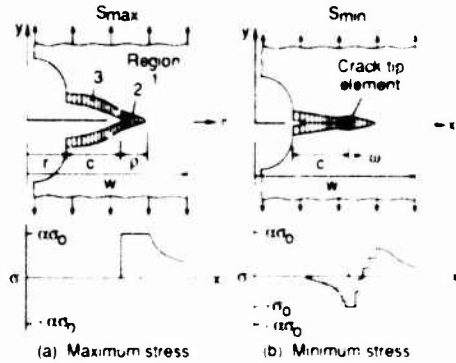


Fig. 2 Schematic of plasticity-induced crack-closure model under cyclic loading

The flow stress  $\sigma_0$  is the average between the yield stress and ultimate tensile strength. For plane-stress conditions,  $\alpha$  is equal to unity (original Dugdale model), and for simulated plane-strain conditions,  $\alpha$  is equal to 3. Although the strip-yield model does not model the correct yield-zone pattern for plane-strain conditions, the model with a high constraint factor is able to produce crack-surface displacements and crack-opening stresses quite similar to those calculated from an elastic-plastic finite-element analysis of crack growth and closure for a finite-thickness plate (see Ref 33). As the crack grows under cyclic loading, residual-plastic deformed material (Region 3) is left on the crack surfaces. During unloading, these surfaces contact each other at the minimum applied stress. The material in the plastic zone and along the contacting surfaces was assumed to yield at  $-\sigma_0$ . (In the original model, the contacting surfaces were assumed to reduce the effectiveness of the crack and reduce the constraint around the crack front. On the basis of three-dimensional finite-element analyses, however, this assumption may need to be studied further but this is beyond the scope of the present paper.) Using the contact stresses, the crack-opening stress is calculated. The crack-opening stress is the applied stress level at which the crack surfaces are fully open and is denoted as  $S'_0$ . The model is able to predict crack-opening stresses as a function of crack length and load history. The crack-

opening stress is then used to calculate the effective stress-intensity factor range,  $\Delta K_{eff}$  (Ref 12). In turn, the crack-growth rate is calculated using a  $\Delta K_{eff}$ -against-crack-growth-rate relation.

In conducting fatigue-crack growth analyses, the constraint factor  $\alpha$  was used to elevate the flow stress at the crack tip to account for three-dimensional stress states. At present, the constraint factor is used as a fitting parameter to correlate crack-growth rate data against  $\Delta K_{eff}$  under constant-amplitude loading for different stress ratios. However, tests conducted under single-spike overloads seem to be more sensitive to state-of-stress effects and may be a more appropriate test to determine the constraint factor.

### 2.1 Effective Stress-Intensity Factor Range

For most damage tolerance and durability analyses, linear-elastic analyses have been found to be adequate. However, for high stress-intensity factors, proof testing and low-cycle fatigue conditions, linear-elastic analyses are inadequate and nonlinear crack-growth parameters are needed (see Ref 10). Herein, the linear-elastic effective stress-intensity factor range, developed by Elber (Ref 12), was used and is given by

$$\Delta K_{eff} = (S_{max} - S'_0) (\pi c)^{1/2} F_1$$

where  $S_{max}$  is the maximum applied stress,  $S'_0$  is the crack-opening stress and  $F_1$  is the usual boundary-correction factor.

### 2.2 Constraint Variations

As a crack grows in a finite-thickness body under cyclic loading (constant stress range) the plastic-zone size at the crack front increases. At low stress-intensity factor levels, plane-strain conditions should prevail but as the plastic-zone size becomes large compared to sheet thickness, a loss of constraint is expected. This constraint loss has been associated with the transition from flat-to-slant crack growth, as illustrated in Figure 3. Schijve (Ref 34) has shown that the transition occurs at nearly the same crack-growth rate over a wide range in stress ratios for an aluminum alloy. Later, Schijve (Ref 35), using Elber's crack-

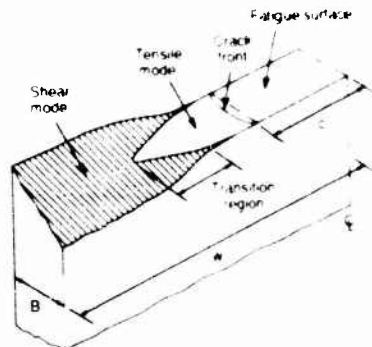


Fig 3 Fatigue crack surface showing transition from tensile- to shear-mode crack growth

closure concept, proposed that the transition should be controlled by  $\Delta K_{eff}$ . This observation has been used to help select the constraint-loss regime (see Ref 31).

In a related effort to study constraint variations using a three-dimensional, elastic-plastic, finite-element analysis, some results are included here to help resolve the constraint-loss issue (see Ref 36). The finite-element code, ZIP3D (Ref 37), was used to analyze center-crack-tension and bend specimens made of a material with an elastic-perfectly-plastic stress-strain behavior. The analyses were conducted on a 2.5 mm-thick sheet with various half-widths ( $w$ ) and a  $c/w$  ratio of 0.5. The crack front was flat and straight-through the thickness. The finite-element model (one-eighth of the specimen) had six layers through the half-thickness with the layer on the centerline of the specimen being 0.15B and the layer on the free surface being 0.025B. The smallest element size around the crack front was about 0.03 mm. The number of elements was 5706 and the number of nodes was 7203. The finite-element model of the specimen was subjected to monotonic loading until the plastic zone extended across the net section.

Because the current model uses a constant flow stress in the plastic zone, a global constraint factor,  $\alpha_g$ , was defined as the average of the normal stress to flow stress ( $\sigma_{yy}/\sigma_0$ ) ratio in the plastic zone. Figure 4 shows a comparison of  $\alpha_g$  as a function of the normalized applied K level for tension and bend specimens. The symbols show the results from the finite-element analyses for various specimen sizes. The upper dashed lines show the results under plane-strain conditions; the lower dashed line shows the plane-stress condition. The global constraint factor was nearly a unique function of the applied K level. Some slight differences were observed near the plane-stress conditions (high K levels). These results show that the global constraint factor rapidly drops as the K level increases (plastic zone size increases) and approaches a value near the plane-stress condition. The solid line is a simple fit to the finite-element results and shows that the constraint-loss regime may be defined by a unique set of K values under monotonic loading and, possibly,  $\Delta K_{eff}$  under cyclic loading. In the current model, the constraint-

loss regime is defined by a set of crack-growth rates because the transition from flat-to-slant crack growth seems to occur at unique rates. This assumption also implies that a unique set of  $\Delta K_{eff}$  values define the constraint-loss regime.

2.3 Constant-Amplitude Loading

In Reference 38, crack-opening stress equations for constant-amplitude loading were developed from crack-closure model calculations for a center-crack tension specimen. These equations give crack opening stresses as a function of stress ratio (R), maximum stress level ( $S_{max}/\sigma_0$ ) and the constraint factor ( $\alpha$ ). To correct the previous crack-opening stress equations for extremely high crack-growth rates, a modification was developed in Reference 17. The new equations give crack-opening stresses that agree fairly well with results from the modified closure model. These equations are used to develop the baseline  $\Delta K_{eff}$ -rate relations that are used in the life-prediction code FASTRAN-II (Ref 39) to make crack-growth and fatigue-life predictions. A typical comparison between the model and the equations for a crack in a titanium alloy is shown in Figure 5. This figure shows crack-opening stresses as a function of crack length for a crack in an infinite plate at low R. To severely test the equations with a rapid change in constraint,  $\alpha$  was selected to be 2.4 for rates less than 1E-04 mm/cycle, and  $\alpha$  was 1.2 for rates greater than 1E-03 mm/cycle. The solid curve shows the calculations from the model. To use the crack-opening stress equations, the R ratio, the  $S_{max}/\sigma_0$  ratio and the constraint factor must be known a priori. In this example, the constraint factor is unknown as a function of crack length. Because rates are used to control the constraint factor in the model, the crack-growth rate must be known to calculate the crack-opening stress. The crack-length-against-cycles results from the model were therefore used to determine the rate for a given crack length. Knowing the rate, then the constraint factor is calculated from

$$\alpha = \alpha_2 + (\alpha_1 - \alpha_2) \frac{[\ln(dc/dN) - \ln(r_2)]}{[\ln(r_1) - \ln(r_2)]}$$

for  $r_1 < dc/dN < r_2$  where  $\alpha_1$  and  $\alpha_2$  are the constraint factors and  $r_1$  and  $r_2$  are the rates, at



Fig 4 Global constraint factors from three-dimensional finite-element analyses



Fig 5 Calculated crack-opening stresses from model and equations

the beginning and end of the constraint-loss regime, respectively. For rates less than  $r_1$ ,  $\alpha = \alpha_1$  and for rates greater than  $r_2$ ,  $\alpha = \alpha_2$ . Once the constraint factor has been determined, then the crack-opening stress is calculated from the equations (dashed curve). For constant  $\alpha$  regions, the results from the equations agreed well with the model. Some differences were observed in the transition region between  $\alpha = 2.4$  to 1.2, but the maximum error in calculating  $\Delta K_{\text{eff}}$  was only 4 percent. The small vertical lines indicate the corresponding life ratio ( $N/N_f$ ), in addition to indicating regions of constant constraint.

## 2.4 Spectrum Loading

For variable-amplitude and spectrum loading, the crack-closure model must be used to compute the crack-opening stress history. Some typical crack-opening stresses under the Mini-TWIST load sequence for a small surface crack in a single-edge-notch-tension (SENT) specimen are shown in Figure 6. In the small-crack simulation, an initial defect size of  $a_i = 3 \mu\text{m}$  and  $c_i = 9 \mu\text{m}$  was used. This size corresponds to inclusion-particle sizes that initiate cracks in some aluminum alloys (Refs 7 and 8). Variable constraint was selected for this simulation. The constraint factor ( $\alpha$ ) was 1.8 for crack-growth rates less than  $7\text{E-}04$  mm/cycle and 1.2 for rates greater than  $7\text{E-}03$  mm/cycle.

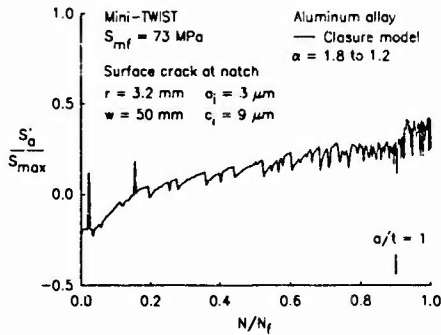


Fig. 6 Calculated crack-opening stresses for small surface crack under spectrum loading.

The figure shows crack-opening stress (normalized by the maximum stress in the spectrum) plotted against the ratio of applied cycles to cycles-to-failure ( $N/N_f$ ). The predicted cycles to failure,  $N_f$ , was about 800,000 cycles. These results show that the opening stresses start near the minimum stress in the spectrum and rise as the crack grows. Crack-opening stresses tended to level off for  $N/N_f$  between 0.7 and 0.9. The rapid jump in  $S'_a/S_{\text{max}}$  for an  $N/N_f$  ratio of about 0.92 was caused by the change in constraint from 1.8 to 1.2 at the higher crack-growth rates. The surface crack became a through crack ( $a/t = 1$ ) at an  $N/N_f$  ratio of about 0.9.

## 3. LARGE-CRACK GROWTH BEHAVIOR

To make life predictions,  $\Delta K_{\text{eff}}$  as a function of the crack-growth rate must be obtained for the material

of interest. Fatigue crack-growth rate data should be obtained over the widest possible range in rates (from threshold to fracture), especially if spectrum load predictions are required. Data obtained on the crack configuration of interest would be helpful but it is not essential. The use of the nonlinear crack-tip parameters is only necessary if severe loading (such as low cycle fatigue conditions) are of interest. Most damage-tolerant life calculations can be performed using the linear elastic stress-intensity factor analysis with crack-closure modifications.

### 3.1 Constant-Amplitude Loading

Under constant-amplitude loading, the only unknown in the analysis is the constraint factor,  $\alpha$ . The constraint factor is determined by finding (by trial-and-error) an  $\alpha$  value that will correlate the constant-amplitude fatigue-crack-growth-rate data over a wide range in stress ratios, as shown in References 30 and 38. This correlation should produce a unique relationship between  $\Delta K_{\text{eff}}$  and crack-growth rate. In the large-crack-growth threshold regime for some materials, the plasticity-induced closure model may not be able to collapse the threshold ( $\Delta K$ -rate) data onto a unique  $\Delta K_{\text{eff}}$ -rate relation because of other forms of closure. Roughness- and oxide-induced closure (see Ref 40) appear to be more relevant in the threshold regime than plasticity-induced closure. This may help explain why the constraint factors needed to correlate crack-growth rate data in the near threshold regime, that is, plane-strain conditions, are 1.7 to 1.9 for aluminum alloys, 1.8 to 2 for titanium alloys and 2.5 for steel. However, further study is needed to assess the interactions between plasticity-, roughness- and oxide-induced closure in this regime. If the plasticity-induced closure model is not able to give a unique  $\Delta K_{\text{eff}}$ -rate relation in the threshold regime, then high stress ratio ( $R \geq 0.7$ ) data may be used to establish the  $\Delta K_{\text{eff}}$ -rate relation.

In the following, the  $\Delta K_{\text{eff}}$ -rate relations for one aluminum alloy and two titanium alloys will be presented and discussed. Similar procedures were used to establish the relationships for all materials used in this study. The large-crack results for 7075-T6 aluminum alloy are shown in Figure 7 for data generated at two different laboratories and at three stress ratios (Ref 20). The data collapsed into a narrow band with several transitions in slope occurring at about the same rate for all stress ratios. Some differences were observed in the threshold regime. For these calculations, a constraint factor  $\alpha$  of 1.8 (nearly equivalent to Irwin's plane-strain condition) was used for rates less than  $7\text{E-}04$  mm/cycle (start of transition from flat-to-slant crack growth) and  $\alpha$  equal to 1.2 was used for rates greater than  $7\text{E-}03$  mm/cycle (end of transition from flat-to-slant crack growth). For intermediate rates,  $\alpha$  was varied linearly with the logarithm of crack-growth rate. The values of  $\alpha$  were selected by trial-and-error. The solid symbols (see upper left-hand portion of figure) denote measured rates at the end of transition from flat-to-slant crack growth (Refs 20 and 41). It has been proposed in Reference 31 that the flat-to-slant crack-growth transition region may be used to

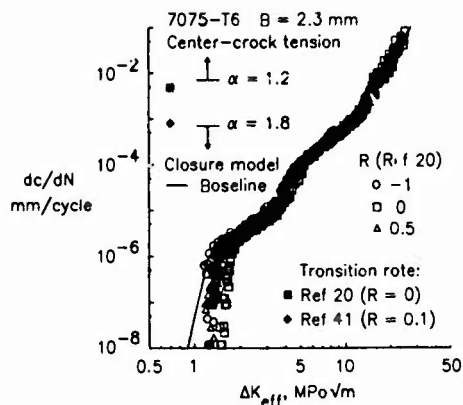


Fig. 7 Effective stress-intensity factor range against rate for large cracks in an aluminum alloy.

indicate a change from nearly plane-strain to plane-stress behavior and, consequently, a change in constraint. In the low crack-growth rate regime, near and at threshold, some tests (Ref 14) and analyses (Ref 15) have indicated that the threshold develops because of a rise in the crack-opening-stress-to-maximum-stress ratio due to the load-shedding procedure. In the threshold regime then, the actual  $\Delta K_{eff}$ -rate data would lie at lower values of  $\Delta K_{eff}$  because the rise in crack-opening stress was not accounted for in the current analysis. For the present study, an estimate was made for this behavior and it is shown by the solid line below rates of about  $2E-6$  mm/cycle. The baseline relation shown by the solid line will be used later to predict small-crack growth rates and fatigue lives under constant-amplitude loading.

Figure 8 shows the  $\Delta K_{eff}$ -rate data for corner cracks in 10 mm-thick Ti-6Al-4V titanium alloy (Ref 23). In these tests, the initial defect size was a 250  $\mu$ m-quarter-circular electrical-discharged machined notch. The data correlated quite well with a constant constraint factor of 1.9. For thick

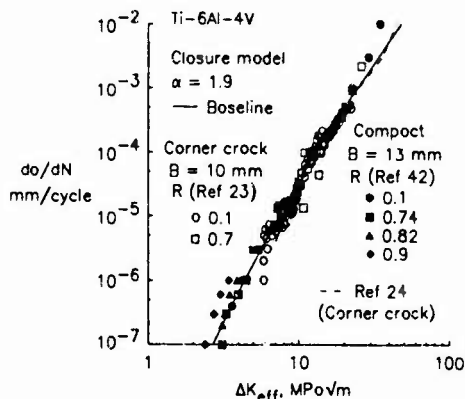


Fig. 8 Effective stress-intensity factor range against rate for small and large cracks in a titanium alloy.

materials, the loss of constraint, as shown for the thin 7075-T6 alloy (Fig 7), may occur at higher values of  $\Delta K_{eff}$  than those shown for the thinner material. Consequently, a constant constraint factor was used over the whole rate range. The solid symbols show the results of 13 mm-thick compact specimens (Ref 42) tested over a wide range of R ratios and down to much lower rates than the corner-crack tests. The baseline relation (solid line), fit to the corner-crack results in the mid-region and the compact results in the low-rate regime, will be used later to predict crack-growth rates for tests with spike overloads repeated every 1000 cycles.

The  $\Delta K_{eff}$ -rate results for IMI-685 titanium alloy compact specimens (Refs 23 and 25) are shown in Figure 9. This material was selected because "roughness-induced" closure was expected to be prevalent. These data also illustrate two difficulties with correlating test data using the linear-elastic effective stress-intensity factor ranges and the plasticity-induced closure model. First, the high R ratio results tend to deviate from the low R ratio results near the end of the tests. These specimens were cycled to failure and the last few data points were taken immediately before the specimen failed. The maximum stress level for the high R ratio test was considerably higher than that used for the low R ratio test; and plasticity effects would have been greater in the high R test than the low R, resulting in higher rates for a given value of elastic  $\Delta K_{eff}$ . However, fitting the  $\Delta K_{eff}$  relation to the low R ratio results (solid line) will allow accurate life prediction for both the low and high R ratio conditions, because the high R ratio tests are predicted to fail at a  $\Delta K_{eff}$  value of 23 MPa√m (fracture toughness  $K_C = 80$  MPa√m). Thus, accurately modelling the upper tail of the high R ratio test would not have greatly affected the number of cycles to failure. The second difficulty with the model occurs in the threshold regime and shows that threshold data (load-reduction tests) begin to form bands of data as a function of R, especially for materials where roughness-induced closure may occur. The steady-state crack-opening stress equations do not account for any

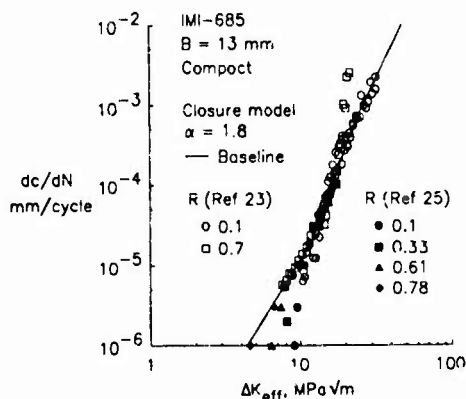


Fig. 9 Effective stress-intensity factor range against rate for large cracks in IMI-685 titanium alloy.

load-reduction effects nor roughness-induced closure which is expected to be dominant in the IMI-685 alloy. Because cracks in the high R ratio tests are expected to be fully open, these results were used to determine the  $\Delta K_{eff}$  relation at the low rates. The baseline relation will be used later to make crack growth predictions under repeated spike overloads.

### 3.2 Spike Overload and Underload

For variable-amplitude or spectrum load crack-growth predictions, the constraint factor should also be verified by some simple tests, such as crack growth after a single-spike overload. Constraint factors appear to be more sensitive to crack-growth delays caused by single-spike overloads than to crack growth under constant-amplitude loading at different stress ratios. Higher values of  $\alpha$  will cause less load-interaction effects, such as retardation or acceleration, than lower values of constraint. Thus, spike-overload tests may be more useful in establishing values of  $\alpha$  than constant-amplitude tests. However, the constraint factors determined by spike-overload tests should also correlate constant-amplitude data (see Ref 43).

A comparison of measured and predicted rates for large cracks after a single spike overload and after a single spike overload followed by an underload are shown in Figure 10. Cracks were grown under constant-amplitude loading ( $R = 0.4$  with  $K_{max} = 19.7 \text{ MPa}\sqrt{\text{m}}$ ) to a crack length of 12 mm. In one case, a single overload,  $K_{OL} = 31.4 \text{ MPa}\sqrt{\text{m}}$ , was applied and then the test was returned to constant-amplitude loading. The second case was identical to the first case, except that an underload  $K_{UL} = -3.9 \text{ MPa}\sqrt{\text{m}}$  was applied immediately after the overload. Two methods were used to measure crack length and rates in the 7475 alloy (Ref 22): the direct-current potential method (solid symbols) and the scanning-electron microscope (open symbols). The predicted results using the closure model with  $\alpha = 1.9$  (curves) agreed well with the test results, especially for the overload-underload case. For the overload case, the experimental rates did not appear to stabilize at the pre-overload rates as quickly as the predictions. These results indicate that the

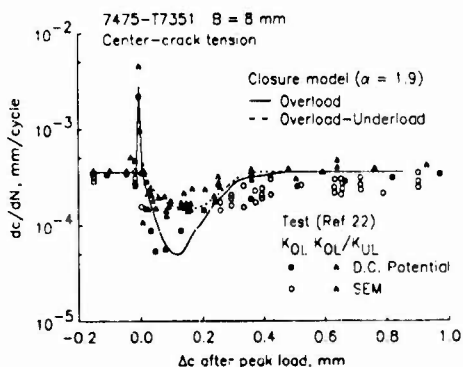


Fig. 10 Measured and predicted rates after an overload and overload-underload sequence.

constraint factor of 1.9 is appropriate for these conditions. But overloads at higher  $K_{OL}$  values would be expected to cause some loss of constraint (lower  $\alpha$ ). Under these conditions, the analyses using an  $\alpha = 1.9$  would be expected to predict higher rates and less retardation than the tests. Thus, variable constraint may be needed to predict the behavior.

### 3.3 Repeated Spike Overloads

Figures 11 and 12 show measured and predicted  $\Delta K$ -rate results for repeated spike overloads applied to compact and corner-crack specimens made of IMI-685 and Ti-17 titanium alloys, respectively. These tests were conducted under constant-amplitude loading ( $R = 0.1$ ) with an overload ( $P_{OL} = 1.7 P_{max}$ ) applied every 1,000 cycles (Refs 23 and 24). The overall trends in the predicted results for the IMI-685 corner-crack configuration agreed well with the test results at low rates. However, the predicted rates tended to be somewhat high in the middle and upper ranges. Although the predicted results for the compact specimen agreed fairly well with the test data, the test results on each individual specimen were

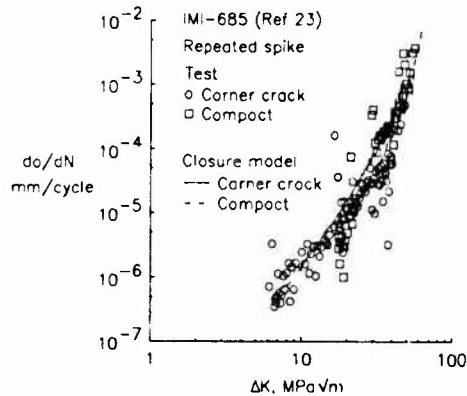


Fig. 11 Measured and predicted rates for IMI-685 titanium alloy under repeated spike overloads.

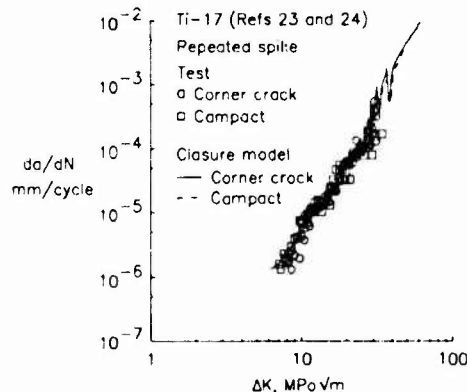


Fig. 12 Measured and predicted rates for Ti-17 titanium alloy under repeated spike overloads.

not modelled very accurately. The measured rates on one of the compact specimens in the beginning of the test were much lower than predicted. The oscillating behavior in the predicted results at high rates was caused by averaging rates over less than 1000 cycles, thus accelerations and retardations during and after the spike overload are being shown. The comparison of measured and predicted rates on the Ti-17 alloy agreed quite well (Fig 12). A comparison of predicted-to-test lives ( $N_p/N_t$ ) for these titanium alloys and Ti-6Al-4V, for the two crack configurations, ranged from 0.57 to 2.12 but most results were within about 20 percent of the test results. These results are presented and discussed in Reference 24.

### 3.4 Spectrum Loading

Wanhill (Ref 18) conducted spectrum crack-growth tests on center-crack tension specimens made of 2024-T3 Alclad material in two thicknesses ( $B = 1.6$  and  $3.1$  mm). Tests were conducted under the TWIST spectrum clipped at Levels I and III with  $S_{mf} = 70$  MPa. The initial crack starter notch half-length was  $3.5$  mm. Comparisons are made between experimental and calculated crack length against flights for Level III; and experimental and calculated crack length against crack-growth rate for Levels I and III.

Crack-length-against-flight data on the  $3.1$  mm-thick specimens tested under the TWIST (Level III) loading are shown in Figure 13. The solid curve is the calculated results from the closure model with the variable-constraint condition ( $\alpha = 2$  to 1) using the baseline  $\Delta K_{eff}$ -rate relation and constraint-loss regime established in Reference 44. To illustrate why the variable-constraint conditions are necessary, example calculations were made for constant constraint conditions of either  $\alpha = 1$  or  $2$  (dashed-dot curves). The model with a low constraint condition ( $\alpha = 1$ ) predicted much longer flights to a given crack length than the test data. Conversely, the predicted results for the higher constraint condition ( $\alpha = 2$ ) greatly under predicted the behavior except in the early stages of growth. Thus, the placement of the constraint-loss regime is crucial to making accurate crack-growth predictions under aircraft spectrum loading.

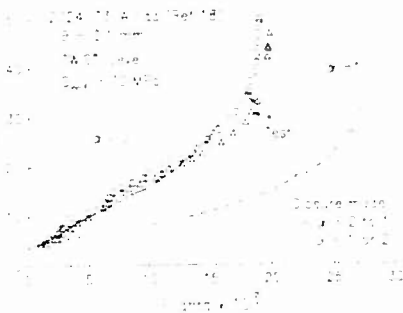


Fig 13 Measured and calculated crack-length-against-cycles under TWIST spectrum loading.

Figure 14 shows a comparison between experimental (Ref 18) and calculated results of crack length against  $dc/dF$  under the TWIST loading (Levels I and III) for the  $1.6$  mm-thick specimens. The crack-growth rate,  $dc/dF$ , is the change in crack length per flight. For both levels, the closure model was able to calculate the initial rates quite accurately (curves). Calculated results under Level III agreed with the test results over nearly the complete range of crack lengths. The calculated results under Level I, however, began to deviate from the test results after a crack length of about  $12$  mm. The ratio of calculated life to test life from an initial crack length of  $3.5$  mm to failure was  $0.61$  for Level I.

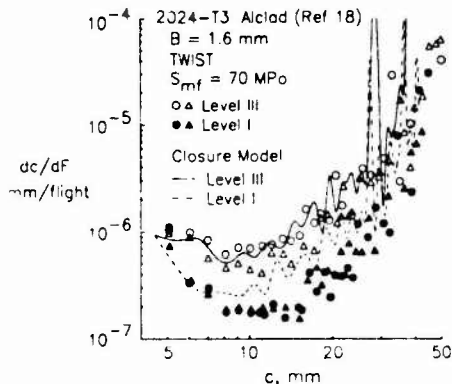


Fig. 14 Measured and calculated rates for large cracks under TWIST spectrum loading.

### 4. SMALL-CRACK GROWTH BEHAVIOR

In the following, comparisons are made between measured and predicted crack-shape changes and crack-growth rates for small surface cracks at a notch in 7075-T6 aluminum alloy under constant-amplitude loading. Comparisons are also presented on measured and predicted rates for small corner cracks at a notch in LC9cs clad aluminum alloy under both constant-amplitude and Mini-TWIST spectrum loading. The plastic-replica method was used to measure the initiation and growth of the small cracks and these results are presented and discussed in Reference 20.

Figure 15 shows the crack-depth-to-crack-length ( $a/c$ ) ratio plotted against the crack-depth-to-sheet-half-thickness ( $a/t$ ) ratio for the 7075-T6 alloy. Measured  $a/c$  and  $a/t$  ratios (open symbols) were determined from an experimental method where specimens were broken at various stages during their life. Results are shown for three stress ratios and for the Mini-TWIST spectrum loading. The spectrum has an overall stress ratio (minimum to maximum stress in the spectrum) of  $-0.23$ . The solid symbols show the sizes and shapes of inclusion-particle clusters or voids which initiated cracks (average size was  $a_1 = 3 \mu\text{m}$  and  $c_1 = 9 \mu\text{m}$ ).

The curves in Figure 15 show the predictions for the different stress ratios using the average inclusion-particle cluster size. In the analyses,

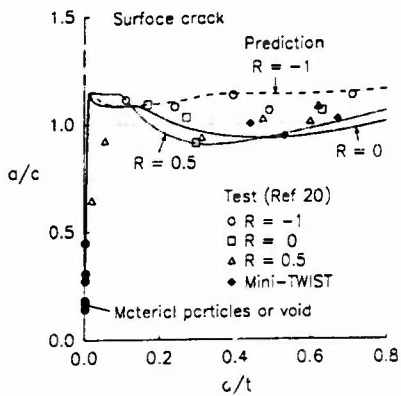


Fig. 15 Measured and predicted surface-crack shape changes in a bare aluminum alloy.

the crack-growth rate relations for  $da/dN$  was different than that for  $dc/dN$  as a function of  $\Delta K_{eff}$  (see Ref 20). The tests and analyses show that small surface cracks tend to rapidly approach an  $a/c$  ratio of about unity for a large part of their growth through the thickness.

Comparisons of experimental and predicted crack-growth rates for small cracks under  $R = -1$  loading are shown in Figures 16 and 17 for 7075-T6 and LC9cs alloys, respectively. For the 7075-T6 alloy, small surface cracks initiated along the notch surface from inclusion-particle clusters or voids. For the LC9cs alloy, small corner cracks initiated in the cladding layer from slip-band formation (cladding thickness was 50 to 70  $\mu\text{m}$ ). Even though the range in maximum stress levels used in each test series are indicated on the figures, no stress-level effect was apparent in the test data and all data have been grouped together. However, a range in stress levels was used in the analyses to show some expected trends with stress level. The dash-dot line shows the large crack ( $dc/dN$ ) results and the dashed line shows the  $\Delta K_{eff}$ -rate curve used in the analyses for  $da/dN$ . The solid curves show the predicted results using an initial defect size

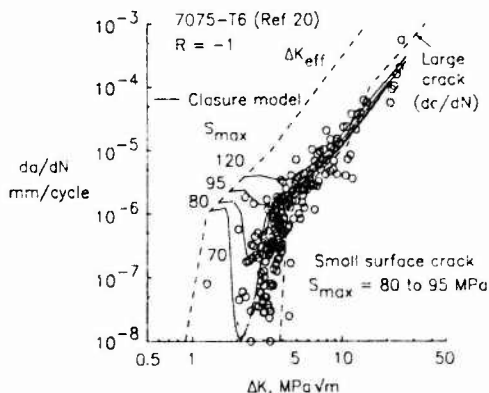


Fig. 16 Measured and predicted small surface crack-growth rates in a bare aluminum alloy.

(3 by 9 by 0.5  $\mu\text{m}$  for 7075-T6; and 77 by 77 by 0.5  $\mu\text{m}$  for LC9cs). All predictions start on the  $\Delta K_{eff}$  curve because cracks at small voids were assumed to be fully open on the first cycle and  $\Delta K$  is equal to  $\Delta K_{eff}$ . For the 7075-T6 alloy (Fig 16), the predictions from the model did not agree very well with the test data for  $S_{max} = 80$  to 95 MPa in the near threshold regime. In Reference 20, part of this discrepancy was attributed to an influence of the acetone used in taking plastic replicas of the notch surface. Fatigue lives for specimens with replicas were much longer (about a factor of 4) than those without replicas. However, the predictions did agree with the test data in the mid- and high-rate range. At 70 MPa, the predictions show that the crack would be nearly arrested (minimum rate) at a  $\Delta K$ -value of about 2  $\text{MPa}\sqrt{\text{m}}$ . At this point the  $\Delta K_{eff}$  was slightly greater than 0.9  $\text{MPa}\sqrt{\text{m}}$ , the effective threshold for small cracks. (Note that the endurance limit for  $R = -1$  was about 70 MPa, see Reference 20.)

For the LC9cs alloy (Fig 17), the predictions from the model agreed well with the test data for  $S_{max} = 70$  to 90 MPa in the early stages of crack growth. The predicted rates seem to be slightly low in the mid- to high-rate range. At 50 MPa, the predictions show a large drop in the crack-growth rates, similar to the 7075-T6 alloy. The crack would have been predicted to arrest if an applied stress of 40 MPa had been used. Again, the effective threshold for small cracks was assumed to be 0.9  $\text{MPa}\sqrt{\text{m}}$  and the endurance limit was about 40 MPa.

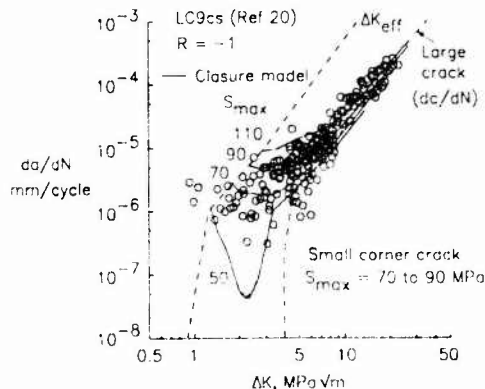


Fig. 17 Measured and predicted small corner crack-growth rates in a clad aluminum alloy.

The measured and predicted small-crack growth rates for the Mini-TWIST loading are shown in Figures 18 for the LC9cs alloy. Here the "average" crack-growth rate is plotted against the "maximum range" stress-intensity factor. The average crack-growth rate is the change in crack length per replica interval (about 30,000 cycles) and the stress-intensity factor range is computed using the maximum and minimum stress levels in the Mini-TWIST spectrum. The predicted values were determined in the following way. Crack length (2a) and cycle results were taken from the analysis at nearly equal cyclic intervals between the initial

crack length and breakthrough ( $a = t$ ). From these values of crack length and cycles, the average rate and maximum range stress-intensity factor were calculated. The predicted rates (solid curve) agreed well with the experimental data for both small- and large- crack behavior.

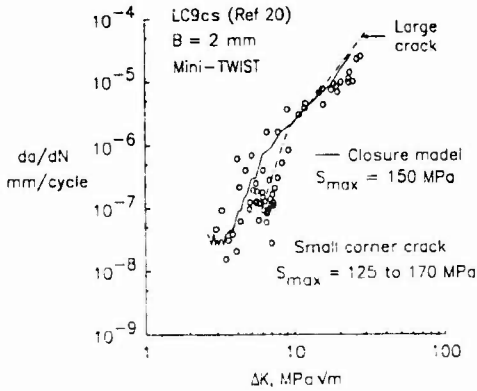


Fig. 18 Small corner crack-growth rates in a clad aluminum alloy under spectrum loading.

5. FATIGUE-LIFE PREDICTIONS

At this point, all of the elements are in place to assess a total fatigue- life prediction methodology based solely on crack propagation from microstructural features. In this approach, a crack is assumed to initiate and grow from a microstructural feature on the first cycle. The crack- closure model and the baseline  $\Delta K_{eff}$ -rate curves are used to predict crack growth from the initial crack size to failure. Comparisons are made with fatigue tests conducted on the single- or double-edge-notch tension specimens. Results are presented for three aluminum alloys and one titanium alloy under either constant-amplitude or various spectrum loadings.

5.1 Constant-Amplitude Loading

Fatigue life (S-N) data for 7075-T6 aluminum alloy are shown in Figure 19 for constant-amplitude loading. A symbol indicates a failure and a symbol with an arrow indicates that a test was terminated before failure. In the analysis, the initial

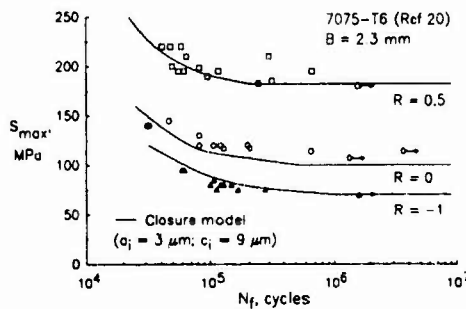


Fig. 19 Measured and predicted fatigue lives for aluminum alloy SENT specimens.

crack size was  $a_i = 3 \mu m$ ,  $c_i = 9 \mu m$  and  $b = 0.5 \mu m$  (defect or void half-height). This crack size is the average inclusion- particle or void size that was measured at actual crack-initiation sites. The effective stress-intensity factor range against rate relation used in the analysis is given in Reference 20 and  $(\Delta K_{eff})_{th}$  was assumed to be  $0.9 MPa\sqrt{m}$ . Using the life-prediction code (Ref 39), predictions were made for constant-amplitude loading. The solid curves show the predicted number of cycles to failure. The predicted lives were in reasonable agreement with the test lives. In addition to predicting fatigue life, the analysis methodology was also able to fit the endurance limit as a function of stress ratio.

Fatigue tests were conducted on Ti-6Al-4V titanium alloy double edge notch tension (DENT) specimens in the AGARD Engine Disc Cooperative Test Programme (Ref 24). These results (symbols) are shown in Figure 20 for two fan disc forgings. To make fatigue life calculations, the baseline  $\Delta K_{eff}$ -rate relation, shown in Figure 8, was used to calculate the life of the titanium specimens. Because no information on crack-initiation behavior was given in Reference 24, life calculations were made on initial crack sizes that would bound the experimental data, like the equivalent-initial-flaw size (EIFS) concept (Ref 45). The solid curves show the calculations for an initial semi-circular surface crack of  $a_i = 5$  and  $25 \mu m$  at the notch root. The solid symbol on the stress axis denotes where the net-section stress is equal to the ultimate tensile strength. Because of the notch configuration, notch strengthening is expected and the upper plateau is an estimate for the maximum net-section stress based on the results from the finite-element analyses (see Fig 4 at the high K levels). In a microstructural analysis, Wanhill and Looije (Ref 46) found that the primary  $\alpha$ -grains were about  $10 \mu m$  in diameter and the transformed and aged  $\beta$ -grains were about  $20 \mu m$  in diameter for these fan disc materials. Further study is needed on these materials to see if cracks of these sizes would be present early in life or to see if the baseline curve (Fig 8) is appropriate for small cracks. For low  $\Delta K_{eff}$  values, small cracks in the titanium alloys may grow faster than large cracks, as observed by Lanciotti and Galatolo (Ref 47).

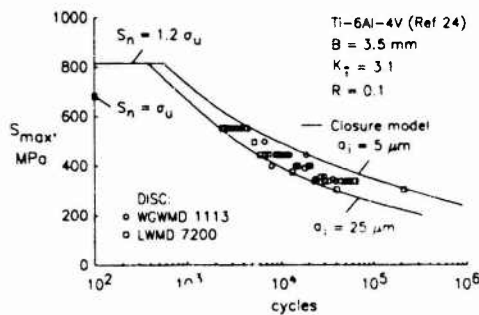


Fig. 20 Measured and predicted fatigue lives for titanium alloy DENT specimens.

## 5.2 Spectrum Loading

Experimental and predicted results for fatigue tests conducted on 7075-T6 bare and LC9cs clad alloy specimens under the Mini-TWIST spectrum are shown in Figure 21. These tests were conducted on SENT specimens (Ref 20). The solid and dashed curves show predictions for each alloy using the initial defect sizes shown. The defect size for 7075-T6 was the average inclusion-particle size that initiated cracks, whereas the initial crack size for the clad alloy LC9cs was somewhat larger than the cladding-layer thickness (50 to 70  $\mu\text{m}$ ). The predicted lives were in reasonable agreement with the test results (symbols) but the predicted lives tended to fall on the lower bound of the test data.

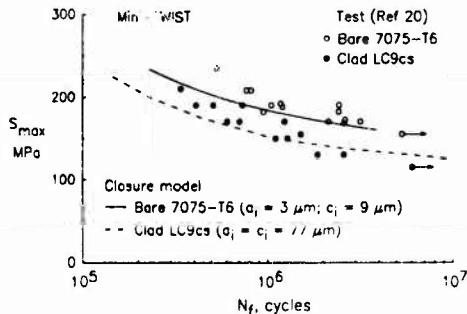


Fig. 21 Measured and predicted fatigue lives for SENT specimens under spectrum loading.

Comparisons of experimental and predicted fatigue lives of notched 2024-T3 aluminum alloy sheet specimens under FALSTAFF, Gaussian and TWIST load sequences are shown in Figure 22. These tests were conducted on SENT specimens (Refs 7 and 19) but they were cycled until a crack had grown across the full sheet thickness instead of failure. The predictions were made using an initial crack size that was the average inclusion-particle size that initiated cracks. The predicted lives agreed well with the test data.

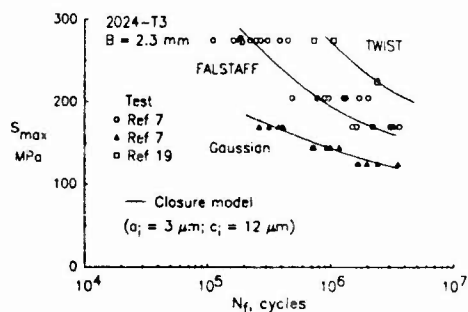


Fig. 22 Measured and predicted fatigue lives to breakthrough for SENT specimens.

## 6. CONCLUDING REMARKS

The "plasticity-induced" crack-closure model was used to correlate large-crack data on several aluminum and titanium alloys under constant-amplitude loading. A constraint factor, which accounts for three-dimensional state-of-stress effects, was used in determining the effective stress-intensity factor range against rate relations. These relations were then used to predict large-crack growth under variable-amplitude and spectrum loading. Comparisons made between measured and predicted small-crack growth rates in two aluminum alloys showed that the closure model could predict the trends that were observed in the tests. Using the closure model and some microstructural features, such as inclusion-particle sizes and cladding-layer thickness, a total fatigue-life prediction method was demonstrated. Fatigue life of notched specimens made of three aluminum alloys were compared with predicted lives under either constant-amplitude or spectrum loading. The predicted results were well within a factor of two of the test data. Fatigue lives for Ti-6Al-4V titanium alloy could also be bounded by using initial crack sizes of 5 and 25  $\mu\text{m}$  in the life-prediction method.

Further study is needed to determine constraint variations along fatigue crack fronts in various materials and thicknesses. These constraint variations are needed to improve life predictions under aircraft spectrum loading, especially for thin-sheet materials. At low rates, the development of the large-crack threshold and its significance for design life calculations also needs further study.

## 7. REFERENCES

- Gallagher, J. P.; Giessler, F. J.; Berens, A. P. and Engle, R. M., Jr., "USAF Damage Tolerant Design Handbook. Guidelines for the Analysis and Design of Damage Tolerant Aircraft Structures", AFWAL-TR-82-3073, May 1984.
- Manning, S. D. and Yang, J. N., "USAF Durability Design Handbook: Guidelines for the Analysis and Design Aircraft Structures", AFWAL TR-83- 3027, January 1984.
- Small Fatigue Cracks, R. O. Ritchie and J. Lankford, eds., The Metallurgical Society, Inc., Warrendale, PA, 1986.
- The Behaviour of Short Fatigue Cracks, K. J. Miller and E. R. de los Rios, eds., European Group on Fracture, Publication No. 1, 1985.
- Rao, K. T. V. and Ritchie, R. O., "Fatigue of Aluminum-Lithium Alloys, Lawrence Berkeley Laboratory", LBL-30176, January 1991.
- Behaviour of Short Cracks in Airframe Components, H. Zocher, ed., AGARD CP-328, 1983.
- Newman, J. C. Jr and Edwards, P. R., "Short-Crack Growth Behaviour in an Aluminum Alloy - an AGARD Cooperative Test Programme", AGARD R-732, 1988.

8. Short-Crack Growth Behavior in Various Aircraft Materials, P. R. Edwards and J. C. Newman, Jr., eds., AGARD Report No. 767, 1990.
9. El Haddad, M. H.; Dowling, N. E.; Topper, T. H. and Smith, K. N., "J Integral Application for Short Fatigue Cracks at Notches", *International Journal of Fracture*, Vol. 16, No. 1, 1980, pp. 15-30.
10. Newman, J. C., Jr., "Fracture Mechanics Parameters for Small Fatigue Cracks", Small Crack Test Methods, ASTM STP 1149, J. Allison and J. Larsen, eds., 1992, pp. 6-28.
11. Leis, B. N.; Kanninen, M. F.; Hopper, A. T.; Ahmad, J. and Broek, D., "Critical Review of the Short Crack Problem in Fatigue", *Engineering Fracture Mechanics*, Vol. 23, 1986, pp. 883-898.
12. Elber, W., "The Significance of Fatigue Crack Closure", Damage Tolerance in Aircraft Structures, ASTM STP 486, 1971, pp. 230-242.
13. Nisitani, H. and Takao, K. I., "Significance of Initiation, Propagation and Closure of Microcracks in High Cycle Fatigue of Ductile Materials", *Engineering Fracture Mechanics*, Vol. 15, No. 3-4, 1981, pp. 455-456.
14. Minakawa, K. and McEvily, A. J., "On Near-Threshold Fatigue Crack Growth in Steels and Aluminum Alloys", *Proceedings of the International Conference on Fatigue Thresholds*, Vol. 2, 1981, pp. 373-390.
15. Newman, J. C., Jr., "A Nonlinear Fracture Mechanics Approach to the Growth of Small Cracks", Behaviour of Short Cracks in Airframe Components, AGARD CP-328, 1983, pp. 6.1-6.26.
16. Newman, J. C., Jr., "A Crack-Closure Model for Predicting Fatigue Crack Growth under Aircraft Spectrum Loading", Methods and Models for Predicting Fatigue Crack Growth under Random Loading, J. B. Chang and C. M. Hudson, eds., ASTM STP 748, 1981, pp. 53-84.
17. Newman, J. C., Jr., Poe, C. C., Jr. and Dawicke, D. S., "Proof Test and Fatigue Crack Growth Modeling on 2024-T3 Aluminum Alloy", *Fourth International Conference on Fatigue and Fatigue Thresholds*, 1990, pp. 2407-2416.
18. Wanhill, R. J. H., "Flight Simulation Fatigue Crack Propagation Evaluation of Candidate Lower Wing Skin Materials with Particular Consideration of Spectrum Truncation", NLR TR 77092 U, July 1977.
19. Blom, A. F., "Short Crack Growth under Realistic Flight Loading: Model Predictions and Experimental Results for AL 2024 and AL-LI 2090", Short-Crack Growth Behavior in Various Aircraft Materials, P. R. Edwards and J. C. Newman, Jr., eds., AGARD Report No. 767, 1990, pp. 6.1-6.15.
20. Newman, J. C., Jr.; Wu, X. R.; Swain, M. H.; Zhao, W.; Phillips, E. P. and Ding, C. F., "Small-Crack Growth Behavior in High-Strength Aluminum Alloys - A NASA/CAE Cooperative Program", 18th Congress International Council of the Aeronautical Sciences, Sept. 20-25, 1992.
21. Zhang, S.; Marissen, R.; Schulte, K.; Trautmann, K.-H.; Nowak, H. and Schijve, J., "Crack Propagation Studies on Al 7475 on the Basis of Constant Amplitude and Selective Variable Amplitude Loading Histories", *Fatigue and Fracture of Engineering Materials and Structures*, Vol. 10, 1987, pp. 315-332.
22. Zhang, S.; Doker, H.; Nowak, H.; Schulte, K. and Trautmann, K. H., "Improvements of Crack Propagation Analysis by More Exact Determination of K<sub>th</sub>-Levels", *Second Symposium on Fatigue Lifetime Predictive Techniques*, ASTM, Pittsburgh, PA., 1992.
23. Raizenne, M. D., "AGARD SMP Subcommittee 33 Engine Disc Test Programme Fatigue Crack Growth Rate Data and Modeling Cases for Ti-6Al-4V, IMI-685 and Ti-17", LTR-ST-1785, National Research Council Canada, Nov. 1990.
24. AGARD Engine Disc Cooperative Test Programme, Mom. A. J. A. and Raizenne, M. D., eds., AGARD Report No. 766, 1988; Pardessus, T., Jany, E. and Raizenne, M. D., eds., AGARD Report No. 766 (Addendum), 1993.
25. Hicks, M. A.; Jeal, R. H. and Beevers, C. J., "Slow Fatigue Crack Growth and Threshold Behaviour in IMI 685", *Fatigue and Fracture of Engineering Materials and Structures*, Vol. 6, No. 1, 1983, pp. 51-65.
26. deJonge, J. B.; Schutz, D.; Lowak, H. and Schijve, J., "A Standardized Load Sequence for Flight Simulation Tests on Transport Aircraft Wing Structures (TWIST)", NLR TR-73029 U, Nationaal Lucht-en Ruimtevaartlaborium, 1973.
27. Lowak, H.; deJonge, J. B.; Franz, J. and Schutz, D., "Mini-TWIST--A Shortened Version of TWIST", LBF Report No. TB-146, Laboratorium für Betriebsfestigkeit, 1979.
28. van Dijk, G. M. and deJonge, J. B., "Introduction to a Fighter Loading Standard for Fatigue Evaluation--FALSTAFF", NLR MP 75017 U, Nationaal Lucht-en Ruimtevaartlaborium, May 1975.
29. Huck, M.; Schutz, W.; Fischer, R. and Kobler, H. G., "A Standard Random Load Sequence of Gaussian Type Recommended for General Application in Fatigue Testing", IABG Report No. TF-570 or LBF Report No. 2909, 1976.

30. Newman, J. C., Jr., "Prediction of Fatigue-Crack Growth under Variable- Amplitude and Spectrum Loading using a Closure Model", Design of Fatigue and Fracture Resistant Structures, P. R. Abelkis and C. M. Hudson, eds., ASTM STP 761, 1982, pp. 255-277.
31. Newman, J. C.; Swain, M. H. and Phillips, E. P., "An Assessment of the Small-Crack Effect for 2024-T3", Small Fatigue Cracks, Ritchie, R.O. and Lankford, J., eds., 1986, pp.427-452.
32. Dugdale, D. S., "Yielding of Steel Sheets Containing Slits, Journal of Mechanics and Physics of Solids", Vol. 8, Vol. 2, 1960, pp. 100-104.
33. Blom, A. F., Wang, G. S. and Chermahini, R. G., "Comparison of Crack Closure Results Obtained by 3-D Elastic-Plastic FEM and Modified Dugdale Model", Proceedings 1st International Conference on Computer Aided Assessment and Control of Localized Damage, Portsmouth, England, June 26-28, 1990, pp. 57-68.
34. Schijve, J., "Significance of Fatigue Cracks in Micro-Range and Macro- Range", Fatigue Crack Propagation, ASTM STP 415, 1967, pp. 415-459.
35. Schijve, J., "Shear Lips on Fatigue Fractures in Aluminum Alloy Sheet Material," Delft University of Technology, Report LR-287, Sept. 1979.
36. Newman, J. C., Jr., Bigelow, C. A. and Shivakumar, K. N., "Three- Dimensional Elastic-Plastic Finite-Element Analyses of Constraint Variations in Cracked Bodies", Engineering Fracture Mechanics, Vol. 46, No. 1, 1993, pp. 1-13.
37. Shivakumar, K. N. and Newman, J. C., Jr., "ZIP3D - An Elastic and Elastic-Plastic Finite-Element Analysis Program for Cracked Bodies", NASA TM 102753, Nov. 1990.
38. Newman, J. C., Jr., "A Crack-Opening Stress Equation for Fatigue Crack Growth", International Journal of Fracture, Vol. 24, 1984, R131-R135.
39. Newman, J. C., Jr., "FASTRAN II - A Fatigue Crack Growth Structural Analysis Program", NASA TM 104159, February 1992.
40. Ritchie, R. O. and Yu, W., "Short Crack Effects in Fatigue: A Consequence of Crack Tip Shielding", Small Fatigue Cracks, R. O. Ritchie and J. Lankford, eds., 1986, pp. 167-189.
41. Vogelesang, L. B., The Effect of Environment on the Transition from Tensile Mode to Shear Mode during Fatigue Crack Growth in Aluminum Alloys, Delft Report LR-286, Delft University of Technology, 1979.
42. Powell, B. E. and Henderson, I., "The Conjoint Action of High and Low Cycle Fatigue", AFWAL-TR-83-4119, Nov. 1983.
43. Newman, J. C., Jr. and Dawicke, D. S., "Prediction of Fatigue-Crack Growth in High-Strength Aluminum Alloy under Variable-Amplitude Loading", Advances in Fracture Research, K. Salama, K. Ravi-Chandar, D. M. R. Taplin and P. R. Rao, eds., Vol. 2, 1989, pp. 945-952.
44. Newman, J. C., Jr., "Effects of Constraint on Crack Growth under Aircraft Spectrum Loading", Fatigue of Aircraft Materials, A. Beukers, Th. de Jong, J. Sinke, A. Vlot and L. B. Vogelesang, eds., Delft University Press, 1992, pp. 83-109.
45. Rudd, J. L., Yang, J. N., Manning, S. D. and Garver, W. R., "Durability Design Requirements and Analysis for Metallic Airframes", Design of Fatigue and Fracture Resistant Structures, ASTM STP 761, P. R. Abelkis and C. M. Hudson, eds., 1982, pp. 133-151.
46. Wanhill, R. J. H. and Looije, C. E. W., "Fractographic and Microstructural Analysis of Fatigue Crack Growth in Ti-6Al-4V Fan Disc Forgings", AGARD Engine Disc Cooperative Test Programme, AGARD Report 766 (addendum), 1993.
47. Lanciotti, A. and Galatolo, R., "Short Crack Observations in Ti-6Al-4V under Constant-Amplitude Loading", Short-Crack Growth Behaviour in Various Aircraft Materials, P. R. Edwards and J. C. Newman, Jr., eds., AGARD R-767, 1990, pp. 10.1-10.7.

## Crack Growth Predictions Using a Crack Closure Model

R.L. Hewitt and P.G. Collins  
Structures and Materials Laboratory  
Institute for Aerospace Research  
National Research Council of Canada  
Montreal Road, Ottawa, Ontario, K1A 0R6

### 1. SUMMARY

Crack growth predictions for through and corner cracks in 7075 1651 plate under constant amplitude loading and corner cracks under two variable amplitude spectra were made using a 'black box' crack closure program. The results were then compared with experiment and various parameters adjusted to give the best match to the experimental results. The optimum parameters chosen will be used for subsequent blind predictions to be made on this material and different but related spectra.

### 2. INTRODUCTION

Use of crack growth prediction programs is no longer restricted to the developers of such programs and those that have many years of experience using them. They are frequently used as 'black boxes' by engineers whose experience may be limited to a university course on the subject. It was therefore considered useful to take a 'black box' program and determine how well a relatively inexperienced user might be able to predict experimental results.

This was done as part of the Canadian contribution to the follow on FICP/HIP 8 Structures and Dynamics Panel Collaborative Program 8.2, Validation of Fracture Mechanics Models for Application in a Damage Tolerance Assessment.

#### 2.1 Background to the Program

At the September 1983 meeting of the HIP 3 subgroup of The Technical Cooperation Program (TICP), it was suggested that a worthwhile collaborative exercise might evolve from application of various crack propagation models to a material with a well defined set of constant amplitude data having equivalent data under variable amplitude loading. Accordingly, the United Kingdom provided constant amplitude crack growth data for several different materials and the results of crack growth tests under two variable amplitude spectra, FWS1 (1) and FWS1 A11 (2). Seven participants then produced crack growth predictions by a method of their choice without reference to the variable amplitude loading results. These predictions were reported in Reference 3 and showed that the ratio of predicted to measured lives ranged from about 0.1 to 25.

An analysis of these results (4) concluded that analyses which are not supported by experimental calibrations may lead to serious errors and listed a large number of factors which had a major influence on the accuracy. These ranged from the level of experience of the analyst to the retardation model and choice of parameter values. The report recommended a new program which would consist of both experimental and analytical phases, where the analytical techniques could first be calibrated by comparison with test results and then used to predict additional test results in the second phase without knowledge of these results. These test results would be for different stress levels and spectra typical of in fleet variations.

Under the FICP/HIP 8 Structures and Dynamics Panel CP 8.2 (Validation of Fracture Mechanics Models for Application in a Damage Tolerance Assessment) the United States Air Force agreed to supply crack growth data and the results of constant amplitude and spectrum loading tests for the first phase, with additional results for related spectra being retained for the second phase. Participants in the member countries were requested to provide the results from the first phase predictions prior to proceeding to the second phase. This report details the Canadian results for the first phase.

#### 2.2 Supplied Data

The material data supplied for this program was in the form of  $da/dN$  versus  $\Delta K$  data originating from tests at stress ratios (R values) of 0.5, 0.1, 0.1, and 0.5, for 7075 1651 aluminum. The tests were conducted on both compact tension and centre cracked tension specimens for positive values of R, and on centre cracked tension specimens for negative values of R. The data was supplied on an IBM compatible floppy disk. Also supplied were two variable amplitude spectra, corresponding to stress spectra for a typical fighter and a typical transport aircraft lower wing skin loadings.

#### 2.3 Predictions Required

Three distinct series of predictions were required, with stress and geometry variations within each series. Series 1 predictions were for constant amplitude loading of a panel with a through crack at a hole. The initial crack dimension, the through stress on the panel and the stress ratio varied, with 11 test configurations in total. For this series, the predicted life and the crack length at failure were requested.

The second series of predictions were for constant amplitude loading of a panel with a corner crack in a hole. The initial crack dimensions, the through stress and the stress ratio varied, with 7 configurations in total. For this series the predicted life, the crack length at failure, the crack aspect ratio at three crack sizes and the crack length and number of cycles to transition (when the crack tip along the bore of the hole reaches the back surface of the plate) were required.

The third series of predictions were for the same geometry as the second series, but under variable amplitude loading. Two normalized spectra were supplied, denoted "fighter" and "transport" spectra. The spectra were also supplied in counted versions, although few details were given on the counting method other than it was a combination of rainflow and range pair counting. For this series, predictions were requested for times to failure and through the thickness penetration, the crack shape aspect ratio at thickness penetration and the critical crack size at failure. Three predictions were required for the fighter spectrum and five for the transport spectrum.

### 3. CRACK GROWTH PROGRAM

#### 3.1 Program

The program used for the predictions was a proprietary program supplied with a user's manual but little documentation of the program.

#### 3.2 Crack Growth Model

The crack growth model used in the program is based on the contact stress model of Dill and Saff (5,6). This is based on the evaluation of the stress intensity caused by crack surface contact and assumes that crack propagation is driven by an effective stress intensity range. An analysis of crack surface displacements during loading and unloading is used to determine the permanent plastic deformation left in the wake of a growing crack and the contact stresses caused by the interference of these deformations are calculated. The effective stress intensity range is then found by subtracting the stress intensity caused by the contact stresses from the applied stress intensity range (5). The model can account for retardation following one or multiple overloads and acceleration following underloads (6).

#### 3.3 Parameter $\alpha$

Although it was originally used to account for the state of stress (plane stress or plane strain or somewhere between), the parameter  $\alpha$  used in the model is described in the user's manual as 'a parameter used to determine the amount of crack retardation' and is used in practice to tune the model. The value of  $\alpha$  lies between -1 and +1, with a value of 0 generally used initially.

#### 3.4 Material Property Data

The program was supplied with material data files for several different materials but also allows the user to input additional material property data files. Since material property data had been supplied with the test data and input of material data often leads to problems of prediction accuracy, it was decided to use the supplied data in this exercise.

The program required crack growth data at a stress ratio of zero and the following material properties:

- Modulus of Elasticity
- Poisson's Ratio
- Cyclic Proportional Limit
- Cyclic 0.2% Offset Yield Stress
- Monotonic 0.2% Offset Yield Stress
- Ultimate Strength
- Ultimate Strain
- Critical Stress Intensity Factor

#### 3.5 Program Treatment of the da/dn File

For constant amplitude loading, the effective minimum stress intensity is primarily a function of stress ratio, R, and the parameter  $\alpha$ . The minimum effective stress intensity,  $K_{min\ eff}$ , at a positive value of R is calculated as

$$K_{min\ eff} = K_{max} * N_r * N_{\alpha} * N_{Yr} \quad (R > 0)$$

where  $N_r$  is a function of R,  $N_{Yr}$  is a function of the ratio of cyclic to monotonic yield stress,  $N_{\alpha}$  is a function of  $\alpha$  and  $K_{max}$  is the stress intensity based on the peak load. If R is

negative the formula becomes

$$K_{min\ eff} = K_{max} * (effkr * c * A * R + B * R) \quad (R < 0)$$

where

$$effkr = K_{max} * N_r * N_{\alpha} * N_{Yr}$$

at a value of R = 0, and A and B are constants.

The program calculates an equivalent da/dn vs  $AK_{eff}$  table from the input da/dn vs AK at R = 0 by adjusting the data using the factor effkr. The data is also adjusted by  $K_{c1}$ , the critical stress intensity and the logarithm of the data is taken to allow linear interpolation between data points. The corresponding equations have the form

$$da/dn_{tabular} = \log \{ da/dn_{R=0} * (K_c - AK) / K_{c1} \}$$

and

$$AK_{eff} = \log \{ AK * (1 - effkr) \}$$

#### 3.6 Stress Intensity Solutions

Stress intensity solutions for common geometries are built into the program and these were the stress intensity solutions used in this investigation.

#### 3.7 Spectrum Input

Loads are input to the program as a series of normalized maxima and minima and number of cycles of that particular pair of load levels. The user's manual indicates that all variable amplitude spectra should be converted to eliminate one effective large cycle being considered as a series of small cycles. It also recommends blocking the spectrum to reduce computation time.

### 4. PREDICTIONS FOR THROUGH CRACKS (CONSTANT AMPLITUDE)

#### 4.1 Selection of Material Property Data

##### 4.1.1 Characterization of Supplied Data

The supplied data consisted of da/dn vs AK data for test specimens at various values of R. These data were generated by the Wright Laboratory using centre cracked tension and compact tension test specimens machined from 7075 T651 aluminum. The data were plotted and 'best fit' curves were manually drawn to fit the data, producing three curves, one each for R = 0.5, R = 0.1, and R = 0. The data for R = 0.1 consisted of only two tests, both at low AK ranges; this data it was not utilized at this stage. The original data and resulting curves are illustrated in Figures 1 through 3.

##### 4.1.2 Conversion of Crack Growth Data

One requirement for the material data file required as input by the program is tabular da/dn versus AK data for a stress ratio of R = 0. This can be obtained from the supplied da/dn versus AK data at non zero values of R through manipulation of the equations presented in section 3.5. The 'best fit' lines to the supplied data were converted to R = 0 data using these equations for values of  $\alpha$  of 1, 0 and -1 respectively. A 'best fit' R = 0 curve was drawn through

each set of data manually. A value of 1 was assumed for the ratio of cyclic 0.2% offset yield stress to monotonic 0.2% offset yield stress since this value was not supplied and it had little effect on the position of the curves.

Since there was little difference in the spread of the data at different R ratios for the different values of  $\alpha$ , the 'best fit' line at  $\alpha = 0$ , as shown in Figure 4, was used in subsequent analyses.

#### 4.1.3 Comparison of Input Data with Raw Data

In order to see how well this R-0 curve fitted the raw data, it was transformed back to data vs AK and plotted over the raw data at R = 0.5, 0.1 and 0.5 as shown in Figures 5 to 7. The program data for 7075 T73 and T76 plate and T76 sheet are also shown for comparison.

One additional data point was added to the curve at the high growth rates because the program log linearly extrapolates higher growth rates from the last two points. These points were made to give a similar slope to the program data for the other 7075 aluminum. The selected curve fits the data at R = 0.1 quite well but overestimates the growth rates at high AK at R = 0.5 and underestimates the same range at R = 0.5. It appears that the threshold for the negative R values is also overestimated. The thresholds for the three 7075 files supplied with the program are all similar and show better agreement with the negative R data. The T73 and T76 sheet data also show better agreement with the data at the higher growth rates.

A comparison of the four crack growth curves at R = 0 is shown in Figure 8. The best fit line follows the T76 plate data at the higher growth rates and the T73 data at intermediate rates and shows a higher threshold. The program data for the 7075 T76 data sets also tend toward the critical stress intensity at a growth rate of  $10^{-2}$  inches per cycle. The best fit line, however, has a  $\Delta K$  of only about 40 ksi  $\sqrt{\text{in}}$  at a growth rate of  $10^{-2}$  inches per cycle compared to a critical value of 51.6 ksi  $\sqrt{\text{in}}$ .

#### 4.1.4 Additional Material Property Data

The program material files also contain eight material properties describing other physical properties of the material as defined in Section 4.4. The values for modulus of elasticity and Poisson's ratio were assumed to be the same as for the existing program material data files for 7075 aluminum, while the monotonic 0.2% offset yield strength and the critical stress intensity were taken as the values supplied with the HCP data. The cyclic proportional limit and the ultimate strength and strain are not used in the analysis for the particular geometry and conditions used for these predictions and nominal values were therefore used. Conflicting data was found on the ratio of cyclic to monotonic yield stress. The ratio was therefore assumed to be 1. The material property values were thus:

Modulus of Elasticity	10000 ksi
Poisson's Ratio	0.333
Cyclic Proportional Limit	60 ksi
Cyclic 0.2% Offset Yield Stress	79 ksi
Monotonic 0.2% Offset Yield Stress	79 ksi
Ultimate Strength	88 ksi
Ultimate Strain	0.02
Critical Stress Intensity Factor	51.6 ksi $\sqrt{\text{in}}$

## 4.2 Spectrum Preparation

The program considers the stress intensity to be constant during application of a block, based on the geometry at the start of the block. It is therefore important that the block length not be very long. The spectrum was therefore input as a block of 10 cycles with a maximum of 1 and a minimum equal to the R value for the required prediction. Since the program outputs hours rather than number of cycles, a block was defined as 1 hour. The number of cycles could then be obtained by multiplying the hours by 10.

## 4.3 Results

The number of cycles to failure and the final crack lengths predicted using the material data input of Figure 8 and a value of  $\alpha$  of 0 are shown in Figures 9 and 10 as three dimensional plots of the ratios of predicted to test lives and crack lengths respectively, while Figures 11 and 12 show similar results for values of  $\alpha$  of -1 and +1 respectively.

Comparison of Figures 9, 11 and 12 shows that using a value of  $\alpha$  of 0 produces slightly more consistent results over the range of R and stress level and Figure 10 shows that there is good correlation with final crack length for an  $\alpha$  of 0. However, it is apparent from Figure 9 that the lives are underestimated as the R ratio is reduced and the stress level is increased. This implies that the crack growth curve is overestimating the growth rates at the higher values of  $\Delta K$  and at the lower values of R. The curve therefore needs to be shifted at higher values of  $\Delta K$  toward the curves for the T76 sheet material supplied with the program.

To investigate the sensitivity to the growth rate curve, predictions were obtained for the three 7075 material data files in the program. The final crack length predictions were a function primarily of the critical stress intensity assumed, being much lower for the T76 plate which has a much lower critical stress intensity. This is shown in Figure 13 which shows the ratio of predicted to measured final crack lengths as a function of critical stress intensity factors of life prediction, both the T73 and T76 sheet data which show similar growth rates, particularly at higher values of  $\Delta K$ , gave very good predictions, while the T76 plate data, which gave a similar curve to the derived T76 sheet data, showed a similar stress dependence to the results obtained with the supplied material data and generally poor agreement with test.

The derived material curve for the T76 sheet material was therefore adjusted so that it followed the T76 sheet data at higher values of  $\Delta K$ , as shown in Figure 14 and the predictions were repeated for an  $\alpha$  of 0. The results are shown in Figure 15 for life and Figure 16 for crack length. Agreement is excellent over the whole range of R and stress, with a mean prediction ratio of 1.05 and a standard deviation of 0.14.

## 5. PREDICTIONS FOR SURFACE CRACKS (CONSTANT AMPLITUDE)

### 5.1 Input Data

The modified material data for the T76 material shown in Figure 14 was used as the material input and the spectrum was input as in Section 4.2. The parameter  $\alpha$  was set to 0.

The program option for an edge crack at the edge of a hole

was used but it should be noted that the program and TTCP nomenclature for the two crack directions (through the thickness and across the plate) are reversed. The TTCP nomenclature is used in this report.

## 5.2 Results

The results for the second series of predictions gave a mean predicted life to test life of 0.93 with a standard deviation of 0.20. The results for total life, life to penetration, final crack length and crack shape at various crack lengths are shown in Figures 17 to 20. Figures 17 and 18 show that the total lives and lives to penetration follow a very similar pattern, with less accurate predictions at a stress ratio of 0.5 and generally lower prediction ratios for the higher stress levels. The mean prediction ratios are higher for the life to penetration than for the total life.

The final crack lengths are predicted quite well as shown in Figure 19, although they are slightly overestimated. The crack aspect ratios are also quite reasonable, although always underestimating the test result. These results show no evidence of any systematic variation.

## 6. PREDICTIONS UNDER VARIABLE AMPLITUDE LOADING

### 6.1 Input Data

The modified material data for the 1651 material shown in Figure 14 was again used for the material input, the parameter  $\alpha$  was set to 0 and the program option for an edge crack at the edge of a hole was used. The spectra, as provided, were first checked to eliminate any non firing points (there were several in the transport spectrum) and then input as simple pairs of maxima and minima as they occurred. The number of repeats of each cycle was set at 1 unless consecutive cycles of the same levels occurred. The TTCP counted spectra were input in a similar manner although there were no non firing points in these spectra.

An additional spectrum was generated from both the lighter and transport spectrum using a range pair counting technique but retaining the order of the original peaks as described by Chang (7). These spectra are referred to as the IAR counted spectra.

### 6.2 Results

Figures 21 to 23 show the predicted to tested total lives using the uncounted, TTCP counted and IAR counted spectra respectively. All three show similar trends, with slightly higher prediction ratios at the lower stress levels, although the IAR counted transport spectrum gives lower predictions than the others. The uncounted spectra give a similar mean prediction ratio (0.93) to the TTCP counted spectra (0.94) with the lowest standard deviation (0.30).

Figure 24 shows that the final crack lengths are overestimated by an average of approximately 30%, even though the final crack lengths for similar constant amplitude tests were within 7% on average. Figure 25 shows the ratio of predicted to test life to penetration. The form of the results is similar to those for the final crack length but there is much more variation. The ratio of predicted to test crack aspect ratios are shown in Figure 26. The crack aspect ratio is generally under predicted as for the series 2 constant amplitude tests.

## 7. DISCUSSION

The initial constant amplitude predictions for through cracks in the 7075 T651 aluminum plates using the supplied data were quite poor, showing a large dependence on both stress and stress ratio. However, by increasing the crack growth rates at higher values of  $\Delta K$  to those of the T76 sheet data supplied with the program, it was possible to get excellent results, both in terms of total life and final crack length using a value of 0 for the parameter  $\alpha$ .

Using the same material data and parameter  $\alpha$ , the predictions for the corner cracks were quite good. However, it appears that the crack growth in the through thickness direction is too low which results in a life to penetration which is too long and a crack aspect ratio which is too small. It may be necessary to use different fatigue crack growth curves for the two directions to improve the predictions, since through the thickness growth rates would be expected to be higher.

The final crack lengths were over predicted for this series whereas for the through cracks the final crack length was very accurate. This is probably related to crack shape, since it is unlikely that the crack front is straight in practice after starting as a corner crack although this is what the prediction assumes once the crack has penetrated the thickness.

The predictions for variable amplitude loading of corner cracks were dependent on the spectrum counting technique but showed similar trends. There was less difference than might be expected, however, especially between the uncounted and TTCP counted spectra. This is probably due to the nature of the spectra which have clearly been filtered significantly. The lighter spectrum in particular is very 'clean' having only three different 'train' levels. This explains the similarity between predictions for the lighter spectrum using all three different counting methods.

The predictions for the uncounted spectra and a value of  $\alpha$  of 0 showed good life predictions and the least scatter and this, coupled with the simplicity, make it the preferred technique for these particular spectra. For spectra with a significant number of cycles which consist of a combination of smaller cycles, a counting technique may be required.

The form of the results for the uncounted spectra are similar to those for the constant amplitude predictions from corner cracks. The crack aspect ratios are under predicted and the predicted life to penetration is too small. However, the difference is much greater than for the constant amplitude predictions, with the predicted life to penetration being 3 times too long in one case. This may well be related to the interaction of the plastic zone and the edge of the plate in addition to the different growth rates in the two directions.

The predicted final crack lengths show the same trend as for the constant amplitude predictions from corner cracks although again the discrepancy is larger. This is probably because there is likely to be more crack asymmetry growing a through crack from a corner crack in variable amplitude loading.

## 8. CONCLUSIONS

A comparison of constant amplitude crack growth predictions for through cracks in 7075 T651 aluminum with test results, initially showed a large dependence on both stress and stress ratio. However, excellent predictions for both life and final crack length could be obtained if the supplied crack growth data was modified to increase the growth rates at higher values of  $K_I$ . These results used a  $\alpha$  value of 0 for the parameter  $\alpha$ .

Using the same parameters for constant amplitude crack growth predictions from corner cracks showed good correlation with test, although the growth in the through thickness direction was under predicted slightly and the final crack lengths were over predicted. This was attributed to different material growth rates in the two directions and crack asymmetry.

Predictions from corner cracks under two variable amplitude loading spectra showed similar trends to those for constant amplitude loading but the errors were larger. However, all the life prediction ratios using uncounted spectra were within the range from 0.57 to 1.34, while the final crack length prediction ratios were within the range from 1.08 to 1.41.

Future bond predictions for this material on similar spectra will be made using the modified material data file, a value of  $\alpha$  of 0 and uncounted spectra. Predictions would be expected to be within a factor of two of test results. If the material is changed or the spectra are significantly different, further validation would be required.

Detailed knowledge of the program is not required to make reasonable predictions, but the user must understand how to properly input the data. Comparison with experimental results is a simple way of confirming this understanding and verifying the validity of the data.

## 9. ACKNOWLEDGEMENTS

This work has been performed under the Statement of Agreement between the Institute for Aerospace Research and the Department of National Defence regarding CF-18 Spectrum Development dated January 1989 and FAR Project 3G3, Aerospace Structures, Structural Dynamics and Acoustics, Sub program 302, Operating Loads and Life of Aircraft. The program is partially funded by the Department of National Defence Financial Encumbrance 8465881 ATR A.

## 10. REFERENCES

1. Various authors, 'ALSTAFF', Description of a Fighter Aircraft Loading Standard For Fatigue evaluation, Joint Publication of I & W, LBI, LMBG and NLR, March 1976.
2. de Jonge, J.B., Schutz, D., Lowak, H. and Schive, J., 'A Standardized Load Sequence for Flight Simulation Tests on Transport Aircraft Wing Structures', LBI Bericht 1-B 106 NLR TR730291, March 1973.
3. TTCP HTP 3 Collaborative Exercise, 'An Assessment of the Accuracy of Various Fatigue Crack Growth

Modeling Techniques Part I - Methods and Results', The Technical Cooperation Program, February 1989.

4. TTCP HTP 8 Collaborative Exercise, 'An Assessment of the Accuracy of Various Fatigue Crack Growth Modeling Techniques Part II - Critical Analysis', The Technical Cooperation Program, June 1991.
5. Dill, H. D. and Sall, C. R., 'Analysis of Crack Growth Following Compressive High Loads Based on Crack Surface Displacements and Contact Analysis' in *Cyclic Stress Strain and Plastic Deformation Aspects of Fatigue Crack Growth* ASTM STP 637, American Society for Testing and Materials, 1977, pp. 141-152.
6. Dill, H. D. and Sall, C. R., 'Spectrum Crack Growth Prediction Method Based on Crack Surface Displacement and Contact Analysis' in *Fatigue Crack Growth Under Spectrum Loads*, ASTM STP 595, American Society for Testing and Materials, 1977, pp. 306-311.
7. Chang, J.B. and Engle, R.M., 'Improved Damage Tolerance Methodology', *J. Aircraft*, Vol. 21, No. 9, pp. 722-730, 1984.

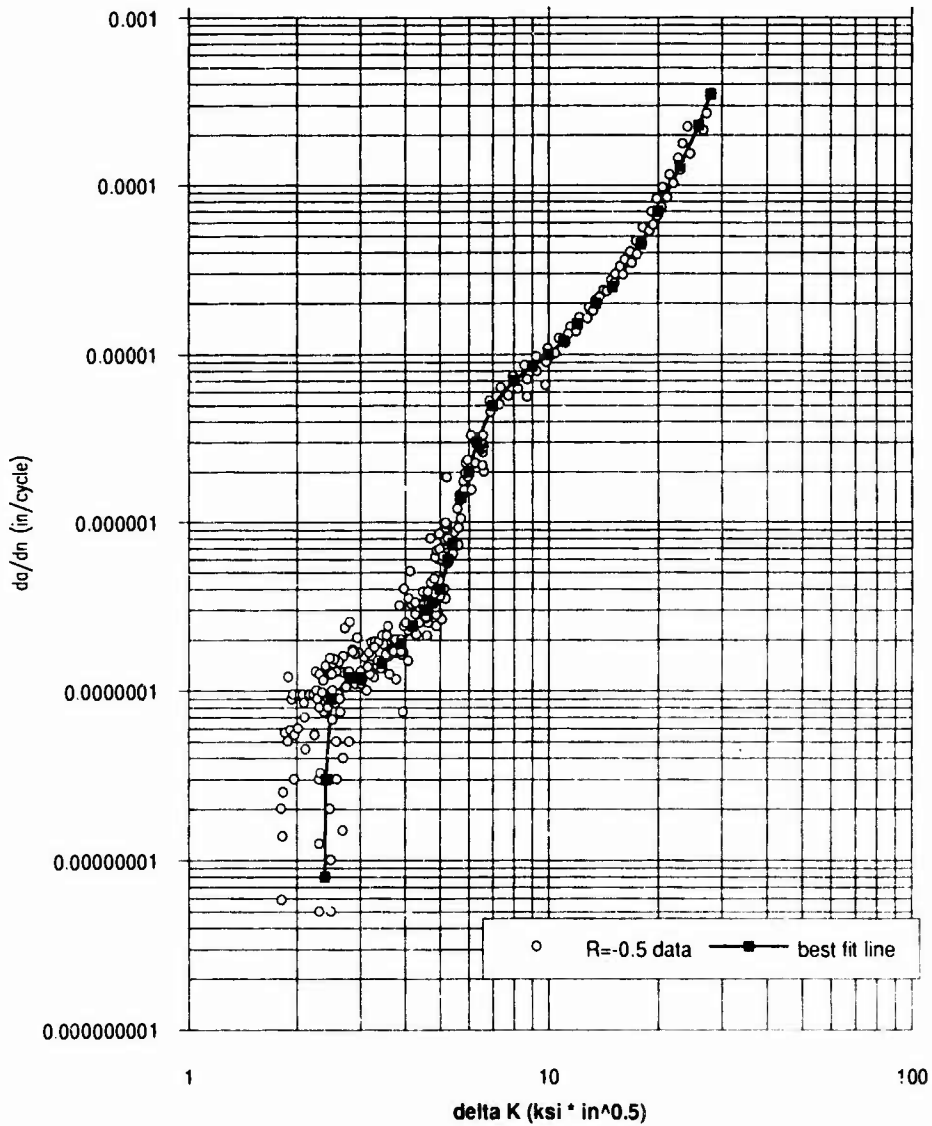


Figure 1:  $da/dn$  versus  $\Delta K$  for  $R = -0.5$  data

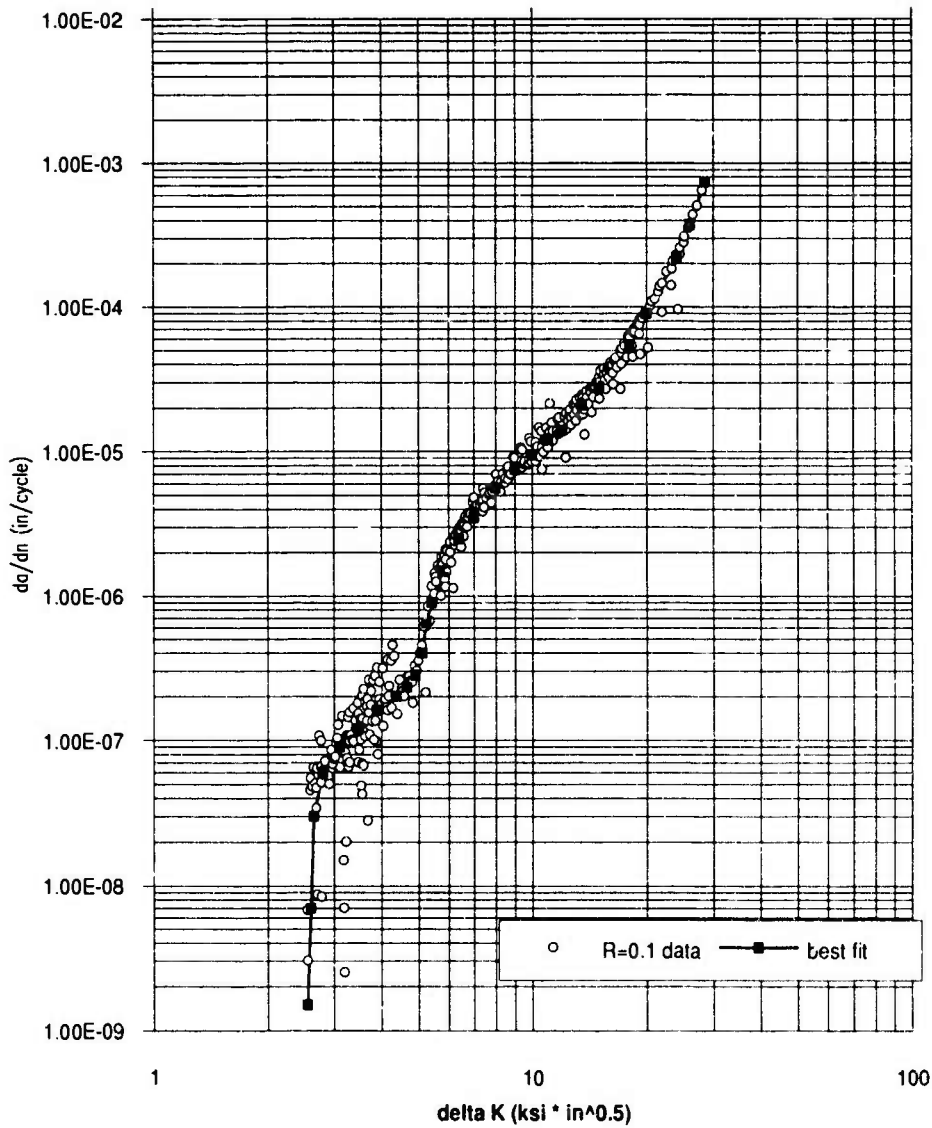
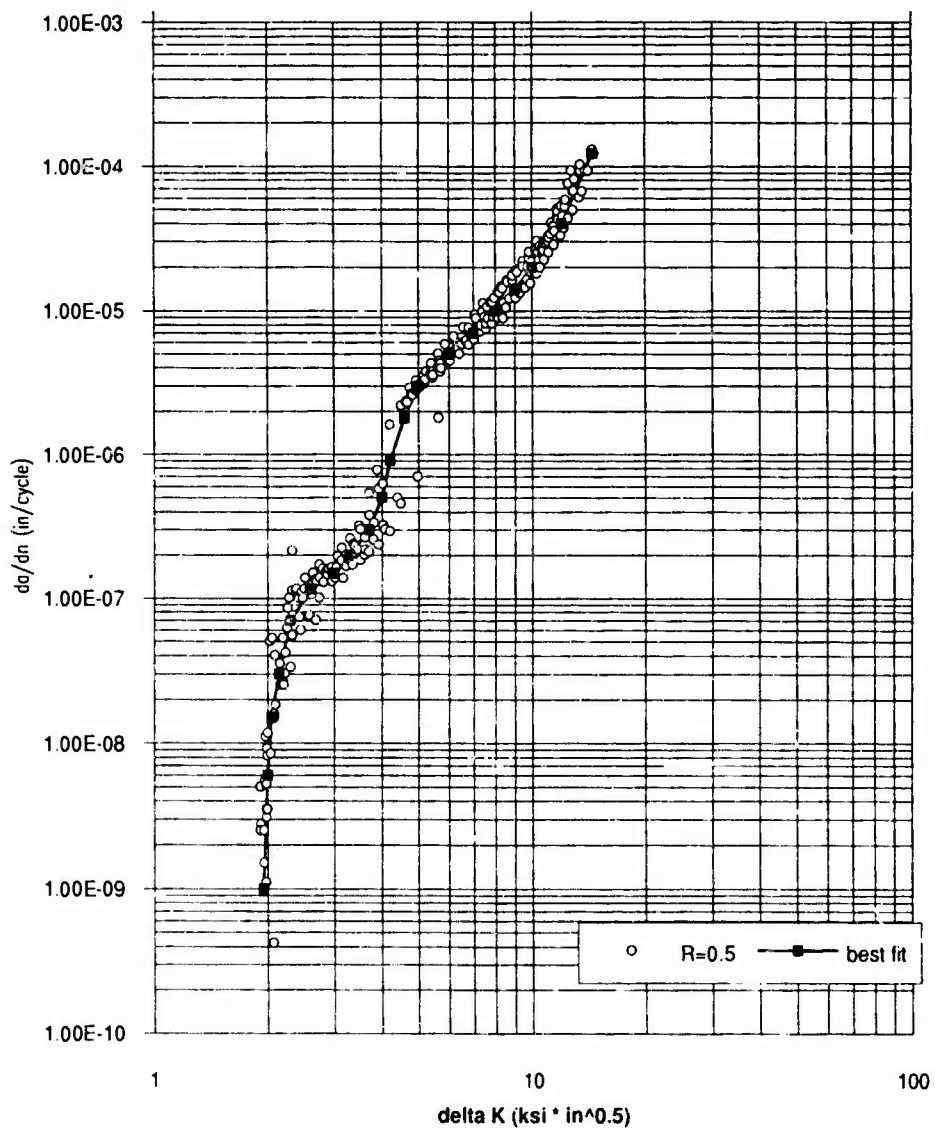


Figure 2:  $da/dn$  versus  $\Delta K$  for  $R = 0.1$  data

Figure 3:  $da/dn$  versus  $\Delta K$  for  $R = 0.5$  data

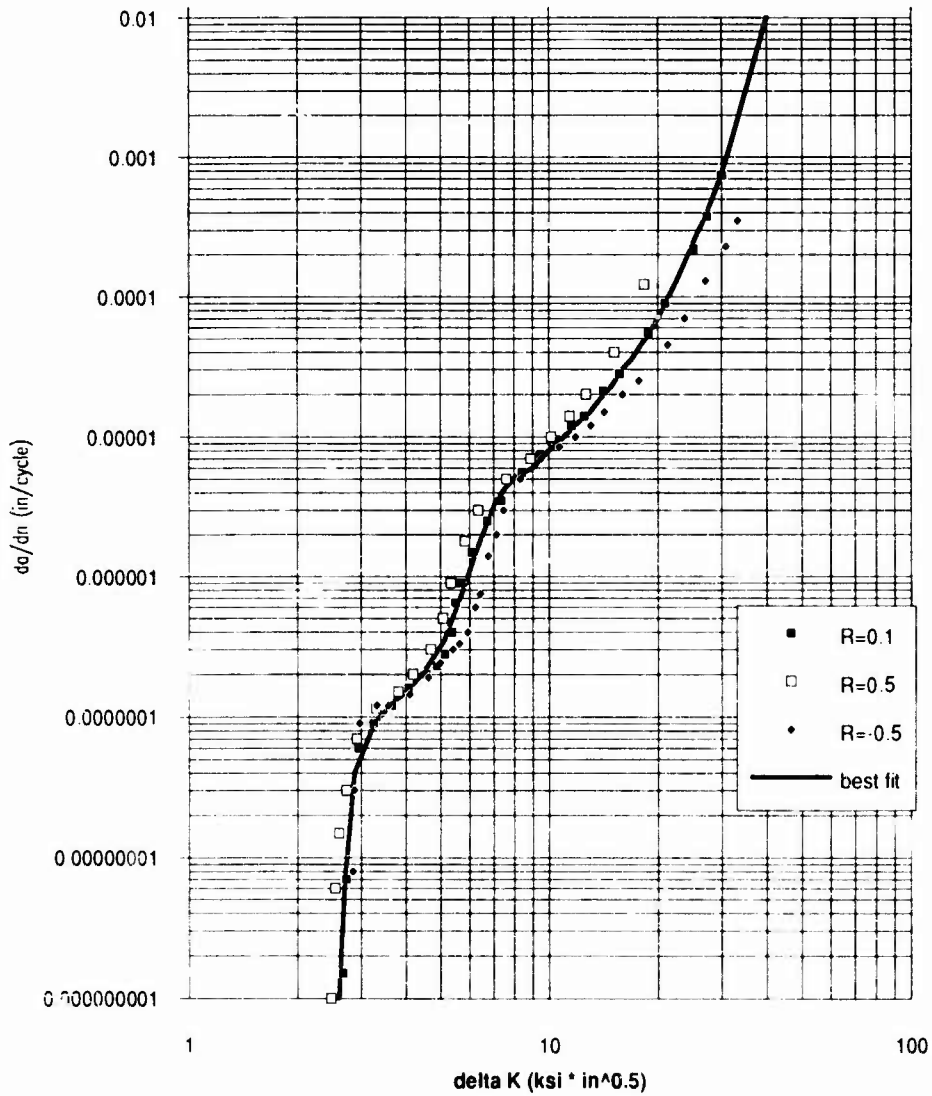


Figure 4:  $da/dn$  versus  $\Delta K$  at  $R = 0$ , originating from data as marked, for  $\alpha = 0$

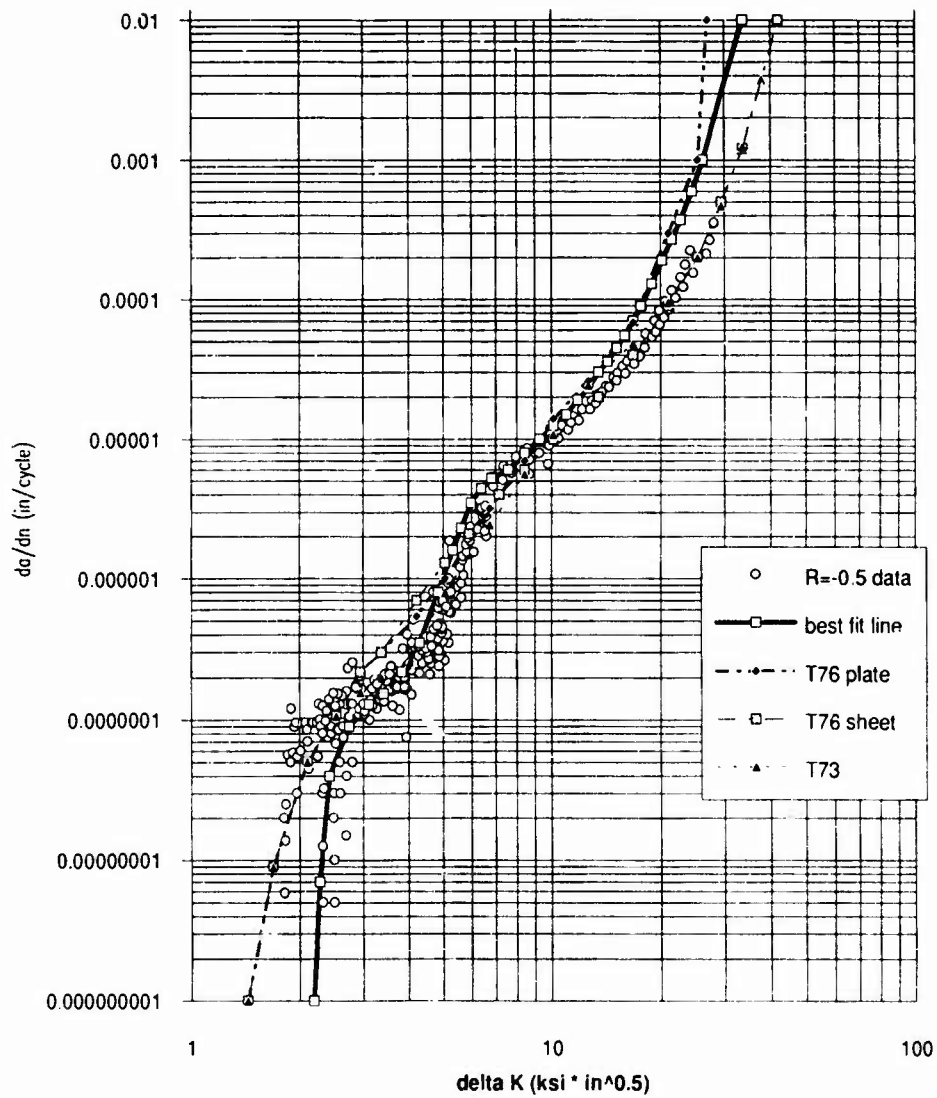


Figure 5:  $da/dn$  versus  $\Delta K$  for  $R = -0.5$  compared with data curves derived from  $R = 0$  curves

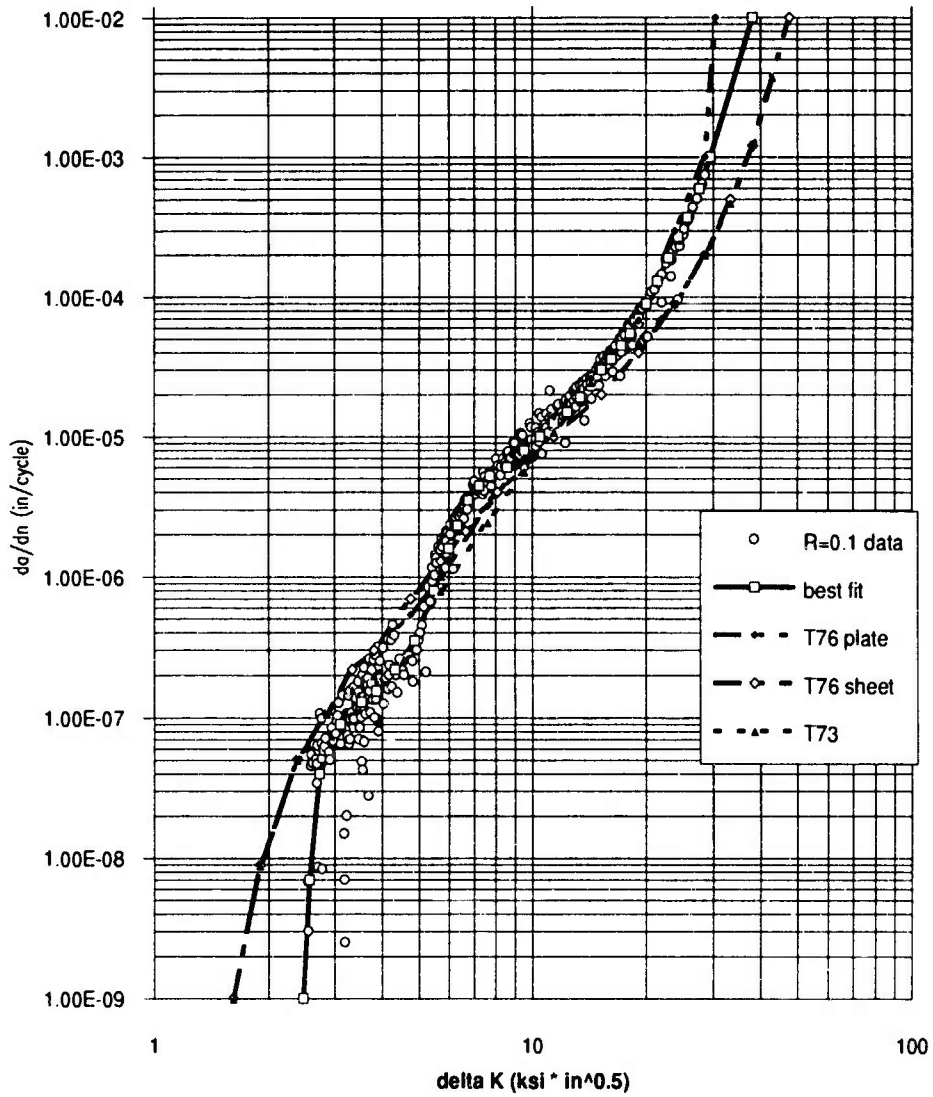


Figure 6  $da/dn$  versus  $\Delta K$  for  $R = 0.1$  compared with data curves derived from  $R = 0$  curves

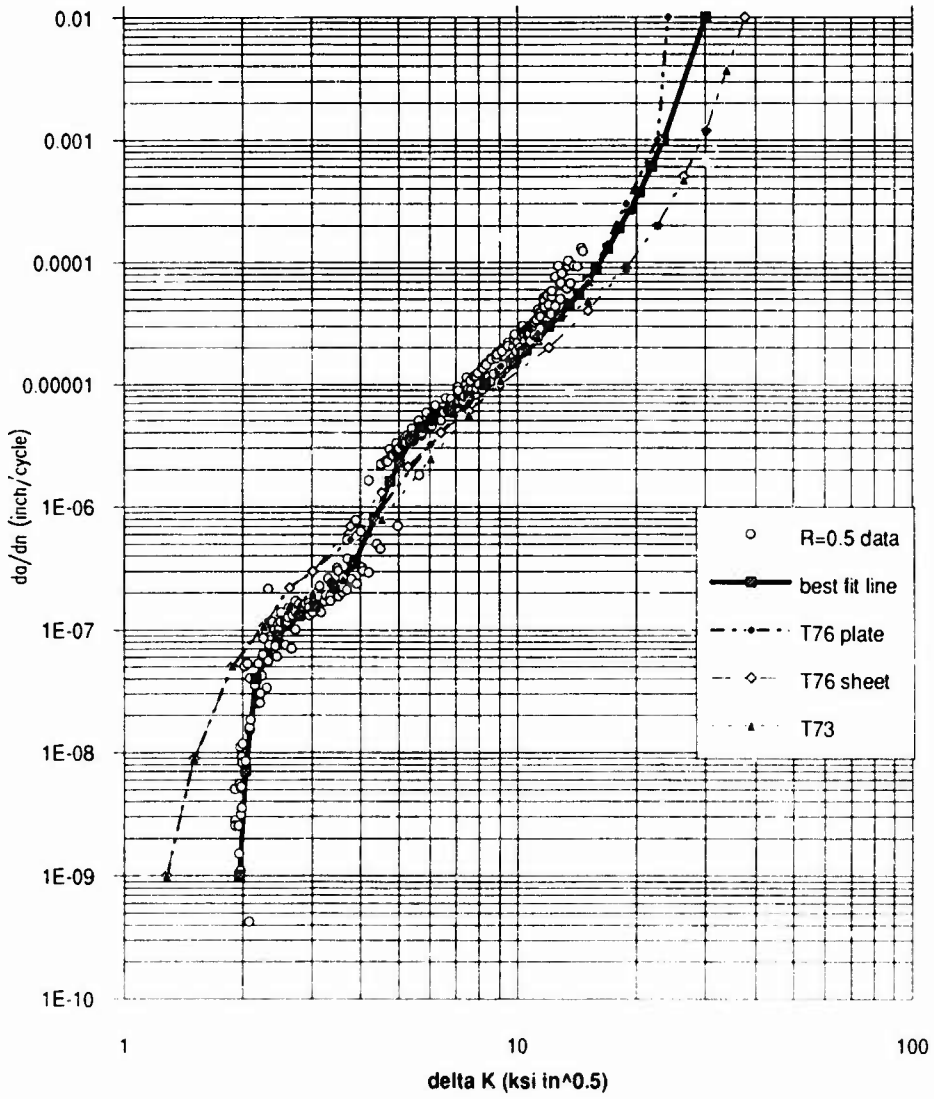


Figure 7:  $da/dn$  versus  $\Delta K$  for  $R = 0.5$  compared with data curves derived from  $R = 0$  curves

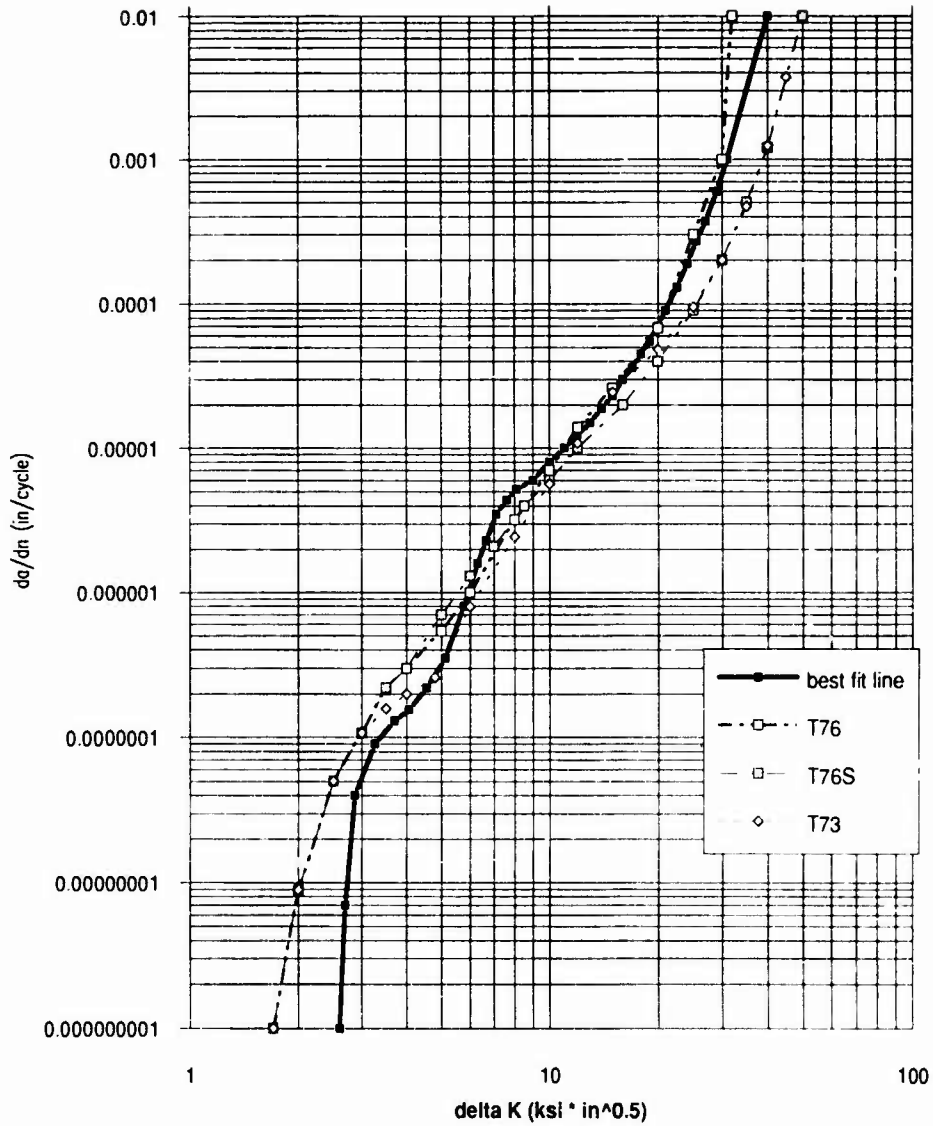


Figure 8: Comparison of crack growth curves at R = 0

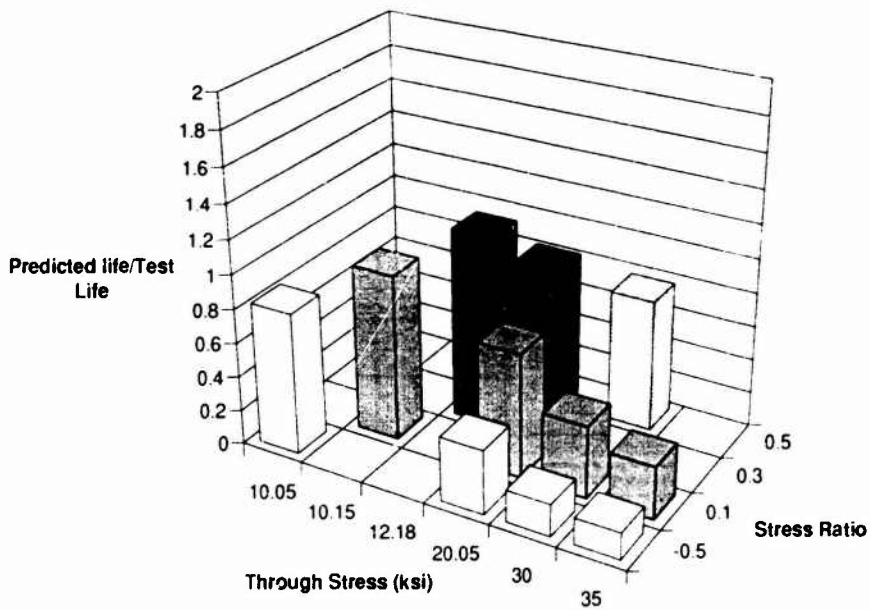


Figure 9: Series 1 life predictions using initial IAR material description and  $\alpha = 0$   
 mean = 0.63, standard deviation = 0.35

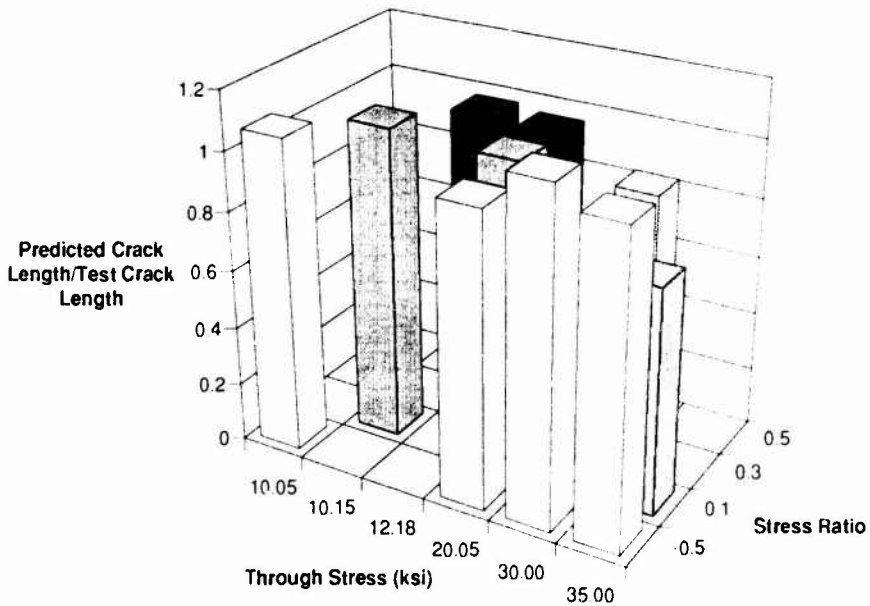


Figure 10: Series 1 crack length predictions using initial IAR material description and  $\alpha = 0$  ( $K_C = 51.6$ )  
 mean = 0.99, standard deviation = 0.12

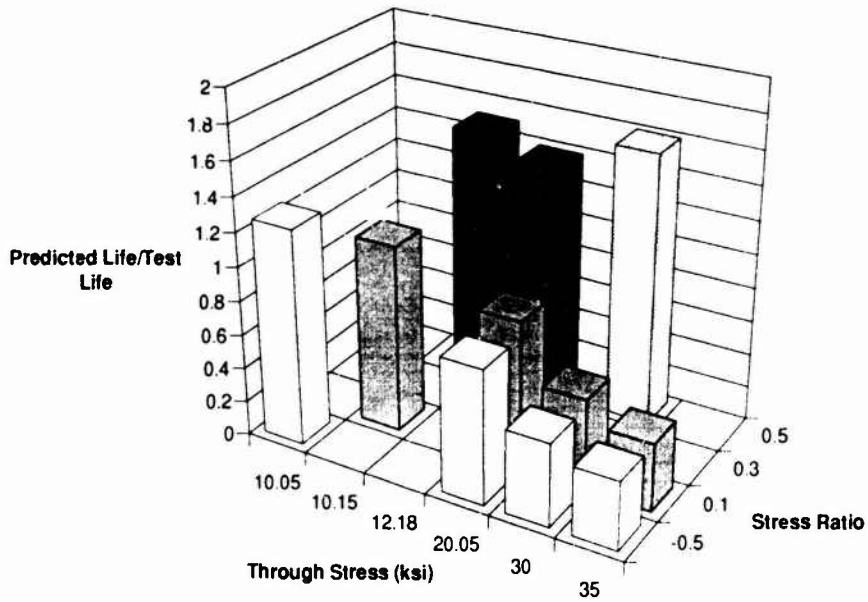


Figure 11: Series 1 life predictions using initial IAR material description and  $\alpha = -1$   
mean = 0.97, standard deviation = 0.50

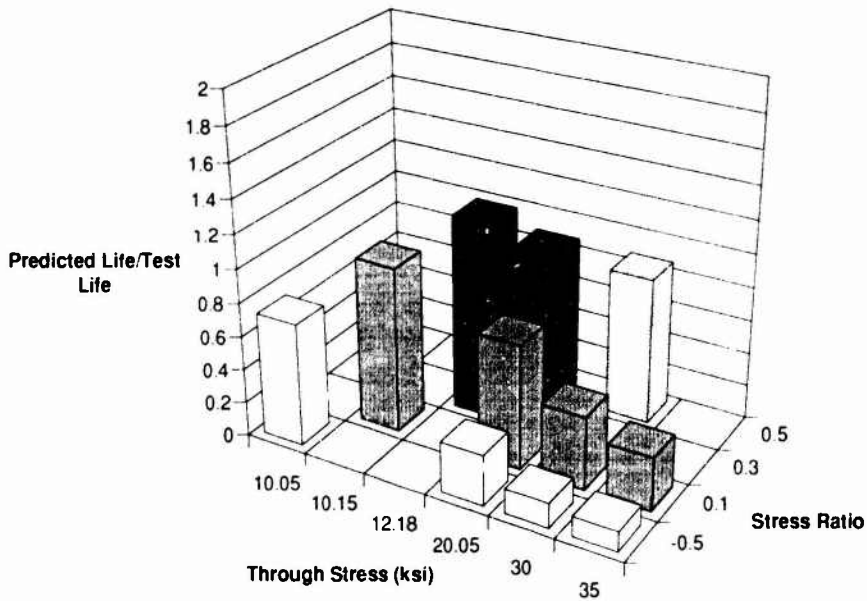


Figure 12: Series 1 life predictions using initial IAR material description and  $\alpha = 1$   
mean = 0.62, standard deviation = 0.38

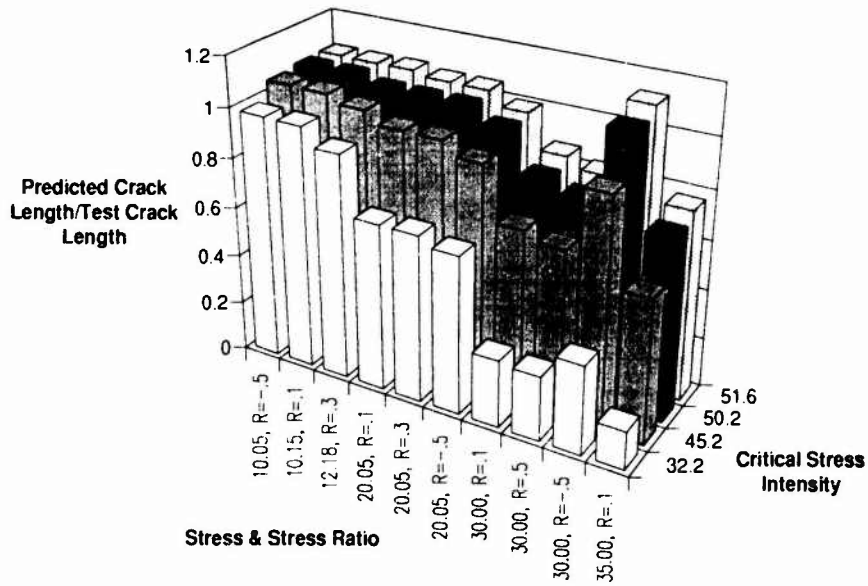


Figure 13: Comparison of predicted/tested critical crack lengths for various critical stress intensities

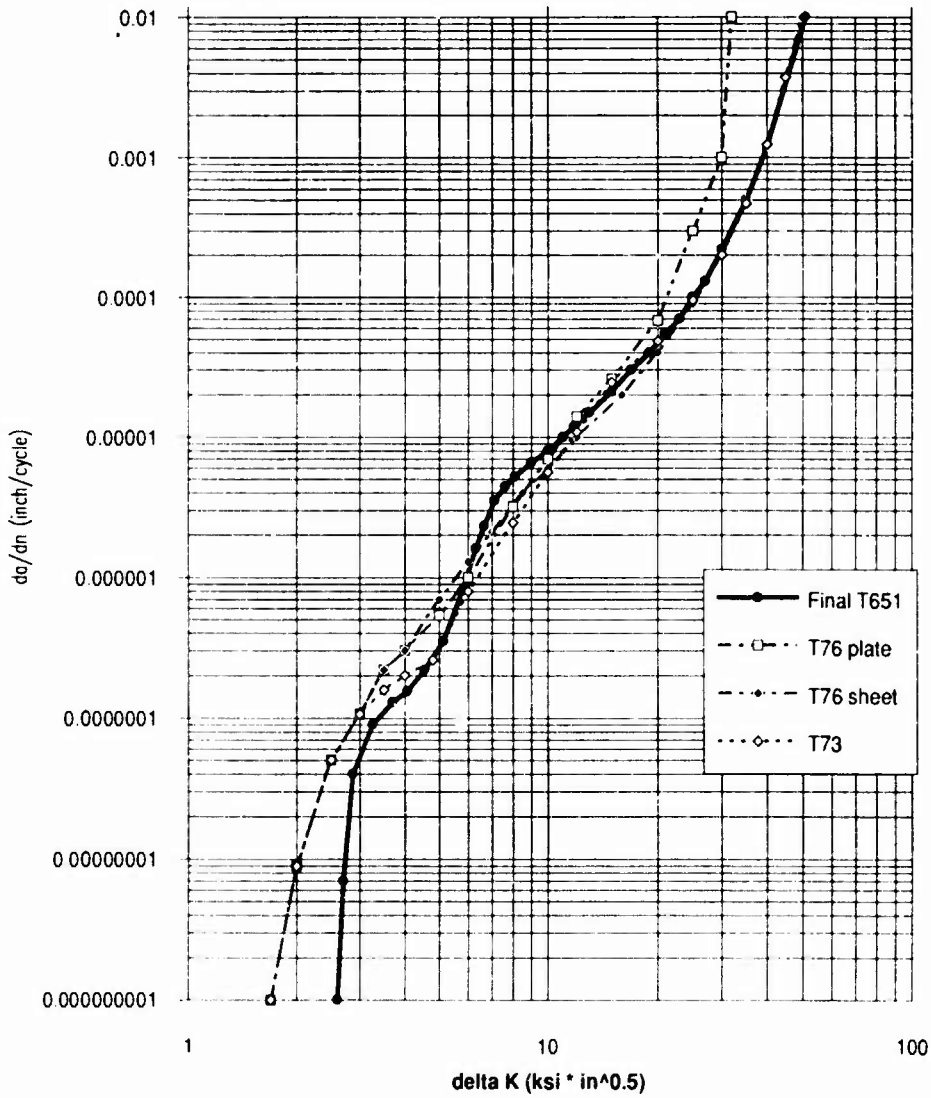


Figure 14: Comparison of final  $da/dn$  versus  $\Delta K$  curve for 7075 T651 at  $R = 0$  with program data

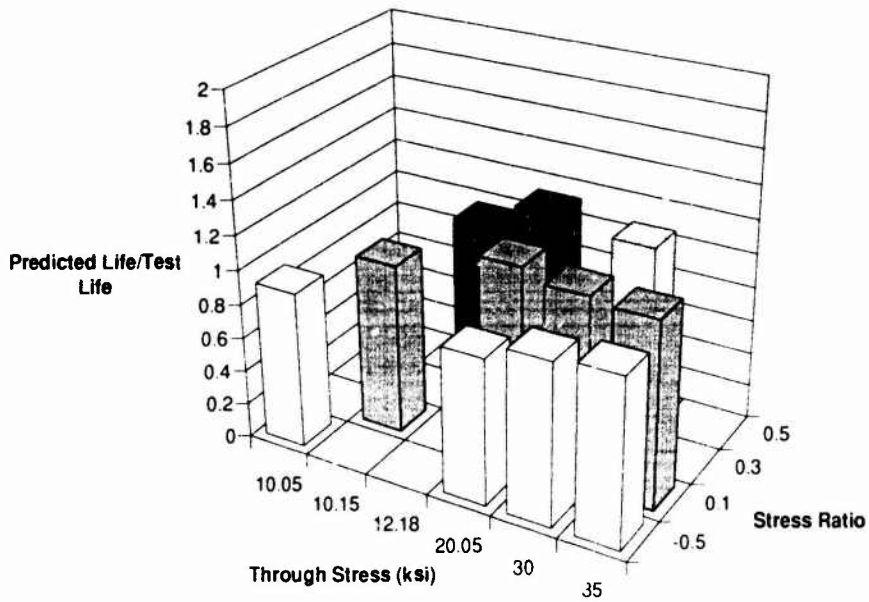


Figure 15: Series 1 life predictions using final IAR material description and  $\alpha = 0$   
 mean = 1.05 standard deviation = 0.14

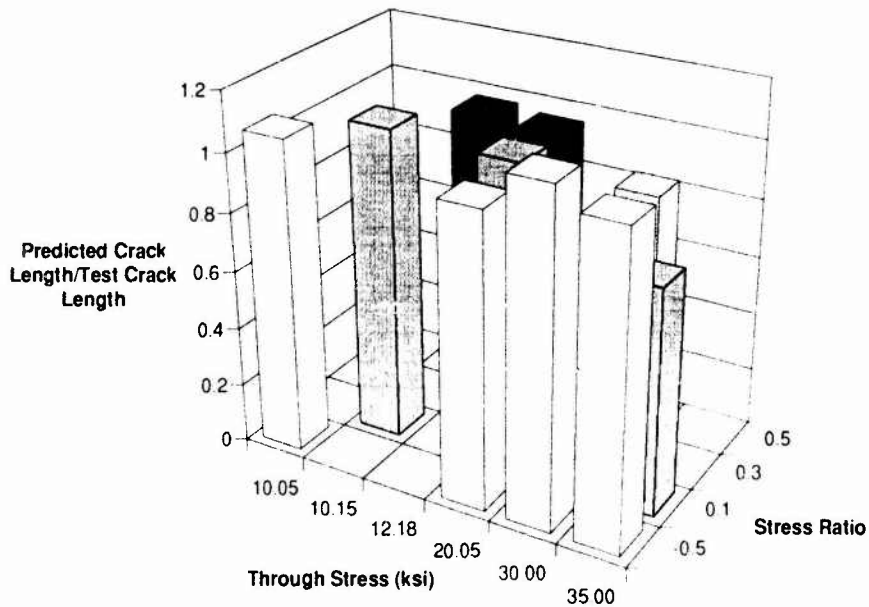


Figure 16: Series 1 crack length predictions using final IAR material description and  $\alpha = 0$   
 mean = 0.99 standard deviation = 0.12

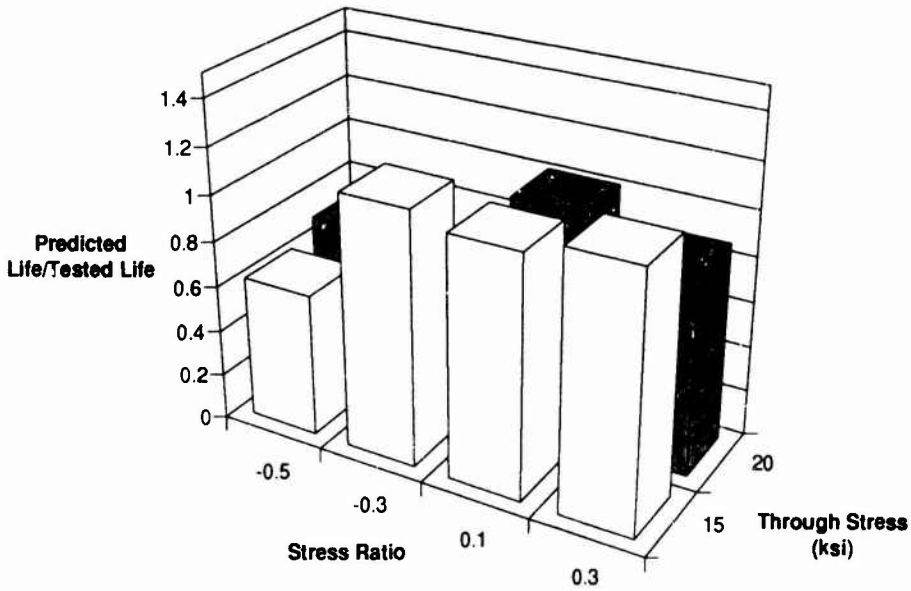


Figure 17: Series 2 life predictions using final IAR material description and  $\alpha = 0$   
 mean = 0.93, standard deviation = 0.20

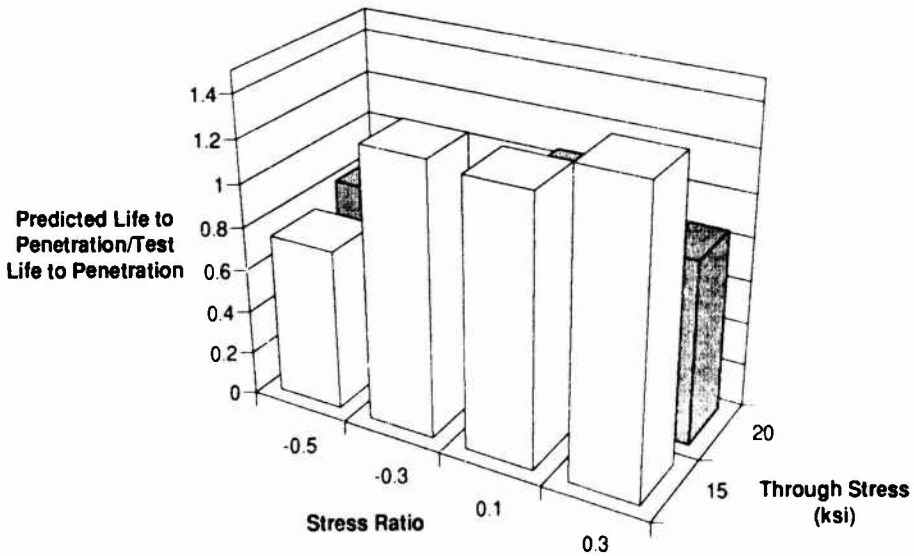


Figure 18: Series 2 predictions for life to crack penetration of plate using final IAR material description and  $\alpha = 0$   
 mean = 1.05, standard deviation = 0.25

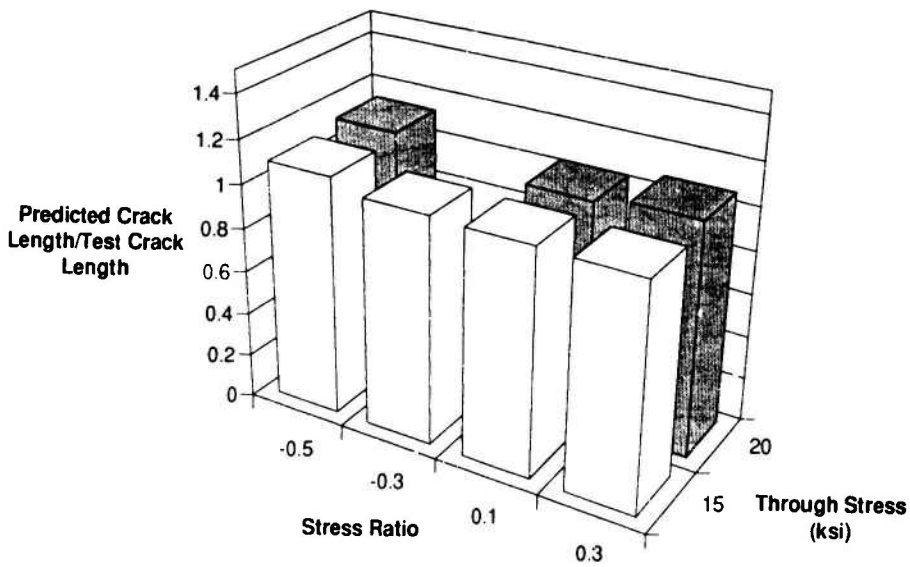


Figure 19: Series 2 crack length predictions using final IAR material description and  $\alpha = 0$   
 mean = 1.07, standard deviation = 0.04

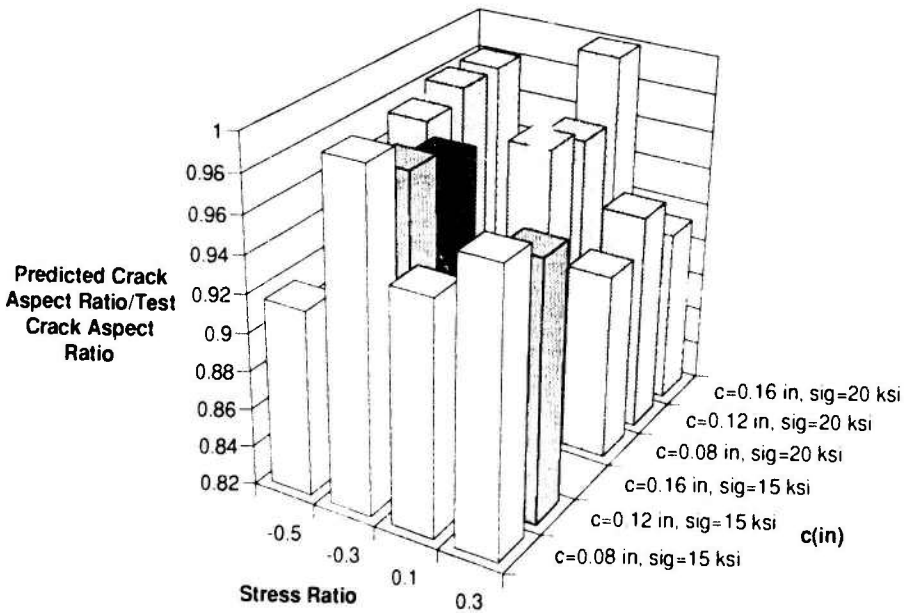


Figure 20: Series 2 crack aspect ratio predictions using final IAR material description and  $\alpha = 0$

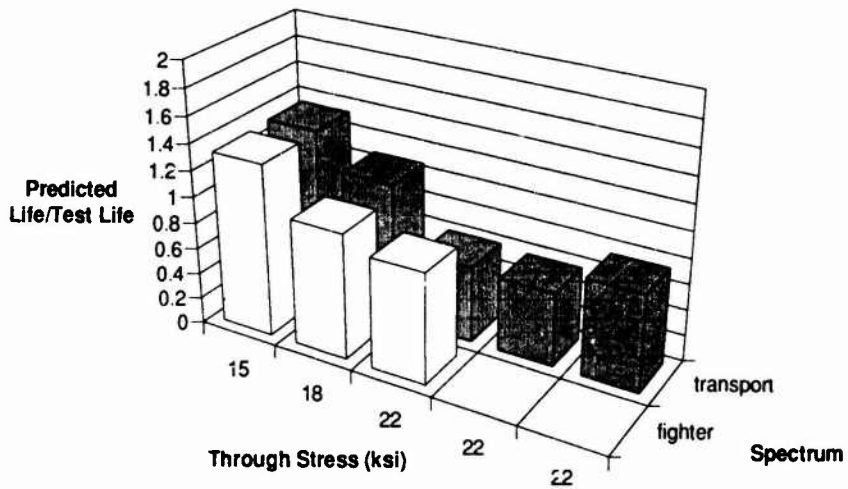


Figure 21: Series 3 life predictions for uncounted spectra using final IAR material description and  $\alpha = 0$   
 mean = 0.93, standard deviation = 0.30

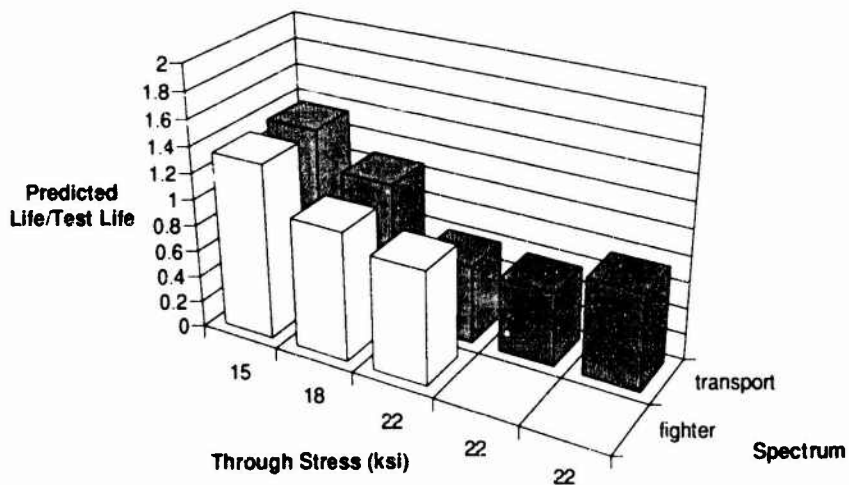


Figure 22: Series 3 life predictions for TTCP counted spectra using final IAR material description and  $\alpha = 0$   
 mean = 0.94, standard deviation = 0.31

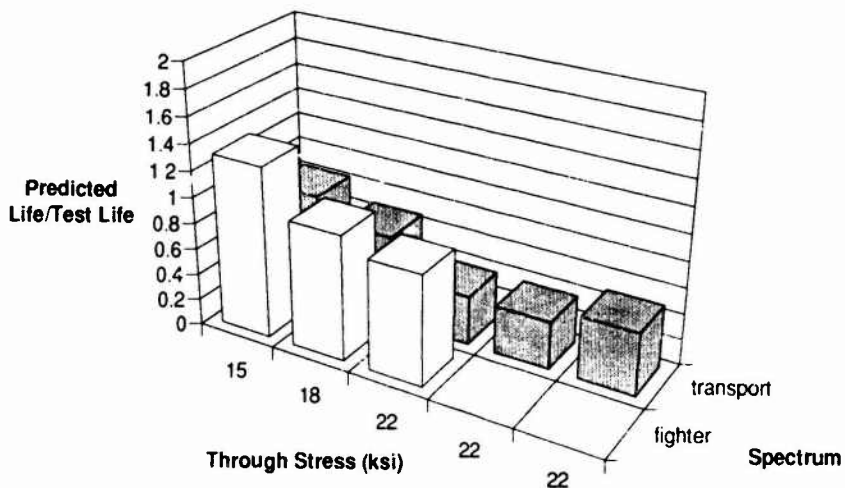


Figure 23: Series 3 life predictions for tAR counted spectra using final IAR material description and  $\alpha = 0$   
 mean = 0.73, standard deviation = 0.32

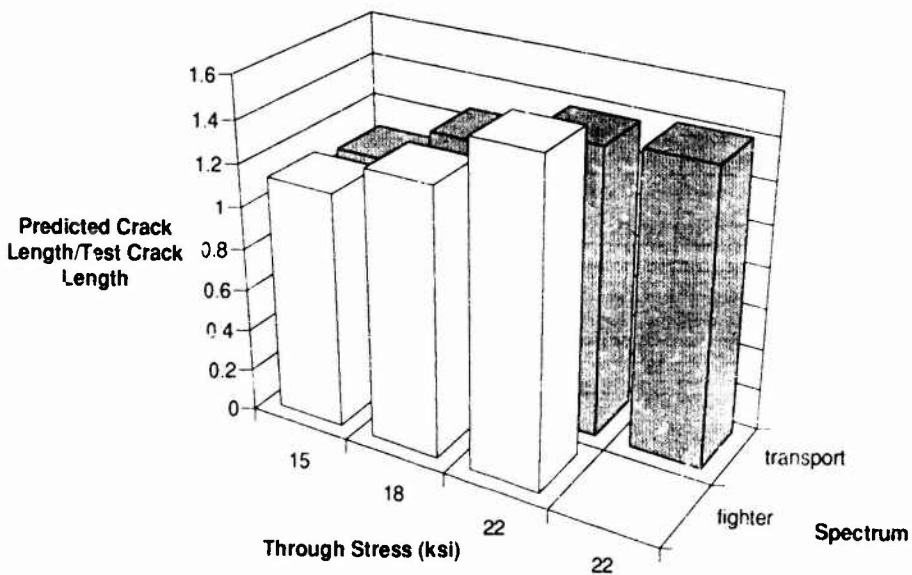


Figure 24: Series 3 crack length predictions for uncounted spectra using final IAR material description and  $\alpha = 0$   
 mean = 1.30, standard deviation = 0.16

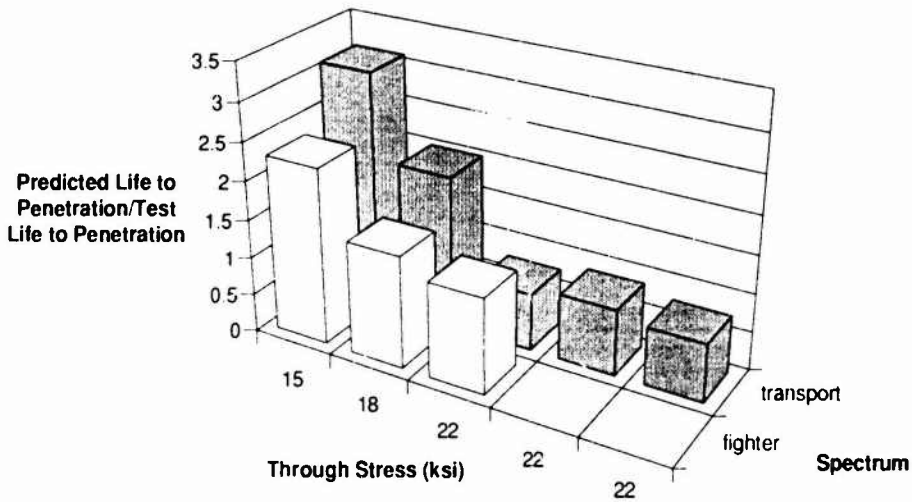


Figure 25: Series 3 predictions for life to crack penetration of plate for uncounted spectra using final IAR material description and  $\alpha = 0$   
 mean = 1.56 standard deviation = 0.85

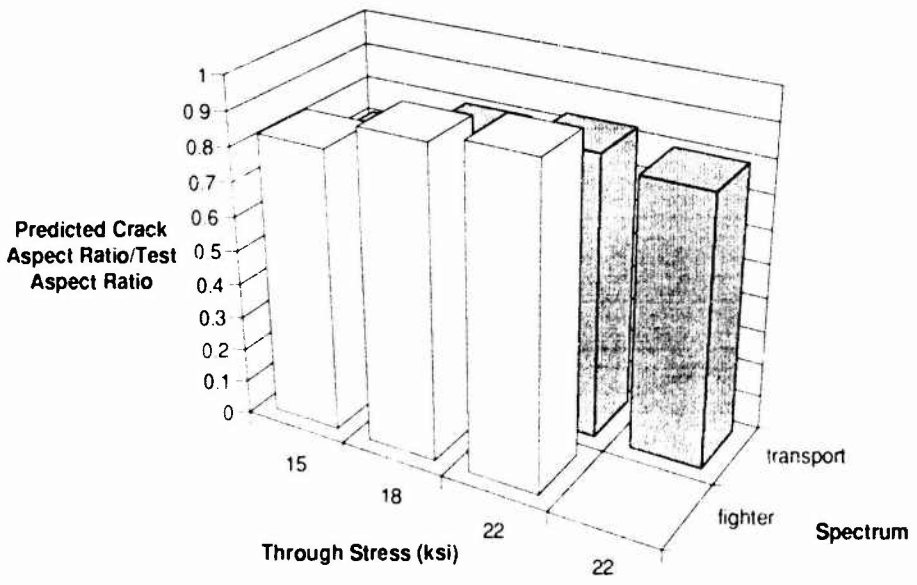


Figure 26: Series 3 predictions of crack aspect ratio at plate penetration for uncounted spectra using final IAR material description and  $\alpha = 0$   
 mean = 0.83 standard deviation = 0.07

## THE CRACK SEVERITY INDEX OF MONITORED LOAD SPECTRA

J.B. de Jonge

National Aerospace Laboratory NLR

P.O. Box 90502, 1006 BM Amsterdam

The Netherlands

**1. SUMMARY**

To assess the consequences with regard to fatigue and damage tolerance of changes in operational usage, a simple means to quantify the relative severity of recorded load spectra is required.

This paper describes the development and validation of the "Crack Severity Index" CSI as a means to express the relative damage in terms of a "crack growth potential" of stress spectra. The CSI is based on a crack-closure crack growth model and takes account of interaction effects by considering the shape of the spectrum.

It is shown that the CSI-concept is a reasonably accurate method to compare the relative severity of manoeuvre dominated spectra in aluminium alloy structure.

**2. INTRODUCTION**

The majority of current fatigue load monitoring systems for military aircraft provide for the determination of service load spectra in one or more significant structural locations, usually indicated as "Control Points". These load spectra are derived either from direct strain measurements or calculated from a few simultaneously recorded flight parameter histories. (1)

In order to assess the consequences of observed changes in service load spectra, a means to quantify the relative "damage" of these spectra is needed. In the past, the usual method was to calculate the cumulative fatigue damage of the spectrum, on the basis of Miner's rule, assuming a "representative"  $K_1$  and an appropriate S-n curve. Unfortunately, the outcome of these calculations turned out to depend heavily on the assumptions made and did not reflect any load interaction effects.

The General Dynamics F16 is the first line Combat aircraft type operated by the Royal Netherlands Air Force. The F16, like most modern fighter aircraft has been designed according to Damage Tolerance Design Criteria. For such aircraft the (possible) amount of crack growth rather than fatigue life consumption defines the severity of a load spectrum.

The NLR has developed a method to express the severity of recorded stress spectra in terms of "crack growth potential". This Crack Severity Index (CSI) is used to assess monitored F16 Service stress spectra as part of the RNLAF F16 Fatigue Management Program.

This paper starts with a description of the background and the development of the CSI-concept. Results of a large number of crack growth tests under widely varying load spectra were used to check the validity of the concept. It is shown that the CSI is a reasonably accurate measure to compare the crack growth damage of manoeuvre dominated

spectra in aluminium alloy structure. In a general discussion, specific aspects of the CSI-concept are reviewed. It is shown that the CSI can also be usefully applied in studies to influence the fatigue consumption by operational measures.

**3. CSI-DEVELOPMENT**

**Stress spectrum.** It is assumed that the stress history in a specific structural area has been recorded over a certain period, say for example during 100 successive flights. This stress history has been analysed using "Rainflow" counting<sup>(2)</sup>; the resulting "stress spectrum" consists of n stress cycles i with max stress  $s_{max,i}$  and minimum stress  $s_{min,i}$ .

**Crack growth law.** The crack growth due to load cycle i is given by a simple Paris-type expression.

$$da_i = C(\Delta K_{eff,i})^m = C[\beta(a)\sqrt{\pi a}]^m (\Delta s_{eff,i})^m$$

a is the crack length,  $\beta(a)$  a geometry function and m a material constant. The effective stress range  $\Delta s_{eff,i} = s_{max,i} - s_{op,i}$ .

The opening stress level  $s_{op}$  is a function of the stress history as will be described further on, but is supposed to be independent of crack length.

**Spectrum crack growth.** Eq. 1 can be rewritten

$$\frac{da_i}{[\beta(a)\sqrt{\pi a}]^m} = (s_{max,i} - s_{op,i})^m \quad (2)$$

or

$$f(a) da_i = (s_{max,i} - s_{op,i})^m$$

with

$$f(a) = \frac{1}{[\beta(a)\sqrt{\pi a}]^m} \quad (4)$$

Under the spectrum a crack with length  $a_0$  will grow to  $a_n$ . Defining the integral of  $f(a)$  as  $F(a)$ , the crack growth can be calculated from

$$F(a_n) - F(a_0) = C \sum_{i=1}^n (s_{max,i} - s_{op,i})^m \quad (5)$$

In this equation, the left hand side is purely defined by the structural geometry crack length and material properties (through the term m). The right hand side includes load-spectrum terms - plus again the material parameter m. Note that the right hand side is independent of crack length (under the assumption that  $s_{op}$  is independent of crack length). We can say that the right hand side

defines the "crack growth potential" of the stress spectrum; two spectra yielding the same value for the "right hand side term" will cause the same amount of crack extension ( $a_n - a_0$ ) starting from a crack with size  $a_0$ ; this right hand side term will be called the Crack Severity Index CSI:

$$CSI = C \sum_{L=1}^n (S_{max,L} - s_{op,L})^2 \quad (6)$$

As the CSI is used to compare different spectra, the value of the constant C is immaterial: In practice, C is chosen so as to yield a CSI = 1 for a "reference" stress spectrum.

The opening stress  $s_{op}$ . It will be clear that the magnitude of  $s_{op}$  has a major influence on the amount of crack growth, and the determination of a simple rationale for calculating  $s_{op}$  is a key element in the CSI-development.

In fighter aircraft, the interest is concentrated on the development of relatively short cracks, emanating from initial flaws of say 1.25 mm in usually relatively thick structure. Hence, for cracks of interest plane strain conditions at the crack tip may be assumed.

Under constant amplitude loading, the opening stress  $s_{op}$  may then be approximated by the expressions given in Figure 1 (Ref. 3).

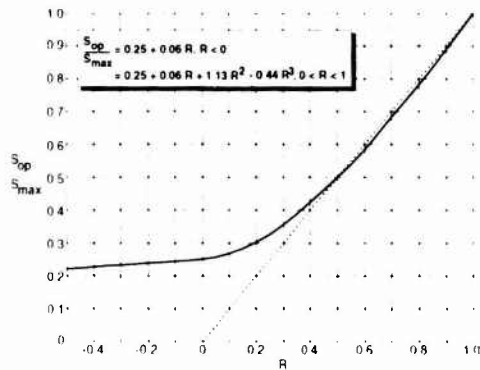


Fig 1  $\frac{s_{op}}{s_{max}}$  as a function of  $R = \frac{s_{min}}{s_{max}}$  for plane strain conditions

Under variable amplitude loading, a much more complicated situation exists as the instantaneous opening stress depends on previous load peaks and valleys and their associated plastic zone sizes near the crack tip. This effect of preceding overloads and underloads on the crack opening stress is currently considered as the cause of so-called crack growth retardation under spectrum loading. To study the behaviour of  $s_{op}$ , an analysis was made of the  $s_{op}$  for typical manoeuvre dominated fighter aircraft load sequences, using the NLR "in house" computer program CORPUS (Calculation of Propagation Under Service loading) (Ref. 3). CORPUS is an advanced program for cycle by cycle calculation of crack growth.

Figure 2 shows typical results for a part of the (relatively long) load sequence analysed. It turned out that after a certain number of flights a "minimum opening stress" has developed, which is purely defined by the highest peak and the lowest valley in the stress sequence: a high load pushes

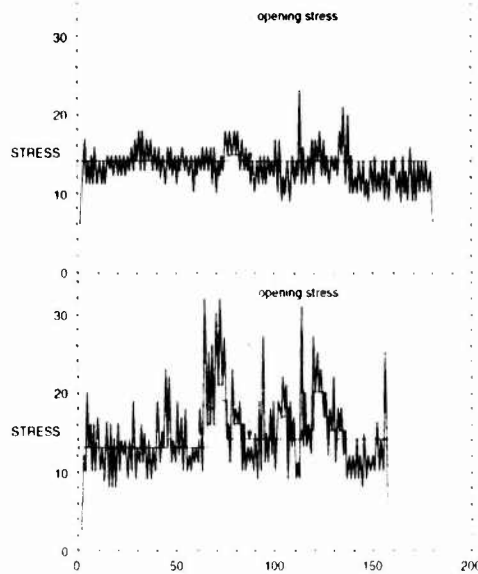


Fig 2 Opening stress levels calculated with CORPUS for two flights in the analyzed sequence

up the opening stress, thus reducing the amount of crack growth associated with the load cycles coming next. The opening stress is lowered again when a low valley occurs. The "memory" of the overload will end with the advance of the crack tip, when the tip grows out of the plastic zone produced by the overload.

On the basis of the above considerations, the following rationale has been adopted for calculating  $s_{op}$ :

$s_{op,i}$  pertaining to stress cycle  $i$  is the largest of:

1.  $s_{op,i}$  determined for  $s_{max,i}$  and  $s_{min,i}$  according to Figure 1
2.  $s_{op,min}$  determined for the highest stress occurring in 30 flights,  $s_{max,30}$  and the lowest stress in 30 flights,  $s_{min,30}$ , whereby  $s_{op,min}$  is related to  $s_{max,30}$  and  $s_{min,30}$  according to Figure 1.

This number of 30 flights represents the estimated average "memory" period for overloads, considering typical plastic zone sizes due to overloads and typical crack growth rates.

The definition given above for  $s_{op}$  implies that a "relevant" CSI-value can only be determined for a stress spectrum covering at least 30 flights: if a CSI has to be determined for a smaller hatch of flights, a value for  $s_{op,min}$  must be assumed, that means it must be assumed that the specific hatch of flights belongs to an overall usage for which the "extremes" of the spectrum are known.

#### 4. VALIDATION OF THE CSI-CONCEPT

In order to validate the CSI-concept calculated CSI-values were compared with results of crack growth tests on simply notched plate specimens, made of 7475 aluminium alloy plate with a thickness of 7.62 mm. Specimens were provided with either a corner crack or a through-the-thickness crack (see fig 3);

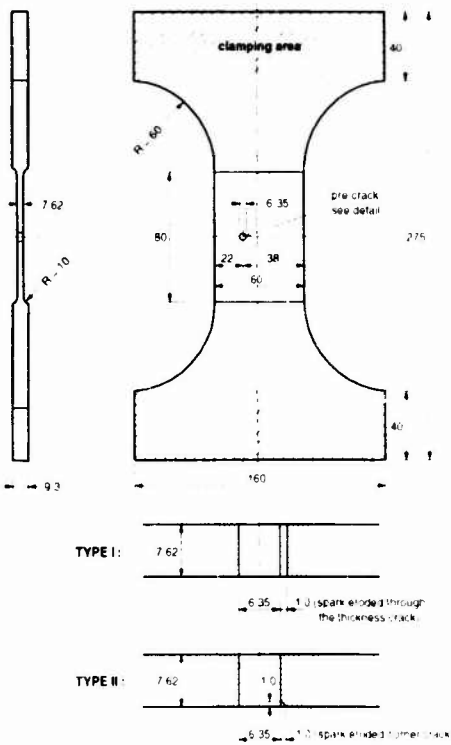


Fig 3 Specimens used for crack growth tests

A number of these tests were defined specifically for the CSI-validation but the majority of tests were done as part of the RNLA F-16 Life Management program. In the following, results of these comparisons will be discussed for a number of the test results that were available.

In these comparisons, the "calculated severity" refers to the CSI value computed for the specific test spectrum, whereas the "observed severity" is the inverse of the crack growth life until a - 16 mm as found in test.

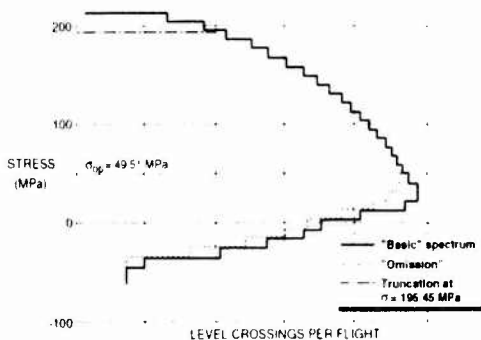


Fig 4 Predicted and observed effect of spectrum changes on spectrum severity

The material constant  $m$  used in the CSI calculations was equal to  $m=3$ .

Figure 4 presents spectra for some tests done specifically for CSI validation. The "basic" spectrum refers to the wing bending moment of a fighter aircraft. In the spectrum indicated as "omission", all load cycles with a  $s_{max}$  lower than the predicted  $s_{op,min}$  (49.51 MPa) were omitted. The CSI-concept predicts that this omission will have no influence on the spectrum severity, and this prediction appears to be fully confirmed by the tests.

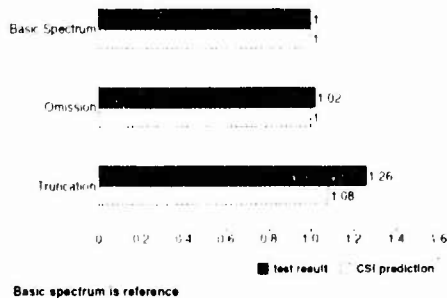
In the "truncated" spectrum the highest peaks were reduced to 195.45 MPa. The increase in severity by a factor of 1.26 was not fully predicted by the CSI, (factor = 1.08) but it may be noted that in any case the CSI predicted an increase in severity due to truncation, whereas all "classical" non-interaction models would have predicted a decrease!

Figure 5 shows different spectra for one structural location, namely the wing root. One spectrum is indicated as "Design", the other three are recorded spectra pertaining to different usages. At first glance, one would expect the Design spectrum to be much less damaging than the actual service usage, but the tests show that the opposite is true: the Design spectrum is the most severe. It turns out that actually the CSI predicted this effect reasonably well. However, the CSI overestimated the severity of usage 3 compared to usage 1 by 20 percent.

Figure 6 shows spectra for three different structural locations. It may be noted that the Horizontal Tail Spectrum is very different from the others as it is nearly symmetrical around zero stress. The horizontal tail spectrum was found in test to be about 16 times less severe than the wing B.M. spectrum. This severity was predicted within 8 percent by the CSI-concept. Undoubtedly, this outcome is remarkably good.

Comparisons for other load spectra, which will not be presented here, revealed equally acceptable results. For a total number of 55 different stress spectra that were studied, the average error in the CSI-prediction was -6.3 percent and the average absolute error was 15.1 percent.

Summarizing, we may conclude that comparison of CSI prediction and test results have shown that the CSI-concept may provide a reasonably accurate means to quantify the relative severity of manoeuvre dominated fighter type load spectra.



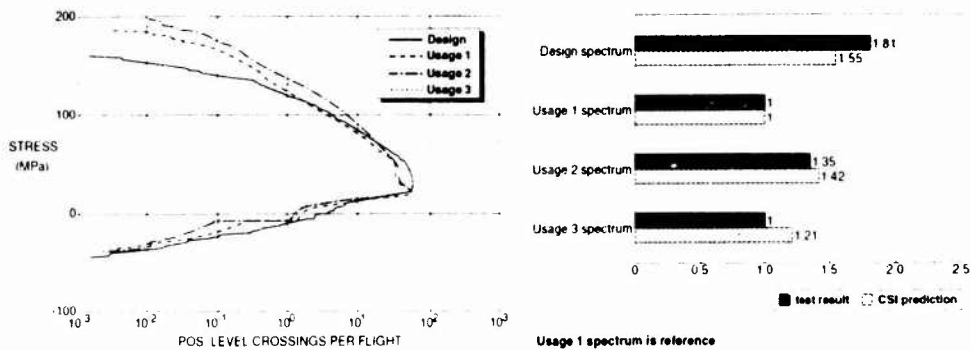


Fig. 5 Comparison of observed and predicted severities for Wing B.M. Spectra pertaining to different usages

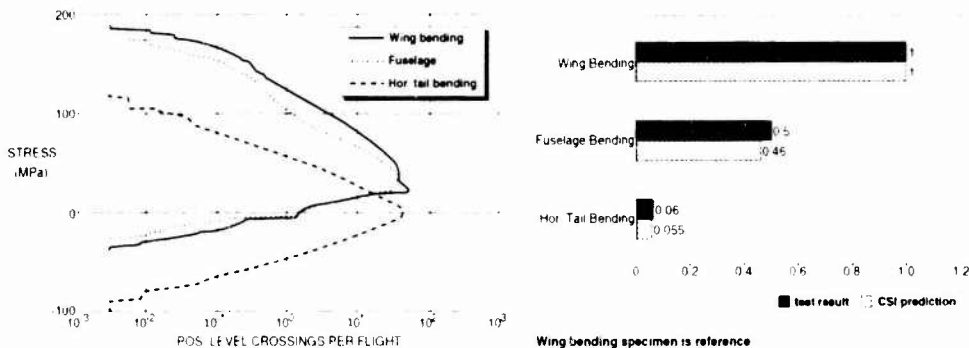


Fig. 6 Predicted and observed severities of spectra for different structural locations

## 5. DISCUSSION

Interaction effects have a major influence on fatigue crack initiation and crack growth under spectrum loading. Very often these effects, specifically the effect of high overloads are of a crack growth retarding nature. Hence, "non-interaction" prediction techniques tend to give conservative results. This expected conservatism combined with their inherent simplicity are cause that "non-interaction" prediction methods are still widely used throughout the aerospace industry. However, it must be realized that this "conservatism" in itself is of no use if one wants to compare the severity of different spectra on a relative basis. A numerical example may illustrate this. Suppose that the crack growth life under spectrum A is predicted to be 2000 flights, while tests yield a life of 5000 flights. The predicted life under a different spectrum B is 2000 flights, while the test life is 4000 flights. Our prediction technique yielded a conservative result in both cases, but the relative prediction was totally wrong, spectrum B was predicted to be less severe than spectrum A, while the opposite is true!

The CSI turned out to give reasonably accurate predictions of the relative severity of widely varying spectra, only because it takes account of

load interaction effects!

The effect of for example a high load remains noticeable during many successive flights. It may be recalled that a valid CSI could only be calculated for a batch of at least 30 flights. In other words, a CSI pertaining to one flight can only be calculated if assumptions are made with regard to the overall spectrum of flights to which our specific flight belongs. This may appear as a shortcoming of the CSI-concept but is actually a direct consequence of the load interaction phenomenon; it must be realized that the damaging effect of a flight is not solely defined by the spectrum content of that flight, but depends on the load sequence that preceded that flight. Any attempt to define damage figures for one flight on the basis of information about the loading history of that flight alone must fail, in case of variable amplitude loadings and structural materials like the common aluminium alloys used in aircraft, which are sensitive for load interaction effects.

As mentioned already in the introduction, the CSI concept has been and is successfully used as a standard tool in the PNAF F-16 Fatigue Load Monitoring Programme (see Ref. 1) as a means to present and assess the observed differences between the usage of various squadrons and to indicate changes in that usage.

Apart from such applications, it was found that the CSI-concept may also be successfully used in studies how to influence the loading severity by changes in aircraft operation. Application of the CSI concept for this purpose will be illustrated in Spiekhout's Paper (Ref. 5) during the present Meeting.

#### 6. CONCLUSIONS

1. A simple means to quantify the severity of a measured load spectrum has been defined, which accounts for load interaction effects.
2. The CSI appears to be a reasonably accurate measure for the relative severity of manoeuvre dominated fighter spectra.
3. The CSI is used as a standard tool in the RNLAFF-16 Fatigue Load Monitoring Programme.
4. The CSI-concept can also be successfully used in studies how to influence the operational fatigue life consumption.

#### 7. REFERENCES

1. Jonge, J.B. de: Monitoring Load experience of Individual Aircraft. Paper, presented at the 17th ICAS Congress, Stockholm, 1990.
2. Jonge, J.B. de: The analysis of Load-Time Histories by means of Counting Methods. In: AGARDograph nr 292. "Helicopter Fatigue Design Guide". 1983. ISBN 92-835-0341-4.
3. Koning, A.U. de: A simple crack closure model for Prediction of Fatigue crack growth rates under Variable Amplitude loading. NLR MP 80006 U, 1980.
4. Spiekhout, D.J.: Load Monitoring of F-16A/B Aircraft using a Smart Electronic Device. AGARD Conference Proceedings CP-506, December 1991.
5. Spiekhout, D.J.: Reduction of Fatigue Load Experience as Part of the Fatigue Management Program for F-16 Aircraft of the RNLAFF Paper presented during the 77th Meeting of the AGARD SMP, Bordeaux, September 1993.

## An Assessment of Fatigue Crack Growth Prediction Models for Aerospace Structures

A. Salvetti, L. Lazzeri, A. Pieracci  
 Department of Aerospace Engineering  
 University of Pisa  
 Via Diotisalvi 2 - 56126 Pisa  
 Italy

### SUMMARY

The current state of crack growth prediction models for aerospace applications is reviewed with special reference to limitations and possible improvements. The present work aims at examining the different crack growth prediction models with reference to effective application for practical use (i.e. with the objective of identifying the experimental data necessary to apply the model) and at quantifying the reliability of the different models. Both crack growth prediction models currently used by aerospace industries and prediction methods under development within the scientific community are considered. An experimental program has been carried out to help achieve the aforementioned objectives.

### LIST OF SYMBOLS

#### Latin Symbols

$a$  = crack length  
 $CA$  = Constant Amplitude  
 $f(x_i)$  = displacement at point  $x_i$  due to the nominal stress in the strip yield model  
 $g(x_i, x_j)$  = displacement at point  $x_i$  due to a unit stress applied at point  $x_j$  in the strip yield model  
 $K$  = Stress Intensity Factor  
 LEFM = Linear Elastic Fracture Mechanics  
 $L_i$  = length of the  $i$ -th element in the strip yield model  
 $OL$  = OverLoad  
 $R$  = ratio of minimum to maximum stress in the load cycle  
 $S$  = nominal stress  
 $UL$  = UnderLoad  
 $VA$  = Variable Amplitude  
 $V_i$  = vertical displacement of the  $i$ -th element in the strip yield model

#### Greek Symbols

$\Delta K$  = Stress Intensity Factor Range  
 $\sigma$  = local stress

#### suffixes

calc = calculated  
 eff = effective  
 exp = experimental  
 max = maximum  
 min = minimum  
 op = opening

### 1. - INTRODUCTION

After the introduction of 'damage tolerance' requirements, at first issued for USAF military aeroplanes [1] and subsequently also for commercial transport aircraft [2], the development of reliable methods for crack growth analysis under Variable Amplitude (VA) fatigue loading has become a crucial point for all aerospace industries. The application of a crack growth model is essential in the different phases of design, certification and operation of aeronautical and aerospace structures. From the point of view of industrial designers, the ideal method should obviously provide reliable predictions, be very easy to handle, should not require too many empirical constants (derived from specific tests) for its use and, lastly, should not require much computer time, because of its extensive use.

A flood of literature has been published in the last twenty years on this subject and has led to considerable understanding of certain problems associated with fatigue crack propagation, at least from a phenomenological point of view. Many methods have been developed and are available to the industrial designer, some of them are quite simple, but others are very complex. Anyhow, still insufficient help and information are too often provided to the user who, besides the general limits of applicability of the models, needs suggestions as to how to identify the most suitable model for his specific problem. Among other things, a very important piece of information for an industrial designer is knowing how far the results of his calculations depend on the scatter of the input data, as well as the sensitivity of the method to changes in the design variables, both in a qualitative as well as in a quantitative way. In a previous research, carried out at the beginning of the 80's [3], a systematic evaluation of the existing models was made. In the following sections, updated crack growth prediction methods are reviewed and evaluated, following the same logic approach, with the help of experimental results, some of which obtained from a specific test program and others from the literature.

### 2. - CRACK GROWTH PREDICTION METHODS

A number of excellent review papers on fatigue crack growth have been published recently; among others, mechanism aspects are well discussed in [4], while papers [5-8] are mostly devoted to the description and analysis of models.

Fatigue crack growth under CA loading is a well established phenomenon, typically analyzed with the use of Linear Elastic Fracture Mechanics (LEFM). On the contrary, the

predictor of fatigue crack growth under VA spectra is a much more complex matter. The basic assumption of the models based on LEFM is to postulate the possibility of correlating CA propagation data to VA loading histories through the identification of a similarity parameter, generally related to the stress intensity factor. Unfortunately, there are so many interaction effects between load cycles of different amplitudes that, even if some of them are quite well understood (at least from a phenomenological point of view), carrying out accurate quantitative predictions is still a formidable task. Among other things, just to quote only the most relevant ones, an ideal prediction model should simulate the following interaction effects:

- crack growth delay, following an overload,
- crack growth acceleration,
- delayed retardation,
- interaction between incompatible crack front orientations,
- development of shear lips,
- interaction with microstructural features (surface roughness)

It is quite clear that a single model should take all these effects into account and therefore it is easy to understand that both simple (but rough) and refined (but complex) methods have been proposed by many researchers.

According to the modelling of the mechanism that is considered to be responsible for the main interaction effects, crack growth prediction methods can be broadly classified in the following groups:

- Non-interaction assumption
- Characteristic K concepts
- Yield zone models
- Crack opening models
- Strip yield models

The simple linear calculation, developed first chronologically speaking, provides usually conservative results, often too conservative, since in a typical wing stress history retardation effects in general largely prevail over acceleration effects. Therefore, most of the methods have been developed to overcome the limited reliability of the non-interaction procedure. The various crack propagation methods are based upon the following two essential elements:

- (i) interaction modelling, i.e. how sequence effects are taken into account, including the selection of the key parameter and the definition of memory effects.
- (ii) how the effective current stress range and R ratio are related to crack increment (crack growth law)

### 2.1 Non-interaction assumption

The non-interaction assumption is based on the hypothesis that a stress intensity factor range occurring in a VA loading history produces the same crack increment as if it were part of a CA loading history. This assumption generally provides conservative predictions, which, depending on the load spectrum, may be often too much conservative. Using the non-interaction assumption, trend effects related to modifications of design variables are generally not predictable. Non-interaction calculations may be carried out in accordance with various crack growth laws or using an interpolation procedure through test data.

### 2.2 Characteristic K concept

It is assumed that it is possible to correlate crack growth in a VA load history with a characteristic stress intensity factor, depending on the spectrum and its stress level. This method is not, strictly speaking, a prediction method, but rather a similitude method useful when experimental data from similar load spectra are available. The results of the calculation, which

are sufficiently accurate in some cases [9-11], are in general sensitive to spectrum variations.

This method is typically applied for block spectra or random gaussian spectra, in the case of flight-by-flight spectra it is not widely used.

### 2.3 Yield zone models

Yield zone models were developed in the 70's in the United States and were the first attempt to take retardation effects after the application of an overload into account. They are based on the assumption that retardation is related to the dimension of the plastic zone created ahead of the crack tip by the preceding OI's. The amount of retardation, i.e. the difference in crack growth produced by the current cycle compared with the growth pertinent to the same cycle if it were part of a CA block, is related to the amount of propagation that is still necessary for the crack to reach the boundary of the plastic zone in which it is embedded. The first and most famous models developed according to these concepts were proposed by Wheeler [12] and Willenborg [13]. These models require as input data the yield stress of the material and CA crack growth data. The Wheeler model also needs an empirical constant, given by the operator as an input datum, which is in practice a parameter regulating the average retardation of the spectrum, it is usually obtained by fitting the model results to test data previously obtained under similar conditions (i.e. material, load spectrum, load severity, etc.).

These models, in practice, simulate only the retardation after OI effect, generally, they are considered as not being accurate, because the interaction modelling based only on plastic zone size evolution is insufficient for such a complex phenomenon. Many modified versions have been proposed for the Wheeler [14-16] as well as for the Willenborg [17-19] models, in an attempt to eliminate the need for an unknown fitting parameter (Wheeler model) and to take into account effects otherwise not predicted by such models, like multiple OI's interaction and UI effect. These updated versions are also based on the same modelling of crack growth mechanics.

Anyhow, they are extensively used by the aerospace industry, mainly due to their simplicity. In particular, since the designer must provide some test data in support of his analysis, whatever the model used, the fitting parameter of the Wheeler model, specific for the material, spectrum and crack interval examined, can be easily evaluated. On the other hand, the Generalized Willenborg model [17] is also quite simple to handle and generally provides conservative predictions, all these reasons justify its wide use in aerospace industries.

### 2.4 Crack opening models

The crack opening models work on the assumption, based on experimental evidence first provided by Elber [20,21], that not all the load excursion is active for propagation, but only a part of it. In particular, it is assumed that propagation takes place only when the crack is fully open, which occurs for a stress level above the minimum stress of the cycle. Such a stress level is named opening stress,  $S_{op}$ , and depends on the previous load history. According to such an assumption, only a part of the nominal stress intensity factor range is active for crack propagation and that part is named effective stress intensity factor range  $\Delta K_{eff}$  ( $\Delta K_{eff} = K_{max} - K_{op}$ ). The  $\Delta K_{eff}$  is considered to be the similarity parameter that allows correlation between CA and VA loading: a cycle of a VA history produces the same growth as a cycle of a CA history with the same  $\Delta K_{eff}$  value.

The various crack opening models available in the literature differ from each other in the interaction assumptions, i.e. how the material remembers the past stress history, as well as in the estimate of the parameters of the utilized crack growth law. The simplest model is the one proposed by Schijve [22],

who assumed that  $S_{op}$  remains constant during each flight of a flight-by-flight sequence. Other models have been proposed in recent years, the most interesting being those of Aliaga [23-25], of Baudin [26, 27] and of De Koning [28, 29]. Such models, considered the most promising ones, receive further attention in the present paper.

## 2.5 Strip yield models

Strip yield models are based on a discrete modelization of the Dugdale-Barenblatt [30, 31] strip yield model. According to the Dugdale assumptions, yielding is supposed to occur in a narrow strip ahead of the crack tip and on the crack flanks. The propagation of a crack interacting with its plastic wake, embedded in a far elastic field, is studied as a superimposition of two elastic problems (see fig. 1). This model has been discretized by many researchers [32-39] in order to study crack propagation through a discrete description of the crack flanks and of the plastic zone. Newman [36] discretized the material surrounding the crack with bars with elastic-perfect plastic behaviour. The problem is governed by the compatibility equations of the vertical displacements ( $V_i$ ) and lengths ( $L_i$ ) of the  $i$ -th bar elements, i.e.  $V_i = L_i \cdot \epsilon_i$  is equal to the residual deformation of the  $i$ -th bar element. The displacements can be determined from the superimposition of two elastic problems, such as

$$V_i = S \cdot f(x_i) + \sum_{j=1}^n \sigma_j \cdot g(x_i, x_j)$$

From the system of compatibility equations, a linear system follows, which can be resolved step-by-step, usually with the Gauss-Seidel method. The boundary conditions are that the  $j$ -th bar in the plastic zone ahead of the crack tip yields in tension at  $\sigma_j = \alpha \sigma_0$  while elements both on the crack flanks and in the plastic zone yield in compression for  $\sigma_j = -\sigma_0$ . If for the  $j$ -th element on the crack flanks  $\sigma_j$  is positive, then such an element is not in contact with its corresponding opposite element and it is posed  $\sigma_j = 0$ . Crack growth is modelled by disconnecting the bar elements ahead of the crack tip. Crack growth calculation is not carried out on a cycle-by-cycle basis, that would be too expensive, but for a fixed crack increment or number of cycles. It is assumed that the parameter  $\alpha$  makes it possible to take the effective three-dimensionality of the stress into account, i.e. the transition from plane strain to plane stress conditions. Calculations carried out by varying the constraint factor  $\alpha$  are reported to simulate the experimental plain strain-plain stress transition very well [39]. Due to the very long calculation time, this model is at present mainly utilized to verify assumptions used in simpler models, although interesting results for flight-by-flight histories have been published.

One of the main features of the model is the identification of the functions  $g(x_i, x_j)$  and  $f(x_i)$ ; Newman reported such functions for the centre crack tension specimen and for a crack emanating from a hole, but displacement functions for other geometries may be obtained from the open literature or using the weight function method [40]. Interesting results have also been obtained with such models in the analysis of short crack growth [40-42].

Strip yield models are still being developed in order to acquire a better definition of the physical meaning and evaluation of the parameter  $\alpha$ .

## 3.- DESCRIPTION OF THE MAIN CRACK OPENING MODELS

In the present investigation particular attention was devoted to the crack opening models, therefore in the following

the PREFFAS, ONERA and CORPUS models are briefly described.

### 3.1 The PREFFAS model

The PREFFAS model [23-25] was devised by Aliaga, Davy and Schaff of Aerospatiale in 1985. The model was proposed for short load sequences, i.e. such that the crack grows inside the plastic zone generated by the highest peak of the block. The authors claimed accurate predictions for simple VA as well as for complex flight-by-flight load histories. Rain-flow effects for the  $S_{max}$ - $S_{op}$  sequence are also considered.

#### 3.1.1 Load interaction modelling

The effect of the previous load history is taken into account, considering that each previous peak produces an opening level, which can be estimated by relating it to the lowest trough included between the peak considered and the current cycle (see fig. 2). The opening stress of the current cycle is the highest opening stress calculated by considering all the previous peaks, utilizing the opening function described below.

The model was originally proposed for short spectra and assumes that the plastic zone associated with the highest peak in the spectrum is dominant, i.e. the boundary of the plastic zone associated with the current cycle never exceeds the maximum extension of the plastic zone. The model evaluates the interaction effects by taking only stress levels and cycle sequence into account. Compressive stresses are set equal to zero.

#### 3.1.2 Opening function

The function that expresses the ratio of the effective stress intensity factor range to the nominal one is supposed to be linear in  $R$ , i.e.  $U(R) = A + B \cdot R$ , the constants  $A$  and  $B$  must be obtained experimentally for each material and thickness. The authors also provide a recommended test procedure to obtain such constants, which cannot be derived through standard crack opening measurements.

#### 3.1.3 Crack propagation law

The crack propagation law, proposed by the authors, is an Elber type law in  $\Delta K_{eff}$ , i.e.  $da/dN = C (\Delta K_{eff})^m$ . Due to the short length of the typical spectrum, the crack length can be considered to be constant during the application of one block. Because of this, the crack growth in a block can be expressed by  $f(a) \cdot \Sigma (\Delta S_{eff})^m$ , where the stress dependent term has the same value for each block, except the first one, where the regime of opening stresses is not yet stable. Therefore, it is much more convenient to evaluate crack growth on a block-by-block basis, rather than on a cycle-by-cycle basis.

#### 3.1.4 Experimental tests needed to apply the model

There are four material dependent parameters to be obtained for applying the method  $A$  and  $B$  for the opening function,  $C$  and  $m$  for the propagation law. CA tests at different  $R$  ratios as well as a block test (1000 cycles with  $R=0.1$  plus a cycle with the same minimum stress level but maximum stress level equal to 1.7 times the maximum stress level of the CA block) must be performed. The latter test is supposed to introduce some correction for OI interaction effects [43] and is fundamental in obtaining the constants  $A$  and  $B$ , values for such constants are given by the authors for 2024-T3 and -1351 (for different thicknesses), 7075, 7010 and 7050 with -16 and -17 heat treatment conditions.

### 3.2 The ONERA model

This model was originally devised by Baudin and Robert of ONERA in 1981 [26], while some modifications were presented in 1984 [27]. The model was proposed for flight-by-flight load histories and initially applied to 2024-T3.

### 3.2.1 Load interaction modelling

The effect of the previous load history is considered through the definition of an equivalent load cycle, based on an appropriate algorithm, such cycle keeps memory of all the previous load history. Plane strain-plane stress transition is taken into account by means of a relationship with the ratio of the Irwin plastic zone size to the thickness of the material. A thickness effect is also considered through a relaxation of the influence of  $K_{min}$  on the interaction rule.

### 3.2.2 Opening function

The opening stress is obtained as a weighted average of two opening function values: the first one is referred to CA load histories (considered to be a particular case of multiple OLs) and the second one for single OL effect. The weight parameter was defined as a fitting parameter when the model was first published [26] and later related to spectrum severity, [27]. The authors obtained the opening functions for 2024-T3 experimentally, in plane stress conditions, [26].

### 3.2.3 Crack propagation law

The suggested crack propagation law is an Elber type one, i.e.  $da/dN = C (\Delta K_{eff})^m$

### 3.2.4 Experimental tests needed to apply the model

To apply the model the opening functions for single OL and for the CA case are needed, as well as the parameters C and m for the crack propagation law. For the evaluation of the C and m constants, the authors use the results of R=0 CA tests.

## 3.3 The CORPUS model

The CORPUS model was proposed by De Koning of NLR in 1981 [28, 29]. At present, the model is considered the most sophisticated and accurate crack opening model. It is based on fractographic observations of crack growth surfaces, which provide support for the hypothesis of a mechanism of plasticity left in the wake of a growing crack. The model is also implemented in the ESACRACK software for crack growth predictions.

### 3.3.1 Load interaction modelling

The interaction is based on the modelling of the behaviour of the plastic zone wake of a crack. Each stress peak is assumed to create a ridge on the crack flanks. The crack is considered to be completely open when the last ridge loses contact; the corresponding stress level is the opening stress for that crack length. The minimum stress of each cycle flattens the existing ridges, i.e. reduces the opening stress level. Each ridge is considered to be active in the determination of the dominating opening stress as long as the crack tip is embedded in the plastic zone of the peak that generated it. Multiple OL effects are taken into account through an experimental relationship. Plane strain-plane stress transition is considered only as far as the dimensions of the plastic zone size are concerned. The effects on the opening level of secondary plastic zones, i.e. plastic zones developing in already stretched material, are also modelled.

### 3.3.2 Opening function

The opening function is based on experimental measurements and also takes the effect of maximum stress into account, the importance of this was pointed out by Newman [36] with the use of the strip yield model and finite element calculations. The same function, relevant to plane stress conditions, is assumed to be applicable for 2024-T3 and 7075-T6 aluminum alloys.

### 3.3.3 Crack propagation law

The suggested crack propagation law is an Elber-type one, i.e.  $da/dN = C (\Delta K_{eff})^m$

### 3.3.4 Experimental tests needed to apply the model

Experimental tests with CA loading at different R values are necessary to obtain the crack propagation law parameters for the material and the thickness under examination, as well as the opening function.

## 4. - EXPERIMENTAL PROGRAM

An experimental program was carried out to support the analysis of the models. The material used was Alclad 2024-T3, 2.54 mm thick, tested in the longitudinal (L-T) orientation. CA tests as well as VA (flight-by-flight spectrum and simple flight simulation spectrum) tests were performed. It was decided to investigate the 'gust-dominated' spectra, typical of transport aircraft, to begin with, but in the follow-on part of the research other spectra will be used.

In particular, simplified flight simulation spectra, similar to those used by Schuyve and Misawa [44], were used, as well as more realistic load sequences, like MiniTWIST [45] and the flight-by-flight wing root design loading history of a medium-range executive aircraft, [46].

### 4.1 Fatigue test apparatus

Two different servohydraulic fatigue machines were used, with capacities of 50 kN and 200 kN, respectively. Each test was completely controlled by a PC, programmed to monitor the load generation and to acquire the crack length measurements at regular intervals, by means of the direct current potential drop technique. The 200 kN machine was used for the executive aircraft flight-by-flight load sequence and for some CA tests. All the other tests were performed on the 50 kN machine.

Centre cracked panel specimens were used, of different width in the central section: all the CA tests and the VA tests under executive aircraft spectrum were carried out on specimens 160 mm wide, while all the MiniTWIST tests and simple flight-simulation tests were carried out on 100 mm wide specimens. The length of the test section was at least equal to twice the width. The initial notch was introduced by means of a jeweller's saw and a natural fatigue crack was nucleated, under a proper CA load, up to 3 mm for narrow specimens and 4 mm for large specimens, then the tests started. Anti-buckling guides were used in all cases.

A detailed description of the tests and of the results obtained can be found in [47].

### 4.2 CA tests

The CA tests were carried out at four different R ratio values (R=0.4, 0.1, 0.4, 0.65). For the analysis of predictions relevant to gust dominated spectra, it was considered of great importance to obtain CA crack growth data also in the low stress intensity factor region. Therefore, some tests were carried out using the load-shedding technique (AK decreasing).

The results obtained are reported in fig. 3; transition points in the  $da/dN$  vs.  $\Delta K$  plot are clearly visible and all the results are consistent with similar results in the literature, [48].

### 4.3 Simple VA tests

Simple VA tests were carried out with simple block spectra, with the aim of obtaining experimental data for situations where only a specific interaction effect was active, a deliberately exaggerated situation. More in particular, the simple VA spectra used were:

(a) the block spectrum required for obtaining the data for the application of the PRELFEAS model. Two tests were carried out, using different maximum stresses of the CA cycles: 56 MPa and 90 MPa.

- (b) a sequence of 200 cycles, starting with a UL - OL (-45 MPa, 110 MPa), while the remaining cycles were a CA sequence (45 MPa, 85 MPa);
- (c) a sequence of 200 cycles, identical to the previous one except that this time the second, the third and the fourth peaks were also set equal to the overload (110 MPa)

The results obtained are reported in fig. 4 in terms of crack length as a function of the number of blocks.

**4.4 Flight-by-flight tests**

Two flight-by-flight load histories were used in the test program: the MiniTWIST and an executive aircraft spectrum. While the first one is a well-known standard spectrum, some comments are worthwhile for the second spectrum, which is characterized by relatively few interaction effects, a light ground stress (about 0.3 times the mean flight stress) and short flights (in average, about 11 cycles per flight: the total length was about 32000 cycles for 3382 flights). Different stress levels, representative of actual operating situations, were used: the MiniTWIST tests were performed for  $S_{lg} = 60, 65$  and  $70$  MPa (3, 6 and 3 tests, respectively), and three stress levels were also used for the executive aircraft spectrum,  $S_{max} = 160, 180$  and  $200$  MPa (1, 4 and 1 tests, respectively). The tests results are reported in figs. 5 and 6.

**5. - ANALYSIS OF THE PREDICTIONS OF THE CRACK OPENING MODELS**

**5.1 Main purpose and objectives of the analysis**

In the past, interesting reviews of crack propagation models have been published [5-8]. The models have been examined in detail, as well as their ability to qualitatively and quantitatively predict certain physical phenomena: single and multiple OL, UL effects, effect of high nominal stresses, plane strain - plane stress transition, delayed retardation, etc. A summary of these analyses, from [5], is to be found in tab. 1.

In the present investigation, particular attention is paid to the evaluation of existing models, carried out through an homogeneous set of test data, obtained both under CA and VA load spectra, and to the assessment of the reliability of the models and their dependence on input data. Crack growth predictions were carried out using input data from the literature (an interesting survey is to be found in [49]) and compared with the results of the predictions carried out on the basis of the CA data obtained in the present test program, this allows a better assessment of the capabilities of the various models and the evaluation of the scatter in the accuracy and reliability of the predictions in the two cases.

As far as the assessment of the reliability of the models is concerned, following the methodology already developed in [3], the ratio  $N_{exp}/N_{calc}$  for a fixed crack growth interval has been evaluated and considered as a random variable assumed to have a log-normal distribution. The median value and the standard deviation of  $N_{exp}/N_{calc}$  may provide more useful information on the predictive ability of the model. A model is commonly classified as "acceptable" when the value of the ratio  $N_{exp}/N_{calc}$  falls within the 0.5 - 2.0 range, [8]. However, the evaluation of a model on this basis only may lead to errors if there is the possibility of self compensating mistakes (e.g. deceleration in the first part of the propagation and acceleration in the final part). To overcome such a setback, the comparison of the experimental to the predicted crack growth rate for the two flight-by-flight load histories was also considered.

The use of different spectra should increase confidence in the evaluation; from this point of view, research is still in progress and will be extended to other load spectra, all belonging to the same group of "transport aircraft" spectra, with similar interaction effects.

**5.2 Determination of experimental parameters for the application of models**

Computer programs were implemented, in accordance with the original references, and checks were made against results in the literature. In the case of the CORPUS model, an interpolation algorithm was also set up, as an alternative to the use of an Elber-type law. The reason for this choice stems from the observation that crack growth under a "gust dominated" spectrum is the result of the application of many small load cycles, which correspond to crack growth rates in the medium-to-small range, below the field of validity of the linear relationship of the Elber law. Therefore, the use of an interpolation procedure seems to be a better solution and is usually adopted by many computer codes which are commercially available, its extension to the other opening models is in progress.

The parameters of the Elber-type equation are obtained by fitting the opening functions used by the models to the experimental data collected in the CA tests. It was necessary to select a given range of data, since the linear behaviour in a log-log plot is relevant only to the Paris region. Sensitivity tests were carried out, by varying the range of crack growth rates considered for the evaluation of the parameters C and m. It is worthwhile pointing out that the related variations of C and m may be such to influence considerably the models predictions. This fact highlights the need for a clear and well-defined procedure to obtain the values of the constants of the crack propagation law from test data for a correct prediction (in the sense of consistency with the model logic structure). Therefore, the data relevant to crack growth rates included between  $10^{-4}$  and  $10^{-3}$  mm/cycle were selected. The following constants were obtained (units: MPa $\sqrt{m}$ , mm/cycle)

- ONERA model  $m=2.857, C=9.415 \times 10^{-7}$ ,
- PREFFAS model  $m=2.780, C=6.327 \times 10^{-7}$ .

while from data in the literature, it was assumed

- CORPUS model ([31,51])  $m=3.7, C=1.26 \times 10^{-7}$ ,
- ONERA model ([29])  $m=3.0, C=8.92 \times 10^{-7}$ ,
- PREFFAS model  $m=3.7, C_1=1.5364 \times 10^{-8}$  for  $R=0.1$  ([49]), opening function constants  $A=0.56$  and  $B=0.44$  ([25]), hence  $m=3.7, C=9.92 \times 10^{-8}$ .

As far as the PREFFAS model is concerned, this method would prove not to be strictly applicable for the material and the thickness under examination according to [23-25], one should find that the experimental data from  $R=0.1$  and  $R=0.1$  plus OL tests provide two parallel data fit lines on a  $da/dN$  -  $\Delta K$  log-log graph, but that was not obtained in the present case, as may be observed from fig. 7. Therefore, following the logic approach of the model, the values suggested by the model's authors were used for the constants A and B, while the slope m was given the value pertinent to CA tests with  $R=0.1$ , C is derived from the A, B and m values.

**5.3 Comparison of the experimental and analytical crack growth predictions**

The first point taken into consideration is the influence of input data on predictions. Figs. 8 show some of the results for flight-by-flight spectra, only one stress level, i.e. the one with the greater number of test curves, was selected. As can be seen, the effect of the input parameters for the description of the crack growth law is different, according to the model taken into consideration. As far as the CORPUS model is concerned, the effect is negligible, notwithstanding the fact that, as far as the input of data from the literature (LD in the figs.) is concerned, an Elber law was used, while an interpolation procedure was used for the present test data (TD) input. On the contrary, for the PREFFAS model considerable improvements in the

accuracy of the predictions can be observed for all the spectra considered, using the material constants obtained according to the above mentioned procedure. Instead, the predictions obtained by means of the ONERA model, in the case of simple VA loading, show a noteworthy decrease in accuracy, even though for these spectra they were already poor. Calculations, carried out in the course of the investigation but not reported in this paper, showed this method is particularly sensitive to the crack growth law: the use of a best-fit Elber law obtained on data relevant to crack growth rates up to  $10^{-2}$  mm/cycle resulted in considerable prediction differences. This was attributed to the change in the slope of the best-fit line that produces differences in the evaluation of the crack growth for small  $\Delta K_{eff}$ , which very often occur in a "gust dominated" spectrum. Besides, differences in crack increments are also related to differences in the memory effects.

For a deeper understanding of the relevant merits of the three opening models, a comparison was made between predictions and test results as far as the average crack growth rate in a block, as a function of crack length, is concerned. Figs. 9 show some of the results: it is clearly evident that predictions based on present test data (TD) are slightly closer to the experimental data than those obtained using data from the literature data (LD). Fig. 9a, relevant to the MiniTWIST spectrum with  $S_{lg} = 65$  MPa, is particularly interesting. CORPUS predictions are the only ones capable of following the trend of the experimental results, while all the other methods predict an average crack growth rate which increases linearly in a log plot. Therefore, for small crack lengths such methods under-estimate the growth rate, while for large crack lengths the opposite occurs: in other words, compensating mistakes may occur in the evaluation of the number of flights required for a given crack growth interval.

As far as the executive aircraft spectrum is concerned, as already specified, it has certain characteristics that make it different from the others: relatively few interaction effects, a light ground stress and short flights. As a consequence, the maximum peak in the spectrum completely controls the opening stress evolution. The logic of most models recognizes the features of such a spectrum as being similar to those of a block spectrum; this is mainly the reason why the CORPUS predictions are less similar to test data than in the case of the MiniTWIST spectrum, fig. 9c.

The simplified VA spectra had been chosen in a manner that proved to be too 'mild': the delay effect was too small and the tests were almost completely CA tests. It is interesting to note that also in this case CORPUS predictions are not very accurate, fig. 9d, in these tests the crack grows for a long period in plane strain conditions.

The aeronautical industry mainly requires crack growth models for the assessment of inspection intervals: it is quite important for a model to provide estimates that are independent of spectrum and crack interval. Therefore, the use of log-normal plots of the random variable  $N_{exp}/N_{calc}$  for a selected interval was considered to be useful for a practical evaluation of the reliability of crack growth models. Two intervals were selected: (a) from the initial crack length to 12 mm and (b) from the initial crack length to 25 mm. A number of results are shown in figs. 10. It is important to point out that PREFAS model results show the lowest scatter and a reasonably log-normal distribution, while the results of CORPUS do not seem to belong to a unique distribution. For comparison, data from [49] are also shown, such results are from various spectra (included MiniTWIST, F27, FALSTAFF, and their variations, all of them for different stress levels) and refer to crack growth intervals different from those considered in this paper. These results are much better than the present ones, both from the point of view of the mean value and the scatter. Anyhow, the present results relevant to the MiniTWIST spectrum are quite consistent with

literature data, while the results from the other spectra seem to belong to a different distribution. A possible reason for this behaviour is assumed to be that such results refer to tests where the crack propagated for a long period in plane stress conditions, which is a situation where the CORPUS model works very well.

The results relevant to the Generalized Willenborg model are shown in fig. 10d, in general, the predictions are conservative and the scatter of the results of this rather simple model is not higher than the one of other models.

#### 5.4 Some simple modifications to the models

Some modifications were made to the models to assess the possibility of extending their capabilities or in an attempt to improve their accuracy.

In particular, the PREFAS program was modified, as already done in [49], in order to take each of the following aspects into account separately:

- (a) disregarding the effects of rain-flow on the  $S_{eff}$  history;
- (b) extreme simplification of the memory effect by keeping the opening stress constant in the whole spectrum, relating the max peak to the minimum stress, which is posed by the model equal to zero.

The modifications introduced did not produce significant changes in the results, as shown in fig. 11, relevant to the MiniTWIST spectrum,  $S_{lg} = 65$  MPa, where the predictions relevant to the modifications are scarcely distinguishable. The conclusion is that such modifications are of little help, because the model contains certain semi-empirical constants that allow a balancing of over- and under-estimates in various parts of the spectrum.

The CORPUS model is the one that receives most credit since it is able to simulate most of the interaction effects. The results of the present investigation revealed a certain lack of accuracy in those cases where a large part of the crack growth occurs in plane strain conditions. The spectra used in the test program are quite 'mild', which has delayed the transition to plane stress conditions. The original CORPUS model takes the transition into account only by varying the size of the plastic zone; in this way, the initial part of the crack growth curve undergoes a small adjustment but does not follow too faithfully the test curve. In the attempt to obtain a better prediction in this area, and following indications of recent papers by Newman [36] and Wang [50], a modification was introduced in the computer program by changing the condition relevant to the beginning and completion of the transition, which is expressed by two values of  $\Delta K_{eff}$  and by using a specific opening function for plane strain conditions, namely the one proposed in [51]. A number of results are shown in fig. 12: an appreciable influence can be observed, which indicates that this is an important point.

## 6 - SUMMARY AND CONCLUSIONS

A research program is in progress at the Department of Aerospace Engineering of the University of Pisa concerning the assessment of currently available crack growth prediction methods. The experimental part of the research is carried out on 2024-T3 Alclad alloy; test results under CA and VA loading have been obtained, to be used as a test case for the models. Particular attention has been devoted to the models based on the crack opening phenomenon and in some cases attempts have been made to modify those aspects, which are supposed not to be covered adequately by the models.

In particular, the following is a summary of our conclusions:

- (a) CA test results obtained in the present investigation are fairly consistent with similar results available in the literature,

(b) the influence of the use of present test data instead of data in the literature is relatively small in the case of CORPUS, while the changes in the predictions obtained with PREFFAS have shown the importance of the range of data selected for obtaining the constants C and m;

(c) the CORPUS model, mainly for the MiniTWIST spectrum but to a minor extent for other spectra, too, is capable of providing the same trend of crack growth rates in relation to crack length as the test data, this is attributed to the more complex logic of CORPUS and is better simulated in the case of spectra with a short period of plane strain conditions;

(d) a relatively simple method, like PREFFAS, is able to provide the industrial designer with virtually good estimates of crack growth interval ratios, in a significant range of spectrum and stress level;

(e) the Generalized Willenborg model, still widely used, even though based on a rough modelling of the crack growth phenomenon, provides in general conservative results, with a scatter not larger than the one of the other methods. Similar conclusions can be drawn for the Wheeler model, which is not, strictly speaking, a 'prediction' method, since it needs to be tuned on the basis of the results of some tests, which anyhow must always be carried out to validate the analysis;

(f) some simple modifications have been made to PREFFAS, with negligible effects on the predictions;

(g) the transition from plane strain to plane stress conditions seems to play an important role, a better description should be introduced in the models, since its effect is important, particularly for 'mild' spectra.

#### ACKNOWLEDGEMENT

The authors gratefully acknowledge the contributions made to this paper by two final-year students Mr. M. Sacchi for the test activity and Mr. A. Verdi for the analysis of data.

#### 7. - REFERENCES

- [1] Anon, 'Airplane Damage Tolerance Requirements', Military Specification MIL-A-83444, U.S. Air Force Aeronautical Systems Division, 1974
- [2] Anon, 'Damage tolerance requirements FAR-25.571', in 'Federal Aviation Requirements, Part 25: Large Aeroplanes', 1978
- [3] Salvetti, A., Cavallini, G. and Lazzeri, L., 'The fatigue crack growth under variable amplitude loading in built-up structures', Final Technical Report, European Research Office, U.S. Army, London, April 1982
- [4] Davidson, D.I. and Lankford, I., 'Fatigue crack growth in metals and alloys: mechanisms and micromechanics', *Internat. Materials Reviews*, vol. 37, No. 2, pp. 45-76, 1992
- [5] Wanhill, R.J.H. and Schijve, J., 'Current status of flight simulation fatigue crack growth concepts', in *Fatigue Crack Growth Under Variable Amplitude Loading*, J. Petit et al. eds., pp. 326-339 (also NLR MP 88001 U), 1988
- [6] Heuler, P. and Schuetz, W., 'Fatigue life prediction in the crack initiation and crack propagation stages', in *Durability and Damage Tolerance in Aircraft Design*, Proc. of the 13th ICAF Symposium, Pisa, G. Cavallini and A. Salvetti eds., EMAS Ltd., Warley, pp. 33-69, 1985
- [7] Schijve, J., 'Fatigue crack closure observations and technical significance', in *Mechanics of Fatigue Crack Closure*, ASTM STP 982, J.C. Newman Jr. and W. Elber eds., pp. 5-34, 1988
- [8] Schijve, J., 'Fatigue crack growth predictions for variable-amplitude and spectrum loading', Delft Un. of Technology, Faculty of Aerospace Eng., Report I.R-537, 1987.
- [9] Gallagher, J.P., 'Steady-state fatigue crack growth rate behaviour', in *Fracture Mechanics*, The University Press of Virginia, Charlottesville, pp. 541-577, 1978.
- [10] Wanhill, R.J.H., 'Engineering application of fracture mechanics to flight simulation fatigue crack propagation', in *Fracture Mechanics in Engineering Applications*, Sijthoff and Noordhoff International Publishers, Alphen aan den Rijn, pp. 241-250, 1979.
- [11] Wanhill, R.J.H., 'Fatigue fracture in landing gear steels', in Proc. of the 15th ICAS Congress, paper ICAS-86-4 9 3, AIAA, New York, pp. 1347-1355, 1986.
- [12] Wheeler, O.E., 'Spectrum loading and crack growth', *J. Basic Eng.*, Trans. of ASME, vol. 94D, pp. 181-186, 1972.
- [13] Willenborg, J.D., Engle, R.M. and Wood, H.A., 'A crack growth retardation model using an effective stress concept', Report AFFDL-TM-71-1-FBR, Air Force Flight Dynamics Laboratory, Dayton, January 1971.
- [14] Pinckert, R.E., 'Damage tolerance assessment of F-4 aircraft', AIAA Aircraft Systems and Technology Meeting, AIAA paper No 76-904, 1976
- [15] Broek, D. and Smith, S.H., 'Spectrum loading fatigue-crack growth predictions and safety factor analysis', NADC-76383-30, Naval Air Development Center, 1976
- [16] Gray, T.D. and Gallagher, J.P., 'Predicting fatigue crack retardation following a single overload using a modified Wheeler model', in *Mechanics of Crack Growth*, ASTM STP 590, pp. 331-344, 1976
- [17] Gallagher, J.P., 'A generalized development of yield zone models', Report AFFDL-TM-74-28-FBR, Air Force Flight Dynamics Laboratory, Dayton, January 1974
- [18] Chang, J.B., Engle, R.M. and Stolpestad, J., 'Fatigue crack growth behaviour and life predictions for 2219-T851 aluminium subjected to variable-amplitude loading', in *Fracture Mechanics Thirteenth Conference*, ASTM STP 743, pp. 3-27, 1981
- [19] Johnson, W.S., 'Multi-parameter yield zone model for predicting spectrum crack growth', in *Methods and Models for Predicting Fatigue Crack Growth Under Random Loading*, ASTM STP 748, pp. 85-102, 1981
- [20] Elber, W., 'Fatigue crack closure under cyclic tension', *Eng. Fract. Mech.*, Vol. 2, pp. 37-45, 1970
- [21] Elber, W., 'The significance of fatigue crack closure', in *Damage Tolerance in Aircraft Structures*, ASTM STP 486, pp. 230-247, 1971
- [22] Schijve, J., 'Prediction methods for fatigue crack growth in aircraft materials', in *Fracture Mechanics Twelfth Conference*, ASTM STP 700, pp. 3-34, 1980
- [23] Ahaga, D., 'Prevision de la fessuration en fatigue sous chargements d'amplitude variable, Modèle PREFFAS', *Aérospatiale Laboratoire Central*, Doc. PV. No. 47 904, 1985

- [24] Aliaga, D., Davy, A. and Schaff, H., 'A simple crack closure model for predicting fatigue crack growth under flight simulation loading', in *Durability and Damage Tolerance in Aircraft Design*, Proc. of the 13th ICAF Symposium, Pisa, G. Cavallini and A. Salvetti eds., EMAS Ltd., Warley, pp. 605-630, 1985.
- [25] Aliaga, D., Davy, A. and Schaff, H., 'A simple crack closure model for predicting fatigue crack growth under flight simulation loading', in *Mechanics of Fatigue Crack Closure*, ASTM STP 982, pp. 491-504, 1988.
- [26] Baudin, G. and Robert, M., 'Crack growth model for flight type loading', in *Aircraft Fatigue in the Eighties*, Proc. of the 11th ICAF Symposium, Noordwijkerhout, J.B. de Jonge and H.H. van der Linden eds., NLR, 1981.
- [27] Baudin, G. and Robert, M., 'Crack growth life-time prediction under aeronautical type loading', in *Life Assessment of Dynamically Loaded Materials and Structures*, Proc. of the 5th European Conf. on Fracture, Lisbon, pp. 779-792, 1984.
- [28] De Koning, A.U., 'A simple crack closure model for prediction of fatigue crack growth rates under variable amplitude loading', in *Fracture Mechanics (Thirteenth Conference)*, ASTM STP 743, pp. 63-85, 1981.
- [29] De Koning, A.U. and Van der Linden, H.H., 'Prediction of fatigue crack growth rates under variable loading using a simple closure model', *Aircraft Fatigue in the Eighties*, Proc. of the 11th ICAF Symposium, Noordwijkerhout, J.B. de Jonge and H.H. van der Linden eds., NLR, (also NLR MP 81023), 1981.
- [30] Dugdale, D.S., 'Yielding of steel sheets containing slits', *Journal of the Mechanics and Physics of Solids*, Vol. 8, pp. 100-104, 1960.
- [31] Barenblatt, G.I., 'The formation of equilibrium cracks during brittle fracture, general ideas on hypothesis, axially-symmetric cracks', *PMM*, Vol. 23, no 3, pp. 434-444, 1959.
- [32] Dill, H.D. and Saff, C.R., 'Spectrum crack growth prediction method based on crack surface displacement and contact analyses', in *Fatigue Crack Growth Under Spectrum Loads*, ASTM STP 595, pp. 306-319, 1976.
- [33] Seeger, T., 'Ein Beitrag zur Berechnung von statisch und zyklisch belasteten Risscheiben nach dem Dugdale-Barenblatt Modell', Report No 21 of the Institut für Statik und Stahlbau, T.H. Darmstadt, 1973.
- [34] Fuehring, H., and Seeger, T., 'Dugdale crack closure analysis of fatigue cracks under constant amplitude loading', *Eng. Fracture Mech.*, Vol. 11, pp. 99-122, 1979.
- [35] Fuehring, H. and Seeger, T., 'Structural memory of cracked components under irregular loading', in *Fracture Mechanics (Eleventh Conference)*, ASTM STP 677, pp. 144-167, 1979.
- [36] Newman, J.C., Jr., 'Prediction of fatigue crack growth under variable-amplitude and spectrum loading using a closure model', in *Design of Fatigue and Fracture Resistant Structures*, ASTM STP 761, pp. 255-277, 1982.
- [37] De Koning, A.U. and Liefing, G., 'Analysis of crack opening behaviour by application of a discretized strip yield model', in *Mechanics of Fatigue Crack Closure*, ASTM STP 982, pp. 437-458, 1988.
- [38] Wang, G.S. and Blom, A.F., 'A modified Dugdale-Barenblatt model for fatigue crack growth predictions under general load conditions', *The Aeronautical Research Institute of Sweden*, Report FFA TN 1987-79, 1987.
- [39] Newman, J.C., Jr., 'Effects of constraint on crack growth under aircraft spectrum loading', in *Fatigue of Aircraft Materials*, Beukers, A. et al. eds., Delft Un. Press, pp. 83-112, 1992.
- [40] Wang, G.S. and Blom, A.F., 'A strip yield model for fatigue crack growth predictions under general load condition', *Engng. Fract. Mech.*, Vol. 40, No. 3, pp. 507-533, 1991.
- [41] Newman, J.C., Jr., 'A non linear fracture mechanics approach to the growth of small cracks', *AGARD-CP-328*, paper 6, 1982.
- [42] Newman, J.C., Jr., Phillips, E.P. and Swain, M.H., 'Predicting the growth of small and large cracks using a crack closure model', *Int. Conf. on Mechanical Behaviour of Materials*, ICM5, Beijing, P.R.C., 1987.
- [43] Schijve, J., 'An evaluation of a fatigue crack growth prediction model for variable-amplitude loading (PREFFAS)', *Delft Un. of Technology, Faculty of Aerospace Eng.*, Report LR-537, 1987.
- [44] Misawa, H. and Schijve, J., 'Fatigue crack growth in aluminium alloy sheet material under constant-amplitude and simplified flight-simulation loading', *Delft Un. of Technology, Dept. of Aerospace Eng.*, Report LR-381, 1983.
- [45] Lowak, H., De Jonge, J.B., Franz, J. and Schutz, D., 'MiniTWIST, a shortened version of TWIST', *National Aerospace Laboratory, The Netherlands*, NLR MP 79018 (also LBF Report TB 146), 1979.
- [46] Lanciotti, A., and Lazzeri, L., 'Effects of spectrum variations on fatigue crack growth', *Int. J. Fatigue*, Vol. 14, pp. 319-324, 1992.
- [47] Lazzeri, L. and Piccirilli, A., 'Fatigue crack growth in Alclad 2024-T3 sheets results of a test program', *ADIA report*, Dept. Aerospace Engng., Univ. Pisa, to be published.
- [48] Wanhill, R.J.H., 'Low stress intensity fatigue crack growth in 2024-T3 and T351', *National Aerospace Laboratory, The Netherlands*, NLR MP 87001, 1987.
- [49] Padmanidana, U.H., 'Investigation of crack-closure prediction models for fatigue in aluminium alloy sheet under flight-simulation loading', *ph. D. thesis*, Delft Univ. of Technology, Faculty of Aerospace Engng., (also Report LR-619), 1990.
- [50] Wang, G.S., Palmberg, B. and Blom, A.F., 'Stress state-related fatigue crack growth under spectrum loading', *Fatigue Fract. Engng. Mater. Struct.*, Vol. 15, No. 7, pp. 695-712, 1992.
- [51] De Koning, A.U., 'A simple crack closure model for prediction of fatigue crack growth rates under variable amplitude loading', *NLR MP 80006 U*, 1980.

MODEL	SINGLE OVERLOAD	MULTIPLE OVERLOAD	OVERLOAD INTERACTION	SINGLE UNDERLOAD	MULTIPLE UNDERLOADS	PREDICTION OF CRACK ARREST	PREDICTION OF NON-STATIONARY CRACK GROWTH	PLANE STRAIN - PLANE STRESS TRANSITION		EFFECT OF HIGH $\sigma/\bar{\sigma}$
								EFFECT OF THICKNESS	RETARDATION REGION AND YIELD LIMIT	
SCHIJVE, [22]	-	+	-	-	+	-	-	-	-	-
DE KONING [28]	+	+	+	+	-	+	-	+	+	+
BAUDIN, [27]	+	+	+	+	-	+	+	+	-	-
ALIAGA, [24]	+	-	-	+	-	+	-	-	-	-
+ = SATISFACTORY / GOOD      - = NOT CONSIDERED / POOR										

Tab. 1 - Comparison of various crack opening models, from [5].

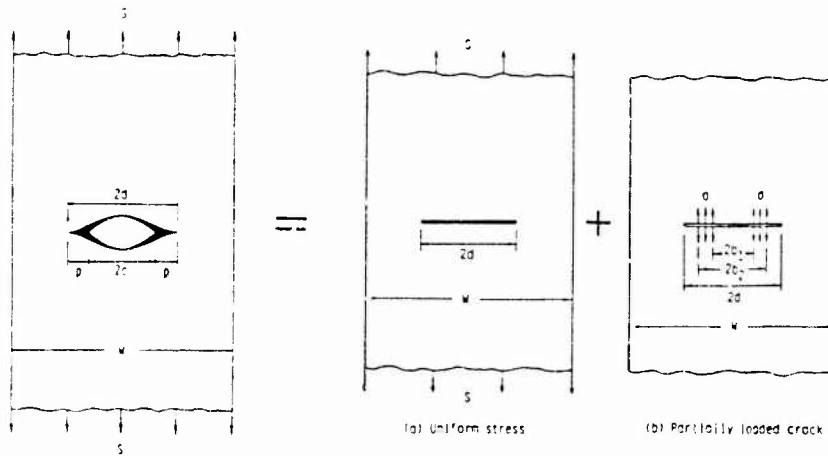


Fig. 1 - Superposition of the two elastic stress fields for the strip yield model analysis, from [3C].

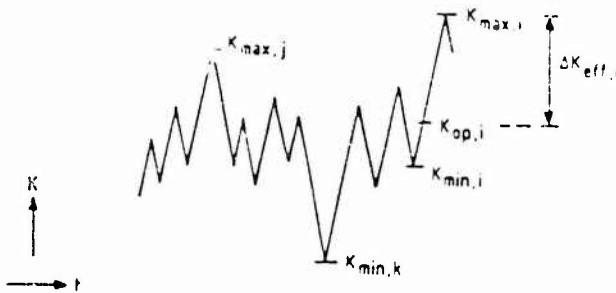


Fig. 2 - Previous cycles effects on the current opening stress according to the PREFAS model, from [43]

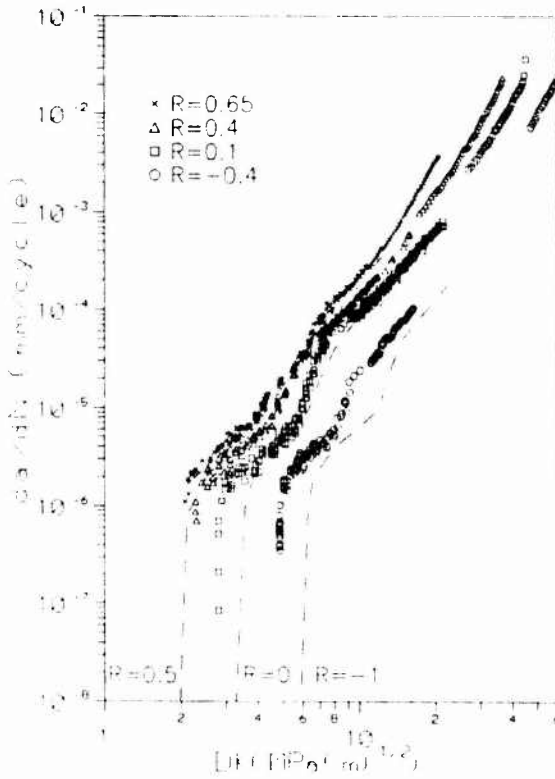


Fig 3 - Results of the CA loading tests - Dashed lines refer to test data in [48]

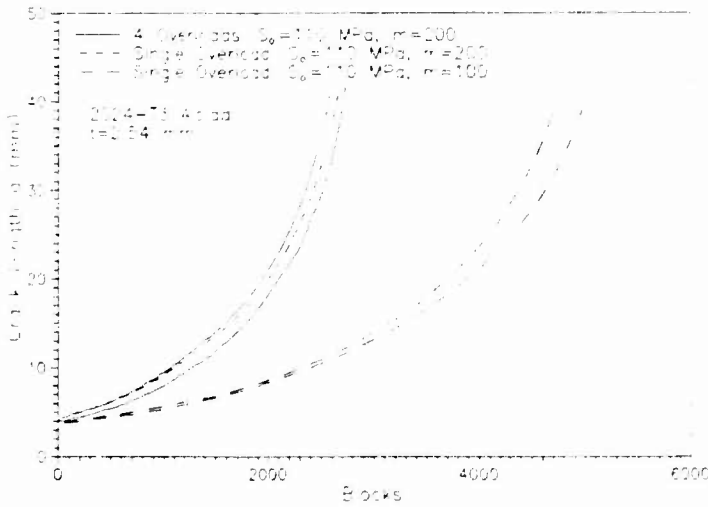


Fig 4 - Results of the simple VA loading tests

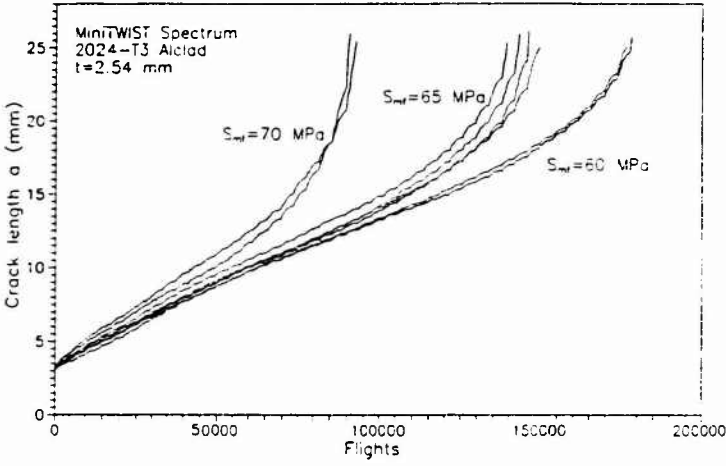


Fig 5 - Results of the miniTWIST loading tests.

Fig 6 - Results of the executive aircraft type loading tests.

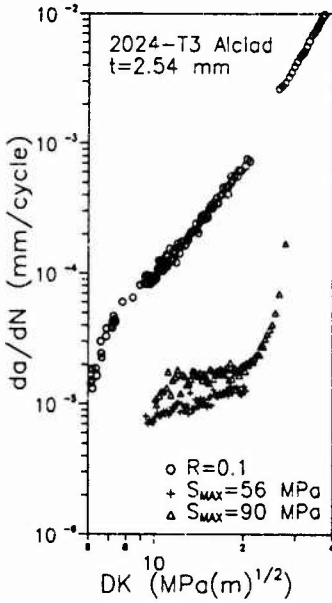
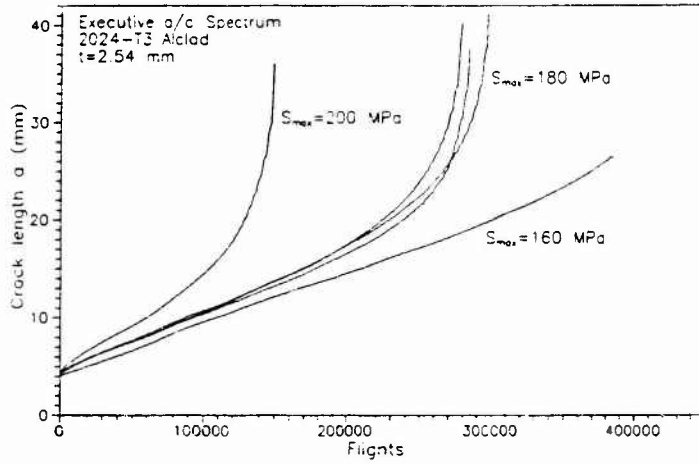


Fig 7 - Block test results for parameters evaluation according to the PREFFAS model.

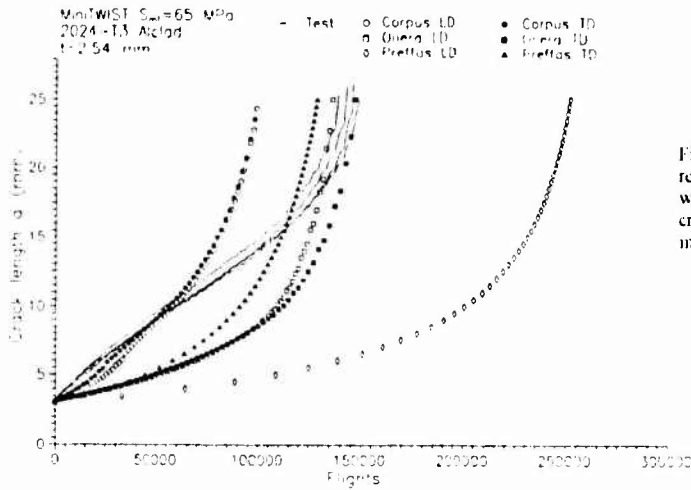


Fig 8a - Comparison of experimental results (miniTWIST,  $S_{max}=65$  MPa) with predictions obtained by means of crack opening models using different input data for material properties.

Fig 8b - Comparison of experimental results (miniTWIST,  $S_{max}=65$  MPa) with predictions obtained by means of yield zone models

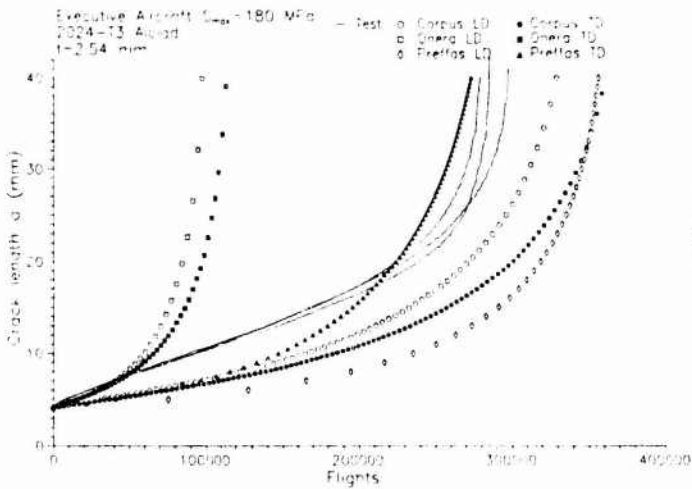
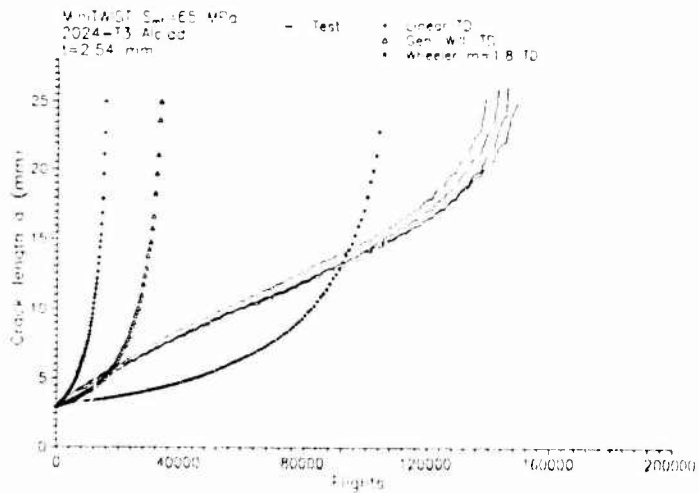


Fig 8c - Comparison of experimental results (executive aircraft spectrum,  $S_{max}=180$  MPa) with predictions obtained by means of crack opening models using different input data for material properties

Fig. 8d - Comparison of experimental results (executive aircraft spectrum,  $S_{max}=180$  MPa) with predictions obtained by means of yield zone models.

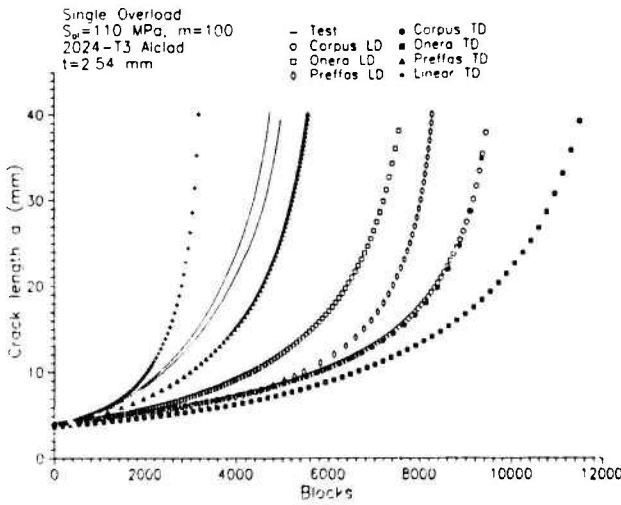
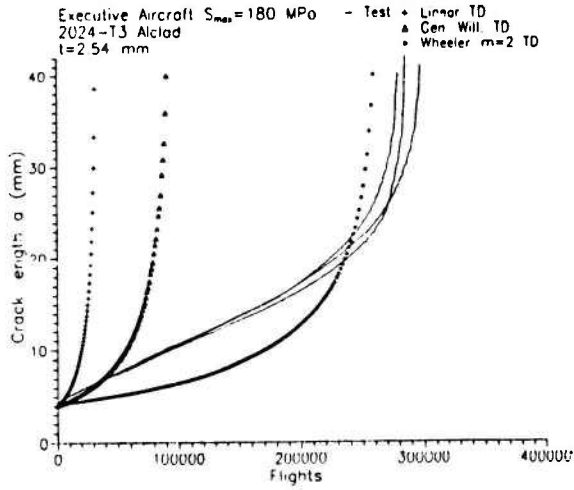


Fig. 8e - Comparison of experimental results (single overload block spectrum) with predictions obtained by means of crack opening models using different input data for material properties.

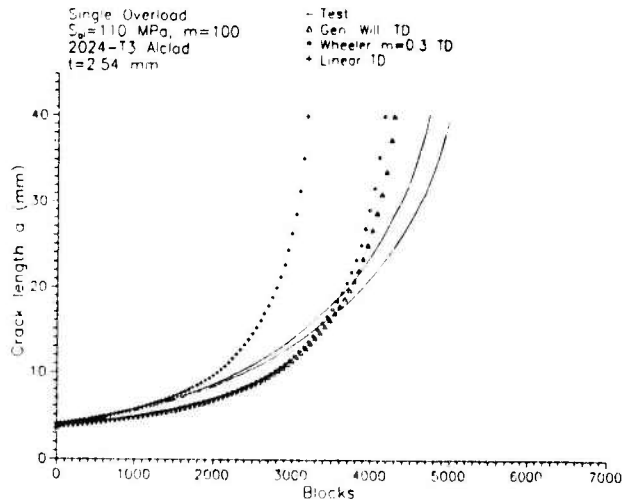


Fig. 8f - Comparison of experimental results (single overload block spectrum) with predictions obtained by means of yield zone models.

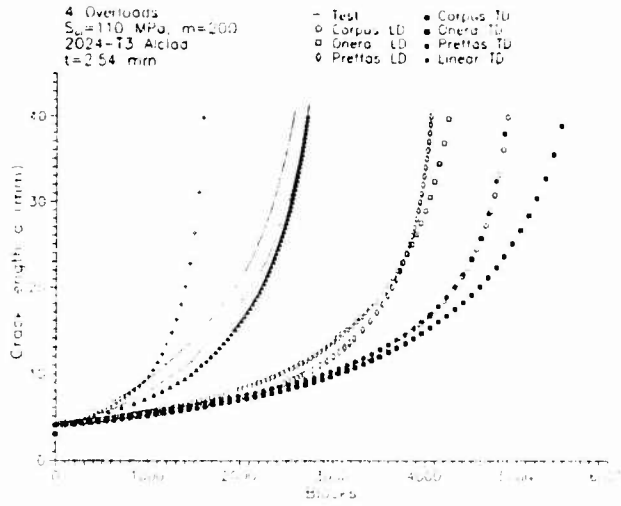


Fig. 8g - Comparison of experimental results (four overloads block spectrum) with predictions obtained by means of crack opening models using different input data for material properties

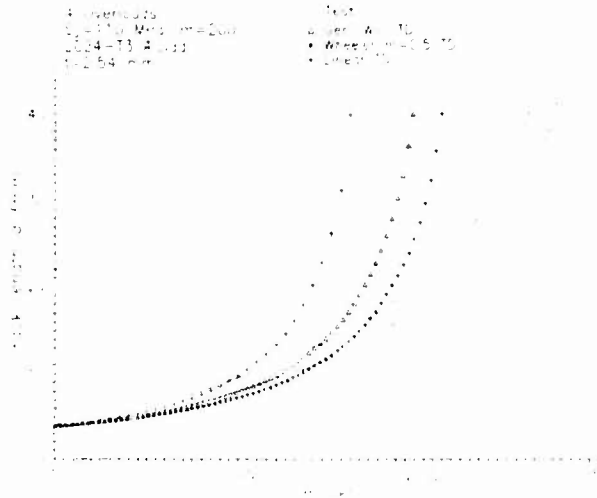


Fig. 8h - Comparison of experimental results (four overloads block spectrum) with predictions obtained by means of yield zone models

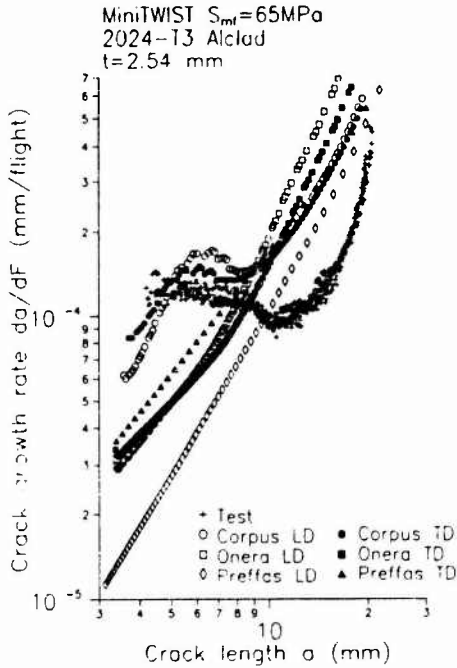


Fig 9a - Comparison of experimental (miniTWIST,  $S_{mf}=65$  MPa) with predicted crack growth rates obtained by means of crack opening models using different input data for material properties.

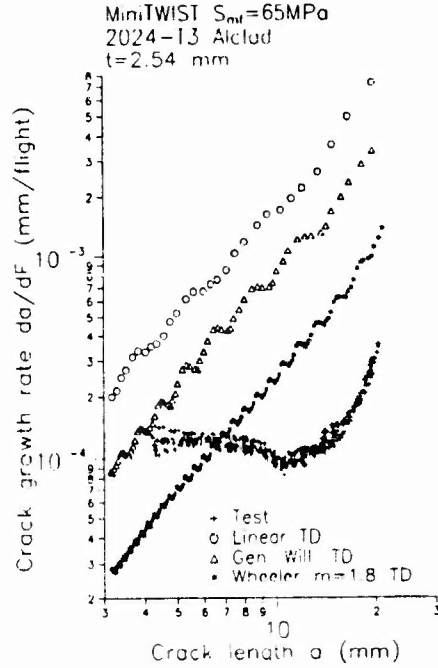


Fig 9b - Comparison of experimental (miniTWIST,  $S_{mf}=65$  MPa) with predicted crack growth rates obtained by means of yield zone models

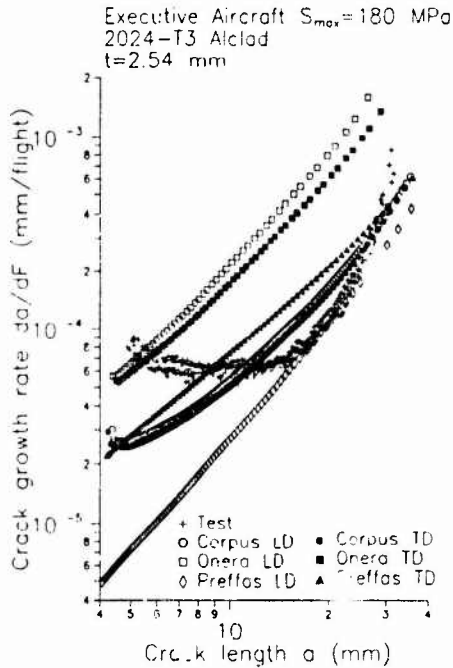


Fig 9c - Comparison of experimental (executive aircraft spectrum,  $S_{max}=180$  MPa) with predicted crack growth rates obtained by means of crack opening models using different input data for material properties.

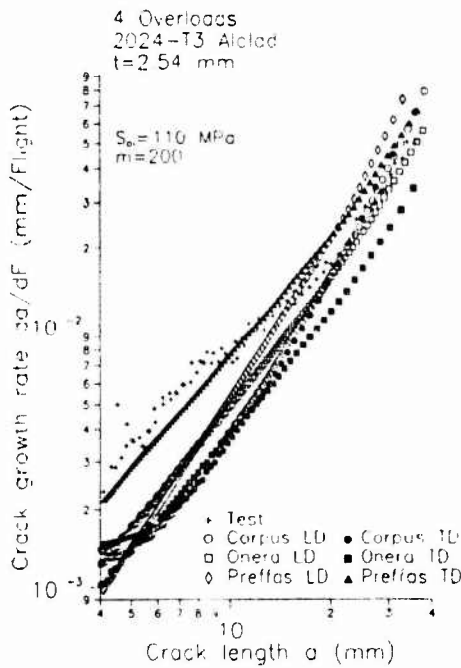


Fig 9d - Comparison of experimental (four overloads block spectrum) with predicted crack growth rates obtained by means of crack opening models using different input data for material properties

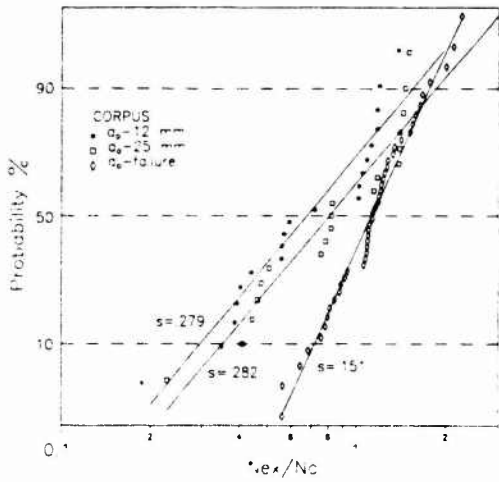


Fig 10a - Distribution on normal probability paper of crack propagation life ratios for the CORPUS model. The results relevant to propagation until failure are from [49]

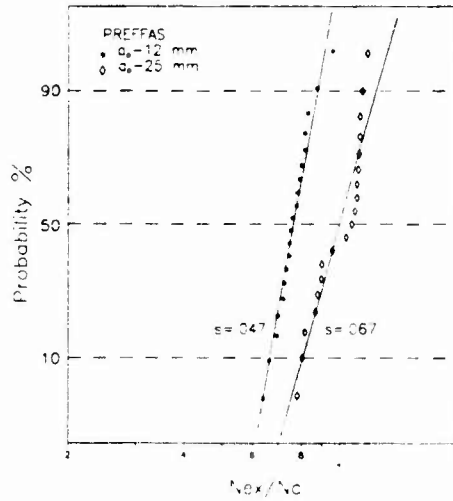


Fig 10b - Distribution on normal probability paper of crack propagation life ratios for the PREFAS model

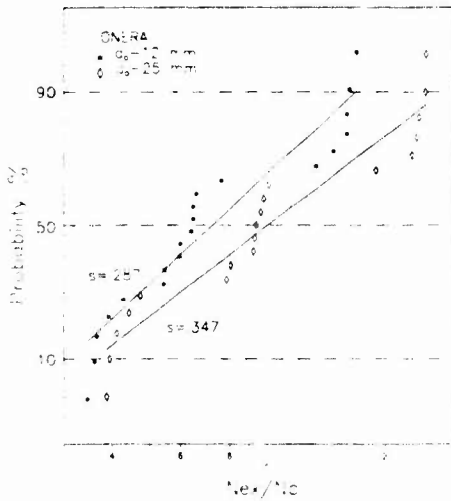


Fig 10c - Distribution on normal probability paper of crack propagation life ratios for the ONERA model

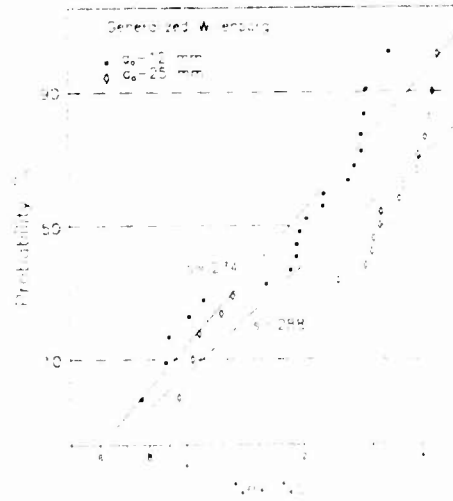


Fig 10d - Distribution on normal probability paper of crack propagation life ratios for the Generalized Willenborg model

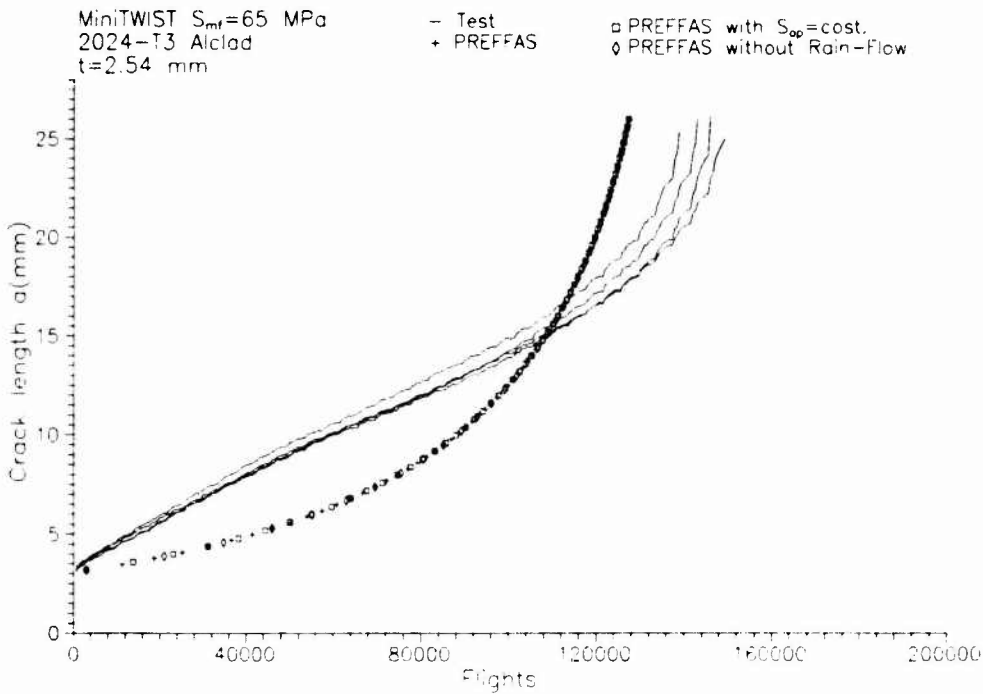


Fig 11 - Effects of some simple modifications to the PREFFAS model.

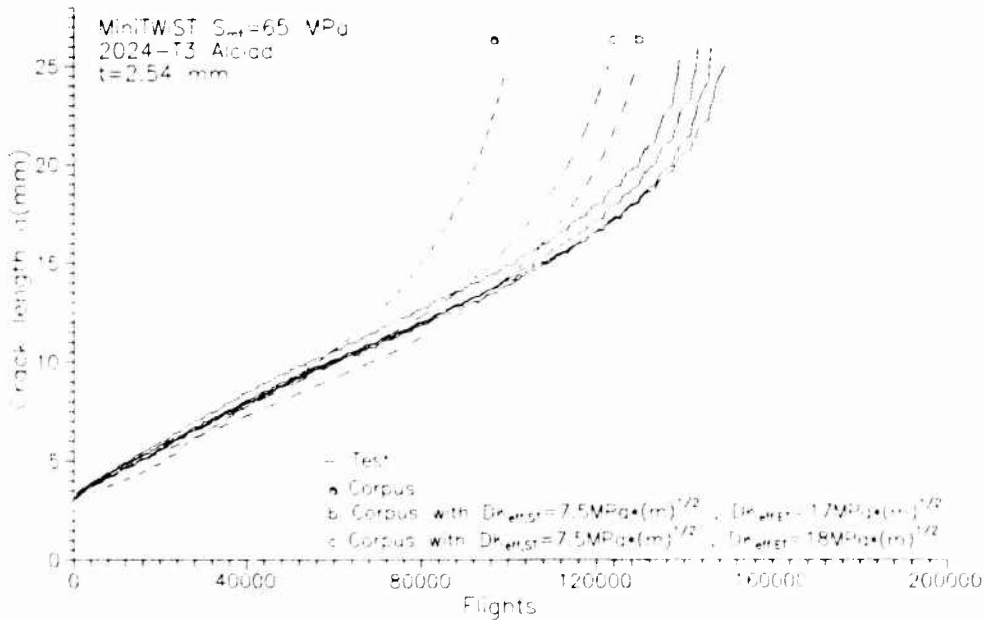


Fig 12 - Effects of variation of plane strain/plane stress transition range in the CORPUS model  
 (ST = start transition, ET = end transition)

# A COMBINED APPROACH TO BUFFET RESPONSE ANALYSES AND FATIGUE LIFE PREDICTION

J. H. Jacobs

R. Perez

McDonnell Douglas Aerospace - East

McDonnell Douglas Corporation

P.O. Box 516, St. Louis, Missouri 63166-0516

United States

## SUMMARY

Experimental measurement and neural network based prediction of wind tunnel model empennage random pressures are discussed. Artificially generated neural network power spectral densities of surface pressures are used to augment existing data and then load an elastic finite element model to obtain response spectrums. Details on the use of actual response spectrums from flight test data are also discussed. A random spectra fatigue method is described which effectively combines buffet and maneuver loads into a time series based on aircraft usage data. A peak-valley damage analysis procedure is employed to compute the aggregate fatigue life of the structure based on the combined load time series information. Applications of the method as a continual learning tool for buffet response spectra is elaborated.

## LIST OF SYMBOLS

AOA	Angle of Attack (degrees)
F	Frequency (Hz)
F(n)	Contribution to power spectrum of $p^2/q^2$ in frequency band n
HCNN	Hybrid Cascading Neural Network
L	Characteristic Length Scale
M <sub>RB</sub>	Root Bending Moment (in-#)
M <sub>RD</sub>	Nondimensional Root Bending Moment
MDA	McDonnell Douglas Aerospace
MLP	Multi-Layer Perceptron
n	Nondimensional Frequency Parameter $f \cdot L/U$
NASA	National Aeronautics and Space Administration
p	pressure (PSI)
PSD	Power Spectral Density
q,Q	Dynamic pressure (PSF)
RBF	Radial Basis Function
RMS	Root Mean Square
U	Free Stream Velocity (in/sec)

NOTE: Bar over symbol means RMS value.

## 1. INTRODUCTION

Aerodynamic vortices develop from the leading edge's of fighter aircraft during high angle-of-attack maneuvers. These vortices impinge upon portions of the aircraft structure causing high frequency vibrations. The high frequency vibrations, known as buffet, induce dynamic stresses into the structure, which in turn, cause rapid accumulation of fatigue damage. Figure 1 shows aerodynamic vortices originating from a forward position on the aircraft creating buffet loading on the aft portion.

Because future aircraft will be more maneuverable, they may be subjected to even more severe buffet environments. Buffet loads, therefore, should be included with maneuver loads in preliminary aircraft design to prevent early fatigue damage and reduce maintenance costs. The ability to accurately predict random pressure environments on the empennage of a fighter aircraft in the advanced design stage has been quite difficult due to the complexity of the interaction between the aircraft geometry, flow field, vortex path, and empennage structure. While existing aircraft test data can provide an estimate of these dynamic and static load environments, more accurate and robust prediction methods must be addressed to avoid costly post-production repairs.

To be able to accurately predict the fatigue life of aircraft structures exposed to buffeting environments, detailed flight test or wind tunnel response data must be obtained. Project limitations and time constraints do not always allow for the gathering of this detailed information at all possible Q and AOA conditions. To alleviate this problem a neural network based learning algorithm has been investigated for possible use in augmenting this information which is required for fatigue life calculations.

Since empennage environments on fighter aircraft are a complex combination of dynamic loads and static maneuver loads, the neural network generated PSD's are combined with maneuver load spectrums to form a total fatigue spectrum. The load history is then used for a peak-valley analysis to compute crack initiation and crack growth fatigue lives.

## 2. BUFFET ENVIRONMENT MODELING

In 1987 a cooperative research effort between NASA LaRC and MDA was initiated to study the effects of vortex-tail interaction process for a 76 degree delta wing with twin vertical tails placed aft of the wing (Ref. 1). The twin tails are illustrated in Figure 2. This geometrically simple configuration was chosen for this initial investigation into buffet environment modeling because it contained the pertinent physics involved in the vortex-tail interaction process and reduced undesired aircraft geometric influences. The experimental investigation measured both the RMS magnitude and frequency of the rigid tail pressures as well as the bending and torsion moments of the flexible tail for various Q, AOA and tail positions.

This set of test data was chosen as the first test bed for using a buffet environment neural network model before implementation on actual aircraft flight test data. The approach was to create a neural network model of the rigid pressure loads on the empennage structure and then use

these loads for finite element analysis of flexible tail response. In this manner, the neural network system verifies the pressure field model and its ability to predict and correlate flexible response with wind tunnel data. Eventually, the method will be used to model actual full scale flight test empennage response data.

Figure 3 represents the RMS buffet pressures near the tip of the rigid tail and the RMS bending moments of the flexible tail for inboard and outboard tail locations as observed during the NASA/MDA test program. The RMS buffet pressure and the RMS bending moment exhibited similar trends as the angle of attack was increased. Near 30° angle of attack there was significant increase in the buffeting levels for both tail positions. These highly nonlinear changes in the RMS pressures and bending moment responses are typical of empennage structures exposed to buffet environments. A distinct change in frequency content of the pressures was also observed as the angle of attack was changed (Figure 4). The peaks represent coherent fluctuations in the flow and are extremely difficult to predict even with today's modern CFD methods but are important for accurate fatigue life predictions.

The data gathered during this joint NASA/MDA program is similar to that of previous model and full scale tests. Several investigators have developed techniques to nondimensionalize both rigid and flexible response information into usable quantities. However, those techniques lack the ability to effectively extrapolate to other test conditions or configurations not investigated (Ref. 2,3). Attempting to use traditional regression techniques to model this type of buffet data is extremely difficult due to the multiple number of noisy parameters that interact in a non-linear manner (Ref. 4). However, neural networks are especially adept at modeling this kind of data because their inter-connected algorithms can accommodate these nonlinearities. They can generally be defined as massively connected, massively parallel networks with the ability to learn. One of their most important characteristics is the ability to generalize from the data they have already seen, which makes them a good candidate for modeling the sparse buffet data (Ref. 5).

The details on the evaluation of specific neural network architecture's to model the buffet data can be found in Reference 6. This paper will only show the applicability of the method for generation of PSD spectrums which can be used for a combined loads fatigue analyses.

It is desired to predict the PSD pressure of the aircraft empennage, caused by upstream vortex impingement, as a function of free stream dynamic pressure, angle of attack, tail chord and span location of the pressure sensors, and positions of the rigid tail relative to the delta wing. In total, three dynamic pressures ranging from 3.3 to 7.7 PSF, fifteen angles of attack ranging from 0 to 40 degrees, five sensor positions, two tail positions, and 49 frequency bands were combined to form 7350 input/output pairs. The neural network architecture developed to model this data is shown in Figure 5. A combination of two types of networks were used which consisted of a Multi-layer Perceptron (MLP) (Ref. 7) and a Radial Basis Function (RBF) (Ref. 8). The overall network is called a Hybrid cascading Neural

Network (HCNN). The HCNN accounts for the wide variation of PSD magnitudes between low and high angles of attack by employing a scaling method which allows for equal emphasis of all training data.

Predictions of this network as compared to the actual test data is shown in Figure 6 for a few representative angles of attack. Its ability to maintain the correct shape and identify modes in the PSD make its increased complexity worthwhile. Individual frequency PSD values varied by approximately 10% for the trained data. However, the integrated overall RMS values were within 5% of the test results.

### 3. BUFFET RESPONSE SPECTRA GENERATION

In general, bending moment response of an empennage structure is directly obtained from full scale flight test data and used for subsequent fatigue calculations. Since the neural network was trained with rigid pressure wind tunnel data, flexible response information was still required for use in fatigue calculations. To demonstrate this, and to correlate with the response of the flexible tail in the wind tunnel, a finite element model was constructed of the flexible tail. The details of the model are discussed in Reference 6. The neural network model of the pressure environment was used to generate pressures over the entire surface of the tail to supply refined pressure distributions to the finite element model. The neural network provides an unbiased method of distributing pressures measured at only five points on the tail over the entire surface of the tail. The level of resolution which is obtainable for the pressure field is illustrated in Figure 7. Two sets of random forced response solutions were run on the NASTRAN finite element model. The first set consisted of a segmented grid of pressures which were simply a PSD value from one of the five sensors based on the best guess distribution of the model test data. The second set used unique PSD information for each grid based on the neural network prediction. Solutions were run for AOA's from 20° to 40° and the results are shown for both tail positions (Fig. 8).

The neural network has comparable results as that of the use of the test data directly. An important benefit of the neural network approach is its ability to continue learning with more information without re-training the whole system. This can be very advantageous for incorporating multiple flight test data over the lifetime of an aircraft.

The method described in the preceding paragraphs is a general approach to modeling sparse buffet type data. This method can be employed in a similar manner on actual flight test response data as is illustrated in Figure 9. In the future, automated procedures will download flight test response data directly into a learning algorithm, such as described within, to fill in missing PSD information for other Q or  $\alpha$  AOA conditions as well as providing future aircraft designers with a valuable tool.

### 4. COMPLETE SPECTRA ASSEMBLY

In order to predict the fatigue life of the structure, the buffet response must be characterized in terms of a stress history. The first step is to generate a PSD curve at each AOA Q

condition using the neural network method. A random buffet load history is then generated for each PSD. The load history is obtained by using a random number generator to select points on the PSD curve. These points defined a random sequence of load levels. Fatigue analysis requires only the peaks and valleys of each load cycle. Therefore, the peak and valley history are extracted from the random sequence of load levels.

Next, the steady state load experienced by the structure at each AOA-Q condition needs to be superimposed with the buffet loads.

The buffet information must be organized into a series of high angle-of-attack maneuvers which represent the way aircraft fly. Flight test data indicate that as an aircraft increases its angle of attack, the Mach number and corresponding dynamic pressure drop. The angle of attack decreases as the maneuver ends, and in general, the Mach number and dynamic pressure remain at or near the lowest level experienced (Ref. 9).

In a possible model of high angle-of-attack maneuvers, the angle-of-attack during each maneuver is ordered in a low-high-low sequence. The corresponding buffet and steady state loads occurring at each AOA-Q condition are then ordered as illustrated in Figure 10. The duration at each AOA-Q condition is determined from fleet usage data which describes the amount of time aircraft spend at various angles-of-attack and dynamic pressure levels.

If low angle-of-attack maneuvers occur, they may induce steady state loads without buffet. These loads can be included as a separate block of cycles or they can be included at the beginning and at the end of each flight. These two options are illustrated in Figure 11.

The final step is to convert the load history to a stress history using standard stress analysis procedures. They can make use of strength of material equations or finite element methods.

## 5. COMBINED LOADS FATIGUE ANALYSIS

Buffet cycles occur in large number because of their high frequency relative to steady state loads. In the analysis and verification of fatigue life, these large numbers can contribute to long test times. Two methods exist for decreasing the number of cycles in the buffet stress histories described in the various section (Ref. 9). One technique is to simply eliminate small cycles that do not cause much damage compared to the rest of the stress cycles, is typically called truncation and is illustrated in Figure 12.

In the second procedure for reducing the spectrum, stress cycles with similar amplitudes and peak stress level are grouped into "blocks". A reduction in spectrum size can be obtained by replacing blocks of constant amplitude cycles with larger amplitude blocks containing fewer cycles. The value of each peak stress is held constant, but the amplitude is increased so that the new spectrum is predicted to do the same fatigue damage as the original spectrum. Figure 13 illustrates an example of this method. In the figure, 110 cycles have been replaced with 55 cycles which cause the

same damage. This procedure is effective, but needs to be verified for the particular application, because excessive reductions in the number of cycles can lead to inaccurate results.

Once the stress history has been determined and the number of cycles reduced with the above procedures, the fatigue life can be predicted. The total fatigue life is composed of a period needed to initiate the fatigue cracks and the remaining life needed to propagate these cracks until failure of the structure occurs.

Crack initiation predictions use stress versus life (S-N) curves for the materials. The stress for each load cycle causes fatigue damage which can be computed with the S-N curve. The damage is added using cumulative damage procedures such as Miner's Rule. Crack growth is predicted using crack growth rate versus stress intensity factor ( $da/dN$  vs.  $\Delta K$  curves for the material). The stress intensity factor for each load cycle is used to predict the crack growth rate. Crack growth is predicted by adding the growth predicted during each cycle. In both segments of the life, the presence of buffet stresses cause a major impact on the total life.

One area of particular concern is the superposition of buffet and steady state loads. The fatigue damage caused when buffet and steady state loads occur simultaneously is much greater than when buffet occurs by itself (Fig. 14). Analytical models need to correctly combine dynamic and static loads in order to predict accurate fatigue life.

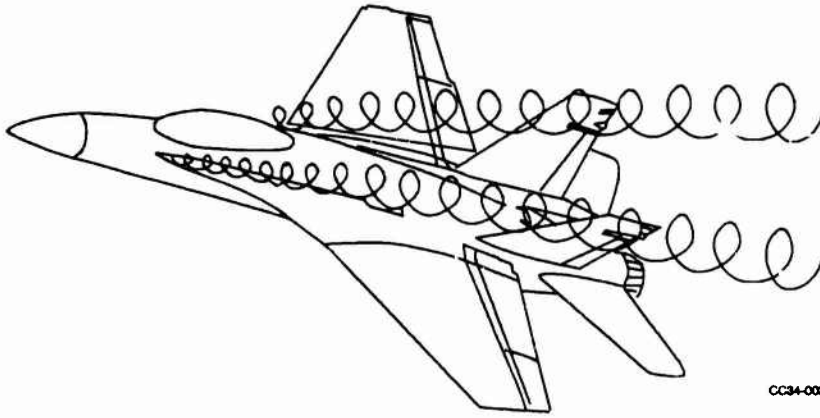
The results of including these combined loads into the calculation of fatigue life is illustrated in Figure 15. In this figure, a series of aluminum test specimens were tested with various combinations of load spectra. As can be seen in the results for crack initiation and crack growth life, the structural life is significantly reduced when the maneuver load cycles are combined with the random buffet load cycles.

## 6. CONCLUDING REMARKS

A method has been established which utilizes buffet response PSD curves to combine with static loads for a combined spectrum life analysis. Neural network learning algorithms have shown the ability to learn and then augment sparse buffet data for needed Q- $\alpha$  conditions. Combining this information with maneuver load time histories provides the necessary information to perform crack initiation and crack growth analysis in order to arrive at more accurate fatigue life predictions. Results from coupon testing shows that structural fatigue life is greatly reduced when buffet loads are included with maneuver load cycles in the excitation spectra. The random PSD method for fatigue life prediction is conservative when compared to actual flight test data but is a simplified way of generating flight-by-flight spectra for test, analysis, and design (Ref. 9). Future work in neural network modeling and fatigue caused by buffet environments will include the effects of upstream geometry, vortex characteristics, and transient maneuvers.

**REFERENCES**

1. Washburn, A. E., Jenkins, L. N., and Ferman, M. A., "Experimental Investigations of Vortex-Fin Interaction", AIAA Aerospace Sciences Meeting, AIAA 93-0050, January 1993.
2. Zimmerman, N.H., Ferman, M. A., Yurkovich, R.N., "Predictions of Tail Buffet Loads for Design Applications", AIAA-89-1378.
3. Mabey, D. G., "Some Aspects of Aircraft Dynamics Loads Due to Flow Separation", AGARD CP R-750, 1987.
4. Ferman, M. A., et. al., "A Unified Approach to Buffet Response", 70th Meeting of Structures and Materials Panel, AGARD CP 17, April 1990.
5. Lippmann, R. P., "An Introduction to Neural Computing with Neural Nets", IEEE ASSP Magazine, April 1987, pp 4 22.
6. Jacobs, J. H., et. al. "The Use of Artificial Intelligence for Buffet Environments", 34th SDM Conference, AIAA-93-1534, April 1993.
7. Rumelhart, D. E., McClelland, J. L., and the PDP Research Group, "Parallel Distributed Processing, Volume 1 - Foundations", Cambridge, MA, MIT Press, 1986, Ch. 8.
8. Chen, S., Cowan, C. F. N., and Grant, P. M., "Orthogonal Least Squares Learning Algorithm for Radial Basis Function Networks", IEEE Transactions on Neural Networks, Vol. 2, No. 2, March 1991.
9. S. T. Harbison, R. Perez, H. G. Smith, C. R. Saff, "Development of Techniques for Incorporating Buffet Loads in Fatigue Design Spectra", Report No. NADC 90071-60 (Vol. I), March 1990.



CC34-0034-311-V

Figure1. Aerodynamic Vortices Acting on an Aircraft

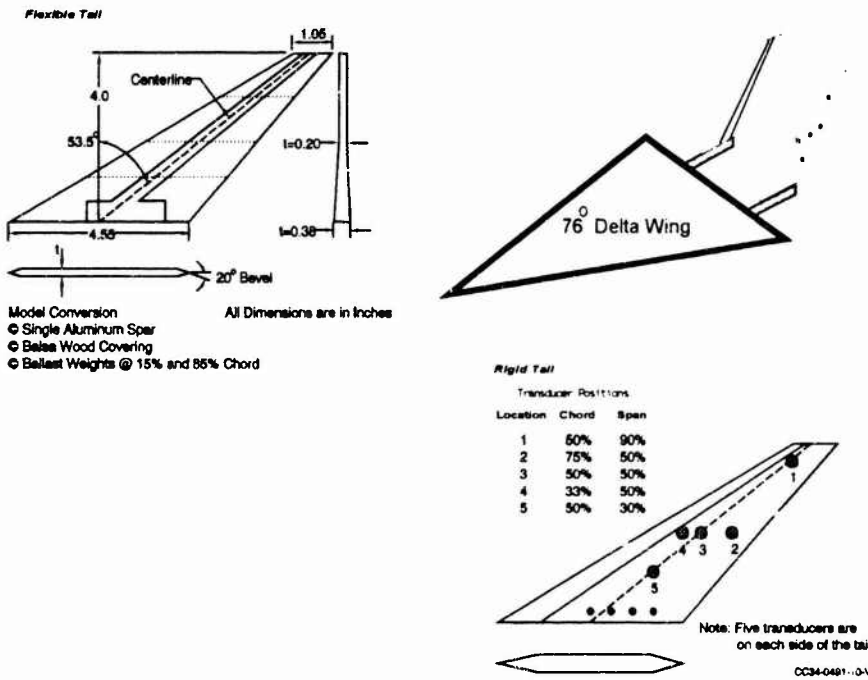


Figure2. Schematic of NASA/MDA Buffet Research Model

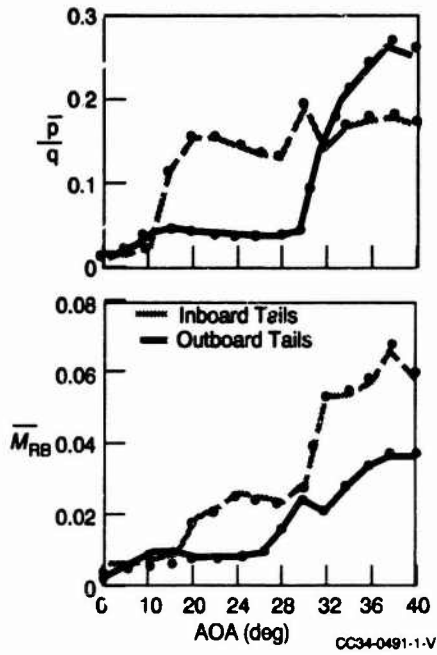


Figure 3. NASAMDA Buffet Model Typical Rigid and Flexible RMS Responses of Vertical Tails

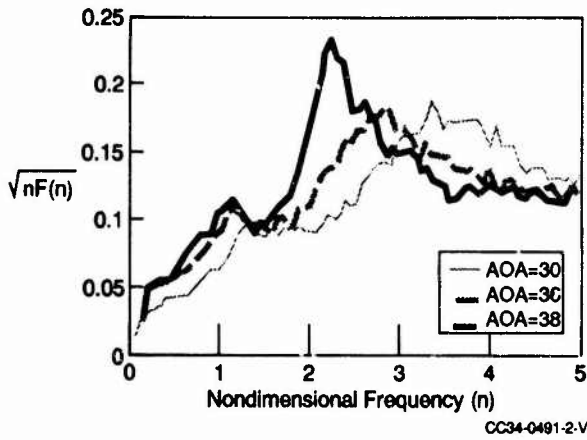


Figure 4. Nondimensional Frequency Response of Rigid Tails for Various Angles of Attack

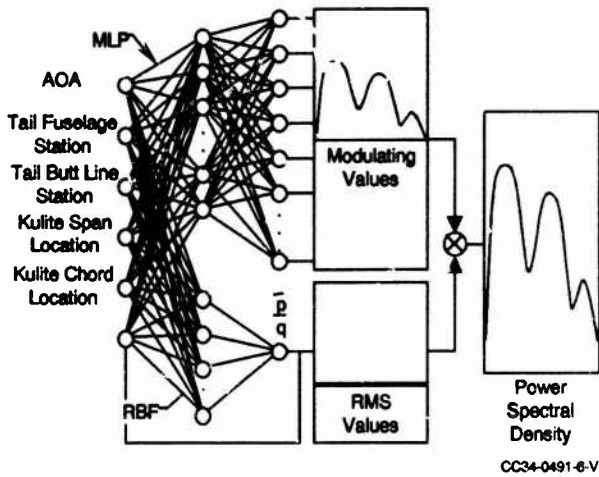


Figure 5. - Hybrid Cascade Neural Network Used for PSD Prediction

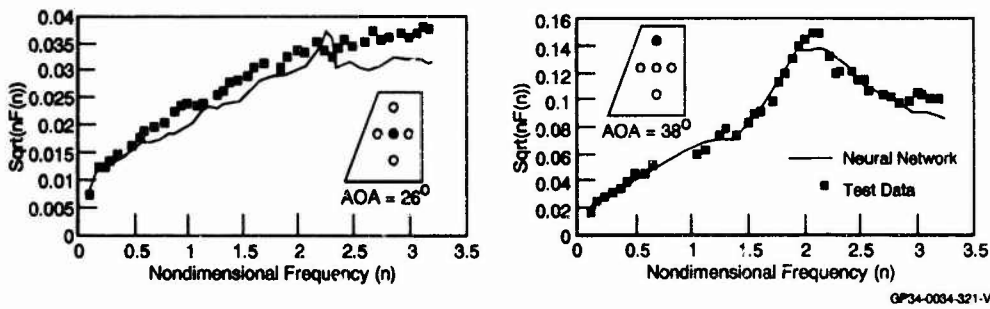


Figure 6. - Comparison of Neural Network Generated and Experimental PSD Curves for Various Conditions

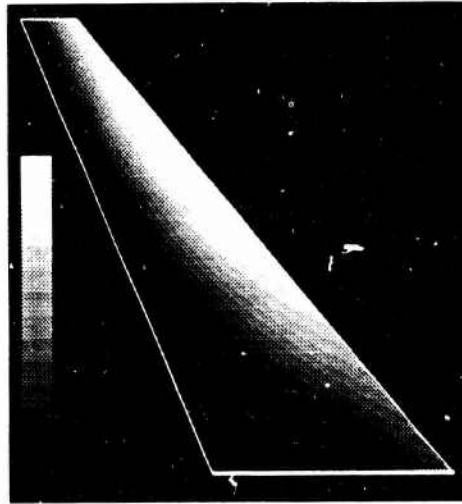


Figure 7. - Surface Contours of RMS Pressure Using Neural Network

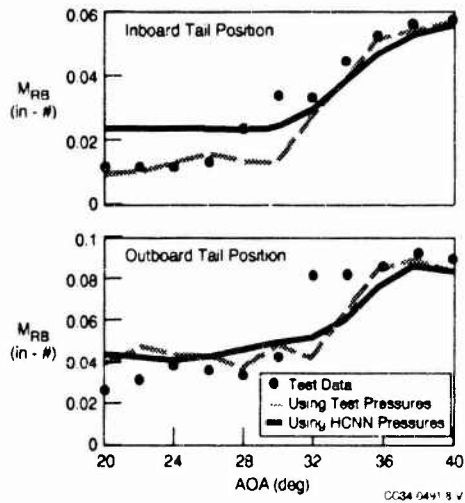
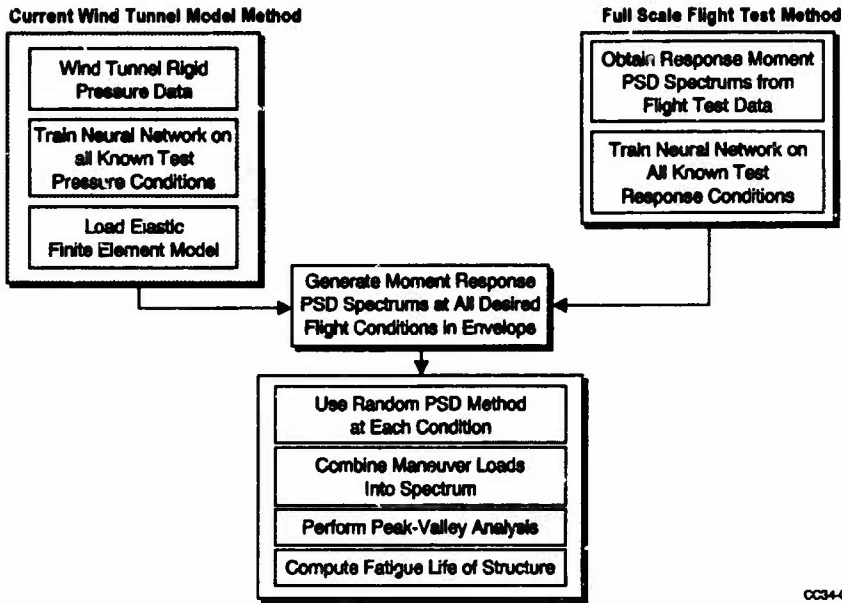
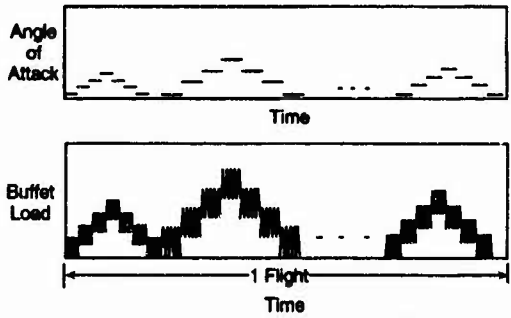


Figure 8. - Comparison of Analytical and Experimental Flexible Response



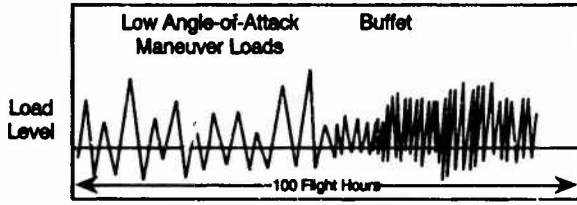
CC34-0034-319-V

Figure 9. - Combined Buffet Analysis and Fatigue Life Prediction Procedure

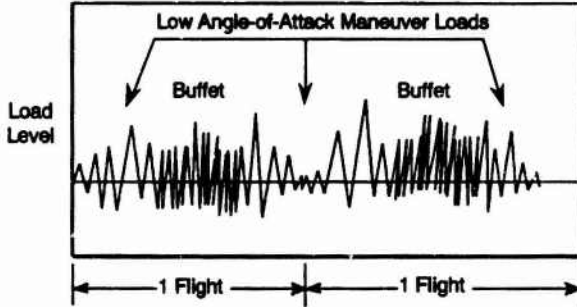


CC34-0034-312-V

Figure 10. Sequence of High Angle-of-Attack Maneuvers Containing the Buffet Loads in a Flight



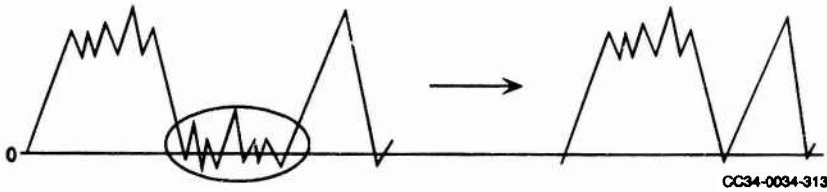
(a) Buffet Added as a Separate Block



(b) Buffet Loads Added In the Middle of Each Flight

CC34-0034-316

Figure 11. Methods for Combining Buffet and Maneuver Loads



CC34-0034-313

Figure 12. Truncation of Small Buffet Cycles

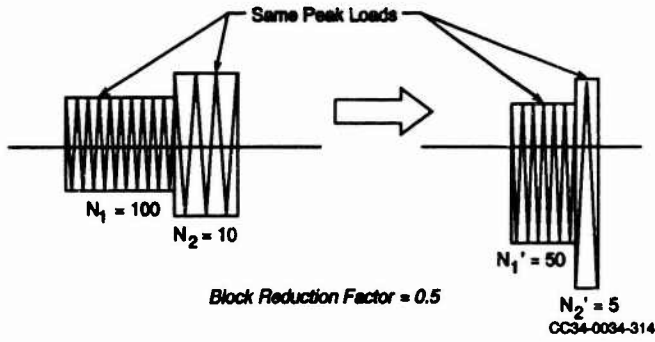


Figure 13. Example of Increased Amplitude Spectrum

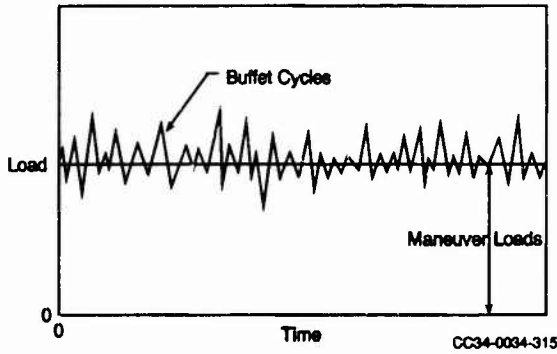


Figure 14. Buffet Load Cycle Incorporation with Maneuver Loads

Spectrum Description	Normalized Crack Initiation Life (Relative to A)	Normalized Crack Growth Life (Relative to A)	Normalized Total Fatigue Life
Maneuver Loads Only	1.0 <sup>(A)</sup>	0.263	1.263
Maneuver Loads at Beginning + Buffet Loads at End	0.227	0.120	0.347
Maneuver Loads in Each Sequence + Buffet Loads	0.193	0.128	0.321

OP94-0064-820-V

Figure 15. Comparison of Individual vs Combined Load Fatigue Lives for Experimental Coupon Tests

## NOTCH FATIGUE ASSESSMENT OF AIRCRAFT COMPONENTS USING A FRACTURE MECHANICS BASED PARAMETER

by

**Chr. Boller and M. Buderath**  
Deutsche Aerospace AG, Military Aircraft Division  
Department LME 221  
PO Box 80 11 60, D-81663 Munich  
Germany

**P. Heuler and M. Vormwald**  
Industrieanlagen-Betriebsgesellschaft mbH (IABG)  
D-85521 Ottobrunn  
Germany

### SUMMARY

Fatigue life evaluation has been performed for flight-by-flight loaded coupons and real aircraft structural components made of 7075-T7351 using the local strain approach and a fracture mechanics based parameter. Results show that this approach can well compete with the traditionally used nominal stress approach. The advantages are a better understanding of material's fatigue behaviour and a less experimental effort required for the determination of baseline data making the local strain approach interesting also for redesign within aircraft mid-life improvement updates.

### LIST OF ABBREVIATIONS

a	crack length
$\alpha$	constraint factor
C	constant in crack growth law
D	damage sum
E	Young's modulus
$\epsilon$	strain
$F_s$	size factor
$I_s$	stress integral
J	J-integral
$K_f$	fatigue notch factor
$K_t$	stress concentration factor
K	cyclic hardening coefficient
m	exponent in crack growth law and damage parameter life curve
MAFT	major aircraft fatigue test
N	number of cycles to initiation of cracks of technical size
n	cyclic hardening exponent
$P_j$	J based damage parameter
$P_{SWT}$	Smith, Watson, Topper damage parameter

Q	constant in damage parameter life curve
q	exponent in Weibull-equation, related to stress
R	stress ratio
S	nominal stress
$\sigma$	stress

### 1 INTRODUCTION

In Europe fatigue assessment of components of military aircraft is conventionally performed on the basis of preliminary parametric fatigue analyses followed by a full-scale fatigue test. Key elements of the fatigue analysis are a stress concentration factor, stress vs. fatigue life (S-N) curves for joints and coupons, baseline aircraft fatigue loads spectra, load cycle counting algorithms and the Palmgren-Miner damage accumulation rule. Based on these elements components are designed where assumptions have to be made when understanding of real material fatigue behaviour is still not fully accomplished. These assumptions therefore mainly require validation in a full-scale fatigue test.

A methodology aiming at better understanding of the fatigue behaviour of components which inevitably contain notches has been given with the local strain approach. According to that approach notch root stress-strain ranges are calculated and used for cumulative damage assessment based on material fatigue data. Thus the failure criterion is equivalent to a given 'technical' crack size. In principle fatigue-relevant effects resulting from mean and residual stresses, different specimen sizes and surface conditions can be accounted for. Various versions of this local strain approach principle have been proposed so far, yet it has to be acknowledged that

the equivalence principle between the notch root and unnotched specimen as well as the linear accumulation of fatigue damage are aspects where improvements are still required.

Application of the local strain approach to aircraft structures has been limited during the past [1,2]. Reasons include the geometric complexity of aircraft structures (e.g. riveted joints) and the influence of various manufacturing (e.g. surface treatments) and environmental (e.g. corrosion) effects. It is interesting to note, however, that the US Navy applies that approach for usage monitoring in combination with full scale test results [3]. On a research level, other examples include studies on life prediction for notched 2024 and 7010 specimens (ONERA), fatigue life evaluation of modified aircraft structures and low cycle fatigue evaluation of aircraft engine parts [4-6].

The traditional nominal stress approach accounts for fatigue-relevant effects globally by testing components for determination of baseline S-N curves. This requires a large amount of component testing and gives no direct access to the prevailing fatigue mechanisms, though it has to be acknowledged that often a detailed modelling of complex structures for fatigue analyses is beyond the scope of practical application.

It is widely accepted that a major part of the fatigue life of components and structures consists of growth of short cracks which may nucleate at a very early stage in life followed by a long crack stage. This has recently led to the development of a fracture mechanics based damage parameter [7] applicable within the framework of local strain approach concepts considering load sequence-driven opening and closure of short cracks and a transient fatigue limit. Thus the damage parameter follows an effective loading parameter concept (equivalent to an effective crack driving parameter used in crack propagation models) and a more realistic modelling is achieved.

In order to assess and validate the progress achieved, predictions for a variety of notched 7075-T7351 aluminum coupons under constant amplitude and fighter aircraft spectrum loading are presented and discussed. Moreover, examples of real aircraft components selected from the major aircraft fatigue test (MAFT) of Panavia's Tornado fighter aircraft are included in order to demonstrate practical applicability.

## 2 THE AIRCRAFT FATIGUE DESIGN PROCESS

Fatigue design of an aircraft structure can be considered as an iteration process between numerical and experimental fatigue life evaluation.

The initial step is to determine fatigue allowables usually in terms of the function of allowable stress (usually maximum stress) versus  $K_f$ , for a defined design life under a given load spectrum. This function is used by designers as a guideline to account for the influence of fatigue in a first approach.  $K_f$ -values for the notches within the aircraft component considered are estimated.

A detailed analysis is then performed on a numerical basis (e.g. by finite element analysis) for the critical areas of the aircraft component considered where  $K_f$ -values can now be determined more precisely. This can lead to  $K_f$ -values higher than those determined initially. Furthermore additional information available in the meantime on the load distribution leads to changes within the load spectrum which finally may require a reevaluation and possibly modification of fatigue critical parts being the second step of the fatigue design process.

Within the next step the numerically optimized aircraft structure is validated experimentally either by testing specific components or in a full scale fatigue test. Areas within the aircraft structure where cracks already occur during the early stage of fatigue testing are reanalyzed with respect to the strains occurring in the respective area. Load levels and distributions are measured in order to obtain a more realistic stress/strain sequence. The new stress sequence is now used for a numerical reevaluation of fatigue life which may end up in a modification of the aircraft component. Fatigue fracture occurring in the later stage of the design life may require modification of the aircraft component as well.

A more detailed description of established fatigue assessment procedures for military aircraft is given in [8].

## 3 RELEVANCE OF IMPROVED NOTCH FATIGUE ASSESSMENT FOR AIRCRAFT COMPONENTS

Fatigue is a major reason for failure in components of aircraft structures. Following a study performed by IABG/DASA, around 70% of failures observed on Tornado-MAFT were related to fatigue. An

analysis of the fatigue failures identifies two major groups each comprising about half of the failures.

About one half is related to fatigue failures resulting from fasteners such as rivets or bolts. For such a type of failures the local strain approach appears not to be suitable for a stringent assessment.

The remaining approximate half of the fatigue failures however are not related to fasteners and are potential areas for application of a local strain based evaluation. In retrospect approximately one third of these failures could be related to non standard surface conditions, notch size effects and damage accumulation problems. Another third is due to insufficient knowledge of load distribution. The remaining third resulted from various effects such as complicated notch geometries, corrosion and various others.

The above analysis demonstrates that areas exist where the development and application of advanced local strain based life prediction approaches appear to be promising.

## 4 ESTABLISHED FATIGUE ASSESSMENT PROCEDURES

### 4.1 Nominal Stress Approach

Fatigue assessment usually applied for European military aircraft is generally based on a nominal stress approach. This requires determination of stress concentration factors  $K$ , S-N curves for joints and components, fatigue loads spectra, load cycle counting algorithms and the Palmgren-Miner damage accumulation rule.

$K$ , which has to be related to a well defined nominal stress is either determined from handbooks, a finite element analysis or a tensile test. Fatigue load sequences are generated on the basis of expected flight envelopes, experimentally determined on aircraft of a similar type or available as standard sequences (e.g. FALSTAFF). Traditionally level crossing load cycle counting has been used, but recently rainflow counting has been recognized to be more realistic. S-N curves for different types of notches and materials are either available from handbooks or have to be determined as part of design guidelines for the specific aircraft considered.

Fatigue life of the structural component is evaluated for the load spectrum considered using S-N

curves for different mean stresses and the appropriate type of specimen, and the Palmgren-Miner damage accumulation rule.

Given the fact that S-N curves are not available for arbitrary values of  $K$ , specific curves have either to be determined by interpolation between the experimentally determined ones or the component's fatigue life is evaluated on the basis of an available S-N curve for a  $K$ -value being slightly above the  $K$ -value of the detail considered.

Whenever possible a relative Palmgren-Miner rule is applied using experimental results for similar notch type components and a similar load spectrum.

### 4.2 Local Strain Approach

The local strain approach starts from the idea, that material's mechanical behaviour in a notch can be assessed on the basis of material data obtained from unnotched specimens. To evaluate fatigue life this requires: 1. a stress concentration factor  $K$ , 2. a load-notch strain relationship, 3. material's stress-strain relationship for cyclic loading and 4. material's fatigue life relationship (Fig. 1).

$K$  is determined as described for the nominal stress approach. The load-notch strain relationship which relates external loads to notch stresses and strains can be evaluated on the basis of a finite elements FE analysis. Alternatively approximation formulae such as Neuber's rule (9)

$$\sigma_{\text{notch}} = K \sigma_{\text{nominal}}$$

can be applied in conjunction with an appropriate equation for the monotonic and cyclic stress-strain curve of the material under consideration. For elastic notch section behaviour which prevails in structural aircraft applications, Eq. (9) can be rearranged to

$$\sigma_{\text{notch}} = K \sigma_{\text{nominal}} \left( \frac{E}{E'} \right)^{1/n}$$

For the case beyond plastic limit load generalized solutions are given in Ref. (10).

Combining the load-notch strain relationship, the material's stress-strain relationship and material memory phenomena the notch root  $\sigma$ - $\epsilon$  path can be predicted for given load sequences. For individual cycles identified during that calculation damage contributions are determined on the basis of material's constant amplitude fatigue life curve and accu-

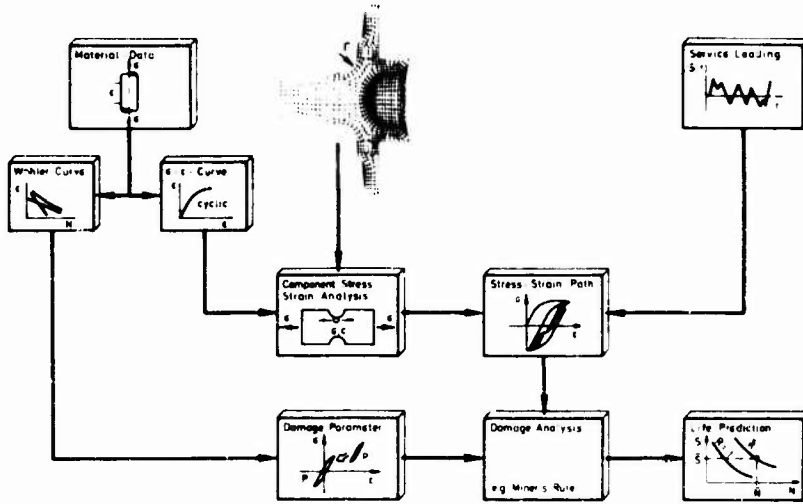


Fig. 1 Local Strain Approach

culated following Palmgren-Miner's rule. Mean stress effects are usually taken into account by use of so-called damage parameters [11] empirically formulated on the basis of constant amplitude test results. A damage parameter being widely applied has been proposed by Smith, Watson and Topper [12] and extended in [13]

$$P_{SWT} = [(\sigma_a + k \sigma_m) \epsilon_a E]^p \quad (3)$$

where  $k$  is a material constant. For application normally the baseline material's fatigue life relationship which may be derived from tests or materials data collections [14,15] is formulated in terms of the damage parameter being used (see Fig. 2).

Although the Smith, Watson, Topper parameter has attracted much acceptance its application suffers from the fact that load sequence effects cannot be accounted for.

To account for the influence of notch size and type of stress, a notch fatigue factor  $K_f$  is used instead of  $K_t$ . Various solutions have been proposed where Peterson's formula

$$K_f = \frac{K_t + a/r}{1 + a/r} \quad (4)$$

has become quite popular, with  $a$  being a material constant and  $r$  the notch radius. Alternative solutions consisting of an appropriate shift of the material's damage parameter life curve by a constant factor are explained in chapter 5.5.

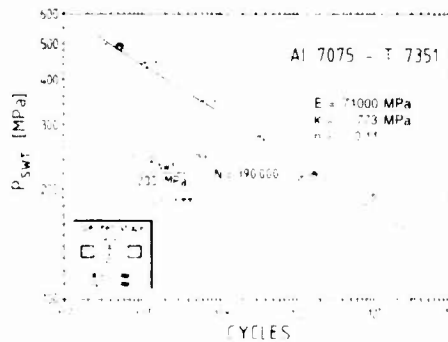


Fig. 2 Material's baseline data,  $P_{SWT}$  damage parameter

## 5 THE FRACTURE MECHANICS BASED PARAMETER

### 5.1 Introduction

Aiming at a closer description of the physical process of fatigue under variable amplitude or spectrum loading, a model for fatigue life prediction has been proposed in Ref. [7] and extended and applied in some further papers [16-19] based on fracture mechanics of short cracks. For years crack closure has been identified as a main driver for load sequence effects on crack growth. Consequently modelling of crack closure and opening levels in order to derive some effective crack driving force represents one of the key elements of that so-called  $P_J$ -model. Since that model had been developed for prediction of technical 'crack initiation' in the framework of local strain based concepts, it predicts effective stress-strain ranges for each cycle identified within the load sequence.

Those effective stress-strain ranges in conjunction with a gradually decreasing fatigue limit are the means that allow for nonlinear cumulative damage effects. Some details of the model are explained in the following.

### 5.2 The $P_J$ Parameter

Since spectrum peak loads may introduce elasto-plastic conditions at notches the cyclic J integral for has been chosen as an elasto-plastic fracture mechanics parameter for the description of crack growth, i.e. damage accumulation. The baseline behaviour may therefore be described by

$$da/dn = C \cdot \Delta J_{eff}^m \quad (5)$$

Considering a nearly semicircular crack shape most common to small cracks,  $\Delta J_{eff}$  can be approximated using Dowling's formula [20]

$$\Delta J_{eff} = \left\{ 1.24 \frac{\Delta \sigma_{eff}}{E} + 1.02 \Delta \sigma_{eff} / n^{0.5} [\Delta \epsilon_{eff} - \Delta \sigma_{eff} / E] \right\} a \quad (6)$$

where  $\Delta \sigma_{eff} = \sigma_{max} - \sigma_{cl}$  and  $\Delta \epsilon_{eff} = \epsilon_{max} - \epsilon_{cl}$ . The term in double brackets in Eq. (6) is independent of crack length and is interpreted as the damage parameter  $P_J$ , leading to

$$\Delta J_{eff} = P_J \cdot a \quad (7)$$

Taking into account the equivalence of crack propagation and damage accumulation calculation,  $P_J$  is applied for cumulative damage analysis just as

other parameters. Accordingly the material's fatigue (strain)-life curve is represented in terms of a  $P_J$ -N-curve which can usually be described by a power law equation (see Fig. 3),

$$P_J^m \cdot N = Q \quad (8)$$

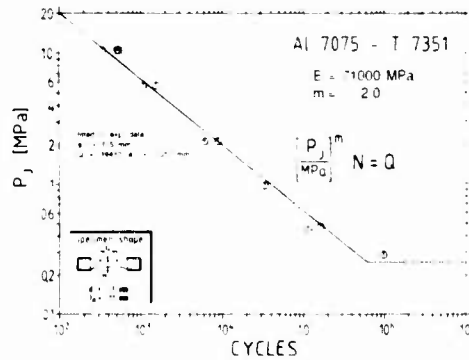


Fig.3 Material's baseline data,  $P_J$  damage parameter

Since  $N$  in Eq. (8) represents the life between  $a_0$  and  $a_r$ , integration of the crack growth law (Eqs. (5) and (8)) allows an estimate of the initial crack size  $a_0$  which is associated with the original strain-life curve via

$$a_0 = (a_r^{1-m} - (1-m) C Q)^{1/(1-m)} \quad (9)$$

It has to be emphasized, however, that Eq. (9) gives a fictitious or equivalent initial crack or flaw size which implicitly takes into account the effects of microstructure, surface finish and specimen size.

### 5.3 Crack Closure and Opening

Opening and closure of short cracks has been investigated by several authors (e.g. [16,21,22]) with the - surprising - result, that the experimental trends are reasonably predicted by Newman's formula originally developed for long cracks [23]. Newman's formula as well as an extension introduced in order to better allow for mean stress dependency of different materials can be found in Ref. [18].

As a second important result of short crack closure examinations, it was found that for elastoplastic loading conditions closure and opening better coincide in terms of strain than in terms of stress, Fig. 4. Consequently crack closure and opening

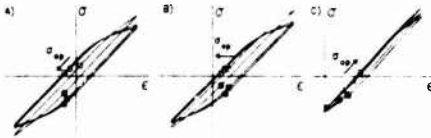


Fig. 4 Crack closure and opening levels as measured for a nickel base superalloy for three limits of strain [31]

strain levels should be considered. For multi-level loading an immediate change of the opening strain level for low-high sequences and a gradual adaptation of the new opening level for high-low sequences had been observed. These findings have been translated into a set of rules for the determination of load sequence dependent strain levels for crack opening and closure which are given in detail in Ref. [16]. The corresponding opening and closure stress levels are calculated using the cyclic stress-strain curve on a cycle-by-cycle basis in connection with rainflow analysis techniques (i.e. memory effects).

#### 5.4 Transient Endurance Limit

A further important feature of the model is the consideration of a transient endurance limit which depends on the accumulated damage. Based on Tanaka's model [24] for the threshold behaviour of short cracks and the above equations, it can be shown how the current endurance limit,  $P_{i,a}$ , depends on the current accumulated damage,  $D = \sum n_i/N_i$ , leading to

$$P_{i,a} = P_{i,a,0} \frac{a^*}{[(a_0^{1-m} - a_0^{1-m}) \cdot D + a_0^{1-m}]^{1/m} + a^* - a_0} \quad (10)$$

where  $a^* = \Delta J_{eff,0}/P_{i,a,0}$  is called an intrinsic crack length. The equivalence between damage and crack length is visualized in Fig. 5 where normalized endurance limit is plotted versus crack length (Kitagawa-Takahashi plot) as well as versus damage  $D$ .

Since the failure crack size was 0.25 mm for the example chosen (specimen diameter 6 mm), the endurance limit for  $D = 1$  is still higher than zero.

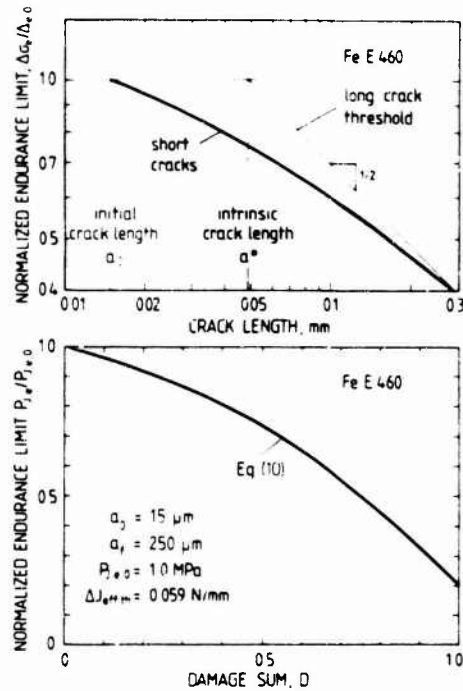


Fig. 5 Crack length dependent endurance limit (Kitagawa-Takahashi plot) (top) and endurance limit as a function of damage sum  $D$  (bottom) for a structural steel

#### 5.5 Notch Size and State of Stress

Size affects the fatigue strength of specimens and components. Size effects due to the statistical distribution of failures can be successfully handled by weakest link principles introducing Weibull's equation describing the probability of failure in terms of life or stress. As shown in [25], the relative fatigue strength of components of different sizes and shapes can be described by a factor

$$F_3 = (I_3/I_{3,ref})^{-1/q} \quad (11)$$

where  $I_3 = \int [\sigma(x,y,z)/\sigma_{max}]^q dV$  is the stress integral representing a measure for the highly strained volume (or surface) under consideration of some (intrinsic) scatter of the material's fatigue strength. With respect to the  $P_i$  parameter concept,  $F_3$  gives

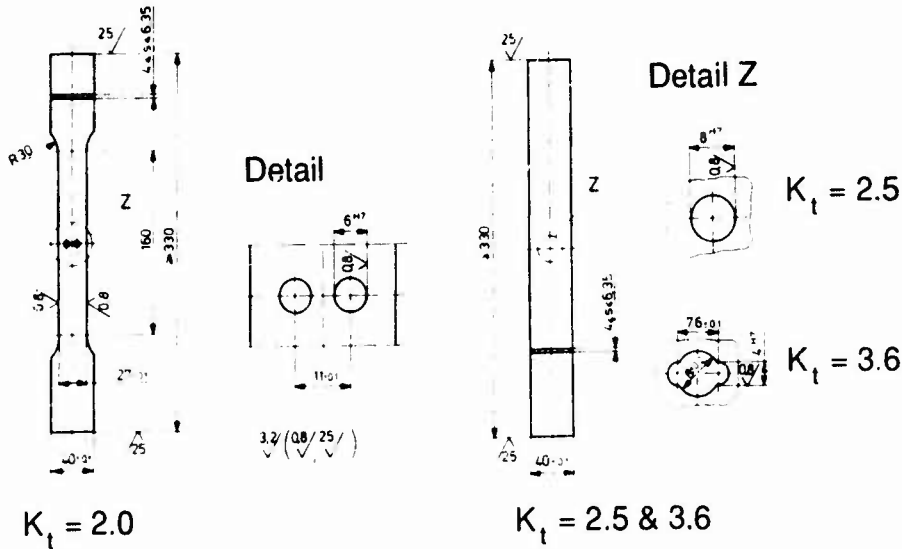


Fig. 6 Coupon geometries and dimensions

a measure for adjustment of the basic  $P_f$ -N curve in terms of  $P_f$ . Since  $P_f$  exhibits a quadratic stress dependency, the actual shift factor is  $F_3^2$ . In terms of crack growth, a different initial equivalent flaw size  $a_0$  can be associated with the adjusted  $P_f$  curve (smaller  $a_0$  for smaller volumes) which unambiguously corresponds to engineering views.

Multiaxial states of stress at notches may influence crack growth by at least two mechanisms: the opening and closure stress levels are different (lower for plain strain when compared to plane stress) and the crack opening displacement may be affected. Crack opening displacement is proportional to the J integral and to the  $P_f$  parameter. In Ref. [18] an approximative solution is given for biaxial stress states which prevail at near-surface areas. For this solution, the constraint factor  $\alpha$  used in Newman's crack opening equations as well as the ratio of biaxial versus uniaxial crack opening displacements have been formulated as a function of the stress ratio  $\sigma_2/\sigma_1$ .

## 6 APPLICATION - TEST DETAILS

### 6.1 Specimens

The approaches discussed above were applied to both a set of spectrum fatigue data of notched

coupons with open holes and two components of the center fuselage of Tornado MAFT made of Al 7075-T7351 alloy.

The experimental results for the notched specimens were taken from earlier studies [26,27]. Specimen geometries and dimensions are given in Fig. 6. Notch factors and other constants are compiled in Table 1. For the majority of tests, crack initiation lives have been determined besides total life. Crack initiation is equivalent to a crack with a fractured surface of about  $0.3 \text{ mm}^2$ .

Two different aircraft components of Tornado with representative fatigue cracks were selected for the present study. The one is a frame of the center fuselage where fatigue cracks originated from corners of a large cutout. Fig. 7 gives an overview of the component, where the notches of consideration have been specially referenced. The other airframe component is a corner segment close to the outboard air intake where a fatigue crack originated on the lower flange side during early stage of MAFT. An overview of this component is given in Fig. 8.

Following the fatigue design procedure used for the Tornado fighter aircraft notches can be related to either one of the three  $K_t$  values 2.0, 2.5 and 3.6 when appropriate. For the components under consideration values of  $K_t = 2.5$  (cutout of frame of

center fuselage) and  $K_t = 2.0$  (corner segment of outboard air intake) had to be set.

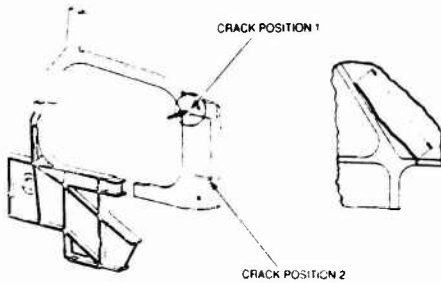


Fig. 7 Crack location in frame of center fuselage

The length of the cracks detected was in the order of 30 mm at the cutout and about 6 mm at the frame close to the outboard air intake. Results of previous inspections as well as a crack growth calculation for a similar detail indicate a high growth rate of the cracks once initiated at the cutout which suggests a crack "initiation" life of about 90 percent of the life reported through inspection.

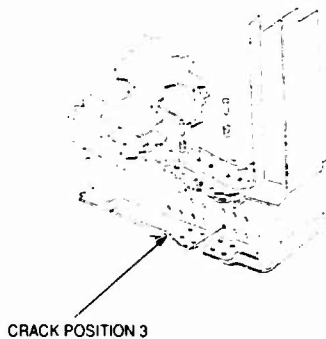


Fig. 8 Crack location in corner segment of outboard air intake

## 6.2 Load Spectra

The load spectra considered have been service load sequences generated for the Tornado design pro-

gramme. Due to slight modifications in the design programme and the component test results available, six different load sequences were selected (Fig. 9):

**Sequence A:** A sequence derived from a typical  $n_t$ -sequence for fighter aircraft and being used to determine the fatigue life of unnotched and notched components. The sequence comprises 200 flights of 15 different flight types. Each flight contains between 48 and 115 load cycles.

**Sequence B:** A sequence derived from 19 different flight types monitored on F-104 G fighter aircraft. The sequence comprises 205 flights with 7 to 169 load cycles per flight.

**Sequence C:** equivalent to B with a different order of flight types.

**Sequence D:** A sequence developed for the design of fighter aircraft tailerons with an overall stress ratio  $R = \sigma_{min}/\sigma_{max} = -0.75$ . The sequence comprises 400 flights with 26 different flight types of approximately 65 load cycles each.

**Sequence E:** A sequence generated from the level crossing spectrum of sequence D. For the new load sequence the mean loads of each load cycle had been set to zero. The sequence comprises 400 flights with 10 different types.

**Sequence F:** This is the sequence used for Tornado-MAFT. It is composed of 1095 different load cases which have been the basis for configuration of 42 different flight types. Each flight type contains about 400 load cycles. One block contains 900 flights. The loads themselves are given in terms of bending moments at a defined coordinate center of the aircraft. To convert the load sequence to a sequence of nominal stresses for the location considered wing position dependent conversion factors were introduced on the basis of fully elastic load transfer behaviour being the ratio of calculated maximum nominal stress vs. the maximum load generated for the specific wing position dependent load cases. Depending on the location considered this led to slightly different load spectra being denoted as F1, F2 and F3 throughout the following.

The above load spectra are shown in Fig. 9 as a result of the peak counting algorithm. For the (nominal stress based) predictions discussed later, however, rainflow counted spectra were applied where the individual mean loads were considered.

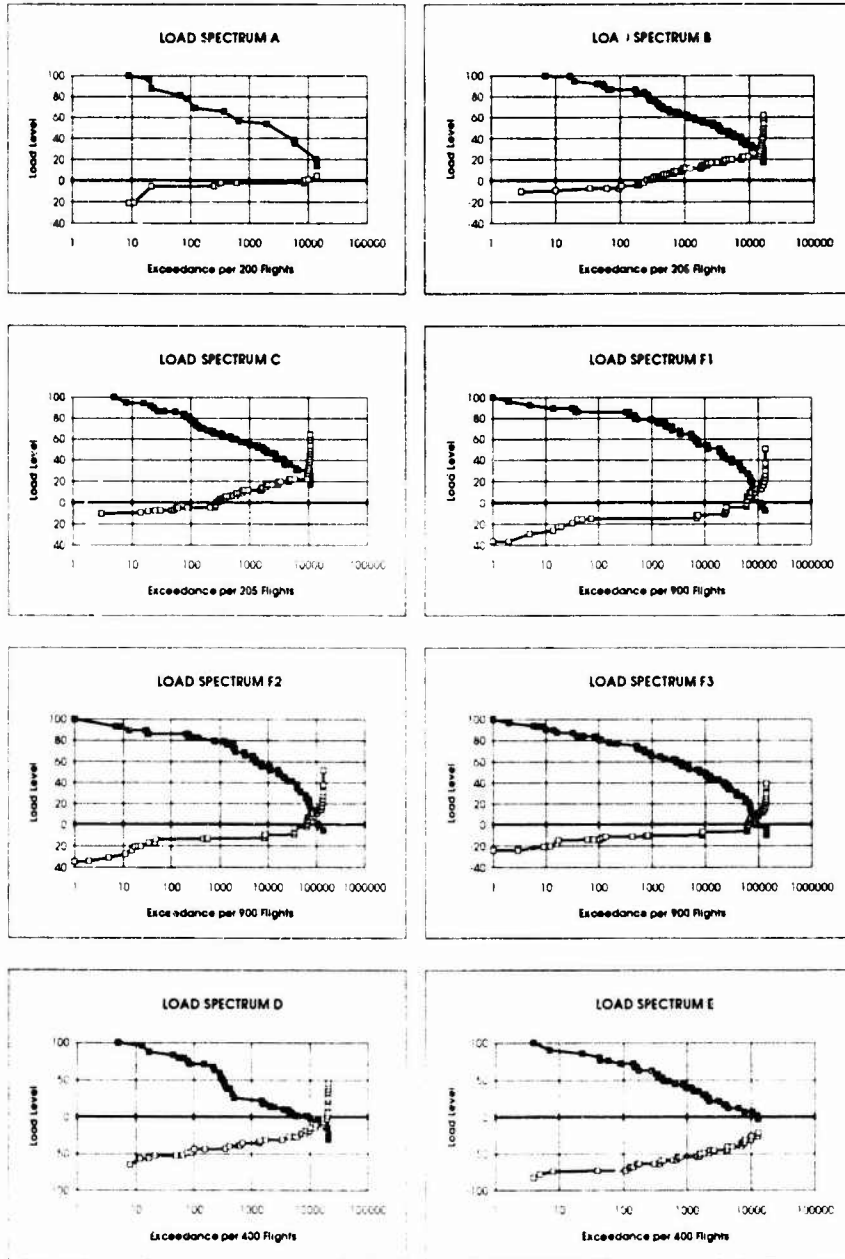


Fig. 9 Load spectra (peak count method)

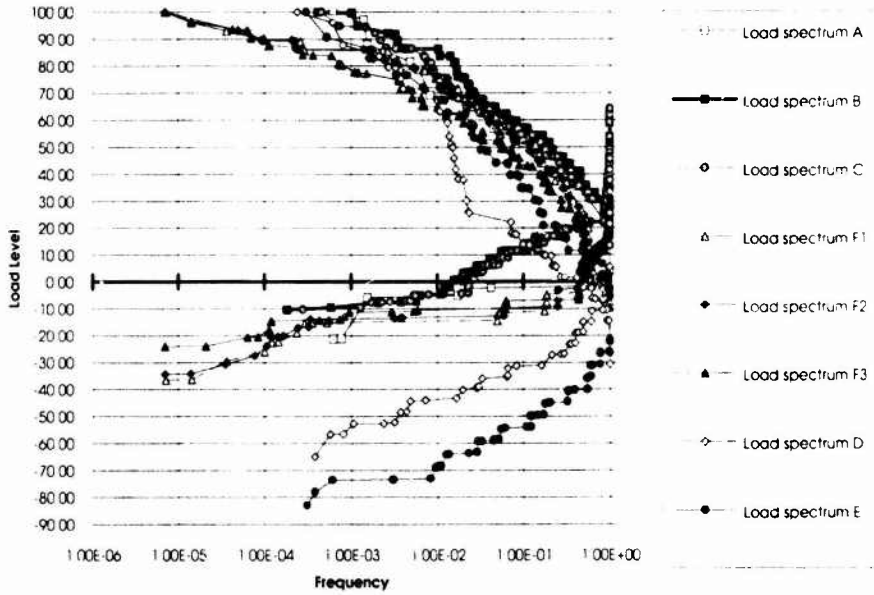


Fig. 10 Comparison of load spectra

A comparison of the normalized load spectra is given in Fig. 10 where load levels and the cumulative frequency have been normalized to the respective maximum values of each spectrum. Typically the taileron sequences D and E differ from the other sequences, but also the peak load distribution of sequences F appears to be less severe than those of sequences A to C. However, sequences F comprise a total number of cycles which is about one order of magnitude larger than the others. Sequence A has been generated during an earlier stage of Tornado design while B and C have been derived on a different fighter aircraft.

### 6.3 Baseline Material Data

Tensile properties of the 7075-T7351 alloy determined on specimens machined from 16 mm and 25 mm thick plates were:  $E = 71000$  MPa,  $\sigma_u = 514$  MPa,  $\sigma_y = 441$  MPa, elongation = 11%. Stress-strain and strain-life data for cyclic constant amplitude loading were determined on unnotched cylindrical specimens. The corresponding coefficients, the specimens' dimensions and the material's fatigue-life curve plotted in terms of  $P_{SWT}$  are given in Fig. 2. The failure criterion selected for

these fatigue tests was  $a_f = 0.5$  mm. The stress-strain relationship used for cyclic loading is written in terms of a Ramberg/Osgood equation:

$$\epsilon_s = \epsilon_{s,e} + \epsilon_{s,p} = \sigma/E + (\sigma/K')^{1/n'} \quad (12)$$

The material's baseline fatigue data in terms of the  $P_f$ - $N$  curve is given in Fig. 3 where  $P_f$  is obtained from strain-life data via Eq. (6). Since according to the  $P_f$  model fatigue life consists of growth of (short) cracks the slope  $m = 2$  of the  $P_f$ - $N$  curve (see Eq. (8)) must be relevant also for the crack growth law which translates to  $n = 4$  in  $da/dN$  vs.  $\Delta K$  diagram due to the quadratic relationship between  $\Delta K$  and  $\Delta J$ . The coefficient  $C = 3.9 \cdot 10^{-4}$  (dimensions mm/cycle and MPa) and the threshold  $\Delta J_{eff,th} = 0.0152$  N/mm have been obtained from long crack data reported in [28]. The equivalent initial crack size corresponding to the  $P_f$ - $N$  curve of Fig. 3 is  $a_0 = 0.057$  mm.

A comparison between the uniform material law for aluminium alloys given in [15], which is based on more than 600 experimental results and the baseline  $\sigma$ - $\epsilon$  and  $\epsilon$ - $N$  data used for the local strain approach shows good coincidence. As baseline data used for

the local strain and nominal stress approach were not available from the same batch, the required set of S-N curves of the notched specimens at different R-ratios was calculated by use of the local strain approach including the  $P_{SWT}$  parameter. These S-N curves were applied for nominal stress based crack initiation life prediction. For two specimen types at two load levels a comparison with experimental data could be made which indicated a reasonable accuracy.

## 7 RESULTS AND DISCUSSION

### 7.1 Crack Initiation Life Prediction

Fatigue life predictions for crack initiation were compared to the experimental results mentioned above. The following models were applied:

- nominal stress approach using S-N curves derived for crack initiation
- local strain approach using  $P_{SWT}$  damage parameter
- local strain approach using  $P_f$  damage parameter.

The nominal stress based predictions used a set of S-N curves for  $R = 0.5, 0, -1$  and  $-2$  as described in chapter 6.3. The curves were fitted to a four-parameter Weibull equation always accounting for the endurance limit. Intermediate R-ratios were considered via interpolation between the above curves.

For the local strain approach the influence of notch size and transient endurance limit was accounted for by different means depending on the damage parameter used. With the  $P_{SWT}$  parameter, a transient endurance limit (or damage below the fatigue limit) was globally accounted for by neglecting the endurance limit. Notch size effects were included by using the fatigue notch factor  $K_f$  instead of  $K_t$  (see Table 1).

Transient endurance limit as well as size effects were considered by the  $P_f$  parameter as described in chapter 5. The relevant constants and coefficients are compiled in Table 1 where a value of  $q = 15$  was used for calculations of  $F_3$  and  $I_3$  [18].

An example of the predicted and experimental spectrum S-N curves of the notched coupons is given in Fig. 11. With two exceptions five tests per load level were available to establish the respective mean value. For all cases the ratio of the experi-

mental mean vs. the predicted fatigue lives were determined and plotted in a bar chart (Fig. 12)

$K_t$	Notch Radius (mm)	$K_f$	$I_3$ (mm <sup>3</sup> )	$F_3$	$\sigma_{y0}$	$\alpha$
2.0	3	1.86	43.0	1.142	0.09	1.6
2.5	4	2.34	16.6	1.217	0.06	1.4
3.5	2	3.08	5.25	1.314	0.13	1.3
1.0	--	1.0	157.4	1.0	---	---

Tab. 1 Coupon notch factors and related constants

where the specimen type, load spectrum and load level is given for each case. To visualize the quality of the different models, the life ratios are plotted in a probability chart (Fig. 13).

For the aircraft components notch size effects were not considered within local strain based calculations because of the relatively large notches. However the influence of multiaxial stresses seemed relevant for the cutouts of the center fuselage's frame. Therefore additional calculations were done to discuss that effect.

The fatigue lives and respective life ratios determined with the different approaches are summarized in Tables 2 and 3.

Following the Tornado fatigue design process the stress concentration factor  $K_t$  for the corner segment was set to 2.0 even though approximations from handbooks yielded a lower value. An additional calculation with  $K_t = 1.5$  was therefore performed.

### 7.2 Discussion

#### Noched Coupons

For the assessment of life prediction hypotheses different criteria can be applied [29]. One important criterion is the spread (or scatter) of life ratios, another one may be the mean life ratio indicating conservative or unconservative predictions on an average or the fact that, for example, predictions are always or predominantly on the conservative side.

With regard to the spread of predictions for the notched coupons, Fig. 13 shows that all three variants exhibit similar numbers with the lowest scatter for the nominal stress approach. Translating

COMPONENT	K <sub>t</sub>	Nom. Stress Approach	P <sub>SWT</sub>	P <sub>J</sub>	
				Without Multiaxiality	With Multiaxiality
Frame in Center Fuselage - Upper Notch - Lower Notch	2.5	265,000	167,360	32,390	55,810
	2.5	70,750	65,770	9,870	16,850
Corner Segment close to Outboard Air Intake	2.0	15,800	22,710	3,500	.....
	1.5		104,850	18,440	

Tab. 2 Predicted flights for aircraft fuselage details using different approaches (crack initiation life)

COMPONENT	K <sub>t</sub>	Nom. Stress Approach	P <sub>SWT</sub>	P <sub>J</sub>	
				Without Multiaxiality	With Multiaxiality
Frame in Center Fuselage - Upper Notch - Lower Notch	2.5	0.04	0.06	0.31	0.18
	2.5	0.14	0.15	1.02	0.60
Corner Segment close to Outboard Air Intake	2.0	0.51	0.35	2.28	.....
	1.5		0.08	0.43	

Tab. 3 Fatigue life ratios for aircraft fuselage details using different approaches (crack initiation life)

quantitative requirements as put forward by different authors [29] into a scatter value (neglecting the absolute life ratios), all concepts may be assessed as acceptable. The mean values however differ significantly. Whereas the nominal stress based as well as the local strain based predictions using P<sub>SWT</sub> deliver unconservative results, the P<sub>J</sub> parameter produced mainly conservative predictions.

Similar trends have been found in [17,18] where an extensive study on a variety of materials including steels and aluminium alloys has been performed. The spread of the P<sub>J</sub> based predictions, however, was markedly smaller than that of the conventional P<sub>SWT</sub> parameter (3.6 for P<sub>J</sub> vs. 5.9 for P<sub>SWT</sub> for the 10% and 90% probability ratio of life ratios). The mean life ratio for P<sub>J</sub> was close to unity whereas for P<sub>SWT</sub> a value of 0.3 was found which is generally in line with the present results.

It is perhaps interesting to note that the nominal stress approach and the P<sub>SWT</sub> based predictions delivered similar results in several cases (Fig. 12) although the consideration of damage contributions below the endurance limit had been different (see

Chapter 7.1). This part of the spectra obviously

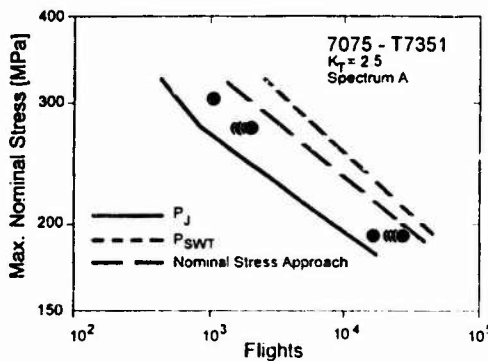


Fig. 11 Comparison of experimental and predicted crack initiation spectrum fatigue lives for notched coupons

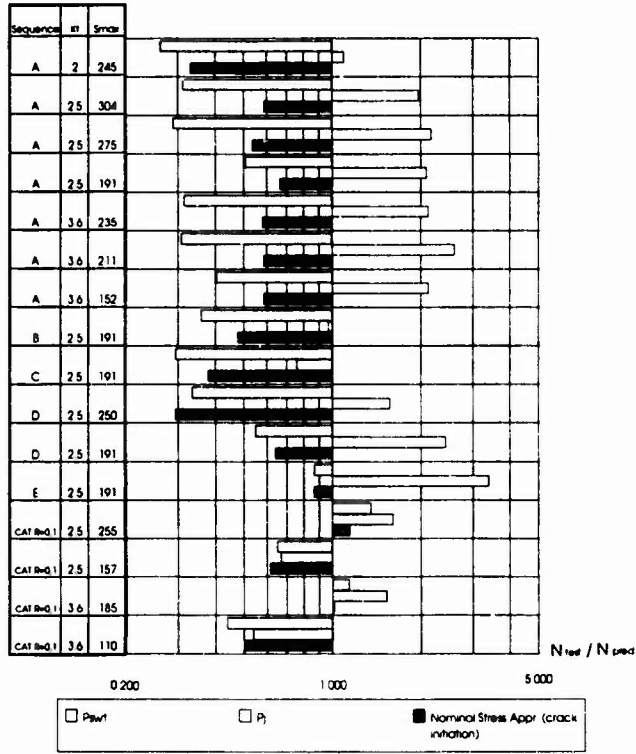


Fig. 12 Life ratios for crack initiation of notched coupons under fatigue loading

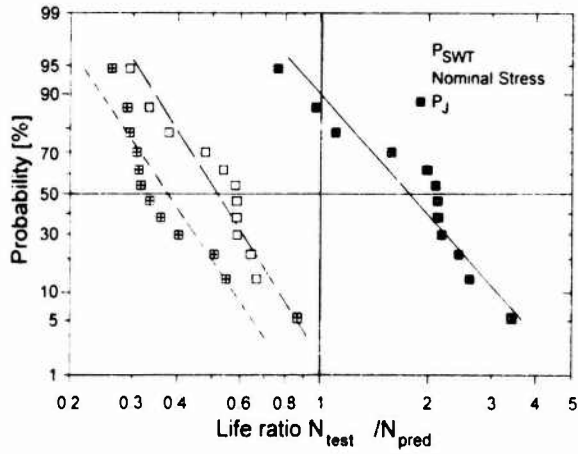


Fig. 13 Distribution of life ratios

does not contribute to the calculated damage to a significant amount within those methods. This has been confirmed for selected test cases.

#### Aircraft Components

Forementioned trends determined for the notched coupons were similar for the aircraft components. The nominal stress as well as  $P_{SWT}$ -based predictions are unconservative whereas the  $P_f$ -based predictions are closer to unity. Considering a biaxial stress state at the cutouts shows a marked influence on the predicted life. With regard to the above results however the approximate nature of that part of the  $P_f$ -model should be kept in mind.

For the corner segment a later analysis indicated the stress concentration factor to be lower than 2.0. Applying a value of 1.5 the  $P_f$ -model again resulted in a better prediction than using the conventional  $P_{SWT}$ -parameter.

The significant underestimation of fatigue life for the upper part of the cutout in the center fuselage's frame may have been promoted by an underestimation of the stress level determined by FE-analysis. The corresponding calculated stress level for the lower notch of the cutout was 17% higher which resulted in a shorter predicted fatigue life even though the experimentally determined fatigue lives were similar for the upper and lower notch. A further crack along a rivet row having occurred in the vicinity of the upper part of the cutout during the final stage of the test life may have contributed to an increase of the applied stress. The short propagation period of the crack initiated at the upper notch gives further support to this assumption.

#### Predictions Based on Handbook Data

Standard design procedures for (German) military aircraft include a nominal stress approach based on S-N data valid for complete specimen separation. Data of that kind is mainly obtained from handbooks [30] and has been used for predictions of the respective total fatigue test lives of the notched coupons and the total test lives of the aircraft components. For the notched coupons, unconservative predictions were obtained with a mean life ratio similar to that obtained with the nominal stress approach based crack initiation fatigue life predictions. Scatter however increased by 60%.

Similar trends are observed for the aircraft components. For the three examples predictions are unconservative and differ significantly with life ratios

between 0.0016 and 0.73. In particular the first number being out of order gives rise to the fore-mentioned assumption of a considerable underestimation of the overall stress level for the respective detail.

## 8 CONCLUDING REMARKS

Fatigue life predictions to crack initiation were performed using the nominal stress approach and two versions of the local strain approach. A so-called  $P_f$ -model for explicit consideration of load-sequence effects based on crack opening and closure phenomena has been outlined which can be applied within the framework of a local strain approach. The spread of life ratios for notched coupons tested under different fighter aircraft spectra was similar for the three variants. Only the  $P_f$ -model, however, resulted in conservative predictions.

In order to demonstrate applicability to fatigue-critical areas of real aircraft, three examples have been selected for Tornado-MAFT.  $P_f$ -based predictions led to the best result which can be taken as a motivation to extend this analysis to further details and materials.

Even if application of the local strain approach to fasteners appears to be impractical, there is a considerable amount of details where such a type of approach is promising. One of these aspects to be noted is the relatively small experimental effort for determination of baseline fatigue data. This makes the local strain based approach potentially interesting not only for prototype design, but also for redesign (e.g. structural or material modification) within aircraft mid-life updates.

## REFERENCES

- [1] Perry F.S.; "Harrier II: A Comparison of US and UK Approaches to Fatigue Clearance"; 77th Meeting of AGARD-SMP, Workshop on "Fatigue Damage and Crack Growth Prediction Techniques", Bordeaux/France (1993) Paper 17
- [2] O'Hara J.; "Fatigue Design, Test and In-Service Experience of the BAe Hawk"; 77th Meeting of AGARD-SMP, Workshop on "Fatigue Damage and Crack Growth Prediction Techniques", Bordeaux/France (1993) Paper 18

- [3] Kelly M., R. Koenigstein; "F/A-18 Structural Fatigue Life Monitoring - The Navy Experience"; pres. at 1992 USAF Structural Int. Progr. Conf., San Antonio, USA
- [4] Bleuzyent C., M. Chaudonneret, J. Falvenot, N. Panganathan, M. Robert; "Validation of Life Prediction Models from Representative Testings on Aluminium Alloy Specimens"; pres. at ICAF-Symp. Stockholm (1993)
- [5] Friedman R., A. Gomza, H. Armen, H.L. Eidinoff; "Fatigue Life under Compression-Dominated Spectra"; in: *Durability and Damage Tolerance in Aircraft Design*, (13th ICAF-Symp.), EMAS (1985) pp. 171-214
- [6] Dowling N.E., A.K. Khosrovaneh; "Simplified Analysis of Helicopter Load Spectra"; in: *Development of Fatigue Loading Spectra*, ASTM-STP 1006 (1989)
- [7] Vormwald M., "Crack Initiation Life Prediction Based on Fracture Mechanics for Short Cracks"; Techn. University Darmstadt, Inst. f. Stahlbau & Werkstoffmechanik, Rep. No. 47 (1989) (in German)
- [8] Bochmann R., D. Weisgerber; "The Role of Fatigue Analysis for Design of Military Aircraft"; 77th Meeting of AGARD-SMP, Workshop on "Fatigue Damage and Crack Growth Prediction Techniques", Bordeaux/France (1993) Paper 15
- [9] Neuber H.; "Theory of Stress Concentration for Shear-Strained Prismatical Bodies with Arbitrary Nonlinear Stress-Strain Law"; *Trans ASME, J. Appl. Mech.* 28 (1961), pp. 544-550
- [10] Seeger T., P. Heuler; "Generalized Application of Neuber's Rule"; *J. Test. Evaluation* 3 (1980), pp. 199-204
- [11] Nihei M., P. Heuler, Chr. Boller, T. Seeger; "Evaluation of Mean Stress Effect on Fatigue Life by Use of Damage Parameters"; *Int. J. Fatigue* 8 (1986), pp. 119-126
- [12] Smith K.N., P. Watson, T.H. Topper; "A Stress-Strain Function for the Fatigue of Metals"; *J. of Materials* 5 (1970), pp. 767-778
- [13] Bergmann J.W.; "On Service-Fatigue Life Prediction Based on Local Stress-Strain"; Techn. University Darmstadt, Inst. f. Stahlbau & Werkstoffmechanik, Rep. No. 37 (1983) (in German)
- [14] Boller Chr., T. Seeger; "Materials Data for Cyclic Loading"; Parts A-E, Elsevier Science Publishers, Amsterdam (1987)
- [15] Bäuml A. jr., T. Seeger; "Materials Data for Cyclic Loading"; Supplement 1, Elsevier Science Publishers, Amsterdam (1990)
- [16] Vormwald M., T. Seeger; "The consequences of short crack closure on fatigue crack growth under variable amplitude loading"; *Fatigue Fract. Engng Mater. Struct.* 14 (1991), pp. 205-225
- [17] Vormwald M., P. Heuler, T. Seeger; "A fracture mechanics based model of cumulative damage assessment as part of fatigue life prediction"; in: *Advances in Fatigue Lifetime Predictive Techniques*, ASTM-STP 1122 (1991), pp. 28-43
- [18] Vormwald M., P. Heuler, C. Krae; "Spectrum fatigue life assessment of notched specimens using a fracture mechanics based approach"; in: *Automation in Fatigue and Fracture Testing and Analyses*, ASTM-STP, to be published
- [19] Vormwald M., P. Heuler; "Examination of Short-Crack Measurement and Modelling under Cyclic Inelastic Conditions"; *Fatigue Fract. Engng Mater. Struct.* 16 (1993), pp. 693-706
- [20] Dowling N.E.; "J-integral estimates for cracks in infinite bodies"; *Engng Fract. Mech.* 26 (1987), pp. 333-348
- [21] Rie K.T., R. Schubert; "Note on the crack closure phenomenon in low cycle fatigue"; *Int. Conf. LCF and El.-Plastic Behaviour Mat.*, Muruch, Elsevier Appl. Science, New York (1987), pp. 575-580
- [22] Du Quesnay D.L., T.H. Topper, M.A. Pompetzka; "The effective stress range as a mean stress parameter"; *Int. J. Fatigue* 14 (1992), pp. 45-50
- [23] Newman J.C. jr.; "A crack opening stress equation for fatigue crack growth"; *Int. J. Fract.* 24 (1984), pp. R131-R135
- [24] Tanaka K., Y. Nakai, M. Yamashita; "Fatigue growth threshold of small cracks"; *Int. J. Fract.* 17 (1981), pp. 519-533
- [25] Boller Chr.; "The Influence of Specimen Size and Surface Roughness on Fatigue Life Evaluations Based on Local Stresses and Strains"; Techn. University Darmstadt, Inst. f. Stahlbau & Werkstoffmechanik, Rep. No. 46 (1988) (in German)
- [26] Weisgerber D.; "Flight-by-Flight Fatigue Tests on Flat Specimens of Ti6Al4V annealed, 7075-T7351 and 2024-T3"; MBB-Report FE 2170/1231 (1974)

- [27] Weisgerber D., P. Hahn; "Fatigue Life Prediction for Fighter Aircraft - Experimental and Theoretical Analyses for Verification of New Life Prediction Procedures" (Part 2); MBB-Report UFE1390 (1977), (in German)
- [28] Huster J.; "Fatigue life prediction under consideration of micro crack growth"; Dr.-Ing. Thesis, Univ. German Fed. Armed Forces, Neubiberg (1988), (in German)
- [29] Schütz W., P. Heuler; "Miner's Rule Revisited"; 77th Meeting of AGARD-SMP, Workshop on "Fatigue Damage and Crack Growth Prediction Techniques", Bordeaux/France (1993) Paper 1
- [30] N.N.; "Luftfahrttechnisches Handbuch (LTH); Handbuch Strukturberechnung (HSB)"; Industrie-Ausschuß Struktur Berechnungsunterlagen (IASB), München (1988)
- [31] Rosenberger A.H., H. Ghonem; "Effect of cycle mean strain on small crack growth in alloy 718 at elevated temperatures", Fatigue Fract. Engng Mater. Struct. 15 (1992), pp. 1125-1139

## Growth of Artificially and Naturally Initiating Notch Root Cracks Under FALSTAFF Spectrum Loading

R. Sunder, R.V. Prakash  
National Aerospace Laboratories, BANGALORE 560 017, India

and

E.I. Mitchenko  
Institute for Strength Problems  
Ukrainian Academy of Sciences Timiryazevskaya, 2, KIEV 252 014, Ukraine

### ABSTRACT

The paper describes an experimental study of notch root fatigue crack growth under FALSTAFF spectrum loading in an Al-Cu alloy. Crack growth rates were measured from crack size as small as 20 microns using optical fractography and replication technique. Fractographic measurements indicate similar scatter levels between notch root short crack and long growth rate data. This is in contrast to surface replica based measurements which are indicative of large scatter. Growth rate variation was noticed between multiple cracks initiating after different periods of natural crack formation. This is attributed to the influence of larger existing cracks on smaller cracks that appear later. In contrast, identical artificially initiating cracks grew at a similar rate.

### INTRODUCTION

Fatigue failures as a rule initiate at stress raisers like holes, fillets, etc.. Even though crack initiation is localized in this manner, a careful study of service failures often indicates that the large crack at failure actually resulted from the merger of multiple cracks that initiated at different locations on the notch surface. A large fraction of total fatigue life can be exhausted in the formation and growth of small cracks at the notch root.

A number of theoretical studies have been carried out on the estimation of stress intensity factors for multiple crack situations involving interaction and coalescence [1-5]. Many studies involved numerical techniques and were usu-

ally restricted to modeling a pair of cracks [6-9]. Statistical techniques have been used to handle the merger of multiple cracks [5,10,11].

A few experimental studies were restricted to the study of the growth and coalescence of two artificially initiated cracks at the notch root [6-9]. Much work has been devoted to the study of the distribution of total fatigue life over crack initiation and growth, including questions of crack density [12-14].

Published experimental data often lack information on the interaction of multiple cracks by way of influencing crack growth rate. In fact ref. 9 which describes experiments on a pair of cracks initiated artificially (and of equal size) concluded that there was indeed no interaction between them.

This paper describes an experimental study on the growth of multiple naturally initiating cracks at the notch root. The study was carried out under a fighter aircraft wing load spectrum to simulate realistic loading conditions. The objective was to track the initiation and growth of small cracks through replication technique, and through optical fractography. It was expected that in contrast to previous work (e.g. ref. 9) which was restricted to multiple cracks of identical size, multiple cracks of different size may interact and thereby influence growth rates. One would expect a related variation in growth rates for cracks when compared with reference to similar size and shape. This can have implications for life prediction as well as nondestructive

inspection. The next section describes the experimental procedure used in the study. This is followed by a summary of test results and discussion.

#### EXPERIMENTAL PROCEDURE

**Material and specimens:** The experiments were conducted on Al-Cu alloy L168 from an Indian manufacturer, which is an equivalent of 2014-T6511. Specimens were cut along the extrusion direction from 200x70 mm bar stock. The geometry and dimensions of the test specimens appears on Fig. 1. A total of three specimens were used in the experiments: Specimen 1 had two similar co-planar crack initiators introduced by electrical discharge machining (EDM). Specimens 2, 3 were tested with a smooth notch surface to ensure natural crack initiation. The notch surface was polished to assist crack tracking using replication technique.

**Testing:** The specimens were tested under a programmed version of the FALSTAFF load spectrum [15]. In this version, the loads are arranged in such a manner so as to cause the formation of discernible striation (beach mark) patterns that can later be recognized by optical fractography. Ref. 15 provides a detailed description of this technique and how it can be used to measure the growth rate of small cracks under the FALSTAFF spectrum. It also provides evidence suggestive of little or no distortion in overall test results due to the rearrangement of the randomized FALSTAFF source load sequence. One complete block of FALSTAFF corresponds to 200 flights. Briefly, the FALSTAFF load spectrum is rearranged into 18 identical multilevel programmed steps, each with one of the 18 major loads in the spectrum. A schematic of the sequence appears on Fig. 2. The major loads are identical to the 18 most severe ones in FALSTAFF, while the programmed steps were shown through analysis and testing to be the equivalent of the rest of the FALSTAFF sequence in damage content [15].

Specimens 1,2 were tested at the same spectrum reference (maximum) nominal stress level of 225 MPa.

This stress level induces monotonic yield at the notch root. However, as the ratio of the lowest to highest stress level in the spectrum is -0.3, reversed yield did not take place. Earlier experiments under FALSTAFF spectrum on the same material had shown [15], that this stress level causes large hysteretic variations in notch root plasticity induced crack closure and also, that the local stress level is sufficiently large to cause early crack initiation. Finally, the selected stress level had in earlier experiments produced excellent fractographic evidence of striation mode crack growth from small sizes right up to a few millimeters from the notch root. The objective of these tests was to compare growth rate behaviour for artificially initiated cracks as opposed to naturally initiating cracks. Specimen 3 was tested at a spectrum reference stress level of 275 MPa. This stress level causes cyclic yield at the notch root. The objective of this experiment was to assess stress level effect on the growth of naturally initiating cracks.

All tests were carried out to failure and no additional instrumentation was used to track crack growth. The testing was carried out on a 100 kN computer controlled servohydraulic testing machine at an average test frequency of 10 Hz. The specimen was held by hydraulic grips, whose wedging action induced uniform displacement, rather than uniform stress conditions. It may be suggested that this difference may have only a negligible effect on short cracks growing out of the notch.

**Crack growth measurements:** Two methods were used to determine notch root short crack growth rates: notch surface replication during the test and optical fractography after failure. During the test, the replica was initially applied to the notch surface once every block of the FALSTAFF spectrum, while maintaining a load equal to 75% of the maximum spectrum load. This was to ensure that those cracks that did appear could be open for the replica to penetrate. Once a crack could be detected, replication was carried

out more often. A Neophot- 2 optical microscope was used to study the fatigue fracture surfaces after failure.

The replica technique is restricted to surface measurements. Fractography assists in tracking growth across the entire crack front. It may be fair to note that fractographic approach gives excellent results everywhere with the exception of the specimen surface, because the surface region is often damaged due to rubbing, debris formation, fallout or abrasive action. As a consequence, crack depth, 'c', rather than surface length, 'a' is a better criterion to assess short crack growth rate. To make this possible, a:c ratio was determined from optical fractography as a function of surface crack length. Using this relationship, replica measurements of surface crack size were translated into crack depth data. The translation assumed that a:c ratio cannot see sudden (discrete) variation - as clearly indicated by the fractographic evidences on growth across the crack front. All growth rates obtained from this study appear in terms of  $dc/dF$ , rather than  $da/dF$ .

Crack growth rate measurements: Growth rates were determined directly from fractography. As mentioned earlier, the programmed FALSTAFF sequence contains eighteen steps, each with a characteristic major load cycle and a number of programmed minor load cycle steps (see Fig. 2). Each of these sets of cycles leaves behind a characteristic 'macro' striation on the fracture surface that can be seen through an optical microscope.

Crack growth rate was determined from replica based growth measurements as the derivative of a parabolic fit through three points. Use of a greater order polynomial or greater number of points would have resulted in loss of data in the earlier stages of crack growth. For example, use of seven point polynomial as per ASTM E-647 would have meant discarding the first three growth data points. The parabolic fit results in the loss of only the first and last points in the growth

curve. Average growth rate estimate from successive crack extension and block interval measurements was discarded after observing a larger degree of scatter than in the case of parabolic fit through three points.

## RESULTS

Fig. 3 shows the fracture surface from specimen 1. One of the artificial crack initiators is clearly visible at the left. Also seen are the striation patterns left behind by the programmed FALSTAFF load sequence. These are visible only at certain locations in view of the poor depth of focus with optical fractography. Locally magnified pictures were used to determine crack growth rates from a crack size under 20 microns right through to failure.

Fig. 4 shows replica based crack growth measurements for the two tests carried out at 225 MPa. In case of the specimen with EDM crack initiators, crack growth was observed almost immediately after commencement of testing: 4 and 6 load blocks respectively for the two initiators. The two cracks merged after 42 load blocks as indicated by a jump in crack size which now appears as a single symbol, representing the sum of the two crack sizes. Also shown on Fig. 4 are replica based crack growth measurements for Specimen 2 with naturally initiating cracks. The replica technique indicated discernible first crack formation and growth after more than 30 blocks of loading, which translates to about 6000 flights. Other cracks appeared subsequently and this along with their merger and growth to failure accounted for the remaining 60 blocks of fatigue loading (12000 flights).

Fig. 5 shows fractographic and replica based crack growth rate estimates for specimen 1. The continuous lines are from replica data while the points are from optical fractography. Growth rate data in the same format for specimens 2 and 3 with multiple naturally initiating cracks at the two spectrum stress levels appear on Fig. 6. A total of 31 crack origins were counted in Specimen 3. A crack origin was identified as the locus

of radial lines passing through a developing crack front. All origins were traced to the notch surface. Figs. 5, 6 are indicative of considerable scatter in short crack growth rates when perceived through replica based measurements. This is consistent with experience cited in the literature [16]. However, scatter is not so apparent in the fractographic estimates of growth rates. Considering the log linear variation of growth rate versus crack depth, the linear fit correlation coefficient is an indicator of scatter. Linear fits through replica based growth rates versus crack depth yielded coefficients ranging between 0.6 and 0.8. This applied to both naturally initiating as well as the artificially initiated cracks. In contrast, log-linear fits of fractographic crack growth estimates versus crack length yielded correlation coefficients always exceeding 0.97. In the case of the two artificially initiated cracks, the coefficient was 0.99. This higher coefficient may be attributed to the larger effective crack size in view of a preexisting EDM notch of finite, well defined size and shape.

In view of the better quality of fractographic growth rate estimates, further analysis was restricted to this source of data. Fig. 7 shows greater detail of multiple crack growth rate data from Specimen 2 ( $S_{ref} = 225$  MPa). We find data points down to a crack depth of 20 microns and less. Data points for a particular crack are denoted by a separate symbol. A total of eighteen crack origin points were detected on this specimen. Data only for ten of these appear on the figure to avoid a cluttered picture. Data for the two slowest cracks are denoted by a continuous line. These were the dominant cracks as shown by the supporting data in Figs. 8 and 9.

Fig. 8 contains linear approximations of growth rate data for specimens 1 & 2. The growth rates for artificially initiated cracks are somewhat less than for the slowest naturally initiating cracks. Lines A and B are for the dominant cracks whose growth rates were denoted by a continuous line

in Fig. 7. This is also apparent from the picture of crack front sizes reconstructed by reverse integration of growth rates and shown for specimen 2 in Fig. 9 at load block 71. We find cracks A and B have already grown to a depth of almost 1.5 mm, while most other cracks are much smaller. As shown by the lines in Fig. 8, the cracks that appeared later grew at a faster rate - under the influence of A and B. Thus, F, the smallest crack shown in Fig. 9 started growing at a rate about ten times higher than that of A (when A was of the same size). As these smaller cracks 'catch up' with the dominant one(s), a through crack finally appears. This is accompanied by a gradual merger of growth rates at the high end. Our observations did not indicate any sign of rapid acceleration after merger.

In contrast to the cracks in Specimen 2, the two artificially initiating cracks in Specimen 1 grew at an almost identical growth rate. Obviously, because their sizes were at any given time similar, their influence on each other was also even. It would be fair to suggest that they had an equal effect on each other, rather than conclude that they did not affect each other. To support the latter claim, one would have to test another specimen with a single (artificially initiated) crack and compare growth rates for the two cases. Equal growth rates would indicate that indeed two coplanar cracks of equal size do not affect each other.

#### DISCUSSION

It must be noted that the replication technique permitted the tracking of all cracks that appeared on the notch surface. Optical fractography could be used to track only those cracks that finally merged to form the dominant crack. Those that were on other planes ended up as non-propagating cracks and could not be studied using fractography. One may conclude that replica technique permits the study of crack formation on the notch surface, while fractography (where applicable) can provide a detailed and high preci-

sion picture of how dominant crack(s) leading to failure developed and propagated.

The fractographic study on specimen 2 revealed as many as 18 crack origins that were not necessarily coplanar. At a higher stress level (specimen 3 at 275 MPa), as many as 31 crack origins were traceable on the fracture surface. This suggests that as applied stress is increased, more cracks will originate at the notch root. It may be suggested however, that from the viewpoint of exhaustion of fatigue life, one needs to consider only the dominant crack(s) which account for the largest fraction of total fatigue life. Their growth occupies a sizeable fraction of total fatigue life. The smaller ones that appear after them would have only a negligible influence over the remaining period.

The observations made above may have implications for assignment of inspection periods and detectable crack sizes in design and operation of airframes. If a potential fatigue critical area is accessible for inspection from all sides where a crack is likely to initiate, one may readily assume that detection will always involve the dominant crack (which will happen also to be the slowest). On the other hand, if the design is of a fastener (inner notch surface concealed) or some other part where the opposite side also may be inaccessible, the design would have to assume the worst case scenario, whereby, when a small crack is detected, a much larger crack is likely to already exist inside that will accelerate the new ones's growth. This problem is more critical for thicker components where a through crack is more likely to be of critical dimensions.

Fractographic estimates of growth rates show negligible scatter and a clear log-linear relationship with crack length. This observation strongly supports the application of Fracture Mechanics to very small cracks. Considering that at higher stress level, crack growth was found to account for total fatigue life, an FM approach to life prediction appears practi-

cal. These observations may appear to contradict those often found in the literature, suggestive of considerable scatter in test results and also the characteristic dip in growth rates after initial accelerated growth, sometimes leading to crack arrest. It may be noted that our tests were carried out under spectrum loading and at stress levels of practical interest, which are rather high. Scatter reported in the literature may be attributed to limitations of growth measurement (replica technique) and the very nature of crack growth under constant amplitude near threshold conditions. Spectrum loading on the other hand has always been known to result in less scatter due to the 'control' exercised on the process by the infrequent overloads.

The artificially initiated cracks appeared to grow noticeably slower than the slowest naturally initiating cracks (Fig. 8). This difference may be attributed to a smaller effective size (given as total depth minus notch depth) of these cracks in the initial stage of growth as they are growing out of an EDM 'notch within a notch'. If this observation is acceptable, it would follow, that one cannot make a useful study of notch root small crack growth using artificial crack initiators.

Finally, it may be noted that the fractographic technique involving specially engineered load sequencing and a material that is conducive to ductile striation formation may not always be a realistic proposition. However, both inputs in this study were of practical relevance and they provided data that may not have been obtained using other methods. Considering the requirement of obtaining a better understanding of spectrum load notch root fatigue of greater application value, it is proposed to extend the same technique to fasteners, including lugs with and without interference fits.

#### CONCLUSIONS

1. The growth of multiple cracks at notches was experimentally studied in L168 Al-Cu alloy coupons. Crack growth was

measured using replication technique and optical photography.

2. Replication technique provides information on the formation and growth of cracks over the entire notch surface. However, the quality of crack growth rate measurements using this technique may not be adequate in view of large observed scatter in results.
3. Fractographic measurements of crack growth rates show excellent consistency and low scatter, that is comparable to long crack growth rates. They also permit identification and tracking of multiple cracks that initiate at the notch root.
4. Cracks growing from identical crack initiators grow at the same rate. However, naturally initiating cracks seldom do so simultaneously. Consequently, cracks that appear later grow faster under the influence of existing fatigue cracks.
5. As applied spectrum stress level is increased, crack initiation sites increase in number. Also, the fraction of total fatigue life consumed in crack growth increases and can reach 100% at a sufficiently high stress level.

**Acknowledgment:** Dr. E.I. Mitchenko's participation in this work enjoyed the support of the Ukrainian Academy of Sciences and the Department of Science and Technology, Govt. of India. Support for the experimental effort was provided by the Aeronautical Development Agency, Govt. of India. The fractographic study involved the participation of Birla Institute of Technology (BITS), Pilani students, Sumeet Saluja and Usha Rani.

#### REFERENCES

1. Isida, M., Analysis of Stress Intensity Factors for Plates Containing Random Array of Cracks, Bull. J.S.M.E., Vol. 13, 1970, pp. 635-642.
2. Heath, B.J., Grandt, A.F., Stress Intensity Factors for Coalescing and Single Corner Flaws Along a Hole Bore in a Plate, Engng. Fract. Mech., Vol. 19, No. 4, 1984, pp. 665-673.
3. Melin, S., Why Do Cracks Avoid Each Other? Int. Journ. Fracture, Vol. 23, 1983, pp.37-45.
4. Murakami, Y., and Nemat-Nasser, S., Interacting Dissimilar Semi-Elliptical Surface Flaws under Torsion and Bending, Engg. Fract. Mech., Vol. 16, No. 3, 1982, pp. 373-386.
5. Chang, R., On Crack-Crack Interaction and Coalescence in Fatigue, Engg. Fract. Mech., Vol. 16, No. 5, 1982, pp. 683-693.
6. McComb, T.H., Pope, J.E., and Grandt, A.F., Growth and Coalescence of Multiple Fatigue Cracks in Polycarbonate Test Specimens, Engg. Fract. Mech., Vol. 24, No. 4, 1986, pp. 601- 608.
7. Grandt, A.F., Thakker, A.B., and Tritsch, D.E., An Experimental and Numerical Investigation of the Growth and Coalescence of Multiple Cracks at Notches, Fracture Mechanics: Seventeenth Volume, ASTM STP 905, J.H. Underwood, R. Chait, C.W. Smith, D.P., Wilhem, W.A. Andrews and J.C. Newman, Eds., American Society for Testing and Materials, Philadelphia, 1986, pp. 239-252.
8. Soboyejo, W.O., Kishimoto, K., Smith, R.A., and Knott, J.F., A Study of the Interaction and Coalescence of Two Coplanar Fatigue Cracks in Bending, Fatigue Fract. Engg. Mat. & Struct., Vol. 12, No. 3, 1989, pp. 167-174.
9. Soboyejo, W.O., On the Prediction of the Fatigue Propagation of Semi-Elliptical Defects, Advances in Fatigue Lifetime Predictive Techniques, ASTM STP 1122, M.R. Mitchell and R.W. Landgraf, Eds., American Society for

Testing and Materials, Philadelphia, 1992, pp. 435-448.

sory Services Ltd., 1982, pp. 3-40.

10. Kitagawa, H., Fujita, T., and Miyazawa, K., Small Randomly Distributed Cracks in Corrosion Fatigue, ASTM STP 642, 1978, pp. 98-114.
11. Suh, C.M., Lee, J.J., Kang, Y.G., Ahn, H.J., and Woo, B.C., A Simulation of The Fatigue Crack Process in Type 304 Stainless Steel at 538 C, Fat. Fract. Engg. Mat. & Struct., Vol. 15, No. 7, 1992, pp. 671-684.
12. Suh, C.M., Lee, J.J., Kang, Y.G., Fatigue Microcracks in Type 304 Stainless Steel at Elevated Temperature, Fat. Fract. Engg. Mat. & Struct., Vol. 13, No. 5, 1990, pp. 487-496.
13. Goto, M., Scatter Characteristics of Fatigue Life and the Behaviour of Small Cracks, Fat. Fract. Engg. Mat & Struct., Vol. 15, No. 10, 1992, pp. 953-963.
14. Hyspecky, P., Strnadell, B., Conversion of Short Fatigue Cracks into a Long Crack., Fat. Fract. Engg. Mat. & Struct., Vol. 5, No. 9, 1992, pp. 845-854.
15. Mitchenko, E.I., Prakash, R.V., and Sunder, R., Fatigue Crack Growth Under Programmed Equivalent of FALSTAFF spectrum, Project Document PDST-9233, National Aeronautical Laboratory, Bangalore, India, August 1992.
16. Newman, J.C., and Edwards, P.R., Short-Crack Growth Behaviour in an Aluminum Alloy - An AGARD Cooperative Test Programme, AGARD Report No. 732, 1988.
17. Schijve, J., Stress Gradients Around Notches, Fatigue of Engg. Mat. & Struct., Vol. 3, 1981, pp. 325-338.
18. Forsyth, P.J.E., The Determination of Fatigue Crack History from Fracture Surface Analysis, Advances in Crack Length Measurement (C.J. Beevers, Ed.), Engg. Materials Advi-

Note: All dimensions in mm.

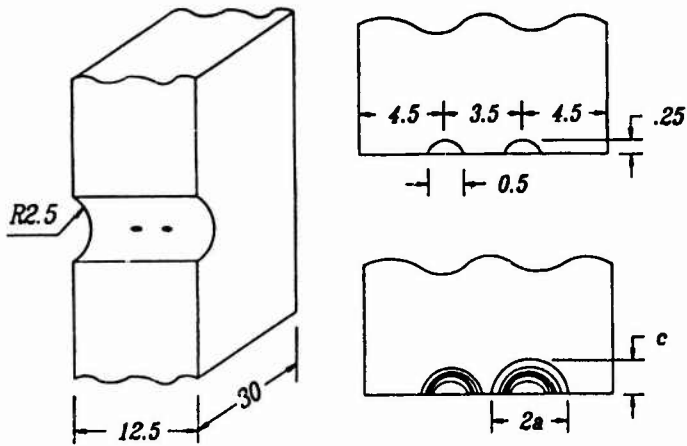


Fig.1. Single edge notch (SEN) specimen with two EDM crack initiators. The other specimens tested were similar, but without the EDM crack initiators.

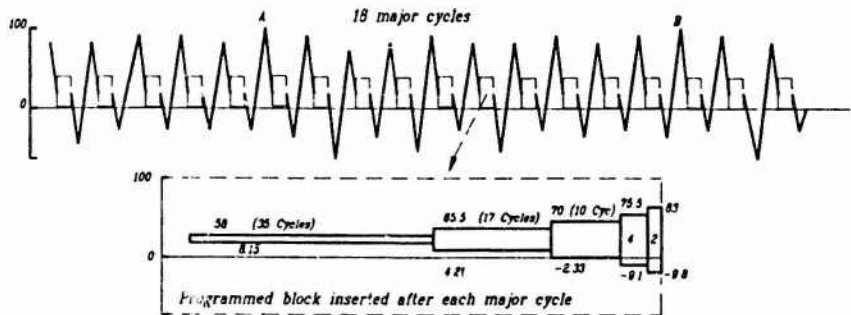


Fig.2. Programmed FALSTAFF load sequence used in experiments. This spectrum was found to provide the same crack growth rates as the full, randomized version [15].



Photomicrograph of a mineral specimen showing a complex, crystalline structure with sharp, angular features and a highly reflective surface.



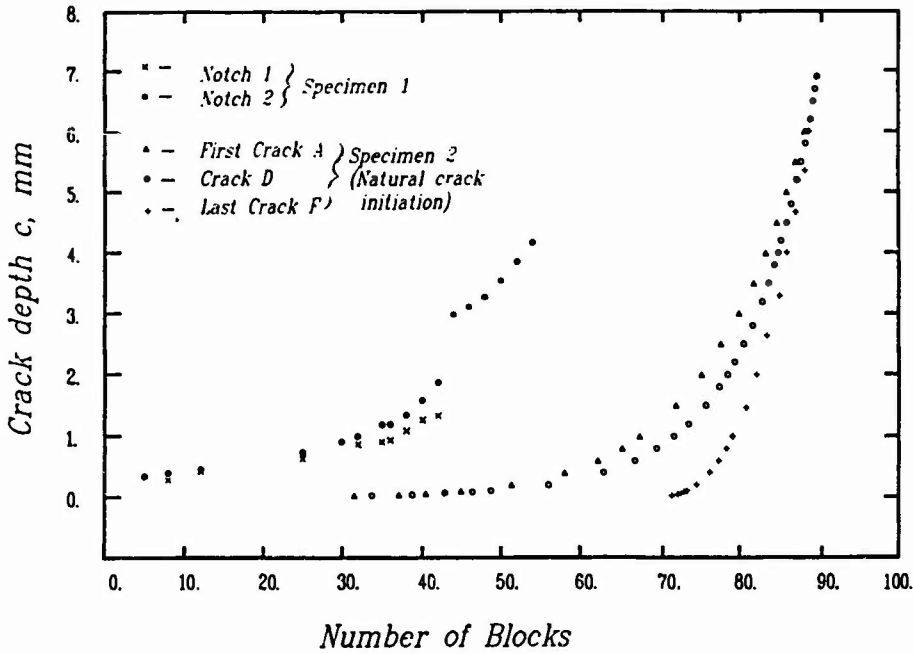


Fig.4. Replica based crack growth measurements under programmed FALSTAFF. Data for Specimens 1 & 2. Spectrum reference stress level 225 MPa.

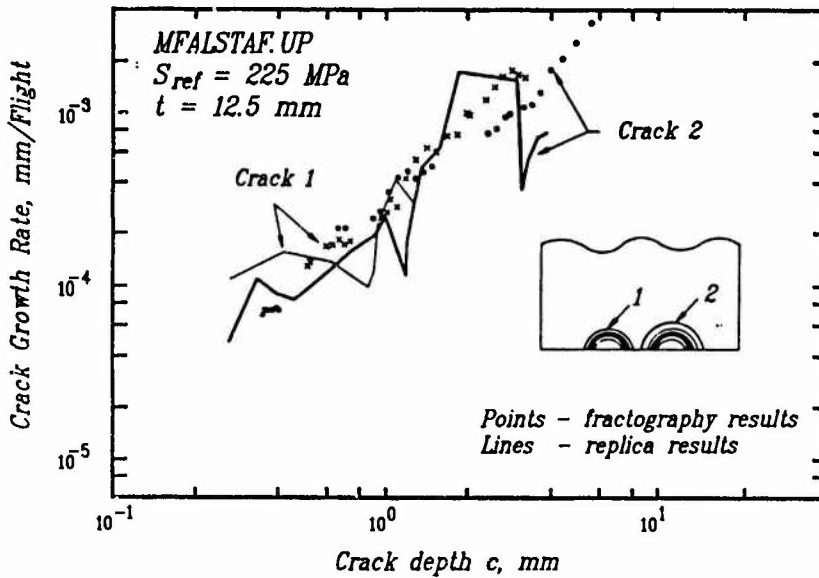


Fig.5. Replica and fractography based crack growth rate estimates for artificially initiated pair of cracks. Specimen 1.  $S_{ref} = 225$  MPa.

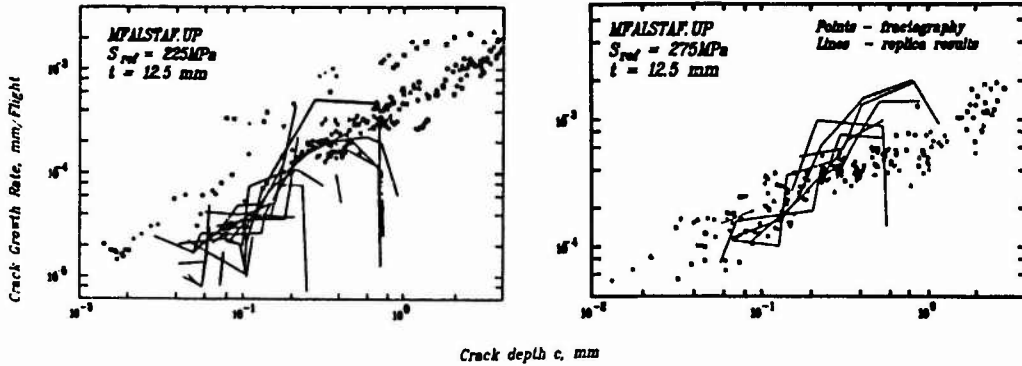


Fig.6. Replica and fractography based crack growth rate estimates for naturally initiating multiple cracks. a) Specimen 3,  $S_{ref} = 275 \text{ MPa}$ . b) Specimen 2,  $S_{ref} = 225 \text{ MPa}$ .

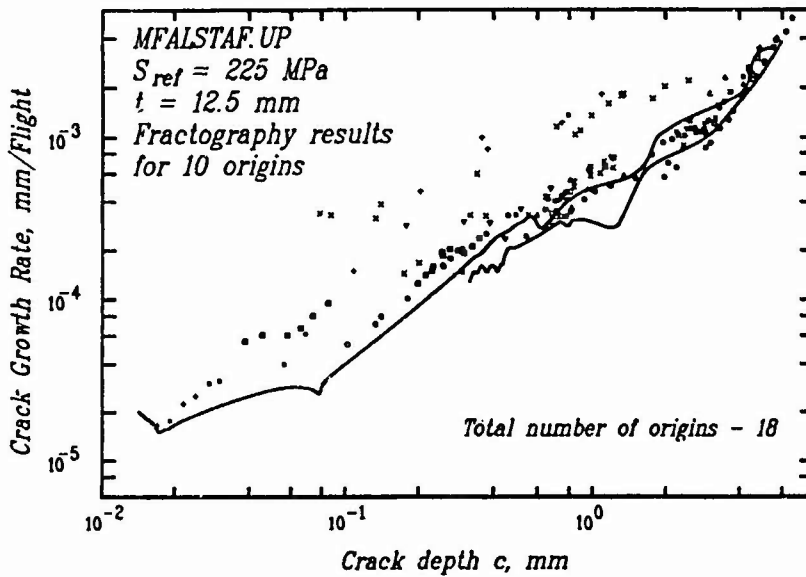


Fig.7. Fractography based crack growth rate estimates for multiple naturally initiated cracks. Data for slowest cracks shown as continuous lines.  $S_{ref} = 225 \text{ MPa}$ .

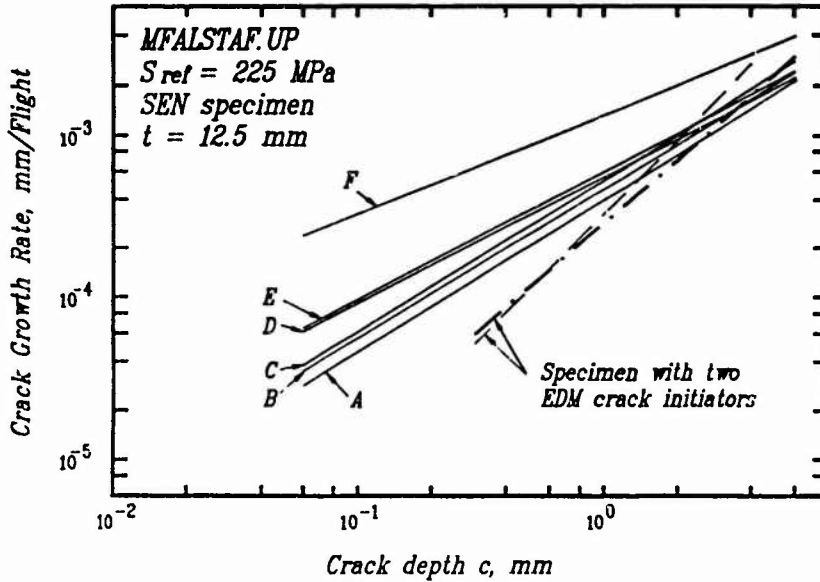


Fig. 8. Summary of crack growth rates measured in specimens 1 and 2 from fractography. Data presented as linear approximations of experimental points. Note the lower initial growth rates for cracks from EDM notches.  $S_{ref} = 225 \text{ MPa}$ .

Block counter - 71.

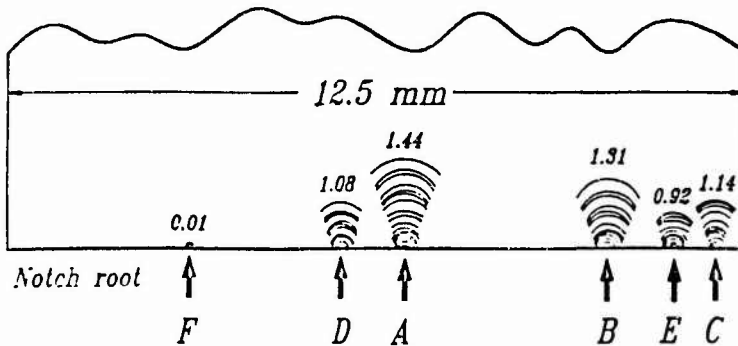


Fig. 9. Schematic representation of traced back intermediate crack front mapping

## **Rotorcraft Fatigue Life-Prediction Past, Present, and Future**

**R. A. Everett, Jr.  
W. Elber**

Vehicle Structures Directorate  
U.S. Army Research Laboratory  
Mail Stop 188E  
Langley Research Center  
Hampton, Virginia 23681-0001  
USA

### **SUMMARY**

In this paper the methods used for calculating the fatigue life of metallic dynamic components in rotorcraft is reviewed. In the past, rotorcraft fatigue design has combined constant amplitude tests of full-scale parts with flight loads and usage data in a conservative manner to provide "safe life" component replacement times. This is in contrast to other industries, such as the automobile industry, where spectrum loading in fatigue testing is a part of the design procedure. Traditionally, the linear cumulative damage rule has been used in a deterministic manner using a conservative value for fatigue strength based on a one in a thousand probability of failure. Conservatism on load and usage are also often employed. This procedure will be discussed along with the current U.S. Army fatigue life specification for new rotorcraft which is the so-called "six nines" reliability requirement. In order to achieve the six nines reliability requirement the exploration and adoption of new approaches in design and fleet management may also be necessary if this requirement is to be met with a minimum impact on structural weight. To this end a fracture mechanics approach to fatigue life design may be required in order to provide a more accurate estimate of damage progression. Also reviewed in this paper is a fracture mechanics approach for calculating total fatigue life which is based on a crack-closure small crack considerations.

### **1. INTRODUCTION**

Over the past several decades rotorcraft have been designed under the safe-life philosophy using the Palmgren/Miner [1,2] nominal stress rule. According to one rotorcraft manufacturer very little has changed [3] philosophically over this time period with most of the changes being made in the mechanics of the calculations where high speed digital computers have replaced slide rules and mechanical calculators. As technology in other areas increases this often allows for more sophisticated aircraft systems that produce different flight operations such as nap-of-the-earth, night flying, and air-to-air combat. These operations will add an even more variable fatigue load environment on rotorcraft than in the past thus requiring a fatigue life analysis that can reliably evaluate the effects of variable amplitude loading on the damage process.

Because of two studies [4,5] done about a decade apart, the safe life approach using the Palmgren-Miner(P/M) linear cumulative rule has been questioned as being the most reliable approach to predicting fatigue life. In the work in reference 4 by Jacoby, the predicted lives of one-third of about 300 tests on all types of structures and materials were considered to be on the unconservative side. The work in reference 5, the hypothetical pitch link problem formulated by the American Helicopter Society(AHS), showed variations in predicted

fatigue life from 9 to 2,594 hours. The AHS pitch link problem caused some people in the international rotorcraft community [6] to review this problem as well as to add a test program on a simulated pitch link so fatigue life calculations could be compared to test results which was not done in the AHS problem [5].

The large differences in the AHS pitch link predicted fatigue lives has resulted from each manufacturer using various conservatisms on the various parts of the fatigue life prediction process. Various reduction techniques in the component fatigue strength curves and the use of top of scatter flight loads are but two of these conservatisms. One of the reasons for conservative design has been a lack of accurate and detailed structural analyses. Over the years advances in computer speed and memory have resulted in more efficient methods for load analysis. However, these methods have been implemented without a better definition of the level of conservatism. As a consequence, the U.S. Army is requiring that the next rotorcraft to be developed have an expected value of six nines reliability for flight critical components.

The exploration and adoption of new approaches in design and fleet management may be necessary to achieve a reliability of six nines with minimum impact on structural weight. Actual fleet loads monitoring may be required to reduce the uncertainty in usage. Some of these new approaches have been implemented in a life cycle management program started during the 1980's [7]. Fracture mechanics fatigue life approaches may be required to provide more accurate estimates of damage progression. Also, flight-by-flight spectrum testing of full-scale parts may be required to reduce the uncertainty of spectrum fatigue life predictions and possibly lower the coefficients of variation. The purpose of this paper is to review the past practice of the rotorcraft safe-life approach, to review some of the aspects of the current six nines reliability fatigue life requirement particularly the recent AHS six nines fatigue life round-robin, and to review a possibly future approach to fatigue life prediction using a fracture mechanics approach where total fatigue life is

predicted using only crack propagation considerations.

## 2. PAST PRACTICES

Since the AHS pitch link problem involved almost all of the U.S. rotorcraft manufacturers as well as two European manufacturers an overview of fatigue life prediction of rotorcraft in the past will be presented by reviewing some of pitch link participants design practices. In the pitch link problem the three key ingredients given to the participants were the mission spectra, the flight loads, and six stress versus fatigue life cycles (S/N) data points. Since the P.M. linear cumulative rule is the basis for rotorcraft fatigue life prediction up to the present, these three ingredients provide all the data that is needed to predict fatigue life. The linear cumulative damage rule states that fatigue failure occurs when the summation of the so-called cycle ratios ( $n/N$ ) is equal to one. In the nominal stress approach, the flight loads are grouped into discrete load levels so the numerator ( $n$ ) of the cycle ratios can be defined. In the design of rotorcraft the denominator ( $N$ ) is determined from fatigue tests on the actual part being designed.

2.1 Mission spectrum (flight loads) The life calculations often start by developing the mission spectrum which defines the maneuvers the rotorcraft will experience as well as the percent occurrence for each of these maneuvers in the mission spectrum. As stated previously, the flight loads from the various maneuvers are used to form the numerator ( $n$ ) of the cycle ratios ( $n/N$ ). Also specified are what is often called the flight profile splits which define the percent time spent at various gross weights, center of gravity, altitudes, rotor speeds and other pertinent data. For the pitch link problem the mission spectrum is shown in Table I.

The flight loads are determined from a flight loads survey on a production configured rotorcraft where the rotorcraft is flown at all of the maneuvers defined in the mission spectrum. These flight loads are usually collected from flights in different air conditions such as smooth, turbulent, hot, cold, wet, dry, etc. These various weather conditions often

require taking loads data on different days which some manufactures require [3]. An example of flight loads on the pitch link for a high speed dive is shown in Figure 1.

The preferred way (in the sense of most conservative) of determining which load values will be used in the damage calculations is termed top-of-scatter loads. From Figure 1 it is seen that the maximum top-of-scatter load is 2352 pounds. When combined with the minimum load during this maneuver, minus 1386 pounds, the maximum load range becomes 3738 pounds which when divided by two gives the top-of-scatter alternating load for this maneuver as shown in Table 2. For the purpose of the damage calculation this load is considered to occur over the entire time of the maneuver. This procedure is performed on all of the maneuvers in the mission spectrum and produces the results shown in Table 2. As it will be seen later, the steady load for all of the conditions that will contribute to the damage using the P/M rule, is fairly close to the steady load used in the pitch links S/N curve, therefore a modification to the alternating loads to account for what is called the Goodman effect is not required. The so-called Goodman effect arises because the fatigue load cycles from the flight loads data are at many different stress ratios, R (ratio of minimum to maximum stress). These loads (stresses) are "corrected" to stress values that give the equivalent damage as the flight load stresses but at the stress ratio used for the component's S/N curve. The linear form of what has been called the Goodman correction was used by most participants in the pitch link problem [3] when it was considered necessary to "correct" the alternating loads.

**2.2 Fatigue strength (S/N curve)** The first step in establishing the design S/N curve which is used to determine the denominator (N) in the P/M rule, is to determine the endurance limit of the component of interest. The endurance limit is determined by first testing a minimum of six full-scale exact replicas of the component to failure at different load levels [3]. In the situations where the complexity of the component and loading is such that more than one failure site is possible, eight or more tests are run by some manufacturers [8]. The endurance

limit is determined by extrapolating each of the six or more tests points to 10 million cycles (for ferrous materials) using a standardized curve. Once the extrapolated endurance limit for each test point is known, the mean and other statistical values of the endurance limit are determined. The standardized shape of the S/N curves is one place where different procedures are used. Most manufacturers use a shape that is determined by running numerous coupon specimens of the component's material with a stress concentration that closest simulates that of the failure site of the actual component [3,8,9]. The methods used to establish the shape of these curves is different for each manufacturer. Some use a Wohler curve [10,11] some a Weibull equation [9], some their own equations [8], and some use two or more procedures depending on which seems to be the most valid for the particular situation [12]. Since each manufacturer uses a different procedure for determining the curve shape that is used to determine the endurance limit, different endurance limits will result thus providing some differences in the final calculated fatigue life.

Probably the greatest difference in fatigue life calculations comes from the method used to reduce the mean endurance limit to the design allowable [6]. Each manufacturer has its own set of reduction factors. The component life is usually calculated using the lowest value of the endurance limit as determined by one of the several reduction factors. Almost all manufacturers use the reduction factor of mean minus three times the standard deviation ( $\text{mean} - 3\sigma$ ). Some manufacturers use 80% of the mean as a reduction factor [3,10] and others used a reduction factor based on an equation by Hald [11]. Table 3 shows a comparison of the mean endurance limit for the pitch link problem as well as the design allowable endurance limit.

**2.3 Fatigue life calculations** With the design allowable fatigue limit determined and the flight loads for the various maneuvers established, the fatigue life can then be calculated using the P/M rule by comparing the flight loads to the endurance limit of the component. The maneuvers where the flight loads are above the endurance limit are considered to be the damaging maneuvers. The numerator in the cycle ratio for the P/M rule for

each maneuver is determined by calculating the number of load occurrences that are experienced by the component over a certain time period (often for one hour). For the pitch link problem with a rotor speed of 324 revolutions per minute and assuming a load frequency of once per rotor revolution, the numerator becomes 145.8 damaging load cycles per hour for the 1.5g right turn ( $324 \times 60 \times 0.0075$ ). The denominator of the cycle ratio is then determined for each maneuver by reading from the component's S/N curve the fatigue life at the stress level for each maneuver. The cycle ratio for each damaging maneuver is formed as just stated and the total fatigue damage is determined by summing all the cycle ratios for each loading condition,  $\sum(n/N)$ . The reciprocal of total fatigue damage,  $1/\sum(n/N)$ , then becomes the fatigue life of the component. If using the top-of-scatter procedure for determining the flight loads gives a too conservative value of fatigue life, then a more formal type of cycle counting is employed.

Again, each company uses a different type of counting method. One manufacturer uses a method that reduces the flight loads into a histogram that contains every load reversal that exceeds the endurance limit [3]. The details of this method are found in Bruhn's Analysis & Design of Flight Vehicle Structures, [13]. One manufacturer did use the rainflow method [10] which has been considered by many to be the more reliable counting procedure for accounting for load sequence effects. Most manufacturers used a method derived to adapt to computer programs that they use to reduce the flight loads data from the actual flight load surveys [8,12].

The final assignment of a fatigue life (sometimes called a safe retirement life) often depends on proven engineering judgment [8,9,14]. Most manufacturers recognize that the P/M rule has often been shown to predict unconservative fatigue lives [4,14] because of such phenomena as load sequence interaction effects and the fact that loads below the so-called endurance limit often produce nonpropagating cracks that can become damaging again when large compressive loads are experienced. Because of this, various

manufacturers also use a reduction factor on the life calculated by the P/M rule [10,14].

### 3. CURRENT DESIGN REQUIREMENT

The intent of this section is to review some of the aspects of the new "six nines" reliability U.S. Army design requirement on the fatigue life of dynamic components. As stated previously this requirement was implemented in the middle of the decade of the 1980's in order to help quantify the overall risk associated with a given component's fatigue life. Prior to this requirement the studies of Jacoby [4] and the AHS pitch link problem of 1980 [5] had shown that the safe life approach using the P/M rule to calculate fatigue life was fraught with difficulties. Some of these difficulties come from the inability of the P/M rule to handle such phenomena as the effects of load interactions on fatigue damage progression. While other problems stem from the fact that different manufacturers will inherently choose different procedures in handling the various ingredients that are needed in calculating the fatigue life (i.e. reduction on mean S/N curve to a design allowable curve). The six nines reliability requirement and the associated concerns about implementing such a philosophy resulted in establishing a round robin in 1988 involving the U.S. Army Systems Command, now called the Aviation and Troop Command (ATCOM), and the U.S. rotorcraft industry. This study was undertaken by the American Helicopter Society (AHS) Subcommittee for Fatigue and Damage Tolerance. The intent of this section is to examine some of the computational methods necessary to determine fatigue life as a function of reliability by reviewing some of the pertinent aspects of the 1988 AHS round robin [15].

3.1 Round robin description The objective of the AHS reliability round robin was to do more than just establish a consistent reliability analysis. Other objectives were to evaluate how the different U.S. rotorcraft industry methods in defining fatigue strength would affect reliability calculations as well as to examine the issue of fleet versus individual aircraft component replacement. A further

objective of the exercise was to contend with the probabilistic complexities associated with defining loads variability to demonstrate the benefits of loads monitoring for achieving six nines reliability. The problem as posed, assumed a normal distribution for fatigue strength under precisely defined cyclic loads and a normal distribution for a simple loading spectrum so that fatigue lives could be calculated to six nines reliability. Of course in actual design practice the probability distribution that best described the flight loads and components fatigue strength would have to be determined (i.e., normal, log-normal, etc.). In order to address all of the above issues the round robin was divided into three phases. In Phase I, the problem was defined such that only one numerical answer was correct. Phases II and III were set up so that the experience of individual contributors could show how differences in assumptions affected the results. Table 4 lists the round robin participants and their appropriate identifier codes.

Phase I - Identical Methods and Inputs. In Phase I of the exercise, all fatigue-related variables were strictly controlled to insure that the participants developed consistent solutions for fatigue lives at the prescribed reliability. For computational purposes, a mathematically defined S-N curve was provided in terms of stress range,  $S_r$  and fatigue limit (fatigue strength at very large loading cycles),  $S_e$ , for a stress ratio  $R=0$ . The loading spectrum used in this round robin was the standardized helicopter load spectra called Felix/28 [16]. To illustrate trends due to overall spectrum severity, a baseline spectrum level was established and other spectrum severities were created by multiplying all loads in the spectrum by a scaling parameter called alpha. To include variability of loads in the reliability analysis, the severity of the spectrum was assumed to have a normal distribution about a mean severity (or mean alpha) level. Again, in design practice the probability distribution that best described the spectrum severity would have to be determined. It is important to recognize that this was a theoretical exercise and that alpha was intended to be a mathematical artifice used to simulate changes in the baseline spectrum which account for differences in usage, pilot technique, weather, vehicle configuration, etc. Thus, for the

purposes of this exercise, alpha is an operational variable that combines both usage and loads variability to discriminate in mission intensity. All of the items just listed that could affect the load spectrum (pilot technique, etc.) would have to be considered when choosing the probability distribution that would best describe the load spectrum.

Based upon these fatigue strength and spectrum loading definitions, the following three problems were proposed and solved by the AHS round-robin participants. For all three problems, it was assumed that fatigue strength was normally distributed about the fatigue limit with a 7% coefficient of variation (COV). Also, for the purposes of the round robin, it was assumed that: (1) Palmgren-Miner's linear damage rule was valid; and (2) Goodman corrections needed to convert the applied stresses to equivalent-damage stresses at  $R=0$  were valid.

Problem 1. Assumed that the loading spectrum does not vary. Fatigue lives were calculated for the mean, mean- $3\sigma$ , and mean- $5\sigma$  fatigue strength curves using the Felix/28 loading spectrum factored by deterministic mean values of the fleet severity parameter, alpha, between 0.3 and 0.9.

Problem 2. Assumed that the loading spectrum severity parameter, alpha, is normally distributed with a 7% COV. The fleet fatigue lives at six nines reliability were calculated for mean values of alpha between 0.3 and 0.9.

Problem 3. Assumed that the severity parameter, alpha, for a subset of helicopters (or individual aircraft) had a normal distribution and could be measured to within a 3% COV. The six nines reliability fatigue lives for the subset of aircraft over a range of alphas were to be calculated. It was further assumed that the mean alphas of the subsets in the fleet were normally distributed with a 7% COV and the mean fatigue lives at six nines reliability for a fleet mean alpha of 0.6 (0.85 for Phase II) were to be calculated.

One of the possible future activities of the AHS Fatigue and Damage Tolerance subcommittee is to

investigate the effects of different COV's on the reliability calculation as well as to address the issue of what value should these COV's be for various component and material combinations.

Phase II Independent Methods and Inputs. In Phase I, the same S-N curve and fatigue limit COV were used by each participant. In Phase II, instead of using a prescribed mathematical expression for the S-N curve, the round-robin participants were provided six constant amplitude test points which were mutually agreed to be typical of the six data points obtained in full-scale helicopter fatigue substantiation testing. Each participant then used this data set to develop an independent S-N curve formulation, fatigue limit, and fatigue limit COV. The three problems in Phase I were solved again to compare the effects of each participant's choice of S-N curve.

Phase III Spectrum Fatigue Tests. In addition to the constant amplitude tests, AVSCOM's Aerostructures Directorate (ASTD), now the Vehicle Structures Directorate (VSD) of the Army Research Laboratory (ARL), conducted spectrum fatigue tests using the Felix/28 loading spectrum over a range of alpha values. The measured alpha versus life curve was used to assess the accuracy of a cumulative damage model and a fracture mechanics model for predicting the measured spectrum fatigue lives. Each participant compared the mean life predictions from Phase II/Problem 1 to the spectrum fatigue test results

3.2 Reliability analysis This section explains the solution methods used to answer the three questions postulated for the round-robin exercise. Problem 1 does not address reliability but was included to assure that all participants properly accounted for loads (alpha) scaling and the Goodman correction when calculating the fatigue life. Problems 2 and 3 were intended to address the probability of failure (POF) for a given distribution of fatigue strength and applied loading. The results were to be presented in terms of reliability or the probability of no failure, (1-POF). Thus, the six nines reliability requirement is equivalent to one failure in a million for each major component in the life of the helicopter fleet. An underlying objective of this

analysis was to demonstrate the advantages of load monitoring for achieving six nines reliability using the results of Problems 2 and 3. See the description of Problem 3 later in this section for an explanation of how load monitoring helps achieve six nines reliability throughout the fleet. The solutions to these problems are presented and discussed in a later section of this paper.

Problem 1. As mentioned earlier, the S-N curve shape, the ultimate strength (180 ksi), and the fatigue limit stress range (40 ksi) were prescribed in Phase I. Figure 2 shows the S-N curve formulation as plotted on a log-log scale. Based upon this straight line definition, the fatigue life equation can be written as

$$N = 500000(S_r - S_c)^{-1.51785}, S_r > S_c \quad (1)$$

and

$$N = 10^{15}, S_r \leq S_c \quad (2)$$

Recall that the coefficient of variation on the fatigue limit was assumed to be 7%. It was further assumed that the standard deviation at the fatigue limit also applies to the fatigue strength distributions at all points on the S-N curve. In other words, the fatigue strength standard deviation was assumed to be constant. The alpha versus fatigue life curves for the mean, mean minus three sigma, and mean minus five sigma fatigue limits were computed using the Palmgren-Miner linear cumulative damage model which was discussed previously. The calculation of a mean minus three sigma fatigue life, provides a reliability of .999 with respect to precisely known loads. The solution process consisted of four basic steps. First, the Felix/28 loading spectrum stresses (mean and amplitude) were multiplied by the alpha scaling parameter. Second, the scaled stresses were adjusted using the Goodman correction. The intent of the Goodman correction is to convert a given stress mean and range into an equivalent stress range which produces equivalent fatigue damage at R=0. Figure 3 describes the Goodman correction for the alpha scaled stress mean and range. The equivalent stress range,  $s_{r^*}$ , is defined as

$$s_r' = \alpha S_u s_r / (S_u - \alpha s_m + \alpha s_r / 2) \quad (3)$$

at the  $R=0$  fatigue life curve for an arbitrary value of  $\alpha$ . Equation (1) is used with  $S_r$  replaced by  $s_r'$  to calculate the fatigue life. Third, for the mean and the reduced-strength definitions of the S-N curves, Palmgren-Miner's Rule is used to calculate the fatigue life for the Felix/28 spectrum. Finally, in the fourth step,  $\alpha$  was plotted versus the number of sequences through the loading spectrum.

**Problem 2.** The purpose of Problem 2 was to include the variability of fatigue strength and applied load in the fatigue life calculations for six nines reliability. For this problem, both strength and load were assumed to be normally distributed with a 7% coefficient of variation. The probability of failure for particular distributions of alpha and strength was considered to be a joint probability of occurrence problem. Joint probability distributions associated with two random variables are discussed in reference 2. The normal distribution curve or probability density function, as depicted in figure 4, is used to calculate the probability that a value of the parameter (strength or load) exists in the interval between  $z_1$  and  $z_1+1$ . The product of the fractional or interval probabilities for load,  $\Delta P_i(\alpha)$  and strength  $\Delta P_j(S)$  defines the joint probability that both occur simultaneously. Thus, the joint probability was given by

$$\Delta P_{ij}(\alpha, S) = \Delta P_i(\alpha) + \Delta P_j(S) \quad (4)$$

This problem was solved numerically by creating a joint probability matrix for normal distributions of alpha and strength, as illustrated in figure 5. These normal distribution curves for alpha and strength were divided into 50 uniform increments from minus five sigma to plus five sigma about the mean. A sensitivity study verified that 50 increments gave results to within 2.5% of the converged solution which required 200 increments.

The procedures which were discussed in Problem 1 were used to compute the fatigue life,  $N_{ij}(\alpha, S)$ , for each combination of alpha and strength in the joint probability matrix. Thus, there is an associated fatigue life for each element in the joint

probability matrix. The reliability is calculated by reordering the  $[\Delta P_{ij}(\alpha, S), N_{ij}(\alpha, S)]$  pairs from the smallest life to the largest life. The reliability at any specified fatigue life is the sum of all values of in the array above that value of life. Figure 6 presents an example of this cumulative joint probability versus fatigue life. As indicated in figure 6, the safe retirement life (or a POF = 0.000001) can be easily calculated by interpolation. This process is repeated for each mean alpha from 0.3 to 0.9. It turns out that only the shaded region of the joint probability matrix in figure 5 contributes to the calculation of six nines reliability. Thus, the number of computations needed to obtain six nines reliability is only about one-eighth of the 2500 load and strength combinations.

There was another method used in the round robin by several participants which gave essentially the same answers as the numerical joint probability/life matrix approach. This alternative method was a closed-form solution which used the following ideas and procedures. Each alpha-sealed and Goodman corrected applied stress range,  $s_r'$ , in the loading spectrum was assumed to be normally distributed with a mean value given by equation (3) and a COV equal to the alpha distribution COV. Furthermore, because  $s_r'$  and  $S_c$  are assumed to be normally distributed, the S-N curve in equation (2) was defined in terms of a new variable,  $\phi = (s_r' - S_c)$  which was also assumed to be normally distributed with a mean,  $\phi_m$ , and a standard deviation,  $\sigma_\phi$ . The S-N equation became

$$N = 500000(\phi)^{-1.51785}, \quad \phi > 0 \quad (5)$$

In the linear damage fraction ( $n/N$ ),  $n$  was defined for each stress range in the loading spectrum. The damage that was exceeded with a POF equal to  $10^{-6}$  (or six nines reliability) at each stress range in the spectrum was determined by using equation (5) to calculate  $N$  when

$$\phi = (\phi_m + 4.75 \sigma_\phi) \quad (6)$$

where,

$$\phi = (s_r' - S_{cm}) \text{ and } \sigma_\phi = (\sigma_{sr}^2 + \sigma_{sc}^2)^{1/2}$$

Finally, the safe retirement life was computed as the reciprocal of the total damage in the loading spectrum.

Although this alternative method has produced answers which are close to those calculated by the "matrix" method, the two methods have not been shown to be theoretically equivalent. One of the differences between the "matrix" method and the closed-form method can be attributed to differences between the normal population statistics for alpha and  $s_r$ . While the alpha-scaled stresses have the same COV as alpha, the alpha-scaled and Goodman-corrected stresses ( $s_r$ ) do not. There was no attempt in the current study to evaluate the limitations of assuming the same COV for alpha and  $s_r$  on the accuracy of the results. However, the closed-form method does require much less computation than the "matrix" method and both approaches were used in the round robin.

Problem 3. Problem 3 was posed to help examine the difference between the safe retirement life for the entire fleet and the safe retirement life based on individual aircraft usage. If the measurements necessary to determine alpha could be made with a 3% COV, then significant maintenance cost savings could be achieved from the longer mean retirement life. This problem is an application of the theorem of total probability where the total fleet has a normal distribution of alpha with a 7% COV. The measurement error on each individual aircraft was assumed to have a normal distribution with a 3% COV. The solution of this problem consists of two steps. First, the safe retirement lives are calculated for each measured alpha. This step is the same as Problem 2, except that the alpha variation has a 3% COV instead of 7%. Second, the mean safe retirement life,  $N_{\text{mean}}$ , is calculated for the prescribed mean alpha using the method of conditional expectation [17] and is expressed in integral form as

$$N_{\text{mean}} = \int N_{\text{ship}}(\alpha) * f_{\text{fleet}}(\alpha) d\alpha \quad (7)$$

where  $N_{\text{ship}}(\alpha)$  is the individual ship six nines life for a 3% COV on applied loads and  $f_{\text{fleet}}(\alpha)$  is the

fleet probability density function for a 7% COV on the mean  $\alpha$ . For this problem  $N_{\text{mean}}$  was calculated using a discretized form of Eq. (7) given by

$$N_{\text{mean}} = \sum N_{\text{ship}}(\alpha) * P_{\text{fleet}}(\alpha) \quad (8)$$

where  $N_{\text{ship}}(\alpha)$  is computed for a 3% COV on applied loads and  $P_{\text{fleet}}(\alpha) = f_{\text{fleet}}(\alpha) * \Delta\alpha$  is computed for a 7% COV on the mean  $\alpha$ . Figure 7 shows a graphical representation of this process.

3.3 Round robin results The results of all three phases of the reliability round robin exercise are presented in this section. Only a portion of the results will be presented. See reference 15 for the complete set of results.

Phase I - Identical Methods and Inputs. In Phase I, all participants used the same S-N curve, spectrum loading sequence, and statistical parameters in solving the three problems. Table 5 presents the fatigue life for Problem 1 for the mean strength for all participants. Table 6 gives the mean minus three sigma and mean minus five sigma strength predictions only for the VSD solutions. All of the other participants solutions for this problem were similar. Tables 7 and 8 present the fatigue life calculations at six nines reliability for Problems 2 and 3, respectively. Fatigue lives in the tables are given in terms of the number of passes through the loading spectrum. For Problems 2 and 3, the first numbers tabulated were calculated using the joint probability/life matrix approach while the numbers in parentheses were calculated using the closed-form method. The results from Phase I confirmed that all participants could calculate about the same answers for all three problems when the S-N curve formulation, loading spectrum, and statistical parameters were identical. The small differences in fatigue lives calculated by the participants can be attributed to two possible sources. First, different answers would occur if the participants used different sizes of incremental sigma's (see description of Problem 2 under Reliability Analysis section) in summing for a given level of probability. Second, the type of numerical integration method

used in summing for a given level of probability would also give slightly different results.

Recall that Problem 2 was set up to calculate fatigue lives at six nines reliability without any knowledge about loads on individual aircraft. On the other hand, Problem 3 assumed that loads (or alpha) could be measured on each aircraft and that the measurement error has a 3%COV. Comparing the fatigue lives at six nines reliability between Problems 2 and 3 may provide some measure of the benefits of loads monitoring. For Problem 3, the calculated six nines reliability fatigue life at a mean alpha of 0.6 was about 4.2 times greater than the six nines fatigue life calculated for Problem 2. Thus, this 4.2 factor could also be used to quantify potential cost savings if retirement lives could be increased through loads monitoring.

Phase II - Independent Methods and Inputs In Phase II, each participant used the constant-amplitude test points provided by VSD to develop an independent S-N curve, fatigue limit, and fatigue limit COV. The form of the fatigue life equation was given as

$$N = A (S_r - S_c)^{-B} \quad (9)$$

where A and B are curve fit parameters. Table 9 presents the parameters from equation (9) and the fatigue limit COV which were used by each participant. Table 10 gives the Phase II fatigue life results for Problem 1 in terms of the number of passes through the loading spectrum for the mean strength. See reference 15 for the complete set of results. As expected, there were differences in the fatigue life predictions. The most significant contributor to these differences appears to be the value of the fatigue limit which was determined from the given constant-amplitude fatigue data. Figures 8 and 9 highlight some of these differences for Problem 1 at alpha's of 0.7 and 1.0, respectively. For alpha equal to 0.7 (fig. 8) the maximum difference in fatigue life predictions is seen to be almost a factor of 30. However, for alpha equal to 1.0 (fig. 9) the maximum difference is less than a factor of three. In terms of current analytical standards for fatigue life prediction a factor of four difference is considered

reasonable. At an alpha of 0.7, many of the loads are below the fatigue limit and small differences in the fatigue limit could result in large differences in the predicted fatigue life. As seen from Table 9, the fatigue limits used by the participants differed by almost 20 percent. The results are consistent with this reasoning in that the longest fatigue life predictions (fig. 9) were calculated by using the highest fatigue limits (Table 9). At the higher alpha's, more of the loads were above the fatigue limit and contribute to fatigue damage. Thus, according to Miner's Rule, less scatter in the fatigue life predictions should be expected, as shown in Figure 9.

Besides the effects of fatigue limit on mean life predictions, the manner in which fatigue strength reductions are applied will contribute to the scatter in life predictions. Recall that in Phase I the statistical variations on strength were based on a constant standard deviation and not a constant coefficient of variation. In Phase II, some of the participants based the strength reductions on a constant COV and not a constant standard deviation. Assuming all other parameters equal, the predicted fatigue lives would be shorter when using a constant COV to account for strength variability. Another slight difference in the statistical analysis was the use of a log-normal distribution for strength by one of the participants. The six nines reliability results from Problem 2 show larger differences among the participants than do the mean fatigue life results of Problem 1. One cause for these differences appears to be the magnitude of the fatigue limit COV that was used. In addition, the differences at higher alpha values may be attributed to the use of a constant COV rather than a constant standard deviation.

Tables 11 and 12 show the Phase II fatigue life predictions at six nines reliability for Problem 2 and Problem 3, respectively. Again, for Problems 2 and 3 the first numbers represent the joint probability/life matrix approach while the numbers in parentheses represent the closed-form method. Figure 10 shows some of the differences in the six nines fatigue lives for Problem 2 at an alpha of 0.6. The maximum difference between the predicted fatigue lives at six nines reliability was almost a

factor of 60. This is about twice the scatter that was obtained in Problem 1 for the mean fatigue life predictions. Comparing the ratio of fatigue lives between Problems 2 and 3 at mean alpha's of 0.8 and 0.85, shows increases in fatigue lives at six nines reliability from as low as 1.8 to as high as 40. Again, the fatigue limit value and the method used for fatigue strength reduction (constant standard deviation versus constant COV) may account for these differences.

**Phase III Spectrum Fatigue Tests.** In this phase, each industry participant used their standard linear cumulative damage methodology and the mean S-N curves derived from the Phase II constant amplitude fatigue tests to calculate mean spectrum fatigue lives. In addition to this approach, VSD used a fracture mechanics approach to calculate mean fatigue lives. The fracture mechanics approach used by VSD is explained in the following section on Possible Future Design Practices. Table 13 presents these mean fatigue life calculations at the same alpha's used to conduct the spectrum tests. Figure 11 shows a comparison between the spectrum test data and the round-robin predictions. Although all the predictions are greater than the test lives, the predictions are within a factor of 4 differences. The relatively small scatter among predictions is consistent with the Phase II/Problem 2 predictions for  $\alpha > 1$ . Also presented in figure 11 are the round-robin predictions for fatigue lives at six nines reliability from Phase II/Problem 2. One clear observation is the larger variation in six nines reliability predictions for alpha values less than one.

**3.4 Round robin conclusions** The purposes of the AHS reliability round robin were twofold. First, it was intended to develop the logic for performing a reliability analysis for fatigue life prediction. Phase I was set up so that only one answer was correct and the results for each participant were compared to assure that a consistent approach was used. Second, in Phases II and III the participants applied the same logic but used their company's standard fatigue methodology to solve for six nines reliability. The intent of these two phases was not to prove that any one answer was "right" or "better" but instead to find out what contributed to the differences.

One of the conclusions of the reliability round robin was that the two major contributors which affected the results were the S-N curve formulation and the method used for strength reduction. This was also a conclusion of the 1980 AHS pitch link round robin. One of the questions which was raised as a result of this round robin was whether the COV or the standard deviation remained constant over the S-N curve. In Phase I, all participants used a constant standard deviation to solve the fatigue life and reliability problems. However, in Phase II some participants used a constant standard deviation while others used a constant COV. There is a real need to establish a uniform methodology for developing S-N curves and coefficients of variation.

Some aspects of the probabilistic approach to six nines reliability were not explored in the reliability round robin. There was no attempt to incorporate confidence levels. By definition (and intent) the problems in the round robin were based upon a 50% confidence level. The aim of the exercise was to develop a methodology which included loads variability but restrained the fatigue analyst's freedom to manipulate conservatism in the measured loads. The need to include confidence levels is a topic which may require further evaluation. Another purpose of this exercise was to try and quantify the benefits of individual component replacement versus fleet replacement. The alpha parameter was devised to account for loads variability in the reliability analysis. While the results showed the potential for increasing mean retirement lives through loads monitoring (with commensurate reductions in costs), no attempt was made in this first round robin to separate usage from other sources of variability in the loads. Additional study is needed to examine how usage should be treated to properly account for operational variability.

All of the questions brought up by the round robin affirmed that much more work is needed before reliability-based fatigue design becomes standard industry practice. The round-robin results did demonstrate that consistent reliability-based design cannot be implemented without the cooperation of

all the rotorcraft industry. In addition to the study areas already mentioned, the reliability round robin further suggested that follow-on efforts to this round robin are needed to:

(1) Extend the statistical and reliability analysis complexity to account for both usage and other sources of load variability, and to assess reliability versus confidence levels. If current flight data recorders largely monitor usage, what does this imply for load accuracy and the merit of individual part replacement?

(2) Apply the reliability methodology to metals using a damage tolerance or fracture mechanics approach.

(3) Repeat the P-M and TLA approaches on other metallic materials with different ultimate strengths and stress concentration factors to develop confidence in the fatigue reliability approach.

(4) Evaluate the effects of coupon versus full-scale testing on data scatter.

(5) Investigate flight loads survey methodology to better define the variabilities of usage and pilotage (simulated mission flights versus maneuver-by-maneuver flights).

(6) Extend the reliability-based fatigue methodology to composites.

Several other sources of work on fatigue life and reliability need to be noted. Two independent sources have stated that the six nines reliability design requirement does not seem to be possible with the safe-life approach of fatigue life prediction [18,19]. One of the sources [18] shows that the large reduction required in the fatigue endurance limit in order to meet "six-nines" would place a severe weight penalty on the component. The other source [19] uses an example problem on a pitch horn and states that only three-nines reliability can be achieved using a safe life approach. In the case of the pitch horn example problem, a redesign of the pitch horn from a single-load-path to a dual-load-path design, showed the dual-load-path pitch horn to have a reliability of nine-nines with a first inspection interval of 1450 flight hours. The dual-load path design was about 12 % heavier than the single-load-path safe-life design.

Sensitivity studies concerning the assumed probability density functions(PDF) chosen to represent the flight loads and fatigue strength of the component, have shown that for even almost undetectable differences in assumed PDF's high reliability estimates can vary substantially [20]. Further work by the same researchers has stated that even a small amount of uncertainty in the safe life fatigue model can result in a substantial reduction in high reliability values for the specified lifetime of a component [21,22].

The work just cited in reference 18 and 19 and the several questions and follow-on studies suggested by the AHS reliability round robin only continue to reinforce the fact that it will take a cooperative effort from both the procuring agencies and the rotorcraft industry before a reliability-based fatigue design can become a standard industry practice. Much of the ongoing efforts of the AHS subcommittee on Fatigue and Damage Tolerance is aimed towards developing a cooperative effort of all parties involved in the design and procurement of rotorcraft.

#### 4. FUTURE DESIGN PRACTICES

The AHS subcommittee on Fatigue and Fracture Mechanics is currently studying the application of a fracture mechanics approach to fatigue life design of rotorcraft. This is part of the follow on activities of the reliability round robin that was just reviewed. In the paper by Krasnowski [23] it was concluded that a damage tolerance method was more suited to a six-nines reliability fatigue life design approach than the safe life method. Krasnowski further stated that a fatigue life prediction model that took into account the fact that the damage process originates from microscopic features, such as metallurgical impurities, would lead to a better procedure for evaluating a reliability fatigue life method. A damage tolerance model based on the crack closure phenomena where the total fatigue life is calculated using crack propagation as the entire fatigue process has been developed by Newman [24]. One of the unique features of this model is that the fatigue cracking process is considered to start from metallurgical features such as inclusion

particles. In a study done by Swain et al. [25] these metallurgical features were shown to be on the order of 0.0006 inches for 4340 steel. This is quite a contrast in size compared to the more traditional damage tolerance approach which uses an initial crack size of 0.05 inches for corner cracks emanating from a hole to calculate a safe inspection interval [26].

The more traditional damage tolerance approach which calculates safe inspection intervals, calculates these intervals by integrating a crack growth rate versus stress intensity factor relationship like

$$da/dN = C (\Delta K)^m \quad (10)$$

where  $da/dN$  is the crack growth rate,  $\Delta K$  is the stress intensity factor range, and  $C$  and  $m$  are curve fit parameters. The main difference between the total life analysis (TLA) and the more traditional fracture mechanics approach is that crack-closure concepts are used to define an effective  $\Delta K$  and the initial crack length was determined from a previous "small" crack study on 4340 steel [25]. From crack-closure considerations,  $\Delta K$  in equation 10 is replaced by  $\Delta K_{\text{effective}}$ . The effective stress intensity factor is usually defined as

$$\Delta K_{\text{eff}} = (S_{\text{max}} - S_0) (\pi a)^{1/2} F \quad (11)$$

where  $S_0$  is the crack-opening stress as calculated from the analytical closure model developed by Newman [24] and  $F$  is the boundary correction factor which accounts for the effects of structural configuration on the stress intensity factors. To calculate the crack growth rate, equation 10 becomes

$$da/dN = C [(S_{\text{max}} - S_0) (\pi a)^{1/2} F]^m \quad (12)$$

Total life is calculated by numerically integrating equation 12 from the initial crack length,  $a_i$ , to the final crack length,  $a_f$ , where  $a_i$  is the initial crack length as determined from the small crack studies and  $a_f$  is the final crack length at failure. Cycles are summed as the crack grows until  $K_{\text{max}} = K_c$ , where  $K_c$  is the fracture toughness. When  $K_{\text{max}} =$

$K_c$ , the summation of the load cycles,  $N$ , becomes the total fatigue life.

The total fatigue life as determined by the TLA method was calculated from a computer algorithm developed by Newman. For this study the initial crack length used to predict the fatigue life was 0.0006 inches. This value was taken from a small crack study on 4340 steel [25] in which initial defect sizes at 34 crack initiation sites were evaluated by scanning electron microscopy of the fracture surfaces. The largest value was about 0.002 inches, the median value was about 0.0006 inches, and the smallest was about 0.00008 inches.

For the AHS reliability round robin fatigue tests were run on 4340 steel specimens at a tensile strength of 212 ksi. The specimens were one inch wide and had an elastic stress concentration factor,  $K_T$ , of 2.42 (based on net section stress). Figure 12 shows the results of these tests as well as the fatigue life predictions from the TLA analysis and the a nominal stress P/M rule analysis. As it can be seen from Figure 12 both the TLA and the P/M analysis predicted the trend of the test data very well. Neither of these analysis employed any probabilistic considerations. The S/N curve used for the P/M analysis was based on a mean regression line of constant amplitude tests at a stress ratio of zero [27]. Both analysis predicted fatigue lives which were slightly on the unconservative side of the test data. If either of these two life prediction methods were used for predicting the design fatigue life of a rotorcraft component, some type of reduction would be taken from the calculated mean life as stated earlier. Figure 13 shows life prediction curves for both of these methods with a reduction factor included to simulate design allowables. For the TLA analysis the lives were calculated using the largest metallurgical feature found in reference Swain. While this design allowables curve predicts life on the conservative side of the test data, it predicts an endurance limit between 40 and 45 ksi which is nominally 20 ksi less than the 80% P/M design allowable value and 25ksi less than the one runout test. To place in perspective the effect of using the current traditional damage tolerance initial crack size (0.05 in) on predicting total life, a curve from

these calculations is also shown in Figure 13. Very conservative lives would be predicted using the 0.05 in. initial crack size.

As a result of P/M analysis predicting lives fairly well for the test lives under the Felix/28 spectrum loads, additional test were run on 4340 steel using the standardized fixed-wing load spectrum called Minitwist [28]. Since this spectrum is often thought of as a highly load interactive spectrum, the test lives from this spectrum should prove difficult for the P/M analysis. The results of these tests and the TLA and P/M analysis are shown in figure 14. For tests above the endurance limit the TLA analysis predicted practically the same lives as the test data while the P/M analysis predicted test lives that were again slightly unconservative. One possible problem with the P/M rule as used in the past was the lack of an adequate load counting technique. With the advent of the rainflow technique some the problems caused by load counting inadequacies may be lessened.

Other studies done by Newman et. al. [29] have shown the TLA analysis using small crack considerations to work very well for other metallic materials such as 2024-T3 aluminum, 2090-T8E41 aluminum-lithium, and Ti-6Al-4V titanium. Before a method like the TLA analysis will replace an industry standard like the P/M rule work will have to be done in predicting the fatigue lives of actual aircraft size components. To this end a rather exhaustive amount of work is being done in the United States using the TLA analysis in crack growth and life predictions in the study of aging aircraft.

One study conducted by Sikorsky Aircraft towards studying the possibilities of life managing rotorcraft using a damage tolerance approach(DTA) is worth noting [30]. Sikorsky evaluated the possible use of the damage tolerance approach for several dynamic components of the HH-53 helicopter. The components studied were considered to be among "the most difficult for achieving damage tolerant management". These parts were from the main rotor and tail rotor hubs as well as some airframe structure. The results showed that if a DTA was used on these selected components reliable detection of cracks as small as 0.005 to 0.010 inches would

have to be established. Furthermore, conservatism such as using 95% of maximum vibratory loads could not be used. Further requirements included "improved stress intensity models for steep stress gradients, verification of stresses and crack growth behavior in threads, and additional crack propagation rate and threshold data for(so-called) small cracks(<0.020 inches)."

Another deficiency noted by the DTA study done by Sikorsky was the lack of usage data for the HH-53 helicopter. The lack of usage data is a general problem that affects the reliability of fatigue life calculations regardless of the fatigue design method used. As noted by Lincoln in reference 31 reliable usage data performs at least two functions. First it will allow an assessment of how pilot techniques may influence the actual life calculations by quantifying the difference in flight loads and usage between the experienced flight test pilot and the total pilot population. Second, it will help the rotorcraft owner to recognize when the usage of a fleet or individual rotorcraft have changed thus requiring possible modifications to their maintenance actions. The use of usage monitors will probably be driven mostly by economic considerations. However, as stated by Lombardo [14] "usage monitoring is a field that will grow in the next few years as operators and manufacturers strive to reduce helicopter operating costs without compromising safety."

In the late 1970's the U.S. Army developed under contract a flight recorder known as the Structural Integrity Recording System called SIRS [14]. However, this system was not put into service. In the early 1990's the U.S. Navy developed a system called the Structural Data Recording Set(SDRS) [14]. This system is currently being tested on an AH-1W Cobra. The systems are intended for production in 1993 with installation planned on all Navy fixed and rotary-winged aircraft. The U.S. Air Force also is developing a usage monitor for the HH-53 helicopter under a contract with Sikorsky Aircraft [30].

The development of a rather unique usage monitoring system was started by the US Army Vehicle Structures Directorate(VSD) of the Army

Research Laboratories(USARL). The intent of this device is to be a low cost system that is small and requires very little hands-on maintenance from the operator. The low cost of the device will allow it to be placed fleet-wide thus maximizing the amount of usage data that will be gathered. This should provide the amount of data that is needed in reliability analysis. The basic concept behind this device is to compare the actual type of maneuver being flown with the design mission spectrum which is usually the 95th percentile spectrum. If the maneuvers actually being flown are less severe than the 95th percentile maneuvers than the recorder known as MIC (Mission Intensity Counter) will indicate that additional life beyond the design life is possible. Of course the reverse is true in the maneuvers being flown are more severe than the 95th percentile design maneuvers. The basic concept of the MIC depends on identifying the maneuver being flown with as few flight parameters as possible. Before a prototype of the MIC can be built several data recognition features need to be addressed. Among these are determining what is the minimum number of maneuvers that need to be identified by the MIC in order to be able to determine if the design life can be modified. The current status of the MIC's development is given in reference 32.

## 5. SUMMARY

Methods used for calculating the fatigue life of rotorcraft in the past(deterministic safe life), current (six nines reliability for safe life) and possible future design approaches have been reviewed. Past practices were addressed by reviewing the AHS pitch link round robin of 1980. The principle causes of the large differences in fatigue life as calculated by the several participants has been shown to be the shape of the S/N curve used by each participant and the reduction factor used on the mean fatigue endurance limit to get the design allowable. Current fatigue design requirements were illustrated by reviewing the 1989 AHS reliability round robin which sought to address some of the issues involved in establishing a six nines reliability fatigue life. The two major contributors which affected the results of this round robin were the same as the pitch link round robin. Another conclusion of this round robin was that

loads monitoring could increase rotorcraft mean retirement lives. Future rotorcraft design procedures were shown to include the possibility of calculating total fatigue life using a fracture mechanics model that used only crack propagation considerations. The need for load monitors was also addressed and several efforts to develop these were noted.

## 6. REFERENCES

- 1 Palmgren, A., "Ball and Roller Bearing Engineering", translated by A. Palmgren and B. Ruley, SKF Industries, Inc. Philadelphia, 1945, pp.82-83.
2. Miner.M.A., "Cumulative Damage in Fatigue," J.Applied Mechanics, ASME, Vol12, Sep1945.
3. Thompson.G.H., "Boeing Vertel Fatigue Life Methodology", AHS specialists meeting on Helicopter Fatigue Methodology, preprint no. 22, March 1980.
4. Jacoby,G.,"Comparison of Fatigue Life Estimation Processes for Irregularly Varying Loads", 3rd Conference on Dimensioning, Budapest, 1968.
5. Arden,R.W.,"Hypothetical Fatigue Life Problem", AHS National Specialists Meeting on Helicopter Fatigue Methodology, Mar 1980.
6. Zhuzhao.S and Hao.K., "The Review of AHS Hypothetical Fatigue Problem and Its Test Investigation(Pitch Link), Nanjing Aeronautical Institute, Nanjing, China
7. Ray,J.,"Army Aviation Mechanical Failures Prevention",U.S.Army Aviation Systems Command, St. Louis MO, USA
8. Altman,B and Pratt J., "The Challenge of Standardizing Fatigue Methodology", AHS National Specialists Meeting on Helicopter Fatigue Methodology, March 1980
9. McCloud.G.W., "A Method of Determining Safe Service Life for Helicopter Components", AHS Specialists Meeting on Helicopter Fatigue

- AHS Specialists Meeting on Helicopter Fatigue Methodology, March 1980.**
10. Aldinio, G. and Alli, P., "The Agusta's Solution AHS'S Hypothetical Fatigue Life Problem", AHS Specialists Meeting on Helicopter Fatigue Methodology, March 1980.
  11. Stievenard, G., "Hypothetical Fatigue Life Problem Application of Aerospace Method", AHS Specialists Meeting on Helicopter Fatigue Methodology, March 1980.
  12. McDermott, J., "Hughes Helicopters - Fatigue Life Methodology", AHS Specialists Meeting on Fatigue Methodology, March 1980.
  13. Bruhn, E.F., "Analysis & Design of Flight Vehicle Structures", Ohio, USA, Tri-State Offset Company, 1965, section C13.
  14. Lombardo, D., "Helicopter Structures - A Review of Load, Fatigue Design Techniques and Usage Monitoring. ARL-TR15, May 1993.
  15. Everett, R.A. Jr., Bartlett, F.D. Jr., and Elber, W., "Probabilistic Fatigue Methodology for Safe Retirement Lives", J.AHS, Vol.37, No.2, April 1992, pp 41-53.
  16. Edwards, P.R. and Darts, J., "Standardized Fatigue Loading Sequences for Helicopter Rotors (Helix and Felix) Part 1, Background and Fatigue Evaluation", Royal Aircraft Establishment, TR 84084, August 1984
  17. O'Conner, P.D.T., "Reliability Engineering", Hemisphere Publishing Corp., New York, 1988.
  18. Amer, K.B., "A 'New' Philosophy of Structural Reliability, Fail Safe Versus Safe Life", J AHS Vol.34 No.1, Jan. 1989.
  19. Krasnowski, B.R., Viswanathan, S.P., and Dowling, N.E., "Design, Analysis, and Testing Considerations of Fatigue-Critical Rotorcraft Components", J.AHS, Vol.35, No.3, July 1990
  20. Neal, D.M., Matthews, W.T., and Vangel, M.G., "Model Sensitivity In Stress-Strength Reliability Computations, U.S. Army Materials Laboratory MTLTR 91-3, Jan. 1991.
  21. Neal, D.M., Matthews, W.T., and Vangel, M.G., Rudalevige, T., "A Sensitivity Analysis On Component Reliability From Fatigue Life Computations", MTLTR 92-5, Feb 1992.
  22. Matthews, W.T. and Neal, D.M., "Assessment of Helicopter Component Statistical Reliability Computations", MTLTR 92-71 Sept 1992.
  23. Krasnowski, B.R., "Reliability Requirements for Rotorcraft Dynamic Components", J.AHS Vol.36, No.3, July 1991.
  24. Newman, J.C. Jr., "A Crack-Closure Model for Predicting Fatigue Crack Growth under Aircraft Spectrum Loading", ASTM STP 748, Oct 1981.
  25. Swain, M.H., Everett, R.A., Newman, J.C. Jr., and Phillips, E.P., "The Growth of Short Cracks in 4340 Steel and Al-Li 2090", AGARD Report 767, Aug 1990.
  26. Gallagher, J.P., Giessler, F.J., and Berens, A.P., "USAF Damage Tolerance Design Handbook, Guidelines for the Analysis and Design of Damage Tolerant Aircraft Structures", AFWAL-TR-82-3073, May 1984.
  27. Everett, R.A. Jr., "A Comparison of Fatigue Life Prediction Methodologies for Rotorcraft", J.AHS, Vol.37, No.2, April 1992.
  28. Lowak, H., de Jonge, J.B., Franz, J., and Schutz, D., "Minitwist, A Shortened Version of Twist", Laboratorium fur Betriebsfestigkeit (LBF), Report No. TB-146, 1979.
  29. Newman, J.C. Jr., Phillips, E.P., Swain, M.H., and Everett, R.A., "Fatigue Mechanics: An Assessment of a Unified Approach to Life Prediction", ASTM STP 1122, 1992.
  30. Tritsch, D.E., Schneider, G.J., Chamberlain, G. and Lincoln, J.W., "Damage Tolerance Assessment of the HH-53 Helicopter", AHS

46th Annual Forum, Vol. II, May 1990.

31. Lincoln, J.W., "Damage Tolerance for Helicopters", 15th ICAF Symposium on Aeronautical Fatigue, June 1989.
32. Lombardo, D.C., "Report on Long-Term Attachment to the U.S. Army to Study Helicopter Structural Fatigue", ARL-TN-11, 1993.

Table 1. Pitch link mission spectrum

Condition			Percent Time
1. Hover-IGE			4.25
2. Ascent			18.50
3. Level flight			54.25
a. 0.4 V <sub>H</sub>			2.40
b. 0.6 V <sub>H</sub>			5.00
c. 0.8 V <sub>H</sub>			23.95
d. 1.0 V <sub>H</sub>			20.50
e. 1.2 V <sub>H</sub>			2.40
4. Pullup (2.0g)			1.00
5. Pushover (0.5g)			2.00
6. Turns			2.50
a. Right			1.25
(1) 1.5g	0.75		
(2) 2.0g	0.50		
b. Left			1.25
(1) 1.5g	0.75		
(2) 2.0g	0.50		
7. Descent			17.50
a. Partial power descent			17.00
b. High speed dive (1.2 V <sub>H</sub> )			0.50
			100.00

Table 2 Flight Loads Data

Flight Condition	Flight	Event	Time (sec)	Cycles	CPS	Max	Min	Sidy	Alt
Hover	1	1	2	11.25	5.63	-80	-850	-435	415
Ascent	1	2	10	54.5	5.45	1380	0	690	690
LF 0.4V <sub>H</sub>	1	3	2	10.7	5.36	910	-460	225	685
LF 0.6V <sub>H</sub>	1	4	2	10.7	5.36	980	-640	170	810
LF 0.8V <sub>H</sub>	1	5	2	10.8	5.4	1070	-680	195	875
LF 1.0V <sub>H</sub>	1	6	2	10.76	5.38	1270	-710	280	990
LF 1.2V <sub>H</sub>	1	7	2	10.7	5.36	2000	-520	740	1260
PU 2.0G	1	8	9.7	52.25	5.39	2134	-1319	406	1727
PO 0.5G	1	9	10	53.95	5.4	1800	-400	700	1100
RT 1.5G	1	10	10	53.95	5.4	2147	-1254	447	1701
RT 2.0G	1	11	10	54	5.4	2236	-1376	430	1806
LT 1.5G	1	12	9.9	54	5.45	2150	-1300	425	1725
LT 2.0G	1	13	10	54.5	5.45	1932	-1214	368	1564
PPD	1	14	10	54	5.4	1340	-550	395	945
HSD 1.2 V <sub>H</sub>	1	15	10	54	.4	2352	-1386	483	1869

Table 3. Pitch link endurance limits.

Manufacturer	Endurance limit mean value (lb)	Endurance limit design allowable (lb)
Aerospatiale	2176	1225
Agusta	2100	1674
Bell	2061	1649
Boeing-Vertol	2106	1685
Hughes	2024	1717
Kaman	2101	1615
Sikorsky	2100	1400

Table 4. AHS Reliability Round Robin Participants

Organization	ID Code
Aerostructures Directorate (AVSCOM)	ASTD
Bell Helicopter Textron	BHT
Boeing Helicopters	BH
Kaman Aerospace Corporation	KAC
McDonnell Douglas Helicopter Company	MDHC
Sikorsky Aircraft Division	SA

Table 5. Fatigue life predictions for mean strength,  
Phase 1 / Problem 1

Alpha	ASTD	BHT	BH	KAC	MDHC	SA
0.3	6.21e9					
0.4	6.21e9					
0.5	14740		14900	14700	16236	14895
0.6	171.1	170.5	168.4	171.0	175.0	168.4
0.7	47.8	50.0	46.85	47.8	48.0	46.85
0.8	18.69	19.3	18.42	18.7	19.0	18.42
0.9	3.49	3.5	3.48	3.49	3.7	3.48
1.0	1.03	1.0	1.02		1.0	1.02

Note: Fatigue lives are in terms of number of passes through the spectrum  
(1 pass = 161034 cycles).

**Table 6. Fatigue life predictions for mean minus 3 sigma and mean - 5 sigma strength, VSD values only, Phase I / Problem 1**

Alpha	Mean -3 $\sigma$	Mean - 5 $\sigma$
0.3	6.21e9	2.67e6
0.4	10850	214.9
0.5	135.0	44.2
0.6	36.9	5.18
0.7	6.72	.891
0.8	1.36	.209
0.9	.294	.096
1.0	.117	.057

**Note: Fatigue lives are in terms of number of passes through the spectrum (1 pass = 161034 cycles).**

**Table 7. Fatigue life predictions for six nines reliability, Phase I / Problem 2**

Alpha	ASTD	BHT	BH	KAC	MDHC	SA
0.3			22697 (23062)			(22663)
0.4	110.7 (105.0)	111.4	105.2 (105.4)		162.6	(105.3)
0.5	21.48 (22.0)	24.05	21.26 (22.1)	(22.3)	23.6	(22.08)
0.6	2.14 (2.19)	2.23	2.01 (2.2)	(2.21)	2.08	(2.20)
0.7	.315 (.35)	.280	.310 (.351)	(.35)	.31	(.35)
0.8	.108 (.114)	.112	.104 (.114)	(.114)	.11	(.11)
0.9	.056 (.058)	.056	.052 (.058)	(.053)	.06	(.06)
1.0	.035 (.036)		.033 (.036)		.04	(.04)

**Notes: 1. Fatigue lives are in terms of number of passes through the spectrum (1 pass = 161034 cycles).**

**2. Fatigue life values in parentheses were calculated using the closed-form method**

**Table 8. Fatigue life predictions for six nines reliability,  
Phase I / Problem 3**

Alpha	ASTD	BHT	BH	KAC	MDHC	SA
0.6	8.88 (8.60)	9.50	8.67	(8.65)	9.14	(8.90)

- Notes: 1. Fatigue lives are in terms of number of passes through the spectrum  
(1 pass = 161034 cycles).  
2. Fatigue life values in parentheses were calculated using the  
closed-form method

**Table 9. Phase II results for S-N curve formulations**

S-N Curve Parameter	ASTD	BHT	BH (1)	KAC	MDHC (2)	SA
A	3.500e6	3.828e6	1.40e9	1.148e8	n.a.	3.855e6
B	1.47164	1.37	2.927	2.31	n.a.	1.3699
S <sub>e</sub>	54.5	49.6	44.75	48.0	n.a.	53.56
COV (S <sub>e</sub> )	.07	.109	.0785	.0831	n.a.	.10

- Notes: 1. Log normal distribution assumed.  
2. Round robin S-N formulation not applicable.

**Table 10. Fatigue life predictions for mean strength,  
Phase II / Problem 1**

Alpha	ASTD	BHT(2)	BH(2,3)	KAC	MDHC	SA(2)
0.5				6.20e9		
0.6		190735.		1.59e6	90356	
0.7	38180.	2316.5	10610.	10900.	1934.0	52354.
0.8	1144.0	649.0	1545.3	1760.0	655.0	1418.8
0.9	376.1	288.0	447.9	580.0	292.0	449.5
1.0	175.8	121.5	175.8	231.0	80.0	205.6
1.1	82.21		59.2	65.2		87.74
1.2	22.37		20.3	22.8		22.23

- Notes: 1. Fatigue lives are in terms of number of passes through the spectrum  
(1 pass = 161034 cycles).  
2. Constant COV for strength reduction.  
3. Modified Goodman correction.

**Table 11. Fatigue life predictions for six nines reliability,  
Phase II / Problem 2**

Alpha	ASTD	BHT	BH	KAC	MDHC	SA
0.3		4786.	17360.			
0.4	257200. (217500.)	324.	1428.0		45914.	(2744.2)
0.5	1166. (1088.)	42.0	121.2	(1340.)	814.0	(326.2)
0.6	283.6 (257.6)	4.8	18.3	(278.0)	180.0	(88.51)
0.7	78.06 (79.56)	.90	4.28	(45.2)	19.0	(10.74)
0.8	12.25 (12.85)	.40	1.73	(8.98)	3.7	(2.20)
0.85	6.82		1.19			(1.09)
0.9	2.88 (3.24)	.25	.878	(2.75)	1.2	(.67)
1.0	.924 (1.01)		.492		.66	(.35)
1.1	.468 (.508)		.679			(.22)
1.2	.288 (.314)		.206			(.15)

- Notes:** 1. Fatigue lives are in terms of number of passes through the spectrum  
(1 pass = 161034 cycles).  
2. Fatigue life values in parentheses were calculated using the  
closed-form method

**Table 12. Fatigue life predictions for six nines reliability,  
Phase II / Problem 3**

Alpha	ASTD	BHT	BH	KAC	MDHC	SA
0.8			3.17	(30.5)		
0.85	25.74 (25.49)	13.55	2.13		9.14	(2.7)

- Notes: 1. Fatigue lives are in terms of number of passes through the spectrum  
(1 pass = 161034 cycles).  
2. Fatigue life values in parentheses were calculated using the  
closed-form method

**Table 13. Fatigue life predictions for mean strength, Phase III.  
( $S_{max} = 70.44$  for  $\alpha = 1.0$ )**

$S_{max}$	Alpha	ASTD	BHT	BH	KAC	MDHC	SA
73.3	1.04	134.7	121.49	109.8		38.74	156.1
80.0	1.14	51.72	18.3	37.5	38.5	13.67	53.7
86.7	1.23	15.3	7.90	15.4	17.5	4.41	15.4
90.0	1.28	9.27	4.60	9.32	9.18	2.56	9.5
93.3	1.32	6.69	2.88	5.46	5.78	1.85	6.8
100.	1.42	2.48	1.23	2.42	2.49	1.03	2.2
120.	1.70	.375	.38	.448	.466		.38

Note: Fatigue lives are in terms of number of passes through the spectrum  
(1 pass = 161034 cycles).

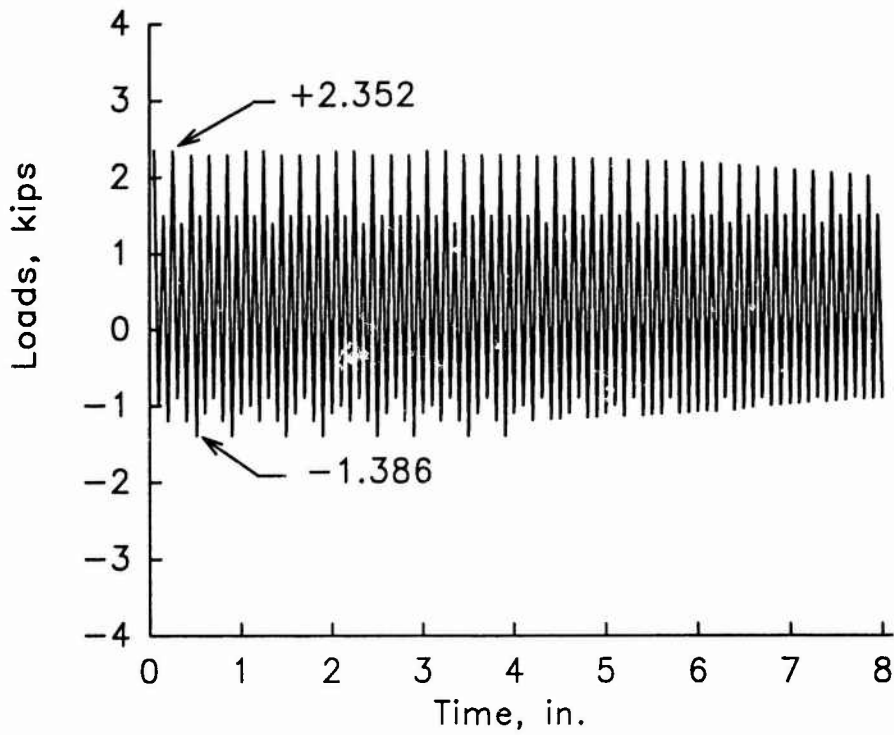


Fig. 1. Flight loads for high speed dive.

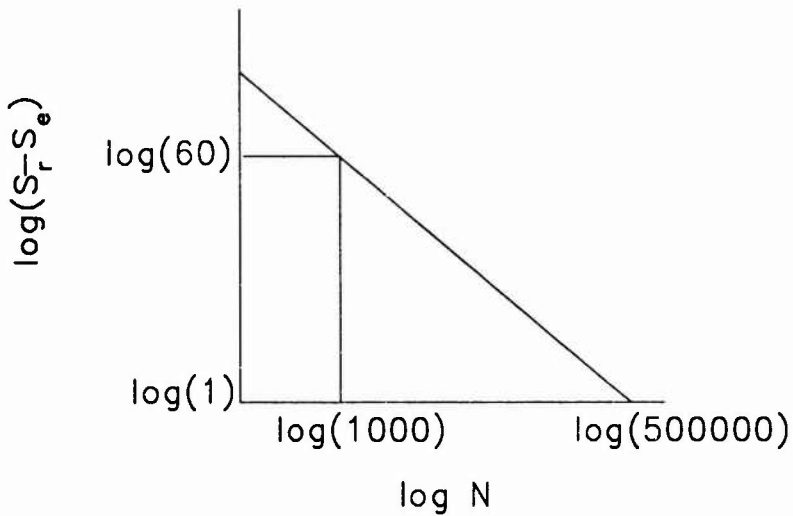


Fig. 2 Theoretical S-N Curve

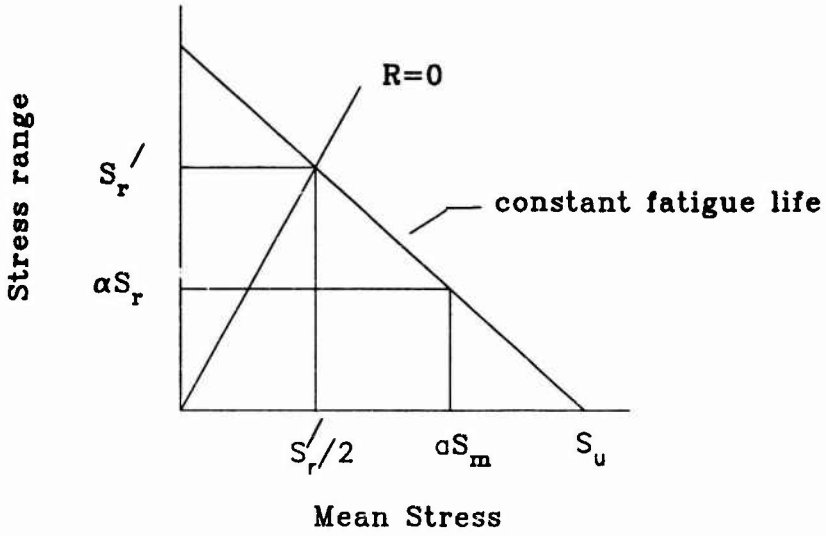


Fig. 3 Linear Goodman diagram

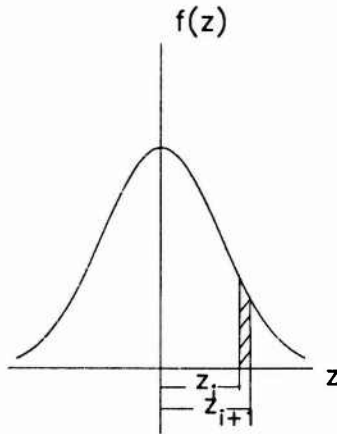


Fig. 4. Probability density function(PDF)

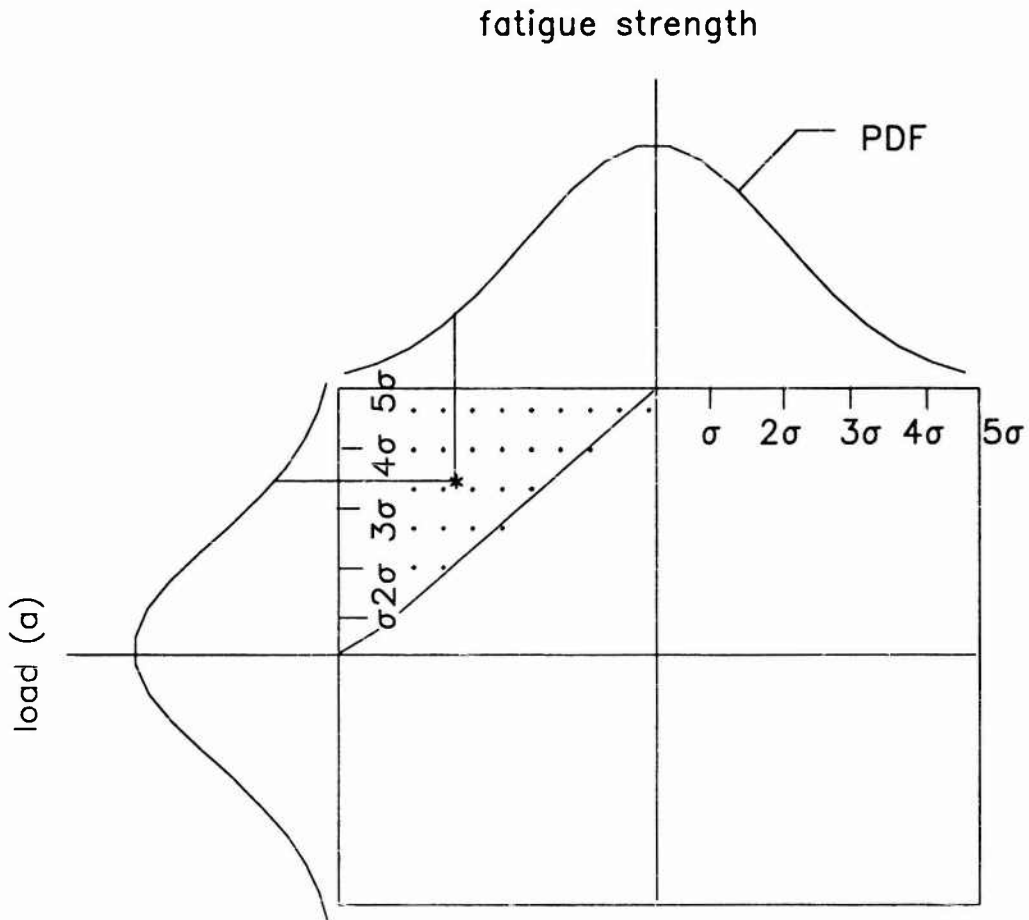


Fig. 5. Joint probability matrix

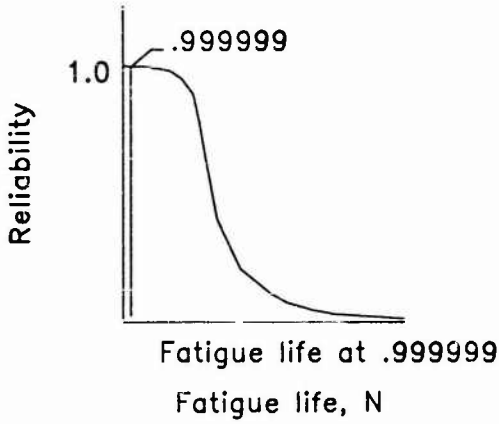


Fig. 6 Reliability versus fatigue life.

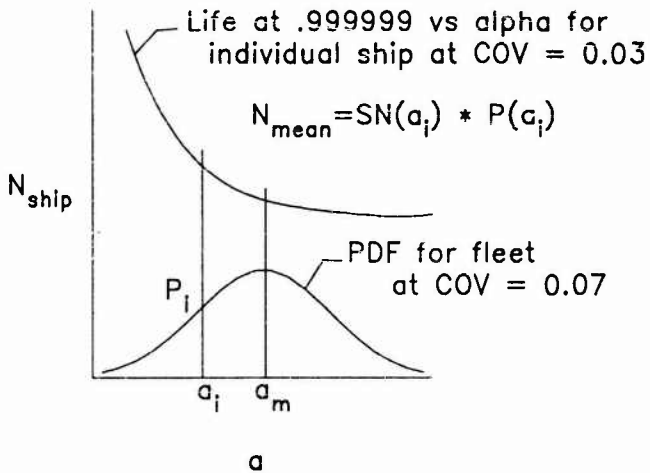


Fig. 7 Total probability process for problem 3.

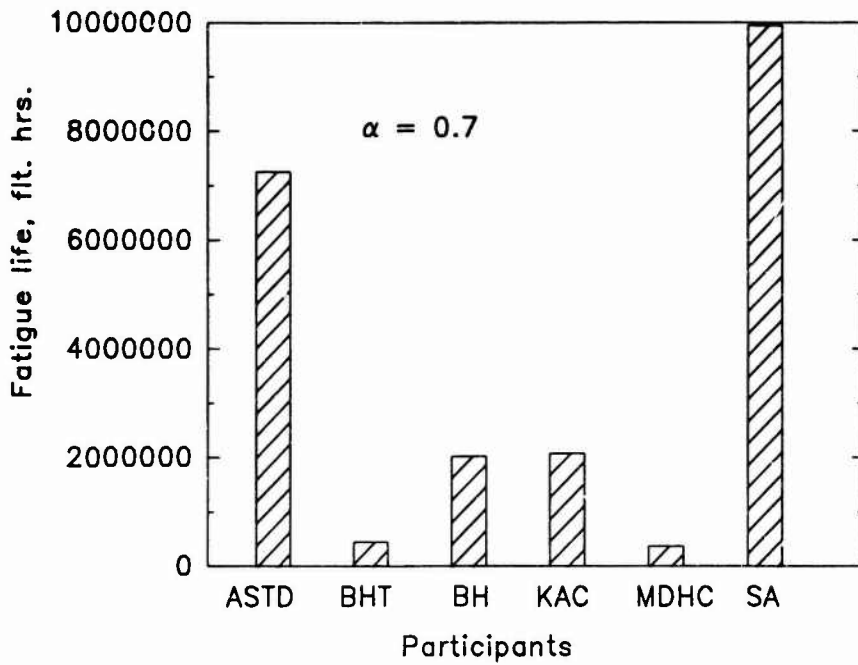


Fig. 8. Phase II/Problem 1 results for mean strength.

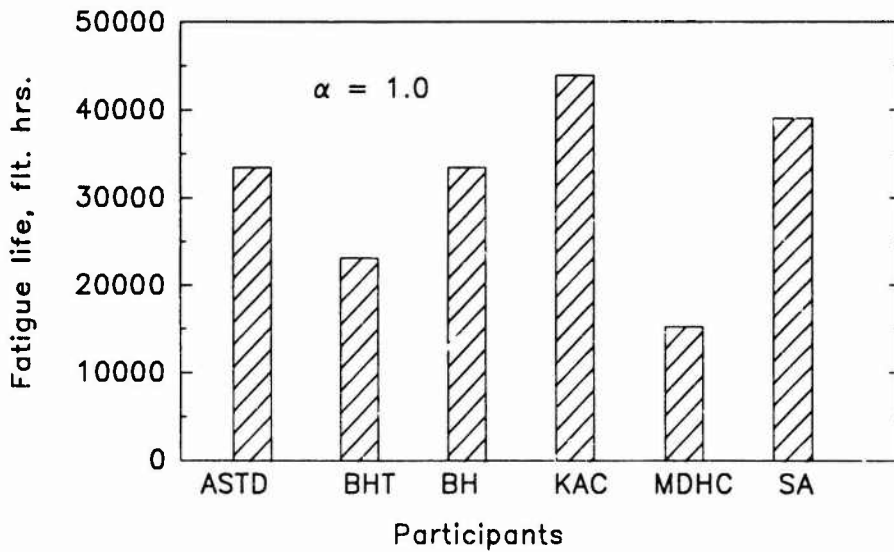


Fig. 9. Phase II/Problem 1 results for mean strength.

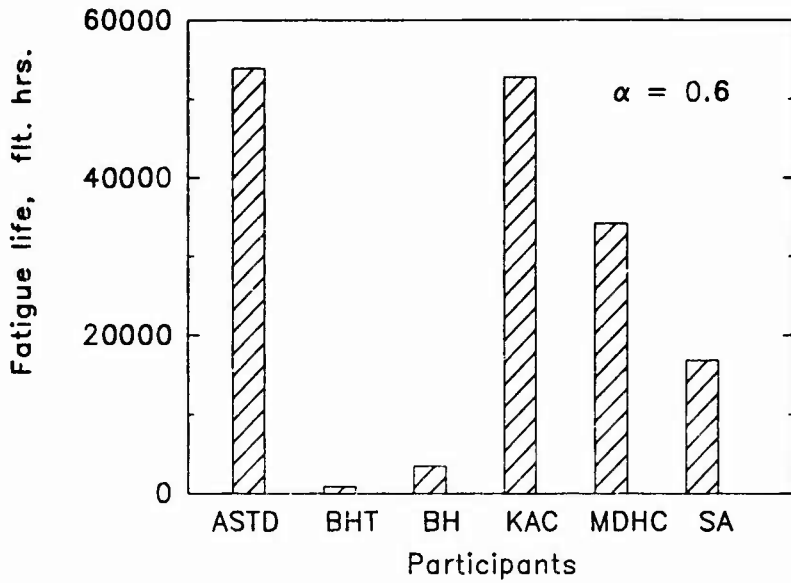


Fig. 10 Phase II/Problem 2 results for six nines reliability.

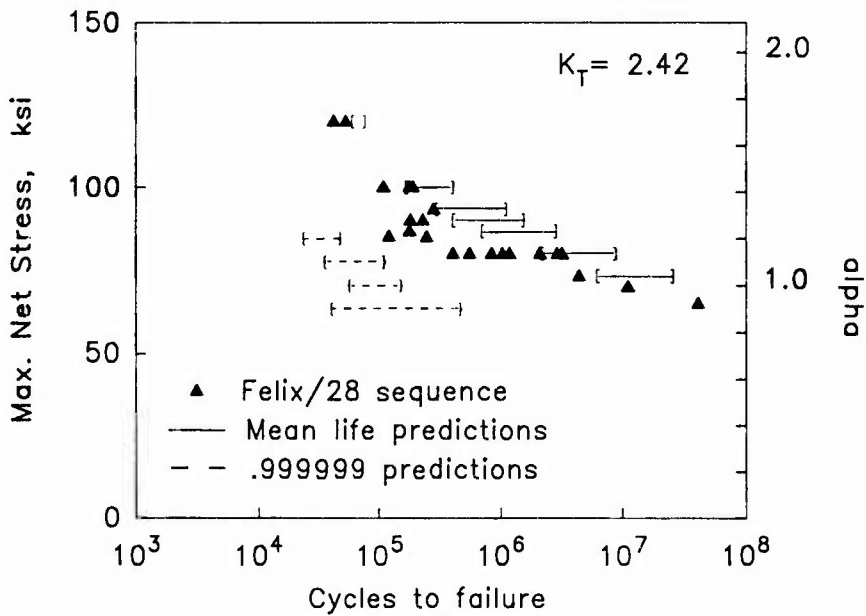


Fig. 11. Round-robin comparisons with spectra tests.

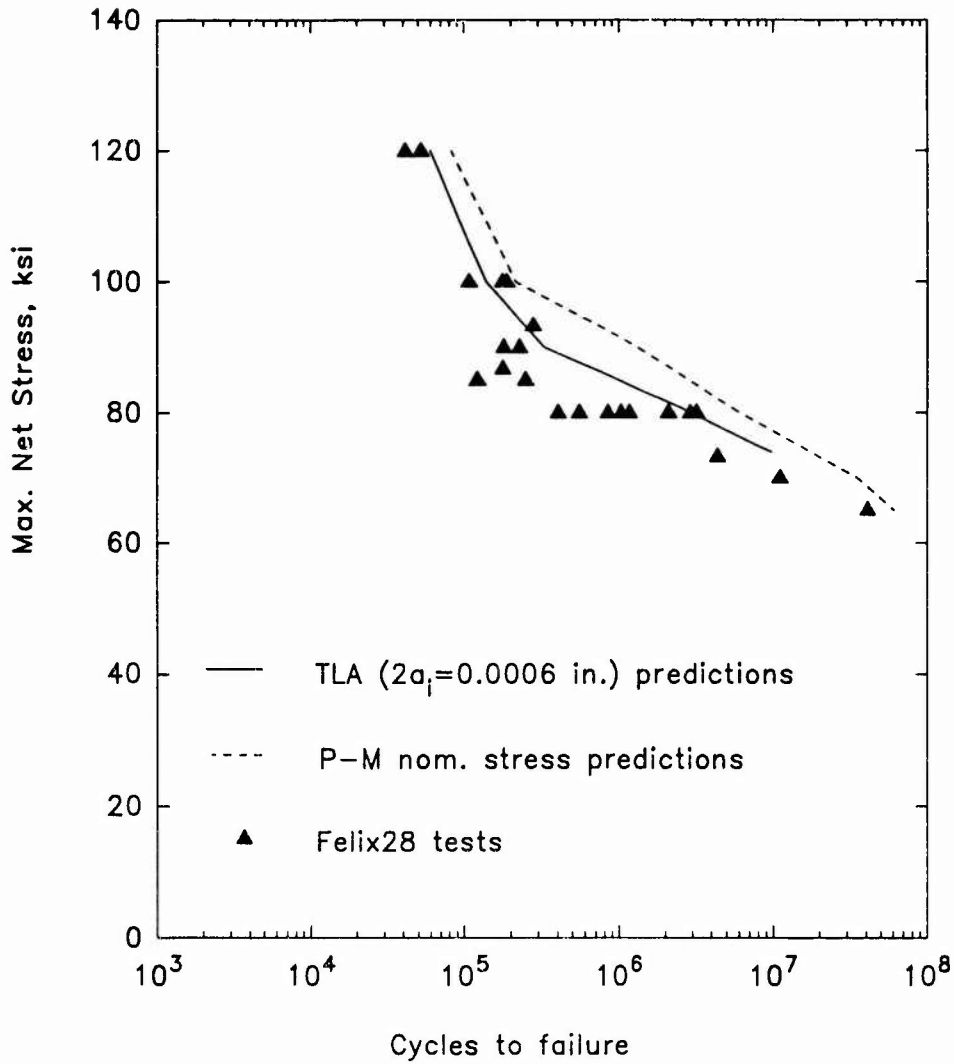


Fig. 12 Fatigue life prediction for Felix/28 tests.

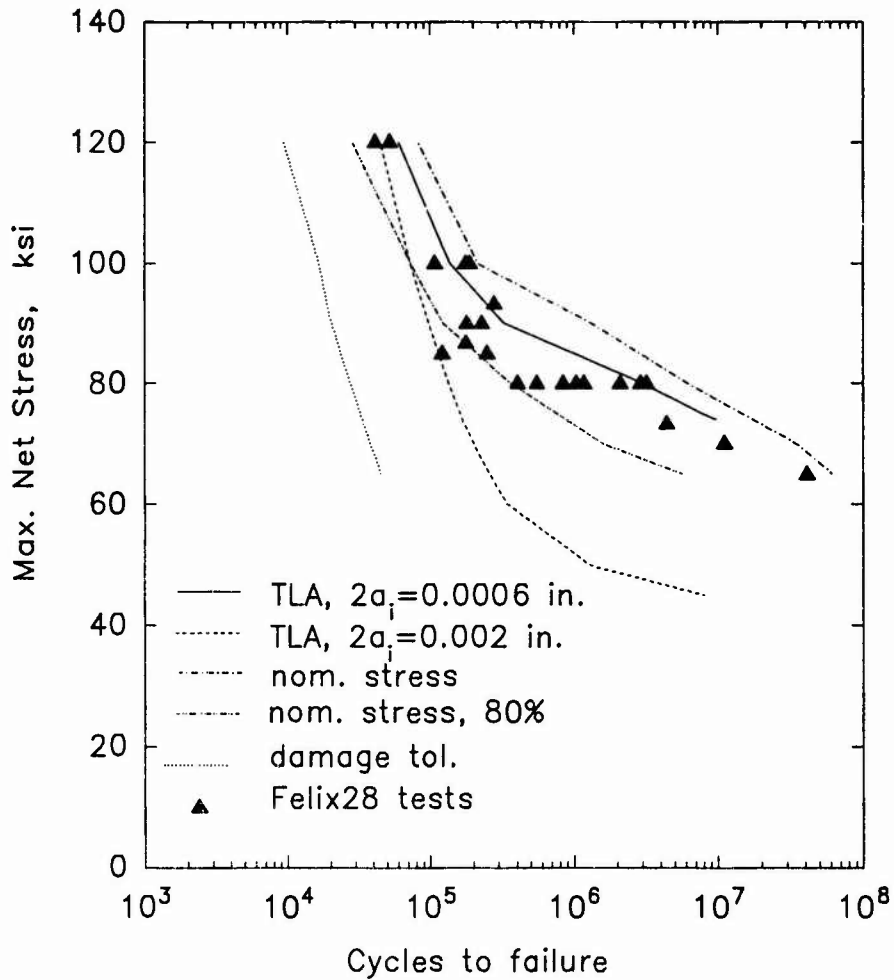


Fig. 13 Effect of conservative assumptions on fatigue life predictions for Felix28 tests.

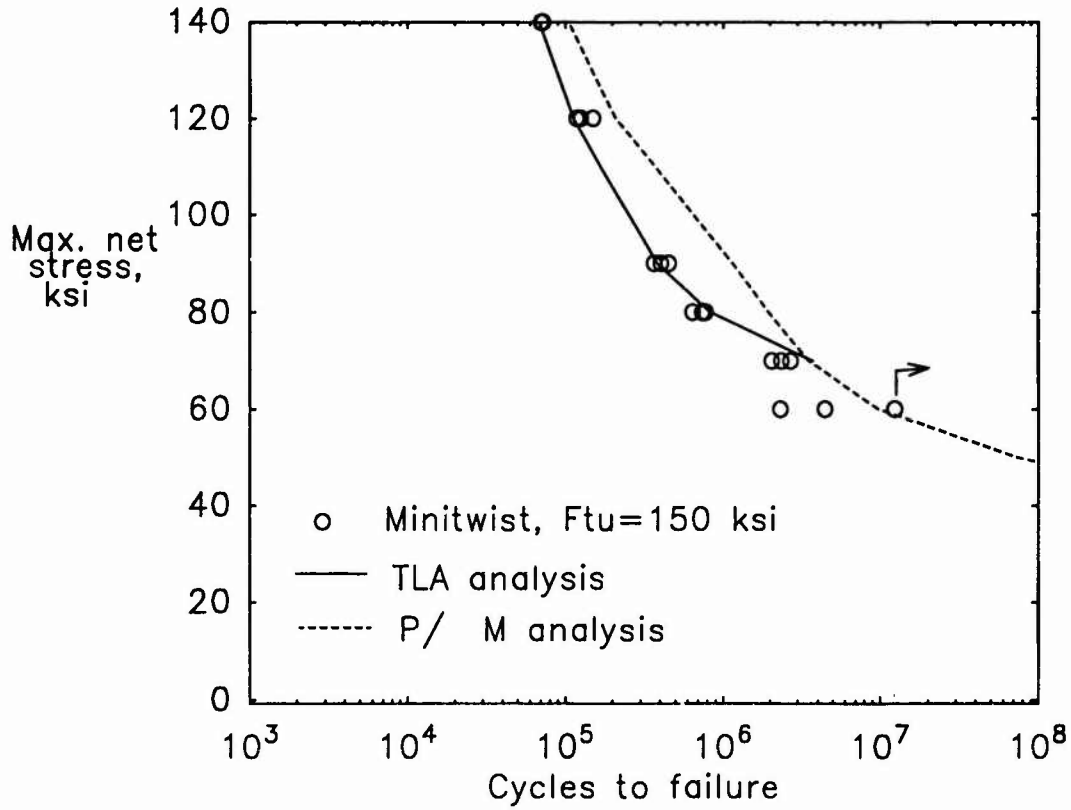


Fig. 14. Minitwist tests and analysis.

# FATIGUE MANAGEMENT AND VERIFICATION OF AIRFRAMES

A.F. Blom\* and H. Ansell#

\* The Aeronautical Research Institute of Sweden (FFA)  
P.O. Box 11021  
S-161 11 Bromma, Sweden  
# Saab Military Aircraft  
S-581 88 Linköping, Sweden

## 1. SUMMARY

The methodology currently used in Sweden for fatigue management and verification of airframes is described. Applications from the new fighter aircraft JAS39 Gripen are included in order to illustrate the various concepts being considered. Additional experience from recent work on the older fighter 37Viggen is also included to highlight certain differences in the detail analyses, stemming from rather different nominal stress levels in the two aircraft. The present paper discusses the handling of load sequences and load spectra development, stress analyses and fracture mechanics analyses, fatigue crack growth modelling, component and full scale testing, service load monitoring regarding both the dedicated test aircraft, which is used to verify basic load assumptions, and also the individual load tracking programme developed for the new fighter.

## 2. INTRODUCTION

While fatigue is recognised as the primary failure mechanism in most structural components, the consequences of such failures (in terms of lives and money) are probably more obvious and severe for aircraft than in any other area. Fatigue and damage tolerance of aircraft are dominant factors throughout the design process, the manufacturing, the structural testing (component level and full-scale), the initial test flights and during the subsequent usage of the aircraft. Without adequate knowledge of relevant loading conditions, resulting stress distributions and material properties no fatigue assessment can be achieved. Further on, such work has to be attached to a specific design philosophy - can the actual component be inspected during service, in the case of damage - can it be repaired or replaced, and in the case of failure, will that cause loss of the entire aircraft? Questions like these, and many more specific detail problems, are dealt with in existing regulations and specifications for military aircraft, e.g. Refs. (1-9). It is far beyond the scope of the present paper to discuss these specifications in any detail (there are also other ones treating, for example, flight and operations tests, vibrations, sonic fatigue and non destructive inspections). Instead, the purpose of this paper is to briefly discuss fatigue management and verification of airframes, with emphasis on the new fighter JAS39 Gripen but with specific examples added from work on the fighter 37Viggen. These two aircraft are designed with some 20 years apart, relying on safe life and/or fail safe methodology for the Viggen fighter but damage tolerance requirements for the Gripen aircraft which, amongst other things, lead to significantly lower stress levels than for the Viggen aircraft. Hence, first order conservative estimates of stress levels and stress intensity factors are normally adequate to verify the design life for the Gripen aircraft while the analytical work carried out to verify the damage tolerance for the Viggen fighter is much more refined.

## 3. DAMAGE TOLERANCE AND DURABILITY

Below we present firstly a short summary of basic definitions, as they are normally interpreted in general terms. Thereafter, we specifically discuss details of these same concepts as applied to the two Swedish fighters being under discussion.

### 3.1 Damage tolerance

Basically, this approach which was developed by the United States Air Force (9), and which is now adopted with or without minor modifications by virtually all countries for both military and civil aircraft, differs from the original Fail-Safe philosophy in that it assumes cracks to exist in the structure already at the very first load cycle. Also, a distinction is made between in service inspectable or non-inspectable structures. Presently, with the exception of landing gear, engines and engine mounts all fighter aircraft structures and all inspectable civil aircraft structures are considered as damage tolerant (9,10). Recently, the damage tolerance approach has also been introduced for engines (11-13), and the concept is also considered viable for helicopters (14).

### 3.2 Durability

While damage tolerance is the principal means to ensure structural safety, durability may be considered as a quantitative measure of the structure's resistance to fatigue cracking under specified service conditions. This means that the economic life-time, including all inspections, replacements or repairs, should exceed or at least equal the design life based on damage tolerance. The traditional means to achieve durability has been through conventional fatigue testing and analysis. However, recently a fracture mechanics philosophy, combining a probabilistic format with a deterministic crack growth approach has been devised (15) for ensuring the U.S. Air Force's durability design requirements for advanced metallic airframes (16)

### 3.3 Initial Flaw Size Assumptions

A damage tolerance analysis implies a thorough identification of all critical areas with due regard to the utilisation of the aircraft and the impact of failure. According to the U.S. Air Force Military Specification (11) these areas should be classified either as Slow Crack Growth, Fail Safe Multiple Load Path, or Fail Safe Crack Arrest structures. If it is possible to prove that the structure is Fail Safe due to Multiple Load Paths (i.e. load redistribution) or Crack Arrest capability, less stringent conditions have to be satisfied.

As a result of material and structure manufacturing and processing operations, small imperfections equivalent to a 0.127 mm radius corner flaw shall be assumed to exist in each hole of each element in the structure. The flaws are assumed to be located in the most unfavourable orientation with respect to applied stresses and material properties. In addition it is assumed that initial flaws of sizes specified in

Ref. (9) can exist in any separate element of the structure. Only one initial flaw in the most critical hole and one initial flaw at a location other than a hole need to be assumed to exist. Interaction between these assumed initial flaws does not need to be considered. The flaw shape is assumed to be through the thickness (straight crack front), quarter circular or semi-circular. However, other flaw shapes with the same initial stress intensity factor are considered appropriate, particularly at locations in the structure where other shapes are more likely to occur.

### 3.4 Damage tolerance methodology

It should be emphasised that the damage tolerance evaluation essentially is analytical but that sufficient testing must be performed to validate the analytical methodology. No strict requirements exist on how the analysis should be performed but the following steps are normally encouraged.

- Based on structural analysis the most fatigue critical areas are identified.
- Stress intensity factors as function of crack geometries (length, depth) and applied loading are computed for the identified areas. Initial flaw size assumptions are specified in the U.S. Air Force Military Specification (9).
- Fatigue crack growth integration is performed on a cycle-by-cycle basis preferably using tabulated constant amplitude fcg-data.
- If a retardation or retardation/acceleration model is used in the crack growth analysis, this model should be shown to be non-unconservative by relevant testing. For example, the original Willenborg model should not be used.
- In the definition of relevant load- and stress spectra, experimental truncation tests (of the scarce extreme loads) should be performed to obtain a spectrum which minimises crack growth life for analysis.
- Extreme loads must be considered for residual strength calculation.
- A certain number of component tests, representative of the structure, should be performed to validate the prediction capability of crack growth in complex structures.
- Based on the analytical predictions of fatigue crack growth, relevant inspection intervals are defined.

These steps are usually complemented not only with full-scale static tests up to at least limit load but also with full-scale spectrum fatigue tests. The latter are typically carried out for at least two design life times in order to detect any cracking at locations which might have been overlooked in the analysis. If no cracking occurs during these lives artificial flaws are introduced at critical areas and then the spectrum loading is carried out for two more design life times. During the latter phase crack growth (from fatigue cracks or artificial flaws) is monitored and compared to analytical predictions. The testing is able to provide such comparisons for several locations as cracked components may either be repaired or replaced by new ones. Eventually, the test ends with a residual strength test of a major structural component.

### 3.5 The Saab JAS39 Gripen aircraft

The basic military concept behind the JAS39 aircraft is that each individual aircraft and each individual pilot should provide multi-mission capability, i.e. instantly be able to perform air-defence as well as air-to-surface attacks or reconnaissance, without any changes to the aircraft itself. This multi-mission capability will result in an

operational flexibility allowing concentration of units in a manner previously not technically possible.

The Gripen is designed to fit into the Swedish Air Force's base system. This means that the JAS 39 is capable of taking off from and landing on road bases. Flight preparation at wartime bases should be possible by conscripted personnel under field conditions.

The aircraft is aerodynamically unstable in certain parts of its operational envelope. Stability is obtained by means of a triplex digital fly by wire control system with a triplex analogue back up system.

#### 3.5.1 Approximate Data of the Aircraft

Engine:	One Volvo Flygmotor RM12 (=General Electric F404) producing 8 tons thrust
Weight:	8 tons
Length:	14 m
Wingspan:	8 m
Speed:	Supersonic at all altitudes
Wing:	Multi-spar design with skins and spars made of CFRP-laminates. Root ribs made of Al-alloy. The structure is bolted together.
Canard, Fin and Control surfaces:	Full core aluminium honeycomb with CFRP laminate skins Some rudders of Al-alloy
Fuselage:	With exception for a few doors it is all metallic, 7475 skins, 7075 extrusions and 7010 forgings.

Most of the attachment fittings joining the various parts of the aircraft are made of 7010 forgings

The CFRP laminates were initially made of Ciba-Geigy toughened epoxy with HTA 7 fibres. Presently also Hercules systems are qualified to be used

#### 3.5.2 The Design Requirements

Design limit load factor	= 9.0
Ultimate safety factor	= 1.5
CFRP laminates not allowed to buckle below	150%LL.

The design and testing requirements essentially agree with the U.S.A.F. military specifications, Refs (3-11)

#### 3.5.3 Damage tolerance requirements for the JAS 39 Gripen

Only so-called Critical parts are required to comply with damage tolerance requirements. A part is classified as critical if its failure alone may cause the loss of an aircraft. The requirements are essentially identical with USAF MIL-A-83444. The main difference is that the residual strength requirement is always 120%LL.

Analysis Goal:	3000 hrs. inspection-free service life
Verification Goal:	4000 hrs. inspection-free service life
Minimum Requirement	No detail to have a shorter inspection interval than 400 hrs

### 3.5.4 Damage tolerance verification policy

Previous experience from a damage tolerance study on the Saab AJ37 Viggen aircraft led to the following policy:

The damage tolerance verification is to be done on full-scale assemblies, where the critical part is correctly built into its surrounding structure.

The critical parts are to be manufactured according to series production standard. (Example: Die forgings are not to be substituted by hand forgings or plate material).

Fatigue testing of critical parts is not allowed to be eliminated just because a damage tolerance verification testing is carried out (Reason: The damage tolerance test is biased, because it interrogates the structure only at the points where artificial flaws have been made. A correct fatigue test does not suffer from that kind of bias.) The fatigue testing shall cover at least four inspection free lives, i.e., 4 x 4000 hrs.

The damage tolerance verification testing shall be done using realistic flight by flight simulation testing, and shall cover at least two inspection free service lives, i.e., 2 x 4000 hrs.

A critical part having initial artificial flaws in accordance with Mil-A-83444 and which survives 2 x 4000 hrs. of realistic service life simulation followed by a residual strength testing to 120%LL is considered to have fulfilled the verification goal: 4000 hrs. of inspection-free service life.

If significant crack growth occurs during the damage tolerance testing, a safe inspection interval is to be established based on crack growth observations.

### 3.6 The Saab 37Viggen aircraft

The Swedish lighter aircraft 37 Viggen, Figure 1, was designed some 30 years ago on a safe life and/or fail safe basis. Some major parts of the aircraft have been re-assessed in terms of a damage tolerance evaluation. The aim of this assessment has been to ensure structural safety, and to investigate the possibilities for extending the original life of the aircraft. This can be carried out because the total life of the aircraft will depend on its durability (see definition above) while the damage tolerance ensures, at all stages, the structural safety of the aircraft.

The purpose here is to summarise some of the damage tolerance analyses and the testing performed on the main wing attachment frames. There are four versions of the main wing attachment frame due to two different versions of the aircraft, attack (AJ) and fighter (JA), and due to major changes in the geometry made after serial production of several aircraft. In this paper focus is on the latest version of the JA frame. Specifically, the aim is to briefly show the complexity of a damage tolerance assessment in a case where the safe original life design has resulted in rather high stresses.

Because of the original safe life design, resulting in quite high stresses, very extensive finite element analyses have been necessary in order to obtain accurate stress distributions in critical sections. These stress distributions have subsequently been used for the evaluation of 3D stress intensity factors. Also, high demands have been placed on the accuracy of the crack growth predictions. Hence,

extensive validation of the crack growth prediction technique has been required.

Structural testing, including artificial flaws, has been carried out with the aim of obtaining crack growth data for correlation to the prediction technique. The stress analyses were mainly verified on basis of traditional static and fatigue testing results available from the design phase of the aircraft.

The approach taken for this study has been to follow the military specification MIL-A-83444 as discussed above. All of the components considered represent primary structures with few or no alternative load paths and have, therefore, been classified as slow crack growth structures. Initial flaw size assumptions follow the requirements of the specification in Ref. (9). A conservative residual strength requirement of 1.2 times limit load has been applied in terms of the linear elastic plane strain fracture toughness,  $K_{Ic}$ , irrespective of actual thicknesses, except for cover sheets where  $K_{Ic}$  values for actual thicknesses were used.

## 4. LOADS

### 4.1 The Saab JAS39 Gripen aircraft

A conceptual model is used which covers design and sizing, structural test verification and service monitoring and involves engineering activities such as mission analysis, external loads analysis, structural analysis and stress analysis. Fig. 1 shows the various parts as a block scheme, while an overview of various computer programmes is illustrated in Fig. 2. Figure 3 shows details of the block scheme shown in Fig. 1.

Design parameters in the mission analysis originate from estimated threats and expected usage and are expressed as a sequence of flights and ground conditions. The conditions are defined by flight mechanics parameters such as load factor, roll rate, speed, control surface deflections, thrust, fuel burn, weapons etc.

Each set of flight parameters defines a certain flight condition. Determining the external loads for those conditions (manoeuvres) at different aircraft configurations requires analysis of e.g. structural dynamic response, aerodynamic pressure distributions at different speeds, angles of attack etc. Ground loads analysis include such events as landing impact, taxiing, braking, turning etc.

The load analysis makes use of techniques like the finite element method to predict dynamic transient response, e.g. landing, computational fluid dynamics for prediction of aerodynamic pressure fields and six degree of freedom flight mechanics model with control system logics to predict in-flight manoeuvres. Numerical predictions are supported by wind-tunnel tests of models.

#### 4.1.1 The global spectrum approach

For fatigue and damage tolerance sizing and test verification, a methodology referred to as the global spectrum approach, in which the design loading of the complete aircraft is defined, has been developed. In this approach the description of each unique manoeuvre is defined as a sequence of instantaneous and balanced load cases. Sequential manoeuvres build up unique missions and sequences of missions build up the expected usage. The load cases consist of linear combinations of unit load cases (including aerodynamic loading, inertia loads, ground loads

etc.) for the finite element model of the complete airframe in a hierarchic way. All information about load case structure and their occurrences in the sequences are stored in a global sequence database. Through this methodology results local load sequences, in terms of loads, stresses, displacements etc., which can be directly used for crack growth calculations or counted, by means of the rain-flow algorithm, in order to be used for classical fatigue analysis or planning of structural test programmes.

This database is updated continuously as a project develops and as flight test data becomes available. The current global sequence for the JAS39A Gripen aircraft consists of 35 different types of unique missions built up by more than 13 000 unique load cases. These unique missions are combined into 60 deterministic sub sequences (defined on basis of pilot training programs and consisting of 12 different taxi load sequences, 35 different flight load sequences and 13 different landing load sequences) which are then combined to a sequence covering 313 complete missions (taxi out, flying, landing, taxi in) containing a total of more than 500 000 load cases. A unique repetition sequence representing an actual service load history of these 313 flights is equivalent to 200 fh and, thus, consists of more than 500 000 states.

The internal loads distribution are obtained by solving a finite element model of the complete aircraft using the external loads representative for the unit load cases in the global sequence description. The finite element models of the single- and twin-seated version of the JAS39 Gripen aircraft are shown in Fig. 4 for which 460 unit load cases are solved and stored in a structural analysis database.

Having access to the global sequence database and the structural analysis database, the engineer is able to obtain local load or stress sequences and rain-flow counted spectra for any member element of the finite element model of the complete aircraft. This is done by an interactive software system which is connected to the two databases. The global spectrum program delivers load sequences for all the loading actuators of the various structural tests. It also delivers the basis for comparison with the results from the loads monitoring registrations on each individual aircraft.

#### 4.1.2 Load calibration

One test aircraft (Test A/C 392) is dedicated to the loads survey programme, figure 5. About 500 strain gauges have been installed. The aircraft has been subjected to about 150 calibration load cases with the purpose to accurately be able to deduce interface loads between wing and fuselage, wing and control surfaces and fin and fuselage. Also shear, torque and bending at three wing sections and at four fuselage sections, as well as bending and torque in the canard pivot, landing gear loads and loads from external stores are measured.

#### 4.1.3 Load interaction

It is well known that the sequential order of the loads in the spectrum is very important for the fatigue life. Models to account for this influence on the fatigue crack growth rates are normally based on plasticity considerations and they may predict rather different results, conservative or not, depending on the model chosen (24). In the flight sequence various parameters influence the crack growth with various amounts. The variations found to have the greatest impact are those involving modifications of the maximum peak loads. These variations include mission mix, high and low load truncation, exceedance curve variations, and test limit load variations. Variations shown to have significant

effects include those which modify all but the highest peak loads throughout the spectrum, such as sequence of missions, compression loads, and peak and valley coupling. Spectra variations shown to produce the least effect are those which modify lesser loads in each mission. These consists of reordering of loads within a mission and flight length variations (25).

#### 4.1.4 Service loads monitoring

For the Swedish fighter JAS39 Gripen, every aircraft will be equipped with a service loads monitoring system, see Fig. 6. The following six loads will be recorded:

- 1 Vertical acceleration at C.G. = Load factor,  $n_z$
- 2 Canard pivot Bending,  $M_x$
- 3 " " Torque,  $M_y$
- 4 Wing Fwd attachment bending,  $M_x$
- 5 " " Aft attachment force,  $S_z$
- 6 Fin Aft attachment bending,  $M_x$

With the exception for the first one, the forces will be measured by means of calibrated strain gauge bridges. Each individual aircraft will be calibrated while flying in detail specified manoeuvres. Nominally identical strain gauge installations on the loads survey aircraft (Test A/C 392), on the major static test structure, on the major fatigue test structure, on two canard pivot test articles and on two fin plus rear fuselage test articles will add confidence to the calibration procedure.

Recorded data will be analysed on board each aircraft using the range pair range count algorithm. After transferring to a ground based computer, comparisons will be made with the corresponding local spectra as delivered from the global spectrum software system.

## 4.2 The Saab 37 Viggen aircraft

### 4.2.1 Geometry and loading

The principal geometry of the JA main wing attachment frame is shown in Fig. 7. The frame can be described simply as an assemblage of two curved U- or J-shaped beams, located a distance of 1600 mm apart and kept together by inner and outer cover sheets. The beams are made of an aluminium die forging and the cover sheets are made of aluminium alloy sheet material. Between the two beams a structural detail, called the middle part, is located as indicated in Fig. 7.

Depending on the aircraft version, the middle part is made of an aluminium die forging or a high-strength steel forging. Also, a lower rear engine attachment is mounted between the two beams, see Fig. 7.

The main wing attachment frame is loaded by the main wing spar. It is the only attachment frame that takes up the bending moment from the wings. Shear loads are distributed on several frames. The loads from the main wing spar are introduced into two attachment holes in each beam and two holes in the middle part. The purpose of the middle part is to distribute a portion of the load to two adjacent attachment holes in each beam, called middle part holes. Furthermore, the main wing attachment frame is loaded by the engine through the rear engine attachment, which transfers vertical loads. Finally, loads are introduced to the frame from the fuselage through the cover sheets. A principal sketch of the loads acting on a quarter of an isolated main wing attachment frame assemblage is shown in Fig. 8. The load,  $P_{1z}$ , at the top of the frame is introduced in combination with extra loads on the engine attachment to compensate for the missing load transfer from the rest of the fuselage when an isolated assemblage is

studied. Obviously, the magnitudes of the loads on the different versions of the main wing attachment frame are different.

#### 4.2.2 Design versus usage spectrum

The load spectrum used both for analytical predictions and for testing of some coupon test specimens and an isolated main wing attachment frame assemblage is shown in Fig. 9. As can be seen, the utilised design spectrum is more severe than the average usage spectrum of the aircraft.

### 5. STRESS SPECTRA AND FRACTURE MECHANICS

Models used for assessment of fatigue life and damage tolerance of fighter aircraft vary from rather simple to highly complex depending on factors such as, if the structural component is primary or secondary, local stress levels, inspectability etc. Typically, simple models are used initially and more sophisticated analysis is resorted to in complex geometries and when safety margins are lower.

#### 5.1 Elimination of insignificant stress cycles

Due to the basics of the global spectrum approach, described above, very many small load cycles are generated. It is therefore advisable to omit certain small cycles which from a fatigue viewpoint have no practical meaning. The system contains interactive facilities to remove insignificant states. By defining omission conditions connected to the earlier defined sequences the reduction of the sequences is immediately displayed. For the component shown in Fig. 10, the original sequence consists of 7813920 states for 3000 flight hours. By omitting cycles with ranges smaller than 20 kN (approximately 10% of the maximum range) the total sequence is reduced by 97.1% to 224250 states. The omission technique adopted also works when more than one load sequence is considered through a lowest common denominator scheme.

Selected parts of the total sequence can be plotted in a variety of forms and on different devices. In Fig. 11 a plot of the beginning of the unreduced sequence is shown on screen format. The sequence shown in Fig. 12 has the above defined omission condition applied. The triangular marks shows where each mission ends. Spectra can be plotted in two forms, either the distribution of ranges or the distributions of peaks and troughs. In Fig. 13, the distributions of ranges are shown for both the original spectrum and the reduced spectrum.

The software has features to facilitate identification of load cases. This can be done by retaining load case identification numbers all the way through the rain flow count operations, omission procedures etc. This technique has proven to be most important when planning for structural testing. For JAS39 every unique load case of the global sequence has been assigned a 9 digits code number according to a systematic scheme.

#### 5.2 The Saab JAS39 Gripen aircraft

The global finite element model predicts the internal loads distribution and the different types of entities that can be obtained depend on mesh and type of elements. The most simple case is to extract a scalar sequence, e.g. a normal force sequence from a flange element. If more complex elements are used, e.g. beams, solids etc., more stress components are available. Since each state in the global sequence represents a certain load case, i.e. a certain

combination of the components, each change from one state to the next state also means a change of the stress intensity factor to another. This complicates the situation if the stress components are not correlated.

The main wing attachments of the Gripen aircraft are shown in Fig. 14. Fig. 15 shows the finite element substructure of one of the three main wing attachment frames and resulting stresses for limit load are shown in Fig. 16 for critical areas. Parts such as the lower flange regions are here modelled by beam elements from which sequences of normal force and bending moments can be obtained. The correlation between the bending moments and the normal force in this region is reasonably good. Figs. 17 and 18 show the bending moments versus normal force. A stress intensity factor solution which is applicable for the complete sequence can thus be obtained from a linear combination of the three entities.

This is most often enough for damage tolerance analysis. Local stress sequences are used together with stress intensity factors that are available for different crack/loading configurations.

Sometimes when predicted crack growth lives initially do not meet the target lives, more sophisticated local modelling can be made and connected to the global model and the global sequence. For the lower flange region a local stress model using solid elements has been solved using the p-version of the finite element method. Figure 19 shows a model of the region and the stress distribution resulting from a load case representing a pull-up manoeuvre. The stress distribution across a section cutting through a highly stressed region is shown in figure 20

The stress intensity factor for a crack in this section is derived using three dimensional weight function technique

Damage tolerance analyses are made for large number of assumed cracks in primary structure. For the JAS39A aircraft more than 1000 crack sites have been analysed. The type of analysis ranges from simplified ones using basic stress intensity factor solutions to more or less advanced ones using p-version FEM either with the crack incorporated in the mesh or by applying 3D weight functions to stress distributions for the uncracked structure. Each analysis is summarised on a damage tolerance analysis sheet. An example of such a summary sheet is given in Fig. 21.

#### 5.3 The Saab 37 Viggen aircraft

The finite element analyses have been made in several steps where the initial step has been to make a global model of the complete component. These global models were able to describe stiffnesses correctly and to indicate where stress concentrations were located. In a few cases the global models were sufficiently detailed to give local stresses, but usually more detailed models were required. A typical example of a global model for a quarter of the main wing attachment frame assemblage (remaining after accounting for the symmetry) is shown in Fig. 22. The model, which is made using a substructuring technique, consists of approximately 75000 degrees of freedom.

Based on the global FE-results, critical areas were identified, which were then subjected to more detailed FE-analyses, including such elements as accounting for bushings and solving contact problems. The boundary conditions for the detailed models were obtained from the

global models in terms of displacements and rotations of nodes along the created cuts through the global models.

The region around the fuel pipe holes in the main wing attachment frame was analysed using the p-version of a newly developed self-adaptive FE-code (26). Also, some stress intensity factors were computed using this technique, which is believed to be the most accurate technique there is for such calculations.

Regions around major attachment holes were analysed using conventional FE-technique but, as already mentioned, contact stresses between wing bolts and bushings, as well as between bushings and frame forgings, were computed using an automatic iterative solution technique. In many cases the detailed analyses were repeated with considerations of more and more details, such as heads of bolts and stiffening effects of middle parts. The reasons for repeating the detailed analyses were seemingly improper or too large deformations and unrealistically high local stresses. For example, by including the bolt head in the model of the middle part hole region, see Fig. 23, the largest principal stress was reduced by 25% due to reduced bolt tilting.

### 5.3.1 Fracture Mechanics and Fatigue Crack Propagation

A difficulty in the damage tolerance analysis has been to obtain relevant stress intensity factors. In many cases the stresses at critical locations have been high (locally) with large gradients in both surface and thickness directions. Stress intensity factor solutions based upon a remotely applied uniform loading are generally not able to describe the local stress gradients. Besides, it is very difficult to define the remote uniform loading.

The most accurate stress intensity factors used were those computed using the adaptive FE-technique, see Fig. 24. However, there were too many critical locations for applying this technique everywhere. Second best stress intensity factor solutions seemed to be those based upon the weight function technique, in which case local stress distributions could be described accurately. Such stress distributions were obtained directly from the FE-analyses and they are valid as long as no major changes due to load re-distributions occur. However, weight functions for 3D geometries are scarce. For 2D geometries it is easier to find accurate weight functions but through-the-thickness cracks were, in general, a far too severe assumption for the critical locations studied.

The solution to the problem was to introduce correction functions based on the 2D weight function solutions such that the 3D solutions for remote loading were modified to approximately account for the local stress distribution in one of the two directions.

Fatigue crack growth predictions were performed using a cycle-by-cycle analysis technique without consideration of plasticity-induced load interaction effects. However, a method for extracting contributing load cycles from an irregular load sequence was used which can be described as a very simplified rain flow counting algorithm.

All available fracture mechanics and crack growth data for the aluminium alloys and the high strength steels involved have been critically reviewed and collected in a data base for easy access. Complementary testing on coupon

specimen level was performed to derive constant amplitude fatigue crack growth data in cases where data were lacking. Figure 25 illustrates the collected data for one of the relevant aluminium alloys.

Additional recent work has shown the wing attachment frame to be fail safe. This was shown by considering the additional dynamic loading transferred to the remaining structure when one of the four aluminium parts fail completely.

### 5.3.2 Verification of Stresses and Crack Growth Prediction Technique

The FE stress analyses were verified by comparisons to experimental results obtained during the traditional static and fatigue testings of the components considered. The comparisons showed that stresses, in general, were computed very accurately even with the global models. Unfortunately, stresses really close to attachment holes could not be assessed due to lack of experimental data.

The technique of modifying 3D stress intensity factors, using 2D weight functions, was verified by comparing such stress intensity factor solutions to solutions obtained using the adaptive FE-technique for a number of typical geometries.

The computer programme used for the crack growth predictions, Ref. (27) was verified as far as possible by comparisons to other computer programmes and also to experimental results (on a coupon specimen level with well-known stress intensity factor solutions) from the literature as well as from test results (on a coupon specimen level) obtained in the current investigation. These comparisons involved both constant amplitude results and results from different types of spectrum loading.

## 6. STRUCTURAL TESTING

Here, we will discuss the testing carried out to substantiate the analytical methodologies used. Such tests include simple coupon tests to study influence of load spectrum truncation etc., component tests to verify numerical predictions and to reveal any unexpected problems, and full scale fatigue and damage tolerance testing of an entire aircraft. The overall test programme for the new fighter aircraft goes on for more than 10 years.

### 6.1 The Saab JAS39 Gripen aircraft

#### 6.1.1 Artificial flaws

In order to monitor the making of artificial flaws on the critical parts to be subjected to verification testing in the JAS39 programme, a manufacturing and quality control specification document was produced. In that document the electro spark method using carbon electrodes is specified as the main method. The specification defines tolerances on the flaw geometry itself as well as its location. The specification also defines machining data such as current and pulse length for electro spark machining or amount of feed between each stroke for the chipping method. Examples of the flaw geometry specifications are shown in Fig. 26. Consider the quarter circular flaw having  $a = 1.27$  mm as per Mil-A-83444. In the Saab manufacturing specification this has been assigned a tolerance  $1.3 < a < 1.5$  mm and a tip radius  $\leq 0.05$  mm. The depth tolerance seldom has been a problem. In cases when the depth has come out below the tolerance,  $a < 1.3$ , the detail has always

been sent back to the workshop to make the flaw deeper. The tip radius was expected to come out between 0.02 and 0.04 mm during electro spark machining. Most of the time, however, the tip radius has come out between 0.04 and 0.05 mm, i.e. very close to the maximum tolerance, and in quite a number of cases it has been necessary to accept tip radii exceeding 0.05 mm (but never exceeding 0.065). Artificial flaws made by chipping have always come out well within the tolerance limits.

An example from a large test programme on unnotched specimens is shown in Fig. 27 for an aluminium specimen subjected to a symmetric fin root spectrum. Here, the crack growth rate first started up at a higher than normal rate and then slowed down to a more normal rate. This can be interpreted as if the artificial flaw is characterised by a negative initiation period. Special attention was paid to artificial flaws on shot-peened surfaces since delayed initiation could be expected. Observed initiation periods for those cases have varied from 800 to 1800 hours for specimens showing a total life of 5000 to 7000 hours. The crack propagation part of the total life has always been larger than the initiation period for all tested stress levels. This is a most important conclusion since it supports the selected principle of verification of the slow crack growth - non inspectable parts even if no identification of crack growth could be detected at artificial flaws in large components at two service lives of fatigue testing. This has also been shown for a most unfavourable crack/geometry case with rapid crack growth rate.

#### 6.1.2 Test programme

The damage tolerance analysis creates the necessary conditions for structural integrity. This integrity also needs to be demonstrated in structural testing according to the sizing approach shown in Fig. 1. Besides from testing for obtaining data for predictions, three main levels of testing are detail testing, major component testing and final full scale verification testing. These three levels are described below.

Detail testing is mainly performed early in the sizing work. It is used to verify detail design of vital structural members and to qualify the application of prediction methods to typical structural configurations. The lower flange region of the main wing attachment frames were studied in that way. Six different crack/geometry configurations were tested according to Fig. 10.

The slow crack growth damage tolerance requirement is applied to all flight safety critical components - even small size units such as tension bolts, hinge bolts for the control surface attachments, control actuators and other small details of the control system. Primary bolts are verified to tolerate semicircular surface flaws with 1.3 (+0.2/-0) mm radius. The verification testing of the tension bolts for the wing and fin attachments have proven very satisfactory damage tolerance.

Major component testing is done for early fatigue and damage tolerance verification. The key point in these tests is that a critical part is tested while properly installed in its nearest boundary structure. This test will spot fatigue critical areas and demonstrate the stable growth of those natural cracks that may initiate and of any artificially made cracks. As an example a test set-up for an attachment of wing to fuselage is shown in Fig. 28. The lower flange region, described above, is here installed in its nearest boundary structure.

Damage tolerance testing of large components involve very many initial flaws, for the rear fuselage tested together with fin and rudder more than 100 flaws were introduced.

The final verification of the fatigue and damage tolerance performance is made with a complete airframe tested for several service lives. A photograph of the static test article is shown in Fig. 29. The test arrangement consisted of 85 independently controlled load channels. A second airframe for fatigue and damage tolerance testing is now installed in the same rig and testing will be started very soon and be subjected to at least four service lives of fatigue testing.

The test program for structural verification of the JAS39 aircraft is shown in Fig. 30 (tests of systems not shown). Component tests for verification of both fatigue and damage tolerance are first subjected to two service lives of fatigue testing, then artificial flaws are introduced, whereafter the test is subjected to a further 2 service lives of fatigue testing. Finally, a residual strength test is carried out with the purpose to verify a load capacity in excess of 120% 1.L. The pure damage tolerance verification tests are performed with artificial flaws introduced from the very beginning and are subjected to two lifetimes of fatigue testing followed by the residual strength test.

Before deliveries of aircraft to the Swedish Air Force, a full scale static test will be performed (this is already completed) and a full scale fatigue test must have simulated one design life. A schematic overview of the entire fatigue and damage tolerance activities for the JAS39 Gripen aircraft, as described above, is shown in Fig. 31.

## 6.2 The Saab 37 Viggen aircraft

### 6.2.1 Structural Testing

As already mentioned, an activity is carried out with the purpose of achieving life extension of this aircraft. For that purpose a complete damage tolerance test programme, similar to the one mentioned above for the Gripen fighter, is currently being performed. Here, the aim is only to show differences in the methodologies used, resulting from the higher stress levels involved for the Viggen aircraft. This is described for the main wing attachment frame assemblage. Due to relatively large displacements (wing root bending moments of up to 520 kNm were applied) the effective test frequency became around 0.2 Hz (testing was conducted at a constant displacement rate). The actual frame tested had already been subjected to four fatigue lives of spectrum loading during the traditional testing to support the original safe life design of 2800 flight hours. No fatigue cracks were reported after the traditional testing. In the present investigation another four fatigue lives were applied subsequent to introduction of defects in the frame. A total of 22 artificial flaws (crack tip radius < 0.02 mm) were introduced by sawing in critical locations of the frame.

The locations chosen for saw cuts were selected based on the FE results, a strain survey using a brittle coating technique, crack growth predictions and inspection considerations. Very good agreement was found between the brittle coating results and the global finite element analysis with respect to both critical locations and magnitudes of the strain field.

Crack growth was monitored both visually and by means of various NDI-techniques, primarily eddy current. Firstly, cracks started to grow from defects introduced at the two fuel pipe holes. This growth was easily observed visually.

and was therefore very useful in verifying the analytical crack growth predictions. A comparison of predicted and experimentally observed crack growth at the upper fuel pipe hole is shown in Fig. 32. Later on, after approximately 12500 simulated flight hours, this crack together with a crack at the lower fuel pipe hole resulted in final failure of the frame.

After some 4000 simulated flight hours, crack growth was observed at one of the wing bolt holes. This is, according to numerical predictions, one of the most critical locations in the frame. However, the predictions for this location are assumed to be overly conservative as friction between the interference fitted bushing and the frame forging was disregarded. Furthermore, it is believed that the interference fitted bushing in the wing bolt hole restrains the crack mouth opening and thereby reduces the effective stress intensity factor range. This would explain the unexpectedly slow crack growth observed at this location.

#### 6.2.2 Inspection Intervals

Based primarily upon crack growth predictions but with due consideration to component testing results and also results concerning the prediction capability (accuracy for various structural details) of the computer programme used, safe periods of crack growth have been established. Inspection intervals have been determined, assuming that the critical locations are depot or base level inspectable. The inspection intervals are then half of the safe crack growth periods. Fig. 33 shows inspection intervals for the JA main wing attachment frame.

### 7. COMPOSITE MATERIALS

An overview of work done in the U.S.A. and recommended certification procedures are summarised for composite structures in Ref. (28). This reference states that draft USAF damage tolerance design requirements for composites are conceptually equivalent to MIL-A-87221. Recognition to the unique property characteristics of composites leads to significantly different defect damage assumptions for composites as compared to metals. Of the assumed flaw/damage types, scratches, delamination and impact damage, the last one dominates design as it is the most severe. The recommended compliance to the draft requirements is summarised in Ref. (28) to allow no significant damage growth in two design lives. This is due to rapid unstable growth after growth initiation. This requirement eliminates in-service inspections. Finally, no full-scale test validation is required as subcomponent test are considered to accurately represent damage tolerance behaviour of full-scale structures.

For the new Swedish fighter JAS 39 Gripen a certification procedure similar to the one mentioned above is being used for the composite structures (wing skins and spars, elevons, leading edge flaps, canards, air inlets, fin and rudder and air brakes). All CRTP-laminate structures were verified by static testing before the first flight. The structures were tested dry, as received from manufacturing. Smaller components such as elevons and rudder were tested at high (+85°C) as well as low (-40°C) temperature besides at room temperature. The wing, the fin and the canard were tested at room temperature besides at room temperature. The wing, the fin and the canard were tested at room temperature only. As all verification testing was done with dry laminates, the requirement was increased to 1.2 times 150%=180% limit load. Subsequently, all those structures

have also passed four design lives of fatigue testing without any fatigue damage.

### 8. DISCUSSION AND CONCLUSIONS

Current development trends concerning loads activities is to incorporate data from more flight systems, influenced by flight conditions, e.g. the gearbox etc, into the global sequence description. Other improvements of the global spectrum approach will be to early verify the mission analysis by a closer connection to the flight simulator. By letting different pilots solve a certain flight task, the variability in manoeuvres can be evaluated early in the project.

Current trends regarding structural analysis is to create more detailed models of vital structures and to incorporate those into the global finite element model as substructures. Special facilities have been implemented into the loads sequence handling system for identification of the most significant load cases. Much more detailed models are being assessed by a parametric approach early on in the analysis phase, to account for the fact that certain dimensions are determined very early and are difficult to modify later on.

Regarding crack growth modelling, retardation has yet not been used for certification purposes. However, recent advances will be utilised for the C-version of the JAS39 Gripen aircraft, to decide which old tests can still be used for the new design.

Other areas which will be studied in more detail within the next few years include: crack growth in mechanical joints, multiaxial loading, constraint effects in three dimensional crack growth, and probabilistic aspects of damage tolerance and the entire structural design methodology.

Structural design of military airframes is driven by damage tolerance requirements. Durability, mostly assessed in terms of conventional fatigue, is achieved by proper inspection procedures, repairs and/or replacements. Structural integrity can only be achieved by detailed knowledge of flight profiles and resulting load spectra, stress distributions and material properties.

The methodology currently used in Sweden for fatigue management and verification of airframes has been described. Models used for assessment of fatigue life and damage tolerance of our fighter aircraft vary from rather simple to highly complex depending on various factors. Typically, simple models are used initially and more sophisticated analysis is resorted to in complex geometries and when safety margins are lower.

Analyses must always be complemented by testing, from coupon specimen level up to full-scale testing. Fatigue management and verification also involve service load monitoring regarding both dedicated test aircraft, used to verify basic load assumptions, and also individual load tracking programmes developed for new fighters.

## REFERENCES

- 1 U.S. Air Force Military Standard, MIL-STD-1530A(11), Aircraft Structural Integrity Program, Airplane Requirements, December 1975.
- 2 Military Specification MIL-A-008860A(USAF), Airplane Strength and Rigidity, General Specification For, March 1971.
- 3 Military Specification MIL-A-008861A(USAF), Airplane Strength and Rigidity, Flight Loads, March 1971.
- 4 Military Specification MIL-A-008862A(USAF), Airplane Strength and Rigidity, Landing and Ground Handling Loads, March 1971.
- 5 Military Specification MIL-A-008865A(USAF), Airplane Strength and Rigidity, Miscellaneous Loads, March 1971.
- 6 Military Specification MIL-A-008866A(USAF), Airplane Strength and Rigidity, Repeated Loads and Fatigue, August 1975.
- 7 Military Specification MIL-A-008867A(USAF), Airplane Strength and Rigidity, Ground Tests, August 1975.
- 8 Military Specification MIL-A-008870A(USAF), Airplane Strength and Rigidity, Flutter, Divergence and Other Aeroelastic Instabilities, March 1971.
- 9 Military Specification MIL-A-83444 (USAF), Airplane Damage Tolerance Requirements, July 1974.
- 10 Swift, T.: "Verification of methods for damage tolerance - evaluation of aircraft structures to FAA requirements", in Proc. of the 12th ICAF Symposium, Centre d'Essais Aéronautique de Toulouse, France, 1983.
- 11 U.S. Air Force Military Standard, MIL-STD 1783, Engine Structural Integrity Program (ENSIP), 1984.
- 12 Cowie, W.D.: U.S. "Air Force Engine Structural Integrity Program (ENSIP) Status", in AGARD/SMP Review: Damage Tolerance for Engine Structures, Vol. 4, in press.
- 13 Cowie, W.D.: "Fracture Control Philosophy", Metals Handbook, Vol.17, Sept.1989.
- 14 Lincoln, J.W.: "Damage Tolerance of Helicopters", Proc. 15th ICAF Symposium, Jerusalem, Israel, 1989.
- 15 Manning, S.D., Yang, J.N. and Rudd, J.L.: "Durability of aircraft structures", in Probabilistic Fracture Mechanics and Reliability, Ed J.W. Provan, Martinus Nijhoff Publishers, Dordrecht, The Netherlands, 1987, pp.213-267.
- 16 U.S. Air Force Military Standard, MIL-STD 1530A, Aircraft Structural Integrity Program, 1975.
- 17 Jarfall, L.: "Fatigue and Damage Tolerance Analysis in the Aircraft Design Process", in Durability and Damage Tolerance in Aircraft Design, Eds. A Salvetti and G.Cavallini, EMAS Ltd, Warley, U.K., 1985, pp. 1-31.
- 18 Jarfall, L., "Verification of Loads, Fatigue Performance and Damage Tolerance of the JAS 39 Gripen", in Aeronautical Fatigue in the Electronic Era, Ed., A. Berkovits, EMAS Ltd., Warley, U.K., 1989, pp. 103-120.
- 19 Ansell, H., "Computer Aided Fatigue and Damage Tolerance Sizing", in proc. 17th ICAS Congress, Stockholm, Sweden, 1990, pp. 693-701.
- 20 Jarfall, L., "Verification of the Damage Tolerance of a Fighter Aircraft, in Fatigue of Aircraft Materials, Eds A. Beukers et al, Delft University Press, 1992, pp 333-349.
- 21 Ansell, H. and Johansson, T., "Design Parameters and Variability in the Aircraft Sizing Process - Aspects of Damage Tolerance, in Durability and Structural Reliability of Airframes, Ed. A.F. Blom, EMAS Ltd, Warley, U.K., in press.
- 22 Palmberg, B., Olsson, M.-O., Boman, P.-O. and Blom, A.F., "Damage Tolerance Analysis and Testing of the Fighter Aircraft 37 Viggen", in Proc. 17th ICAS Congress, International Council of the Aeronautical Sciences, AIAA, Washington, D.C., U.S.A., 1990, pp. 909-917.
- 23 Palmberg, B., Olsson, M.-O., Boman, P.-O. and Blom, A.F., "Damage Tolerance Assessment of the Fighter Aircraft 37 Viggen Main Wing Attachment", J. of Aircraft, pp. 377-381, 1993.
- 24 Blom, A.F. "Modelling of Fatigue Crack Growth", in Advances in Fatigue Science and Technology, Eds C.Moura Branco and L. Guerra Rosa, NATO Advanced Study Institutes, Series E, Vol.159, Kluwer Academic Publishers, Dordrecht, The Netherlands, 1989, pp.77-110.
- 25 Dill, H.D. and Saff, E.R.: "Effects of Fighter Attack Spectrum on Crack Growth", Performed by McDonnell Douglas Corporation for Air Force Flight Dynamics Laboratory, Wright-Patterson Air Force Base, Ohio, U.S.A., Report AFFDL-TR-76-112, 1977.
- 26 Andersson, B., Falk, U., Babuska, I., "Accurate and Reliable Determination of Edge and Vertex Stress Intensity Factors in Three-Dimensional Elastomechanics", in Proc. 17th ICAS Congress, International Council of the Aeronautical Sciences, AIAA, Washington, D.C., U.S.A., 1990, pp. 1740-1746.
- 27 Palmberg, B. "LIFE Crack Growth Prediction and Evaluation Program LIFE Version VAX APOLLON 04" The Aeronautical Research Institute of Sweden, Bromma, FFAP-H-1000, March 1989.
- 28 Whitehead, R.S. "Certification of Primary Composite Aircraft Structures", in Proc. 14th ICAS Symposium, Ed. D.L. Simpson, EMAS Ltd., Warley, U.K., 1987, pp. 585-617.

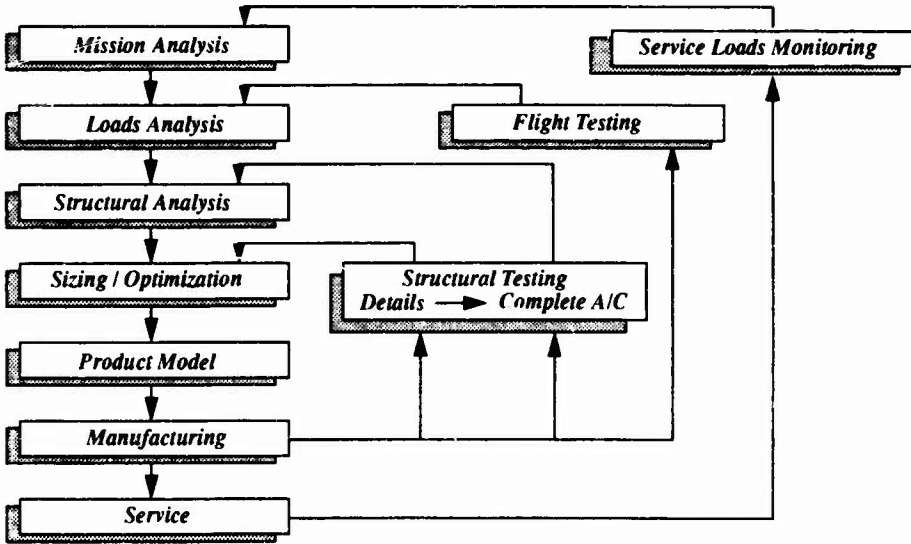


Figure 1 Block scheme of conceptual model for JAS39 Gripen aircraft

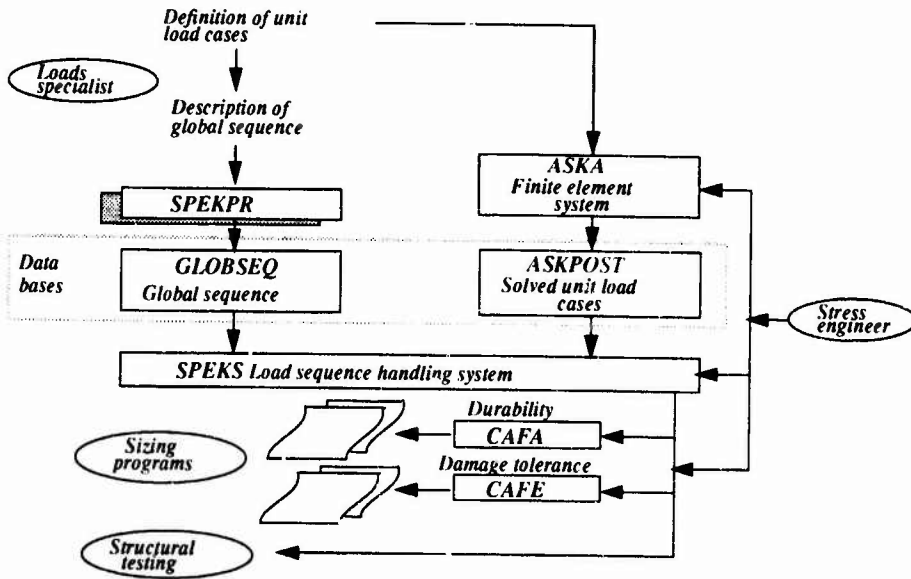


Figure 2 Computer programmes used in the sizing system

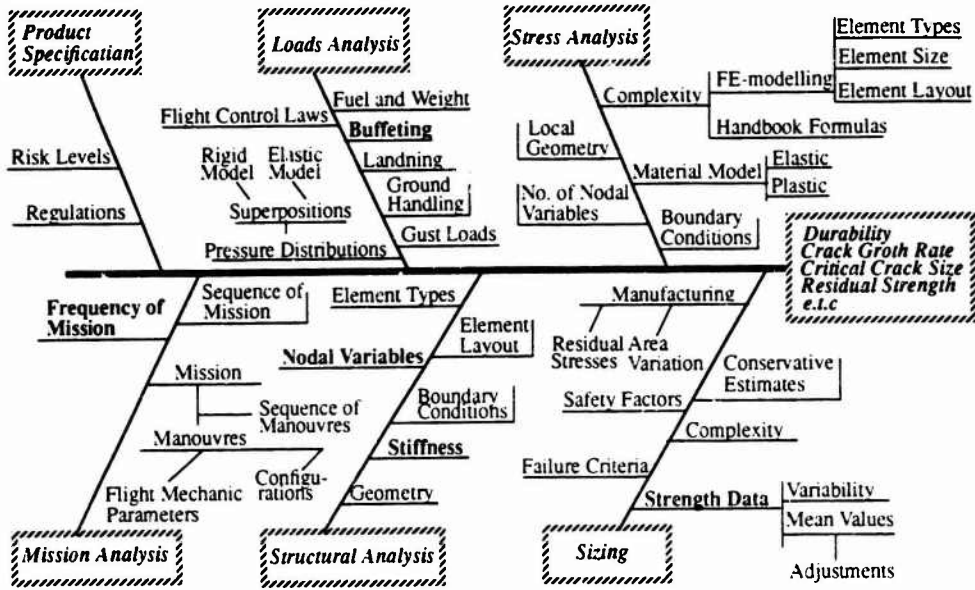


Figure 3 Model parameters and response variables in the design stage

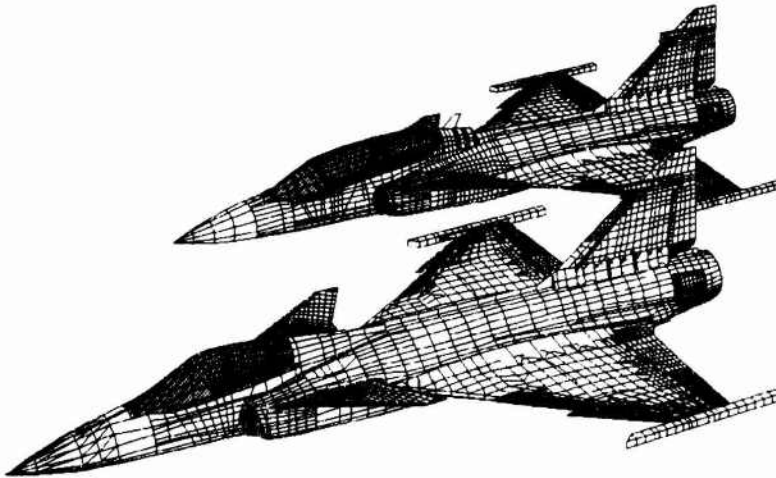


Figure 4 Structural models of the single and twin seated version of the JAS39 Gripen aircraft

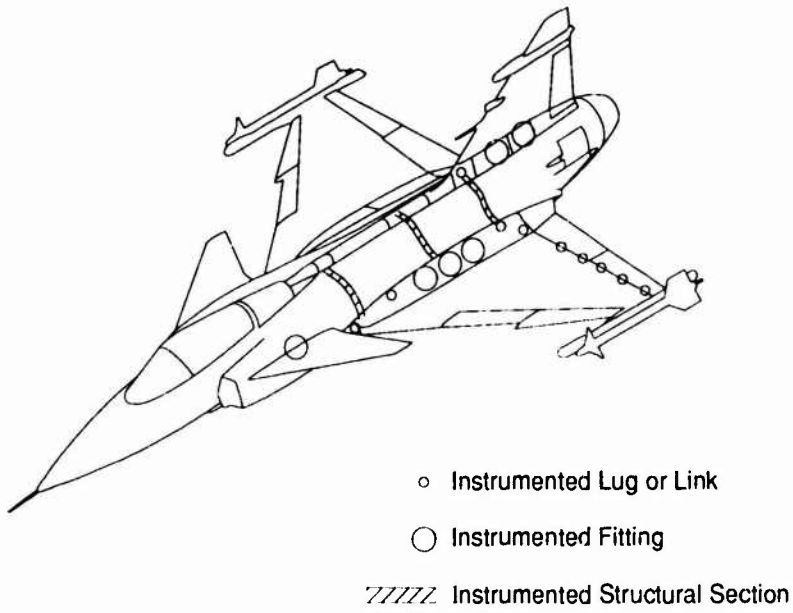


Figure 5 Calibrated regions of the loads survey test aircraft

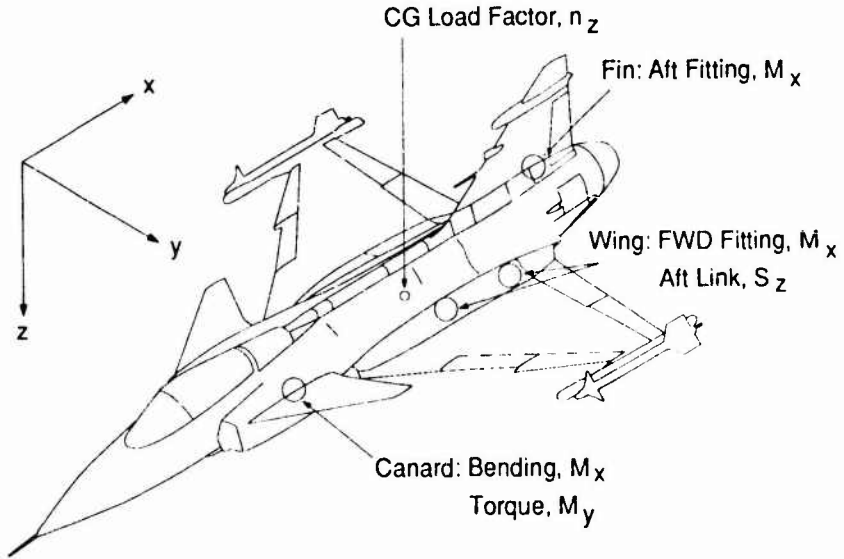


Figure 6 Service loads monitoring on each aircraft

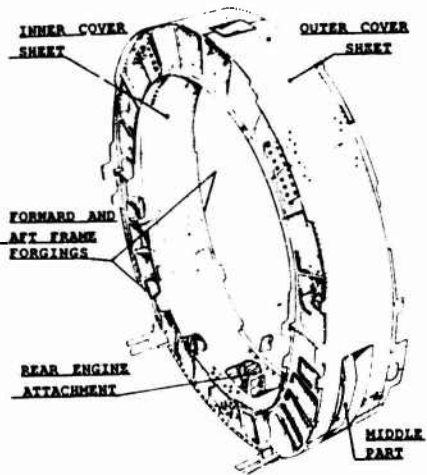


Figure 7 JA37 Viggen main wing attachment frame assemblage

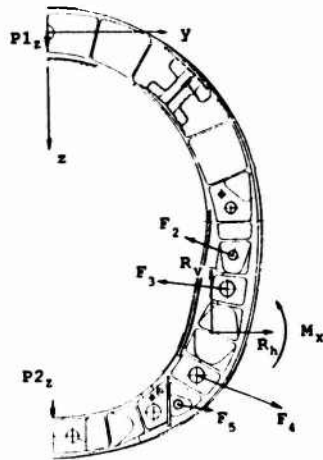


Figure 8 Schematic showing the loads applied

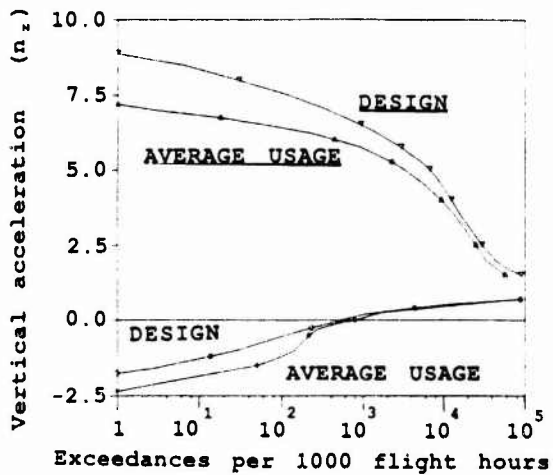
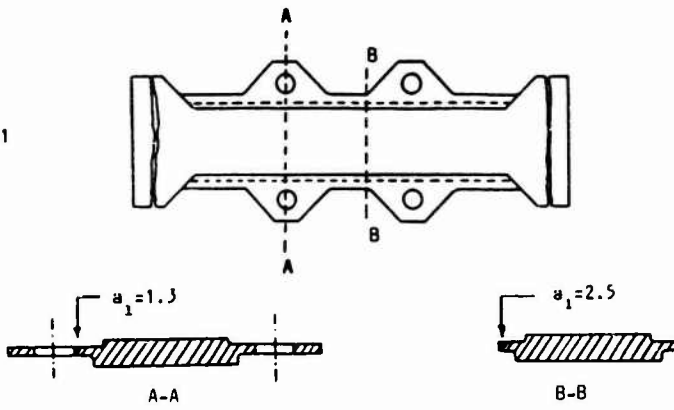
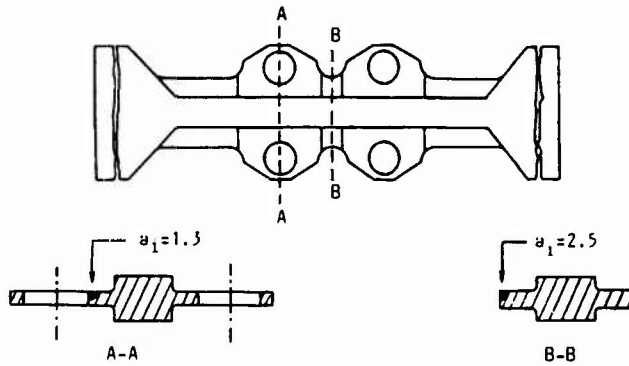


Figure 9 Comparison between design spectrum and in-flight recorded spectrum for the average JA37 Viggen aircraft

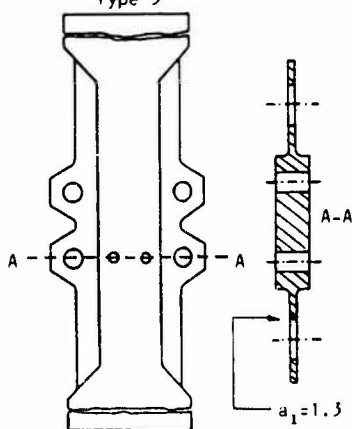
Type 1



Type 2



Type 3



Type 4

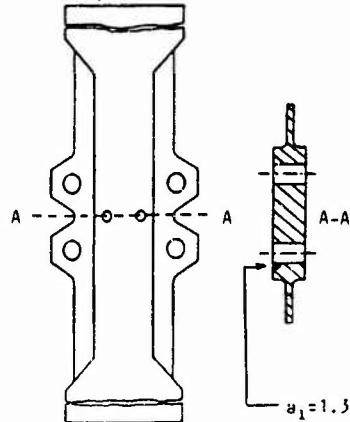


Figure 10 Different crack/geometry configurations of the JAS39 lower flange region of the main wing attachment frames

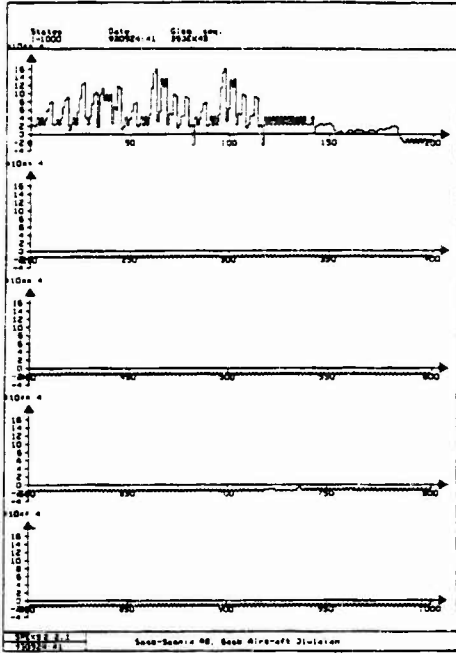


Fig. 11 Part of the unreduced local flange force sequence

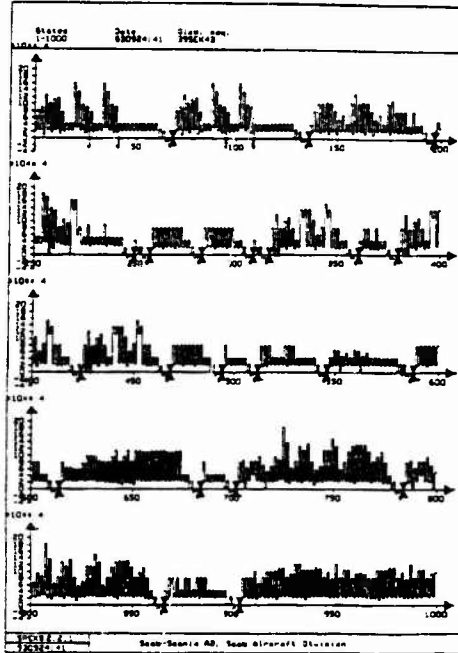


Fig. 12 Part of the reduced local flange force sequence. Triangular marks show where each mission ends

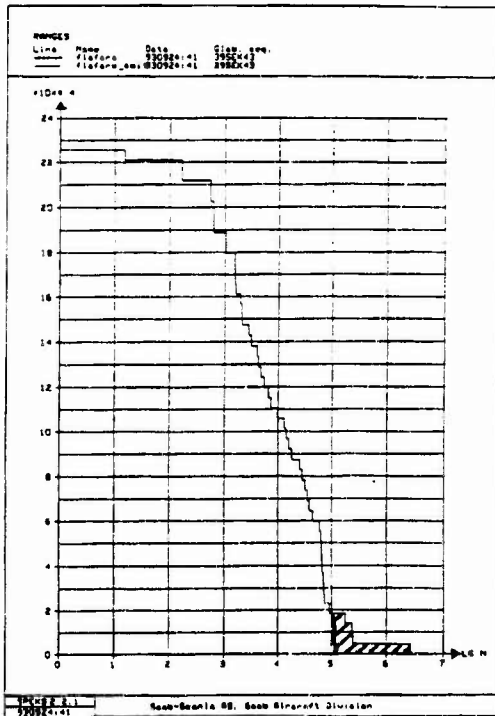


Figure 13 Distributions of ranges for original and reduced sequences

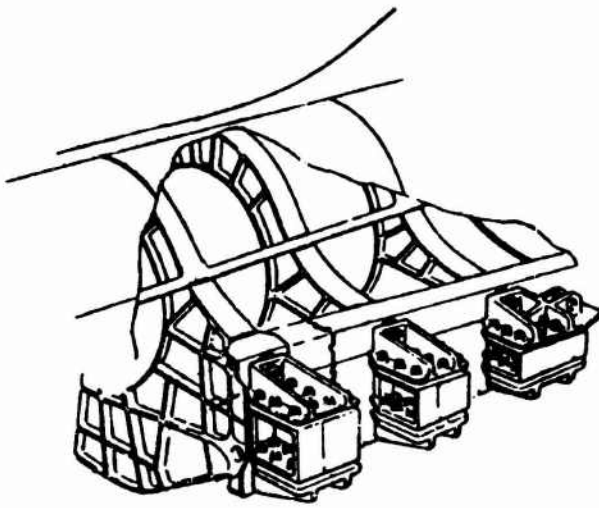


Figure 14 Main wing attachment frames of the JAS39 Gripen aircraft. The frames are machined die forgings of aluminium 7010 alloy. The wings are attached to the frames with steel bath-tub fittings

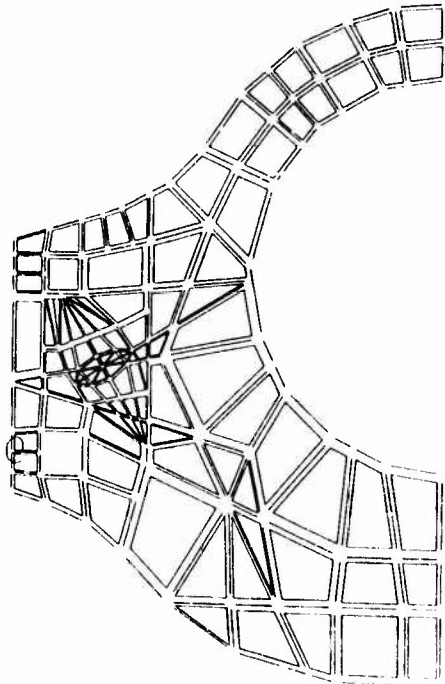


Figure 15 Finite element substructure of wing attachment frame

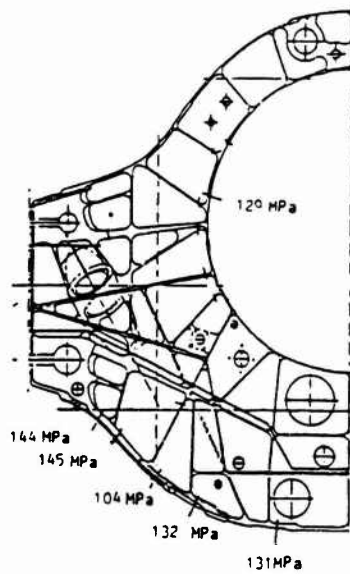


Figure 16 Stresses at lower flanges due to limit load

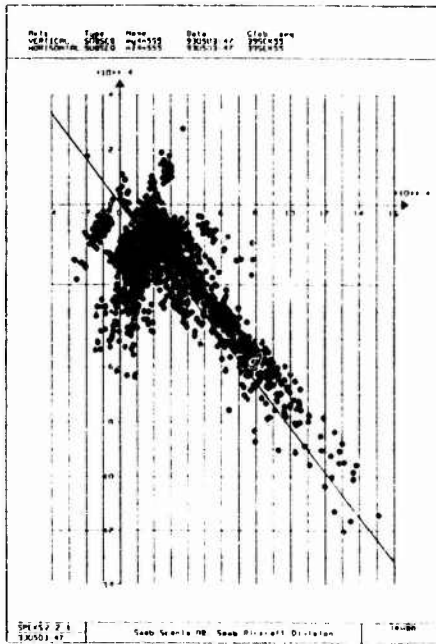


Fig. 17 Correlation between bending moment  $M_y$  and normal force  $P_z$  in lower flange section

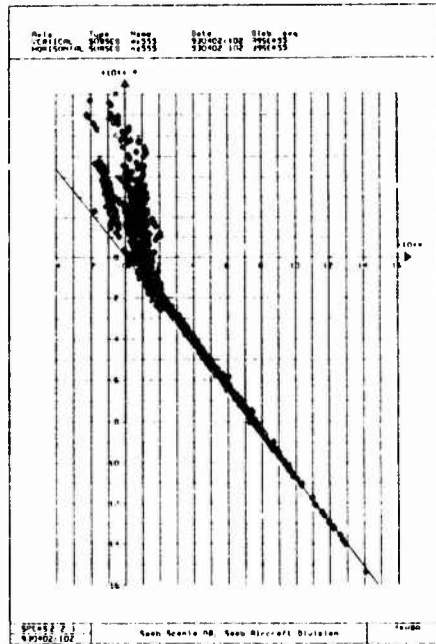


Fig. 18 Correlation between bending moment  $M_x$  and normal force  $P_z$  in lower flange section

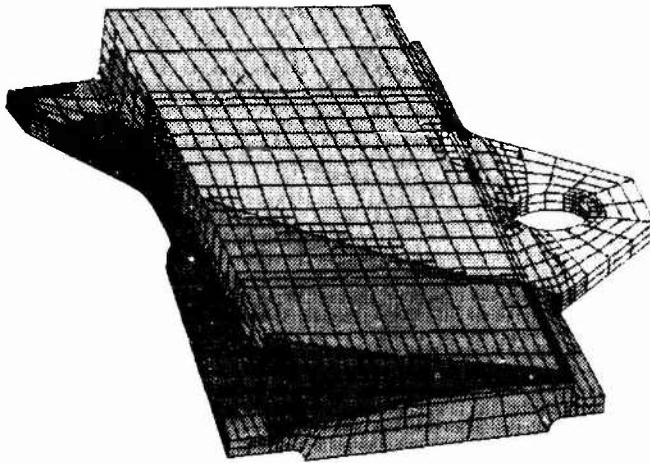


Figure 19 p-version FE model of lower flange region

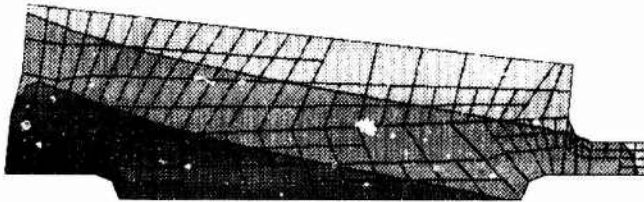


Figure 20 Stress distribution across a highly stressed region of the lower flange

### JAS39 Damage Tolerance Review Sheet

<b>Category</b> Slow crack growth - Non inspectable	<b>Analysis code No</b> 2.2.1 C <b>Drawing No</b> 1903152-001, 1903154-131
<b>Inspection free Interval</b> One service life	<b>Material</b> Al 3644-74 die forging
<b>Special inspection requirements</b> No	<b>Description</b> Rear fuselage Wing attachment frame X <sub>85</sub> 10250 Lower flange
<b>Limit load case</b> <b>Limit load stress</b>	LC 349 AP05 111.1 MPa, ref. a/c 39.157.02.5 s2.9
<b>Spectrum</b> <b>Max spectrum peak stress</b>	Glob. seq. 39SEK55, loc. spec. SA157009, ref. a/c 39.157.02.5 s2.10 108.4 MPa, ref. a/c 39.157.02.5 s2.9
<b>Fracture toughness data</b>	$K_{Ic} = 1450 \text{ N/mm}^{3/2}$ at $t = 4 \text{ mm}$ , ( $K_{Ic} = 900 \text{ N/mm}^{3/2}$ )
<b>Crack growth data</b>	SD 37-3644 page 3. (forging, TL-orient.)
<b>Crack growth model</b>	Non interacting
<b>Stress intensity factor model</b>	
<b>Initial crack shape and size</b>	Quarter-circular corner crack, $a = 2.54 \text{ mm}$
<b>Critical crack at 150% LL shape and size</b>	Through-the-thickness crack, $a = 17.5 \text{ mm}$
<b>Critical crack at 120% LL shape and size</b>	Through-the-thickness crack $a = 19.8 \text{ mm}$
<b>Crack growth period</b>	57039 fh
<b>Applicable testing</b>	Test No: 5.1.7.3 Wing to fuselage attachment Test No: 5.1.18 Lower flanges in wing attachment frames

Figure 21 JAS39 Gripen damage tolerance review sheet

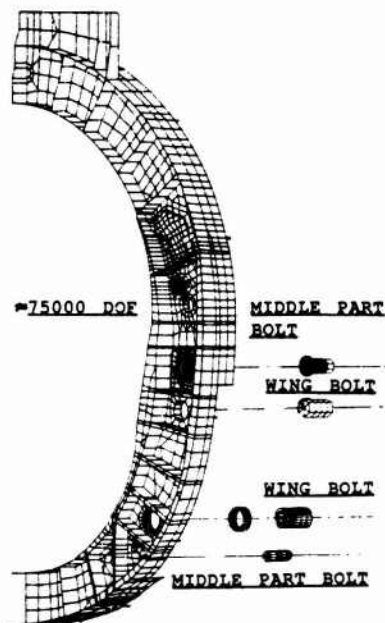
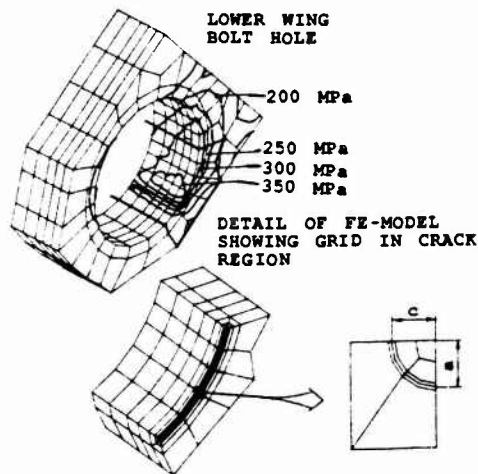


Fig. 22 FE model of the JA37 main wing attachment



STRIP RESULTS, UNIFORM  $p=6$

a (mm)	c (mm)	$K_{Ia}$ (MPa $\sqrt{\text{mm}}$ )	$K_{Ic}$ (MPa $\sqrt{\text{mm}}$ )
1.3	1.3	472.8	572.5
1.3	1.6	514.6	602.9
2.0	2.6	621.9	749.2
2.0	3.0	647.4	778.8

Fig. 24  $K_I$  determination using p-version FEM

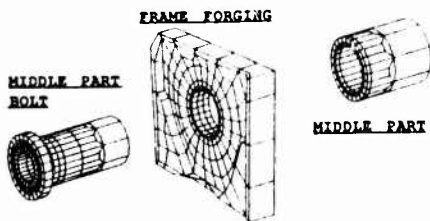


Fig. 23 FE model of the middle part bolt, including the bolt head, a region of the frame forging, and a portion of the middle part

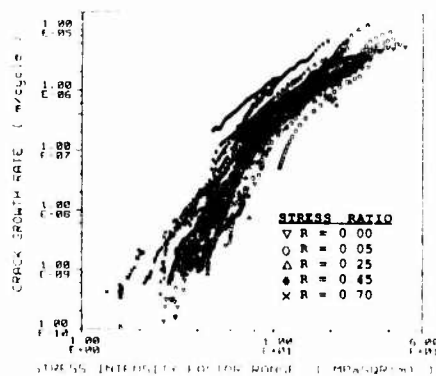


Fig. 25  $F_{cg}$ -data for 7075 Al-alloy

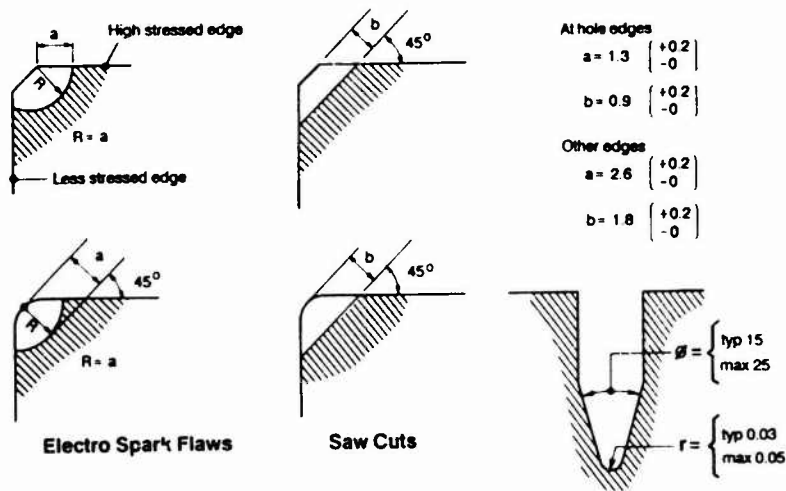


Figure 26 Geometry specifications for artificial flaws

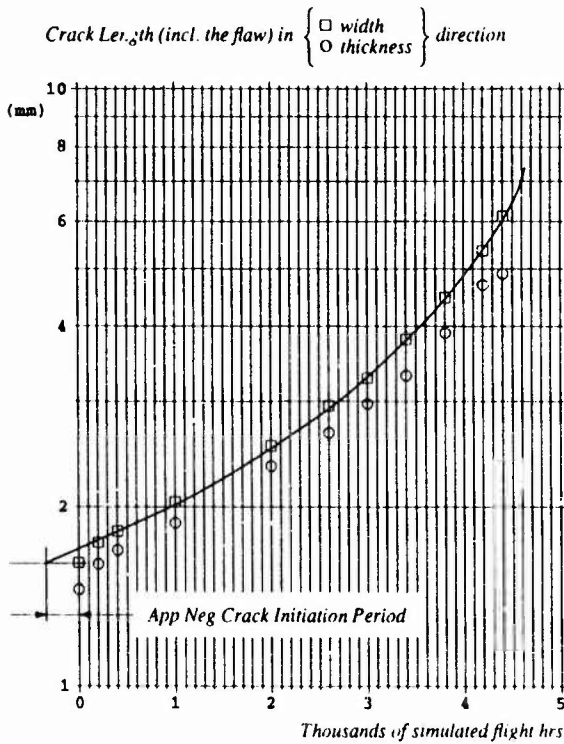


Figure 27 Apparent negative initiation period from an artificial flaw (no shot peening)

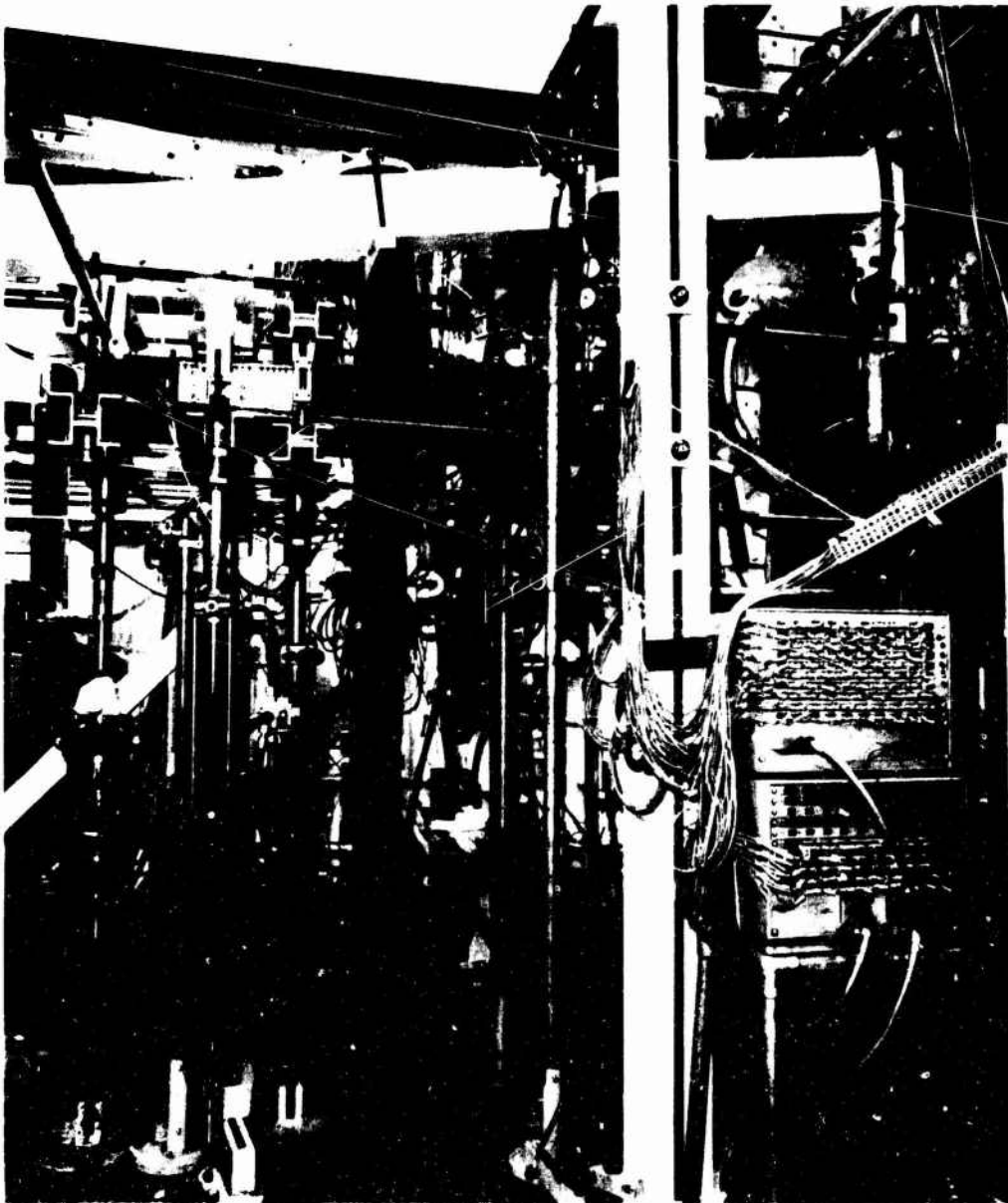


Figure 28 JAS39 Gripen test set up for attachment of wing to fuselage

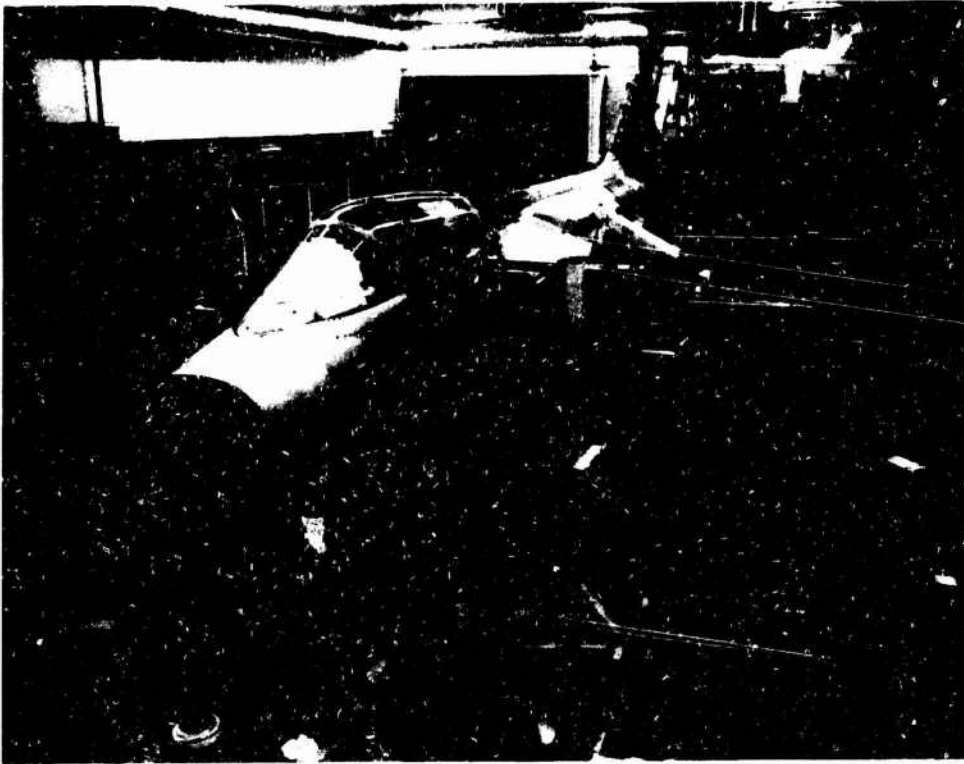


Figure 29 JAS39 Gripen full scale static test. Fatigue testing will be performed in the same rig

# JAS 39 GRIPEN: STRUCTURAL VERIFICATION TESTING

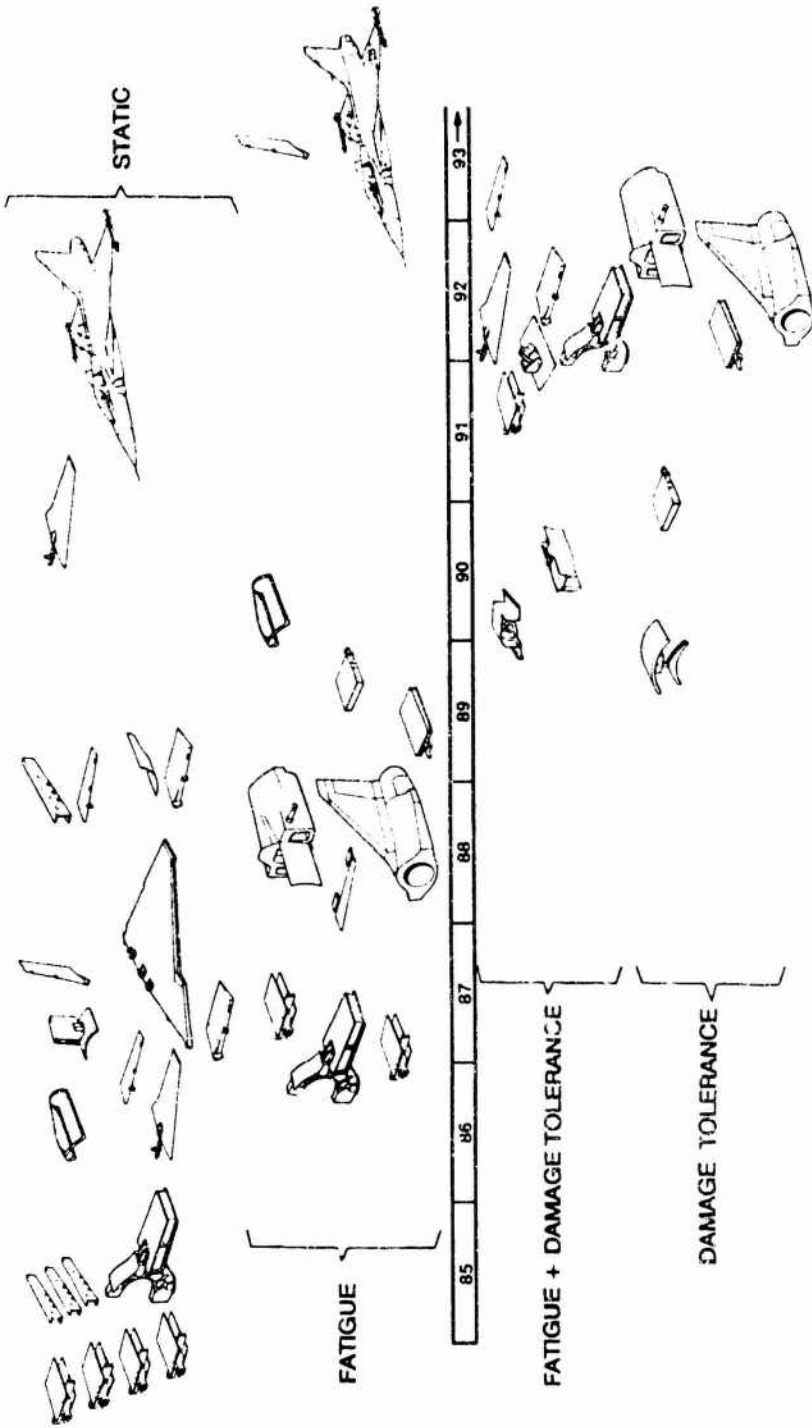


Figure 30 Test program for structural verification of JAS39 Gripen

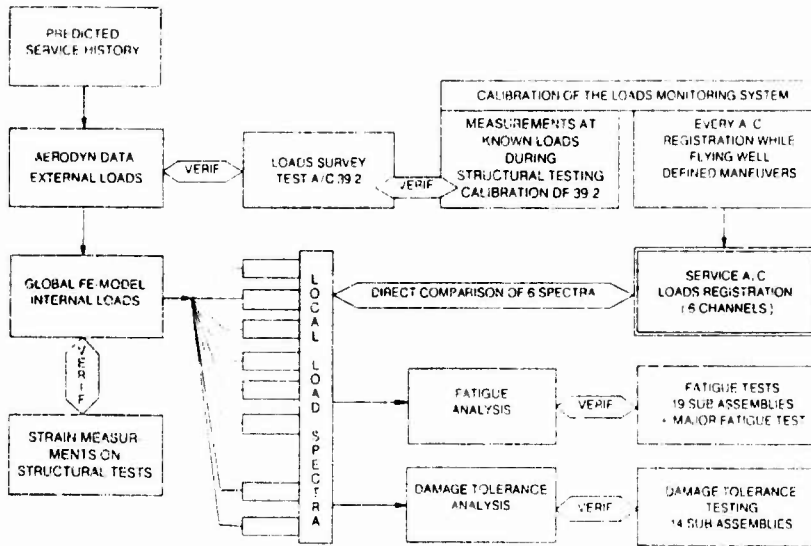


Figure 31 JAS39 Gripen structural life assurance

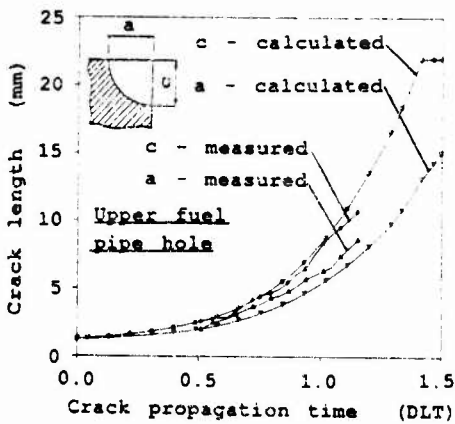


Fig. 32 Comparison between predicted and measured crack size in JA37 main wing attachment as function of design life time (DLT)

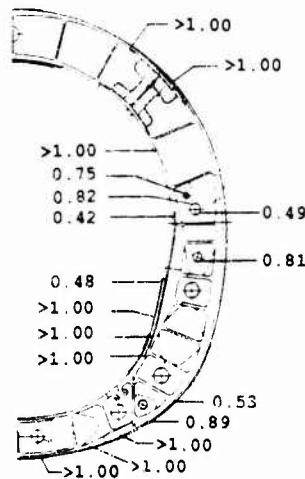


Fig. 33 Suggested inspection intervals in DLT for JA37 main wing attachment to ensure structural safety according to damage tolerance requirements for slow crack growth structures

## RISK ANALYSIS OF THE C-141 WS405 INNER-TO-OUTER WING JOINT

1991 USAF Structural Integrity Program Conference  
 San Antonio, Texas  
 2-5 December 1991

by

**R.E. Alford, R.P. Bell, J.B. Cochran and D.O. Hammond**  
 Lockheed Aeronautical Systems Co.  
 Georgia Department 73-25  
 Zone 0160  
 86, S.Cab. Drive  
 Marietta, G. 3006  
 United States

### INTRODUCTION

It is evident that weapon system management benefits greatly from the use of probabilistic risk assessment methods. The C-141 WS 405 inner-to-outer wing joint provides an actual case of how this technology was implemented by Lockheed and USAF engineers to determine conditions of inspection and repair for the C-141 fleet.

longer under more severe conditions, the current tools of structural analysis must go beyond the specifics of strength, durability, and fracture mechanics and into the realm of probabilities, i.e. risk assessment.

### BACKGROUND

The C-141 aircraft was delivered to and deployed by the Air Force during the 1960's. Constructed mostly of 7075-T6 aluminum alloy, the C-141 was designed to provide 30,000 flight hours of service. Currently, however, the force is averaging over 34,000 flight hours. In the 1970's the C-141 was stretched and given refueling capability, and it was this model, the C-141B, that rapidly became the workhorse of MAC. Today it is reasonable to expect the C-141 to provide reliable airlift well into the 21st century. Consequently, since the C-141 and other weapons systems are being called upon to last

### WING STATION 405 JOINT

The C-141 WS 405 wing joint connects the outer wing to the inner wing. This structure has met design goals of 30,000 flight hours, but it is rapidly deteriorating as aircraft usage continues to accumulate. The structural assessment explained herein was performed using standard risk analysis programs adapted to address the wing joint problem. In the 1980's fatigue cracking manifested itself in the WS 405 joint, and it was at this time that inspections, redesigns, and repairs were engineered. However, by 1989 generalized cracking was prevalent throughout the fleet elevating the WS 405 joint issue to one of safety. It was this concern for safety that prompted the risk assessment of the joint.

**RISK ANALYSIS METHODOLOGY**

The following resources and information are required to perform a structural risk analysis. Field inspection results are necessary to determine the initial cracking data from which the analysis can proceed. In the case of the 405 joint this information was obtained mainly from directed bolt hole eddy current (BHED) and x-ray inspections. Inspected structure included the lower rear beam cap attachment to the tie down fitting and the front and rear beams of the wing joint region. Also, the fastener holes in the joint area were reworked and inspected by BHED. Multi-element and multi-site damage were both confirmed by these inspections. Furthermore, the data revealed that approximately 50% of the cracks found in the rear beam lower cap were in excess of the critical crack length. Another required resource for risk analysis is the crackgrowth data for the area of concern. These data are needed to reduce the actual fleet crack data to corresponding lengths for average force aircraft. Flaw distribution data is also required to generate the strength data for the components being analyzed. To determine the distribution of bolt loads and stresses of the various components, a non-linear finite element model analysis of the WS 405 joint area was performed. Finally, load exceedance data is needed to calculate the probability that an aircraft will sustain or exceed a given load.

**CRITERIA**

The objective of this procedure was to determine a method for evaluating the safety of the C-141 fleet during the force management program initiated because of the cracking problem. As previously discussed, risk analysis was the method selected. Moreover, the risk of failure was defined as the probability of the load exceeding the strength at a given point in time. The following failure criteria, as set forth during a C-5 SAB review, was adopted, "If a structural member fails, for whatever reason, then the risk of catastrophic failure on a single flight of no more than one in ten thousand is acceptable."

**BLANK DECISION TREE**

Early in the analysis it was necessary to establish a failure tree such as the one in figure 1. Although it is important that the tree reasonably simulates possible failure paths, it is not possible to include every detail. For example, three elements will require six possible failure combinations and four elements twenty-four combinations. Considering that it takes one day to run the finite element model (FEM), one day to reduce data to plots of bolt loads and stresses, and at least two days to generate the crackgrowth curves, it is evident that the failure modes must be simplified to every extent possible.

At this point the failure tree is only an estimate of what the final result will be based on the FEM data. Obviously, several iterations are required to finalize the tree. Field inspection results also play a large role in the failure tree construction. Figure 2 shows the critical components of the 405 joint represented by this failure tree. This outboard view of the region shows the beam caps, splice fitting, and chordwise joint. The decision tree of figure 1 represents only the rear beam area. A separate analysis was conducted on the front beam using the same methodology.

**EXAMPLE RISK CALCULATIONS**

Figure 3 presents an example of how risk calculations are performed on a single element. Assume, as the chart depicts, that there are a certain number of parts which contain cracks. For each crack size there is a strength which this member can sustain but will fail if exceeded. The chart designates these elements as S1 through S5. For each part there is an associated strength and percentage of the total number of parts at this strength level. For example, 30% of all the parts have a strength level of 50 KSI as indicated by the designation S4. Also shown are the probabilities that a load of a given magnitude will be applied to an element. If these loads, L1 through L4, are applied randomly to

all members the risk can be determined. From the chart it is clear that all the loads are greater than the strengths of the 5<sup>th</sup> of the parts designated S1. Therefore, the probability of failure of these parts is the probability that the load will occur times the number of elements or  $(1.00 \times 0.05)$ . Similarly, the 10<sup>th</sup> of the parts with strength S2 may incur loads L2, L3, or L4 which will result in failure of these parts, and hence their probability of failure is  $(L2+L3+L4) \times (S2)$  or 0.04. This process is carried out for every element, and the final failure probability is the sum of these values.

#### CRACK DATA and PROBABILITY OF DETECTION

A distribution of cracks determined by a TCTO inspection of the 405 joint is shown in figure 4. This inspection was performed along the aft tab of the rear beam cap concentrating on the area near the ground tie down fitting. Early in the analysis and prior to inspections, using a linear finite element model, this region had been cited as a possible failure area. This turned out to be a reasonable predictor of the actual facts. In figure 4 the critical crack length shown is for limit design load, and the cracks indicated above the line are therefore incapable of sustaining limit load stress. Consequently, these long cracks shed load to adjacent areas.

A further important component of risk assessment is the probability of detection of crack data. Prior to any analysis a probability of detection curve must be applied to the fleet crack data to account for the cracks not found during inspection. This analysis used the estimated probability of detection based on the "Have Cracks Will Travel" program. The risk analysis of the 405 joint was heavily dependent on this probability of detection data since development of a new curve would have been a cost intensive procedure.

#### WEIBULL, DISCRETE CRACKS, and STRENGTH DISTRIBUTIONS

Initial cracking data for the chordwise joint and splice fitting was simulated using a Weibull distribution. This statistical analysis method was chosen for its ability to predict future crack initiation from a small sample of actual data. However, log-normal data regression would also be acceptable and was used to predict beam cap crack initiation. Weibull plots display cumulative crack distributions adjusted to average flight hour values. From this distribution cracks can be generated and grown out to flight hours of interest.

Figure 5 shows a discrete crack frequency distribution generated from a Weibull distribution of the inspection data. Both the chordwise joint and splice fitting were simulated using a Weibull distribution, while the beam cap distribution was generated from a previously existing log-normal fit. The cap data was simply updated and used in this assessment. It turned out that after normalizing the crack data to average flight hour levels the fit to actual fleet data was excellent. Furthermore, data obtained subsequent to this analysis during current repair actions continues to match the predicted distribution. The data shown in figure 5 is for a single element at a single point in time. Distributions such as this one need to be generated for each element at each time for which the risk is to be calculated.

Each element in the analysis requires a strength distribution curve so that for a given crack length an resulting strength can be determined. A theoretical strength curve is shown in figure 6 using the approach of Fedderson. This method allows strength predictions for both the linear elastic range between approximately 80% of the yield strength out to 1/3 of the width and also for the areas outside of the linear elastic fracture mechanics range. Knowing the frequency distributions of crack lengths and the resulting strengths remaining in each element, a probabilistic strength distribution can be built.

**NON-LINEAR FINITE ELEMENT MODEL**

The non-linear finite element model was an essential component of the WS 405 wing joint risk analysis. A linear model would have been sufficient for bolt load calculations and normal slow crackgrowth stresses, but for severed parts a non-linear model was required. The 405 joint model consisted of 10,000 elements with each non-linear run taking approximately one day. The model was originally constructed to provide information on standard crackgrowth stresses, and it was later modified to generate non-linear data. However, by creating load versus stiffness curves for each bolt load and iterating run by run until sufficient accuracy was achieved, non-linear calculations were only required on about 250 bolts.

**CRACKGROWTH DATA**

Figure 7 shows three crackgrowth curves typical of the chordwise panel splices. From the failure tree there are three ways that the chordwise joint can fail, and these failure modes correspond to the three crackgrowth curves. As shown, it can fail with all structure intact, it can fail due to extra load carried because of a failed beam cap, and it can fail due to prior failure of both the beam cap and the major splice fitting. The crackgrowth data is also used to reduce the field inspection data to desired flight hour values. This is a necessary step since each aircraft is at a different flight hour value when an inspection is performed.

**LOADS CURVE**

Figure 8 shows a typical load exceedance curve from which probabilities are taken. The probability of incurring a specified stress level is calculated as  $1-e^{-N}$  with  $N$  being the number of occurrences. The stress level is plotted along the x axis with the probability of exceedance plotted along the y axis. Again, for every element in the failure tree a load exceedance curve must be generated.

**DECISION CHARTS**

The next two figures, 9 and 10, show typical results of the risk analysis discussed in this report. The numbers shown are not actual calculated values but merely serve as an illustration of the process. Figure 9 shows the probability of failure for an average aircraft at 33,400 flight hours. The second chart shows the resulting reduction in risk due to an x-ray inspection of the joint area. It is important to remember that the validity of the analysis depends on the accuracy of the probability of detection data. A primary value of these decision charts is that they clearly show which areas must be protected to ensure safety.

**SUMMARY**

The risk assessment of the C-141 WS 405 wing joint has provided valuable input for decisions regarding a real aircraft problem. Cooperation between Lockheed and the Air Force combined with a reliable database has yielded a force management approach that is capable of safely executing corrective actions to the 405 joint problem.

## WS 405 RISK ASSESSMENT FAILURE DECISION TREE

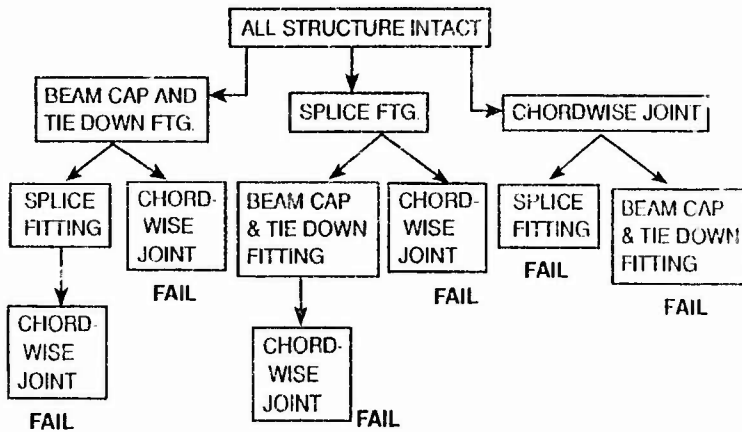


Figure 1

## STATEMENT OF CONDITION

Summary of Cracked Holes,  
C-141 Force, WS 405 at  
Rear Beam

NDI: BHEC

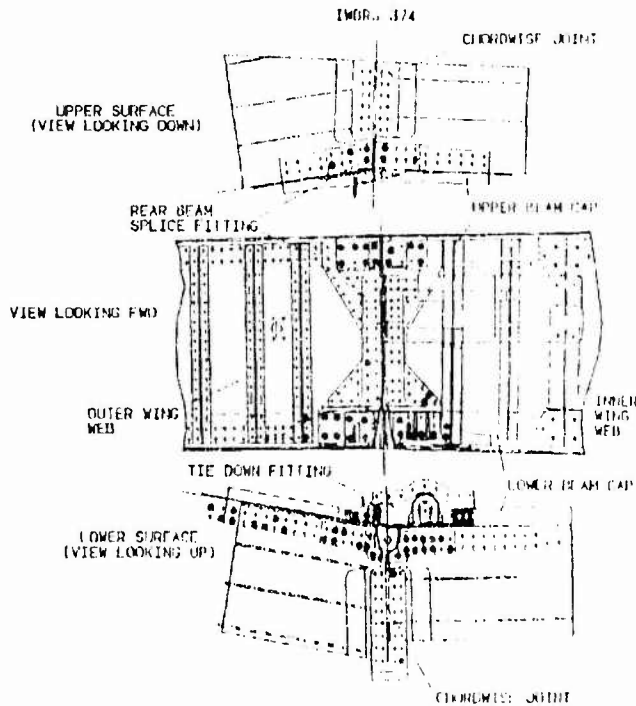


Figure 2

# Risk Assessment Basics

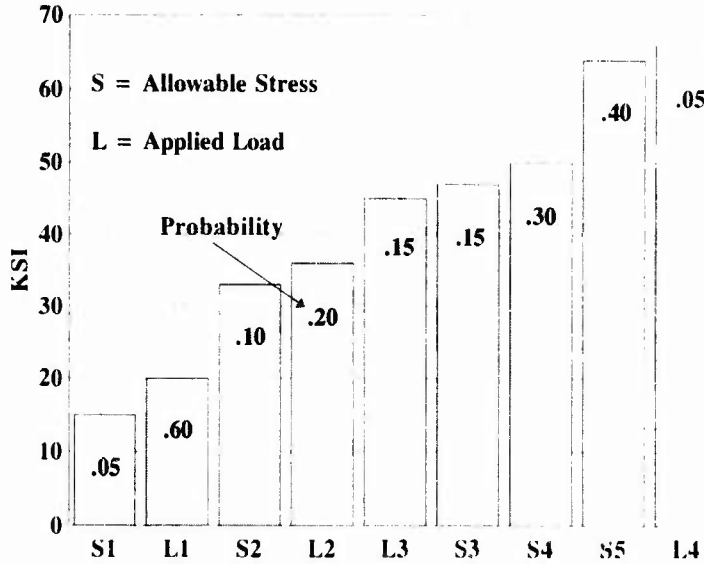
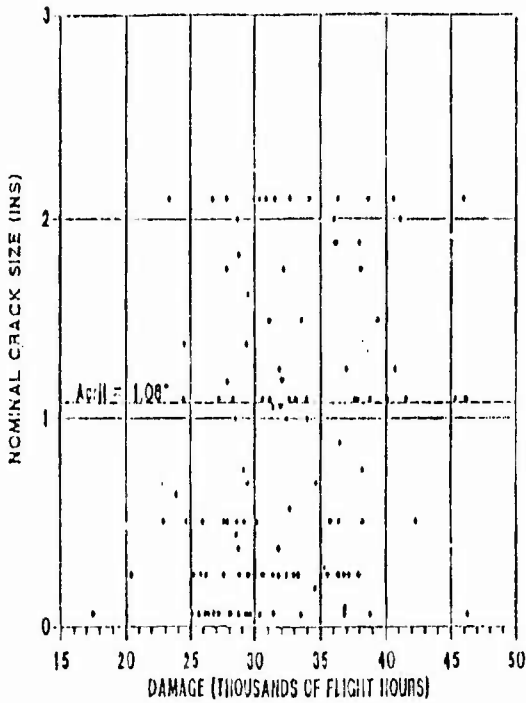
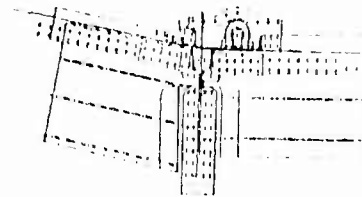


Figure 3



## CRACKS FOUND BY TCTO 753 IN WS 405 AREA



LOWER SURFACE  
(VIEW LOCATIONS UP)

Figure 4

# WS 405 Risk Assessment

## Typical Crack Frequency Distribution Generated from Weibull Analysis

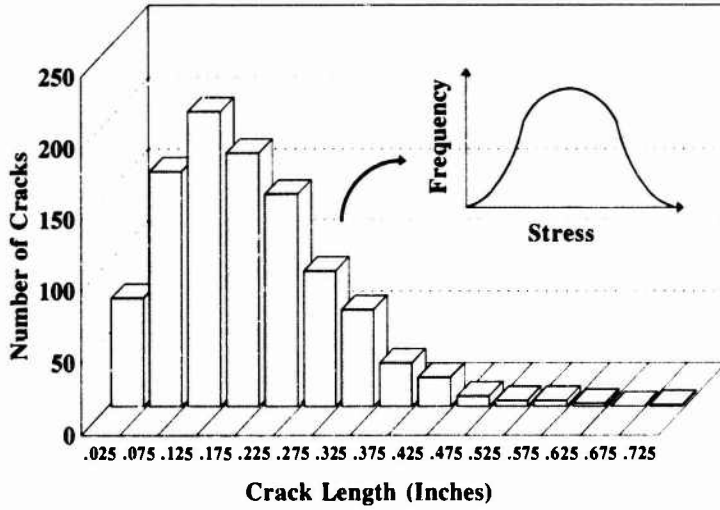


Figure 5

### Residual Strength Diagram for a Single Element

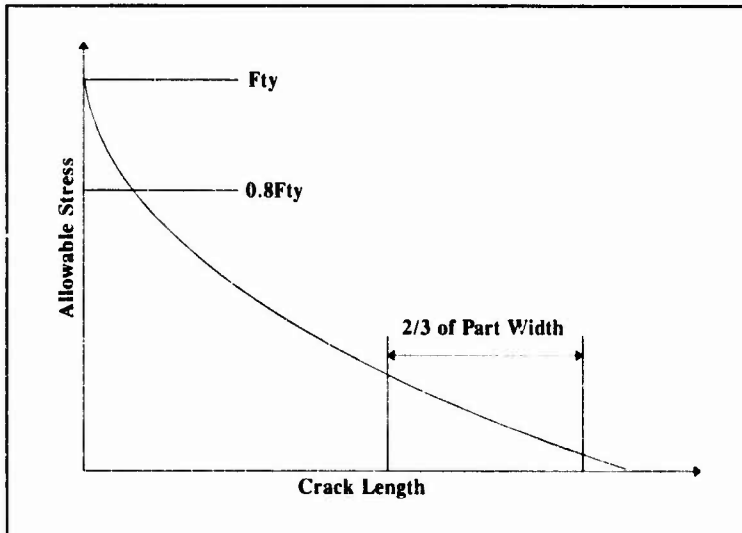


Figure 6

# WS 405 Risk Assessment

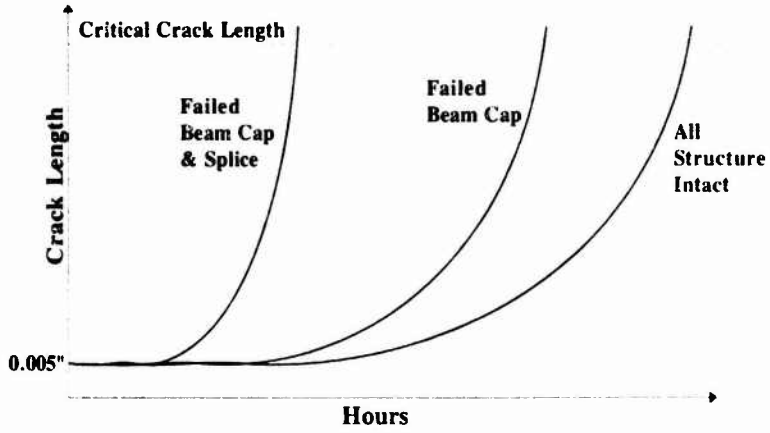


Figure 7

## Loads vs. Probability

---

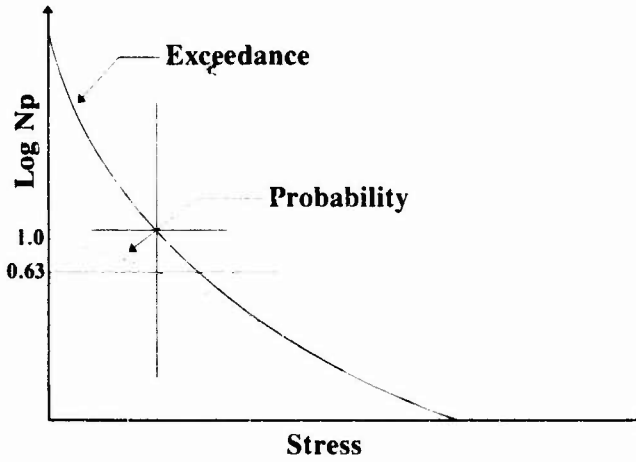


Figure 8

**WS 405 RISK ASSESSMENT  
FAILURE DECISION TREE  
BEFORE INSPECTION**

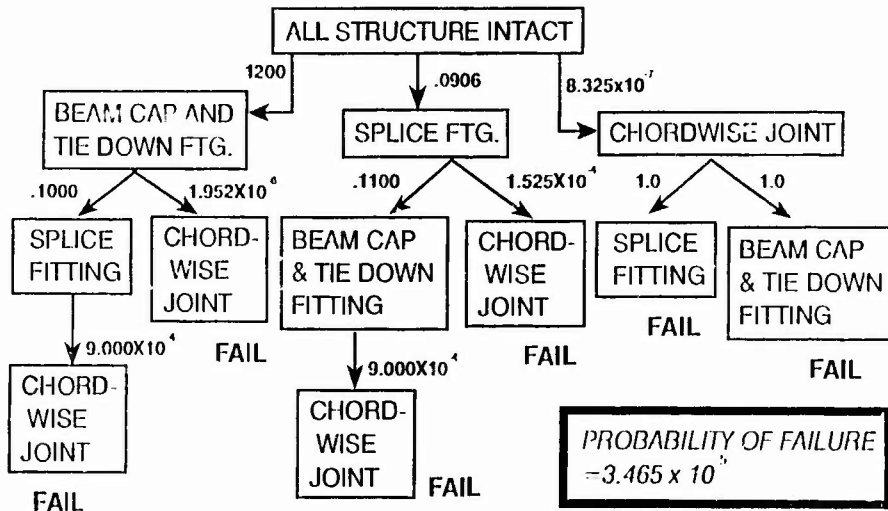


Figure 9

**WS 405 RISK ASSESSMENT  
FAILURE DECISION TREE  
AFTER INSPECTION**

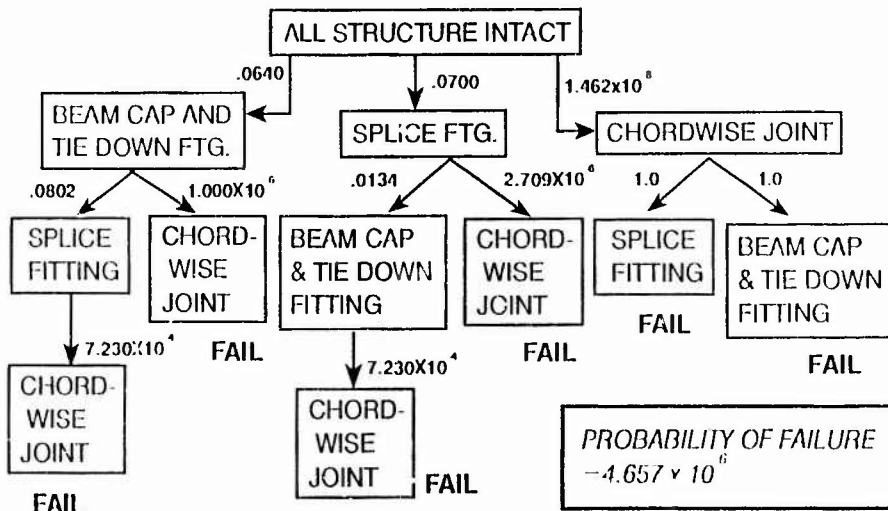


Figure 10

# ASSESSMENT OF IN-SERVICE AIRCRAFT FATIGUE MONITORING PROCESS

by

**R.J. Cazes**  
 Dassault Aviation  
 Breguet  
 78, Quai Marcel Dassault  
 92214 Saint Cloud  
 France

## ABSTRACT

Maintaining the structural integrity of aircraft depends on the initial definition of an inspection program (updated during the entire aircraft operational period) to detect structural damage that may occur in service.

Prediction of possible fatigue damage due to applied loads and conditions of use encountered in service is based on an analysis of the probability of incipient cracks and on an evaluation of the development of undetectable faults assumed to exist between two inspections.

The validity of evaluation models is generally demonstrated based on comparisons with results obtained on elementary test pieces subjected to predicted (or recorded) local load conditions in service and used to identify the influence of events such as rare overloads, or frequent repetitive small loads, etc...

This paper presents the principles for processing in flight signals collected in order to predict structural damage by making in flight integrated calculations, considering influences such as:

- load signals precision (frequency of points taken...),
- elimination of low amplitude variations, ...,
- cycle counting methods for the damage calculation ("Rainflow", sequence lengths processed, ...),

related to performances of damage prediction models, constraints on industrial construction costs and minimizing tasks of in flight data recordings.

## 1 - INTRODUCTION

The structural behavior of aircraft in service concerning fatigue and tolerance to damage is one of the main aspects of the cost effectiveness of their commercial and operational use. The cost of maintenance programs, defined to respect safety and structural dimensioning standards, is directly related to the precision with which loads encountered in service are known, and the accuracy with which their effects on structural integrity can be evaluated.

Defining efficient structural monitoring requires that preventive or remedial service work is minimized, while maintaining maximum operational availability and life. The essential coherence of inspections to be carried out, suited to the individual nature of each type of usage for aircraft in service, makes use of principles used during the structural design in regard with the planned usage objectives.

This paper presents the basis for an application of the conceptual structural analysis principles to the in-service evaluation of fatigue damage initiation (probability of incipient fatigue defect) and damage tolerance capability (propagation of undetected faults assumed to be existent at any time).

For this purpose, the impact of load parameters, as used during the structural design, is estimated with respect to dispersions that are inescapable in fatigue, inherent to the microstructure of the material and the uncertainties in fatigue behavior prediction models.

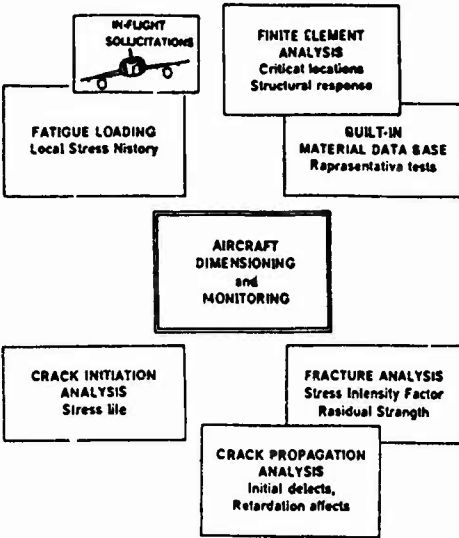
These results, quantified in usage times, help to define constraints for the acquisition of significant parameters in terms of the necessary (and only necessary) precision, volume and reasonably justified cost of data processing considering industrial production constraints, and finally minimization of tasks by systematically preparing results.

**2 - APPLICATION OF THE STRUCTURAL ANALYSIS CONCEPT**

**2.1 - Structural design to fatigue and damage tolerance**

Different concepts are involved for the in fatigue structural design. Main of them are hereunder summarised :

**AIRCRAFT FATIGUE AND DAMAGE TOLERANCE**

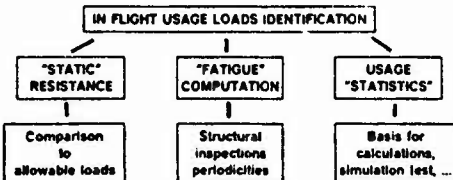


**2.2 - Objectives of monitoring in service**

Maintaining the in service aircraft structural integrity relies to the definition of a program of inspections in order to detect structural degradations that are likely to occur in service.

The definition of this program, is directly linked to the results of the previous (sheduled) inspections and to the knowledge of the in service encountered loads.

**AIRCRAFT IN SERVICE MONITORING**



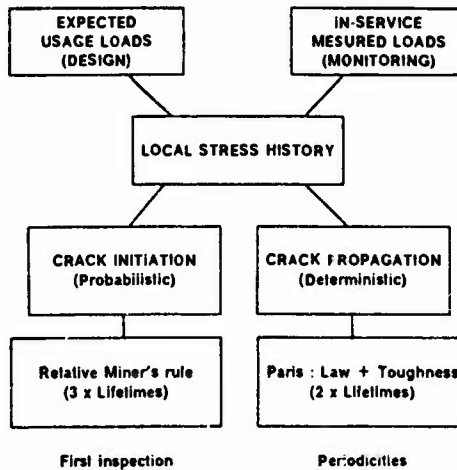
Real conditions of use on aircraft consists in a basic data set to :

- detect if allowable structural loads are exceeded in service,
- update inspection programs in order to maximize the economically viable structural life,
- define usage statistics for confirmation/revision of calculation bases, when taking them into consideration in the structural response model.

**2.3 - Study presented**

The proposed study starts from the involved "Fatigue and Damage Tolerance" design basis as hereunder proposed :

**STRUCTURAL FATIGUE EVALUATION PROCESS**



It will be pointed out the significance of the precision of in service loads stress acquisition (or reconstitution), or assumed types of structural degradations (cracks profiles).

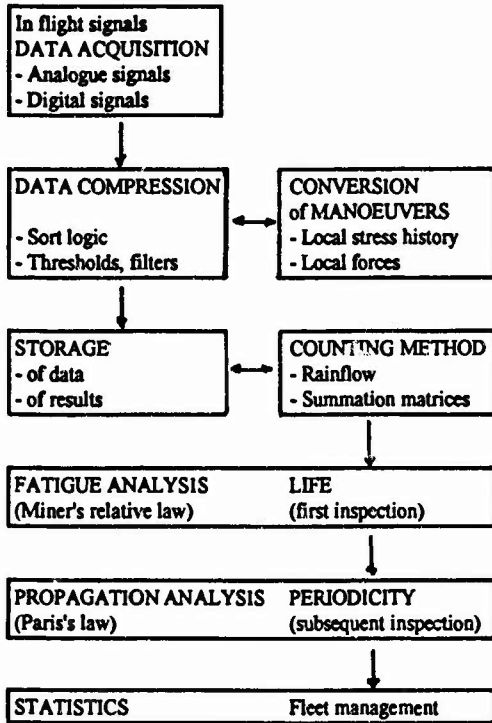
The results obtained help to define conditions for an identification of in-flight parameters consistent with their influences on the in fatigue structural behavior [1] and uncertainties in the prediction models [6]. The presented Principles have been implemented for the definition of aircraft MIRAGE 2000 monitoring system. Findings of MIRAGE 2000's experience will be presented as a conclusion.

### 3 - IN FLIGHT SIGNAL PROCESSING

#### 3.1 - Signal processing steps

The following diagram describes the functions carried out (entirely or partly) in flight, in order to calculate local damage due to in service loads such as loads gusts (transport aircraft) or such as loads in resources and manoeuvres (military aircraft).

#### SIGNAL PROCESSING



The specific nature of each step in terms of precision, the number of representative selected parameters, the "fineness" of tables of stored values, can affect volumes of informations to be processed, or even the feasibility of processing for operation without long and expensive systematic actions to be carried out by users.

Some of the most significant aspects are presented in this paper.

(\*) Flight analysis parameters :

- flight conditions (Mach, Zp,...)
- control deflections
- weight configurations

#### 3.2 - Generating structural responses

##### 3.2.1 - Principle

"Pilot" damage monitoring areas are selected beforehand. Knowledge of structural local stress in flight due to real aircraft operating conditions may be found by :

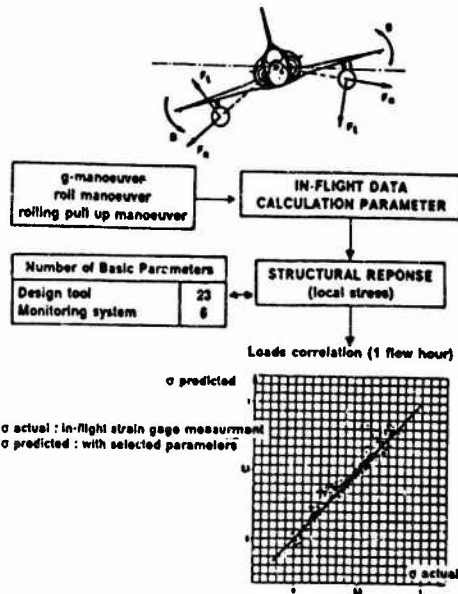
- direct measurement of the local stress or significant structural force (strain gauge, ...)
- reconstitution of variations of the local stress and/or representative forces.

When local structural information is not collected directly, the feasibility may be considered on modern types of aircraft without specific devices for data collecting : for example, on board existing parameters for Electrical Flight Control Systems can be used to calculate structural forces in pitch, roll and yaw manoeuvres.

##### 3.2.2 - Conversion of signals into local stresses

For a military aircraft such as the MIRAGE 2000, the used dimensioning model is based on values of about 16 main "aerodynamic" parameters associated with mass configuration parameters as in the left bottom (\*) summarized. A preliminary parametric study [2] allowed to reduce the number of basic parameters to 7 (6 analogue + 1 digital) without significant discrepancy as shown hereunder :

#### STATION LOAD ANALYSIS



Starting from such an "approached" reconstitution of in service encountered loads, the resulting "STATIC" and "FATIGUE" magnitudes of accuracy are :

**COMPUTATION ACCURACY**

STATIC	Normalised value
Basic complete model	1
6 parameters	$0.9 < F_{max} < 1.1$

FATIGUE	Normalized value D
Basic complete model	1
6 parameters	$0.95 < D < 1.05$

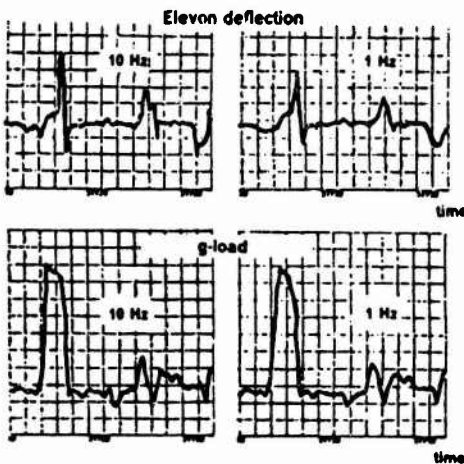
This approach does not generally require the installation of specific gauges on the aircraft, and should be recommended especially when a computer model was built for aircraft structural responses at the time of the design.

**3.3 - Signal acquisition (analogue parameter)**

A fatigue load is qualified by a succession of its component minima and maxima. Acquisition of these extremes as accurately as possible may be therefore a controlling condition at the source for the quality of the resulting fatigue evaluation.

The following chart is a simulation of the influences of inputting, at different sampling frequencies, a real signal from a combat aircraft flight . It concerns variations of the g-load factor (slow variations = 0.5 Hz) or a control surface angle ("fast" variations = 10 Hz).

**FILTER SAMPLING FREQUENCY**



Computed results according frequencies are hereunder summed up (MIRAGE 2000's example) :

Sampling frequency	G-Load history		
	50 Hz	10 Hz	1 Hz
Static maximum (normalised value)	1	0.99	0.98
Damage value (Miner's law)	1	1.00	0.98

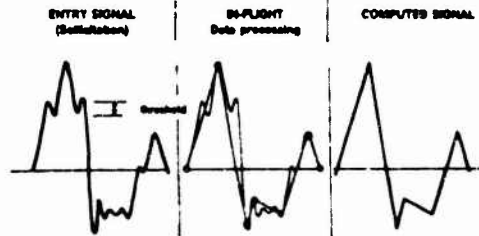
Sampling frequency	Elevon deflexion		
	50 Hz	10 Hz	1 Hz
Static maximum (normalised value)	1	0.96	0.72
damage value (Miner's law)	1	0.98	0.80

This type of preliminary analysis concerning sampling frequencies can produce a significant "saving" of in real time flight parameters processing. It concerns one of the most critical items for the monitoring device feasibility... and its cost/efficiency ratio.

**3.4 - Compression of data volumes acquired in flight**

A first sort carried out in real time eliminates intermediate values from the signal to be processed, and keeps only extreme values. Also low amplitude alternations (minimum, maximum) are generally only kept above a given variation amplitude "threshold" (omission of small cycles).

**DATA REDUCTION THRESHOLDS**



Increasing the sort "threshold" can reduce the volume of stored data, without a significant influence on Miner's prediction (see example below: on a typical combat aircraft flight).

Normalized results	Threshold for "G-Load" data			
	0.5 g	1 g	1.5 g	2 g
Volume of data storage	1.	0.72	0.57	0.52
Damage evaluation	1.	0.97	0.96	0.93

Remark : the resulting "omission of small cycles" parameter is however controlling [1], particularly in the case for gust loads on transport aircraft, in terms of life to incipient cracks or propagation (see comparative table below established for underlying load history)

LIFE RATIO Tests (*)	Small cycles omitting	
	Initiation	Propagation
Mini TWIST	x 2	x 2
Short FALSTAFF	x 1	x 1

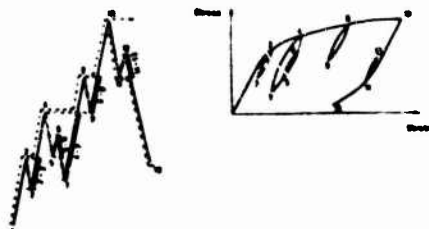
(\*) Ref. 1 - Fig.7

The estimate of this "small cycles influence" on the quality of fatigue predictions should be considered from the preliminary stage of stress design. A result would be the choice of data threshold to be recommended in order to obtain a results precision homogeneous with other parameters.

### 3.5 - Cycle counting method

The order of successive maxima and minima will have to be reorganized in order to carry out the processing for the fatigue and crack propagation for the local stress sequence. The "Rainflow" method [3] is one of the most representative methods for the local stress/deformation behavior as illustrated below

### DAMAGING CYCLES FROM TIME SERIES DATA



Several counting techniques are currently available for peak-through detection in a variable amplitude time history signal. Among them, "Rainflow" method provides a description of loads data compatible with the illustrated stress/strain behaviour of fatigue critical area. Moreover, after storage of identified cycles by the mean of matrix summations, it is possible to reconstitute representative loads sequences from the recorded Rainflow matrices [4]

In principle, "Rainflow" procedure is performed at the end of the signal recording, after the storage of each flight by flight data (extremes should have to be stored in their chronological order)

A comparative computation (carried out using a fighter aircraft load history) makes it possible to consider a progressive Rainflow storage procedure, when memorizing a limited number of selected previous extremes, without significantly affecting the quality of theoretical computed damage

Such a preliminary investigation allows a flight by flight "Rainflow" procedure at the end of each flight or during the flight at any time (manoeuvre dominated spectra)

### 3.6 - Crack initiation and propagation prediction calculations

#### 3.6.1 - The Miner model (crack initiation)

Miner's cumulative law applied universally for damage appearance by the  $m/N = 1$  formulation should be used with the recalibration concept (Miner's relative law) on test results under multiple levels stress histories.

However, this method is generally incapable of taking account of the "small cycles" influences on fatigue lives. Miner's computed damage values are quite the same while the on tests initiation lives vary significantly (see section 3.4)

More over, it doesn't reflect the beneficial effects of overloads, the harmful effects of truncating forces, as shown hereunder

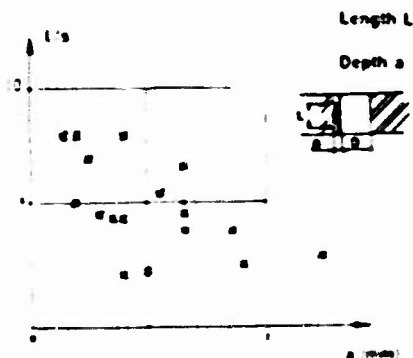
LIFE RATIO Tests (*)	High loads truncation	
	Initiation	Propagation
TWIST	x 1/3	x 1/3
FALSTAFF	x 1/1,5	x 1/2

(\*) Ref. 1 - Fig.5 and 6

**3.6.2 - The stress intensity factor (normalization)**

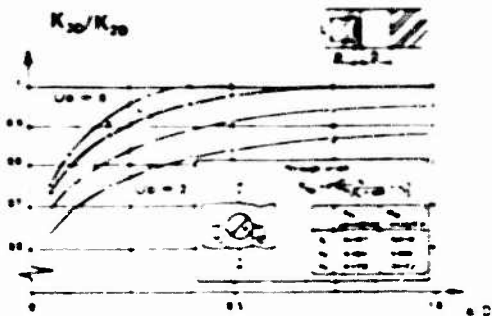
The following diagram considers cases of fatigue defects in service actually observed [5], on MIRAGE III combat aircraft semi-elliptical fatigue cracks on bores in thick tensioned base plates. Identification of defect depths using eddy currents devices reveals a high profile dispersion (L/a eccentricity)

SCATTER OF CRACKS PROFILES



Resulting variations in the stress intensity factor (noted K in the hereunder diagram) create propagation rates that vary (when considered as depending on  $\Delta K$ )  $\propto C(\Delta K)^2$  in a ratio of  $\times 0.5$  to  $\times 1.5$  magnitudes

SCATTER OF STRESS INTENSITY FACTORS



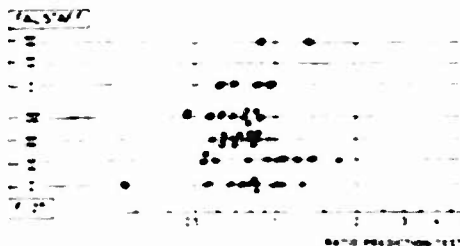
**3.7 - Optimum damage monitoring reliability**

The dispersion concept, inherent to any repeated physical observation highly, concerns the fatigue behavior of materials. The distribution of experimental results is often characterized as a Gaussian normal law with mean value and standard deviation, the orders of magnitude of which are representative of the maximum significance that could be obtained from simulation models

For example, in S-N curves, interpretation of a standard deviation of 0.10 (frequent on aluminium alloys) in a normal log distribution, will give a factor of 2 on the life at about 3 standard deviations (associated probability = 0.001).

In terms of prediction/tes. ratios, the results presented below [6] are prepared for loads representative of stresses at the intrados of transport type aircraft wings ("TWIST" or "F27" load and 2500 flight sequences) or military aircraft wings ("FALSTAFF" load and 200 flight sequences). Several variations of each load type have been considered by a different distribution of severe flights, omission of small cycles, or truncation of the high levels encountered loads during the flight sequences

RELIABILITY OF CRACK PREDICTION PATTERNS



RATIO (%)	Mean value	Standard deviation
"F27"	0.8	0.25
"FALSTAFF"	0.9	0.25

(\*) Ref. [6] - Table 29 - AED-BA results (ONERA's model)

Interpretation of a reduction factor of 2 on the calculated life will produce a non-conservative forecast with a deviation of  $1 - 0.72 = 0.28$  namely 2.8 standard deviations (associated probability = 0.01 in normal law)

This means that variations of influence parameters calculated relatively of small amount when compared with the "standard deviations" presented above will not be considered as representative of a significant physical phenomenon, but only within the dispersion envelope of the structural behavior prediction model

### 3.8 - Usage "statistics"

The Rainflow method keeps numbers and levels of recorded maxima and minima. Building up of count summations by "class" matrices then enables the use of structural behavior prediction models.

These summation matrices built up by flight phase, flight or group of flights, are used to count load factor occurrences, force spectra or local stresses, etc.

Random drawing methods help to generate flights and loading cycles in order to carry out representative tests of conditions encountered in service, to evaluate the structural behavior (maintenance anticipation), to prepare updated data (modify theoretical initially assumed calculation basis).

## 4 - CONCLUSION

### 4.1 - Application to aircraft monitoring system

The generalization of monitoring structural damage to aircraft in service is a phenomenon that will soon increase in coming years with the development of efficient on-board computer systems.

Moreover access to information already available in flight for other purposes, for example Electric Flight Controls Systems (EFCS) gives an unprecedented opportunity to learn about real forces on aircraft during use.

In regard with predicting structural behavior in "fatigue" and "tolerance to damage", this paper has emphasized the necessary cohesion (and precision/imprecision homogeneity) on the various signal acquisition and processing parameters. The criteria for this processing, done in flight, are defined with respect to inescapable effects such as dispersions of responses of materials under fatigue loads, the influence of ignoring small force cycles and uncertainties in prediction models.

Such a study have been achieved for the basic definition and industrial development of the Dassault Electronic's system "SPEES" as implemented on several French Air Force aircraft for in service damage or loads evaluation.

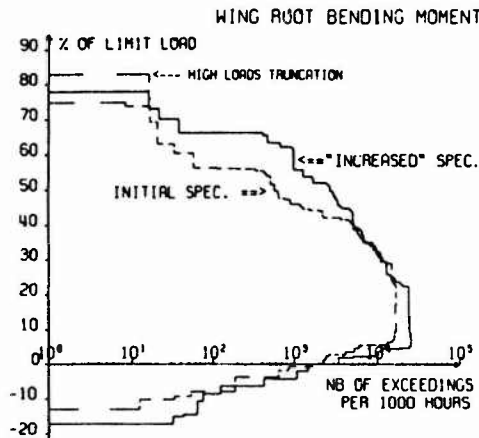
Choices (acquisition frequency, signal sort thresholds, result matrix dimensions, etc...) have been made considering their impact on calculated forces and lives, and with the objective of minimizing tasks for users.

### 4.2 - MIRAGE 2000's experience results

The MIRAGE 2000 performed her maiden flight in 1979 and has been demonstrated to comply with required Technical Specifications with important static strength margin (1,7 limit load withstood without failure) and high durability (5 x life times simulated on a Full Scale Test Article without failure).

However, as a result of in-service usage data processing, the aircraft was found to be much more severely handled (since pilots rely on the automatic protections provided by the EFCS) than expected from the initial design Technical Specifications (see figure below).

#### MIRAGE 2000 : FATIGUE RESISTANCE SPECTRA



The in-fatigue spectra and usage processed data, combined with stringent static design conditions due to new capabilities increasing weight and load inventories (such as underwing 2,000 l. fuel tanks or under-fuselage additional stores), were the basis of strengthening the structure for the current production aircraft.

Consequently, the MIRAGE 2000 structure capability has been raised up to 9 g in a wide range of interception and combat aircraft, and including an outstanding fatigue resistance.

In service recorded data have been processed, when considering the presented stress histories effects, for defining the subsequent loading conditions of a fatigue test of a production line random wing. Three life times have been completed in March 93 before appearing the first cracks in their early stage. Test is going ahead (a fourth lifetime and residual strength tests) for damage tolerance capability demonstration.

**LIST OF REFERENCES**

- [1] J. SCHIJVE  
"The significance of flight-simulation fatigue tests".  
13th Symposium of the International Committee on  
Aeronautical Fatigue, (1985), Pisa, ITALY.
- [2] R.J. CAZES et P. DEFOSSE  
"Aircraft tracking optimization of parameters  
selection".  
AGARD - SMP - 72th meeting, 1991, JAPAN.
- [3] AFNOR - projet de recommandation A03-406  
"Fatigue sous sollicitations d'amplitudes variables  
Méthode "Rainflow" de comptage des cycles  
Principe et utilisation"  
SF7M, Commission de Fatigue des métaux, 1992,  
Paris, FRANCE.
- [4] B.H.E. PERRETT  
"An evaluation of a method of reconstituting fatigue  
loading from rainflow counting"  
14th Symposium of the ICAF, 1987, CANADA.
- [5] R.J. CAZES (\*)  
"Fatigue and Non Destructive Inspection".  
GIFAS, French Aerospace Conference, 1991,  
AUSTRALIA.
- [6] BAUDIN ET ROBERT  
"A check of crack propagation models against test  
results generated under transport and military  
aircraft flight simulation loading".  
GARTEUR ACTION GROUP 04, 1989,  
ONERA, FRANCE.

(\*) R.J. CAZES  
Dassault Aviation (DEC/CS)  
78, Quai Marcel Dassault  
92214 - Saint-Cloud  
FRANCE

# THE ROLE OF FATIGUE ANALYSIS FOR DESIGN OF MILITARY AIRCRAFT

by

**R. Bochmann and D. Weisgerber**  
 Deutsche Aerospace AG, Military Aircraft Division  
 Department LME 221  
 PO Box 80 11 60, D-81663 Munich  
 Germany

## 1. SUMMARY

A brief overview of the fatigue design method employed at DASA (Deutsche Aerospace AG) for combat aircraft is here presented. The efficiency of the fatigue analysis - as embedded in the overall design process - is discussed and compared with full scale testing. Furthermore, possible improvements in the method are suggested.

## 2. INTRODUCTION

For the fatigue design of military aircraft most of the European A/C industry has not adopted the damage tolerance procedure used by the US industry but stays with conventional safe life concept. Since the requirements are specified by the customer, i.e. the Ministry of Defence or Air Force, a generally good confidence in the 'safe life' design may be presumed in Europe. However, a periodic critical review of the analysis methods should be performed, and finally a comparison of full scale test results and service experience with the initial predictions may lead to a revision or refinement of the analysis methods.

A brief description of the fatigue verification process presently used at DASA is given below, and in particular the problem areas are discussed and possible improvements proposed.

## 3. BASIC DATA AND ANALYSIS METHOD

### 3.1 Requirements Specified by the Customer

The fatigue life requirements specified by the customer or operator normally comprise of:

- required service life
- peace time missions including breakdown and configurations
- manoeuvre spectrum (provided as g-exceedances)
- safety factor (scatter factor) for test and analysis

### 3.2 Analysis Methods Used for Metallic Structure

In spite of many reservations expressed in numerous publications Miner's cumulative damage rule is still used at DASA, and is obviously still the most widely used analysis method - certainly due to the simple and universal applicability. A study performed at DASA

already in 1978 (Ref.1) revealed an acceptable accuracy for typical fighter aircraft spectra (Fig.1).

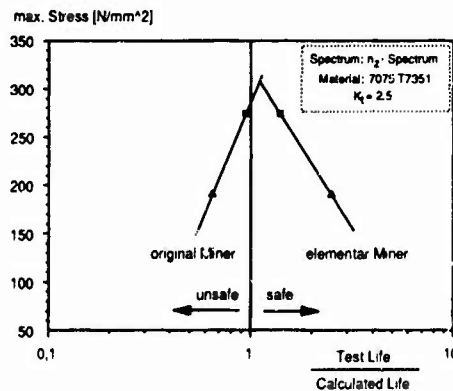


Fig 1 Example for Miner's Rule compared to Test Results

A computer programme has been developed that uses the Weibull equation of the form shown below to approximate the S-N data.

$$S = C1 + (C2 - C1) / \exp((\lg N / C3) C4)$$

or

$$\lg(N) = C3 * (\ln((C2 - C1) / (S - C1))) / C4$$

where:

S = nominal stress  
 N = number of cycles to failure  
 C1, C2, C3, C4 = constants derived by regression analysis of test results

An example is presented in Fig.2

Programme inputs are the maximum and minimum loads of each discrete load step together with the occurrences in the spectrum. The stress level is determined by input of a scaling factor. In addition, an iteration routine allows a quick assessment of the stress level for any predetermined damage sum.

If appropriate full scale or component test results of previous projects are available a relative Miner's rule has been frequently adopted for similar structural details. Thereby, a damage calculation is performed with the test spectrum up to failure. From the database a S-N data-set is selected that best fits the structural detail of the test specimen as well as that of the structure to be analysed.

The resultant damage sum for the test failure is then also applied to predict the allowable stress for the structure to be analysed.

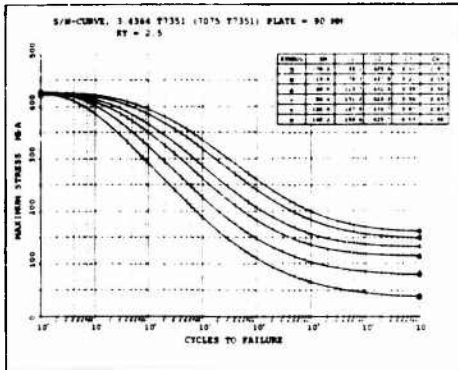


Fig 2 Example for S-N Curve

**3.3 S-N Data for Metallic Structure**

A sufficient database of S-N data is essential to analyse all type of structure. The S-N data are derived from coupon tests and cover:

- standard aircraft material
- geometric notches
- riveted and bolted joints
- lugs
- other effects (e.g. welding, surface treatment, chemical milling etc.)

Furthermore, test results of full scale tests and component tests are available.

In this context the life improvement processes like shot-peening and cold-expanding of holes should be mentioned. The policy adopted is to use these processes not for initial design but as a cost-effective potential to increase the fatigue life of structure that failed during fatigue testing.

**3.4 Consideration of Temperature and Corrosion**

The effect of in-service environment on fatigue is considered to be negligible for most of the structure. It is assumed that the applied surface protection will sufficiently prevent corrosion and, if required during the service life a re-protection will be carried out.

The temperature spectrum due to aerodynamic heating is to be based on the peace time missions. A degradation of the fatigue properties in consequence of this spectrum is

unlikely to be encountered for the typical aircraft materials. However, for areas close to other sources of heating, e.g. engines, a reduction of the fatigue characteristics must be taken into account. Consideration is also to be given to the occurrence of thermal stress cycling as a result of temperature variations on different materials jointed together.

**3.5 Fatigue Analysis Policy for CFRP**

For CFRP structure, whether the components are undamaged or predamaged (delaminations), fatigue analyses have not been performed up to present.

The reasons are:

- The design allowables (strains) are significantly below the allowables determined by fatigue.
- Reliable analysis methods are not yet available.
- Extensive fatigue testing of CFRP components under representative loading have neither shown any development of damages nor the growth of artificially introduced delaminations.

In spite of the superior fatigue properties of CFRP for future projects consideration should be given to the following:

- Repeated buckling of CFRP structure may cause fatigue damage. Therefore, buckling should be avoided up to the maximum service spectrum load.
- In the case of conventional joints failures have been observed at fasteners.
- At repair patches, damage growth may occur - particularly under hot/wet condition - if the bonding is insufficient.
- Generally in CFRP structure, damage will develop under fatigue loading (Fig.3). Consequently, with changes of the design allowables or the life requirements the necessity of a fatigue analysis should be considered.

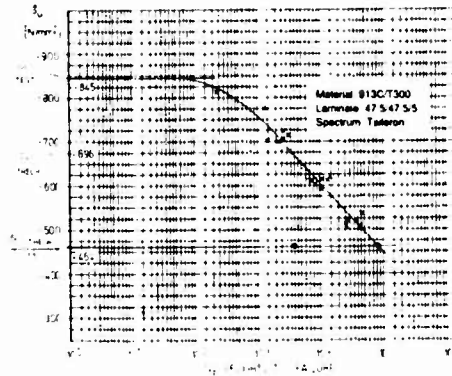


Fig 3 Fatigue Life Curve for CFRP 913C/T300 (Ref.2)

#### 4. PRELIMINARY FATIGUE ALLOWABLES

Already early in the development phase fatigue allowable stress levels are being established for the various parts of the aircraft. The loading spectra used are either the g-spectrum for all aircraft structure predominantly loaded in linear correlation to the load factor  $n_z$ , e.g. wing box and large areas of the centre fuselage, or component spectra of previous projects modified, if required, to take into account obvious differences regarding the usage.

The allowable stresses are usually given in nominal stresses in the net section. They are presented in a graphical form stress vs. stress concentration factor  $K_t$  (Fig.4) or as allowable stress levels for typical riveted and bolted joints and also for lugs of various geometries and sizes.

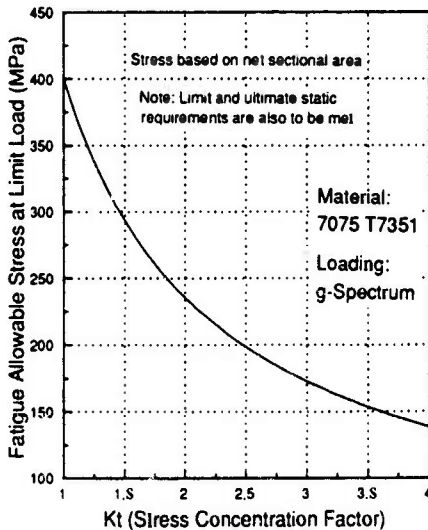


Fig.4 Allowable Stress vs  $K_t$

For the major load carrying components, e.g. fitting of wing/fuselage attachment, the results of early development fatigue tests are used for final design or, a read-across from previous tests on components of similar structure and material is possible.

Generally, the early assessments of fatigue allowables have a tendency to be pessimistic.

As soon as more accurate loading spectra are available, particular from computer simulations of typical manoeuvres, the allowables are updated.

#### 5. USE OF FATIGUE ALLOWABLES

Since commonly FEM calculations are performed only for load cases that are defined by static design

requirements these have to be used also for fatigue design. If the most severe load case for a particular component, covering the whole flight parameter envelope, would be chosen for fatigue design, an arbitrary conservative result would be achieved.

To avoid extreme conservatism, those load cases are selected for use in conjunction with the fatigue allowables which lie within the envelope of the peace time missions. The main parameter to be considered are load factor  $n_z$ , roll rate, mass, configuration, altitude and speed. Since the envelope for static design is much wider it is often difficult to identify suitable cases. In practise those cases close to the envelope of the mission requirements are included. However, 'exotic' cases that are unlikely to occur during the aircraft life of the majority of the fleet are deleted.

A further problem is the occurrence of combined stresses. In this case the maximum principal stress is used in conjunction with the fatigue allowables.

The fatigue allowable stress has to be compared with the calculated stress of the considered section and should give a ratio  $S_{allow}/S \geq 1.0$  which may be regarded as a measure for the fatigue quality.

It is the stress engineers responsibility to apply the allowable stress correctly during stress analysis. Advice from the fatigue specialist is available whenever requested. For the major load carrying components the involvement of the fatigue specialist is mandatory.

#### 6. DETAILED FATIGUE ANALYSIS

The major structural components and joints are usually subjected to a detailed fatigue analysis using final design information with regard to:

- loading spectra
  - derived from manoeuvre simulations and using rainflow counting method
- stresses
  - using detailed stress assessment or strain gauge measurements obtained from full scale static test or early strain gauge readings from the full scale fatigue test

Since the analysis is performed late in the design progress a shortfall in predicted fatigue life can have a considerable effect on the structural qualification process.

#### 7. QUALIFICATION TESTS

At the end of the fatigue verification process a full scale airframe test will prove the accuracy of the fatigue design and form the basis for the in service fatigue life monitoring. The test loading has to be based on the customers requirement. The load simulation covers all

load variations that are likely to effect the structural fatigue life, including manoeuvres, gusts, buffet, airbrake operations, landing impact and ground operations, cabin pressure and also tank and air intake pressure. In Fig. 5 an example is shown for the test loading of an unsymmetrical manoeuvre that is obtained from a computer simulation. The manoeuvre is represented by the time slices i to 4.

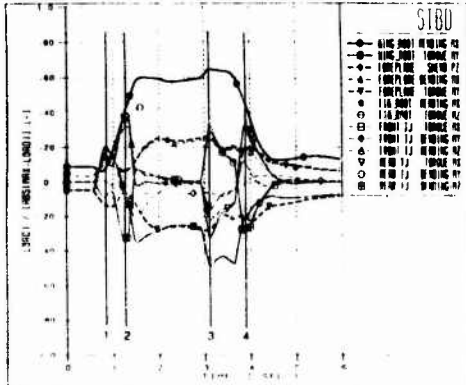


Fig 5 Test Simulation of an Unsymmetrical Manoeuvre

Due to economic restrictions buffet and gusts are usually tested in a simplified manner on a damage equivalent basis. Also the tank and air intake simulation is simplified with the purpose to achieve locally a reasonable superposition of loading caused by manoeuvre and pressurization.

Besides the full scale airframe fatigue test a number of component qualification tests are required for these items which are not embodied in the airframe test specimen, or replaced by a dummy, or not representatively loaded.

Failures during fatigue qualification testing usually induce a modifications of the relevant structure. The immediate embodiment of the modification in the test specimen is the preferred solution. If an unrepresentative repair is embodied in order to carry on testing the life of the modification has to be qualified separately.

**8. IN SERVICE FATIGUE LIFE MONITORING**

Once in service the fatigue life of the individual aircraft life will be monitored relative to the qualification tests. This requires the installation of a sophisticated fatigue life monitoring system.

**9. CRITICAL REVIEW OF FATIGUE VERIFICATION PROCESS**

**9.1 General**

The quality of the assessment of fatigue allowables is largely affected by the availability of sufficient accurate loading spectra for the individual parts of the aircraft. Consequently, the fatigue specialist always attempts to use the best available information during development progress. If the derivation of a particular spectrum is doubtful, then usually a somewhat pessimistic approach is applied. On the other hand, in order to accomplish the aircraft mass requirements also the fatigue specialist is often encouraged to give up the 'pessimistic assumption', whether or not this will finally prove to be true. The problem encountered during early development may be emphasized by the histogram shown in Fig. 6.

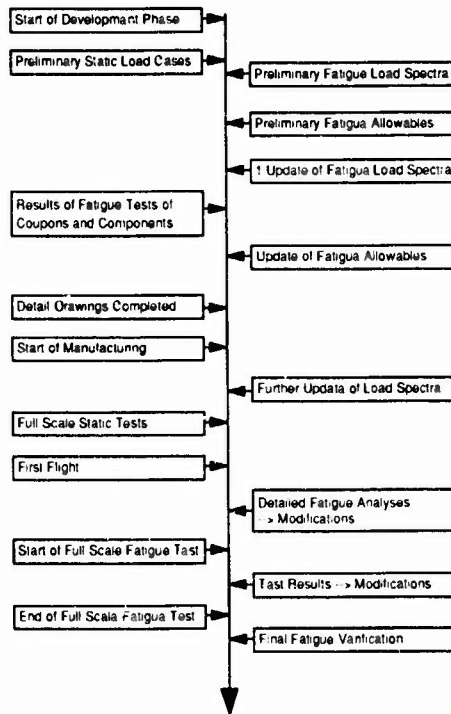


Fig 6 Chronology of Fatigue Verification Process

Also the stress engineer who has to apply the fatigue allowables is faced with the problem of tight time schedules and the need to perform detail stress calculation for areas recognized to be dimensioned by the fatigue allowables.

Another point worth discussing is the fatigue analysis method used. It is certainly disappointing to realize that

today in principal the same approach is used as more than 20 years ago (Ref. 5 to 9).

However, if reviewing the proposed alternatives during this period only the local strain concept seems to have a promising prospect. The reasons why it is not used during the development phase are simply:

- a large portion of fatigue critical sections are joints where the local strain concept has not yet proved to be applicable.
- a general superiority compared to the nominal stress approach has not always been achieved (Ref. 3).

In Fig. 7 to 9 some statistical evidence derived from the full scale fatigue test for the TORNADO aircraft is presented.

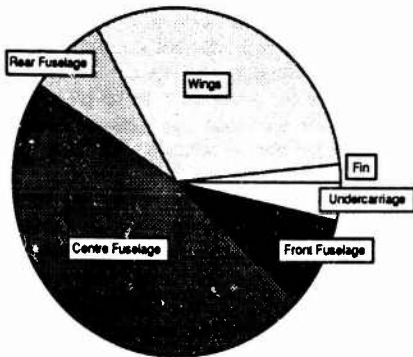


Fig. 7 Distribution of Damages in Major Structure Parts (Ref. 4)

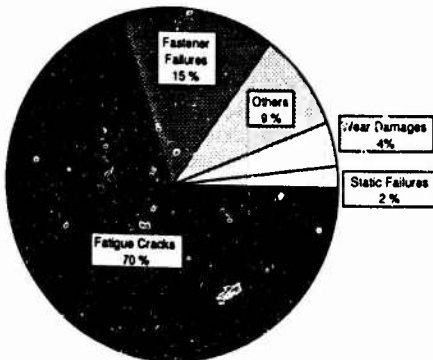


Fig. 8 Type of Damage (Ref. 4)

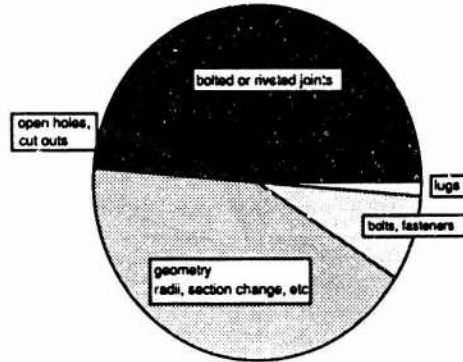


Fig. 9 Distribution of Fatigue Cracks

### 9.2 Major Load Carrying Components

The major load carrying components in general receive special attention with regard to detail fatigue design. The loading spectrum is usually of good accuracy and early development tests - static and/or fatigue - are often performed and necessary modifications can immediately be introduced into the design. Therefore, no significant fatigue problems are encountered for these components.

### 9.3 General Structure

Whenever an unexpected failure occurs during a full scale test or in service the question has to be raised: Why has the criticality not been recognized during the design stage?

It is common experience that a considerable number of unexpected cracks will develop during full scale testing in sections that had not been identified to be critical. A few of them may be attributed to unpredictable assembly stresses or internal stresses due to manufacturing processes or even to excessive scatter of fatigue properties in a particular material. However, for the majority of cracks the problems must be traced back to the fatigue analysis process.

An attempt has been undertaken to survey and categorize the fatigue cracks developed during the TORNADO major aircraft fatigue test. The graph in Fig. 10 contains the cracks discovered on the centre fuselage up to 12000 simulated flight hours (75% of the required test life).

From that graph it can clearly be seen that a large portion of the fatigue critical sections were not recognized because the stress analysis was not sufficient, whether it was not detailed enough, or the FE model inaccurate, or for whatever reason. Another considerable portion was categorized to be 'bad detail design'. The majority of these details are secondary structure and therefore, the structural integrity of the aircraft is not directly affected. Nevertheless, since inspections, repairs or modifications

may be necessary these are important from an economic point of view.

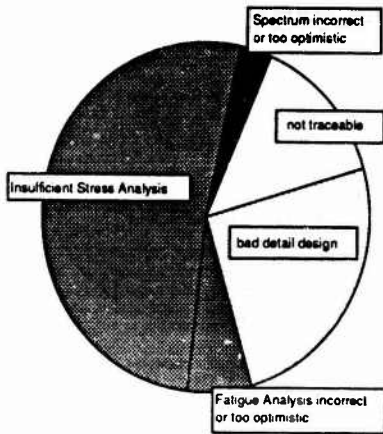


Fig 10 Reasons for Not Recognizing the Fatigue Critical Sections (Survey of Centre Fuselage only)

The number of failures traced back to 'fatigue analysis' and 'load spectrum' are fairly small. An explanation for the latter is probably the tendency to use pessimistic assumptions if the spectrum is not clearly defined. Finally, the fatigue analysis method obviously plays a minor role with regard to the results of the full scale fatigue test.

## 10. DISCUSSION

If it is assumed that the above findings about unexpected fatigue failures are typical for A/C design, at least for a similar type of aircraft, then some essential conclusions should be drawn.

### Loading Spectra

As initially mentioned the basic loading spectra and in consequence the local spectra used to assess allowable stresses are usually in an accuracy range of good to conservative compared to the final definition applied to the full scale testing. However, care should be given to structural areas significantly loaded by spectra of different sources, e.g. manoeuvres and landing loads, to account for changes of mean load in the load history. Today, computer simulations of flight manoeuvres allow the generation of spectra for the major loading actions, including the loading and movement of control surfaces. Unfortunately, the computer models are generally too late available as to form the basis for the assessment of the fatigue allowable stresses.

As a consequence, it would be desirable to obtain early in the development phase computer simulations of acceptable accuracy. Complete load sequences

according to the mission requirements could then be built up and used for fatigue analysis.

### Stress Analysis

The stress analysis was found to give the major contribution to the unrecognized fatigue critical sections. This is rather disappointing since it is common opinion that the FEM analysis is an excellent tool to determine the strength of the structure. However, obviously it is not always successful for fatigue design and therefore, an attempt is made to investigate the reasons:

Since the total structure will be represented by a mesh of finite elements an important criteria for accuracy is how fine is the mesh. Does it sufficiently cover details, particular in a complex structure. For a number of cracks this was not the case and the criticality was therefore not recognized, as has been shown by strain gauge measurements on the full scale specimen and/or fine mesh recalculations for the relevant sections.

Another difficult problem is the representation of joints. The stiffness of the joints have to be predicted for embodiment into the model. The effect of stiffness deviations on the overall accuracy may have caused some of the fatigue failures.

Furthermore, the stress engineer has to transform the loads or strains/stresses of the finite elements into nominal stresses which have to be compared to the fatigue allowable stresses. For a complicated structure this is not an easy job and requires experienced engineers. An early assistance from the fatigue specialist may be helpful in many cases.

It is obvious that each of the above mentioned points can lead to either over- or underestimating of stresses and consequently, in the case of underestimating a fatigue problem may be encountered. A stress analysis error in a member of a statically indeterminate structure with multiple redundancy can - to some degree - be tolerated from a static strength point of view since during static testing the load will be redistributed as soon as nonlinear deformation occurs. However, in case of fatigue loading - which represents the inservice loading - the full load spectrum will normally be acting and fatigue damage according to the correct stress level will be accumulated. Finally, also a non-technical aspect should be mentioned. Since often a tight time schedule is pressing the stress engineer to release the drawings, he may sometimes primarily check the static strength and - knowing the problems of predicting accurate local fatigue stresses - be forced to rely on the results of the full scale fatigue test.

### Detail Design

With increasing complexity of the structure also the danger of unfavourable detail design increases. A great deal of knowledge and experience regarding optimum design against fatigue is required to avoid these fatigue

problems. A 'feeling' for load flow, structural deformation and material capability are important to deal with complex structures.

Comprehensive information in the design handbook are certainly of great help, particular for young design engineers with little experience.

In spite of all precautions taken to avoid these failures happening it is certainly wise to accept that a perfect detail design throughout the complete structure will remain a dream.

#### *Fatigue Analysis*

The fatigue incidences attributed to incorrect fatigue analysis are dominated by a typical crack pattern. The cracks developed in the flange of a frame, perpendicular to the short transverse direction. Thus, the degradation of the fatigue properties in the ST direction has been disregarded. Therefore, care must be taken not to miss any structural details that are detrimental to the fatigue characteristics.

Whether for a safe life design Miner's rule will soon be superseded by a more sophisticated method remains doubtful. Further improvements or modifications of Miner's rule - e.g. adjustments based on results of flight-by-flight component tests - seems to be more likely. In this context the generation of an international database (as proposed previously, Ref. 10,11) covering flight-by-flight test results for structural details and also for full scale specimens would be greatly appreciated. It should contain all information necessary to allow the re-analysis of the test failure. Thereby, it will be possible to adjust the relevant analysis parameter.

#### 11. CONCLUDING REMARKS

For the major load carrying parts, attracting special attention with regard to fatigue, generally no significant problems are expected for the final built standard.

For general structure it can clearly be concluded that the fatigue analysis alone is by far not the weakest link in the total fatigue verification process, at least for a fighter aircraft. The main potential for improvement can be assumed in the stress analysis field. In consequence of the problems discussed also a change in design principle from 'safe life' to 'damage tolerant' would not automatically result in an improved efficiency of the analysis. This does, of course, not question the basic differences between the two philosophies.

As an obvious conclusion it has to be repeated that comprehensive full scale testing of the total airframe or components remains an essential part of the fatigue verification process.

However, for present and future projects a gradual improvement of the analytical part of the fatigue verification process is expected. This optimistic outlook is mainly based on the fast development of computer

software and associated tools used in the disciplines loads, stress and fatigue analysis.

#### REFERENCES

- 1.) MBB-Report UFE 1459, 1978, "Lebensdauervorhersage für Kampfflugzeuge. Experimentelle und theoretische Untersuchungen zur Überprüfung neuer Lebensdauerberechnungsverfahren, Teil 2".
- 2.) Arendts F.J., K.O. Sippel, D. Weisgerber, 1980, "Constant Amplitude and Flight-by-Flight Tests on CFRP Specimens, AGARD-CP-288
- 3.) Buxbaum O., H. Oppermann, H.-G. Köhler, D.Schütz, Chr. Boller, P. Heuler, 1983, "Vergleich der Lebensdauervorhersage nach dem Kerbgrundkonzept und dem Nennspannungskonzept", LBF-Bericht Nr.FB-169
- 4.) IABG Internal Report B-TF 2860, 1991, "TORNADO - IDS, Major Airframe Fatigue Test, Final Report"
- 5.) Maxwell R. D. J., 1971, "The Practical Implementation of Fatigue Requirements to Military Aircraft and Helicopters in the United Kingdom, Proc. 6th ICAF Symposium, Miami Beach USA
- 6.) Schivje J., 1972, "The Accumulation of Fatigue Damage in Aircraft Materials and Structures", AGARD-CP-118
- 7.) Schütz W., 1972, "The Fatigue Life Under Three different Loading Spectra - Tests and Calculations", AGARD-CP-118
- 8.) Schivje J., 1973, "Aspects of Aeronautical Fatigue", AGARD-LS-62
- 9.) Schütz W., 1973, "Fatigue Life Prediction - A Somewhat Optimistic View of The Problem", AGARD-CP-118
- 10.) Heuler P., W. Schütz, 1985, "Fatigue Life Prediction in the Crack Initiation and Propagation Stages", Proc. 13th ICAF Symposium, Pisa Italy
- 11.) Schivje J., 1985, "The Significance of Flight-Simulation Fatigue Tests", Proc. 13th ICAF Symposium, Pisa Italy

## DAMAGE TOLERANCE MANAGEMENT OF THE X-29 VERTICAL TAIL

by

J. Harter  
Wright Laboratory  
Wright-Patterson AFB  
Dayton, OH 45433  
United States

### SUMMARY

During high angle-of-attack (aoa) less than 25 degrees, the X-29 experienced severe vertical tail buffet. Fin tip accelerometer data exceeded 110 g's at approximately 16 Hz. The U.S. Air Force Flight Dynamics Directorate was asked to provide technical support to ensure that the entire X-29 flight test program could be safely conducted.

The Flight Dynamics Directorate transitioned an in-house developed crack growth life prediction program (MODGRO - Ref 1) to the X-29 program office and NASA/Dryden as well as an extensive technical support. Three dimensional crack growth analyses were conducted between flight days to track possible damage growth based on actual strain data collected at critical areas of the vertical tail. The entire high aoa flight test program was completed as planned using MODGRO to predict damage accumulation and used the data to manage flight maneuvers to maximize useful flight data and minimize structural risk.

A follow-on flight test program was conducted with the X-29 to assess Vortex Flow Control. Repair to the tail was required to complete this mission. Analysis and verification testing of the repair was performed by the Flight Dynamics Directorate. At the end of that flight test program, less than 10% of the repair life was used.

### 1 BACKGROUND

Many current high performance aircraft have experienced vertical tail buffet at high aoa. Under high aoa conditions, turbulent air flow from the aircraft forebody can impinge on the vertical tail causing high frequency loading. This buffeting action has the potential to severely reduce the service life of aft, vertical control surfaces. The X-29 demonstrator aircraft #2 first encountered significant vertical tail buffet on 9 May 1990 during flight #42 at angles-of-attack between 20 and 35 degrees. This buffet condition occurred for 15 seconds and resulted in fin tip accelerations in excess of 110 g's and a dominant first bending mode of 16 Hz. This condition resulted in vertical tail loads approaching their design limits and the decision was made to temporarily avoid this flight condition. However, this decision severely impacted the X-29 flight test program since military utility flights were to be conducted at high aoa to demonstrate the maneuverability of the aircraft. Damage tolerant analyses of the tail were performed for the assumed most critical location to estimate the crack growth life of the vertical tail at various g levels. An initial flaw size of 0.03 inch was chosen based on field experience and confidence with existing non-destructive evaluation (NDE) methods. In this case, an eddy current inspection method was used.

Preliminary analyses established inspection intervals at the most critical areas of the tail. These analyses used the limited fin tip acceleration data that was available for the tail and a simple transfer function to estimate local stress levels. Additional strain gage instrumentation was installed on the vertical tail while the aircraft was down for its next scheduled maintenance and stress analyses were performed to determine the actual stresses at several locations on the tail. These analyses were then correlated with subsequent flight test data and more detailed crack growth predictions were performed to more accurately establish the damage tolerance of the vertical tail.

### 2 APPROACH

Analysis of the in-flight accelerometer data during buffet revealed that the vertical tail was primarily experiencing the first bending mode at a natural frequency of 16 Hz. There was some indication of the second bending mode and first torsion mode at higher frequencies but at much lower amplitudes. Several areas of the tail were considered as possible areas for crack initiation and growth (FIGURE 1.0), but the aft root fitting (location #4) was considered to be the most critical since the tail was primarily being loaded in pure bending during buffet. The aft tail mount was considered to be most highly loaded due to the fact that the tail is swept aft, shifting the center of pressure and mass toward the rear fitting. This was supported by static test data supplied by the manufacturer (Grumman). Grumman also supplied a transfer function relating fin tip acceleration to stress at the aft fitting. This was accomplished by relating acceleration to deflection and deflection to root bending moment and finally to the gross section stress in the aft attachment. The 15 second fin tip acceleration trace obtained during flight #42 was normalized (FIGURE 2.0) and used as a loading spectrum for crack growth analysis. Various maximum g levels were modeled by multiplying the normalized spectrum by the stress level corresponding to a given acceleration.

Prior to performing any damage tolerance analysis for the aft tail attachment, a reasonable initial crack length must be assumed. The assumed size should, of course, be large enough to have a high probability of detection. Since NASA had safety of flight responsibility for the aircraft, they were responsible for any type of aircraft inspection. It was determined that eddy current inspections would be performed at three locations on the tail (locations 3, 4, and 6 - FIGURE 1.0). Inspections of areas 1 and 2 would have required the removal of blind fasteners which had a higher probability of causing crack initiation than the buffet loads. Location #5 was considered less critical than location #4. The NASA

inspector initially claimed to be able to detect any flaw larger than 0.005 inch using a hand held probe inside fastener holes. U.S. Air Force experience has indicated that a more realistic size is on the order of 0.03 - 0.05 inch. After discussions with NASA and Grumman engineers, it was decided to use the Air Force crack growth prediction program, MODGRO, assuming an initial 0.03 x 0.03 inch corner flaw at location #4. It was also agreed that an immediate inspection of locations 3, 4, and 6 would be conducted and subsequent inspections would follow if and when the time spent in buffet exceeded 1/2 the predicted time to failure for the highest fin tip acceleration measured since the last inspection. The predicted life (time in buffet) is shown in FIGURE 3.0 as a function of maximum g level. This approach was very conservative assuming that location #4 was indeed the most critical location, but it was felt that the limited available data warranted a conservative approach to assure safety. In any case, this approach returned the aircraft to flight at high aoa.

While the above approach returned the X-29 to high aoa flight, subsequent flights and frequent inspections demonstrated the need to obtain more data to remove some of the conservatism from the analyses. While the aircraft was nearing the next standard 100 hour overall inspection, Air Force, NASA, and Grumman Engineers decided to install strain gages covering all six critical areas on the right side of the tail during the scheduled down time. These gages would provide detailed strain information for these locations. Grumman was contracted to perform stress analyses for each location and used flight test data from the new gages to calibrate their analyses. Flight #55 was the first flight after the installation of the gages and was flown at low aoa to obtain less dynamic strain for calibration purposes. Flight #57 was the next flight in which a 25 second buffet event occurred at high aoa. TABLE 1.0 shows the maximum strains and calibrated notch stresses for this event. As can be seen, the initial assumption that location #4 was the most critical location was incorrect. In fact, applying the rule-of-thumb that the difference in crack growth life is approximately equal to the cube of the stress ratio in aluminum results in a factor of 27 between the life at location #4 compared with location #2. Location #2, which is just above the drag chute bracket, is non-inspectable in practice since blind fasteners must be drilled out for inspection. A detailed view of location #2 is given in FIGURE 3.0. Grumman engineers performed both crack initiation and crack growth analyses for location #2 using the 25 second buffet event. Constant load amplitude test data for 2024-T851 aluminum (X-29 tail material) coupons with open holes were also available from Grumman. These data provided cycles-to-failure information at several load levels. Since Grumman is primarily a U.S. Navy contractor, their aircraft are generally certified by crack initiation analyses. Since the Air Force requires damage tolerant analysis for safety of flight, MODGRO was used to determine an initial corner crack size that would yield a predicted life matching the Grumman test data. The resulting initial crack length was 0.01 inch for the 2024-T851 aluminum skin material. This size also happens to be the same as the generally accepted size defining crack initiation. This was pure coincidence since a much smaller initial crack size is usually required to predict total life with damage tolerant analysis alone. However, this material is relatively brittle and

Grumman had also predicted a short initiation time for the flight #57 event. In lieu of any inspection of location #2, an initial 0.01 x 0.01 inch initial corner crack was assumed at the lower fastener hole (FIGURE 4.0). Since all locations on the vertical tail are matched on both the left and right side, the event in flight #57 was also inverted to model the loads on both sides of the tail. The mean stress was rarely zero, probably due to the fact that at various aoa, left or right rudder are applied to maintain heading or perhaps the vortices favor one side over the other. The strain trace from flight #57 is given in FIGURE 5.0. The minimum crack growth life from the initial flaw size was predicted to be 330 repeats of the buffet event seen in flight #57 (FIGURE 6.0). After more discussions between Air Force, Grumman, and NASA, a life of 165 repeats of the event was agreed on to provide a safety factor of two for the analysis. Time in buffet prior to flight #57 was counted by using the flight #57 event, correlation between maximum stress at location #2 and fin tip acceleration, maximum stress ratio between previous events and flight #57, and the time spent in buffet in the previous flights. Once the correlation between stress at location #2 and fin tip acceleration was determined, the equivalent time in buffet (based on flight #57) for each previous flight was determined as follows:

$$\text{Equiv. Time} = [\text{Max Stress}/\text{Flt 57 Max Stress}]^3 \times \text{Buffet Time}$$

A review of previous flight test records resulted in approximately 45 equivalent buffet events up to flight #57. Therefore, after flight #57, approximately 30% of the tail life was used.

A special version of MODGRO was supplied to NASA/Dryden to be used to predict crack extension using actual flight test data. Between flight days, buffet stress data was downloaded to an IBM compatible PC and crack growth predictions were made using both the given and inverted versions of the stress spectra. Crack growth was predicted from the last predicted crack size and each spectrum was input twice to provide a safety factor of two on life. The most conservative prediction was used as the new crack size. To provide a metric for the percent life expended, the crack growth curve for flight #57 was used as a reference in that the number of repeats of the flight #57 event corresponding to the current crack size was divided by the life (330 repeats). The aircraft completed the original flight test program at approximately 96% tail life. A second flight test program was desired to study the potential of vortex flow control to supplement the vertical tail yaw control. The fasteners at location #2 were drilled out, eddy current inspected, reamed 0.03 in, re-inspected, coldworked, and interference fit fasteners were re-installed. The Air Force Flight Dynamics Directorate conducted a test program to verify the repair and developed new input data files for MODGRO. The damage accumulation from an 0.03 inch initial corner flaw was tracked by the Air Force program office. Crack growth predictions were not made as frequently as was done previously since the repair was considered better than the original structure. At the end of the program approximately 7% of the repair life had been expended.

### 3. CONCLUSIONS

The X-29 demonstrator aircraft was not designed using damage tolerance requirements, but after the tail buffet problem was discovered, it was possible to employ the damage tolerance philosophy to provide a means to continue the program safely. Without the use of damage tolerance analysis methods, it is extremely doubtful that the responsible organizations (NASA, U.S. Air Force, and Grumman) would have continued operations under high load conditions. Although location #4 was not the most critical location, the use of a conservative initial approach quickly led to the discovery of the high notch stress at location #2. The subsequent detailed analysis of location #2 provided a means to manage future flights. The Air Force and NASA used MODGRO as a tool to manage the X-29 test program after flight #57. More severe flights were conducted earlier than they would have been and

experience gained from certain maneuvers allowed them to be modified or deleted to complete other important tests of the aircraft. It is very difficult to quantify the success of the damage tolerant design philosophy by pointing out aircraft that have not experienced a structural failure. However, its use in the X-29 program has clearly been invaluable.

### REFERENCES

1. Harter, J.A., "MODGRO, Users Manual, Version 1.2", AFWAL-TM-88-157-FIBE, Feb, 1988

TABLE 1.0 : Flight Test Results

Location	Gage	Strain (micro-inch)		Knotch Stress (ksi)
		Flt 55	Flt 57	
Fwd Skin	91033	680	700	
Radius	91034	610	600	16.1
(1)	91035	580	600	
Aft Skin	91029	170	600	
Radius	91030	820	1500	
(2)	91031	900	1500	77.5
	91032	1160	2000	
Mid Rudder	91026	300	1200	
Hinge	91027	400	1200	19.0
(3)	91028	500	1300	
Aft	91037	650	700	
Pedestal	91038	620	700	24.4
(4)	91039	520	800	
Fwd Pedestal	91040	590	500	
(5)	91041	980	850	17.9
Upper Hinge	91024	290	900	
(6)	91025	200	700	32.0

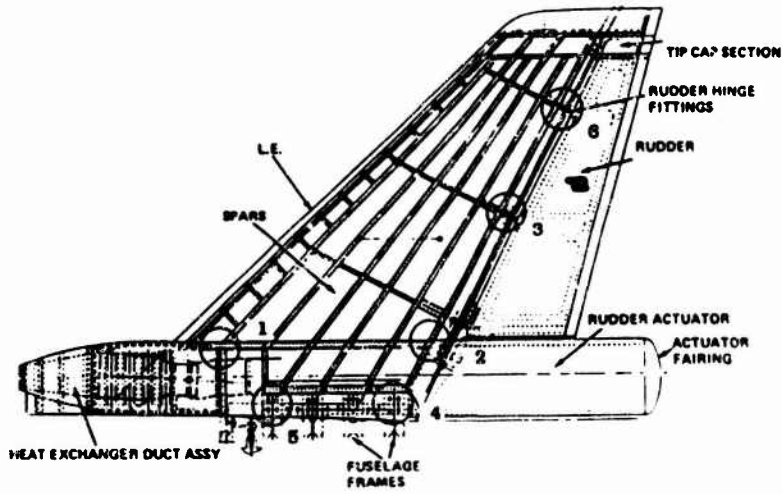


FIGURE 1.0 : Vertical Tail Critical Locations



1025 Cycles  
15 Second Event  
68.3 Cycles/Second

FIGURE 2.0 : Flight #42 Flt Tip Accelerometer Trace

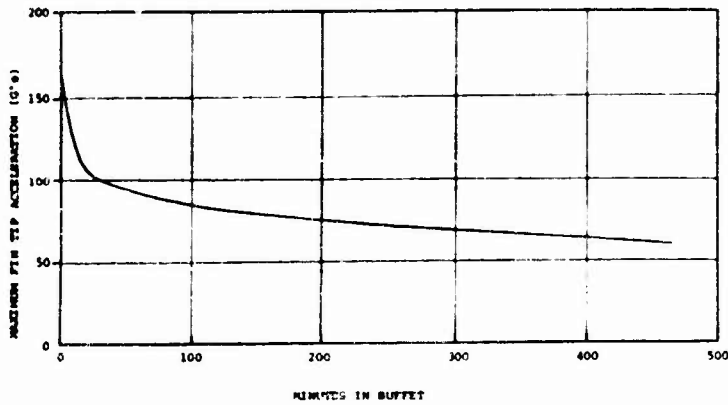


FIGURE 3.0 : Air Tail Mount (Location #4) Crack Growth Life

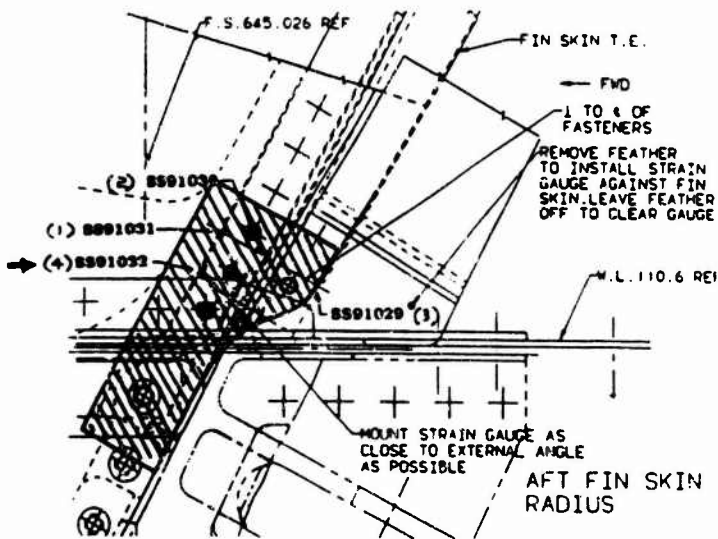


FIGURE 4.0 : Detailed View of Location #2



532 Cycles  
 25 Second Event  
 21.3 Cycles/Second

FIGURE 5.0 : Flight #57 Strain Gage 91032 Trace

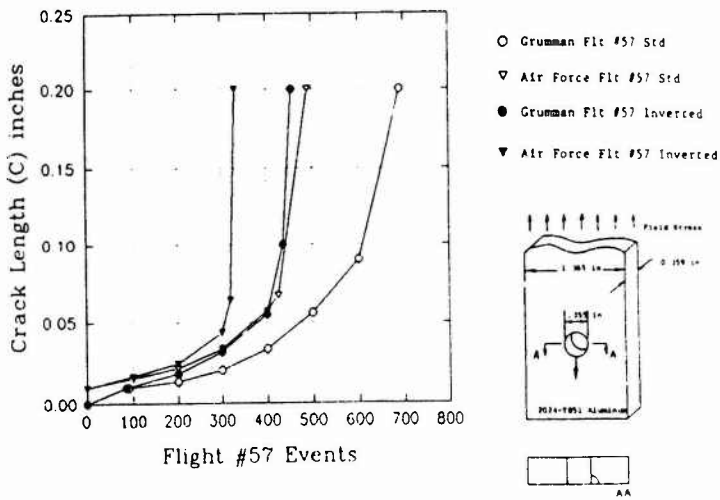


FIGURE 6.0 : Total Life at Location #2

## HARRIER II: A COMPARISON OF U.S. AND U.K. APPROACHES TO

### FATIGUE CLEARANCE

F S Perry

British Aerospace Defence Limited, Military Aircraft Division  
Hertford House, PO Box 87, Farnborough Aerospace Centre  
Farnborough, Hants, GU14 6YU, UK

#### 1. SUMMARY

The different approaches adopted for the fatigue clearance of the Harrier II in United States Marine Corps and Royal Air Force usage are discussed.

Brief accounts are given of the impact differing analysis methodologies and national airworthiness requirements have had on fatigue design, test and monitoring of the airframe.

#### 2. INTRODUCTION

Harrier II is a general name adopted for the second generation aircraft evolved from the Harrier GR.Mk.1 airframe designed by Hawker Siddeley Aviation (HSA) at Kingston upon Thames in Surrey, England. The GR.Mk.1 (later re-designated the GR.Mk.3) design was itself founded on extensive experience gained from its forerunners, the P.1127 and Kestrel aircraft.

The design of the Harrier II was initiated in response to a United States Marine Corps (USMC) requirement for an aircraft with payload and radius capabilities superior to those of the USMC version of the GR.Mk.1, the AV-8A. The new aircraft, designated AV-8B, was developed by the McDonnell Aircraft Company, MCAIR, as prime contractors, with HSA (now British Aerospace, BAe) sub-contracted to design and produce the air-centre and aft fuselage.

The Royal Air Force, RAF, had a similar requirement for a VSTOL-capable aircraft to replace its fleet of Harrier GR.Mk.3 aircraft and decided eventually to purchase the AV-8B aircraft, essentially as an existing design. In the RAF the aircraft was re-named the Harrier GR.Mk.5.

This Paper examines the considerations given to fatigue in the structural design and clearance of the AV-8B and the policies adopted in the UK to ensure safe operation of the Harrier GR.Mk.5 aircraft in RAF operational duties. Particular attention is paid to areas where the US and UK approaches contrast as a result of separate airworthiness requirements and differing methodologies evolved by the design authorities.

#### 3. DESIGN AND CLEARANCE AGAINST FATIGUE - HARRIER I

The structural design of the Harrier GR.Mk.1 aircraft, which entered service with the RAF in the late 1960's, used the results from a full scale fatigue test of the prototype aircraft, the Kestrel. Fig 1, supplemented by numerous tests of detail parts, systems and assemblies. There followed full scale tests of the single and two-seater aircraft at HSA's Kingston plant. All stages of this process were guided by the UK airworthiness requirements contained in Ref 1.

The primary consideration in the design was one of minimum weight, although a 3000 hour fatigue life was specified. A limited fatigue evaluation was carried out at the design stage, but mainly concentrated on detail design to ensure that the life requirement was achieved. This course proved to be highly successful as the full scale fatigue tests went on to demonstrate that the airframe had an endurance twice that specified.

While specific fatigue calculations were restricted in scope during design, a clear value was seen in analysis of data from the fatigue tests. Accordingly, the results were the subject of detailed fatigue analysis using Miner's cumulative damage rule and an S-N equation for bolted joints derived by the Royal Aeronautical Establishment (Farnborough), RAE(F), Ref 2.

The substantial work, Ref 3, published in 1962 by a former RAE employee, RB Heywood, which correlated an extensive range of fatigue data, formed the basis for more refined analysis techniques adopted by HSA Kingston. In 1968, a summary of the empirical S-N equations was compiled with a view to formulating a comprehensive procedure for the fatigue analysis of airframe components. This later became practicable with the introduction of mini-computer technology and a program was developed offering a wide range of analysis facilities.

The principal input data to the program were:

- o stress concentration factor
- o notch root radius
- o nominal mean and alternating stresses

The endurance of the notched component was obtained for the given stresses by an iterative process using master diagram (constant life) data for the plain material and complementary strength reduction relationships for the notched alloy.

When interpreting the results of testing, nominal stress levels or parameters within the generalized equations were modified to 'fit' the S-N data to a known test failure point. By this 'calibration' of the equations, read-across to in-service aircraft could be effected. Fig 2 illustrates manipulation of the S-N curve by, in this instance, variation of stress concentration parameters.

Fatigue life predictions, using available S-N data without the benefit of full-scale fatigue test results, were shown to be unreliable. This was variously attributed to inadequate knowledge of the critical location, the local stress distribution and the spectrum of applied loads (which would also preclude full-scale testing).

#### 4. DESIGN AND CLEARANCE AGAINST FATIGUE - AV-8B

The Detail Specification for the AV-8B, Ref 4, stated that the aircraft should have a fatigue life of 6000 hours. In order to meet the enhanced payload and range requirements, substantial changes were required to the structure of the Harrier I on which the aircraft was broadly based. The new design took account of Harrier I test and in-service data, an AV-8A service life extension programme (designated AV-8C) and experience gained from a prototype aircraft, the YAV-8B.

The requirements necessary to prove that the design would meet the specified fatigue life were set out in Ref 5 and were founded on established US military specification requirements, Ref 6.

The principal materials used in the airframe are shown in Fig 3. The structure comprised conventional metallic assemblies complemented by extensive use of composite materials, particularly in the forward fuselage, wing and tailplane. The use of the new materials in major airframe components required that a design and clearance programme for composites was developed in addition to the more traditional routes adopted for the metallic structure.

##### 4.1 Fatigue Spectra

Data gathered from USMC operations of the AV-8A fleet and YAV-8B aircraft were used to assemble an

AV-8B normal acceleration spectrum. The following key requirements set out in the Detail Specification for the AV-8B directed this process:

- o "Mean + 3 $\sigma$ " normal acceleration spectrum
- o 9:1 ratio of symmetric to asymmetric manoeuvres
- o maximum wing up-bending moment flight condition
- o a flight-by-flight test sequence

Fatigue meter data were collated and a mean normal acceleration spectrum generated for the AV-8A fleet. A 1000 flying hour AV-8B spectrum was derived by increasing the count at each fatigue meter level by three times the standard deviation for that level. This "Mean + 3 $\sigma$ " spectrum, shown in Fig 4, formed the basis for much of the design and testing of the AV-8B airframe.

The third requirement of the Specification was significant. A "worst-point-in-the-sky" condition, based on the maximum wing up-bending case, was stipulated which applied loads that generally would be higher than those routinely encountered in service. This ostensibly conservative approach enables a reduction in duration of qualification testing and is the major difference between US and UK philosophies. A test factor of two - and so a duration of 12000 hours - was agreed by the customer's technical authority, NAVAIR, to cover scatter in fatigue performance of the metal structure.

In design calculations a factor of four was applicable where testing would determine the true life of structure, where no testing was scheduled a life factor of eight was applied.

##### 4.2 Design Calculations - KtDLS Approach

In the design of the AV-8B, the resistance of the structure to fatigue loadings was a major consideration. Numerous fatigue calculations were performed and for many components fatigue strength, rather than static strength, was the overriding design criterion. To avoid the need for repetitious, complex and time-consuming damage calculations on every component of the critical structure, a system based on allowable stresses was employed. This enabled engineers not fully conversant with the intricacies of fatigue analysis to apply a checking procedure similar to that used in routine static stressing.

Component stress spectra and allowable stresses were generally developed by the process shown in Fig 5

for each critical component of the airframe, Table 1. The allowable stresses were derived as "KIDLS" values (DLS = Design Limit Stress) to provide a measure against which the combined stress concentration (Kt) at a notch and peak nominal stress in the region could be compared.

**TABLE 1: AV-8B COMPONENT FATIGUE SPECTRA LOCATIONS**

Wing/Fuselage
Flap
Aileron
Inboard pylon forward wing back-up fitting
Forward Fuselage
Cockpit crosstie
Lids fence
Alt Fuselage - Frame 40 to 43 area
Rudder top hinge
Stabilator
Vertical tail
Main landing gear
Nose landing gear
Outrigger landing gear
Speedbrake
Outboard pylon

The fatigue analysis used in the calculation of these allowables was based on local strain analysis, using Neuber's rule, Ref 7, supported by a sizeable series of laboratory fatigue testing to establish stress-strain and strain-life data. Further element testing provided substantiation of the fatigue life prediction calculations.

The use of local strain methodology in preference to traditional S-N based data for fatigue analysis was another area of divergence from UK (HSA) procedures. But in this case, the difference was matter of company methodology, rather than national airworthiness requirements.

#### 4.2.1 A Brief Overview of the Local Strain Method

Local strain analysis is a more rational basis for fatigue analysis than calculations based on nominal stress, as the degradation of a metal by fatigue is initiated by microscopic, irreversible, displacements within the material. The analysis attempts to model the strains of the material at a notch, taking account of local yielding and, if the load history is preserved, residual stresses from previous cycles.

The input data required to estimate the time to crack

initiation (assumed when crack reaches 0.25 mm) are:

- o nominal stress history
- o elastic stress concentration factor
- o stress-strain parameters
- o strain-life parameters

Strain-life data are obtained from tests of plain specimens under strain controlled conditions. The method assumes that the specimen is representative of the behaviour of material at the root of a notch in actual structure.

By solving Neuber's equation and the stress-strain relationship for each reversal in the nominal stress history, a local strain sequence at the notch root is generated. The associated local stress at each strain point is also recorded. A hysteresis loop identification routine is then used in conjunction with the strain-life equation to calculate damage values for each strain cycle in sequence. A simple summation of the damage values gives the total damage due to the stress history.

Fig 6 shows these steps in graphical form.

#### 4.2.2 Determination of Stress Concentration Factors

A key parameter in local strain and conventional fatigue analyses is the geometric stress concentration factor. It was noted previously that HSA found that fatigue life predictions often tended to be unreliable due, in part, to uncertainties concerning the local stress distribution at the critical feature. In the design of the AV-8B much effort was dedicated towards ensuring accurate values of stress concentration factors were used in the calculations. Allowances were made for a number of parameters, including:

- o thickness
- o countersink
- o bearing stress
- o variation of load direction in lugs
- o edge distance
- o interference fit
- o cold working
- o surface treatment

This attention to local stress condition, allied with accurate field stresses obtained from finite element modelling, removed a significant source of inaccuracy which had prevented satisfactory life prediction calculations on the Harrier I.

Nevertheless, while major improvements in fatigue analysis can be made by the use of modern analysis

techniques, scatter in fatigue performance will always prevent accurate predictions of when an individual part will fail.

#### 4.2.3 A cursory comparison of Local Strain and S-N Analyses

Although differences in MCAIR and BAe fatigue analysis methodology were not directly related to the US and UK airworthiness requirements, it is interesting to compare briefly the principles and benefits of the methods.

In both local strain analyses and more traditional S-N methods the life to crack initiation is considered. Further similarities exist between local strain analysis and the S-N method used by BAe Kingston. Indeed, the principle proposed by Heywood of relating notched material behaviour to plain specimen life data is very similar to the local strain method. Heywood states that,

*"For alternating stresses the cyclic plastic strain reduces the theoretical maximum stress in the notch, and it is reasonable to assume that the reduced value corresponds precisely to the stress in the plain specimen, for the same cycles to failure."*

Where Heywood used stress as the basis for read-across (because of the vast mass of data available), local strain methodology uses strain.

A major argument often advanced for using local strain analysis over stress-based methods is the ability to account for residual stress effects at the notch root. This is not possible with S-N analysis, but in many cases it is debatable whether this shortfall is important. Often the load history is not available - and where it is, the sequence effects usually serve to cancel each other. Unlike transport aircraft, for example, fighter aircraft experience extremely complex load histories where high positive and negative loads occur often and evenly throughout the aircraft's life.

Local strain analysis does have a distinct benefit in components which do not experience this random mix of loading, where one load direction predominates with occasional significant changes of sign. Components subjected to upper wing loadings can fall into this category.

The generalized S-N equations do not allow such refinement, but some significant benefits are gained by their use. A vast amount of S-N data has been compressed into a number of equations covering the entire range of mean and alternating stress, and the

effects of stress concentration, notch sensitivity, notch size and fretting. This enables fatigue calculations to be carried out on most aluminium and steel alloys without recourse to expensive laboratory fatigue tests.

The treatment of mean stress is a notoriously difficult problem and outside the scope of this Paper, but it receives a rational treatment in the generalized S-N equations with the introduction of a mean stress reduction factor,  $K_m$ . This enables due allowance for mean stress effects to be made automatically in routine analysis. The treatment of mean stress in Neuber's analysis varies, two rules are in regular use: the Morrow correction and the Smith-Watson-Topper parameter. Both have been tried in the MCAIR analysis system and the latter is currently favoured.

The question of the relative accuracies of the local strain and S-N approaches is difficult to assess. The different applications of the methods (design and in-service read-across) by the BAe and MCAIR preclude a direct comparison. In any event, the "accuracy" of fatigue calculation is a rather notional concept as fatigue data are obscured by scatter in results and a profusion of secondary environmental and physical effects.

A subjective assessment suggests that, when sensibly applied, there is little to choose between the two methods. In both cases the nominal accuracy depends on the suitability of the fundamental materials data. The local strain method is comparatively new and so the library of strain-controlled test data is not as extensive as that available for S-N data. Conversely, the generalized S-N equations were derived over 30 years ago and must be re-validated when applied to materials now in common use.

#### 4.2.4 The KtDLS Method in Operation

To date, evidence from the AV-8B indicates that the KtDLS method has been instrumental in producing a rugged, well designed aircraft. This must be the fundamental measure of the worth of the system, as to be cost-effective it must result in a better product. A significant benefit is also derived from its use as a routine stressing tool. A wide-spread awareness of fatigue is promoted amongst engineers, encouraging the control of fatigue to be an integral part of the design process.

It is not a panacea, though. Fundamental difficulties in fatigue analysis are not removed, particularly that of predicting where cracking will start. A re-design will attend to those areas which analysis shows to be deficient in fatigue strength, but it is almost inevitable

that the areas which eventually give rise to fatigue problems will be those that were overlooked in the design review.

A good example of this dilemma is provided by the original design of the fin forward attachment fitting of the AV-8B. Fig 7 shows a sketch of the component. The front spar of the fin is attached to the two lugs grown out of the fitting. Clearly, this is a crucial joint and naturally its fatigue strength was assessed using the KtDLS method. The lugs were identified as potential fatigue initiation points and subsequent fatigue analysis indicated that they had been efficiently designed with adequate fatigue strength. However, on the AV-8B Full Scale Development Fatigue Test a failure of the port fitting occurred at about a third of the required life.

The failure originated, not from the lug bore, but from the corner root fillet radius, causing complete separation of the lug from the fitting. A retrospective KtDLS analysis of this section, which involved a special detailed finite element analysis to quantify the stress concentration, showed that the fatigue strength was indeed inadequate and premature failure might be expected.

This experience showed that the KtDLS method is a reliable guide to fatigue performance (the lug and the fillet were correctly identified as non-critical and critical, respectively), but that detail designers must remain alert to the often insidious nature of stress concentrations.

#### 4.3 Clearance of Composite Structures

The use of carbon fibre composite material on the AV-8B was the result of an accumulation of experience gained on F-4, F-15 and F-18 aircraft. As confidence and knowledge grew, the extent of CFC components increased, from the rudder on the F-4 to the AV-8B, where about 25% of the structural weight is CFC material.

A comprehensive description of the development of CFC structure for the AV-8B is given in Ref 8. The design and clearance of the wing box, the primary CFC component of AV-8B, will be briefly examined here.

The torque box comprises eight CFC spars and a mixture of CFC and metal ribs (where out-of-plane loads are high) attached to monolithic upper and lower skins. As is typical for composite constructions of any complexity, a "building block" approach was used in the design and clearance of the structure. Throughout the programme, summarized in Fig 8,

particular attention was paid to the reduction in material properties resulting from adverse environmental conditions and inadvertent damage. The progressive build-up from simple elements, to joints, to sub-assemblies also allowed examination of the structural interaction effects which frequently result in the complex and unpredictable failure of composite structures.

Except for the centre-line wing joint (see Fig 9), fatigue was not a principal criterion in the design process. It is well known that, unlike metals, an adequate static load carrying capability in CFC structures normally confers satisfactory fatigue strength. The use of conservatively low design strains ensured that cyclic loads encountered in-service, even in conjunction with barely visible impact damage, would not cause propagation of damage.

Another noted property of composite construction, its sensitivity to out-of-plane loads, attracted special consideration in the design of the wing box. Where point loads were introduced into the structure, at pylon attachments for example, carefully designed metal fittings were used to minimize out-of-plane loads in the CFC structure. At the wing centre-line, quite high "kick" loads were caused by the wing anhedral and the design allowables were reduced in this area in compensation. A sub-assembly fatigue test of the joint was carried out to validate the design.

The AV-8B Full Scale Development fatigue test, although part of the overall qualification of the airframe, was aimed principally at clearing the metallic components. The combined full clearance of mixed metal and CFC structure by a single test is very difficult to achieve and was unnecessary in this case. For the CFC components, the stress factoring required to complete the test in an economic time-scale increases the risk of premature and unrepresentative failure of the metal components. The CFC components had been qualified by the rigorous building-block series of tests and on the full scale test their main purpose was to obtain the correct loading distributions on the metal components. Nevertheless, the completion of testing without incident on the CFC components provided further confidence in the overall integrity of the design.

In summary, the key axioms in the philosophy adopted in the design and clearance of the AV-8B CFC structure may be summarized as follows:

- o establish a sound database by extensive testing of elements and sub-structures, including environmental effects

- o design for static strength and keep design limit strains low
- o be alert to the threat posed by out-of-plane loadings

#### 4.4 The AV-8B Full Scale Development Fatigue Test

The fatigue life of the AV-8B airframe was proved by a Full Scale Development Fatigue Test (FSDFT) which was commissioned in early 1982, before the AV-8B aircraft went into service.

A series of metallic component fatigue tests was carried out to verify critical design features before full scale testing was undertaken. A list of these components is given in Table 2. Each component was subjected to 24000 hours of the spectrum loading that would be experienced on the full scale test.

**TABLE 2: AV-8B METAL COMPONENT FATIGUE TESTS**

<p>Centre wing back-up fittings          Centreline rib radius block          Flap link          Inboard flap hinge          Inboard aileron hinge          Pylon fitting seal          Cross tie          Horizontal stabilator attach lug</p>
---

For the FSDFT, a near structurally complete test article, FTV1, was installed in a free-standing test frame. The most notable missing component was the tailplane, which was subject to a separate full scale fatigue test.

The test was scheduled for 12000 hours of loading based on the 1000 hour flight-by-flight "Mean + 3 $\sigma$ " spectrum. The test loadings were applied as a randomized sequence and comprised positive and negative 'g' excursions with a 10% asymmetric content. The symmetric loads were based on the "worst-point-in-the-sky" maximum wing up bending design condition, known as WB01, a 7'g' symmetric pull-up followed at 0.95M at 9000 ft.

During the derivation of fatigue load spectrum an analysis of USMC wing stores usage showed that the loads associated with the WB01 design case was overly conservative. It was agreed with NAVAF that the test symmetric bending moments should be based on the "worst-point-in-the-sky" flight condition, but combined with a more representative stores

configuration. This decision reduced the fatigue test symmetric load case to 88% of the basic WB01 design case. Supporting analysis confirmed that the test loadings remained conservative with respect to average USMC usage. The AV-8B test condition is summarized in Table 3.

**TABLE 3: AV-8B TEST CONDITION**

<u>Configuration</u>		
Aircraft Mass : 22950 lb		
Fuel State : 60% internal fuel		
Fuselage Stores : Guns and ammo		
Centre-line pylon + Mk 82 SE		
Wing Stores : Inboard pylon + 2 x Mk 82 SE		
Intermediate pylon + Mk 82 SE		
<u>Flight Condition</u>		
Mach No.	Altitude	cg
0.95	9000 ft	12.30% MAC

#### 4.4.1 Test Results and Conclusion

The test reached 250 hours by 22 March 1982 and was completed on 2 August the same year. Apart from failures at the inboard and intermediate wing pylons, the failure of the port fin attachment lug was the only major incident to occur during the test. It was concluded from this exceptionally favourable outcome that, subject to appropriate structural modification to rectify these areas, the main components of the AV-8B airframe were structurally adequate to meet the safe life requirement of the aircraft in USMC service.

#### 4.4.2 Major Component Fatigue Testing

A full scale test of an airframe aims to provide a general clearance of the principal structural component. However, constraints imposed by the rig and method of load application and control inevitably limit the extent of clearance obtained. To overcome this difficulty on the AV-8B a series of auxiliary tests were carried out. The components are identified in Fig 3.

#### 4.5 Fatigue Monitoring In-Service

The culmination of effort spent in the design and testing phases minimizing the risk of fatigue problems is reached when the aircraft enters service.

To maintain this low probability of structural fatigue failure, the fatigue life consumption of every AV-8B is monitored by a software simulation of the conventional aircraft fatigue meter resident on each aircraft's mission computer. Data from the inertial navigation system are converted to an equivalent normal acceleration signal at the nominal fatigue meter location. Cumulative normal acceleration exceedances, displayed post-flight on the cockpit digital display unit, are read off and fatigue index values calculated by application of a fatigue meter formula.

The limitations of fatigue meter based systems are well known and, for the AV-8B, an improved fatigue tracking system was proposed by MCAIR to extend the area of monitored structure and so reduce conservatism in fatigue life calculations.

Five structural control points were selected, Fig 10, to monitor fatigue usage on the wing, tailplane, fin and main landing gear. The proposed system favoured calculation of component loads from aircraft trajectory parameters rather than direct load measurement. The ease of retrofit, zero weight penalty, reliability and flexibility of the parametric solution were seen as its key advantages over the strain gauge based alternative.

To reduce the amount of on-board processing - load equations, derived with the aid of flight load measurement programme data, were optimized by removal of less significant terms. The on-board processing proposed also contained a peak-trough identification routine to reduce the load histories to their turning point values in preparation for transfer to a ground-based fatigue index computation routine.

#### 4.6 Summary of AV-8B Fatigue Life Clearance Philosophy

Base design on successful AV-8A Harrier structure

Derive fatigue design loads from  $Me_{an} + 3\sigma$  AV-8A normal acceleration data

Design to comprehensive set of fatigue allowable stresses

For composites, carry out rigorous "building block" development test programme

Prior to full scale fatigue test carry out component tests on critical areas

Test full scale article to 2 lifetimes of "worst-point-in-the-sky" maximum wing up heading case, with

excursions beyond DLL

Carry out supplemental tests of major sub-components not cleared by the full scale test

Monitor usage in-service on an individual aircraft basis

### 5. CLEARANCE AGAINST FATIGUE - HARRIER GR.Mk.5

The AV-8B, re-named the Harrier GR.Mk.5, was purchased by the Royal Air Force as a replacement for its Harrier GR.Mk.3 fleet. BAe was designated as prime contractor to the UK Ministry of Defence for the supply and in-service support of the aircraft. With the exception of some detailed structural modifications, the airframe was that of the AV-8B.

As the GR.Mk.5 was purchased as an existing design there was no stated fatigue life requirement for the airframe, but this did not discount the need for the safe life to be established in its intended role in the RAF.

The optimum clearance route was contemplated at considerable length by the UK Ministry of Defence and its technical advisor, RAE(F). From the outset, it was the opinion of the UK Authorities that, though much of the clearance programme of the AV-8B would contribute to the process, there were such marked differences in US and UK procedural requirements that the results of the AV-8B FSD fatigue test could not be used directly to clear the GR.Mk.5. This opinion was largely informed by experience gained from the RAF Phantom F4 aircraft programme.

#### 5.1 The Phantom Experience

Three full scale fatigue tests had been carried out to US requirements before the Phantom entered service with the RAF. The UK requirements for the design of aircraft, contained in Ref 1, stipulated that full scale fatigue testing of an aircraft should be done under realistic load conditions for a duration of up to five times the specified fatigue life. Clearly, such a test is costly and for an aircraft previously designed and tested, albeit to foreign airworthiness requirements, it was reasonable to examine the possibility of obtaining clearance from extant data. However, in the case of the Phantom the differences in US and predicted UK load spectra, particularly the deliberate inclusion in the US tests of loads higher than would be expected in normal operations, led the UK Authorities to conclude that a UK fatigue test was

essential.

The comparison of "hard" US and "soft" UK normal acceleration spectra in Fig 11 shows the significant high load content of the US spectrum. The peak load in the US test was 118% DLL against 95% DLL in the UK test. The omission of low load level cycles from the US spectrum is another important difference.

The decision to proceed with an additional UK test was vindicated by the value of the information it produced. Most surprisingly, where failures occurred on both tests, the UK test tended to experience lower lives, even under the apparently more benign load spectrum. The test lives of two key failures of the wing are given in Table 4. The relative severity of the two spectra is taken into account in the ratio of Fatigue Index (FI) values at failure in the right hand column. (100 FI is equivalent to 4500 hours of US spectrum testing.) This shows that in the worst case the UK specimen had a safe life of only one fifth of that demonstrated by the US test.

**TABLE 4: PHANTOM - COMPARISON OF US/UK WING FAILURES**

FEATURE	FAILURE TIME		FI RATIO US : UK
	UK TEST	US TEST	
OUTER WING SKIN	7526	11800	3.7
CENTRE WING PYLON HOLE	5258	11800	> 5

These results highlighted the inability of simple cumulative damage calculations to read-across between spectra of markedly different shape. It may be speculated that the increased number of low load level cycles in the UK test promoted fretting fatigue actions, while the high loads in the US test introduced beneficial compressive stresses which retarded crack growth.

Compelling evidence of the benefits of testing to a representative spectrum is given in Table 5. This strongly indicates that the UK test provided information more characteristic of the in-service fatigue performance of the structure.

**TABLE 5: PHANTOM WING FAILURES SERVICE VS TESTS**

SERVICE FAILURE LOCATION		
OUTER WING	UK TEST	US TEST
SKIN AT 35% SPAR ATTACH	YES	NO
SKIN AT 41% SPAR ATTACH	YES	YES
SKIN AT ROOT RIB ATTACH	YES	NO
SKIN AT RIVETED RIB ATTACH	YES	NO
SKIN DRAIN HOLES	YES	NO
SPAR FLANGE (59% SPAR)	YES	NO
REAR SPAR LOCK LUG BORE	YES	NO
REAR SPAR LOCK LUG ROOT RADIUS	YES	YES
CENTRE WING		
WING FOLD RIB #13 LUG BORE	YES	NO
WING FOLD RIB #14 LUG ROOT RAD	YES	NO
BL 132.5 PYLON HOLE	YES	YES
CENTRELINE SPLICE PLATE	YES	NO

### 5.2 GR.Mk.5 Main Airframe Fatigue Test (MAFT) Philosophy

The possibility that undesirable life enhancement effects may be introduced by the "worst-point-in-the-sky" spectrum had been recognized by NAVAIR at the time of the AV-8B test, but the high loads in the "Mean + 3σ" spectrum were considered to occur with sufficient frequency not to produce these effects.

The UK Authorities were clear, though, that a second fatigue test of the structure was necessary to UK requirements and to a RAF normal acceleration spectrum. In 1980, Bae and its subcontractor, MCAIR, began work on the initial proposal for the new fatigue test scheduled to start in June 1985. The test would be carried out at MCAIR St Louis and utilize much of the AV-8B FSDFT hardware.

While work progressed towards the test set up, the MoD became attracted to the idea of postponing the test start date for several years to allow time for in-service loads to be obtained from the early years of operations. This strategy held a further benefit in that more consideration could be given to the clearance route for the CFC structures of the airframe.

It was estimated that a delay in testing of, say, 6 years would require an interim clearance of at least 1500 safe hours to allow RAF operations to proceed without interruption. To this end, a detailed study was undertaken by the RAE(F) to quantify the read-across that might be obtained from USMC flying and the

## AV-8B FSDFT.

Unfortunately, at that stage RAE(F) could underwrite an interim of 1000 safe hours only and the case for a delay in testing was severely undermined. In the light of this constraint, the MoD, RAE(F) and BAe agreed that the test should proceed without waiting for in-service load data. The thorough US development programme for the CFC components was deemed sufficient to qualify the structures in RAF usage and modification of the test loads for this purpose was judged neither desirable or necessary. The test would, therefore, be to traditional UK conditions, namely: realistic loads, a duration equivalent to five times the required safe life and clear metallic components of the airframe only.

Further reappraisal of the test programme led to the transfer of the test from its proposed site in St Louis to the new BAe Structural Test Facility.

### 5.3 Generation of the GR.Mk.5 MAFT Loadings

#### 5.3.1 Normal Acceleration Spectrum

The normal acceleration spectrum was derived from RAF usage data of the Harrier GR.Mk.3 fleet. The RAF had compiled a draft Statement of Operating Intent (SOI), Ref 9, which set out the planned usage of the GR.Mk.5 in terms of 13 sortie profile codes (SPCs). The SPC descriptions in the SOI were compared, according to flying intensity, with the seven SPCs flown by the existing GR.Mk.3 fleet and an approximate read-across table generated. This correlation of SPCs is summarized in Table 6.

**TABLE 6: HARRIER GR.Mk.3 and GR.Mk.5 SPC CORRELATION**

GR.3 SPC	GR.5 EQUIVALENT GROUPING DESCRIPTION	% Usage	
		GR.5	GR.3 <sup>a</sup>
1	A Display	0.5	0.5
2	BCJ Air Test, General Handling, IF	10.5	8.9
3	DM Ferry, VSTOL Practice	3.5	12.3
4	EK LL Nav/Rece or SAP, III-to Navex	30.5	26.9
5	FLH SAP, Tac Recee with bounce, Weapon Training	42.0	28.0
6	I Air Combat Manoeuvring	5.0	21.8
7	G Ultra Low Level Flying	8.0	1.0

The 'g' spectra for each Harrier GR.Mk.3 SPC coupled with the GR.Mk.5 utilizations in Table 6 were used to assemble an overall normal acceleration spectrum for the GR.Mk.5. In contrast to AV-8B, the exceedance values at each 'g' level in the overall spectrum were purely 'mean' values with no allowance for variation in the sample.

It will be seen that approximately 50% of the GR.Mk.5 usage comprised low-level and/or ground attack. This coupled with minor adjustments to the 'g' spectrum to account for predicted performance improvements of the GR.Mk.5 in ground attack and combat, led to the severe normal acceleration spectrum, which is shown in Fig 12 and compared to spectra from related aircraft.

#### 5.3.2 Generation of Manoeuvre Sequence and Loads

As with the AV-8B FSDFT, the MAFT load spectrum was to be a flight-by-flight sequence. Extensive use of the technology developed for the Hawk T.Mk.1 fatigue test was employed in its derivation.

The exceedances in the cumulative normal acceleration spectrum were de-accumulated and the counts sub-divided into component flight profiles. It was known that a typical RAF sortie would consist of climbs, descents, cruise at various heights and an active phase comprising ground attack and/or air combat. For each flight, the 'g' counts were arranged in a sequence according to these phases of the sortie and manoeuvres assigned to each count. The manoeuvre set was an adaptation of those developed for the Hawk T.Mk.1 full scale fatigue test.

A typical manoeuvre sequence is shown in Table 7.

An awareness of the need to formulate a spectrum which would simulate in-service conditions as far as possible directed all stages of the spectrum development process. An example of this philosophy was the retention of a large number of gust loads in the manoeuvre sequence, in spite of damage calculations which indicated they would not cause fatigue problems to the structure.

Once the manoeuvre sequence had been finalized, the major component loading generated by each manoeuvre was determined from flight simulation and loads model data. Again, the degree to which load sequences were idealized for test purposes was guided by the need for a representative spectrum.

**TABLE 7: TYPICAL MAFT MANOEUVRE SEQUENCE**

SORTIE CODE C (QFI Check)

'g' Manoeuvre Type

- Ground Condition
- 2 Atmospheric Gust (Up)
- 0
- 4 Maximum Rate Turn
- 1
- 2 Atmospheric Gust (Up)
- 0
- 5 Tight Turn
- 1
- 3 Loop
- 1
- 3
- 0 Atmospheric Gust (Down)
- 2
- 1
- 4 Roll Off The Top
- 1
- 4 Tight Turn
- 1
- 4 Half Roll and Pull Through
- 1
- 3 Vertical Roll
- 0
- 3
- 1 Atmospheric Gust (Down)
- 3
- 1
- Ground Condition
- Ground Condition
- Ground Condition
- END

In contrast to the fixed, 90% symmetric / 10% asymmetric, randomized load sequence of the AV-8B FSDFT the GR.Mk.5 MAFT loading was based on a full manoeuvre simulation - the majority of manoeuvres having some asymmetric load content.

A summary of the derivation procedure is given in Fig 13

### 5.3.3 Flight Condition

The loads of the GR.Mk.5 MAFT were based on the flight conditions, stores configuration, mid-sortie mass and fuel state shown in Table 8, all of which were representative of average service usage.

**TABLE 8: HARRIER GR.Mk.5 TEST CONDITION**

<u>Configuration</u>		
Aircraft Mass : 21190 lb		
Fuel State : 60% internal fuel		
Fuselage Stores : Guns (no ammo)		
Centre-line pylon		
Wing Stores :		
Inboard pylon + CBLS Mk.3 + 4 x 3 kg bombs		
Outrigger pylon + AIM-9L + LAU-7		
Intermediate pylon		
Outboard pylon		
<u>Flight Conditions</u>		
Mach No.	Altitude	cg
0.65	Sea Level	10.20% MAC
0.85	Sea Level	10.20% MAC

The manoeuvre loads were predominantly based on the 0.65M flight condition. It was found that this condition resulted in a very benign rear fuselage load spectrum and a second test condition at 0.85M was needed to ensure that the tailplane and rear fuselage were more fully exercised by the test.

Fig 12 showed the severity of the GR.Mk.5 normal acceleration spectrum compared to that of other aircraft, including the AV-8B. The picture is somewhat different when the GR.Mk.5 and AV-8B bending moment spectra are compared, Fig 14. The 0.95M point in the sky of the AV-8B results in far more severe wing root bending moment values than the more benign case selected for the GR.Mk.5.

### 5.3.4 Repeated Programme Duration

The length of the repeated test load programme chosen for the GR.Mk.5 MAFT was 25 equivalent flying hours (EFH) - based on Hawk T.Mk.1 experience. This was considered by BAe to be a suitable length for test control and analysis purposes, while being of sufficient duration to restrict the possibility of bias due to the inadvertent introduction of hidden sequence effects. It was considerably shorter than the 1000 hour repeated spectrum chosen for AV-8B testing and some debate took place with RAE(F) on the relative merits of long and short programmes.

It was concluded that long programmes are necessary for transport aircraft where the flight load histories contain distinct load events, but are less important for the complex load histories of combat aircraft.

The shorter programme length of the GR.Mk.5 also reflects a subtle difference in the aims of the UK and US tests. The UK test is used, not only to establish the safe life limit of the airframe, but also to provide a comprehensive basis for the support of the aircraft in-service. Structural modifications and repairs identical to those used in-service are applied to, and lified by, the test. A prolonged test programme complicates read-across to the fleet - fatigue life assessments are more easily accomplished by reference to repetitions of a short programme than by fractions of a lengthy programme. As the emphasis of US testing is more tuned to the quick and early determination of the ultimate safe life, this complication is not as relevant. A long programme may be adopted, thus avoiding the inevitable "rounding" adjustments caused by the use of a short spectrum to represent all in-service flying.

#### 5.4 MAFT Experience

The MAFT was eventually commissioned in May 1990 and has now reached 9500 equivalent flying hours out of the scheduled 30000 equivalent flying hours. There have been a number of incidents on the test which were not presaged by the AV-8B FSDFT findings.

An interesting incident was discovered at 7000 hours when the starboard wing forward attachment fitting failed. Cracking in the aft outboard base of the titanium fitting caused total separation of one of the attachment lugs, Fig 15.

It was readily apparent from a comparison of the fatigue loadings in this region why the fitting remained intact on the AV-8B test, while failure was more likely on the GR.Mk.5 MAFT. The attachment arrangement on the wing rib is shown in Fig 16. The distribution of loadings between the three attachments for the GR.Mk.5 and AV-8B up-bending cases is compared in the table in the lower half of the illustration. Under the AV-8B case the centre and rear attachments are in tension but, due to the aft CP position of WB01, the front is in compression. Since the majority of positive 'g' loadings on the AV-8B FSDFT were derived from this condition, the fitting was subjected to a most benign fatigue spectrum. In contrast, the GR.Mk.5 up-bending load condition placed the joint in tension and so the fitting was exercised more vigorously.

This serves as a reminder that test loads are inevitably idealizations of reality and involve certain compromises. Where the aim is for a "worst" rather than a representative case, there will always be a risk that the over-testing of the major part of the airframe will be accompanied by an undesired side-effect of local under-testing.

#### 5.5 Extent of Clearance Gained from MAFT

The MAFT is the corner-stone to the fatigue clearance of the Harrier GR.Mk.5 but, in common with the AV-8B and all full scale fatigue tests, the extent to which the components of the structure are tested varies.

Among the major airframe components not fully cleared by the MAFT is the tailplane. Unlike the AV-8B FSDFT, a tailplane is fitted to the MAFT - but the loading applied is derived from quasi-steady state manoeuvres only and contains no allowance for vibration loading. This consideration is particularly important to the tailplane which, due in part to the unusual engine thrust configuration of the Harrier, experiences significant vibration loads.

A large proportion of the tailplane is fabricated from CFC material and, in common with other CFC components, this portion of its structure is considered to have an infinite life. A safe life must be obtained, though, for the metal constituents of the structure.

A detailed examination has been made of existing data provided by the development testing of the AV-8B. The differing US requirements have proved a fundamental barrier to read-across of lives from AV-8B testing. Once the results of the AV-8B FSDFT were deemed inappropriate for clearance of the GR.Mk.5, then much of the supplemental testing and calculations, which were also based on the worst-point-in-the-sky tenet, were necessarily unacceptable to the UK Authorities. Only in regions where testing had been extended beyond the "two lifetimes" standard was there any possibility of obtaining a satisfactory read-across.

Another factor which contributed to the difficulties of read-across on the tailplane was the lack of reliable loading spectra for the GR.Mk.5 components. While there was a high degree of confidence that the manoeuvre simulations were accurate, detailed loadings on control surfaces were not known. The lack of such data was a prime reason for delaying the MAFT until such time as in-service loading data could be incorporated into the spectrum. Once a decision had been taken to proceed with the test without delay then the possibility of a more

comprehensive clearance disappeared.

A third problem in read-across calculations, alluded to when discussing the KIDLS approach to design, was the difficulty in choosing an area for fatigue analysis. Full scale fatigue tests are needed because it is so difficult to predict where fatigue cracks may initiate. The results of AV-8B component testing were of no great assistance in this respect as few fatigue failures occurred.

A programme is now in hand to obtain loading data from flight testing and to carry out additional testing of the tailplane and other components not covered by MAFT. The flight test measurements will provide magnitudes of loading for the test but the average occurrences of these loads during RAF operations will have to be estimated. It is expected that in-service data collected from the FMCs (see Section 5.7) will be used to confirm the accuracy of the assumed spectrum.

Time-scales have been somewhat more prolonged than originally supposed and an interim clearance route based on fatigue prediction calculations will be necessary to cover continued flying of the aircraft prior to completion of this additional testing. The uncertainty inherent in life predictions will be reflected in the adoption of conservative safety factors which will lead to low but, it is hoped, acceptable lives.

#### **5.6 Summary of AV-8B and GR.Mk.5 Test Philosophies**

The US test of the airframe was undertaken prior to the aircraft's entry into service with the USMC and early enough to allow modifications to production components in the event of test failures. There was no overriding concern for the representative nature of the test spectrum; it was a randomized sequence, severe in terms of loading and occurrences, intended to highlight fatigue hot-spots early enough to avoid costly in-service modifications.

The GR Mk 5 MAFT philosophy was founded on different principles. Above all, it conformed to UK requirements that emphasize the need to represent as exactly as possible the aircraft's average in-service loading environment. A full five lifetimes of testing is necessary to cover the effects of scatter and ensure an acceptably low risk of in-service failure. This, and a prevailing desire to ensure modifications and repairs are incorporated on the specimen in a precise reflection of in-service practice, act to elongate the real time-scale. It is worth observing that the AV-8B test was complete within 6 months, while the test of a

GR Mk 5 towtrainer, the Harrier T Mk 2, took (for various reasons) 15 years to complete.

Experience to date suggests that the UK approach yields more reliable information about the fatigue performance of the structure in service. Timed, as it was on the GR Mk 5, to start after the aircraft has entered service, it has the significant disadvantage (though of being unable to influence design) of the aircraft before full scale production is well underway. Unstated UK requirements Ref 10 now favour an early pre-production fatigue test to approximate loadings, with a later, more accurate test benefiting from in-service load measurement programmes.

#### **5.7 Fatigue Monitoring In-Service**

Like its sister the AV-8B, the GR Mk 5 is fitted with a software fatigue meter. The benefits of simplicity, convenience and low operating cost obtained by the use of a fatigue meter are undeniable but the system is nevertheless rudimentary. The structure covered is limited and the reliance is placed on administrative procedures to ensure the aircraft's role is correctly interpreted by the fatigue meter formula.

The loss of a RAF Buccaneer in the 1980 triggered the search for a replacement of the 30 year old fatigue meter technology. A contributory cause to that accident was a change in role of the fleet which had undermined the original clearance obtained from the full scale fatigue test. The simple fatigue meter did not alert the operator or designer to the catastrophic implications of these changes.

Acting on advice from the RAFF, the RAF specified a requirement for a device fitted fleet wide to replace the fatigue meter which would automatically and directly provide fatigue monitoring coverage of all major airframe components. Due to the conveniently concurrent time-scales of the system development and aircraft production, the Harrier GR Mk 5 project was chosen as the sponsor for the device.

From the earliest conception of the Fatigue Monitoring and Computing System (FMC) strain gauge technology was considered the optimum basis for the system. In particular, experience from a comprehensive and long established O&M programme, known as SUMS, carried out on the RAF's fleet of Tornados, aircraft had engendered a conviction that strain gauges would provide a more reliable means of measuring service loads than indirect techniques using track load parameters. BAE who were responsible for the installation of the hardware on the GR Mk 5, were tasked to specify

locations for the strain gauges

It was known that the system would be limited to 16 strain gauge channels, so a prime consideration in the selection of candidate locations was the need to measure broad loading actions rather than local loads or strains at hot-spots. This would increase the opportunities for read-across to areas of structure not initially identified as fatigue critical. Quite severe constraints were placed on the number of suitable locations in this respect by the requirement to install gauges on all aircraft. Internal gauging of the wing, for example, could not be effected within the production programme and a full "Skopinski" calibration exercise on each aircraft was impractical. Further factors which influenced the position of gauges were ease of access for repair and, somewhat conflictingly, security from accidental damage.

The general arrangement of the FMCS equipment is shown in Fig 17. The position of the bridge conditioning modules, which are near to strain gauge locations, provide an indication of the structural coverage.

The prime purpose of the FMCS is fleet-wide fatigue monitoring. All processing necessary for this task is carried out onboard the aircraft. Fatigue index values are computed in real-time and transferred after flight to ground-based systems. In most instances further processing of data on the ground will be unnecessary, but where re-analysis is required, sufficient part-processed data are transferred with the FI values to allow validation or retrospective adjustments to be made. In cases where access to raw data is needed, the facility exists to record unprocessed strain gauge signals.

When FMCS enters service it is likely that it will play an important part in the clearance of the major items not covered by the MAFT. General levels of load can be obtained from flight tests, but until a database of in-service frequency of occurrence data is accumulated, clearance will rest on assumed usage. In this quasi-OLM role, FMCS will provide the first comprehensive set of in-service structural usage data ever obtained for any mark of UK Harrier aircraft.

The choice to use strain gauges on FMCS was based on the experience of their use on Tomado, where they have proved reliable, versatile and durable. There are differences in the two systems, though, which lead to certain areas of risk for FMCS. The Tomado SUMS system is fully calibrated, which has allowed many gauges to be placed in areas away from vulnerable attachment positions. Only eight aircraft are instrumented so service personnel are able to take

extra care with these aircraft without adversely affecting overall servicing times. The system itself is maintained by BAE personnel so there has been no need for strain gauge expertise in the RAF. Data generated by the SUMS system are also processed exclusively by BAE.

In these respects FMCS is a different prospect for the RAF. A knowledge and awareness of strain gauge technology is under development and attention is now being paid to the storage and analysis of the vast amount of data that will be generated by FMCS. Ultimately, there is little doubt that FMCS will be the RAF's most powerful fatigue management tool.

## 6. DESIGN AND CLEARANCE AGAINST FATIGUE - HARRIER T.Mk.10

The RAF operated a number of two-seat Harrier variants alongside the Harrier GR.Mk.3 aircraft in a demanding dual fighter/trainer role. Keen to maintain this operational format, the RAF has ordered 13 T.Mk.10 two-seat derivatives of the Harrier GR.Mk.5.

There is a high degree of commonality between the T.Mk.10 and the GR.Mk.5, but this procurement differs in that the new structure of the T.Mk.10 has been designed to UK requirements. A direct purchase "off-the-shelf" of the USMC AV-8B trainer, the TAV-8B was precluded by the significantly more exacting role specified for the T.Mk.10. The rear fuselage, in particular, has been strengthened in response to GR.Mk.5 MAFT results and instances in-service of acoustic fatigue damage.

A full scale fatigue test of the T.Mk.10 was deemed unnecessary due to the broad commonality of structure with the GR.Mk.5. The most extensively changed structure is the front fuselage which is fabricated largely from CFC material and has been judged cleared by element testing carried out for the TAV-8B aircraft. The remainder of the metallic structure has been cleared by BAE using Neuber based KUDS calculations incorporating fatigue life factors of five for areas shared with the GR.Mk.5 aircraft and 10 for new, enhanced structure.

## 7. CONCLUSIONS

Whatever fatigue analysis and test techniques are adopted in the design and clearance of metallic structures, an underlying consciousness must be retained of the impossibility of accurate fatigue life prediction. Modern stress analysis techniques have

removed some areas of uncertainty which had previously rendered many fatigue calculations worthless, but scatter in fatigue performance can not be eliminated.

The introduction of stressing procedures which incorporate allowable fatigue stresses has provided an excellent means of promoting a general recognition amongst stress engineers of the threat metal fatigue poses to structural integrity. But the principle adopted by HSA in the original design of the Harrier that high stress concentrations should be avoided rather than sanctioned by calculation must remain a priority in aircraft design.

The experience from the early days of the Harrier through to AV-8B and GR.Mk.5 has shown the overriding importance to successful fatigue resistant designs of experience gained from forerunners, prototypes and full scale fatigue testing. For the foreseeable future, testing will be invaluable in locating those areas of the structure which are prone to fatigue cracking. Experience has shown that fatigue problems are fickle and defy designers attempts to anticipate them.

The nature of test loadings and the duration of the test are areas where US and UK philosophies diverge. However, it is not unreasonable to regard the AV-8B and GR.Mk.5 tests as complementary parts of an overall programme which has yielded benefits for the USMC and the RAF. Depending on the objective of the test each approach has its merits. A short, sharp test is useful at the early design stage to highlight particularly poor design features which should be deleted before production is underway. A more prolonged test, where every attention is paid to the simulation of actual operations, is essential if reliable indications are needed of likely fatigue problems in-service.

An area where US and UK authorities agree is the treatment of CFC components. CFC materials exhibit a larger variability in mechanical properties than metals and are more susceptible to adverse environmental conditions. For these reasons a full scale fatigue test of the airframe is not a viable clearance route for CFC structures. Qualification is achieved incrementally through testing of progressively more complex elements and substructures. Routine inspection of the CFC structure in-service provides additional assurance that structural integrity is not compromised by this concession.

There is also general recognition that the fatigue meter is no longer able to monitor fatigue usage on

modern, highly manoeuvrable combat aircraft. There is no firm consensus, though, on the most suitable means of broadening the fatigue monitoring envelope. The UK Authorities strongly believe strain gauges are essential to establishing the accurate loading histories on major airframe components, while others consider that load predictor equations are satisfactory. But there is no doubt that either option will reduce the penalty incurred by the continued use of the fatigue meter - whether it be unnecessarily massive structure or reduced operational safety.

## 8. REFERENCES

1. Design Requirements for Service Aircraft AvP 970.
2. Heywood RB. "Correlated Fatigue Data for Aircraft Structural Joints." RAE Report No. Structures 184, June 1955.
3. Heywood RB. "Designing Against Fatigue." Chapman and Hall Ltd. 1962.
4. Detail Specification for the Design of Full Scale Development Model AV-8B Aircraft. SD-563-3-1
5. Contract Engineering Data and Test Requirements for Model AV-8B Aircraft Weapons System. Addendum 484 to MIL-D-8706B(AS).
6. Airplane Strength and Rigidity Requirements, Repeated Loads and Fatigue. MIL-A-8866(AG) May 1966.
7. Neuber H. "Theory of Stress Concentration for Shear-Strained Prismatic Bodies with Arbitrary Nonlinear Stress Strain Laws." Journal of Applied Mechanics Dec 1961.
8. Riley BL. "AV-8B/GR Mk 5 Airframe Composite Applications." Twenty-second John Player Lecture 1 Mech E Proceedings Vol 200 No 50 1986.
9. Harrier GR.Mk.5: Draft Statement of Operating Intent. D/DD OR4(RAF) 13/5: 7 14 April 1982.
10. Design and Airworthiness Requirements for Service Aircraft, Vol 1 - Aeroplanes. Defence Standard 00-970.

**9. ABBREVIATIONS**

B Ae	British Aerospace
CFC	Carbon Fibre Composite
DLS	Design Limit Stress
DLL	Design Limit Load
FI	Fatigue Index. A non-dimensional number which, via damage calculation, is used to quantify severity of loading relative to a defined datum (normally a full scale fatigue test spectrum).
FMCS	Fatigue Monitoring and Computing System
FSDFT	Full Scale Development Fatigue Test
HSA	Hawker Siddeley Aviation
K <sub>t</sub>	Geometric Stress Concentration Factor
MAFT	Main Airframe Fatigue Test (GR.Mk.5)
MCAIR	McDonnell Aircraft Company
OLM	Operational Loads Measurement
RAE(F)	Royal Aircraft, later Aerospace, Establishment (Farnborough)
RAF	Royal Air Force
S-N	Stress-Endurance
SOI	Statement of Operating Intent
SUMS	Structural Usage Monitoring System
USMC	United States Marine Corps

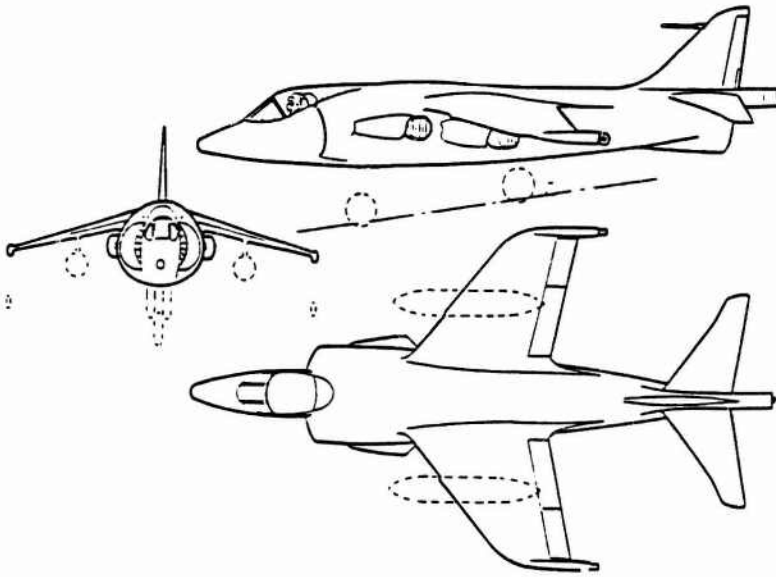


Figure 1. The Hawker Siddeley Kestrel

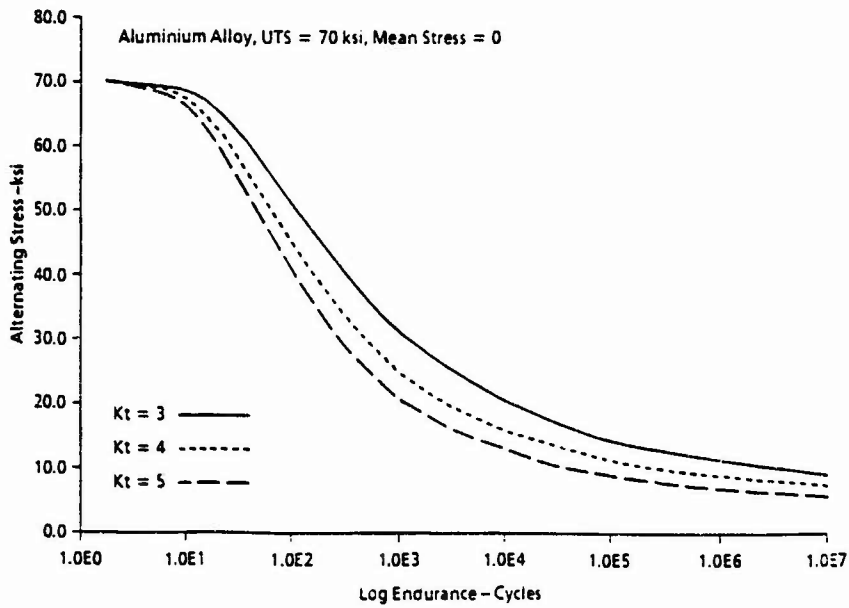


Figure 2. Heywood's Generalized S-N Equations  
Effects of Varying Kt

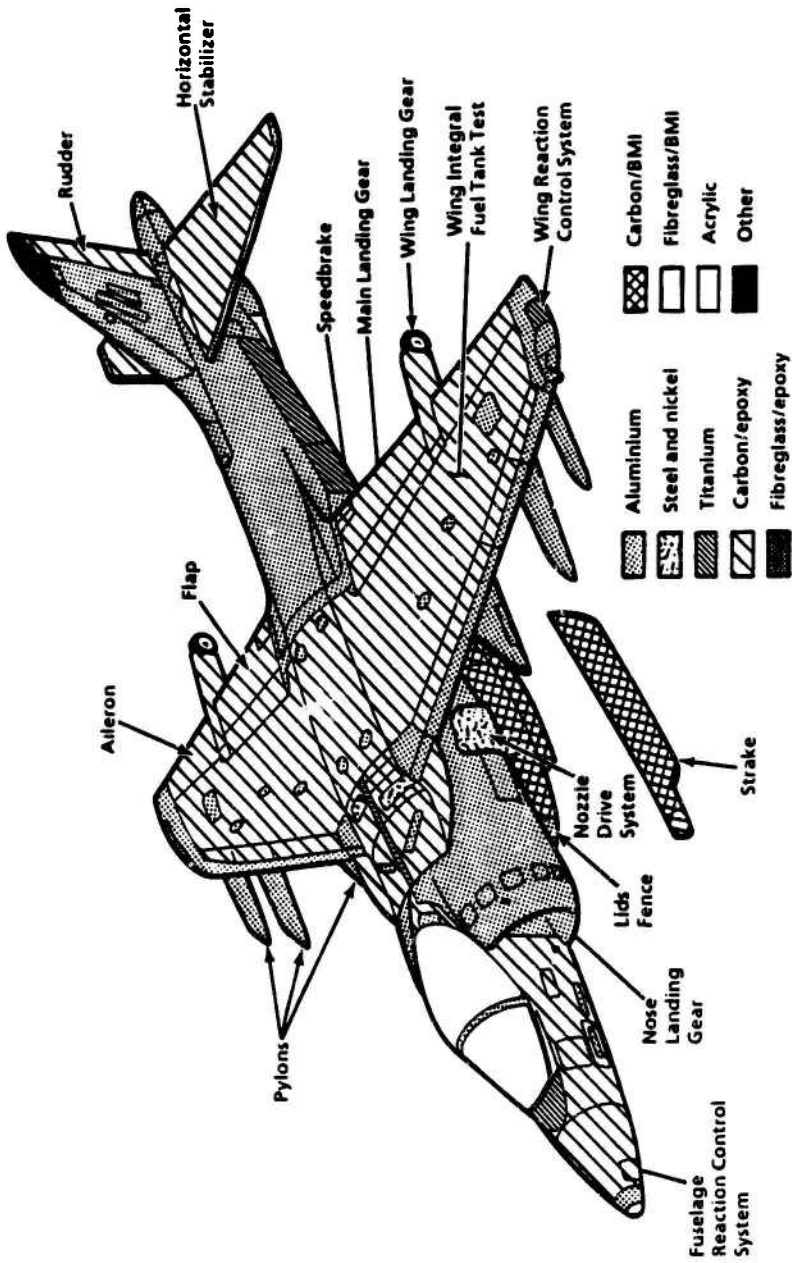


Figure 3. AV-8B Material Usage and Component Fatigue Tests

Fatigue Design Condition  
Maximum Positive Wing Bending Moment

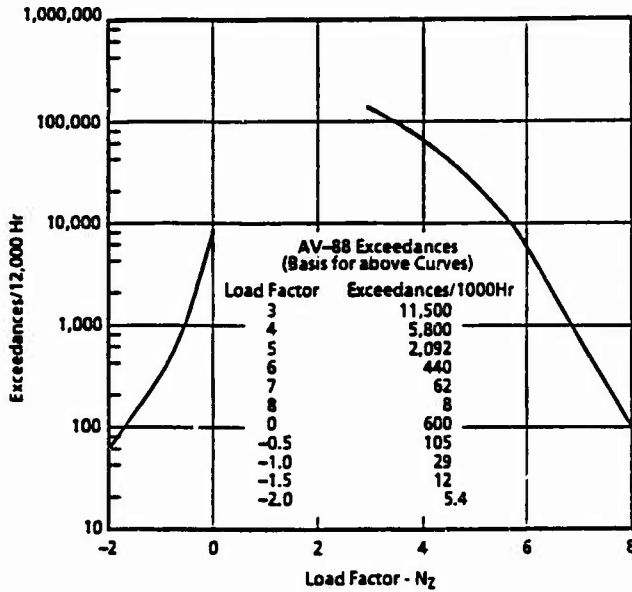


Figure 4. AV-8B Normal Acceleration Spectrum

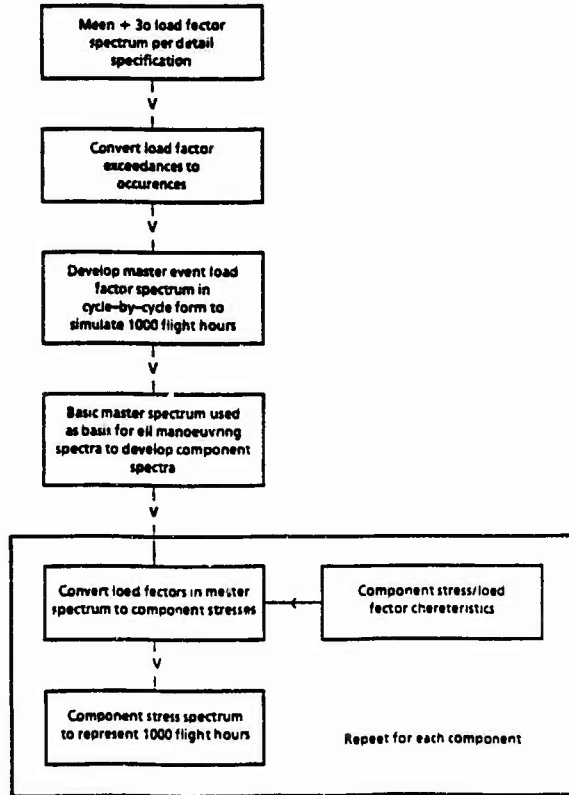


Figure 5. AV-8B Component Fatigue Spectrum Development

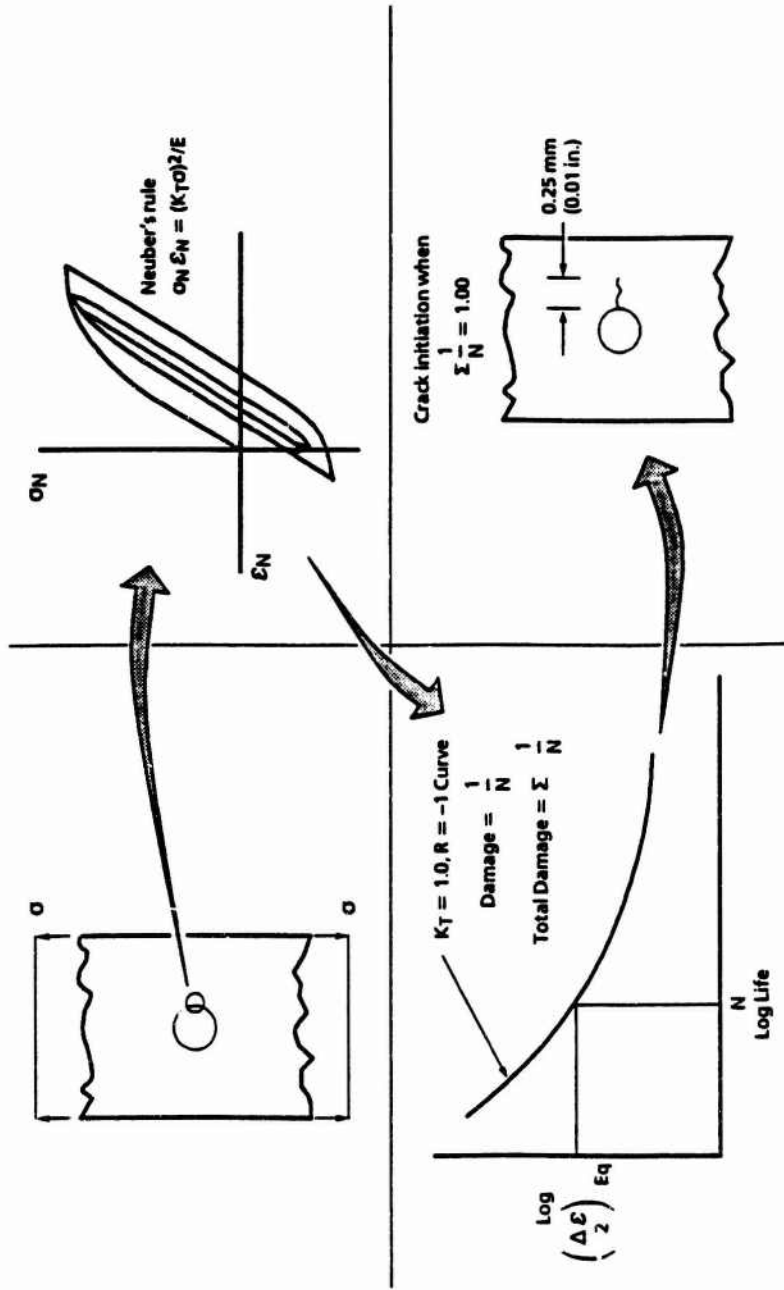
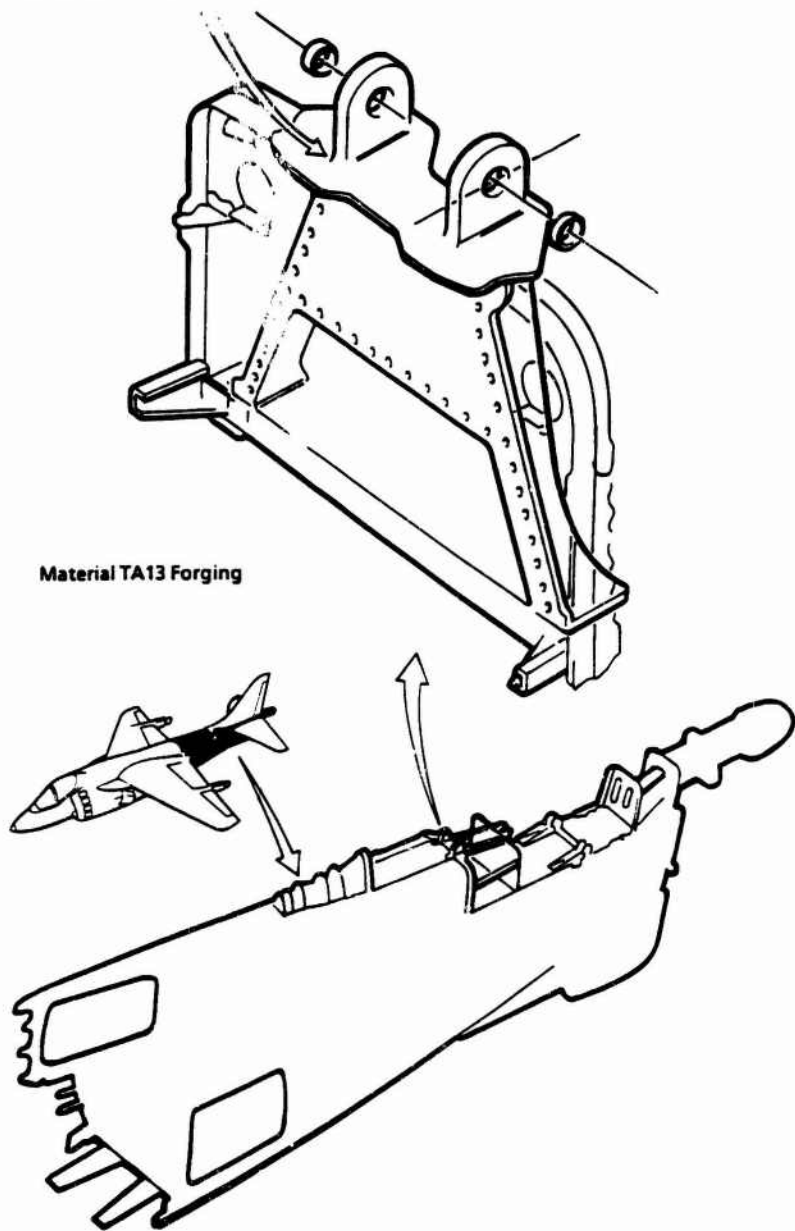


Figure 6. AV-8B Local Strain Analysis Procedure

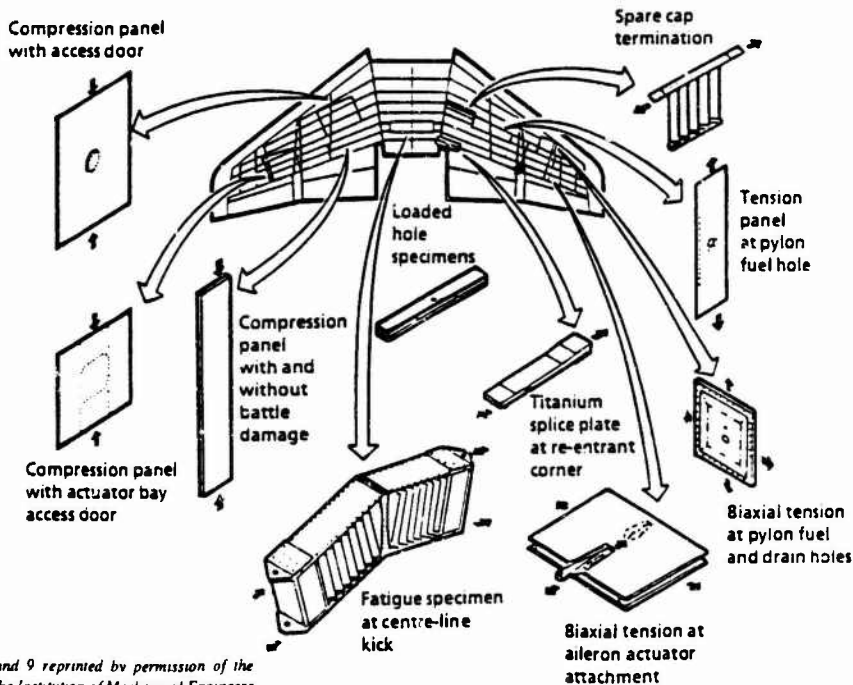
**Complete Separation of Port Attachment lug  
at .20/.25 inch Root Radius**



**Figure 7. AV-8B Forward Fir Fitting**

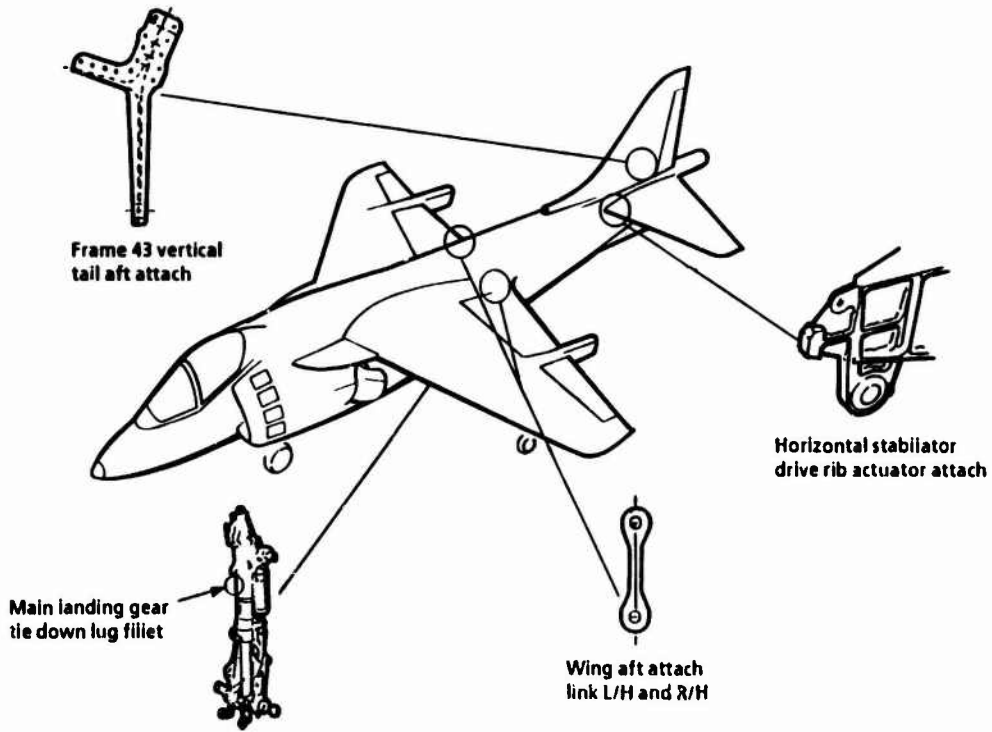
1974 1975	Preliminary Design	
1975  ↑ to ↓ 1977	Design allowables	
	Joints	
	Skins	
	Substructure	
	Box beams	
1977	Operational hazards	
1978	Static wing YAV-8B flight demo	
1980 1981	FSD static airframe	
1981 1982	FSD fatigue airframe	
1984 on	Production deliveries	

Figure 8. AV-8B Composite Wing Development Programme



Figures 8 and 9 reprinted by permission of the Council of the Institution of Mechanical Engineers from I Mech E Proceedings 1986 Vol 200 No 50.

Figure 9. AV-8B Skin Test Specimens



**Figure 10. AV-8B Improved Fatigue Tracking System  
-Structural Control Points**

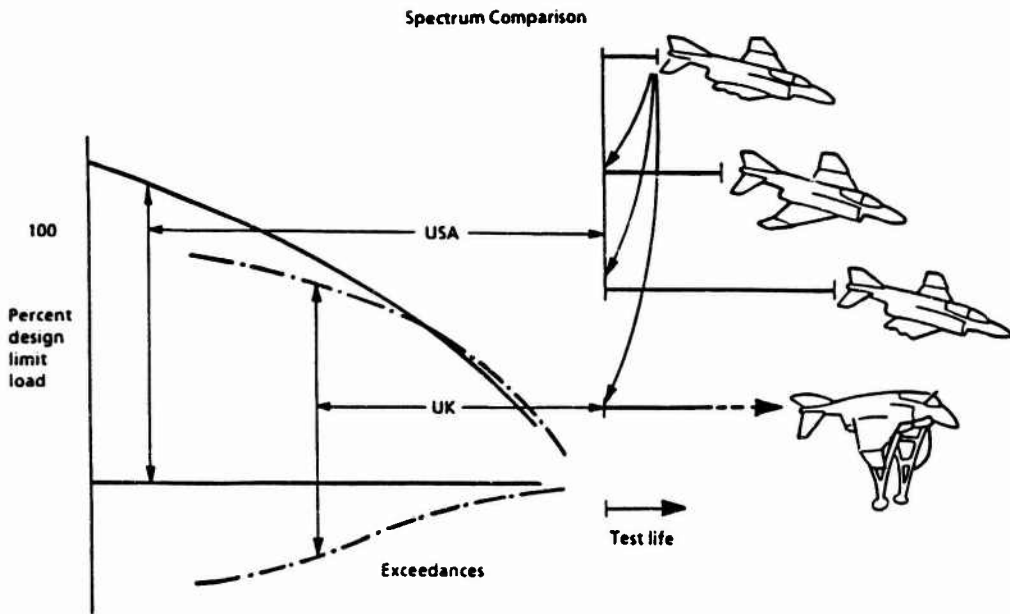


Figure 11. Phantom Comparison of US and UK Normal Acceleration Spectra

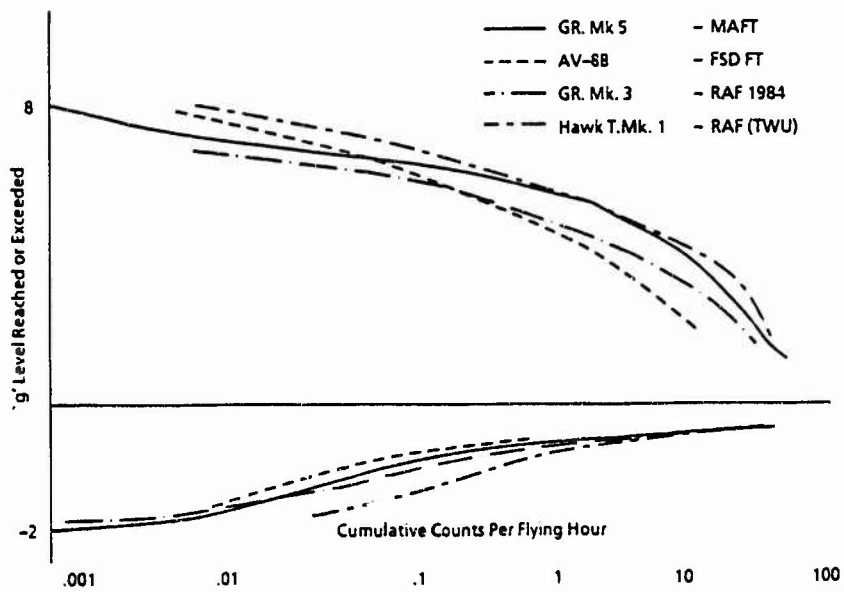


Figure 12. Harrier GR. Mk. 5 Normal Acceleration Spectrum and Comparison With Other Spectra

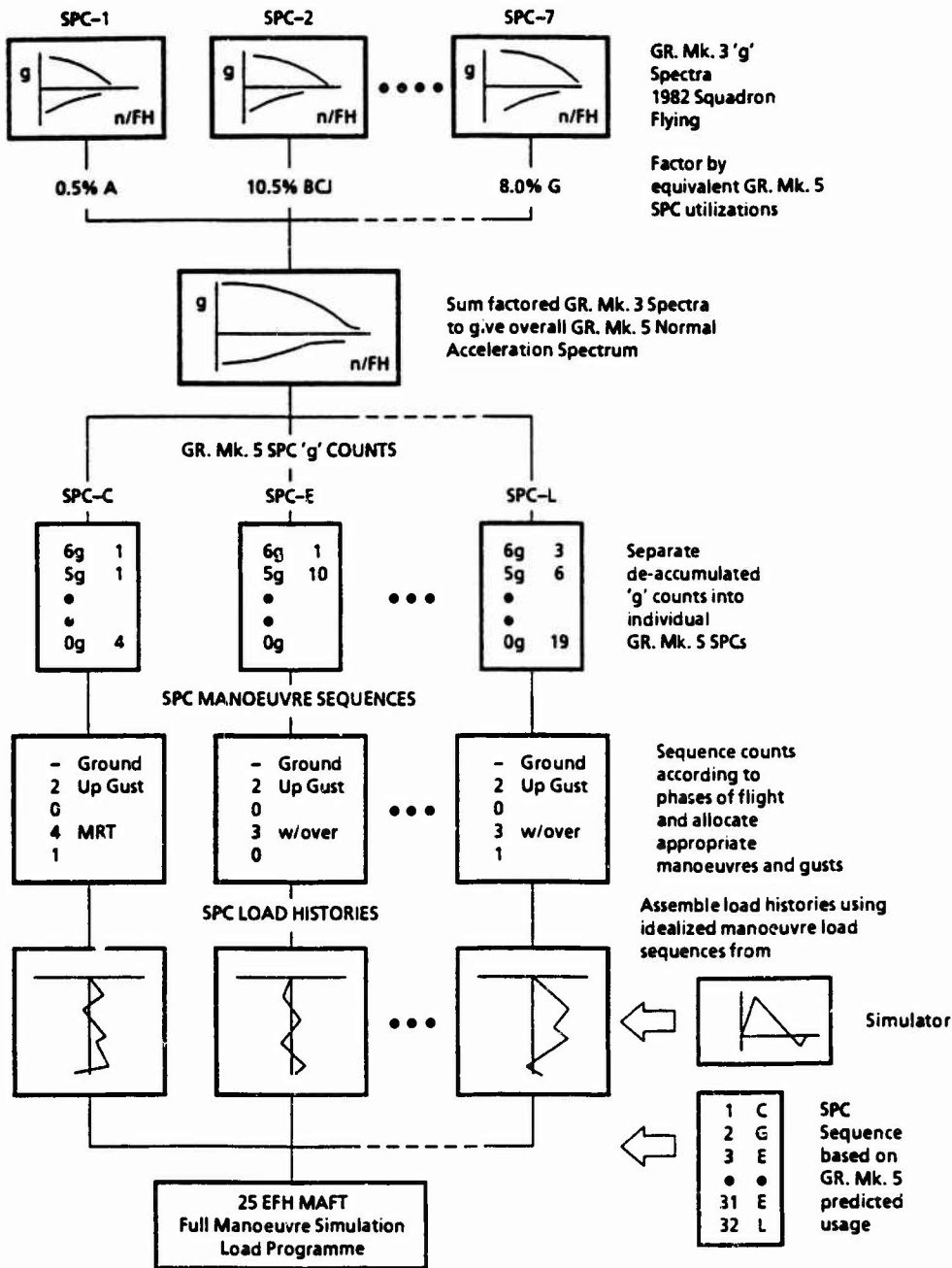


Figure 13. GR. Mk. 5 - Derivation of MAFT Loading Spectrum

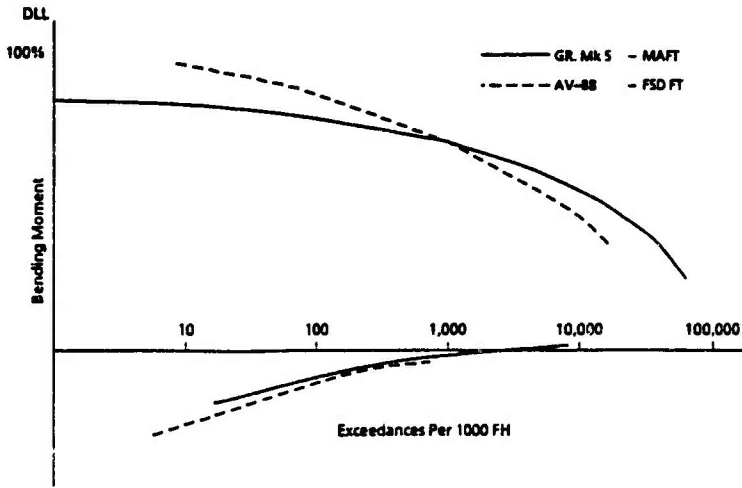


Figure 14. Comparison of GR. Mk. 5 and AV-8B Wing Root Bending Moment Spectra

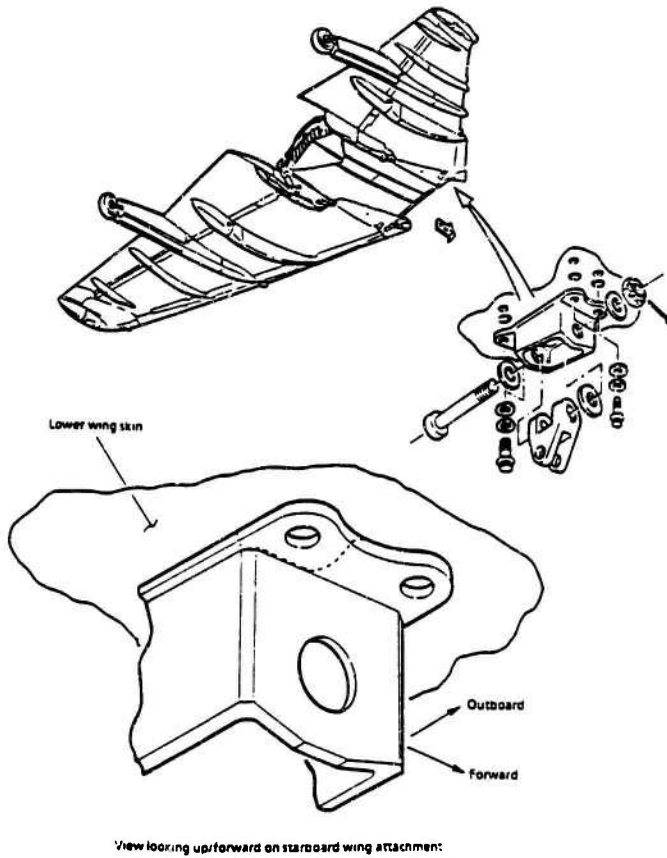
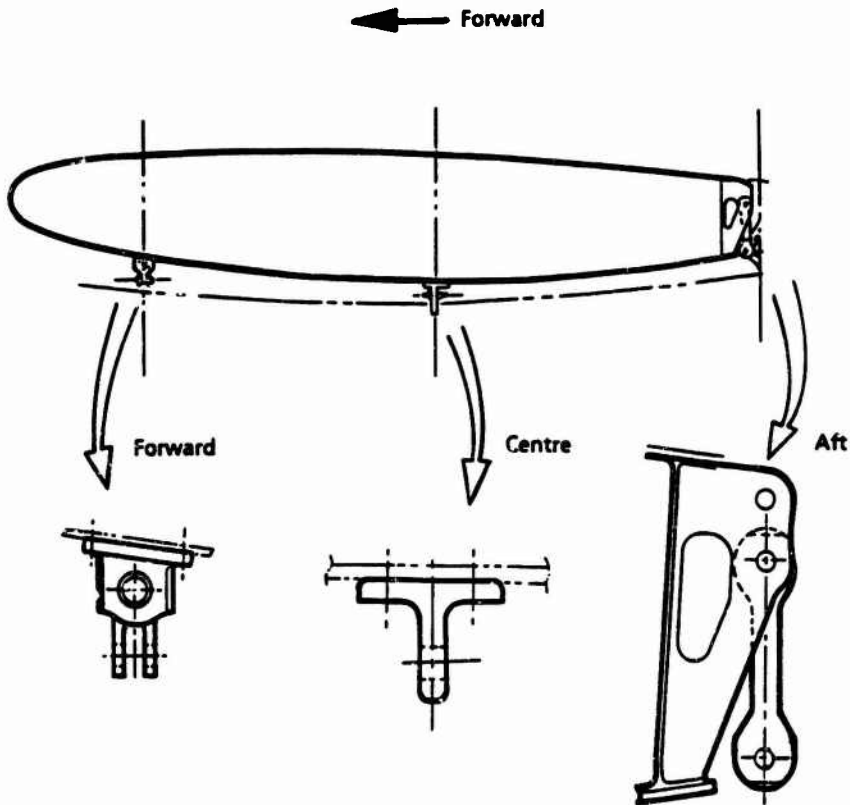


Figure 15. GR. Mk. 5 MAFT Cracking of forward Wing Attachment Fitting



Wing attachment reaction (per side)  
Expressed as percentages of GR. Mk. 5 MAFT loading

Up Bending Case	FORWARD (Fr 19A)	CENTRE (Fr 23)	AFT (Fr 29)
GR. Mk. 5 MAFT	10%	19%	21%
AV-8B WB01	-1%	31%	42%

Figure 16. AV-8B/GR. Mk. 5 Wing Attachment Rib

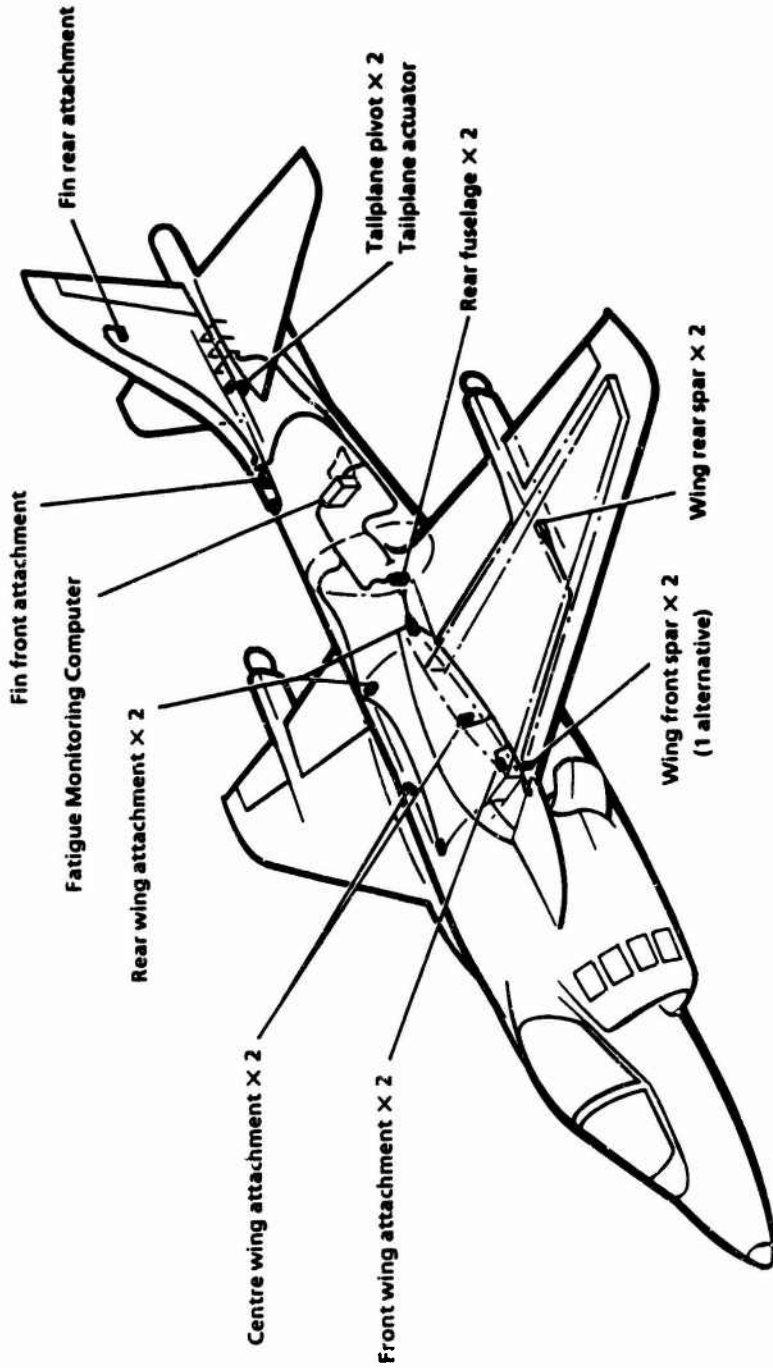


Figure 17. GR. Mk. 5 FMCS General Arrangement



## FATIGUE DESIGN, TEST AND IN-SERVICE EXPERIENCE OF THE BAe HAWK

John O'Hara  
Structures Unit  
British Aerospace Defence Ltd.,  
Brough, North Humberside HU15 1EQ  
United Kingdom

### SYNOPSIS

The BAe Hawk family is designed primarily to UK regulations, including the safe life S-N fatigue philosophy. S-N data pertinent to key structural features was assembled at the design stage, and fatigue coupon / element tests were conducted in confirmation. The Hawk TMk.1 Full Scale Fatigue Test (FSFT) has continued to lead the RAF fleet, and the test loading has been validated by a major Operational Loads Measurement (OLM) exercise. Incidents arising on the FSFT or in-service are handled by several approaches including S-N and fracture mechanics calculations, testing, statistical analysis, and modifications and / or routine inspections are introduced when necessary. The development of the fatigue life clearances of the BAe Hawk family is discussed with particular emphasis on the confirmatory testing and in-service loads measurement necessary to ensure and maintain fleet aircraft fatigue life clearance.

### 1. INTRODUCTION

The current new derivatives of Hawk are developments of a successfully established aircraft, the Hawk TMk.1. Developments in engine, airframe, and avionics technology have enabled the design to progressively meet market and customer requirements for ever greater capability, reliability, and low maintenance costs. The design has evolved to include a naval version with carrier capability, together with operationally capable single seat and twin seat variants. The structural problems posed encompassed both the static and fatigue/fracture aspects, often leading to the need for extensive analysis and confirmatory test programmes. The Hawk Full Scale Fatigue Test (FSFT) has to date proved successful in identifying areas requiring modification and/or routine inspection, and it is noteworthy that no Hawk aircraft has been lost due to structural failure. Validation of the FSFT loading spectrum was obtained from the Hawk TMk.1 Operational Loads Measurement programme which comprised more than 400 flights covering the range of aircraft utilisation. This paper discusses the treatment of the fatigue life clearance of the Hawk TMk.1, by calculation, test, modification, inspection, and monitoring. The fatigue clearance of the naval T-45 Goshawk, designed to Mil Spec regulations and presenting different structural challenges, is also discussed.

### 2. HAWK T-Mk.1 DESIGN REQUIREMENTS

Specification 281 D&P was issued by the Controller for Aircraft in March 1972, and was strongly based on the requirements of (1). It called for a new tandem seated jet to cover the course of training between basic and OCU (operational conversion unit) stages, encompassing general handling, instrument flying, navigation, formation flying and weapons training.

Emphasis was placed upon the need for low operating costs and high reliability, and this was reflected by the stringent fatigue requirement for the primary structure of 6000 flying hours, factor 5, to the spectra of Figure 1, with a design aim that this be inspection free. Furthermore, it was specified that all aircraft equipment should comply with the vibration requirements of (2).

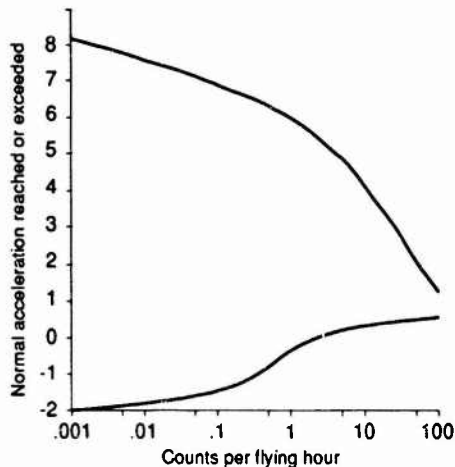


Figure 1a  
Hawk T-Mk.1 Normal Acceleration Design Spectrum

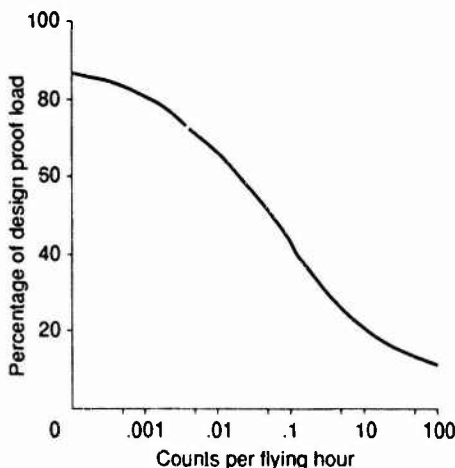


Figure 1b  
Hawk T-Mk.1 Fin Fatigue Load Design Spectrum

### 3. HAWK T-Mk.1 DESIGN PROCEDURE

The structural analysis of Hawk followed rules and employed methodologies which are current today, of note was the early use of finite element modelling in the form of the force method.

Fatigue was an important consideration in the structural design and special attention was paid to the selection of materials possessing good resistance to crack initiation, stress corrosion and crack growth. Titanium interference-fit fasteners were specified in key wing and fin areas, particularly skin to spar connections, and the one piece integrally machined wing skins minimised the number of possible crack initiation locations. Furthermore, the low wing configuration placed the wing to fuselage attachment links principally in compression during flight, thus conferring good fatigue resistance.

Fatigue analyses were based on traditional Miners S-N methodology, combined with elastically calculated bolt load distributions where appropriate. Design spectra, including those of Figure 1, were derived from detailed data and operating experience on RAF Gnat, Hunter and Harrier aircraft, covering the planned RAF Hawk training schedule ranging from general handling and low level navigation exercises to advanced weapons training and air combat practice. Fatigue element and coupon tests were commissioned to confirm the fatigue design of key structural features such as the wing centre line joint, Figure 2, including assessment of life sensitivity to possible build tolerances and the effect of interleaf.

Vibration analyses were performed to the Category 4 levels of (2), which were reflected in all pertinent aircraft equipment procurement specifications.

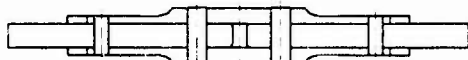


Fig. 2 - Wing Centre Line Joint Fatigue Test Specimen commissioned during the design stage

### 4. TEST CONFIRMATION OF HAWK T-Mk.1 DESIGN

Static strength testing of the airframe was performed on a T-Mk.1 aircraft structure, with the tailplane and aileron tested separately. Figure 3 shows the test wing and fuselage at the preparation stage prior to assembly. Note the fitment of load pads to enable load application via hydraulic jacks and winch trees. Over 700 strain gauges were fitted to the test article to enable maximum information to be derived, including comparison of theory with practice and assessment of variation in structural response with load level. In general, the test article demonstrated more than adequate static strength, indicating substantial scope for future growth.

The T-Mk.1 Full Scale Fatigue Test (FSFT) indicated that the design was sufficient to meet the design requirements, whilst suggesting that fatigue enhancement of the wing was necessary to provide scope for significant service life extension, and for the mass growth that would ensue from uprating the aircraft's capability. Figure 4 shows the installation of the FSFT for the naval Hawk version, the

T-45A Goshawk, in the Brough Structural Test Facility. The Hawk T-Mk.1 FSFT configuration is along similar lines.

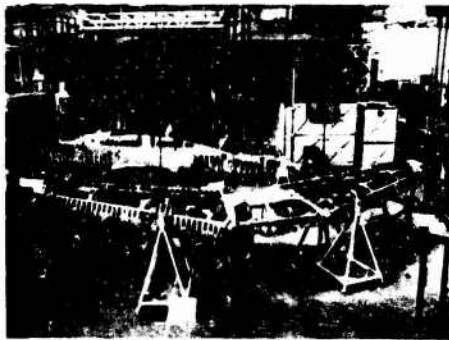


Fig.3 - Hawk T-Mk.1 Static Strength Article prior to assembly and test, at British Aerospace, Kingston

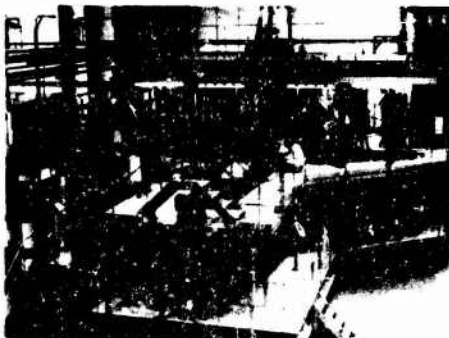


Fig.4 - Installation of Goshawk full scale fatigue test article, at British Aerospace, Brough

### 5. HAWK T-Mk.1 VIBRATION OLM PROGRAMME

Thirty-four accelerometers were fitted to the first production Hawk, XX154, see Figure 5. Recordings were taken over a twelve flight programme, and power spectral densities derived for particular flight conditions at different structural locations for a variety of aircraft configurations, see Figure 6. This work led to the construction of equipment procurement vibration spectra for different zones of the aircraft, and these are still in use today.

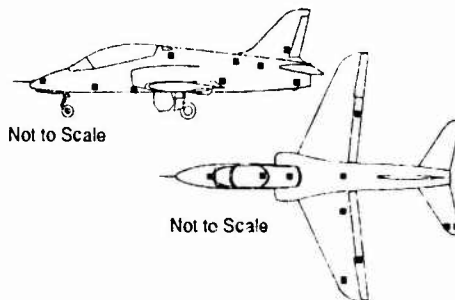


Fig.5 - Views showing the accelerometer locations for the vibration trials aircraft

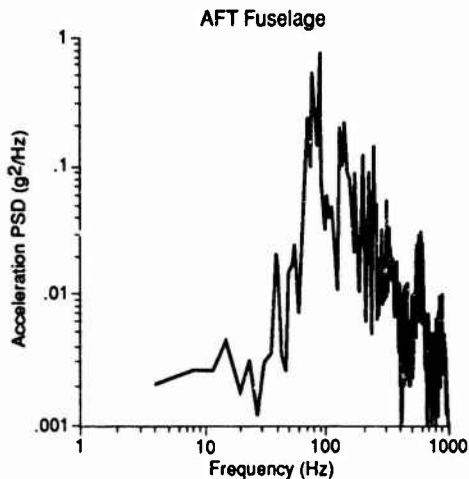


Fig.6a - Hawk Vertical Vibration PSD during turn into Buffet  
Note: Window 4Hz

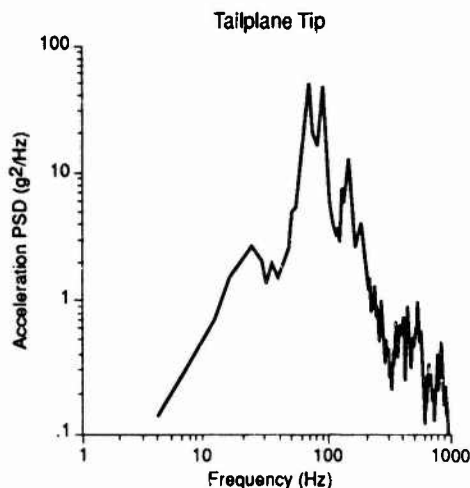


Fig.6a - Hawk Vertical Vibration PSD during turn into Buffet  
Note: Window 4Hz

## 6. HAWK TMk.1 OPERATIONAL LOAD MEASUREMENT

The TMk.1 OLM programme was one of several, including Tornado, Jaguar and Buccaneer, to be commissioned by the UK Ministry of Defence in the early 1980's. The principal aims were :-

- to compare the Hawk TMk.1 FSFT loading with in-service loading at specified structural locations, including confirmation of the efficacy of the wing fatigue meter formula.
- to identify particularly damaging flight regimes.

## 6.1 OLM Instrumentation

The programme employed two instrumented aircraft and encompassed more than 400 flights covering the range of Hawk TMk.1 utilisation. A Plessey Structural Usage Monitoring System (SUMS) was installed in each aircraft, recording 14 strain gauge bridge outputs (see Figure 7) and 16 aircraft parameters (see Table 1) on one C90 cassette tape. Flight durations are typically one hour, and the following measures were introduced to maximise the amount of useful recorded data :-

- the recording system start-up was delayed until selection of 95% throttle angle setting, as opposed to engine switch-on, to minimise pre-flight expenditure of recording time, which was limited to 67.5 minutes at full sampling rates.
- a data compression facility was incorporated, with the SUMS equipment automatically selecting either fast or slow recording rates dependent on flight conditions. A low sampling rate (data compression) was used for those parts of a flight which result in structurally insignificant conditions. The decision to switch from the full recording rates of Table 1 occurred when relevant trigger parameters fell below preset threshold values.

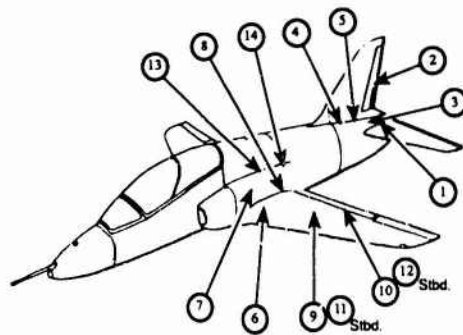


Fig.7 - Hawk OLM Strain Gauge Locations  
Refer to Table 1 for details

The strain gauges of Figure 7 were located as for the Hawk TMk.1 FSFT to provide readacross and to facilitate meeting the two principal aims 6(a) and 6(b) above. The low stress gradient nature of the gauge locations, together with the good accuracy of properly installed modern day strain gauges, the checks provided by two identically gauged aircraft, and consideration of cost led to the decision not to load calibrate the OLM aircraft. This decision proved, in the main, to be reasonable. However, the collection and analysis of a very large body of data often involves dealing with surprising or conflicting information, which only strain gauge load calibration may be able to resolve. One of the conclusions of the programme was that load calibration should be included in future OLM exercises.

Symbol	Location / Parameter	Sampling Rate
S01	Tailplane Port Top Skin	32
S02	Tailplane Starboard Top Skin	16
S03	Tailplane Jack Hor	16
S04	Fin Front Spar Root	16
S05	Fin Rear Spar Root	16
S06	Port Wing Auxillary Spar , Web	8
S07	Port Wing Front Spar , Rib 1-2	8
S08	Port Wing Rear Spar , Rib 1-2	8
S09	Port Wing Front Spar , Rib 7	16
S10	Port Wing Rear Spar , Rib 8-9	8
S11	Starboard Wing Front Spar , Rib 7-8	8
S12	Starboard Wing Rear Spar , Rib 8-9	8
S13	Top Longeron Port , Frame 12-14	8
S14	Top Longeron Port , Frame 20-21	8
S15	Fin Front Spar Root - Reversed	-
S16	Fin Rear Spar Root - Reversed	-
S17	Tailplane Hinge Port	-
S18	Tailplane Hinge Starboard	-
NAC	• Normal Acceleration	8
IAS	• Indicated Airspeed	2
AL1	• Pressure Altitude	4
LAC	• Lateral Acceleration	8
TPA	• Tailplane Angle	8
AAP	• Aileron Angle - Port	8
AAS	• Aileron Angle - Starboard	8
RUD	• Rudder Angle	8
FLA	• Flap Angle	8
P6	• P6	8
THA	• Throttle Angle	8
VAS	• Vertical Acceleration - Starboard Wing	8
CWP	Central Warning Panel	1
UND	Undercarriage Down	1
ABP	Airbrake Position	1
UNU	Undercarriage Up	1

- Notes:-
1. Sampling rates are quoted in samples per frame. The SUMS equipment records at 2 frames per second.
  2. The sampling rates given apply when the SUMS equipment is operating in uncompressed mode.
  3. Gauges S15, S16, S17 and S18 are strain gauge outputs derived from other strain gauges.
  4. \* - Parameter which is part of the standard ADR system.

Table 1 - Hawk OLM Measurement Details

## 6.2 Analysis Procedure

Comparison of in-service fatigue loading with that of the FSFT was performed using S-N damage calculations at each of the strain gauge locations. Mean S-N curves were selected to represent the structural feature monitored most closely by each strain gauge on the basis of shape, such as high or low load transfer. They were set to predict either actual FSFT arisings, or imaginary incidents upon the application of the next FSFT loading cycle, using rainflowed strain histories.

On completion of each OLM flight, the C90 cassette was despatched to BAe Brough together with the appropriate MoD form 725 giving details of mission type, aircraft configuration, take-off and landing weights together with fatigue meter readings. The cassette was replayed and copied to disk, and a quick look chart containing a plotted time history of each strain gauge and aircraft parameter produced. A portion of a typical quick look chart is shown in Figure 8. Corrupt data, including spikes and dropouts, were removed,

and each strain gauge history rainflowed prior to dedicated S-N analysis. The use of S-N curves fitted to FSFT performance, as discussed above, enabled direct comparison of in-service and FSFT damage rates, thus providing confirmation of the fleet clearance conferred by the FSFT.

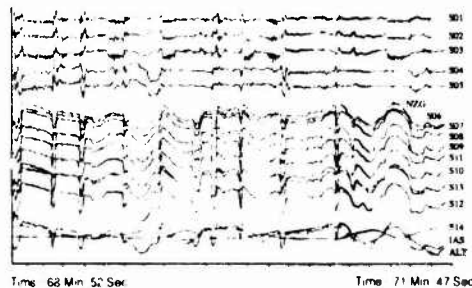


Fig 8 - Segment of Hawk OLM quick look chart

Fatigue monitoring of in-service Hawk TMk.1 wings is provided by a fatigue meter, which cumulatively records exceedances of discrete normal acceleration levels, and is located close to the centre of gravity of the aircraft. Figure 9 indicates the variation of incremental bending moment with wing span location, due to rolling during asymmetric manoeuvres, leading to the lowering of the allowable wing fatigue stress in the outboard direction when the flight spectrum is not solely symmetric.

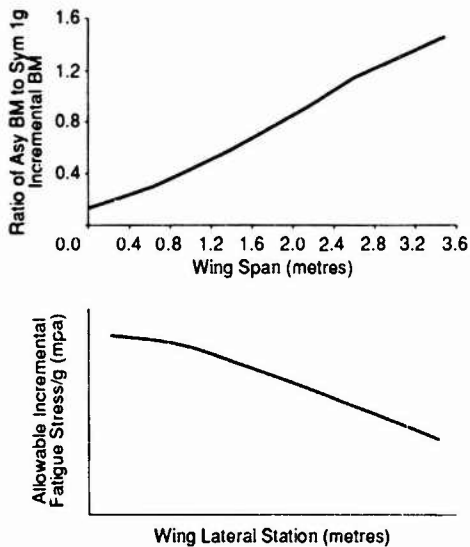


Fig.9 - Effect of Wing Spectrum Asymmetric Content

Therefore, since the fatigue meter records only the symmetric acceleration component,  $N_z$ , of any particular manoeuvre, it was important to establish that the fatigue damage rates per F.I. (wing fatigue accrualment is measured by the fatigue meter in terms of Fatigue Index units), calculated for each of the FSFT wing strain gauge histories, were at least as great as those inferred from the OLM strain gauge measurements.

### 6.3 Analysis Results

The analysis concluded that the fatigue meter was in fact adequately monitoring the aircraft, inferring sufficient asymmetric manoeuvre content for the FSFT loading spectrum.

The analysis also showed that the FSFT fin loading adequately covered the most damaging normal service usage, again supporting the degree of asymmetric content within the FSFT loading spectrum.

The position regarding the fuselage and tailplane was less clear cut. Inspection of tailplane strain gauge flight traces showed significant vibration activity during certain mission types, which was surprising in view of the length of time the TMk.1 had been in service bearing in mind it had not been reported by any aircrew. Analysis highlighted three main vibration modes and calculation indicated that such loading, whilst not particularly damaging in real terms, substantially undermined the then achieved FSFT tailplane clearance. A

special empennage OLM vibration trial was commissioned, employing much higher digital recording rates as well as analogue measurements to ensure that the vibration mechanism was properly understood. Figure 10 illustrates the problem of selecting digital sampling rates for strain gauges in vibration environments, highlighting the possibly serious underestimation of strain magnitudes produced by slow sampling rates. The results of this special programme formed the basis of the Interim FSFT which brought the clearance of both tailplane and fuselage up to that of the fin and wing without incident, as predicted by calculation.

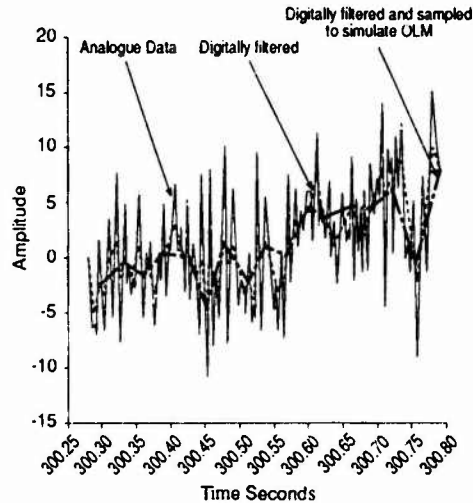


Fig.10 - Comparison of OLM & Analogue Derived Response to Buffet

In general, substantial scatter was observed between damage rates calculated from notionally similar flights. This scatter was evident over the full range of mission types, justifying the large number of 400 successful flights specified at the outset of the programme.

It is likely that the scatter within specific mission types arose principally from two main sources :-

- naturally occurring differences between similar flights.
- insufficiently precise mission labelling.

Mission identifiers, known as Sortie Pattern Codes (SPC), may each encompass variations of one particular flight type, and, bearing in mind the marked sensitivity of calculated fatigue damage to changes in load levels and utilisation profile, one may deduce that b) above may contribute significantly to the total scatter. Possibly, greater focus of mission descriptions would reduce such uncertainty.

### 7. POST OLM ANALYSIS

Following the successful conclusion of the Hawk TMk.1 OLM programme, attention was focused on the unmonitored structure, which attracts an additional life factor of 1.5 compared with structure monitored by the fatigue meter, (3). Since fatigue damage accrualment varies markedly with

utilisation, and given the large body of data covering key structure over the full range of TMk.1 utilisation, analyses were conducted to establish whether monitoring of the wing only was adequate. These analyses showed that the usual additional unmonitored factor of 1.5 was adequate for the tailplane and fuselage where stress levels were sufficiently low. However, it was considered prudent to introduce passive monitoring of the TMk.1 fin, using OLM derived damage coefficients for each SPC, to cater for those fin structures which might be subject to utilisation spectra markedly departing from the design spectrum. Consequently, a SPC dependent fatigue damage formula has been issued for in-service Hawk TMk.1 fins.

Current MoD policy is moving towards retention of the 1.5 additional factor in cases where an OLM programme has been conducted and regularly revalidated (4), increasing this factor in the absence of such programmes. Conversely, (4) discusses the possibility of reducing the 1.5 factor in cases of OLM derived passive monitoring. Note however that this alleviation has not been introduced for Hawk TMk.1 fins.

Further Hawk TMk.1 OLM programmes are likely to be commissioned as circumstances dictate, either in response to marked changes in utilisation, or as data collection exercises in pursuit of solutions to specific fatigue problems.

## 8. TREATMENT OF FSFT AND IN-SERVICE ARISING

Where the test loading has been representative, all significant fatigue incidents so far have arisen first of all on the FSFT. One recent arising, currently under investigation and involving several separate bolt failures, may be caused by tensile residual stresses induced by heavy asymmetric landings. This class of residual stress problem, induced by occasional overloads outside the scope of the fatigue design spectrum, is difficult to identify on even the most comprehensive OLM programme, and is likely to remain a source of unexpected arisings on many types of aircraft in years to come.

### 8.1 Investigation Procedure

Generally, following the discovery of a new problem, fleet structural integrity is maintained by the application of some or all of the following.

- the crack may be removed and subjected to metallurgical examination, including assessment of the initiation process and striation counting where possible.
- stress analysis of the component is conducted/confirmed, often involving finite element analysis and/or strain gauging, and appropriate S-N analyses performed.
- strain tracking crack initiation methodology may be employed to account for the effect of spectrum shape, especially useful in the case of compression induced tensile residual stresses.
- coupon/element tests may be performed in confirmation.
- LEFM is used to predict crack growth history.

a), b), c), d) and e) above are used to explain the presence of the crack and to specify any in-service inspection intervals.

Stress levels and/or S-N and da/dN data may be 'tuned' in line with the observed crack discovery time and the results of a) above. In cases of doubt concerning the read across of FSFT loading to in-service usage, some ground and/or flight strain measurements may be commissioned.

### 8.2 Fleet Action

Regular inspections will almost always be introduced. They may be employed temporarily to maintain fleet structural integrity until a suitable repair or modification is embodied, or included in routine inspection schedules if a philosophy of repair or modification on condition is adopted.

#### 8.2.1 Inspection Requirements

Inspection specifications usually comprise the following.

- an inspection procedure / technique.
  - an initial inspection time / life point.
  - a regular inspection interval.
- b) and c) above depend critically on the efficacy of the method specified in a). Additional factors of safety above those usually specified are incorporated where the inspection method is considered to be less than normally reliable, owing, for example, to poor access or low sensitivity.

The initial inspection point, after which regular inspection is required, may be set solely by consideration of incident times. However, it is often more efficient to first of all inspect on a fleetwide basis to establish the population values, obtaining the current lives of both affected and unaffected components, and employ statistical techniques to predict a 'safe' initial inspection point based on a nominal level of confidence.

Following such a fleetwide inspection, let

$x_1, x_2, \dots, x_m$  be the lives of cracked components

$z_1, z_2, \dots, z_n$  be the lives of uncracked components

Let  $y = f(x, \beta)$ ,  $x > 0$ , be the probability density function of time to cracking  $X$  of the component, where  $\beta$  is the vector of distribution parameters.

(eg.  $\beta = (\mu, \sigma)$  in the case of a normal distribution)

Then  $\beta$  may be estimated by maximising the Likelihood function

$$L = \prod_{i=1}^m f(x_i, \beta) \prod_{j=1}^n g(z_j, \beta) \quad \text{where} \quad g(z, \beta) = \int_z^{\infty} f(s, \beta) ds$$

and the maximum likelihood estimate of the 'safe' first inspection point  $S_a$  is then obtained from the solution to

$$1 - g(S_a, \beta) = a$$

where  $a$  is the preset level of risk (often of the order of  $10^{-3}$ ).

Log-normal and two parameter Weibull distributions have been successfully employed on Hawk problems in setting the value of  $S_a$ . Note however, that whilst both distributions often yield very similar values of  $S_a$ , the hazard function, or age specific failure rate,

$$h(t) = \lim_{\Delta t > 0} \frac{\text{Prob}(t < X < t + \Delta t \mid t < X)}{\Delta t}$$

of the log-normal distribution is non-monotonic, suggesting that the distribution may not in certain cases be suitable for predicting future population behaviour, restricting its use to the estimation of  $S_a$ .

Probable errors in the estimates of  $\beta$  and  $S_a$  may be derived from likelihood theory.

### 9. T-45 GOSHAWK FATIGUE DESIGN

The T-45A Goshawk is a naval version of the Hawk TMk.I, and has been designed by BAe and MDC to be crack free for 14400 flying hours, factor 4.

The structural analysis procedures follow US Mil Spec regulations, as opposed to UK Av P and DEF STAN requirements, including the use of the Neuber crack initiation method to establish adequate fatigue life.

Fatigue allowable stresses were derived from minimum life spectra determined by truncation analysis, as shown in Fig.11. A comprehensive coupon/element fatigue test programme was commissioned in support of the initial fatigue calculation effort, including checks on spectrum sensitivity to confirm minimum life spectrum configurations and testing of a large wing panel to confirm damage tolerance.

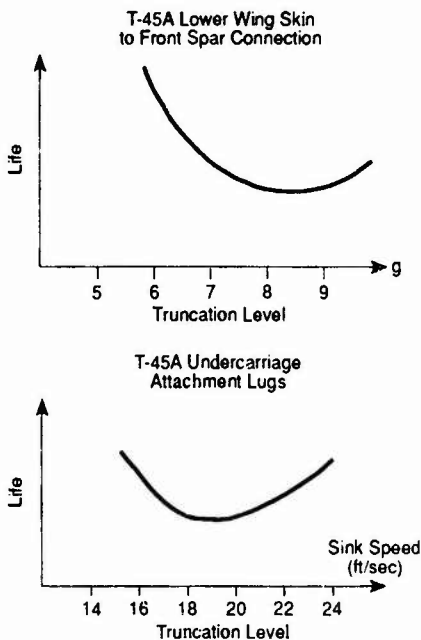


Fig.11 - Typical Life v Truncation Level Analyses

Particular attention was paid to the influence of the much greater landing loads encountered during carrier operations on spectrum shape and severity. The incorporation of the effects of residual stresses on time to crack initiation proved to be particularly beneficial, especially in cases of tensile residual stress which can profoundly affect the initiation time at features considered to be experiencing mainly compressive applied stresses.

This latter point was amply demonstrated during the design of the wing. Calculations, shown in Fig.12, indicated early crack initiation in the upper wing skin at certain access panel attachment holes, caused by substantial tensile residual stresses induced by high  $N_z$  manoeuvres. Simple coupon tests were commissioned, Fig.13, and confirmed the calculations which indicated that a 30% reduction in notch stress level was required in order to meet the specification. The option of installing titanium interference fit fasteners was not available owing to the need for routine in-service panel removal, and hole cold-working is not efficacious in such compression problems. Several different designs of steel bush were evaluated, and cracked at 30% to 50% of the life requirement with the skin still uncracked, thus not meeting specification. Following further investigations, Copper-Beryllium interference fit bushes were tested and complied with specification.

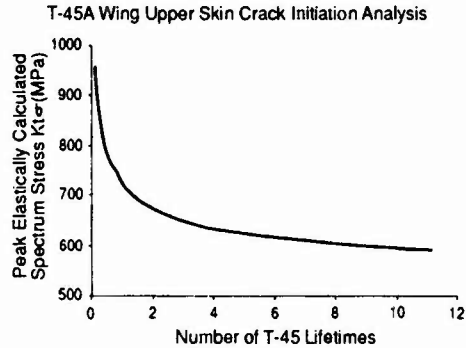


Fig.12 - T-45A Wing Upper Skin Crack Initiation Analysis

Holes 'A' & 'B' unbushed in early tests which confirmed the problem. Further tests performed with bushes to identify the fatigue solution.

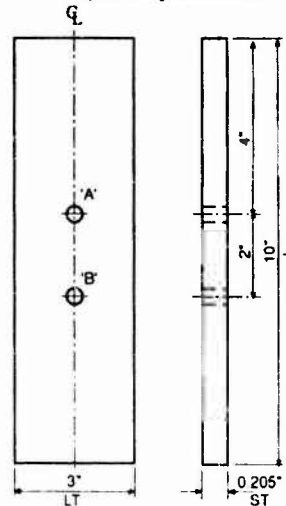


Fig.13 - T-45A Upper Wing Skin Coupon Specimen to Assess Compression Induced Fatigue

T-45A and Hawk aircraft possess many common structural characteristics. However, a significant structural difference lies in the method of undercarriage attachment. Compared with Hawk, much greater energy absorption capability is required of the T-45A landing gear. In response to this requirement, the wing structure has undergone some reconfiguration, including the adoption of a one piece landing pick up rib running from the auxiliary spar to the rear spar, necessitating a split in the front spar shown in Fig. 14. The structure was considered less amenable to accurate analysis than usual, due to the complex interaction of landing and flight loads at several significant locations.

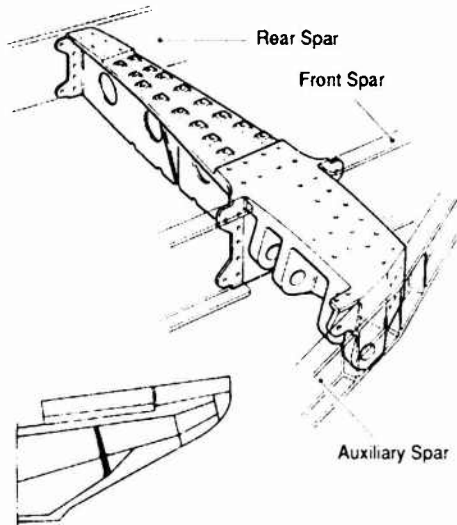


Fig.14 - View showing split in T-45A wing front spar

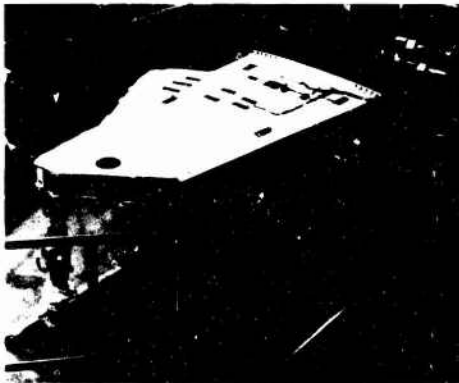


Fig.15 - View on top surface of T-45A Pre-production Wing Fatigue Test Rig



Fig.16 - General view of T-45A Pre-production Wing Fatigue Test Rig

Thus, a major fatigue test was commissioned and performed by BAe to investigate the structural integrity of this configuration, Figs. 15 & 16, and was scheduled to protect the first hatch of production aircraft in case design changes were required. Two important incidents arose towards the end of testing :-

- a) cracking in the lower flange of the front spar at the second fastener hole just outboard of the landing rib, Fig. 17.
- b) cracking of the lower skin edge at the main landing gear cut-out radius, Fig. 18.

Incident a) was caused by over-zealous stepping down of the spar flange thickness as it terminated outboard of the landing rib, and was cured by a small increase in thickness.



Fig.17 - View showing lower flange of front spar outer  
Crack runs from 2nd fastener hole Outboard of Rib 7  
towards free edge

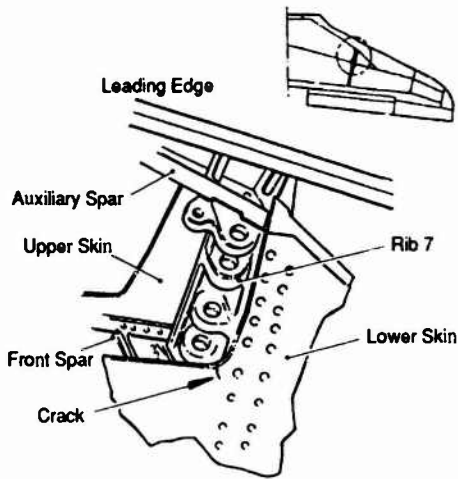


Fig. 18 - View showing crack in lower skin inboard of Rib 7

Incident b) arose even though the incremental stress/g was reduced to approximately 65% of the surrounding region value. Finite element analysis indicated that the crack had initiated at a point where flight induced stresses (mainly tensile) and landing induced stresses (mainly compressive) each concentrated substantially, though not each at their peak concentration. This unusual circumstance led to significant stress ranges within the fatigue spectrum. Coupon testing, Fig. 19, identified high strain energy density, due to the shallow stress gradient induced by the large notch radius, as the principal cause of earlier than expected crack initiation, magnifying the effective fatigue stress level by approximately 1.3. Research is currently underway at BAe into this mechanism, which tends to occur at holes above a certain diameter and at appropriately shallow notches, and initial results are encouraging. Extensive finite element analysis identified the necessary design changes, including separation of the flight and landing stress concentrations, to the cut-out profile within space constraints, which was proven by confirmatory fatigue and static testing. Details are given in Fig. 20 and Fig 21, including the benefits of the local thickening adopted as part of the solution.

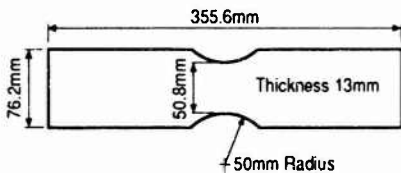


Fig. 19 - Lower Wing Skin Coupon Test Specimen

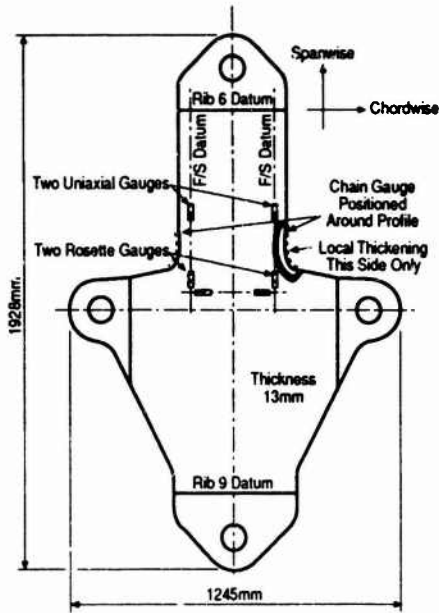


Fig. 20 - T-45A Lower Skin Stress Analysis Specimen

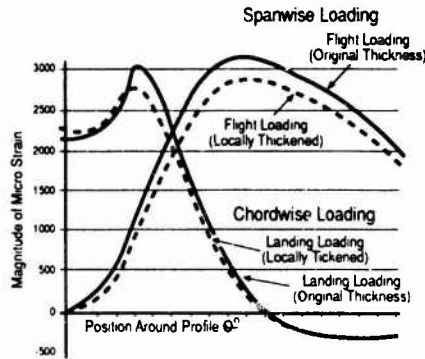


Fig. 21a - Cruciform Static Specimen Plot of Measured Strain v Position Around Profile

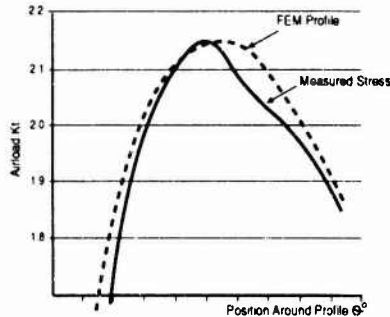


Fig. 21b - Comparison of FEM & Measured Stress from Cruciform Specimen for Spanwise Loading

The above illustrates the value of pre-production large scale tests in cases of greater than usual uncertainty, where the cost is more than outweighed by the potential savings on post-design freeze modifications and design changes.

The T45A has now entered service with the US Navy, and the Full Scale Fatigue Test is currently underway.

## 10. CONCLUSIONS

The structural design of Hawk is based strongly on the need for good fatigue life, which has been achieved by a combination of calculation, test, and flight measurement. OLM has played a key role in both the maintenance of Hawk TMkl fleet fatigue life clearance, and the current MoD standpoint on life factors suggests that it will feature ever increasingly in the management of aircraft fleets. The T45A Goshawk pre-production fatigue test illustrated the considerable savings that can be achieved by identifying features requiring attention prior to manufacture.

## ACKNOWLEDGEMENTS

The author is indebted to the Ministry of Defence for permission to publish. Thanks are also due to colleagues at BAe Brough for helpful discussions and to Mr J Ward for preparing the illustrations.

## REFERENCES

- (1) Av P 970 Design Requirements for Service Aircraft
- (2) BS 3G 100 Specification for General Requirements for Equipment in Aircraft December 1969
- (3) Defence Standard 00-970 Lcaflet 201/3 Fatigue Damage Tolcrance Substantiation of Fatigue Life October 1987
- (4) Cardrick, A. DRA Working Paper MS1-92-WP-015 The Chance of Finding a Crack - A Guide to the Fatigue Factors used for British Military Aircraft December 1992

**REDUCTION OF FATIGUE LOAD EXPERIENCE AS PART  
OF THE FATIGUE MANAGEMENT PROGRAM FOR F-16  
AIRCRAFT OF THE RNLAf**

**D.J. Spiekhouf**

National Aerospace Laboratory NLR  
P.O. Box 90502, 1006 BM Amsterdam  
The Netherlands

### 1. SUMMARY

Load monitoring of the F-16 fleet of the RNLAf is carried out by NLR using an electronic device capable of analyzing the signal of a strain gage bridge on one of the main carry through bulkheads. This is done on a sample of the fleet. By making use of the information stored in a large centralized data base system, "individual airplane tracking" is done.

Six times per year, the fatigue damage experience of the fleet is reported to the air staff, expressed in the so called "Crack Severity Index".

From the measurements it is known, that the RNLAf is operating its F-16 fleet in a very damaging way.

For this reason, it was decided to investigate the possibilities how to decrease the severity of flying. In this program much attention has been given to the "stress per G" relation during a flight. In particular the influence of flying with more favourite take off store configuration has been studied.

### 2. INTRODUCTION

Load monitoring of the F-16 fleet of the Royal Netherlands Air Force, RNLAf, is carried out by means of an electronic device which analyses the signal of a strain gage bridge on one of the major carry through bulkheads of the fuselage. Beside this strain gage bridge, also altitude, airspeed and loadfactor are being recorded. A debriefing form has to be filled in for each recorded flight.

"Individual Airplane Tracking" is possible by making use of information, like mission code and take off store configuration, which is stored in a large centralized data base system. The latter information is available for all flown F-16 flights by the RNLAf.

The loads department of the National Aerospace Laboratory in the Netherlands, NLR, is responsible for this load monitoring program and the processing and analysis of recorded data.

Six times per year the damage experience per aircraft, squadron and/or air base is reported to the air force. By using this information the RNLAf can closely monitor the fatigue experience of the fleet and take appropriate actions.

The results over the last years did show, that a number of squadrons within the RNLAf are operating far more damaging with the aircraft than has been assumed for the maintenance schedule given in the Fleet Structural Maintenance Plan, FSMP.

For this reason, a working group was established in order to reverse the trend of the more damaging flying from year to year.

As part of the activities of this working group, NLR developed a software program to recalculate the damage of a recorded flight for a different take off store configuration than the original one, but assuming the same loadfactor history. Further, the influence of flight limitations on loadfactor, airspeed and/or altitude can be studied. As a result, advices have been given to the RNLAf for lowering the fatigue experience of the fleet.

In the next chapter of this paper the load monitoring, as it is carried out today by the RNLAf, will be described. Individual airplane tracking and fatigue management will be presented in the next two chapters. In chapter 6 a description will be given of the method used for calculating the fatigue damage of a flight, in terms of crack growth. This is the so called "Crack Severity Index" concept.

In chapter 7 the different steps, which have been taken to investigate the possibilities for reducing the damage of a flight, will be discussed. The paper ends with some concluding remarks.

### 3. LOAD MONITORING TODAY IN THE RNLAf

For many years, the NLR has been engaged in the load monitoring of the Lockheed F-16 aircraft of the RNLAf. From 1990 on, the originally available equipment such as Mechanical Strain Recorder and Flight Loads Recorder, has been replaced by instrumentation specified by NLR. Data collection and data analysis is carried out by NLR. An overview of the load monitoring program is given in reference 1.

In 1992, the one channel version of the load monitoring recorder has been replaced by a more modern four channel version of the system, which has been manufactured in Switzerland by Spectralab, see figure 1.

The new system has the advantages of more memory capacity, a higher resolution and a real clock. The additional channels in the new system are used for recording loadfactor, altitude and airspeed. The signals for altitude and airspeed are taken from the data bus in the aircraft. So far, the signal for the loadfactor has been provided by an additional acceleration sensor on top of the instrumentation package. These additional three signals are needed for a recalculation of the fatigue damage of a flight which will be discussed later on.

The Spectrapot Data Collector performs a data compression during flight by searching for peaks and troughs in the signal of the strain gage bridge. This bridge is located on one of the major load carrying bulkheads in the airframe and therefore a

good measure of the fatigue loading of the wing and the centre section of the fuselage.

At the moment of occurrence of a peak or a trough, also the values in the signal of the loadfactor, airspeed and altitude are recorded. This is a result of the so called master/slave recording method. In figure 2 the data flow in the RNLAFF-16 load monitoring program is given.

In the last years also the number of aircraft with "provisions for" has been increased from 5 to 7 per squadron.

Discussions are being held, to further increase the number of aircraft with "provisions for" and the number of instrumentation packages per squadron.

#### 4. INDIVIDUAL AIRPLANE TRACKING

As mentioned before, the load monitoring program itself is only carried out on a sample of the fleet. For the RNLAFF it was found that there is no need for a fleet wide installation, because in general the aircraft are used randomly in a squadron by all pilots and for all mission types.

In this set up it is essential that long term "non standard" operation of an aircraft is monitored separately. Over the last years there is an increase of this kind of operation, mostly outside the Netherlands. Examples are the low altitude operation in Goose Bay, Canada, the pilot training in Tucson, USA and the "Deny flight" operation from Villa Franca, Italy. Also "special flying" in exercises like "Red Flag" and during "Air Display" flights has been recorded. In the load monitoring program, these "non standard" squadron flights are being handled as special mission types for the RNLAFF.

"Individual Airplane Tracking" can be done by a combination of recording in a sample of the fleet and by a usage monitoring "on paper" for the total fleet, see reference 2.

From the measurements and debriefing forms in the load monitoring program the fatigue damage per mission type per squadron and per time period becomes available. The fatigue damage is expressed in the so called "Crack Severity Index", which is explained in more detail in reference 3.

The individual mission mixture per tail number in a squadron is known from a centralized maintenance data base system, CAMS. In this data base system information like mission code, squadron, flight duration and take off store configuration is stored for each F-16 flight made by the RNLAFF. Each month the data are sent to NLR by means of a modem connection with the air force.

For individual airplane tracking, the severity of flying per mission type per squadron has to be combined with the mission mixture of an individual aircraft. In this way the fatigue damage or CSI value per tail number is calculated for a given time period.

#### 5. FATIGUE MANAGEMENT

For the air staff of the RNLAFF, management of the load monitoring program itself is carried out by NLR. In the sample program it is essential that a sufficient number of flights for each mission type are recorded for each half year and for each squadron. It is the task of the squadrons to fill in the associated debriefing forms and also to change the Spectrapot equipment into another aircraft with "provisions for" in case of long term maintenance of an aircraft. There is a continuous effort from the air staff and NLR personal to increase the number of recorded flights.

The results of the fatigue damage calculation per tail number are presented six times per year to the air staff of the

RNLAFF. Of course, it is possible to provide the information more often. However, for management purposes a two monthly interval seems to be sufficient.

The results are given in "standard" tables, which together give an overview of the fatigue damage experience of the fleet.

In the first place, a comparison is being made between the flown mission mixture of a squadron in the last two months and the last three years, with the assumptions made for the FSMP. From figure 3 it is clear that in actual operation large differences occur.

With respect to the take off store configuration, per squadron a comparison is being made between the actually flown take off store configurations and the "most preferable take off store configurations" as defined by the RNLAFF.

In figure 4 the variation of the CSI value over the total life of each aircraft is given. For each aircraft the history is known in terms of flight hours flown in each squadron. Since 1985 also the individual mission mixture flown in each squadron is available. In this way a cumulative damage or CSI value over the whole life of the aircraft is calculated.

From figure 4 it is clear that there is a need for mission mixture management per aircraft within a squadron. Of course, the information can be presented per squadron and per air base. An example is given in figure 5.

The air staff uses all this information to supply the air bases and squadrons with their own fatigue damage results. Sudden changes in the experienced fatigue damage are raising questions and do initiate additional investigations into the cause of the increase of the fatigue damage experience.

#### 6. CRACK SEVERITY INDEX CONCEPT (CSI)

An important "tool" in the calculation of the fatigue damage of a flight is the so called "Crack Severity Index" concept, which has been developed by NLR some years ago. In reference 3 more detailed information is given about the CSI development and the specimen tests which have been carried out for validation of the concept.

The CSI value is used for quantification of the fatigue damage of recorded stress spectra in terms of crack growth potential. The concept is based on modern concepts with regard to crack growth prediction, including crack closure and associated crack growth retardation. An important quantity is the minimum crack opening stress. This opening stress is a function of the maximum and the minimum stress in the spectrum under consideration. It is important to realize that the calculated CSI value is a relative damage figure for a specific location and loading spectrum.

In the F-16 load monitoring program of the RNLAFF, the CSI concept has been applied to the location of the strain gage bridge used in the program. As a reference, a batch of 488 RNLAFF F-16 flights recorded in 1985, have been taken

As mentioned before, the minimum crack opening stress is of major importance for taking into account the interaction effect caused by the large load cycles. It is based on the load cycle which occurs once in thirty flights.

In the reports to the air staff a distinction has been made between the so called normalized CSI or nCSI and spectrum CSI or sCSI. The nCSI is based on the minimum crack opening stress of the reference batch of flights flown in 1985. In the case of the sCSI, the crack opening stress is calculated for all the flights flown in the last half year by a squadron. The resulting crack opening stress is used for calculating the

severity per flight and per mission type. In this way load interaction effects between mission types are taken into account. In figure 6 an example is given of the importance of such an approach. For example, a 50/50 percent mixture of severe ACT and RANGE flights has a combined fatigue damage per hour of about half that of the ACT mission type alone. This effect is caused by the high crack opening level resulting from the ACT mission type. As a result, the large number of load cycles in the RANGE mission type hardly contribute to the crack growth. See also figure 7.

## 7. DECREASE OF FATIGUE DAMAGE CONSUMPTION

As mentioned before, a number of squadrons are operating more severely with its F-16 aircraft than has been assumed for the Fleet Structural Maintenance Plan. It may be added that in comparison with other air forces the RNLAf also is flying more severe. In terms of maintenance this means that more fatigue cracks are found during inspections and that there is more additional downtime of the aircraft.

In order to reduce the fatigue experience of the RNLAf F-16 fleet, a working group has been established. First priority has the reduction of the fatigue damage to the one assumed for the FSMP. This means that the trend of an increasing load experience over the last years has to be reversed.

For the RNLAf it is important that the operational training value for the pilots will not be reduced. This means that reducing the loadfactor load experience is not the first choice.

In the last year, most work has been done on reducing the "stress per G relation", mostly by making use of more favourable take off store configurations. This work will be described in chapter 7.2. First, however, the effect of reducing the maximum allowable loadfactor will be discussed.

### 7.1 Limitation of maximum loadfactor

One of the "standard" answers to the question of how to reduce the fatigue damage experience, is a limitation of the maximum allowable loadfactor during operation of the aircraft. From chapter 6 it may already be clear that one has to be very careful if the large load cycles within a load spectrum are being changed. This, because of the large influence of those cycles on the crack opening stress level. Instead of increasing the crack growth life of the structure, the result may be a shorter crack growth life. Specimen tests have been carried out by NLR making use of recorded load sequences during normal operational flights. In figure 8 the results are shown. By reducing the maximum allowable loadfactor from 9 G to about 8 G, it was found that the "truncated" load sequence was about 25 percent more severe.

In figure 9 the results are shown of an analysis of the influence of the maximum allowable loadfactor on the crack growth life of the reference batch of 488 flights. By reducing the maximum allowable loadfactor, the fatigue damage of the load sequence increases to a maximum at a maximum allowable loadfactor of about 5.5 G. For a lower maximum loadfactor the damage decreases, but it is only at about 4 G that the original damage is reached again! It is clear that this is not the right way to go.

### 7.2 Reducing the "stress per G" relation

Most attention has been given to the reduction of the crack growth damage by manipulating the take off store

configuration. The stress per G ratio is very variable as a result of changing aircraft mass by burning fuel and mass distribution, which means store and fuel location.

Of course, there are more parameters influencing the stress per G relation. For example Mach number and roll speed. In figure 10 the variation of stress per G is shown in a batch of about 250 recorded flights. For the same loadfactor, a large variation of stress can be seen. It has to be mentioned here, that the stress is taken at the location of the strain gage bridge used in the load monitoring program.

Figure 11 gives an example of the stress per G variation during a flight with an external centreline fuel tank. During flight, the fuel in this tank is the first to be used. Next, the fuel in the internal wing tanks are burned and the remaining part of the flight is flown on fuel from the internal fuselage tanks.

During the first part of the flight the stress per G relation is not changing so much, there after the ratio is decreasing slowly as a result of burning fuel from the internal fuselage fuel tanks. The more or less constant stress per G in the first part of the flight is caused by a little decrease of the stress per G from the external centreline tank followed by the counteracting effect of burning fuel from the internal wing fuel tanks.

Most attention in the project so far has been given to the reduction of the stress per G relation by changing the take off store configuration. For this reason, NLR developed a computer program for calculating loads in a few sections of the wing. The formulae used have been received from Lockheed, the former General Dynamics.

The formula for calculating the stress at the location of the strain gage bridge used in the load monitoring program, has the following form:

$$\begin{aligned} \text{Stress (at location of strain gage bridge)} &= \\ &C1 * \text{shear force} && \text{(in wing root)} \\ + &C2 * \text{bending moment} && \text{" " " " } \\ + &C3 * \text{torsion moment} && \text{" " " " } \end{aligned}$$

Each of these sectional loads is a function of loadfactor, mass, Mach number, angle of attack, roll and yaw velocity/acceleration, etc. This computer program has been used as a "tool" for comparing different take off store configurations.

In figure 12 an example is given. For a large number of "points in the sky", which are combinations of airspeed, altitude and fuel quantity, the stress is calculated for two different take off store configurations. Clearly visible for all "points in the sky" is the favourable effect from the additional external stores. From this investigation "most favourable take off store configurations" have been selected for the most important mission types.

Although the "point in the sky" calculation did promise some improvement, it still was a question how much of this would happen under actual operational conditions. In order to investigate this, the computer program for calculating the "points in the sky" was extended in order to recalculate actually recorded load sequences.

From the load monitoring program the sequence of peaks and troughs in the strain gage signal of a flight is available. At each peak and trough also airspeed, altitude, mass and mass distribution are known.

A few assumptions have to be made. In the first place the

amount of stress resulting from asymmetric manoeuvring is kept the same. Also the flight duration is taken as a constant. In principle it is also possible with the computer program to recalculate a flight with limitations on airspeed, altitude and/or loadfactor.

For the resulting new load sequences, the fatigue damage is calculated using the CSI method. In figure 13 results are given of a recalculation for a batch of ACT flights. In this example only external stores are replaced. The external tank configurations are kept the same. The favourable effects are clearly visible. Based on these results, "most preferable take off store configurations" have been selected.

As a begin, the RNLAf has decided to fly as much as possible with four missiles or dummy missiles at the outboard wing stations.

More investigations are planned for the near future. The effect of Mach number and the time at which manoeuvring takes place will be studied in more detail.

In the end, the favourable effects of changes in the take off store configuration usage should be seen in the results of the load monitoring program.

From the recorded flights, which are stored in the data base, it can already be seen that use of a more favourable take off store configuration gives indeed a lower nCSI value. An example is given in figure 14.

## 8. CONCLUDING REMARKS

- An overview has been presented of the load monitoring of the F-16 fleet of the RNLAf. By making use of a combination of a sample measuring program and the information stored in a centralised data base, fatigue experience per individual tailnumber becomes available.
- A description has been given of the "tools" which are present for detailed calculation of the fatigue damage of a flight and the recalculation of a flight for another take off store configuration.
- More research is needed to investigate the possibilities of a further reduction of the fatigue severity of operational usage. For example effects of Mach number and time of manoeuvring in a flight.

## 9. REFERENCES

1. Spiekhout, D.J., Load monitoring of F-16 aircraft of the RNLAf with a smart electronic device. AGARD conference proceedings CP-506, Fatigue Management, december 1991. Also NLR report TP 91116 U.
2. Jonge, De, J.B., Load experience variability of fighter aircraft. NLR report TP 89172 U, june 1989.
3. Jonge, De, J.B., The crack severity index of monitored load spectra. Paper presented during the 77th Meeting of the AGARD SMP, Bordeaux, september 1993.



Fig 1 Spectrapot-4C data collector

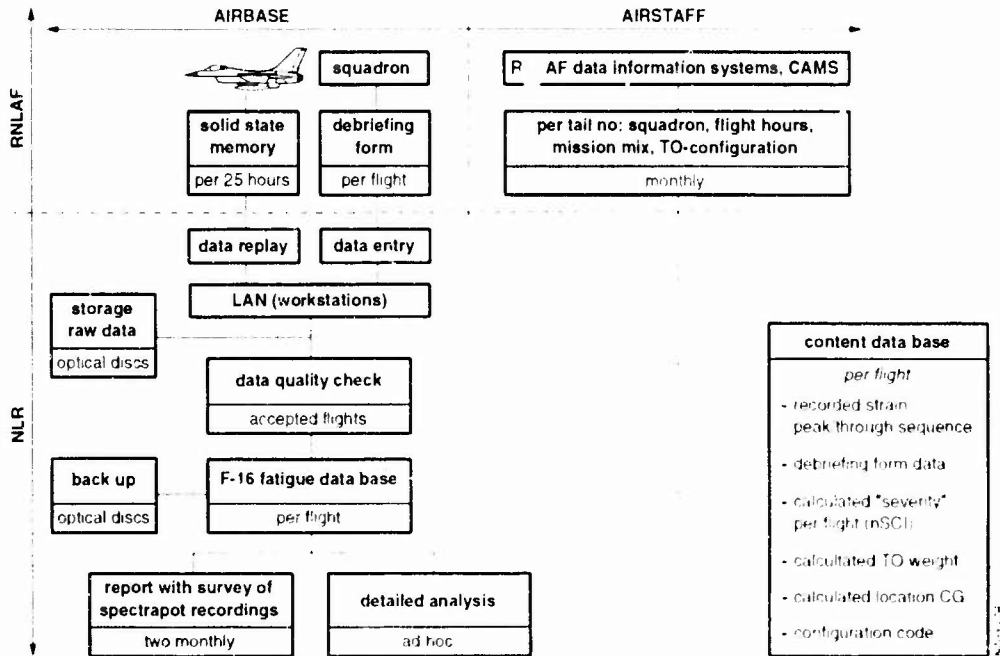


Fig 2 Data flow in F-16 load monitoring program

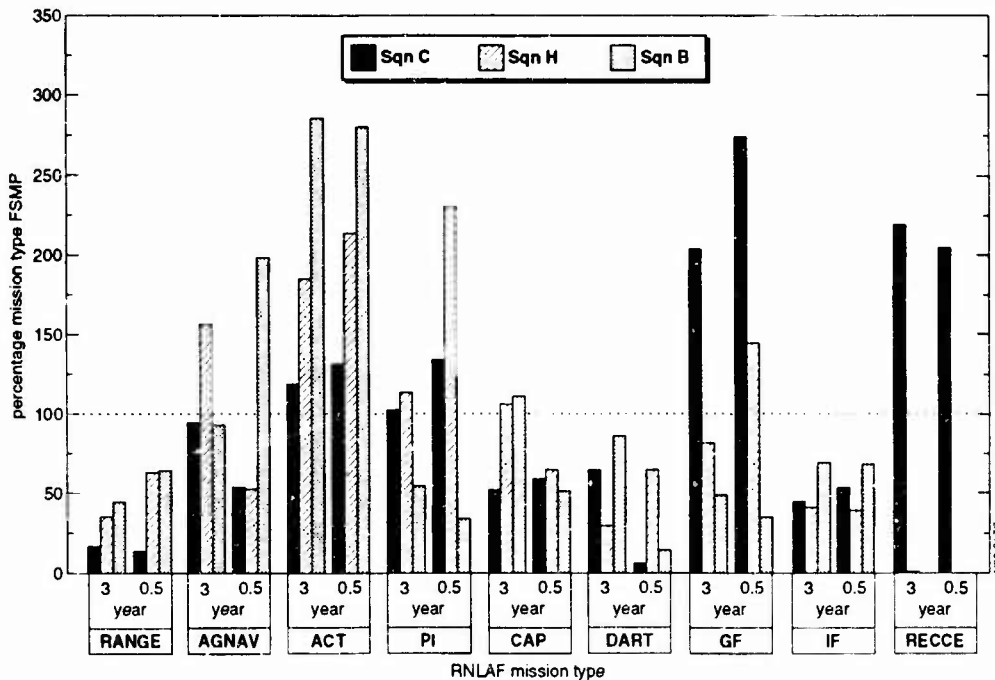


Fig. 3 Mission mixture variation per squadron

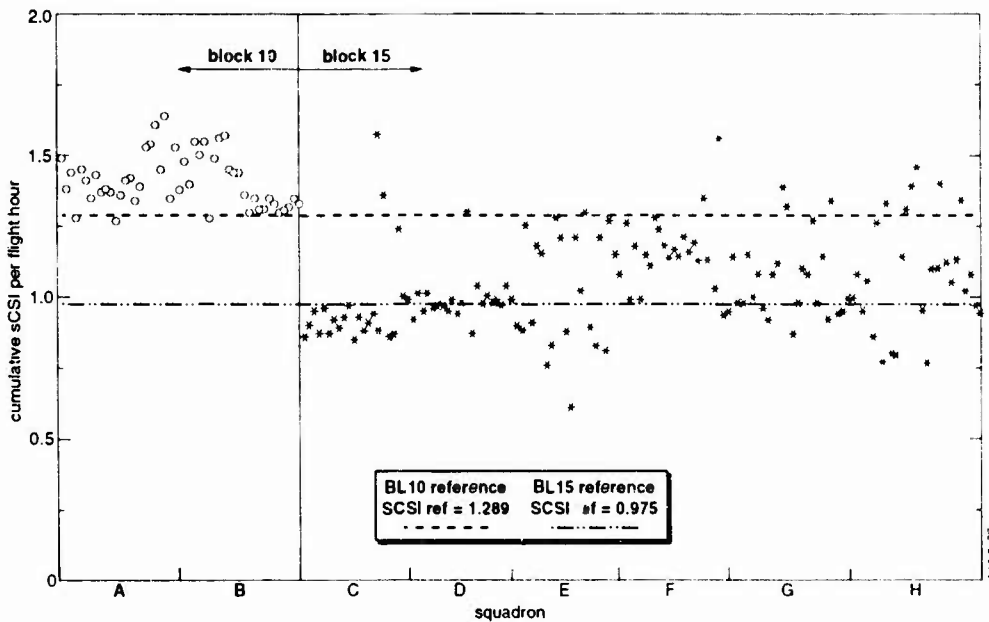


Fig. 4 Cumulative fatigue damage per tailnumber

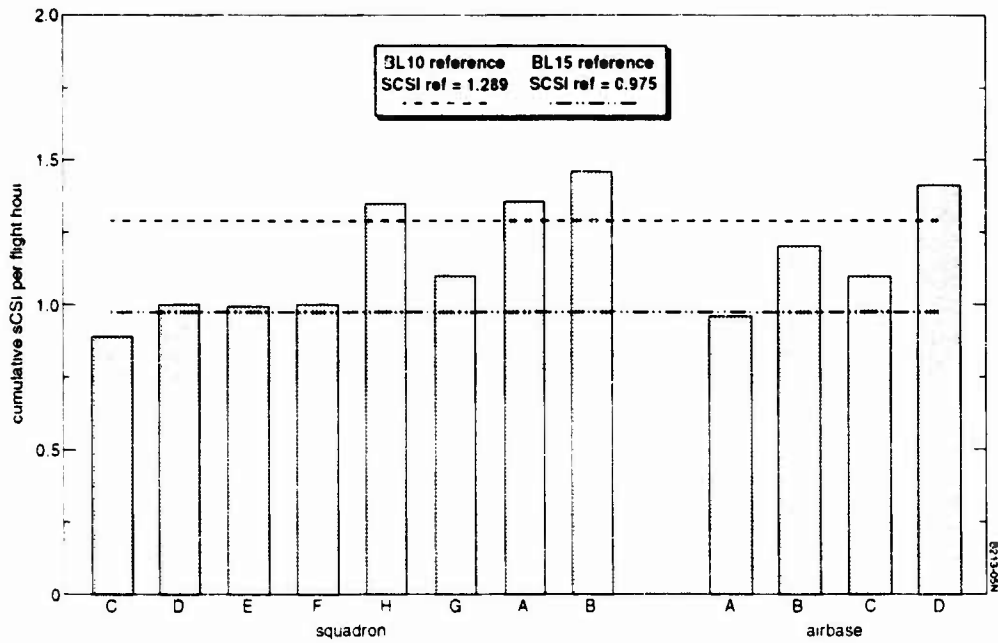


Fig. 5 Cumulative fatigue damage per squadron, airbase

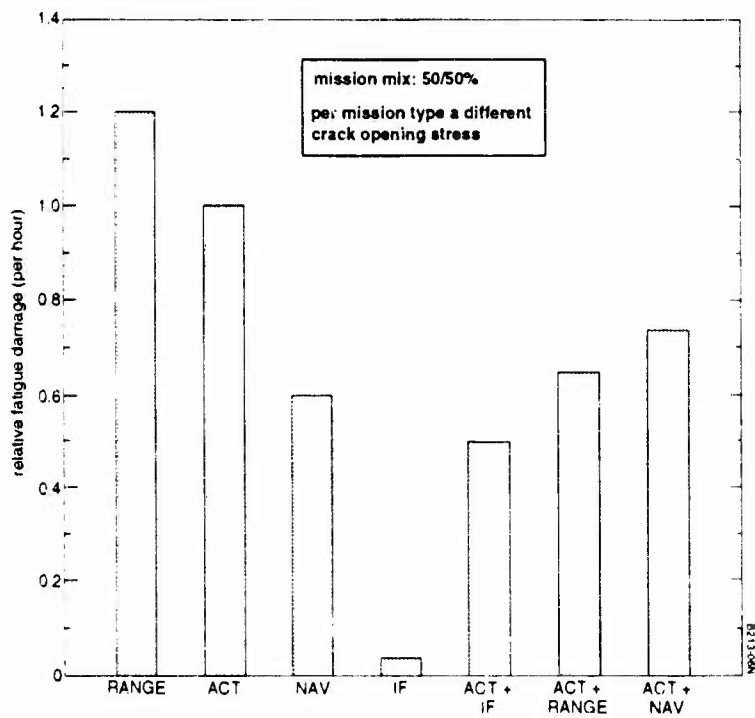


Fig. 6 Example of influence of mission mixture

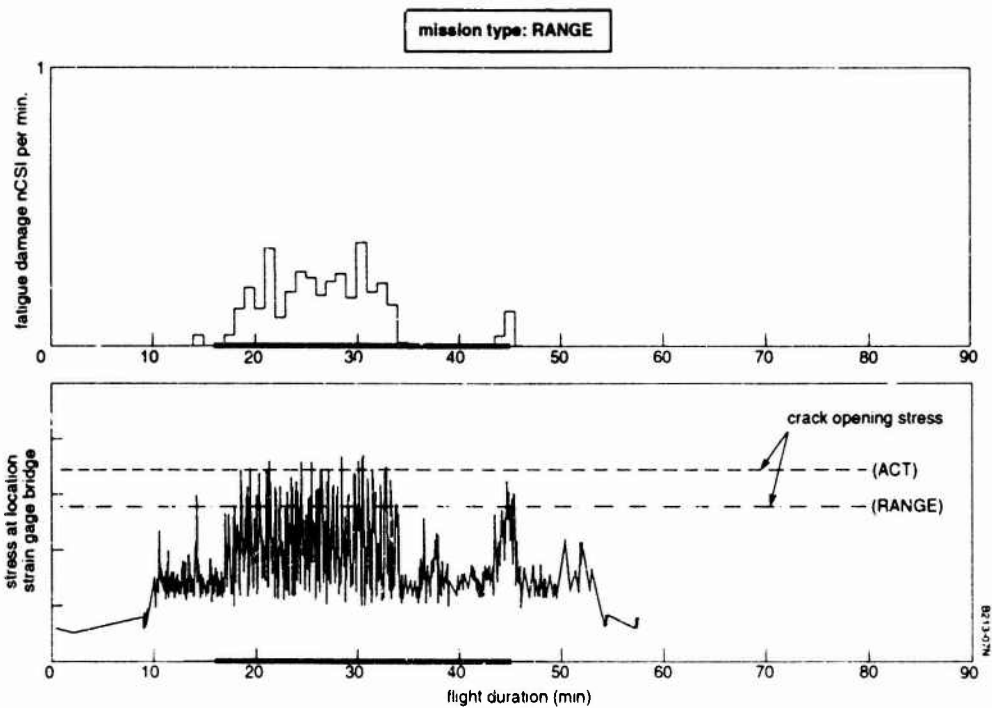


Fig. 7 Example of fatigue damage cumulation during a flight

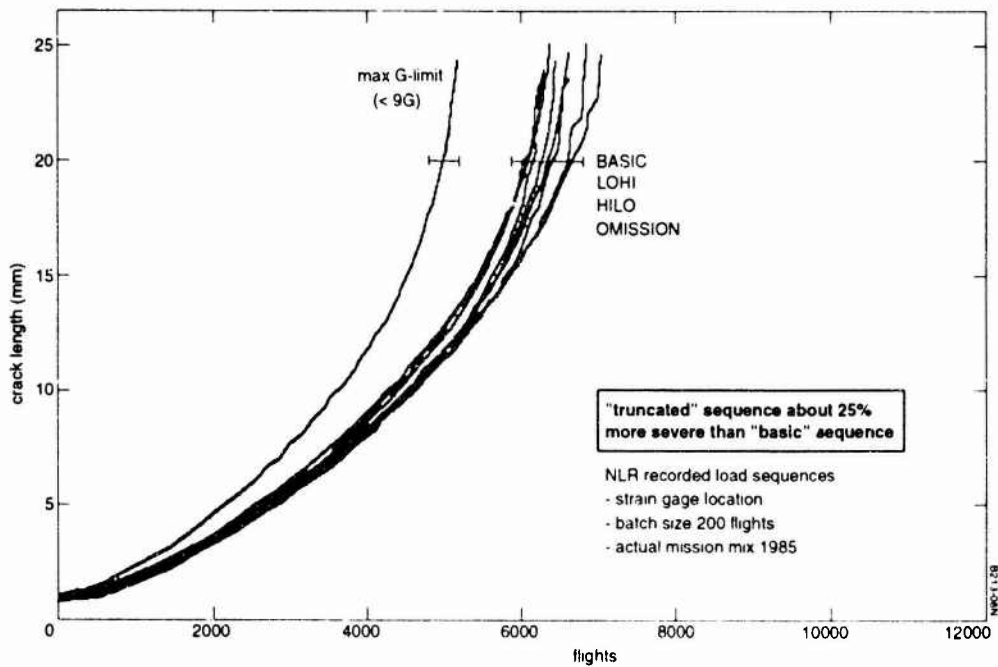


Fig. 8 Crack growth specimen test results

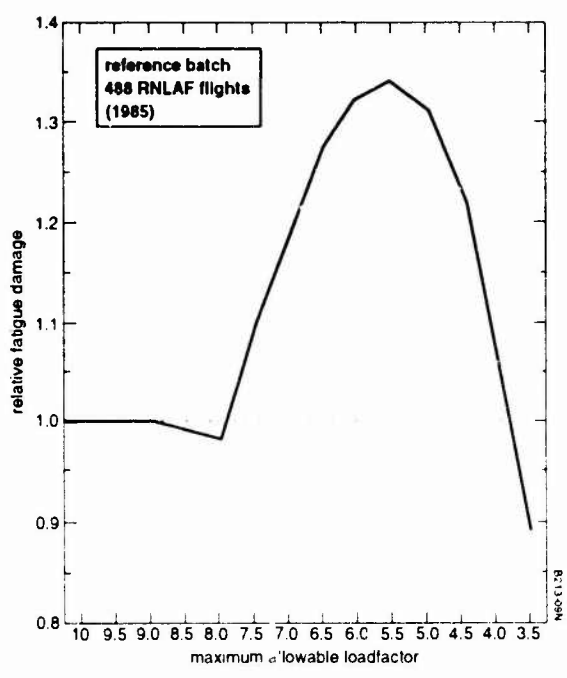


Fig. 9 Influence limitation maximum allowable loadfactor

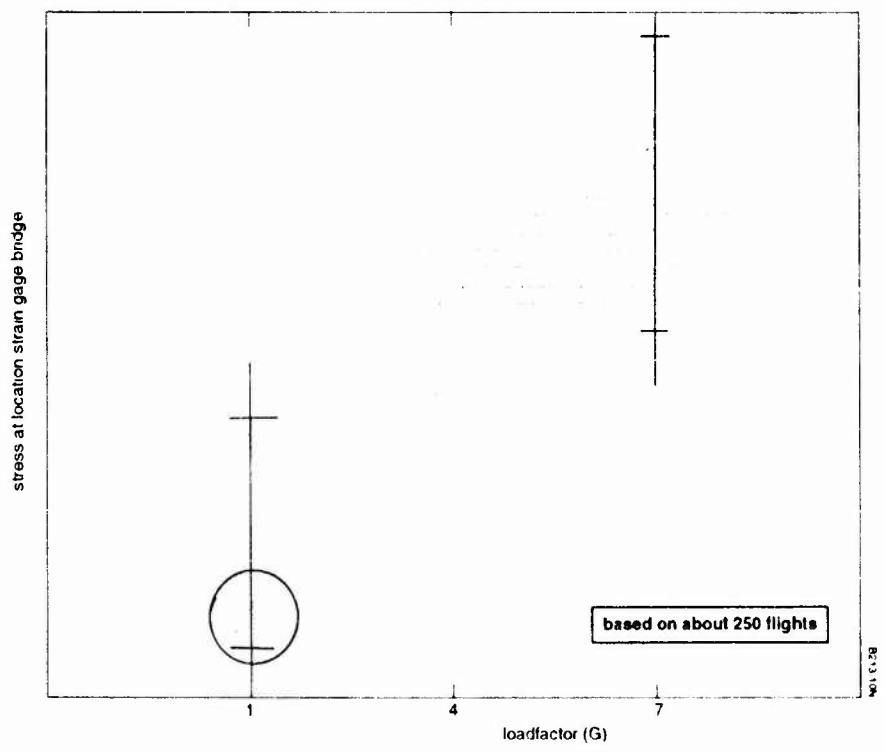


Fig. 10 Variation of stress per G relation

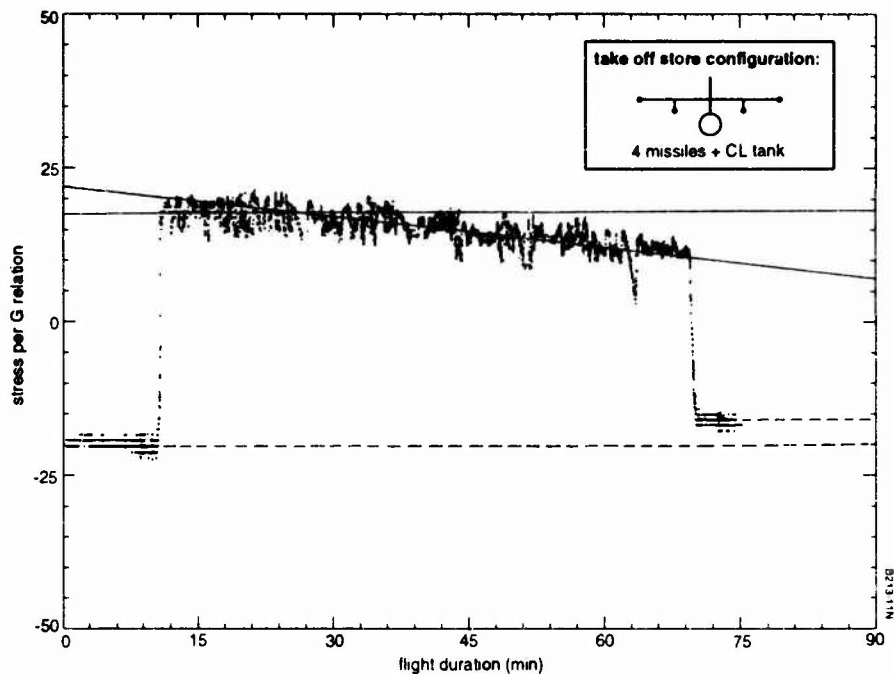


Fig. 11 Variation of stress per G relation during flight

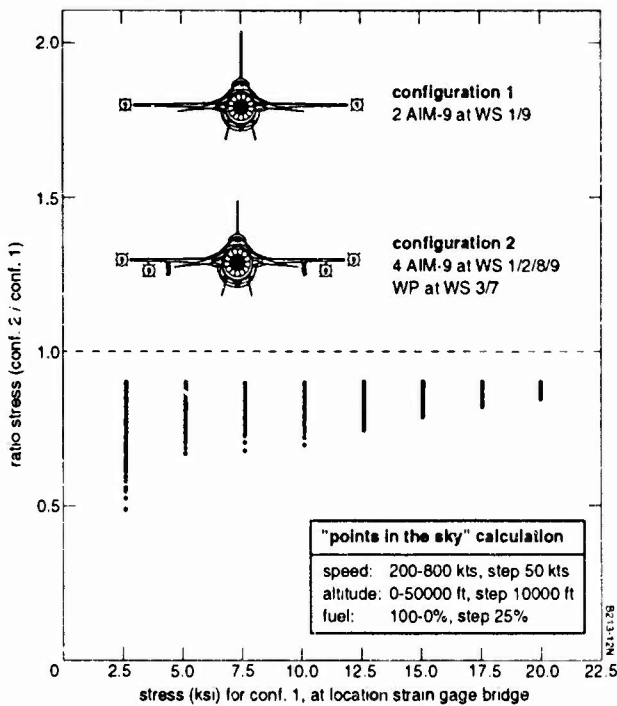


Fig. 12 Comparison for two take off store configurations

take off store configuration	air base			
	D	A	B	C
	97	102	103	103
	88	90	89	94
	73	71	69	78
	113	122	126	120
	85	86	85	91
	76	75	74	82
	63	59	57	68

- launcher + dummy
- ▮ UW-launcher
- \* dummy
- weapon pylon

remark: tank configuration is the same as in the original batch of flights

Fig. 13 Example batch of recalculated ACT flights per air base (in percentage of nCSI of original batch of flights)

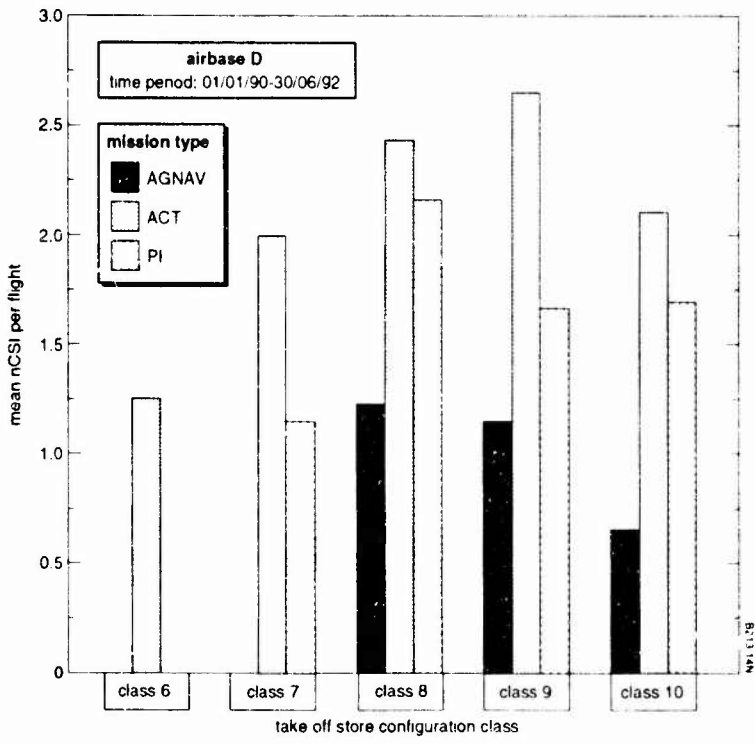


Fig. 14 Influence take off store configuration class on fatigue damage

## AN OVERVIEW OF THE F-16 SERVICE LIFE APPROACH

by

**J.W. Morrow and G.T.Herrick**

Lockheed Fort Worth Company  
Mail Zone 2846  
P O Box 748  
Fort Worth  
Texas 76101  
United States

*This Paper was not available at the time of printing, but included is the authors' material used at the presentation during the AGARD Workshop held in Bordeaux.*

### **Introduction to F-16 Airframe**

- The F-16 Airframe Has Been Designed According to the Latest USAF Philosophy which was Adopted in the 1970s
- It has a Modular Structural Arrangement and Maximum Use Has Been Made of Aluminum
- It is the First Aircraft Designed for Fracture Requirements in Mind, from its Inception
- It is the First Aircraft Designed to Withstand 9.0g Loads and it is Certified to 8,000 Service Hours
- It Has Completed Flight-By-Flight Durability and Damage Tolerance Test Programs with No Catastrophic Failures
- Fracture Control Program Has Been Implemented for Designated Critical Parts
- Force Management Program in Place to Monitor Crack Growth and Enable the USAF to Maintain Operational Readiness
- Capability Additions Have Grown Basic Flight Design Gross Weight from 22,500 Pounds (1975) to 28,750 Pounds (1992)
- Maneuverability and Pilot Comfort Features Have Contributed to Significant Increase in Maneuver Activity Levels by All Users

### **Vu-Graph 1**

*Presented at an AGARD Meeting on An Assessment of Fatigue Damage and Crack Growth Prediction Techniques, September 1993.*

## ***F-16 Requirements for Airframe Structural Durability and Safety***

- **MIL-A-1530A - Aircraft Structural Integrity Program (ASIP)**
  - Defines Overall Requirements to Achieve Structural Integrity
- **MIL-A-8866B - Airplane Durability Requirements**
  - Identifies Durability Design Requirements Applicable to Airplane Structure
- **MIL-A-83444 - Airplane Damage Tolerance Requirements**
  - Identifies Damage Tolerance Design Requirements Applicable to Airplane Safety of Flight Structure
- **MIL-A-8867B - Airplane Strength and Rigidity Ground Tests**
  - Identifies Ground Tests Required for Substantiation of Aircraft Structural Integrity

***As Interpreted by F-16 Structural Design Criteria Documents***

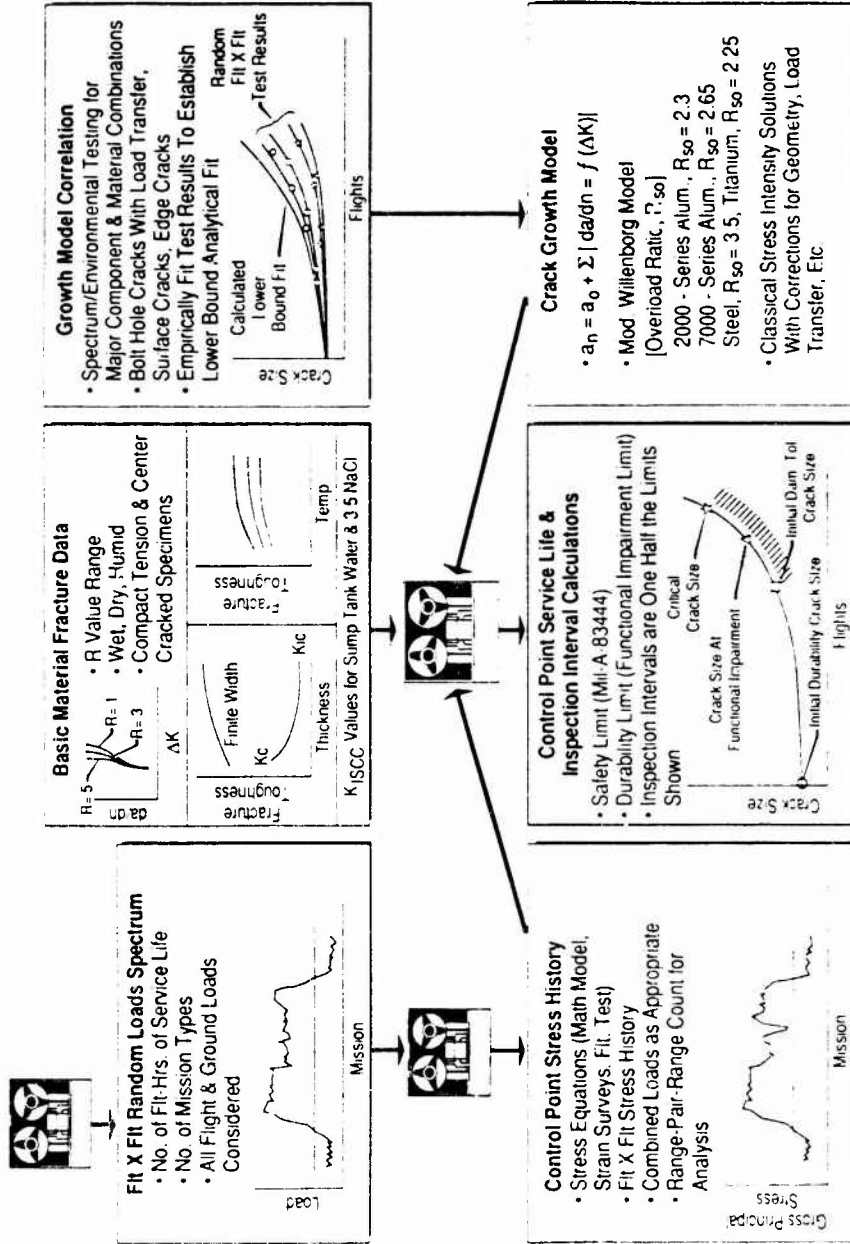
### **Vu-Graph 2**

## ***F-16 Design Approach***

- **"Safe Life" Approach Abandoned by USAF**
  - Does Not Account for Initial Flaw
  - Poor Correlation Between Test and Service
- **Safety and Durability Requirements Decoupled**
- **Safety - Damage Tolerant Design**
  - Fall-Safe
  - Slow Crack Growth
  - Fracture Mechanics
- **Durability - Designed Such That:**
  - Economic Life > Required Design Life
  - Time to Functional Impairment > Required Design Life
- **Resulted In:**
  - Use of Tougher Materials
  - Lower Operating Stresses
  - Improved NDI Procedures
  - More Realistic Testing

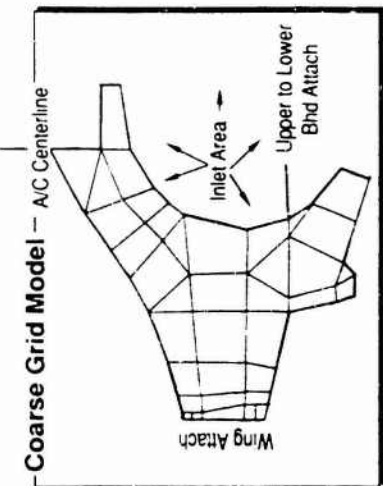
### **Vu-Graph 3**

# Metals Crack Growth Analysis Methodology

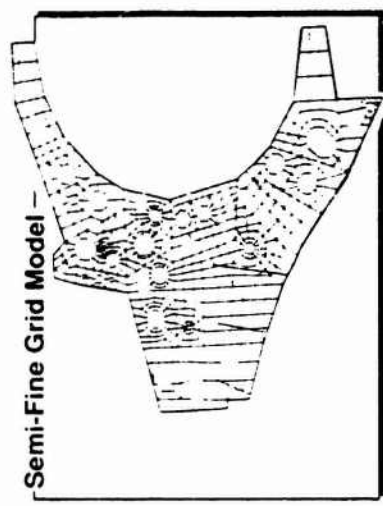


**Vu-Graph 4**

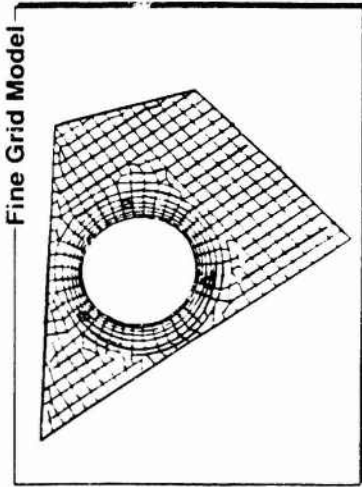
# Fatigue/Fracture Bulkhead Web Analysis



Webs in the Coarse Grid Model Consist of 1-4 Elements, Therefore Holes are not Geometrically Modeled. Element Thicknesses, However, are Reduced when Holes are Present to Compensate for Reduced Web Stiffness.



The Semi-Fine Grid Model Contains Major Web Penetrations Along with Real Thicknesses. Small Penetrations such as Satellite Holes, However, are not Modeled.



Fine Grid Model

The Fine Grid Model Contains Actual Structure Geometry Including Satellite Holes.

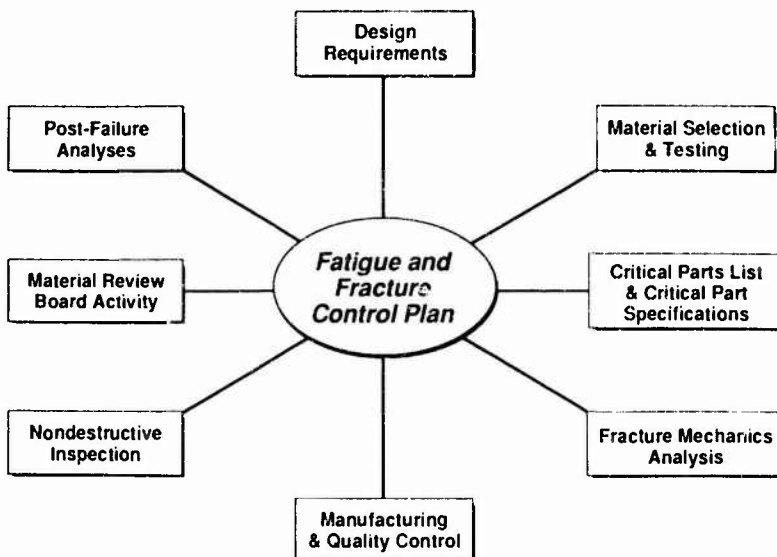
Vu-Graph 5

## Test Policy Comparisons

<u>Pre 1969/70</u>		<u>F-16 Policy</u>
Block	Test Spectrum	• Flight by Flight (F x F)
Production Aircraft	Selection of Test Article	• Early RDT&E Aircraft
No Policy	Test Schedule	• FSD Requirements Are: - One Lifetime Prior to Prod. Go-Ahead, Two Lifetimes (Or Economic Life) Prior to First Production Delivery
4 Lifetimes	Test Duration	• Two Lifetimes (Or Economic Life) Durability • Two Lifetimes (With Pretlaws) Damage Tolerance Plus Residual Strength Loading
No Policy	Post Test Inspection	• Teardown Inspection • Fractography
4 Lifetimes Without Fatigue Failure	Acceptance Criteria	• Final Analysis Using Test Results • Economic Life > Design Life • Meets Damage Tolerance Reqmts

Vu-Graph 6

## Fatigue and Fracture Control Plan



Vu-Graph 7



## ***F-16 Fleet Management Recording Systems***

- **Crash Survivable Flight Data Recorder (CSFDR)**
  - Signal Acquisition Unit (SAU) on Every Airplane
  - Crash Survivable Memory Unit (CSMU) on Every Airplane
  - Performs Onboard Data Compression and Data Storage
    - *Type 1 - Data for Mishap Investigation Analysis*
      - Last 15 Minutes or More of Flight Data
      - Up to 5 Special Events
      - Baseline Data at Liftoff
      - Data Extracted as Required
    - *Type 2 - Data for Individual Airplane Structural Tracking*
      - $\Delta$  Nz W Exceedances and Other Usage Information
      - Data Extracted at 75 and 150 Hour Phased Inspections
    - *Type 3 - Data for Structural Loads and Service Life Analysis*
      - Retains Data for Last 7 to 10 Flights
      - Data Extracted at 75 and 150 Hour Phased Inspections
    - *Type 4 - Data for Engine Usage Analysis*
      - Retains Data for Last 7 to 10 Flights
      - Data Extracted at 75 and 150 Hour Phased Inspections
- **Standard Flight Data Recorder (SFDR)**
  - Baselined Off of CSFDR
  - Replaces Z8002 Microprocessor with MIL-STD-1750

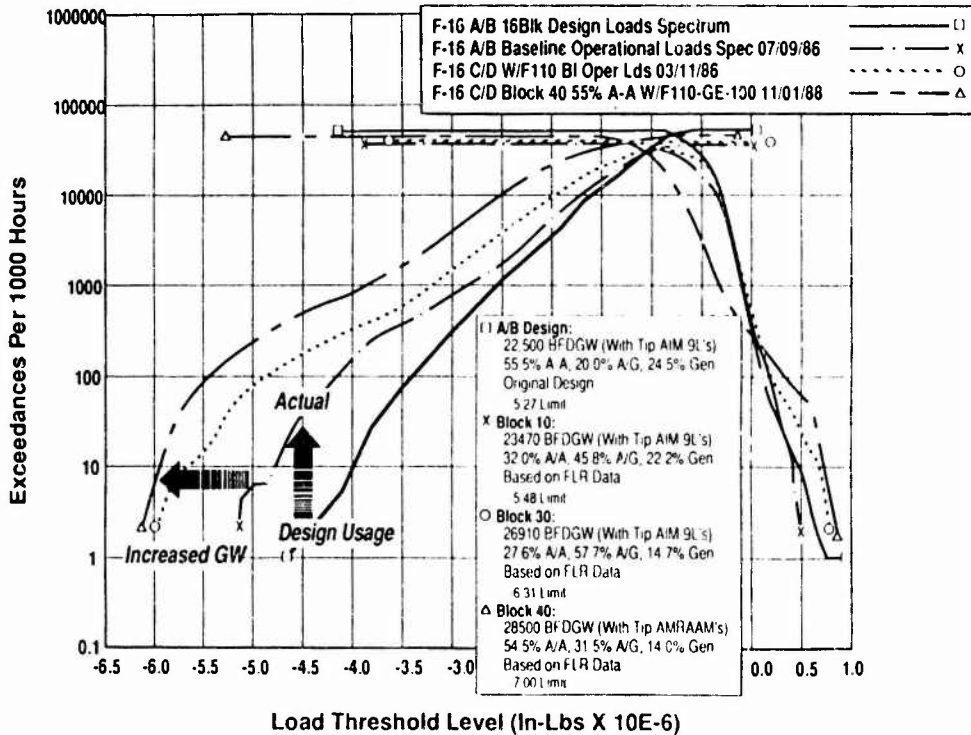
Vu-Graph 9

## ***Lessons Learned Summary***

- 1. Assume Realistic Effectiveness for Removable Panels and Covers**
- 2. Insufficient Edge Distance a Recurring Design Detail Problem with Today's Compact Fighter Designs**
- 3. Do Not Ignore Effects of Residual Stress for Structure Loaded Primarily in Compression**
- 4. Keep Load Paths Straight. Eliminate Section Changes. Both Frequently Ignored**
- 5. Design Connectors for Systems Routing to Provide Adequate Edge Distance for Satellite Holes (2 to 3D). Position Satellite Holes Out of Maximum Tension Stress Field. Locate Routing Holes in Low Stress Areas. Use Single Large Routing Hole Instead of Multiple Holes**
- 6. Hard to Inspect/Difficult to Replace Structure Should Be Designed with an "Upper Bound" Usage Spectrum**
- 7. Program Memorandums Must Be Used to Establish Design Criteria/Guidelines for Service Life Just as They Are for Static Strength**
- 8. Fine Grid FEM Stress Analysis Is Required to Accurately Predict Stress Equations for Service Life Analysis in Areas of Complex Load Sharing and Areas Having Stress Gradients**
- 9. Use of Extruded Shapes and Forged Shapes in Primary Structure Should Be Fully Investigated with Respect to Fracture Properties**
- 10. Material Properties Testing and Development Testing Must Be Accomplished Early in the Design Process**
- 11. Use of Generalized Allowable Stresses Okay for Design with Light to Moderate Usage. Overrated for Tough Requirements. Detail Allowable Curves or Detail Analysis Required**
- 12. Full Scale Testing Must Be Scheduled to at Least Be Concurrent with Final Design Release**
- 13. Still Difficult to Out Guess Weight and Usage Changes as Systems Mature**

# Still A Challenge - Combined Impact of Weight and Maneuver Activity

## Peak Load Exceedance Comparison Fuselage Station 373.8 Bending Moment



Vu-Graph 11

**REPORT DOCUMENTATION PAGE**

1. Recipient's Reference	2. Originator's Reference AGARD-R-797	3. Further Reference ISBN 92-835-0734-7	4. Security Classification of Document UNCLASSIFIED/ UNLIMITED
5. Originator	Advisory Group for Aerospace Research and Development North Atlantic Treaty Organization 7 rue Ancelle, 92200 Neuilly sur Seine, France		
6. Title	AN ASSESSMENT OF FATIGUE DAMAGE AND CRACK GROWTH PREDICTION TECHNIQUES		
7. Presented at	the 77th Meeting of the AGARD Structures and Materials Panel, held in Bordeaux, France 29th—30th September 1993.		
8. Author(s)/Editor(s) Various	9. Date March 1994		
10. Author's/Editor's Address Various	11. Pages 284		
12. Distribution Statement	There are no restrictions on the distribution of this document. Information about the availability of this and other AGARD unclassified publications is given on the back cover.		
13. Keywords/Descriptors			
Crack propagation Cracking — fracturing Fatigue — materials Aircraft Fatigue tests	Predictions Damage Fractures — materials Mathematical models		
14. Abstract			
Fatigue is an important consideration in structural design and monitoring of continued airworthiness of military aircraft.			
This Workshop titled "An Assessment of Fatigue Damage and Crack Growth Prediction Techniques" provided a forum for an in-depth discussion of the correlation between in-service experience and results from analytical predictive models, specimen level tests, component tests and full-scale tests. Additionally, it made possible an examination of the operating standards that different countries adopt with respect to various elements in the design process for assessment of fatigue damage.			

<p>AGARD Report 797 Advisory Group for Aerospace Research and Development, NATO AN ASSESSMENT OF FATIGUE, DAMAGE, AND CRACK GROWTH PREDICTION TECHNIQUES Published March 1994 284 pages</p> <p>Fatigue is an important consideration in structural design and monitoring of continued airworthiness of military aircraft.</p> <p>This Workshop titled "An Assessment of Fatigue, Damage and Crack Growth Prediction Techniques" provided a forum for an in-depth discussion of the correlation between in-service experience and results from analytical predictive models, specimen level tests, component tests</p> <p>P I O</p>	<p>AGARD-R-797</p> <p>Crack propagation Cracking — fracturing Fatigue — materials Aircraft Fatigue tests Predictions Damage Fractures — materials Mathematical models</p>	<p>AGARD Report 797 Advisory Group for Aerospace Research and Development, NATO AN ASSESSMENT OF FATIGUE, DAMAGE, AND CRACK GROWTH PREDICTION TECHNIQUES Published March 1994 284 pages</p> <p>Fatigue is an important consideration in structural design and monitoring of continued airworthiness of military aircraft.</p> <p>This Workshop titled "An Assessment of Fatigue, Damage and Crack Growth Prediction Techniques" provided a forum for an in-depth discussion of the correlation between in-service experience and results from analytical predictive models, specimen level tests, component tests</p> <p>P I O</p>	<p>AGARD-R-797</p> <p>Crack propagation Cracking — fracturing Fatigue — materials Aircraft Fatigue tests Predictions Damage Fractures — materials Mathematical models</p>
<p>AGARD Report 797 Advisory Group for Aerospace Research and Development, NATO AN ASSESSMENT OF FATIGUE, DAMAGE, AND CRACK GROWTH PREDICTION TECHNIQUES Published March 1994 284 pages</p> <p>Fatigue is an important consideration in structural design and monitoring of continued airworthiness of military aircraft.</p> <p>This Workshop titled "An Assessment of Fatigue, Damage and Crack Growth Prediction Techniques" provided a forum for an in-depth discussion of the correlation between in-service experience and results from analytical predictive models, specimen level tests, component tests</p> <p>P I O</p>	<p>AGARD-R-797</p> <p>Crack propagation Cracking — fracturing Fatigue — materials Aircraft Fatigue tests Predictions Damage Fractures — materials Mathematical models</p>	<p>AGARD Report 797 Advisory Group for Aerospace Research and Development, NATO AN ASSESSMENT OF FATIGUE, DAMAGE, AND CRACK GROWTH PREDICTION TECHNIQUES Published March 1994 284 pages</p> <p>Fatigue is an important consideration in structural design and monitoring of continued airworthiness of military aircraft.</p> <p>This Workshop titled "An Assessment of Fatigue, Damage and Crack Growth Prediction Techniques" provided a forum for an in-depth discussion of the correlation between in-service experience and results from analytical predictive models, specimen level tests, component tests</p> <p>P I O</p>	<p>AGARD-R-797</p> <p>Crack propagation Cracking — fracturing Fatigue — materials Aircraft Fatigue tests Predictions Damage Fractures — materials Mathematical models</p>

<p>and full-scale tests. Additionally, it made possible an examination of the operating standards that different countries adopt with respect to various elements in the design process for assessment of fatigue damage.</p> <p>Papers presented at the 77th Meeting of the AGARD Structures and Materials Panel, held in Bordeaux, France 29th—30th September 1993.</p> <p>ISBN 92-835-0734-7</p>	<p>and full-scale tests. Additionally, it made possible an examination of the operating standards that different countries adopt with respect to various elements in the design process for assessment of fatigue damage.</p> <p>Papers presented at the 77th Meeting of the AGARD Structures and Materials Panel, held in Bordeaux, France 29th—30th September 1993.</p> <p>ISBN 92-835-0734-7</p>
<p>and full-scale tests. Additionally, it made possible an examination of the operating standards that different countries adopt with respect to various elements in the design process for assessment of fatigue damage.</p> <p>Papers presented at the 77th Meeting of the AGARD Structures and Materials Panel, held in Bordeaux, France 29th—30th September 1993.</p> <p>ISBN 92-835-0734-7</p>	<p>and full-scale tests. Additionally, it made possible an examination of the operating standards that different countries adopt with respect to various elements in the design process for assessment of fatigue damage.</p> <p>Papers presented at the 77th Meeting of the AGARD Structures and Materials Panel, held in Bordeaux, France 29th—30th September 1993.</p> <p>ISBN 92-835-0734-7</p>

AGARD holds limited quantities of the publications that accompanied Lecture Series and Special Courses held in 1993 or later, and of AGARDographs and Working Group reports published from 1993 onward. For details, write or send a telefax to the address given above. *Please do not telephone.*

AGARD does not hold stocks of publications that accompanied earlier Lecture Series or Courses or of any other publications. Initial distribution of all AGARD publications is made to NATO nations through the National Distribution Centres listed below. Further copies are sometimes available from these centres (except in the United States). If you have a need to receive all AGARD publications, or just those relating to one or more specific AGARD Panels, they may be willing to include you (or your organisation) on their distribution list. AGARD publications may be purchased from the Sales Agencies listed below, in photocopy or microfiche form.

NATIONAL DISTRIBUTION CENTRES

**BELGIUM**

Coordonnateur AGARD – VSL  
Etat-Major de la Force Aérienne  
Quartier Reine Elisabeth  
Rue d'Evere, 1140 Bruxelles

**CANADA**

Director Scientific Information Services  
Dept of National Defence  
Ottawa, Ontario K1A 0K2

**DENMARK**

Danish Defence Research Establishment  
Ryvangs Allé 1  
P.O. Box 2715  
DK-2100 Copenhagen Ø

**FRANCE**

O.N.E.R.A. (Direction)  
29 Avenue de la Division Leclerc  
92322 Châtillon Cedex

**GERMANY**

Fachinformationszentrum  
Karlsruhe  
D-7514 Eggenstein-Leopoldshafen 2

**GREECE**

Hellenic Air Force  
Air War College  
Scientific and Technical Library  
Dekelia Air Force Base  
Dekelia, Athens TGA 1010

**ICELAND**

Director of Aviation  
c/o Flugrad  
Reykjavik

**ITALY**

Aeronautica Militare  
Ufficio del Delegato Nazionale all'AGARD  
Aeroporto Pratica di Mare  
00040 Pomezia (Roma)

**LUXEMBOURG**

See Belgium

**NETHERLANDS**

Netherlands Delegation to AGARD  
National Aerospace Laboratory, NLR  
P.O. Box 90502  
1006 BM Amsterdam

**NORWAY**

Norwegian Defence Research Establishment  
Attn: Biblioteket  
P.O. Box 25  
N-2007 Kjeller

**PORTUGAL**

Força Aérea Portuguesa  
Centro de Documentação e Informação  
Alfragide  
2700 Amadora

**SPAIN**

INTA (AGARD Publications)  
Pintor Rosales 34  
28008 Madrid

**TURKEY**

Milli Savunma Başkanlığı (MSB)  
ARGE Daire Başkanlığı (ARGE)  
Ankara

**UNITED KINGDOM**

Defence Research Information Centre  
Kentigern House  
65 Brown Street  
Glasgow G2 8EX

**UNITED STATES**

NASA Headquarters  
Attention: CF 37, Distribution Center  
300 E Street, S.W.  
Washington, D.C. 20546

The United States National Distribution Centre does NOT hold stocks of AGARD publications. Applications for copies should be made direct to the NASA Center for Aerospace Information (CASI) at the address below.

SALES AGENCIES

NASA Center for  
Aerospace Information (CASI)  
800 Elkridge Landing Road  
Linthicum Heights, MD 21090-2934  
United States

ESA Information Retrieval Service  
European Space Agency  
10, rue Mario Nikis  
75015 Paris  
France

The British Library  
Document Supply Centre  
Boston Spa, Wetherby  
West Yorkshire LS23 7BQ  
United Kingdom

Requests for microfiches or photocopies of AGARD documents (including requests to CASI) should include the word 'AGARD' and the AGARD serial number (for example AGARD-AG-315). Collateral information such as title and publication date is desirable. Note that AGARD Reports and Advisory Reports should be specified as AGARD-R-*nnn* and AGARD-AR-*nnn*, respectively. Full bibliographical references and abstracts of AGARD publications are given in the following journals:

Scientific and Technical Aerospace Reports (STAR)  
published by NASA Scientific and Technical  
Information Program  
NASA Headquarters (JTT)  
Washington D.C. 20546  
United States

Government Reports Announcements and Index (GRA&I)  
published by the National Technical Information Service  
Springfield  
Virginia 22161  
United States  
(also available online in the NTIS Bibliographic  
Database or on CD-ROM)



Printed by Specialised Printing Services Limited  
40 Chigwell Lane, Loughton, Essex IG10 3TZ

Aucun stock de publications n'a existé à AGARD. A partir de 1993, AGARD détient un stock limité des publications associées aux cycles de conférences et cours spéciaux ainsi que les AGARDographies et les rapports des groupes de travail, organisés et publiés à partir de 1993 inclus. Les demandes de renseignements doivent être adressées à AGARD par lettre ou par fax à l'adresse indiquée ci-dessus. *Veuillez ne pas téléphoner.* La diffusion initiale de toutes les publications de l'AGARD est effectuée auprès des pays membres de l'OTAN par l'intermédiaire des centres de distribution nationaux indiqués ci-dessous. Des exemplaires supplémentaires peuvent parfois être obtenus auprès de ces centres (à l'exception des États-Unis). Si vous souhaitez recevoir toutes les publications de l'AGARD, ou simplement celles qui concernent certains Panels, vous pouvez demander à être inclus sur la liste d'envoi de l'un de ces centres. Les publications de l'AGARD sont en vente auprès des agences indiquées ci-dessous, sous forme de photocopie ou de microfiche.

CENTRES DE DIFFUSION NATIONAUX

## ALLEMAGNE

Fachinformationszentrum,  
Karlsruhe  
D-7514 Eggenstein-Leopoldshafen 2

## BELGIQUE

Coordonnateur AGARD-VSL  
Etat-Major de la Force Aérienne  
Quartier Reine Elisabeth  
Rue d'Evere, 1140 Bruxelles

## CANADA

Directeur du Service des Renseignements Scientifiques  
Ministère de la Défense Nationale  
Ottawa, Ontario K1A 0K2

## DANEMARK

Danish Defence Research Establishment  
Rysvangs Alle 1  
P.O. Box 2715  
DK-2100 Copenhagen Ø

## ESPAGNE

INTA (AGARD Publications)  
Pintor Rosales 34  
28008 Madrid

## ETATS-UNIS

NASA Headquarters  
Attention: CF 37, Distribution Center  
3010 E. Street, SW  
Washington, D.C. 20546

## FRANCE

O.N.E.R.A. (Direction)  
29, Avenue de la Division Leclerc  
92322 Châtillon Cedex

## GRECE

Hellenic Air Force  
Air War College  
Scientific and Technical Library  
Dekelia Air Force Base  
Dekelia, Athens TGA 1010

## ISLANDE

Director of Aviation  
c/o Flugrad  
Reykjavik

## ITALIE

Aeronautica Militare  
Ufficio del Delegato Nazionale all'AGARD  
Aeroporto Pratica di Mare  
00040 Pomezia (Roma)

## LUXEMBOURG

Voir Belgique

## NORVEGE

Norwegian Defence Research Establishment  
Attn: Biblioteket  
P.O. Box 25  
N-2007 Kjeller

## PAYS-BAS

Netherlands Delegation to AGARD  
National Aerospace Laboratory NLR  
P.O. Box 90502  
1006 BM Amsterdam

## PORTUGAL

Força Aérea Portuguesa  
Centro de Documentação e Informação  
Alfragide  
2700 Amadora

## ROYAUME UNI

Defence Research Information Centre  
Kensington House  
65 Brown Street  
Glasgow G2 8EX

## TURQUIE

Milli Savunma Başkanlığı (MSB)  
ARGE Daire Başkanlığı (ARGE)  
Ankara

Le centre de distribution national des États-Unis ne détient PAS de stocks des publications de l'AGARD.

D'éventuelles demandes de photocopies doivent être formulées directement auprès du NASA Center for Aerospace Information (CASI) à l'adresse suivante:

AGENCES DE VENTE

NASA Center for  
Aerospace Information (CASI)  
800 Elkridge Landing Road  
Linthicum Heights, MD 21090-2934  
United States

ESA Information Retrieval Service  
European Space Agency  
10, rue Mario Nikis  
75015 Paris  
France

The British Library  
Document Supply Division  
Boston Spa, Wetherby  
West Yorkshire LS23 7BQ  
Royaume Uni

Les demandes de microfiches ou de photocopies de documents AGARD (y compris les demandes faites auprès du CASI) doivent comporter la dénomination AGARD, ainsi que le numéro de série d'AGARD (par exemple AGARD-AG-315). Des informations analogues, telles que le titre et la date de publication sont souhaitables. Veuillez noter qu'il s'agit de spécifier AGARD-R-*num* et AGARD-AR-*num* lors de la commande des rapports AGARD et des rapports consultatifs AGARD respectivement. Des références bibliographiques complètes ainsi que des résumés des publications AGARD figurent dans les journaux suivants:

Scientific and Technical Aerospace Reports (STAR)  
publié par la NASA Scientific and Technical  
Information Program  
NASA Headquarters (JTT)  
Washington D.C. 20546  
Etats-Unis

Government Reports Announcements and Index (GRA&I)  
publié par le National Technical Information Service  
Springfield  
Virginia 22161  
Etats-Unis  
(accessible également en mode interactif dans la base de  
données bibliographiques en ligne du NTIS, et sur CD-ROM)

